

The Institute for Solid State Physics
The University of Tokyo

Activity Report 2020

S

S

T

ISSP

Activity Report 2020

Contents	Pages
Preface	1
Research Highlights	2 - 39
Joint Research Highlights	40 - 55
Progress of Facilities	56 - 63
Conferences and Workshops	64 - 67
Subjects of Joint Research	68 - 155
Publications	156 - 194



Preface

We would like to offer the readers the scientific activity report of the Institute for Solid State Physics (ISSP) for the Japanese FY 2020.

ISSP was established in 1957 as a joint usage/research institute attached to the University of Tokyo. In every era, we aim to lead the frontier of “condensed matter physics and materials science” and contribute to science and technology from the view of basic research. We have promoted activities focused on research, education, and joint usage/research.

The first and second parts of the report, Research Highlights/Joint Research Highlights, exhibit experimental and theoretical achievements in condensed matter physics and materials science. In 2020, the number of adapted joint usage/research is 1,042 and the total number of researchers is 931, which was reduced by the COVID-19 pandemic.

The third part includes the reports on progress of facilities in 2020 as follows. (1) In International MegaGauss Science Laboratory, the pulse magnets can generate up to 87 Tesla (T) by non-destructive manner, and from 100 T up to 1200 T, the world strongest as an in-door record, by destructive methods to promote materials science under high magnetic field. (2) In the Supercomputer Center (SCC), the System B was replaced in October 2020, which has larger total computational power. In Center of Computational Materials Science, the website "MateriApps" for information on application software in computational science has been constructed to support community members. (3) In Neutron Science Laboratory, it is really good news that JRR-3 has restarted in February 2021 after long shutdown and the normal General User Program is scheduled to come back from July 2021. The technical progress of High Resolution Chopper (HRC) spectrometer has been proceeded under high pressure and low temperature environment in cooperation with KEK. (4) The Laser and Synchrotron Research (LASOR) center has 10 groups in 2020 where ISSP has integrated the two streams, namely the extreme lasers and synchrotron radiations, into the common platform. In Synchrotron Radiation Laboratory, operand spectroscopy is available by using lasers at Harima branch.

In the following parts, seven reports of international and domestic online conferences and workshops owing to COVID-19 pandemic, subjects of joint research, and list of publications have been presented.

The fourth international external evaluation was held by hybrid-style from December 7 to 10, 2020 for the proposal of the next Joint Usage/Research Center during FY2022~2027. The activities toward the current five missions, the activities of two cross-sectional groups established after the last evaluation, and the establishment of a materials data commons (materials data science research) and a quantum materials nanostructure laboratory as future plans were proposed and evaluated by the international evaluation committee with important and useful comments.

All these facts confirm that ISSP continues to develop successfully and dynamically as the global center of excellence of condensed matter physics and materials science. We appreciate continuous support and cooperation of communities for our activities.



July, 2021
MORI Hatsumi
Director of the Institute for Solid State Physics
The University of Tokyo

Research Highlights

Vapochromism Induced by Intermolecular Electron Transfer Coupled with Hydrogen-Bond Formation in Zinc Dithiolene Complex

Mori and Ozaki Groups

Reversible control of electronic functionalities of molecular materials using external stimuli and perturbations is important not only for applications to next-generation switching devices and sensors but also from the viewpoint of basic science to elucidate the mechanism and to establish the material design criteria. Recently we have demonstrated a proton-electron coupled phenomenon in H (hydrogen)-bonded π -conjugated molecular crystals [1-3], in which magnetism and electrical conductivity were switched by proton (deuteron) dynamics in an intermolecular H-bond. If control of the functionalities, such as optical properties, other than magnetism and electrical conductivity by modulating the electronic states through H-bonding is well established, it will impact various research fields and greatly expand the design criteria of functional materials. As one of the functional molecular materials with optical properties responsive to external stimuli, vapochromic materials, which respond with color changes when exposed to solvent vapors, have been actively studied as good candidates for their use as chemical sensors because they can directly visualize external environmental changes. In this study, we focused on a novel Zn complex, $(\text{Ph}_4\text{P})_2[\text{Zn}(4\text{-mxbdt})_2]$ (**1** in Fig. 1; 4-mxbdt = 4-methoxybenzene-1,2-dithiolate) to realize the control of vapochromic behavior by direct modulation of electronic states through H-bonding. Based on the detailed single-crystal structure analyses and first-principles calculations considering intermolecular interactions using the periodic structure model of the crystal, we disclosed a new mecha-

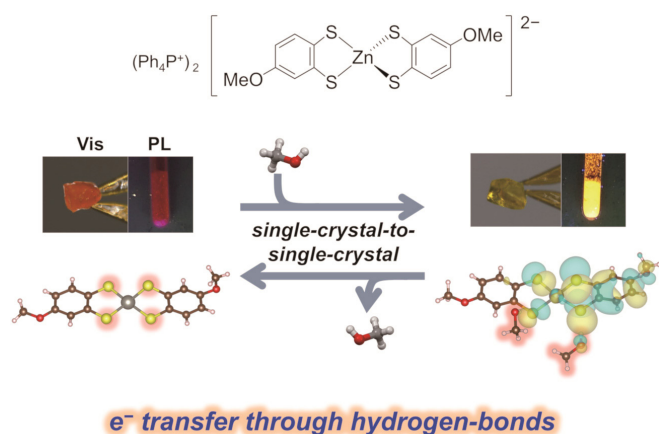


Fig. 1. A novel vapochromic mechanism by intermolecular electron transfer coupled with hydrogen-bond formation was realized in a zinc dithiolene complex crystals, $(\text{Ph}_4\text{P})_2[\text{Zn}(4\text{-mxbdt})_2]$ (**1**, left) and $1 \cdot 2\text{CH}_3\text{OH}$ (right).

nism of vapochromism in **1**, that is, not molecular structure and arrangement changes but electron transfer via H-bond formation for the first time [2].

The Zn complex **1** was synthesized by complexation of zinc(II) chloride and the ligand precursor in methanol. Yellow block-like crystals were obtained by the slow evaporation of the crude mixture. From the X-ray structural analysis, the yellow crystal was determined as $(\text{Ph}_4\text{P})_2[\text{Zn}(4\text{-mxbdt})_2] \cdot 2\text{CH}_3\text{OH}$ ($= 1 \cdot 2\text{MeOH}$) (Fig. 1). In this crystal, the $[\text{Zn}(4\text{-mxbdt})_2]$ complex showed tetrahedral coordination without a π -stacking structure because of the presence of bulky Ph_4P^+ cations, and thus there were no significant intermolecular interactions between the complexes. The spaces in the loosely packed structure were filled with two methanol molecules per formula. These methanol molecules formed $[\text{S} \cdots \text{H}-\text{O}]$ H-bonds with S atoms on the $[\text{Zn}(4\text{-mxbdt})_2]^{2-}$. Interestingly, drying the crystals overnight under vacuum induced the color change from yellow to orange, maintaining its high crystallinity (Fig. 1).

We quantitatively evaluated the color change of each crystal by UV-vis absorption spectra. Visible-light absorption edges of the orange crystal **1** and yellow crystals, $1 \cdot \text{H}_2\text{O}$ and $1 \cdot 2\text{MeOH}$, were estimated to be 2.29 eV (541 nm), 2.41 eV (514 nm), and 2.45 eV (506 nm), respectively. A blue shift of the absorption edge (0.12–0.16 eV) upon methanol or water vapor absorption was observed, which is consistent with the visually observed color changes. We also evaluated the photoluminescence properties of these crystals. Significantly, a blue shift was observed in the photoluminescence spectra (0.10–0.14 eV) for both $1 \cdot \text{H}_2\text{O}$ and $1 \cdot 2\text{MeOH}$, similar to the

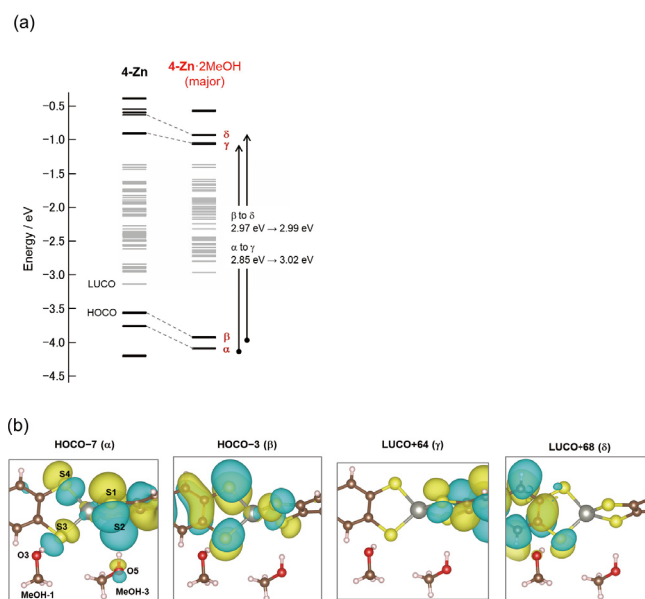


Fig. 2. (a) Crystal orbital energies of **1** and $1 \cdot 2\text{MeOH}$ (major) and (b) corresponding crystal orbitals in $1 \cdot 2\text{MeOH}$ (major). Crystal orbitals from -3.2 eV to -1.3 eV (left; gray lines) are mostly on Ph_4P^+ cation molecules.

UV-vis absorption spectra. The apparent color changed from red to yellowish-orange. These experimental data demonstrate that crystal **1** is a novel vapochromic material having both visible-light absorption and photoluminescence changes when exposed to methanol or water sorption with reversible SCSC (single crystal-single crystal) transformations. Remarkably, this is the first report of metal-dithiolene-based vapochromic materials with SCSC transformations.

Then, we focused on the mechanism of vapochromism in this crystal, **1**·2MeOH. DFT calculations based on the experimentally observed crystal structures using OpenMX software revealed the mechanism of the Fig. 2(b) H-bonding structures in **1**·2MeOH. In **1**·2MeOH (major), energy gaps for both α to γ and β to δ transitions increased (α to γ : 2.85 eV to 3.02 eV, β to δ : 2.97 eV to 2.99 eV), where the α and β orbitals were more stabilized than γ and δ (Fig. 2 (a)). This is because of the fact that the occupied orbital groups (α and β) have a large weight on the H-bonding S atoms, on which the largest changes in the number of electrons were estimated by Mulliken population analysis, compared with the unoccupied orbital groups (γ and δ). Considering the orbital shape around the H-bond, these crystal orbitals are derived from the hybridization of the frontier orbitals (HOMO-1, HOMO, LUMO, and LUMO+1) of the $[\text{Zn}(4\text{-mxbd})_2]^{2-}$ complex with the LUMO of the absorbed vapor molecules at higher energies. This hybridization leads to the above-mentioned electron transfer to stabilize both the α/β and γ/δ orbitals.

In conclusion, a novel mechanism of vapochromism based on the intermolecular electron transfer coupled with H-bond formation was realized in the newly obtained zinc dithiolene complex crystal, $(\text{Ph}_4\text{P})_2[\text{Zn}(4\text{-mxbd})_2] \cdot 2\text{CH}_3\text{OH}$. According to the mechanism proposed in this study, molecules in which molecular orbitals for visible-light absorption are significantly distributed to H-bonding parts can be promising candidates for a new class of vapochromic materials. The findings here provide important insights to expand the scope of molecular designs for vapochromic as well as other stimuli-responsive materials.

References

- [1] S. Yokomori, A. Ueda, T. Higashino, R. Kumai, Y. Murakami, and H. Mori, *Cryst Eng Commun.* **21**, 2940 (2019).
- [2] S. Yokomori, S. Dekura, T. Fujino, M. Kawamura, T. Ozaki, and H. Mori, *J. Mater. Chem. C*, **8**, 14939 (2020).
- [3] S. Yokomori, S. Dekura, A. Ueda, R. Kumai, Y. Murakami, and H. Mori, *J. Mater. Chem.* (to be published).

Authors

S. Yokomori, S. Dekura, T. Fujino, M. Kawamura, T. Ozaki, and H. Mori

Nonlinear Anomalous Hall Effect in Organic Massive Dirac Fermion System

Osada Group

When an electron system has a conduction band with a finite Berry curvature and no time reversal symmetry, it may exhibit the intrinsic anomalous Hall effect (AHE) even at zero magnetic field. This topologically nontrivial transport phenomena disappears in equilibrium state of the system with time reversal symmetry. However, the AHE may revive

as a nonlinear transport phenomenon in the non-equilibrium state carrying finite electric current.

In this study, we predicted the nonlinear AHE in a layered organic conductor α -(BEDT-TTF) $_2\text{I}_3$, and confirmed it experimentally. This is the first example of topological transport phenomena in organic conductors. We focused on the "weak" charge ordering (CO) state in α -(BEDT-TTF) $_2\text{I}_3$, where the inversion symmetry is broken. This compound exhibits a phase transition to a CO insulator at 135 K at ambient pressure. This CO transition is suppressed by pressure, and a two-dimensional (2D) massless Dirac fermion (DF) state appears above the critical pressure $P_c \sim 1.3$ GPa. The CO state just below P_c is called the weak CO state.

First, we experimentally established the fact that the weak CO state is a 2D massive DF state with a pair of tilted gapped Dirac cones [1]. We used the temperature-dependent peak structure of the interlayer magnetoresistance, which is peculiar to the layered DF system. The magnetic field dependence of the peak temperature observed in the weak CO state is explained only by the massive DF with a finite gap. Therefore, a finite Berry curvature appears in the weak CO state.

Next, we investigated the nonlinear AHE in the current-carrying state in the 2D massive DF system [2]. Under the time reversal symmetry, the sum of Berry curvature over occupied states is canceled out between the Kramers pair of Dirac cones, resulting in no AHE in the equilibrium state. However, if the Dirac cones are tilting, this Berry curvature balance is broken between the Dirac cone pair in the current-carrying state with non-equilibrium distribution. It revives finite AHE as the current-induced nonlinear AHE. The efficiency for the appearance of this current-induced phenomenon is represented by the Berry curvature dipole (BCD) of the system. We demonstrated the anisotropy and rectification characteristics (non-reciprocity) of the nonlinear AHE in the 2D tilted massive DF system. The generated Hall current exhibits unidirectionality even under an external AC field. Furthermore, we quantitatively estimated the nonlinear AHE expected in the weak CO state in α -(BEDT-TTF) $_2\text{I}_3$, and concluded that it is within the measurable range.

In real α -(BEDT-TTF) $_2\text{I}_3$, there may exist two types of

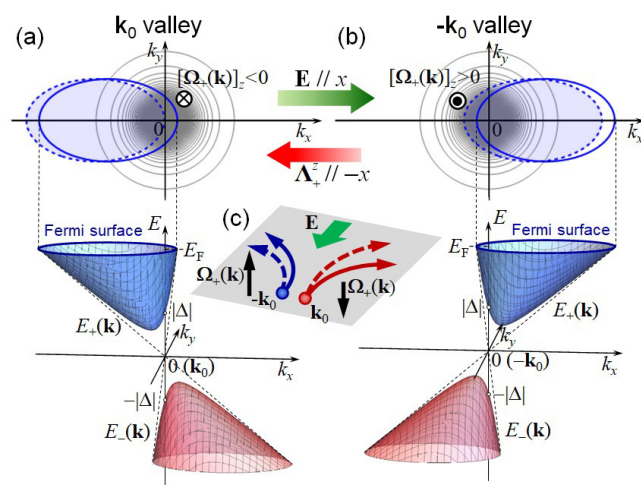


Fig. 1. Current-carrying state in the 2D massive DF system with tilted Dirac cones around (a) k_0 and (b) $-k_0$. Lower panels depict the band dispersion and upper panels illustrate the Berry curvature (contours) and the Fermi surface of the conduction band. The hatched region indicates occupied states in the current-carrying state. (c) Schematic of the nonlinear AHE. The balance of average anomalous velocity of electrons around k_0 and $-k_0$ is broken (dashed arrows) in the current-carrying state.

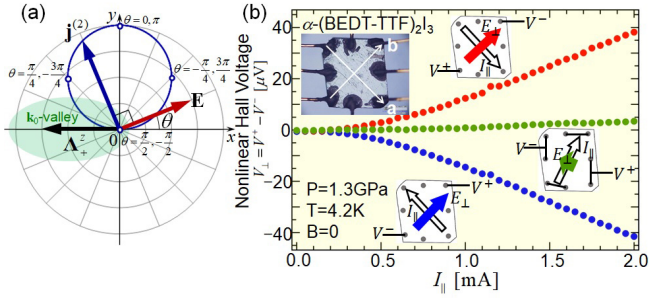


Fig. 2. (a) Dependence of anomalous Hall current $\mathbf{j}(2)$ on the electric field direction θ in the current-carrying state. (b) Nonlinear AHE observed in the weak CO state in α -(BEDT-TTF) $_2$ I $_3$. It shows the rectifying characteristics, that is, the same Hall voltage against reversed current.

CO domains, which cancel the nonlinear AHE under current. So, we proposed the "current-field-cooling" technique, for macroscopic emergence of nonlinear AHE [2]. It utilizes the current-induced orbital magnetization (orbital Edelstein effect) to enhance the formation of single type of CO domains.

Finally, we attempted an experimental confirmation of the nonlinear AHE in the weak CO state in α -(BEDT-TTF) $_2$ I $_3$. We performed transport measurements in the weak CO state at 1.25 GPa and 4.2 K, and extracted the nonlinear signal from current-reversed data. We successfully observed nonlinear AHE with estimated order and rectifying characteristics only below the CO transition temperature [3].

References

- [1] K. Yoshimura, M. Sato, and T. Osada, J. Phys. Soc. Jpn. **90**, 033701 (2021).
- [2] T. Osada and A. Kiswandhi, J. Phys. Soc. Jpn. **89**, 103701 (2020); *ibid.* 128002 (2020).
- [3] A. Kiswandhi and T. Osada, arXiv: 2103.00300.

Authors

T. Osada, A. Kiswandhi, K. Yoshimura, M. Sato, K. Uchida, and T. Taen

Thermal Hall Effects of Spins and Phonons in Kagome Antiferromagnet Cd-Kapellasite

Yamashita, Hiroi, Kawashima, and Sakakibara Groups

The trajectory of an electron bends as it moves through a magnetic field. This Hall effect has been thought to not appear in insulators because of the apparent absence of mobile electrons. But recent reports of a thermal version of this effect, known as the thermal Hall effect, in numerous insulators has led to broad attention from researchers to understand its origin as well as potential applications for thermal current control.

Thermal current in an insulator is carried by spins and phonons. This leads us to ask how these charge neutral carriers can be bent by magnetic fields and how one can separate these two effects. To clarify the issue, we investigate the magnetic insulator Cd-kapellasite CdCu $_3$ (OH) $_6$ (NO $_3$) $_2$, a kagomé antiferromagnet [1]. In Cd-kapellasite, Cu $^{2+}$ ions form a kagomé structure with a dominant nearest-neighbor antiferromagnetic interaction $J/k_B = 45$ K. The geometrical frustration effect of the

kagomé structure suppresses the magnetic order down to $T_N = 4$ K, realizing a spin liquid state in a wide temperature range $T_N < T < J/k_B$.

We find clear thermal Hall signals in the spin liquid phase in all samples. The thermal Hall conductivity (κ_{xy}) is larger in a higher-quality sample with a larger longitudinal thermal conductivity (κ_{xx}), whereas the temperature dependence of κ_{xy} is similar (Fig. 1(a)). At 15 T, κ_{xy} and κ_{xx} are found to show a peak at almost the same temperature, a telltale sign of a phonon contribution κ_{xy}^{ph} in κ_{xy} at high fields. In addition, we find that the field dependence of κ_{xy} turns to be nonlinear at low temperatures and at low fields (Fig. 1(b)), concomitantly with the appearance of the field suppression of κ_{xx} , indicating the presence of a spin contribution κ_{xy}^{sp} in κ_{xy} at low fields. This is the first observation of both κ_{xy}^{ph} and κ_{xy}^{sp} in the same magnetic insulator.

Remarkably, by assembling the κ_{xx} dependence of κ_{xy}^{sp} data of other kagome antiferromagnets, we find that, whereas κ_{xy}^{sp} stays a constant in the low- κ_{xx} region (the "intrinsic" line in Fig. 2), κ_{xy}^{sp} starts to increase as κ_{xx} does in the high- κ_{xx} region (the "extrinsic" line in Fig. 2). This κ_{xx} dependence bears similarity to that of the anomalous Hall effect in ferromagnetic metals; the intrinsic mechanism by the Berry curvature is dominant in a moderate dirty metal, whereas the extrinsic mechanism by skew scatterings is dominant for a superclean metal. This good analogy indicates the presence

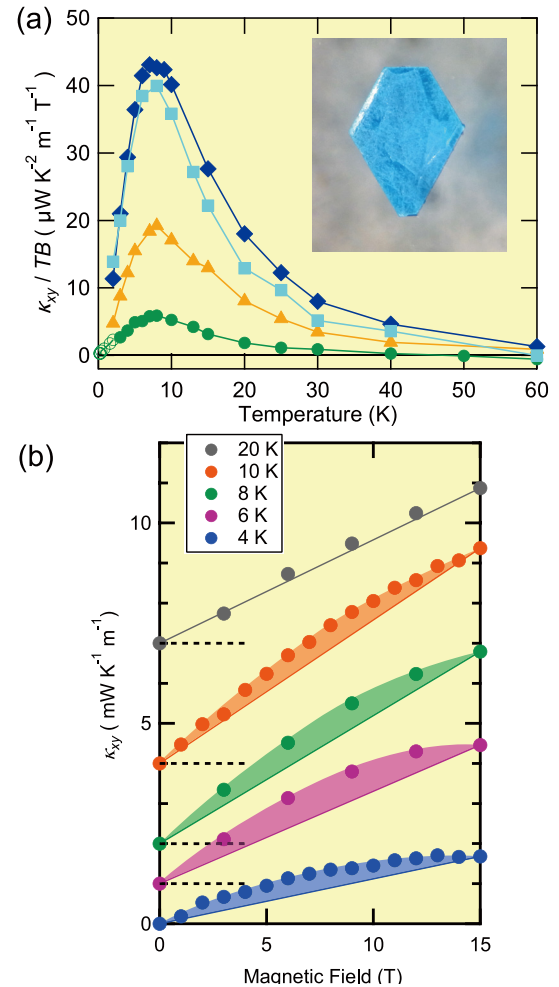


Fig. 1. (a) The temperature dependence of the thermal Hall conductivity of Cd-kapellasite of different samples at 15 T [1]. All the samples show a peak at the same temperature, but with different magnitudes. (b) The field dependence of κ_{xy} at different temperatures. The non-linear part (colored region) shows the spin contribution.

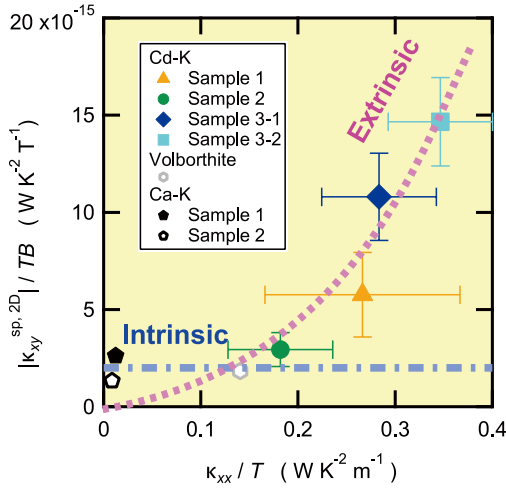


Fig. 2. The dependence of the spin thermal Hall conductivity per the 2D kagomé layer ($\kappa_{xy}^{sp, 2D}$) on the longitudinal thermal conductivity (κ_{xx}) of Cd-kapellsite [1], Volborthite [2], and Ca-kapellsite [3]. The blue and pink dashed lines are guides to the eye for the intrinsic and extrinsic contributions, respectively.

of a similar duality of intrinsic-extrinsic mechanisms for the spin thermal Hall effect of an insulator.

Furthermore, we find that both κ_{xy}^{ph} and κ_{xy}^{sp} disappear in the antiferromagnetic ordered phase at low fields, showing that phonons alone do not exhibit the thermal Hall effect. A high field above approximately 7 T induces κ_{xy}^{ph} , concomitantly with a field-induced increase of κ_{xx} and the specific heat, suggesting a coupling of the phonons to the field-induced spin excitations as the origin of κ_{xy}^{ph} .

References

- [1] M. Akazawa *et al.*, Phys. Rev. X **10**, 041059 (2020).
- [2] D. Watanabe *et al.*, Proc. Natl. Acad. Sci. USA **113**, 8653 (2016).
- [3] H. Doki, M. Akazawa, H.-Y. Lee *et al.*, Phys. Rev. Lett. **121**, 097203 (2018).

Authors

M. Akazawa, M. Shimozawa^a, S. Kittaka^b, T. Sakakibara, R. Okuma, Z. Hiroi, H.-Y. Lee^c, N. Kawashima, J. H. Han^d, M. Yamashita

^aOsaka University

^bChuo University

^cKorea University

^dSungkyunkwan University

Presence and Absence of Itinerant Gapless Excitations in the Quantum Spin Liquid Candidate EtMe₃Sb[Pd(dmit)₂]₂

Yamashita Group

The presence or absence of itinerant gapless excitations in the organic quantum spin liquid (QSL) candidate EtMe₃Sb[Pd(dmit)₂]₂, probed by a finite residual linear term in the thermal conductivity $\kappa_0/T \equiv \kappa/T$ ($T \rightarrow 0$), has been controversial hot topic. We find that κ_0/T strongly depends on the cooling process. A finite κ_0/T is observed in a slow-cooled sample, but not in a rapid-cooled sample [1]. These results provide evidence that the true ground state of EtMe₃Sb[Pd(dmit)₂]₂ is a QSL with itinerant gapless excitations.

The organic Mott insulator EtMe₃Sb[Pd(dmit)₂]₂ possesses a nearly isotropic triangular lattice of localized spin-1/2 on the Pd(dmit)₂ dimers. This geometrical frustration effect caused by the triangular lattice and a proximity effect of the Mott transition are believed to enhance the zero-

point fluctuation not to allow the spins to order. While the presence of a finite linear residual thermal conductivity, $\kappa_0/T \equiv \kappa/T$ ($T \rightarrow 0$) has been shown [2], recent experiments [3, 4, 5] have reported the absence of κ_0/T in some samples. (Fig. 1). However, in the experiments reporting the absence of κ_0/T , the phonon thermal conductivity is strongly suppressed [3]. In sharp contrast, a large phonon thermal conductivity with a phonon mean free path reaching almost the boundary limit is observed in the experiments showing the presence of the κ_0/T . Therefore, it is not clear if the absence of κ_0/T shows absence of the gapless spin excitations or if the gapless spin excitations are simply suppressed when the phonons are strongly scattered.

Here we show that both the magnitude of the phonon thermal conductivity and the presence/absence of κ_0/T strongly depend on the cooling process of the sample. When cooling down very slowly, a sizable κ_0/T is observed. In contrast, when cooling down rapidly, κ_0/T vanishes and, in addition, the phonon thermal conductivity is strongly suppressed. These results suggest that possible random scatterers introduced during the cooling process are responsible for the apparent discrepancy of the thermal conductivity data in this organic system. The present results provide evidence that the true ground state of EtMe₃Sb[Pd(dmit)₂]₂ is likely to be a quantum spin liquid with itinerant gapless excitations.

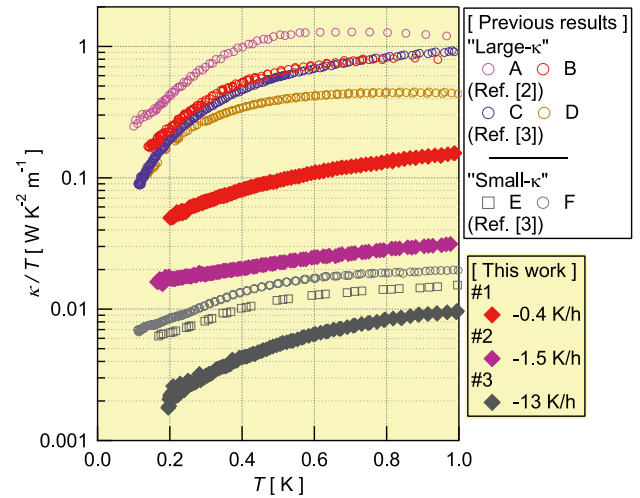


Fig. 1. Temperature dependence of the thermal conductivity divided by the temperature of EtMe₃Sb[Pd(dmit)₂]₂. The data of the previous reports [2, 3] are also plotted.

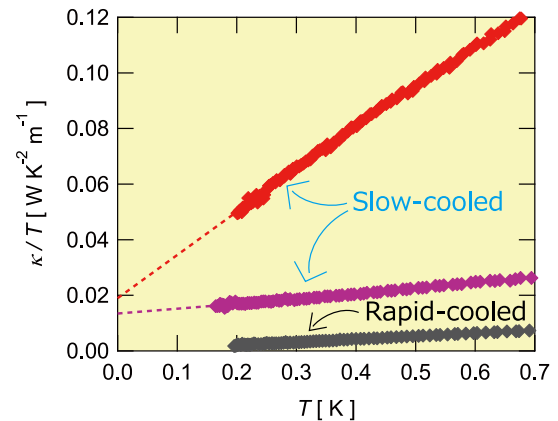


Fig. 2. Low-temperature data of κ/T plotted as a function of T . The dashed lines show an extrapolation of the data.

References

- [1] M. Yamashita *et al.*, Phys. Rev. B **101**, 140407(R) (2020) * Editor's suggestion.
 [2] M. Yamashita *et al.*, Science **328**, 1246 (2010).
 [3] M. Yamashita, J. Phys. Soc. Jpn. **88**, 083702 (2019).
 [4] P. Bourgeois-Hope *et al.*, Phys. Rev. X **9**, 041051 (2019)
 [5] J. M. Ni *et al.*, Phys. Rev. Lett. **123**, 247204 (2019).

Authors

M. Yamashita, Y. Sato^a, T. Tominaga^a, Y. Kasahara^a, S. Kasahara^a, H. Cui^b, R. Kato^b, T. Shibauchi^c, and Y. Matsuda^a
^aKyoto University
^bRIKEN
^cThe University of Tokyo

Sample Dependence of the Half-Integer Quantized thermal Hall Effect in a Kitaev Candidate α -RuCl₃

Yamashita and Uwatoko Groups

Non-trivial topology in a condensed-matter state realizes a quantization of a physical quantity. One of the most fundamental examples is the quantized Hall conductivity in a quantum Hall system, where the quantized Hall conductivity is given by the Chern number determined by the topology of the system.

A new intriguing case of this topological quantization is now found in a magnetic insulator, a Kitaev magnet. In the Kitaev model, localized spin-1/2 moments on a two-dimensional (2D) honeycomb structure are coupled each other by bond-dependent Ising interactions. The frustration

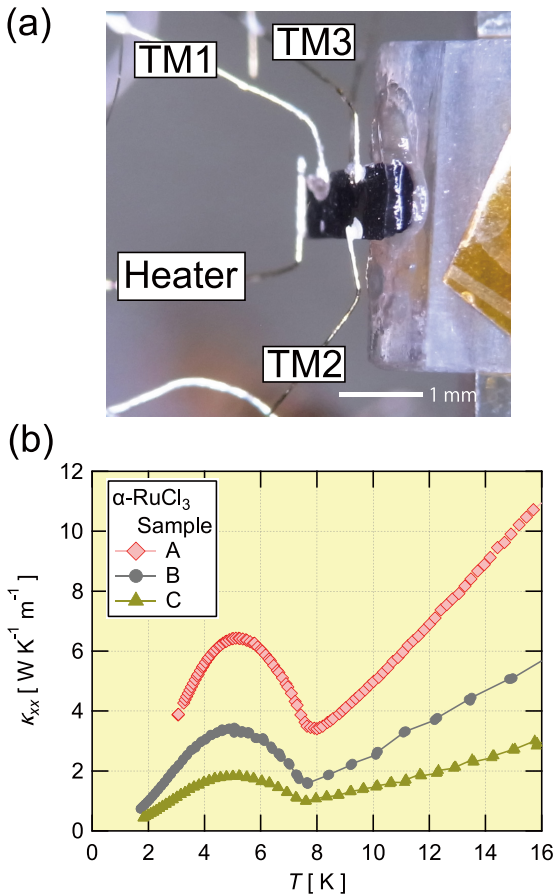


Fig. 1. (a) A setup picture of the thermal conductivity (κ_{xx}) and the thermal Hall (κ_{xy}) of α -RuCl₃ (sample A). The sample was tilted to the base plate so that the magnetic field oriented to 45 degree to the c axis. (b) The temperature dependence of κ_{xx} of different samples (A, B, and C) at zero field.

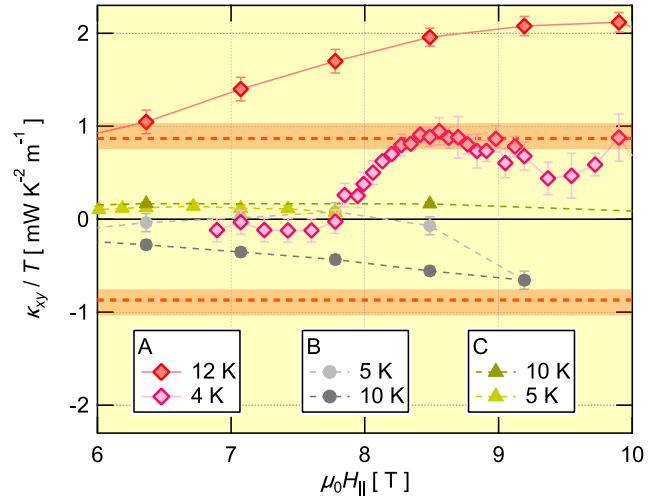


Fig. 2. The in-plane field dependence of κ_{xy}/T of all the samples. The dotted lines show the value corresponding to the half-integer quantized thermal Hall effect $\kappa_{xy}^{2D}/T = q_t C/2$, where $q_t = (\pi/6)k_B^2/\hbar$. The sign of κ_{xy} of sample A is inverted for a clarity.

effect of this Kitaev Hamiltonian prevents the spins from ordering even at the zero temperature, realizing a quantum spin liquid state. Remarkably, this ground state of the Kitaev Hamiltonian is exactly solvable. The ground state has been shown to be characterized by the two kinds of elementary excitations; itinerant Majorana fermions and localized Z₂ fluxes. In a magnetic field, this itinerant Majorana fermions have topologically non-trivial gapped bands with the Chern number $C = \pm 1$, giving rise to a quantized chiral edge current protected by the field-induced gap. In contrast to a quantized chiral edge current of electrons in a quantum Hall system, this chiral edge current is carried by the charge neutral Majorana fermions. Therefore, this quantized chiral edge current has been predicted to appear in the 2D thermal Hall conductivity as $\kappa_{xy}^{2D}/T = q_t C/2$, where $q_t = (\pi/6)k_B^2/\hbar$.

In this work [1], we reveal that it is necessary to protect the chiral edge current from severe scattering effects on phonons to stabilize the quantized thermal current. We investigate the sample dependence of the longitudinal (κ_{xx}) and transverse (κ_{xy}) thermal conductivity of three single crystals of α -RuCl₃ – a promising candidate realizing the Kitaev spin liquid [2]. We find the half-integer quantized thermal Hall effect in a sample showing the largest κ_{xx} among the three crystals (sample A in Fig. 1). On the other hand, the other samples with smaller κ_{xx} show κ_{xy} much smaller than the value expected for the quantization (Fig. 2). Given that κ_{xx} is mostly given by phonons, the different magnitudes of κ_{xx} in different samples reflect the different scattering strengths on phonons; phonons in a sample with smaller κ_{xx} are exposed in stronger scattering effects. Therefore, the dependence of κ_{xy} on κ_{xx} shows that the chiral edge current in the Kitaev magnet is sensitive to scattering effects on phonons.

Further, we find that a sample with a larger κ_{xx} shows a larger decrease of the magnetic susceptibility below the Néel temperature, in addition to a larger field-increase effect of κ_{xx} , showing that magnetic scattering effects are more strongly suppressed by magnetic fields in a sample with a better quality. These results suggest that suppressing this magnetic scattering effect plays an important role to realize the quantized thermal Hall effect.

References

- [1] M. Yamashita *et al.*, Phys. Rev. B **102**, 220404(R) (2020).
 [2] Y. Kasahara *et al.*, Nature **559**, 227 (2018).

Authors

M. Yamashita, J. Gouchi, Y. Uwatoko, N. Kuritaa, and H. Tanakaa
^aTokyo Institute of Technology

Ultralow Temperature NMR of CeCoIn₅

Yamashita and Takigawa Groups

We have established the experimental procedures to measure high-field spin-echo NMR signals down to ultralow temperatures (~ 1 mK) with ensuring the thermal equilibrium between the sample and the cryostat [1]. This technique allows us to observe a peak in $1/T_1T$ of ^{59}Co NMR signals at ~ 20 mK, showing a magnetic transition in CeCoIn₅.

Understanding the role of enhanced quantum fluctuations near a magnetic quantum critical point (QCP) has been a central issue in condensed-matter physics, because such quantum fluctuations are believed to mediate various exotic phenomena, such as non-Fermi liquid behaviors, enhancements of effective mass, and unconventional Cooper pairings. Many studies of unconventional superconductivity near a magnetic QCP have been performed in heavy-fermion materials. Among the various heavy-fermion materials, CeCoIn₅ has been attracting broad attention because of its d -wave superconducting state with the high transition temperature of 2.3 K and the proximity to a putative magnetic QCP. However, no antiferromagnetic (AFM) state corresponding to the QCP has been observed, shrouding the origin of the QCP in mystery.

Recently, we have reported anomalous decrease in the de Haas–van Alphen (dHvA) amplitudes of CeCoIn₅ below 20 mK for 6–10 T [2]. An appearance of a field-induced AFM phase has been put forward to explain the decrease of the dHvA amplitude, because additional dissipation by

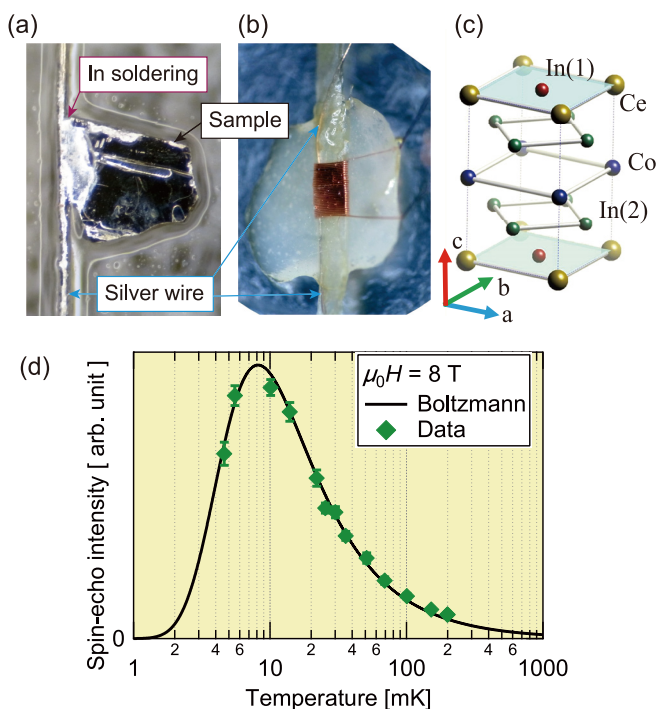


Fig. 1. (a) A picture of the sample with a silver wire (100 μm diameter) soldered by indium. (b) Cu wires were wound around the sample for NMR measurements. The silver wire was thermally anchored to the cryostat. (c) Crystal structure of CeCoIn₅. NMR measurements were performed at ^{59}Co ($I = 7/2$) nuclei. (d) The temperature dependence of the spin-echo intensity at 8 T. The solid line shows the calculation from the Boltzmann distribution of the nuclear spins.

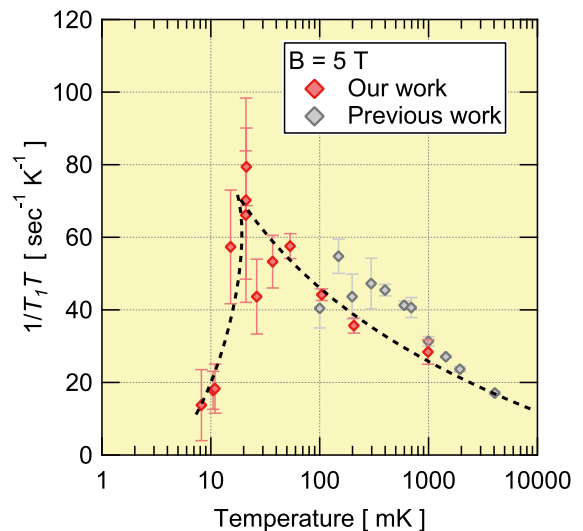


Fig. 2. The temperature dependence of $1/T_1T$ at 5 T. The data of the previous report [3] is also plotted. The dashed line shows a guide to the eyes.

magnetic breakdowns in the AFM phase can provide the most plausible explanation for the decrease of the dHvA amplitude. However, direct evidence of magnetic order has yet to be observed.

In this work, we performed spin-echo NMR measurements down to 5 mK to find the magnetic order. It is a very challenging issue to observe NMR signals down to ultralow temperatures without heating the sample. First, we made a strong thermal connection between the sample and the cryostat by indium soldering a silver wire to the sample (Fig. 1). Second, we find that the temperature dependence of the spin-echo intensity $I_{SE}(T)$ provides a good measure of the sample temperature. By taking into account the population difference of the nuclear spins in different energy levels which have the Boltzmann distribution, one can find the temperature dependence of $I_{SE}(T)$ as shown by the solid line in Fig. 1d. We confirm that the NMR signal follows the Boltzmann curve when the heating caused by the NMR pulses is negligible (Fig. 1d), allowing us to find a pulse condition without heating the sample.

Having established the NMR pulse conditions without heating of the sample, we investigate the temperature dependence of the longitudinal relaxation time (T_1). We find a pronounced peak in $1/T_1T$ at 5 T, implying an appearance of magnetic order as suggested by our previous dHvA measurements [2]. On the other hand, the NMR spectrum shows no change below 20 mK. Moreover, the peak in $1/T_1T$ disappears at 6 and 8 T in contrast to the results of the quantum oscillation. We discuss that an antiferromagnetic state with a moment lying in the a – b plane can be a possible origin for the peak in $1/T_1T$ at 5 T.

References

- [1] M. Yamashita *et al.*, Phys. Rev. B **102**, 165154 (2020).
- [2] H. Shishido *et al.*, Phys. Rev. Lett. **120**, 177201 (2018).
- [3] T. Taniguchi *et al.*, JPS Conf. Proc. **30**, 011107 (2020).

Authors

M. Yamashita, M. Tashiro, K. Saiki, S. Yamada, M. Akazawa, M. Shimosawa^a, T. Taniguchi^b, H. Takeda, M. Takigawa, and H. Shishido^c

^aOsaka University

^bIMR, Tohoku University

^cOsaka Prefecture University

Dynamics of Composite Domain Walls in Multiferroics FeGdO₃

Tsunetsugu Group

Domain Walls (DW) are topological defects with mesoscopic size and understanding their dynamics is important for both experimental and theoretical interests. We have theoretically studied the steady state dynamics of DW driven by magnetic field in a system with multiple orders coexist [1].

Our target system is the multiferroic compound FeGdO₃ and its low-temperature phase is characterized by three order parameters: antiferromagnetic moments of Fe spins N with biaxial anisotropy and isotropic Gd spins n and one component of electric polarization P . Their coupling $cN \cdot nP$ leads to composite DWs, i.e. two order parameters need to flip together in each DW, and therefore there exist 3 different types of composite DWs: N - n , N - P , and n - P .

We have studied the dynamics of these composite DWs driven by magnetic field based on the phenomenological time-dependent Ginzburg-Landau theory. Neglecting fluctuations inside the DW, we have investigated by numerical calculations the time evolution of their one-dimensional motion. With the help of anisotropic exchange couplings, the applied magnetic field couples to N and thus drives N - P and N - n DWs. One important finding is the difference between these two types in the scaling of DW steady state velocity $v(c, H)$. In its weak field expansion $v(c, H) = \alpha(c^2)H + \beta(c^2)H^3 + \dots$, the coefficients exhibit a singularity at $c = 0$ for N - n DW, and this is related to n 's internal isotropy.

As a big surprise, it turns out that a composite DW

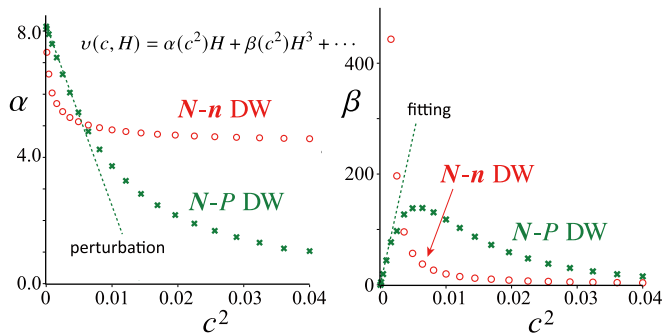


Fig. 1. Velocity of composite DWs driven by magnetic field expanded in H . α is the linear mobility. c is the interaction strength.

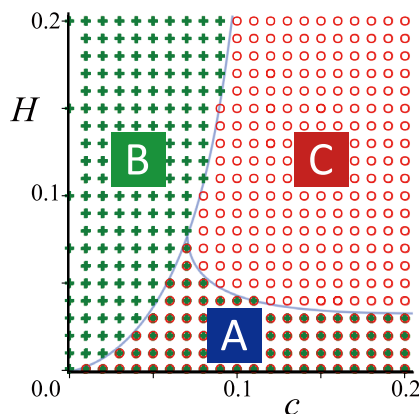


Fig. 2. Stability phase diagram of composite DWs driven by magnetic field H . B: N - n DW is unstable, C: N - P DW is unstable, A: both DWs are stable.

becomes unstable in strong magnetic field and splits into a pair of different types: N - $P \rightarrow N$ - $n + n$ - P and N - $n \rightarrow N$ - $P + n$ - P . In both cases, n - P DW is immobile but its partner succeeds to the moving part after splitting. The possibility of this type of splitting was pointed out as an impurity effect [2], but we have found that it may occur in a pure bulk as a dynamical instability. An important point is that the non-flipping component is also dragged by the flipping ones due to the coupling c -term. With increasing the driving field, its modulation grows and finally creates a pair of kink and anti-kink, which is DW splitting. This type of dynamical instability may appear, in principle, in any systems with more than two types of order parameters. It is an interesting challenge to observe in experiments this splitting of composite DW.

References

- [1] K. Kawahara and H. Tsunetsugu, J. Phys. Soc. Jpn. **90**, 014703 (2021).
- [2] Y. Tokunaga *et al.*, Nat. Mater. **8**, 558 (2009).

Authors

H. Tsunetsugu, K. Kawahara

Fermi-Liquid Correction in Current Noise through a Correlated Quantum Dot

Kato Group

Artificially generating, controlling, and measuring quantum states on semiconductor substrates is the key to realizing quantum information technology, such as quantum computers and quantum communications. On the other hand, the development of technologies to generate and control artificial quantum states has brought about a paradigm shift in material science. As a result, it has become possible to thoroughly explore the physical phenomena that give rise to nontrivial features of matter by artificially reproducing the quantum states in matter, rather than simply investigating the properties of natural matter as has been done in the past. Furthermore, through advanced control technology, it has become possible to precisely investigate the behavior of quantum many-body states in complex environments, such as nonequilibrium states, which were previously not easy to access.

Along with superconductivity and the quantum Hall effect, the Kondo effect is one of the fundamental many-body effects of electrons. The primary mechanism of the Kondo effect was elucidated in 1964 and has been thoroughly investigated since then. The Kondo effect occurs not only in dilute magnetic materials, where the phenomenon was originally discovered, but also in a variety of physical systems. Recently, many studies on the Kondo effect have been carried out in various physical fields, such as condensed states of light-trapped cooled atoms and quarks. However, the actual state of these systems often deviates from the ideal state assumed in the mathematical analysis. In other words, it is known that the symmetries possessed by physical states (time-reversal symmetry and particle-hole symmetry) are broken and play a significant role in the low energy states. However, the correction on the local-Fermi-liquid state beyond the linear response had remained a difficult problem until recently [1].

Consider a situation in which electrons are confined in a quantum dot, which is a device of several tens of

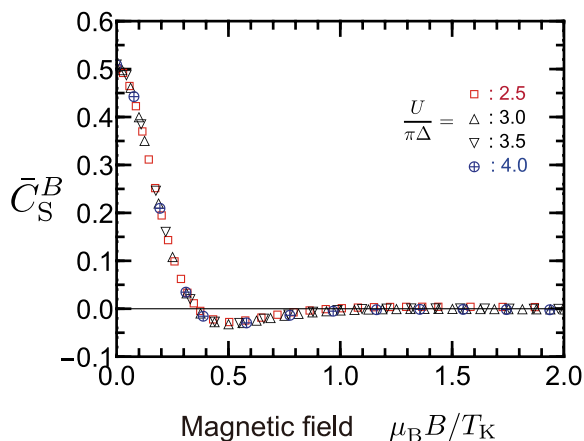


Fig. 1. Bias-voltage nonlinear coefficient of current noise \bar{C}_S^B as a function of magnetic field B normalized by the Kondo energy scale (Kondo temperature) T_K for several choices of the Coulomb interaction $U/(\pi\Delta)$ is plotted. Here the current noise is given in the form $S = \frac{4e^2}{h} |eV| \left[S_1 + \bar{C}_S^B \left(\frac{eV}{T_K} \right)^2 \right] + \mathcal{O}(V^5)$. It is found that all the data points are on a universal curve.

nanometers in size made of a semiconductor or other material. In a quantum dot made of carbon nanotubes, for example, the shape of the electron confinement region is highly symmetric. As a result, in addition to the spin of the electrons, a magnetic moment is generated in the quantum dot due to the orbit of the electron motion. By attaching electrodes to this quantum dot, the number of confined electrons can be tuned, and the local-Fermi-liquid state can be controlled in a state of broken electron-hole symmetry. Using quantum field theory and mathematical methods, we have clarified that the local-Fermi-liquid corrections, which are caused by the three-electron correlation, play an essential role in the correlated quantum dot beyond the conventional theory on the local Fermi liquid. This three-electron correlation is particularly pronounced in quantum dots with multiple orbitals. For example, in the Kondo effect caused by electron spin alone, it is difficult to observe the local-Fermi-liquid corrections because the Kondo effect itself disappears when the number of electrons is changed.

Exploiting numerical simulations and field theory techniques, we have clarified that the local-Fermi-liquid corrections can be observed in actual experiments based on the transport quantities such as nonlinear current, current noise, and thermal conductivity [2]. We have also found that there is a scaling universality in the nonlinear current noise behavior when a magnetic field is applied to a quantum dot. Application of magnetic field breaks the time-reversal symmetry of the quantum dot and gives rise to the local-Fermi-liquid corrections in nonlinear transport quantities. It is also found that the local-Fermi-liquid corrections have a universal scaling property independent of the details of the nanoscale materials, similar to the conventional local-Fermi-liquid (see Figure).

This research has significantly advanced our understanding of the physical mechanisms that give materials their nontrivial features through the interaction of electrons. The Kondo effect is the most fundamental quantum many-body effect, and it appears in the properties of various materials. Therefore, it is expected to be helpful in designing new materials and exploring new materials in the future. In addition, the study of artificially controlled quantum many-body states in nanoscale materials requires highly sensitive observation techniques, which will contribute to the development of technologies to generate and control quantum states.

Recently, our collaborators have succeeded in an experiment to verify the local-Fermi-liquid correction effect using current measurement on a carbon nanotube-based quantum dot [3].

As described so far, the results of this research are fundamental to the physics of condensed matter. However, it is expected that they will lead to the development of materials science and quantum information technology.

References

- [1] C. Mora, C. P. Moca, J. von Delft, and G. Zarand, Phys. Rev. B **92**, 075120 (2015).
- [2] Y. Teratani, R. Sakano, and A. Oguri, Phys. Rev. Lett. **125**, 216801 (2020).
- [3] T. Hata, Y. Teratani, T. Arakawa, S. Lee, M. Ferrier, R. Deblock, R. Sakano, A. Oguri, and K. Kobayashi, Nat. Commun. **12**, 3233 (2021).

Authors

R. Sakano, Y. Teratani^a, and A. Oguri^a

^aOsaka city university

Sub-Atomic Lattice Distortion of an Atomic Layer Compound Visualized by Moiré Pattern

Komori Group

Chemical and physical properties are greatly affected by lattice distortion through the change of the electronic structures. At solid surfaces, the local distortion induced by the adsorbates, subsurface impurities and hetero-interface modify reactivity, growth and other atomic processes. By mapping the amplitude and direction of the local distortion, we can elucidate the details of the atom processes including surface reactivity. However, it has been technically difficult to observe the local distortion directly using microscopy methods. While scanning tunneling microscopy (STM) with atomic resolution is one of the ideal tools for studying the local structure, its lateral resolution is still insufficient to measure the distortion of the order of a few % of the lattice constant [1]. One of the ways to improve the lateral resolution is a use of the moiré pattern in the STM images [2]. In the present study, we demonstrate that the local lattice distortion of a hexagonal iron-nitride monatomic film grown over a flat and wide Cu terrace can be visualized by analyzing the moiré pattern. [3]

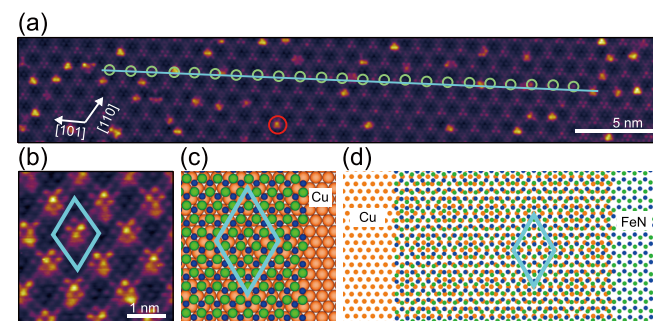


Fig. 1. (a,b) Topographic STM images of the hexagonal iron-nitride monolayer on Cu(111). Cyan line in (a) is drawn along the moiré pattern. The lattice orientation of the iron-nitride monolayer is indicated by green circles in (a). The red circle in (a) indicates the point protrusion. (c) Schematic model of the hexagonal iron-nitride monolayer on Cu(111). Green, blue and orange balls indicate Fe, N and Cu atoms, respectively. The Cu(111) lattice is rotated by 0.28° from the iron-nitride lattice. (d) Moiré pattern between the hexagonal iron-nitride monolayer and Cu(111) obtained by the schematic model in (c). Cyan rhombuses in (b), (c) and (d) show the unit cell of the moiré pattern [3].

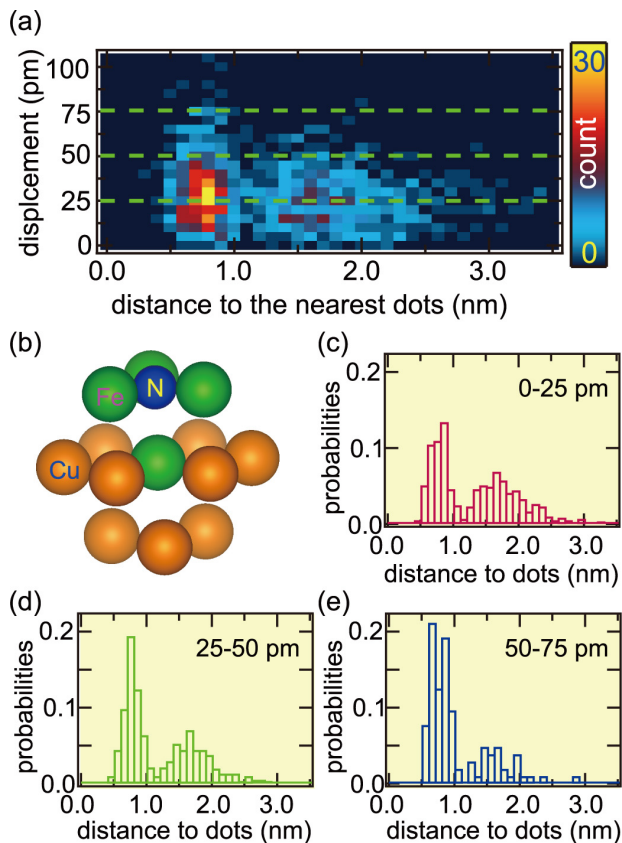


Fig. 2 (a) Two-dimensional histogram of the displacement of the moiré pattern center and the distance to the nearest point protrusion. (b) Proposed schematic model of the point protrusion. (c–e) Histograms of the distance from the centers to the nearest point protrusions for three regions of the displacement 0–25 pm in (c), 25–50 pm in (d), and 50–75 pm in (e). The counts are normalized by the total counts in each region [3].

Observed topographic STM images of the surface are shown in Fig. 1(a, b). A uniform iron-nitride film grows over the Cu(111) terrace larger than $100 \times 100 \text{ nm}^2$, and a hexagonal moiré pattern with the periodicity of $\sim 1.3 \text{ nm}$ can be seen in the images. The green circles in Fig. 1(a) show the positions of the surface atoms along the [101] direction, and the cyan line is plotted along the moiré pattern. The latter is tilted from the lattice orientation of the hexagonal iron nitride monolayer by $1.1 \pm 0.1^\circ$. A schematic model of the iron nitride monolayer on Cu(111) is displayed in Fig. 1(c). We assume that Fe atoms are observed as protrusions by STM. This model can reproduce the overall characteristics of the moiré pattern in the image including the 1.1° tilt as in Fig. 1(d). In the STM images, we notice larger and higher protrusions, which randomly distribute on the surface, than the atomic protrusions as indicated by the red circle in Fig. 1(a). We call them point protrusions.

A detailed analysis of the moiré pattern reveals that the center of the moiré pattern does not form a regular periodic lattice. The center positions randomly fluctuate from a hypothetical regular lattice points. Figure 2(a) shows a two dimensional histogram of the displacement of the moiré pattern center from the lattice point and the distance from the center of the moiré pattern to the nearest point protrusion. Our structural model of the point protrusion is given in Fig. 2(b). The histograms of the distance from the centers to the nearest point protrusions are made depending on the displacement to see the correlation more clearly as in Fig. 4(c–e). For the centers with a large displacement, the distance to the nearest point protrusion is relatively short compared to those with a small displacement. The point

protrusions are preferentially formed in the regions with large lattice distortion of the iron nitride monolayer.

References

- [1] S. Ohno *et al.*, Surf. Sci. **554**, 183 (2004).
- [2] M. Ritter *et al.*, Phys. Rev. B **57**, 7240 (1998).
- [3] T. Hattori *et al.*, Nano Lett. **21**, 2406 (2021).

Authors

T. Hattori, N. Kawamura, T. Miyamachi, and F. Komori

Steps as a Disorder on Atomic-Layer Superconductors

Hasegawa Group

Two-dimensional (2D) superconductors, whose thickness is thinner than the coherence length, exhibit peculiar properties. Compared with bulk superconductors, 2D superconductors are susceptible to disorder since induced electron localization enhances repulsive electron-electron interaction, which suppresses the Cooper pairing. As demonstrated with thickness-dependent critical temperature of amorphous superconducting thin films, changing parameters such as disorder, thickness, and perpendicular magnetic field lead to a superconductor-insulator transition (SIT). The zero-temperature transition is one of the typical examples of quantum phase transitions, and has been investigated extensively to elucidate its universal properties.

Recent technical advancements have allowed us to fabricate highly crystalline 2D superconductors, some of which has only mono-atomic layer thickness. In the case of such highly-ordered 2D superconductors it has been reported that during the SIT induced by the magnetic field application metallic phase appears in between. So far, the properties of this peculiar quantum metallic phase have been investigated mainly by transport measurements but the mechanism is still controversial. In order to understand its details atomistic real-space measurements are crucial. In the present study, we studied superconducting properties of striped-incommensurate (SIC) phase of the Pb/Si(111) system; one of the monoatomic-layer superconductors, formed on vicinal Si substrates. Since the substrate is tilted, uniformly distributed steps, whose spacing is equivalent or even smaller than the coherence length, should behave as a dispersed disorder on the ultimately thin superconductor. We investigated how the steps affect the superconducting properties and the magnetically induced SIT by using low-temperature scanning tunneling microscopy (STM).

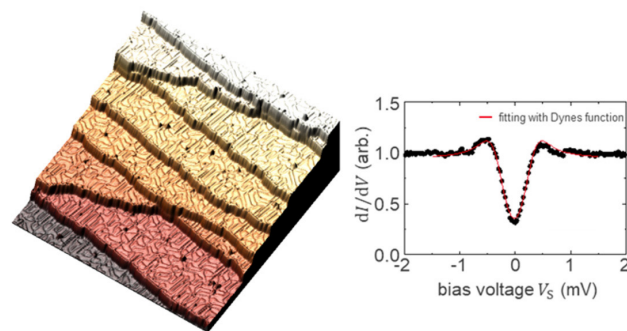


Fig. 1. (left) 3D-rendered STM image of striped incommensurate (SIC) phase of Pb/Si(111) system formed on a 1.1° -tilted vicinal substrate. (right) tunneling spectrum taken on a terrace of vicinal SIC phase taken at 0.36 K showing a superconducting gap of 0.30 meV.

Carrier Density Control in Oxide Quantum Wells

Lippmaa group

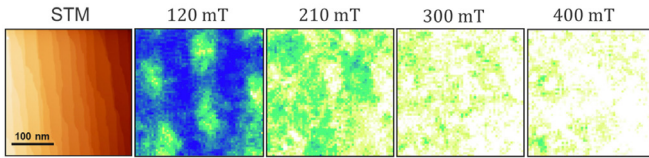


Fig. 2. STM image of the vicinal SIC superconducting phase and zero-bias-voltage maps, which correspond to the spatial distribution of the density of states (DOS) at the Fermi level, taken under the perpendicular magnetic field of 120, 210, 300, and 400 mT.

Figure 1 shows a 3D-rendered STM image of the SIC phase formed on a 1.1° -tilted vicinal Si(111) substrate taken at 0.36 K. A characteristic SIC stripe pattern can be seen on the terraces. In the image, the vertical scale is severely exaggerated; the step height corresponds to 0.31 nm whereas the averaged terrace width is 16 nm. A tunneling spectrum taken on a terrace shows a superconducting gap that can be well fitted with the Dynes function. The fitted superconducting gap, 0.30 meV, is almost same as that taken on SIC phase formed on a flat substrate, indicating the Cooper pairing is not affected by the presence of the steps.

In our previous studies on the role of steps on superconductivity, we found that the steps basically behave as a Josephson junction connecting the neighboring terraces, and the strength of the decoupling strongly depends on the phases [1, 2]. Among the Pb monolayer phases, the steps of the $\sqrt{3} \times \sqrt{43}$ phase decouple terraces significantly to make the terraces superconducting nano stripes [2]. On the other hand, the decoupling of the SIC phase is rather weak so that vortices are just pinned at step edges. In the case of the vicinal one, as the terrace width (16 nm) is much shorter than the coherence length of the flat one (38 nm), more than one steps are involved on the formation of a vortex.

Figure 2 shows an STM image and zero-bias-voltage maps, which correspond to the spatial distribution of the density of states (DOS) at the Fermi level, taken under various magnetic fields. At 120 mT, the vortices are observed elongated along the step direction. The DOS at the core of the vortices is not fully recovered to that of the normal metal. These are the characteristic features of an Abrikosov-Josephson vortex. The oval shape of the vortices is due to the reduced coherence length along the step-crossing direction caused by the limited mean free path due to the presence of the steps. Because of the reduced coherence length, the critical magnetic field, which is inversely proportional to the coherence length, is enhanced on the vicinal superconductor.

At the magnetic field of 210 mT, the number of vortices increases as well as the background DOS. The vortices are no longer distinct, and significant corrugation in DOS is discernible. By further increasing the magnetic field, DOS gradually increases and its distribution becomes homogeneous. Around 330 mT, DOS exhibits saturation, indicating the breaking of superconductivity. According to the transport measurement performed on the same phase the vortex liquid phase and quantum metallic phase are observed at these magnetic fields. The observed blur vortices and inhomogeneous DOS contrast presumably corresponds to thermally activated or quantum diffusing vortex liquid phase.

References

- [1] S. Yoshizawa *et al.*, Phys. Rev. Lett. **113**, 247004 (2014).
- [2] F. Oguro *et al.*, Phys. Rev B **103**, 085416 (2021).

Authors

Y. Sato, M. Haze, S. Yoshizawa^a, T. Uchihashi^a, and Y. Hasegawa

^aNational Institute for Materials Science

Two-dimensional carrier confinement in a quantum well at an oxide heterointerface offers new ways of controlling the transport behavior of oxide materials by applied external fields. Magnetic tunability has been attributed to Rashba-type spin-orbit coupling in an asymmetric electron distribution, the enhancement of spin-orbit coupling close to a filling-dependent Lifshitz transition, or a change in the effective disorder experienced by carriers when the quantum well width changes. Electric fields, on the other hand, can be used to change the quantum well filling, by accumulating or depleting carriers at an interface, or to modify the width of the electron distribution in the depth direction.

Oxide quantum wells are usually formed by growing a thin epitaxial LaAlO₃ layer on SrTiO₃, in which case the quantum well forms at the surface of the SrTiO₃ substrate due to, at least in part, the change of lattice polarity at the interface. Instead of using the polar LaAlO₃ layer, it is also possible to form quantum wells by depleting oxygen from the surface or by delta-doping SrTiO₃ with a (La,Sr)O_x monolayer. All these techniques produce a metallic quantum well with qualitatively similar properties, but the LaO_x delta-doping technique has several advantages in allowing a broad range of carrier densities to be explored. In contrast, the carrier number is essentially fixed by the polarity discontinuity at LaAlO₃/SrTiO₃ interfaces, while oxygen-deficient surfaces can only be maintained in ultra-high vacuum conditions.

In our recent work [1], we have studied the possibilities of constructing oxide quantum wells based on embedded (La,Sr)O_x layers in SrTiO₃. The heterostructures were grown by Pulsed Laser Deposition on SrTiO₃ single crystals as illustrated in Fig. 1. The carrier number in these heterostructures is controlled by two parameters: the number of La atoms in the delta-doping layer, and the thickness of a SrTiO₃ capping layer. Since SrTiO₃ surfaces exposed to air are strongly depleted, a space-charge layer forms in the cap layer and the thickness of the capping layer can be used to partially deplete the carriers in from the quantum well. Almost complete carrier depletion occurs when the capping

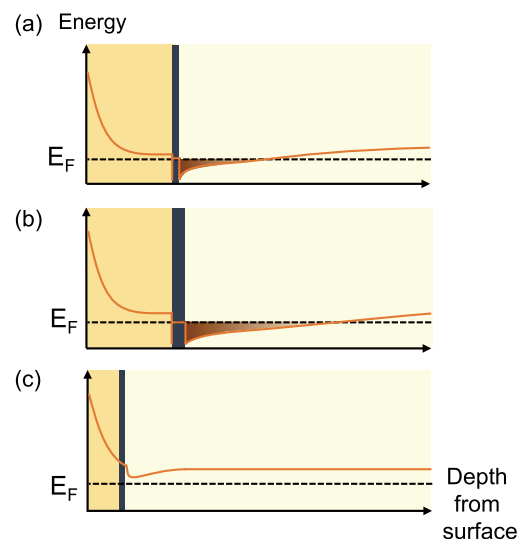


Fig. 1. Formation of a quantum well in SrTiO₃ around a LaTiO₃ delta doping layer. Due to surface depletion, carriers are depleted from the quantum well if the distance is small (c). Saturated metallic behavior is obtained only for capping layers thicker than 10 nm (a).

Sandwich Structure Formation of BN-Covered Silicene on ZrB₂/Si(111) by Adsorption of NO and Thermal Processes

Yoshinobu Group

Atomic layer materials have attracted much attention in physics, chemistry and materials science. Silicene is a silicon analogue of graphene. A honeycomb silicene layer has been prepared on suitable substrates such as Ag, ZrB₂, Ir, ZrC surfaces. It has been reported that a silicene layer grown on these metallic surfaces has relatively strong interaction with the substrate because of the orbital mixing between metal bands and Si sp-bands. Towards the functionalization of silicene for device applications, several theoretical and experimental investigations have been carried out concerning the interaction between the silicene and other atoms/molecules. Here, we investigated the adsorption and thermal reaction processes of NO with the a silicene monolayer on the ZrB₂/Si(111) substrate using synchrotron radiation X-ray photoelectron spectroscopy (SR-XPS) and density-functional theory (DFT) calculations. SR-XPS experiments were carried out at BL13 of KEK-PF.

Figure 1 shows a series of O 1s, N 1s, Si 2p and B 1s XPS spectra of these processes. The initial surface is a clean silicene monolayer on ZrB₂/Si(111) (see each XPS for the clean surface). NO is dissociatively adsorbed on the silicene surface at 300 K. At an early stage of NO exposure, an atomic nitrogen is bonded to three Si atoms most probably by a substitutional adsorption with a Si atom of silicene (N≡Si₃). An atomic oxygen is inserted between two Si atoms of the silicene (Si-O-Si). After a large amount of NO exposure (1500 L), the two-dimensional honeycomb silicene structure becomes destroyed judging from the decay of typical Si 2p spectra for silicene (see Fig. 1c). The oxidation state of Si becomes Si⁴⁺ predominantly and the XPS peaks

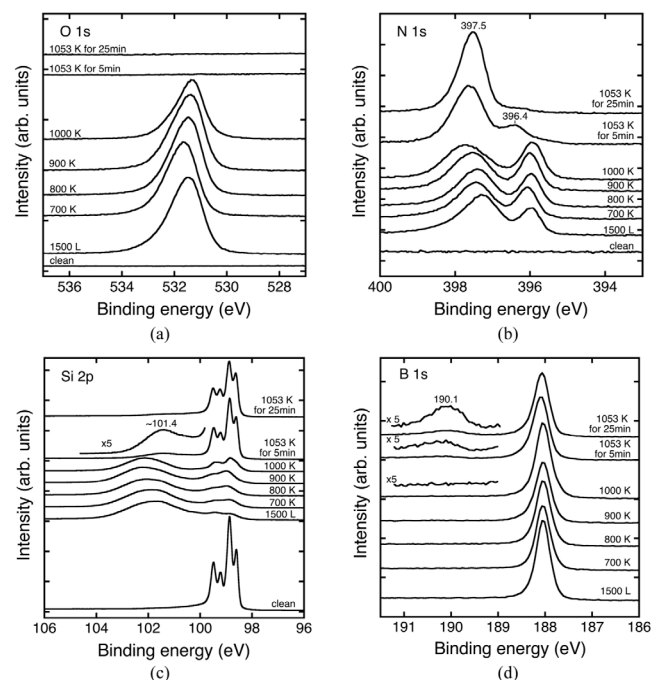


Fig. 1. A series of XPS spectra of the 1500 L NO/silicene/ZrB₂/Si(111) surface as a function of heating temperature. (a) O 1s spectra ($h\nu = 700$ eV), (b) N 1s spectra ($h\nu = 560$ eV), (c) Si 2p spectra ($h\nu = 260$ eV), and (d) B 1s spectra ($h\nu = 700$ eV). After quick heating to each temperature, the sample was cooled down to room temperature, and XPS measurements were carried out. Note that at 1053 K, the heating duration time was 5 min and 25 min.

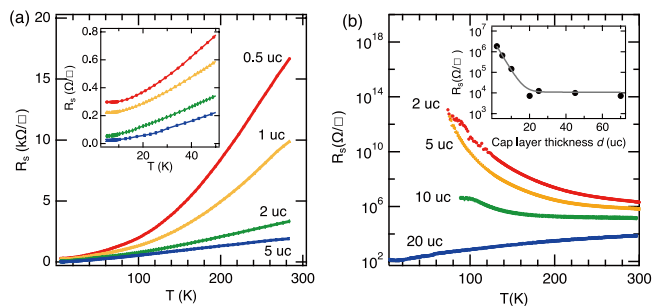


Fig. 2. Variation of the sheet resistance of SrTiO₃/LaTiO₃/SrTiO₃ heterostructures with the LaTiO₃ delta-doping layer thickness (a) and SrTiO₃ capping layer thickness (b). Layer thicknesses are given in unit cells (4Å).

layer thickness drops below 4 nm (10 unit cells). Above 10 nm capping thickness, surface depletion no longer affects the carrier density in the quantum well and the carrier density is set by the number of La atoms in the delta-doping layer. The built-in carrier density in the quantum well is thus set by two layer thickness parameters that are easy to control with precision in the growth process. When the heterostructures are formed into gated field-effect transistors, additional fine-tuning of the carrier density over a narrow range is possible by applying a suitable gate voltage. The electrostatically-gated heterostructure devices are thus particularly well suited for studying filling-dependent Lifshitz transitions, i.e. varying the Fermi energy in the quantum well across the Ti 3d conduction band $d_{xz,yz} - d_{xy}$ level crossing.

The effects of the doping and capping layer thicknesses on the transport behavior of the heterostructures are shown in Fig. 2. When a thick capping layer is used and the surface depletion effect can be ignored, metallic conductivity is obtained from the LaO_x layer coverage exceeds about 0.3 monolayers and a gradual reduction of the sheet resistance is observed as the La coverage is increased. For a single unit cell of LaTiO₃, the quantum well carrier density was on the order of 10¹³ cm⁻². In all cases, however, the Hall resistance was nonlinear, indicating that a significant depth distribution of carriers exists. Approximately 1/4 of the carriers are distributed to a distance of 10 nm or more from the interface. These ‘deep’ carriers do not suffer from interfacial scattering and reach a mobility of over 10⁴ cm²/Vs at 4K.

The built-in carrier concentration can be further adjusted by changing the cap layer thickness, as shown in Fig. 2b. As the cap layer thickness is reduced to 10 unit cells or less, the heterostructures become semiconducting and finally insulating. These experiments show that it is possible to tune the carrier density continuously close to the lowest densities where metallic conductivity can be sustained.

Reference

[1] J. N. Lee, X. Hou, R. Takahashi, and M. Lippmaa, Appl. Phys. Lett. **116**, 171601 (2020).

Authors

J. Lee, X. Hou, R. Takahashi^a, and M. Lippmaa^a

^aNihon University

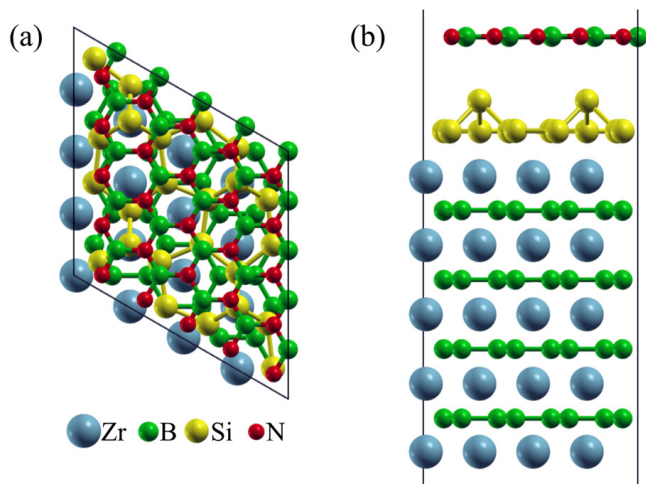


Fig. 2. (a) top view and (b) side view of the optimized structure of a sandwich structure of a hexagonal BN sheet on the silicene/ZrB₂ substrate

of ZrB₂ substrate are decreased in intensity, indicating that complicated silicon oxinitride species have developed three-dimensionally on the ZrB₂/Si(111) substrate at 300 K. By heating above 900 K, the oxide species start to desorb from the surface probably as SiO, but nitrogen-bonded species still exist (Figs. 1a and 1b). After heating at 1053 K for 5 min., no oxygen species is observed on the surface (Fig. 1a); SiN species are temporarily formed as a metastable species and BN species also start to develop (Fig. 1b). In addition, the silicene structure is partly restored on the ZrB₂/Si(111) substrate (Fig. 1c).

After the prolonged annealing at 1053 K for 25 min., the XPS spectra show a single peak at 397.5 eV for N 1s (Fig. 1b) and an emerging peak at 190.1 eV for B 1s state (Fig. 1d). Since the B 1s peak at 190.1 eV can be ascribed to the B atom in the hexagonal BN structure according to the reference XPS spectra of BN, we conclude that the hexagonal BN structure has developed on the silicene on ZrB₂. By DFT calculations, the geometrical structure has been optimized as shown in Fig. 2; a hexagonal BN sheet weakly interacts with the silicene layer on the ZrB₂ substrate. The calculated binding energy of the N 1s state in the hexagonal BN is 397.61 eV on average, while there is a variation of the binding energies depending on the relative position of N atoms with respect to the Si atoms of silicene, and the minimum and maximum binding energies are 397.41 and 397.81 eV, respectively. The good agreement between the experimental and calculated binding energies supports the formation of the hexagonal BN structure after the prolonged annealing at 1053 K. Thus, the sandwich structure of BN-covered silicene on the ZrB₂/Si(111) substrate is formed by adsorption of NO at 300 K and prolonged heating at 1053 K.

Reference

[1] J. Yoshinobu *et al.*, *J. Chem. Phys.* **153**, 064702 (2020). doi: 10.1063/5.0011175

Authors

J. Yoshinobu, K. Mukai, T. Ozaki, Y. Yamada-Takamura^a *et al.*
^aJapan Advanced Institute of Science and Technology

Functional Characterization and Study on the Molecular Mechanism of Ion-transporting Rhodopsins

Inoue Group

Rhodopsin is photo-receptive heptahelical transmembrane protein in which a retinal chromophore is covalently bound to a conserved lysine residue in the seventh transmembrane helix (TM7), and animal and microbial rhodopsin families are known so far. Animal rhodopsins are present in animal retina to transfer visual signals to brain and are also related to non-visual light sensing in various tissues. Microbial rhodopsins show diverse functions: light-driven ion pump, light-gated ion channel, phototactic sensor, light-dependent regulation of gene expression and enzyme, and so on. Both types of rhodopsins are being widely used in optogenetics to control various cellular events, such as neural activity, gene expression, dynamic protein localization, and so on, by light.

In 2020, we reported the functional characterization of schizorhodopsin (SzR) which was found in metagenome assembled genomes of Asgard archaea which is thought to be the closest living prokaryote to the last common ancestor of eukaryotes [1]. The ion-transport activity assays revealed that SzRs function as light-driven inward proton (H⁺) pumps [2]. The inward H⁺ transport of SzRs are significantly higher than that of another inward H⁺ pumping rhodopsin, xenorhodopsins (Fig. 1). The high-speed atomic force microscopy revealed the trimeric structure of SzR in lipid bilayer. The photocycle of SzR in which K, L, L/M and M intermediates are included was determined by the laser flash photolysis spectroscopy. The transient absorption change of a pH indicator (cresol red) indicated that the substrate H⁺ is released to the cytoplasmic milieu and taken up from the extracellular side on the M-accumulation and decay, respectively. This suggests that no metastable trapping of H⁺ released from retinal Schiff base (RSB) occurs on any amino acid residues, and it was supported by the low-temperature Fourier transform infrared spectroscopy. This is quite

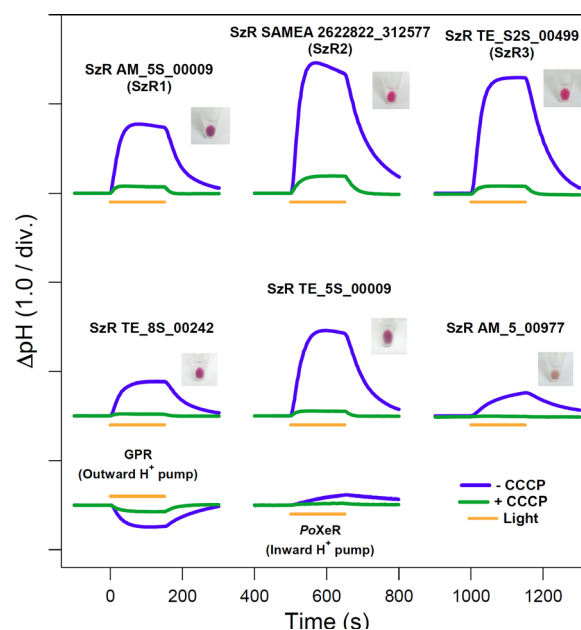


Fig. 1. Inward H⁺ transport activity of six SzRs (top and middle) compared with outward H⁺ pumping GPR and inward H⁺ pumping XeR (PoXeR) (bottom).

Omnidirectional Control of Large Electrical Output in a Topological Antiferromagnet

Nakatsuji Group

The net magnetization defines the signal size of memory devices and sensors, and thus the manipulation of magnetization is essential for the broad application of ferromagnets. However, the magnetization itself causes a dilemma. While its size matters to obtain strong responses upon its reversal, the large magnetization simultaneously suppresses the range of its directional control due to the demagnetizing field. To overcome the demagnetization/shape barrier, one needs to carefully tune the crystalline and interfacial effects [1]. Thus, it would be ideal to find alternative magnets that carry no magnetization but strong responses.

The antiferromagnet Mn_3Sn hosts a large Berry curvature in momentum space owing to the topological metallic state. The Berry curvature can be manipulated by the ferro ordering of the cluster magnetic octupole and remains large even with negligible magnetization. This feature enables disproportionately large transverse responses such as anomalous Hall effect (AHE)[2] and anomalous Nernst effect

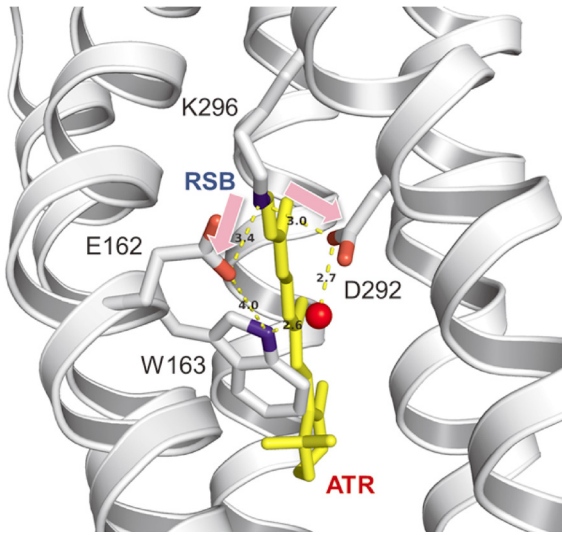


Fig. 2. Trp163 of C1C2 plays a role regulating the branching ratio of H^+ transfers between RSB and counterions, Glu162 and Asp292.

different from XeR, in which protonation of the proton accepting aspartate on the cytoplasmic side is involved in H^+ transfer from the RSB to the cytoplasmic milieu. A comprehensive amino-acid mutation experiment suggested that Cys75 and Glu81 in the transmembrane helix (TM) 3 and Asp184 in TM7 is critical for the inward H^+ transport of SzR.

Channelrhodopsins (ChRs) are light-gated cation channels which nonspecifically transports various cations according to the electrochemical potentials of cells. In order to reveal the cation transport function of ChR, we investigated a mutant of a member of ChR, C1C2, in which a tryptophane residue in TM3 was substituted with phenylalanine (C1C2 W163F). Trp163 of C1C2 is highly conserved in most microbial rhodopsins, but its relationship to the channel function is not known. C1C2 W163F showed greatly attenuated channel activity, while outward proton pumping activity became more prominent. This result indicates that Trp163 plays a critical role in suppressing the outward proton pumping function and increasing channel activity by regulating the branching ratio of proton transfer to the two counterions Glu162 and Asp292 respectively (Fig. 2) [3].

We also reported the theoretical and experimental studies on the Cotton effect observed in the visible CD spectrum of sodium pump rhodopsin (KR2) [4]. KR2 shows a visible CD spectrum whose peak is significantly red-shifted from that of its absorption spectrum. The transition density fragment interaction (TDFI) method quantitatively revealed that this shift is caused by the excitonic coupling between retinal chromophores in pentamer of KR2 [4].

References

- [1] P.-A. Bulzu, A.-Ş. Andrei, M. M. Salcher, M. Mehrshad, K. Inoue, H. Kandori, O. Bėja, R. Ghai, and H. L. Banciu. *Nat. Microbiol.* **4**, 1129 (2019)
- [2] K. Inoue, S. P. Tsunoda, M. Singh, S. Tomida, S. Hososhima, M. Konno, R. Nakamura, H. Watanabe, P.-A. Bulzu, H. L. Banciu, A.-Ş. Andrei, T. Uchihashi, R. Ghai, O. Bėja, and H. Kandori. *Sci. Adv.* **6**, eaaz2441 (2020)
- [3] Y. Nagasaka, S. Hososhima, N. Kubo, T. Nagata, H. Kandori, K. Inoue, and H. Yawo. *Biophys. Physicobiol.* **17**, 59 (2020)
- [4] K. J. Fujimoto and K. Inoue, *J. Chem. Phys.* **153**, 045101 (2020).

Authors

K. Inoue, T. Nagata, H. Yawo

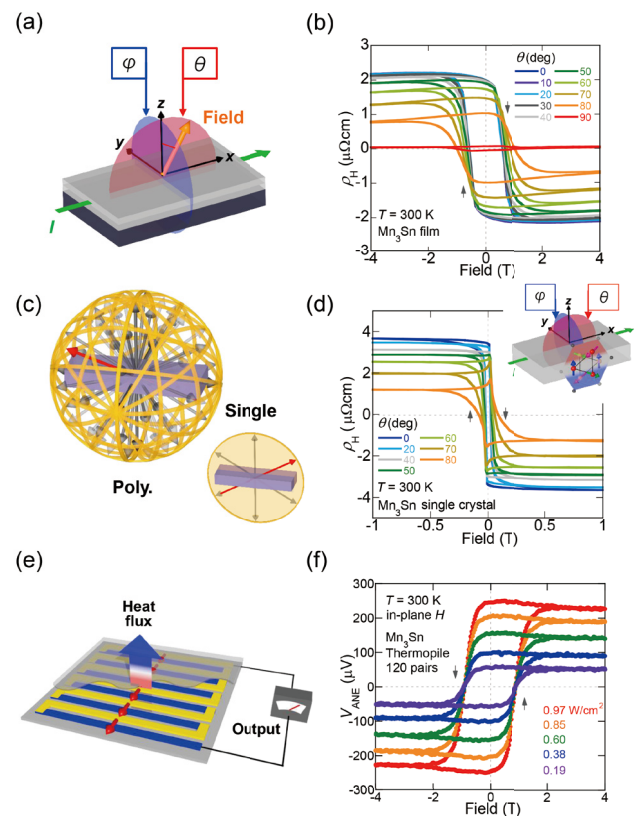


Fig. 1. (a) Schematic illustration of the rotation planes. θ and ϕ are the angles from the normal direction within the planes parallel and perpendicular to the electric current direction, respectively. The orange arrow represents the direction of the external magnetic field. (b) Field dependence of the Hall resistivity obtained for the Mn_3Sn film with various angles θ at 300 K. The black arrows indicate the field sweep direction. (c) Schematic illustrations of the 3D omnidirectional property for randomly oriented multi-grains and the 2D omnidirectional property for a single crystal/grain. The red arrow represents the direction of the magnetic order parameter. (d) Field dependence of the Hall resistivity obtained for the Mn_3Sn single crystal with various angles θ at 300 K. Inset: Schematic illustrations of the rotation planes for the single crystal. (e) Schematic illustration of heat flux sensor. (f) Field dependence of the Nernst voltage V_{ANE} for the Mn_3Sn thermopile made of 120 pairs of $\text{Mn}_3\text{Sn}/\text{Au}$ wires under several values of the heat flux q_{heater} at 300 K.

(ANE)[3], opening up the possibilities for replacing ferromagnets with antiferromagnets in magnetic devices. As the first step for spintronics applications, we fabricated Mn₃Sn thin films [4]. And more recently, we demonstrated electrical manipulation of the magnetic ordering in the Mn₃Sn/heavy metal bilayer devices [5], which has triggered extensive research activities into the interface properties of Mn₃Sn thin film.

In this study [6], we report the omnidirectional behavior in Mn₃Sn due to negligible shape anisotropy. Moreover, we demonstrate a new method for multi-level data recording and a magnetically robust ANE-type heat flux sensor.

We have fabricated the polycrystalline Mn₃Sn thin films on the thermally oxidized Si substrate by dc magnetron sputtering methods [4]. With these thin films, we measured the anomalous Hall effect as a function of magnetic field angles, θ and ϕ (Fig. 1(a)). As shown in Fig. 1(b), the field dependence of AHE obtained for various θ exhibits a multi-stable signal. Namely, the spontaneous Hall signal gradually decreases with increasing θ , indicating that the polarization direction of the magnetic octupole essentially follows the field direction rather than being restricted within the xy plane. Notably, the rotation for both θ and ϕ angles shows the same angular dependence, indicating that the magnetic octupole can be freely (omnidirectionally) orientated in all directions (Fig. 1(c)) as a result of the negligibly small shape anisotropy and polycrystalline arrangement.

Interestingly, single-crystal/grain samples also show the multi-stable signals as a function of the field angle, but only for field rotations within the kagome layer (Fig. 1(d)). Ferromagnets with magneto-crystalline anisotropy sufficiently larger than the shape anisotropy can show similar multi-stable behavior in their polycrystalline form. However, in the single crystal samples, the magnetization is restricted to one direction due to the substantial magneto-crystalline anisotropy, and therefore only a binary signal can occur. The new multi-level recording method found in Mn₃Sn may allow writing and reading beyond two units of information (0 and 1), namely, a device comprising a single grain of nanometer scale can hold three or more units of information.

Taking advantage of the small shape anisotropy and the omnidirectional property, we developed a ANE heat flux sensor consisting of micro-fabricated Mn₃Sn wires (Fig. 1(e)). This sensor exhibits the heat flux sensitivity comparable to that made of ferromagnetic materials while being resistant to magnetic field disturbances (Fig. 1(f)).

References

- [1] R. Skomski and J. M. D. Coey, *Scr. Mater.* **3**, 112 (2016).
- [2] S. Nakatsuji *et al.*, *Nature* **527**, 212 (2015).
- [3] M. Ikhlas, T. Tomita *et al.*, *Nat. Phys.* **13**, 1085 (2017).
- [4] T. Higo *et al.*, *Appl. Phys. Lett.* **113**, 202402 (2018).
- [5] H. Tsai, T. Higo *et al.*, *Nature* **608**, 580 (2020).
- [6] T. Higo *et al.*, *Adv. Funct. Mater.* **31**, 2008971 (2021).

Authors

T. Higo, Y. Li^a, K. Kondou^b, D. Qu, M. Ikhlas, R. Uesugi, D. Nishio-Hamane, C. L. Chien^a, Y. Otani, and S. Nakatsuji

^aJohns Hopkins University

^bRIKEN-CEMS

Large Hall Signal due to Electrical Switching of an Antiferromagnetic Weyl Semimetal State

Nakatsuji, Otani, and Miwa Groups

The topologically protected properties in Weyl semimetals have been extensively studied in recent years. The Weyl points act as sources and drains of Berry curvature, leading to significant responses such as anomalous Hall effect (AHE) and anomalous Nernst effect (ANE) [1-3]. In nano-scale technology, such large topological responses may play a significant role in developing next-generation electronic devices.

Recently, the electrical manipulation of the topological state has been demonstrated in antiferromagnetic Weyl semimetal Mn₃Sn [4]. Mn₃Sn is a metallic antiferromagnet with the hexagonal D019 structure and ABAB-stacking of Mn kagome lattice along [0001]. The geometrical frustration leads to a 120-degree structure made of Mn magnetic moments with a negative vector chirality (Fig 1(a)). This non-collinear structure can be viewed as a ferroic order of a cluster magnetic octupole made of six neighboring Mn moments. The polarization of the magnetic octupole determines the distribution of Weyl points in momentum space and thus the polarity of AHE (Fig 1(b)). Figure. 1(c) shows the schematic image of the current switching in Mn₃Sn/heavy metal heterostructures. Taking Mn₃Sn/W as an example, with an applied electrical current in the multilayer, a spin current generated by the spin Hall effect in the W

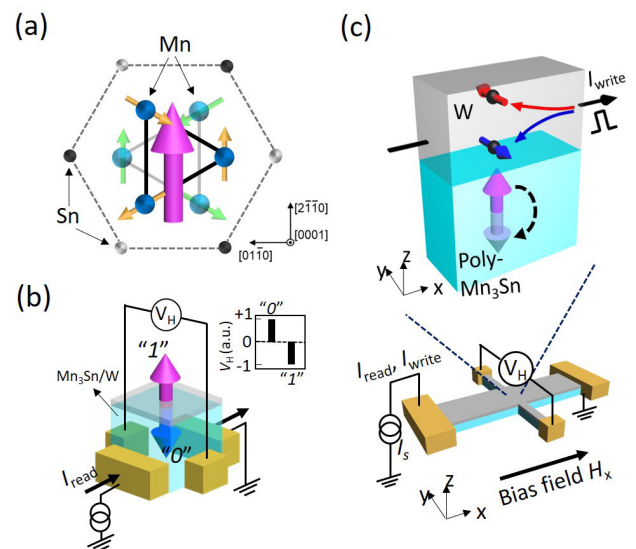


Fig. 1. (a) Crystal and spin structures of Mn₃Sn. Blue and light blue spheres represent Mn atoms on the kagome bilayers, forming an octahedron. Black and gray spheres represent Sn atoms. The non-collinear spin structure consisting six Mn magnetic moments (yellow and green arrows) can be viewed as a ferroic ordering of a magnetic octupole (purple arrow). (b) Hall voltage measured in Mn₃Sn/W devices. The sign of readout voltage is determined by the out-of-plane component in the polarization direction of the magnetic octupole of Mn₃Sn (purple and blue arrows), namely, “0” or “1” state. (c) Bottom: Schematic image of Mn₃Sn/heavy metal devices and the setup of electrodes. The samples are fabricated in 16 μm × 96 μm Hall bar structure with Au/Ti electrodes. Top: Schematic image of the current switching in Mn₃Sn/W bilayer. An electrical current flowing in the W layer generates a spin current by the spin Hall effect of W. This spin current induces a spin-orbit torque in the Mn₃Sn layer and switch the polarization direction of the magnetic octupole. Here, red and blue thin arrows represent the spin moments of the spin current. Purple and light purple thick arrows represent the polarization direction of the magnetic octupole.

layer exerts the spin-orbit torque on the Mn₃Sn spin texture, causing the switching of the polarization direction of the magnetic octupole. This manipulation of AHE enables us to store the information from the electrical signal, “0” or “1” state, into the magnetic octupole of Mn₃Sn. Thus, Mn₃Sn can work as a non-volatile memory, in which the information can be written and read by current. Moreover, the antiferromagnetic structure of Mn₃Sn allows electronic devices with higher density and computing speed than those made of conventional ferromagnets [5]. For applications, it is essential to enhance the readout signal of the switching. This study demonstrates that the switching signal of Mn₃Sn can grow dramatically by adjusting the crystal orientation and interface condition of the Mn₃Sn/heavy metal structures. Moreover, by increasing the read current, the readout voltage may go well beyond 1 mV, a milestone for future memory technology.

To find the largest readout signal, we prepared four different multilayer stacks: (i) Ru(2)/Mn₃Sn(40)/Pt(5), (ii) Mn₃Sn(40)/Pt(5), (iii) Ru(2)/Mn₃Sn(40)/W(5), and (iv) Mn₃Sn(40)/W(5), all units in nm, deposited on a Si/SiO₂ substrate. For the sample (i)-(iii), the stacks are annealed at 450 °C for 0.5 h after the fabrication of the Mn₃Sn layer. The samples (iv) Mn₃Sn(40)/W(5) is annealed at 450 °C for 0.5 h after the fabrication of the W layer. Using these thin films, a Hall bar structure (16 μm × 96 μm) is fabricated, with Ti/Au electrodes attached (Fig 1(c)). Figure. 2(a) shows the AHE signal in W devices with and without the Ru layer. By removing the Ru layer, the AHE becomes 1.6 times larger than that observed in devices with the Ru layer. Similar enhancement of the AHE also occurs in Pt devices. This enhancement comes from the crystal orientation change of Mn₃Sn. The X-ray diffraction analysis shows that the kagome plane of Mn₃Sn tends to align in-plane in the presence of the Ru underlayer. After removing the Ru layer, Mn₃Sn layer becomes completely polycrystalline. The out-of-plane component of the magnetic octupole is more than one with the Ru layer, resulting in a larger AHE. Next, we investigated the electrical switching in W devices. In these experiments, both electrical current and bias field are applied along the longitudinal direction (*x*-direction) and the transverse Hall voltage V_H is detected in the *y*-direction, as shown in Fig. 1(c). A strikingly large switching Hall voltage, $\Delta V_H^{\text{current}} \sim 70 \mu\text{V}$, is observed in Mn₃Sn/W devices (Fig. 2(b)). This Hall signal is 3 times larger than that observed in the Ru/Mn₃Sn/W devices, more pronounced than the 1.6 times difference of the AHE caused by removing the Ru layer. We attribute this enhancement in current switching to the different annealing process because only the Mn₃Sn/W samples is once annealed after the W deposition. This additional annealing process may affect the interface condition. Finally, since the Hall voltage is proportional to the

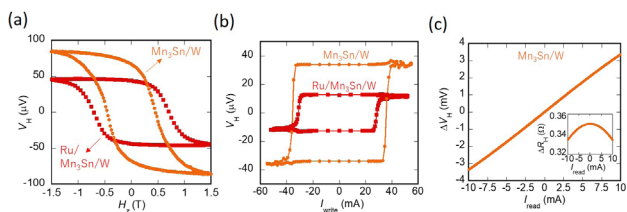


Fig. 2. (a) Hall voltage V_H as a function of a perpendicular magnetic field H_z for Ru/Mn₃Sn/W and Mn₃Sn/W devices, respectively. (b) V_H as a function of the write-current I_{write} under a bias field $\mu_0 H_x = 0.1$ T applied along the electrical current direction for Ru/Mn₃Sn/W and Mn₃Sn/W devices, respectively. (c) Switching Hall voltage ΔV_H as a function of the read current I_{read} in the Mn₃Sn(40)/W(5) sample. Inset: Hall resistance ΔR_H as a function of the read current I_{read} .

read current within a suitable temperature range, we tried to enhance the read current to maximize the readout signal (Fig. 2(c)). We found that the readout switching Hall voltage ΔV_H can exceed 1 mV when applying 3 mA read current. This observed mV order Hall voltage is a significant advance in the electrical switching technology, and our results may pave the path for designing a new type of memory device using the robust topological properties of Weyl antiferromagnets.

References

- [1] H. B. Nielsen and M. Ninomiya, Phys. Lett. B, **130**, 389 (1983).
- [2] S. Nakatsuji, N. Kiyohara, and T. Higo, Nature, **527**, 212 (2015).
- [3] M. Ikhlas, T. Tomita, T. Koretsune, M. Suzuki, D. Nishio-Hamane, R. Arita, Y. Otani, and S. Nakatsuji, Nat. Phys. **13**, 1085 (2017).
- [4] H. Tsai, T. Higo, K. Kondou, T. Nomoto, A. Sakai, A. Kobayashi, T. Nakano, K. Yakushiji, R. Arita, S. Miwa, Y. Otani, and S. Nakatsuji, Nature **580**, 608 (2020).
- [5] T. Jungwirth *et al.*, Nat. Nanotechnol. **11**, 231 (2016).

Authors

H. Tsai, T. Higo, K. Kondou^a, S. Sakamoto, A. Kobayashi, T. Matsuo, S. Miwa, Y. Otani, and S. Nakatsuji

^aRIKEN, Center for Emergent Matter Science (CEMS)

A Tunable Stress Dilatometer and Measurement of the Thermal Expansion under Uniaxial Stress of Mn₃Sn

Nakatsuji Group

The hexagonal antiferromagnet Mn₃Sn with triangular spin structure exhibits large spontaneous electronic responses associated with Weyl fermions [1], which has attracted tremendous attention due to its potential for spintronic applications [2]. The single crystals of this compound are known to be stable in their off-stoichiometric compositions. Depending on the composition, three distinct kinds of magnetic phases can emerge as a function of temperature, namely the high-temperature triangular spin structure phase ($\mathbf{q} = 0$) [3], the intermediate-temperature incommensurate spin spiral phase ($\mathbf{q} \neq 0$) [4], and the low-temperature cluster spin glass phase [5]. The topological transport properties vanish in the incommensurate phase, whose origin remains elusive. A theoretical study suggests that out-of-plane antiferromagnetic exchange interaction may destabilize the triangular spin structure [6].

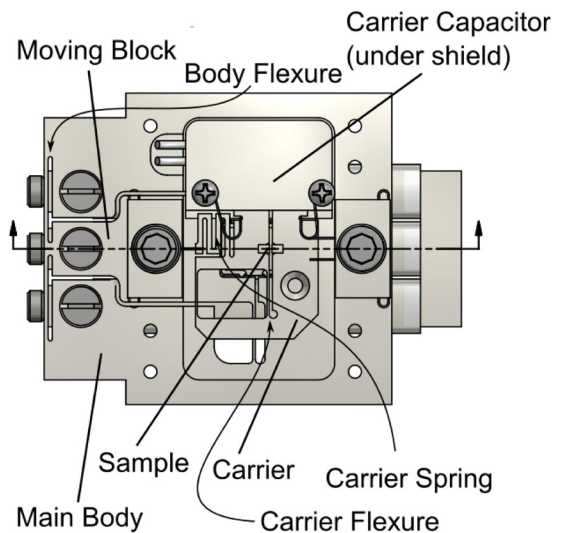


Fig. 1. Uniaxial stress dilatometer

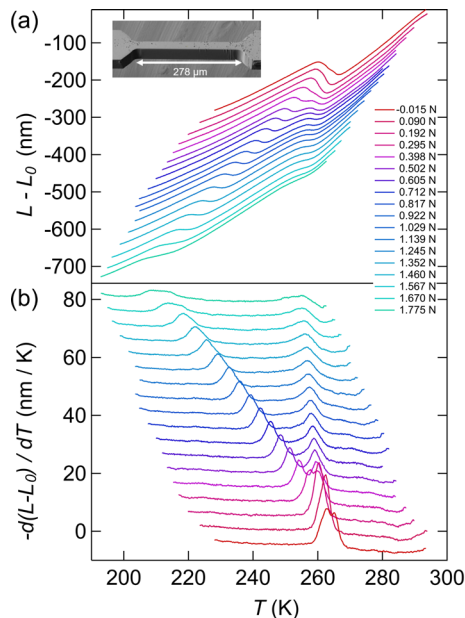


Fig. 2. Thermal expansion of Mn_3Sn under uniaxial pressure. (a) Sample's c -axis length change $L-L_0$ vs. temperature under various applied uniaxial forces. Inset shows the sample used for the measurements. (b) Derivative of c -axis length change $-d(L-L_0)/dT$ vs. temperature (bottom panel) under various applied uniaxial forces.

A long-wavelength incommensurate spin structure can originate from various mechanisms, such as competition between short-range and long-range exchanges in CeSb [7], and Fermi surface nesting in hexagonal rare-earth elemental metals [8]. In the latter case, Fermi surface nesting is largely determined by the lattice constant ratio c/a , which is tunable by alloying or uniaxial pressure. Uniaxial pressure is a clean tuning parameter compared to chemical doping. Here, we explore the evolution of the magnetic phase diagram of Mn_3Sn under c -axis uniaxial pressure.

In collaboration with Dr. Clifford Hicks and Dr. Kent Shirer from Max Planck Institute for Chemical Physics of Solids (MPI CPfS), Dresden, Germany, we developed a piezoelectric-based uniaxial stress dilatometer that provides *in-situ* stress tunability, as shown in Fig 1. This device allows high-sensitivity thermal expansion measurements, offering a compelling route to thermodynamic information on magnetic phase evolution under large and homogenous applied stress. The sample is sculpted into a paddle using a focused ion beam and then epoxied across the central gap of the sample carrier, as seen in the inset of Fig 1a. Applying voltage to the piezo stacks displaces a spring and delivers uniaxial stress to the sample, while the sample's length change was estimated from the displacement of the parallel plate capacitor attached to the carrier.

Figure 2a shows the temperature dependence of c -axis length change $L-L_0$ of Mn_3Sn at various applied uniaxial forces. At zero force, the sample exhibits a first-order transition from triangular to spiral spin structure on cooling below $T_H = 267$ K, accompanied by a discontinuity in $L-L_0$. Under uniaxial force, the transition splits into two, as shown in Fig. 2b. The peak in $-dAL/dT$ that shifts to lower temperatures with an increasing uniaxial force corresponds to the response of the central narrow portion of the sample. With an elastic compressive stress of $\sigma_z \sim 1.5$ GPa, the transition is suppressed by $\Delta T \sim -50$ K. Below $-\sigma_z \sim 0.5$ GPa, T_H has a linear dependence on σ_z , with $\partial T_H/\partial \sigma_z = 33.3$ K at zero stress. We estimate an entropy change of $\Delta S \sim 0.1$ mJ mol⁻¹ K⁻¹ from Clausius-Clapeyron relation, using the magnitude of the discontinuity in ΔL and $\partial T_H/\partial \sigma_z$. This value of ΔS

is consistent with that estimated from heat capacity data. Above $-\sigma_z \sim 0.5$ GPa, $\partial T_H/\partial \sigma_z$ does not deviate appreciably from its ambient pressure value; this information cannot be extrapolated solely based on the zero pressure $\partial T_H/\partial \sigma_z$. Overall, we found that the transition is insensitive to stress compared with its response to chemical doping, suggesting that the lattice is not the primary driver of the transition. This device is compatible with other probes, such as transport and spectroscopy, opening a new avenue to study phases of matter under extreme conditions [9].

References

- [1] T. Chen, T. Tomita, S. Minami, M. Fu *et al.*, Nat. Comm. **12**, 572 (2021).
- [2] H. Tsai, T. Higo *et al.*, Nature **580** (2020).
- [3] T. Nagamiya, S. Tomiyoshi, and Y. Yamaguchi, Solid State Commun. **42** (1982).
- [4] J.W. Cable *et al.*, Solid State Commun. **88** (1983).
- [5] W. J Feng, D. Li *et al.*, Phys. Rev. B **73** (2006).
- [6] S. Dasgupta and O. Tchernyshyov, Phys. Rev. B **102** (2020).
- [7] M. E. Fischer and W. Selke, Phys. Rev. Lett. **44** (1980).
- [8] A. Andrianov *et al.*, Phys. Rev. B **62** (2000).
- [9] M. Ikhlas, K. Shirer *et al.*, Appl. Phys. Lett. **117** (2020).

Authors

M. Ikhlas, K. Shirer^a, P.-Y. Yang^a, A. P. Mackenzie^a, C.W. Hicks^a, and S. Nakatsuji

^aMax Planck Institute for Chemical Physics of Solids

Large Transverse Thermoelectric Effect in Iron-Based Binary Ferromagnets

Nakatsuji and Miwa Groups

Thermoelectricity provides vital technology for versatile energy harvesting and heat current sensors. So far, thermoelectric technologies are focused on the longitudinal Seebeck effect. Its transverse counterpart, the anomalous Nernst effect (ANE), has recently gained significant attention, owing to several potential benefits [1,2]. Namely, the transverse geometry of the Nernst effect enables simplified structures of thermoelectric generators with enhanced conversion efficiency once the suitable materials become readily available. Moreover, the transverse geometry is hypothetically better suited for thermoelectric conversion, as the Ettingshausen heat current should support the Nernst voltage while the Peltier heat current may suppress the Seebeck voltage [3]. A server obstacle here is that the anomalous Nernst effect is too small compared to the Seebeck effect for real-life thermoelectric applications. Thus, it is essential to design a new class of materials that exhibit a large ANE without an external magnetic field.

To find candidate compounds efficiently, we carried out a high-throughput calculation to screen materials and found two candidate iron-based cubic compounds, Fe_3X ($X = \text{Ga}, \text{Al}$),

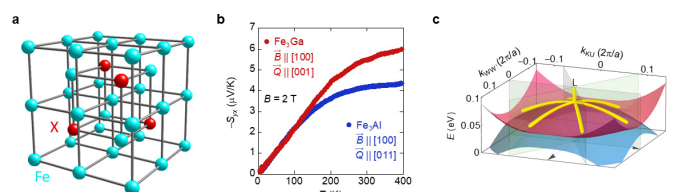


Fig. 1. (a) Crystal structures of Fe_3X ($X = \text{Ga}, \text{Al}$) (b) Temperature dependence of the Nernst signal $-S_{yx}$ in Fe_3X ($X = \text{Ga}, \text{Al}$) under a [100] magnetic field of 2T. (c) The nodal web in momentum space formed by nodal lines (yellow) of nearly flat energy dispersion around the L point.

Al) (Fig. 1a). We discovered record high spontaneous transverse thermoelectric effects at room temperature in these materials, reaching about $6 \mu\text{VK}^{-1}$ in Fe_3Ga and $4 \mu\text{VK}^{-1}$ in Fe_3Al (Fig. 1b). We then succeeded in fabricating Fe_3Ga and Fe_3Al thin films that display an ANE of about $4 \mu\text{VK}^{-1}$ and $2 \mu\text{VK}^{-1}$ at room temperature with an applied in-plane temperature gradient. For an out-of-plane temperature gradient, these thin films exhibit a zero-field ANE, with a coercivity B_C of the in-plane magnetization being about 40 Oe in Fe_3Ga and 20 Oe in Fe_3Al , respectively. These features are suitable for designing low-cost, flexible thermoelectric generators.

The comparison between experiment and theory indicates that the Fermi energy tuning to the nodal web is the key to the substantial enhancement in the transverse thermoelectric coefficient. Figure 1(c) shows a schematic of the nodal web, a flat band structure made of interconnected nodal lines. The Berry curvature is particularly enhanced at the momenta connecting the edge of the nodal web around the L point at the Brillouin zone boundary, extending over a quasi-2D area spanned by the web. The strongly enhanced Berry curvature occurs near the momenta originally belonging to the flat nodal web, such as the one around the L point.

Our innovative iron-based thermoelectric material represents a significant step toward commercializing thermoelectric generators that can power small devices such as remote sensors or wearable devices. It is vital to enhance the coercivity further to achieve stable performance in daily use. Finally, it would be an interesting future direction to look for an enhanced output by combining the ANE with the spin Seebeck effect, both of which occur in the same transverse geometry. [4]

References

- [1] A. Sakai *et al.*, Nat. Phys. **14**, 1119 (2018).
- [2] M. Ikhlas, T. Tomita *et al.*, Nat. Phys. **13**, 1085 (2017).
- [3] M. Mizuguchi, and S. Nakatsuji, Sci. Technol. Adv. Mater. **20**, 262 (2019).
- [4] A. Sakai, S. Minami, T. Koretsune, T. Chen, T. Higo *et al.*, Nature **581**, 53 (2020).

Authors

A. Sakai, S. Minami^a, T. Koretsune^b, T. Chen, T. Higo, Y. Wang, T. Nomoto^c, M. Hirayama^d, S. Miwa, D. Nishio-Hamane, F. Ishii^a, R. Arita^{c,d}, and S. Nakatsuji

^aKanazawa University

^bTohoku University

^cUniversity of Tokyo

^dRIKEN CEMS

Electrical Manipulation of a Topological Antiferromagnetic State

Nakatsuji, Otani, and Miwa Groups

The Weyl semimetal features nodal points formed by two linearly dispersive non-degenerate bands. These touching points or Weyl nodes act as topologically protected monopoles or antimonopoles of underlying Berry curvature, resulting in large anomalous Hall effect (AHE) and chiral anomaly. The electrical manipulation of Weyl nodes is among the key topics of technological innovation utilizing a novel topological state. Moreover, electrical manipulation of an antiferromagnetic Weyl metal is considered a significant advancement, given the prospects of antiferromagnetic (AF) spintronics for realizing high-density, ultrafast devices [1].

We demonstrate the electrical switching of the AF Weyl

state using Mn_3Sn /nonmagnetic metals (NM = Pt, W, Cu) bilayer devices and the spin-orbit torque (SOT) switching method [5]. The inverse triangular spin structure of Mn_3Sn can be viewed as a ferroic ordering of cluster magnetic octupoles. The magnetic octupole's polarization direction determines the location of Weyl nodes and the associated distribution of the Berry curvature in the momentum space (Fig. 1(b) right) [2]. With an electrical current applied to the Pt layer, a spin polarized current generated by the spin Hall effect of Pt induces the SOT on the Mn_3Sn layer and causes the switching of the polarization direction of the magnetic octupole (Fig. 2a). The measurement configuration and optical micrograph of the fabricated bilayer Hall bar devices are shown in Fig. 2(b). We first perform the magnetic field switching of the Hall voltage V_H by using an out-of-plane magnetic field H_z and a read current of

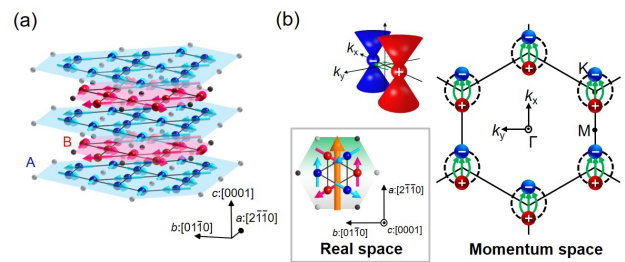


Fig. 1. (a) Mn_3Sn crystal structure and inverse triangular spin (ITS) structure. The Mn magnetic moments (light blue and pink cylindrical arrows) lie within the kagome layer with the ABAB stacking sequence and form the ITS structure at room temperature. This spin structure can be viewed as a ferroic ordering of cluster magnetic octupoles. (b) Bottom-left: cluster magnetic octupole (orange cylindrical arrow) consisting of the six spins on the kagome bilayer. Right: schematic of the Weyl point distribution near the Fermi energy in momentum space (k_x - k_y plane at $k_z = 0$); the corresponding magnetic structure is shown in the left-side figure. The red and blue spheres correspond to Weyl nodes acting as sources (+) and drains (-) of the Berry curvature (green arrows). Inset: three-dimensional schematic of a pair of Weyl nodes.

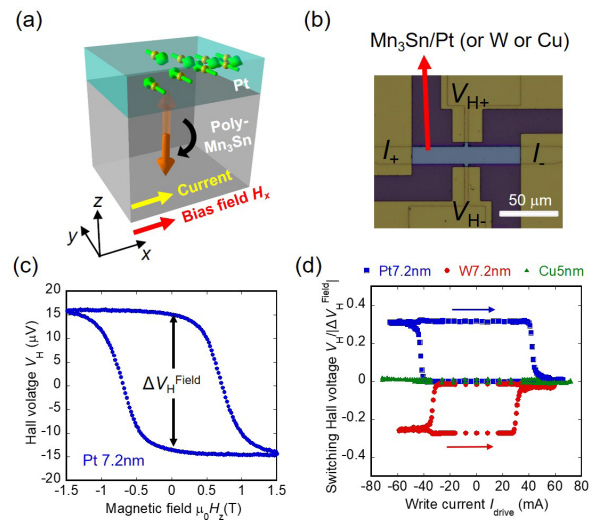


Fig. 2. (a) Schematic image for the spin-orbit torque switching. Under a write current and a bias field along the x -direction, the spin-polarized current in Pt (green cylindrical arrows on yellow spheres) exerts a spin-orbit torque, causing the polarization axis of the cluster magnetic octupole to switch (orange cylindrical arrow) in the polycrystalline Mn_3Sn . (b) Measurement configuration and optical micrograph of the Mn_3Sn -nonmagnet bilayer Hall bar devices. (c) Hall voltage V_H vs. magnetic field along the z -direction H_z obtained for the $\text{Mn}_3\text{Sn}/\text{Pt}$ 7.2 nm device at room temperature. (d) Hall voltage V_H vs. write current I_{write} for the Pt 7.2 nm, Cu 5 nm, and W 7.2 nm devices at room temperature. The Hall voltage is normalized by the zero-field Hall voltage $|\Delta V_H^{\text{field}}|$ obtained from the magnetic field dependence measurements for each sample.

0.2 mA, and a clear hysteresis of V_H with the zero-field change of $\Delta V_H^{\text{field}} (= V_H(+H_z \rightarrow 0) - V_H(-H_z \rightarrow 0))$ is observed (Fig. 2(c)). To examine the possible SOT switching of Mn_3Sn , we pass a 100 ms write-pulse current I_{write} along the x -direction; then, we wait for 600 ms after the pulse current and measure V_H with a 0.2 mA read current. Figure 2(d) shows V_H as a function of I_{write} in Pt, W, and Cu devices. For the NM = Pt (spin Hall angle $\theta_{\text{SH}} > 0$) and a bias field H_x parallel to the current direction, a clear negative (positive) jump appeared in the Hall voltage for a positive (negative) current larger than a critical threshold write-current I_c . The magnitude of the jump reaches $\sim 30\%$ of the total Hall voltage change $|\Delta V_H^{\text{field}}|$ in the field sweep measurements. To confirm that the observed switching of V_H is related to the SOT due to the spin Hall effect in the NM layer, we prepared NM = W ($\theta_{\text{SH}} < 0$) and Cu ($\theta_{\text{SH}} \sim 0$). For NM = W, the switching polarity is opposite to the Pt case, while for NM = Cu, hysteresis is absent with the electrical current cycle. The difference in switching polarity between Pt and W devices and the absences of switching in Cu devices cannot be explained by the current-induced Oersted field but agree well with the sign of θ_{SH} of the NM layer. These results demonstrate that SOT from the NM layer induces the perpendicular switching of the AF domain and thus manipulates the direction of the Weyl nodes.

In recent years, utilizing antiferromagnets in spintronics devices have attracted significant attention as its vanishing small stray fields and much faster spin dynamics than ferromagnets [1]. We achieved the electrical switching of the AF Weyl metal using the same protocol as the one used for ferromagnetic metals [3, 4]. The critical write current density in the NM layer is considerably smaller than that in the NM/FM devices. These results indicate that topological antiferromagnets offer the unmatched potential for spintronic applications that may surpass today's ferromagnetic counterparts [5].

References

- [1] T. Jungwirth *et al.*, Nat. Nanotechnol. **11**, 231 (2016).
- [2] S. Nakatsuji, N. Kiyohara, and T. Higo. Nature **527**, 212 (2015).
- [3] I. M. Miron *et al.*, Nature **476**, 189 (2011).
- [4] L. Liu *et al.* Science **336**, 555 (2012).
- [5] H. Tsai, T. Higo, K. Kondou, T. Nomoto, A. Sakai, A. Kobayashi, T. Nakano, K. Yakushiji, R. Arita, S. Miwa, Y. Otani, and S. Nakatsuji, Nature **580**, 608 (2020).

Authors

H. Tsai, T. Higo, K. Kondou^a, Takuya Nomoto^b, A. Sakai, A. Kobayashi, T. Nakano^c, K. Yakushiji^c, R. Arita^a, S. Miwa, Y. Otani, and S. Nakatsuji

^aRIKEN CEMS

^bThe University of Tokyo

^cAIST

Weyl-Fermion-Induced Anomalous Transport in the Chiral Antiferromagnets Mn_3X , ($\text{X} = \text{Sn}, \text{Ge}$)

Nakatsuji Group

The blooming field of spintronics has bridged astonishingly complex antiferromagnetic structures to the realm of energy-efficient memory technologies. However, a significant obstacle to overcome is the tiny response of the antiferromagnetic structure to external magnetic fields [1]. The recent discoveries of large room-temperature anomalous transport effects in antiferromagnets Mn_3X ($\text{X} = \text{Sn}, \text{Ge}$) [2,3] signifies an experimental breakthrough in this direction,

bringing the study on strongly correlated topological phases to the main stage of basic science and technological innovation. These anomalous transport properties are considered fingerprints of Weyl fermions in the momentum-space band structure [4]. Therefore, understanding the role of magnetic Weyl fermions in driving the transport properties of chiral antiferromagnets is all the more important for making real-life applications with topological states of matter.

In this work, we establish Weyl fermions as the origin of the large anomalous Hall and Nernst effects in Mn_3X systems by combining our previous reports with a new, comprehensive set of transport measurements and theoretical analysis of high-quality Mn_3Sn and Mn_3Ge single crystals [5]. In particular, Mn_3Ge provide an ideal experimental platform for identifying transport signatures stemming from Weyl fermions; in this compound, the inverse triangular covers a wide temperature range down to at least 0.3 K, approximately one-thousandth of the Néel temperature. This feature allows a clear-cut detection of the Weyl-fermion-induced transport anomalies at sufficiently low temperatures, where spin fluctuations are essentially suppressed.

The fingerprint of Weyl points in magnetotransport is known as the chiral anomaly. With a magnetic field, the Weyl crossings are quantized into Landau levels (LLs), and the lowest LL are divided into left- and right-movers of opposite chirality. These two groups do not mix, leading to separate number conservation of the three-dimensional left- and right-handed Weyl fermions. Once an electric field parallel to the magnetic field is applied, the conservation of chirality no longer holds due to mixing the left-and-right movers. In such a case, charge pumping between the Weyl nodes of opposite chirality generates the positive longitudinal magnetoconductivity (LMC) or the negative magnetoresistivity (LMR) only when the electric current and magnetic field are parallel to each other. This strongly anisotropic behavior of LMC provides transport evidence for Weyl fermions.

Our findings of magnetotransport signatures specific to chiral anomalies in Mn_3Ge and planar Hall effect in Mn_3Sn provide concrete evidence for the presence of Weyl fermions in both materials. Figure 1a shows the field dependence of the magnetoconductivity observed in Mn_3Ge at 0.3 K. For applied fields $B > 2\text{T}$, the magnetoconductivity becomes positive for the parallel configuration and is nearly quadratic in magnetic field. The B^2 dependence of the positive LMC is likely a result of strongly tilted type-II Weyl cones with the applied magnetic field perpendicular to the tilt axis. We

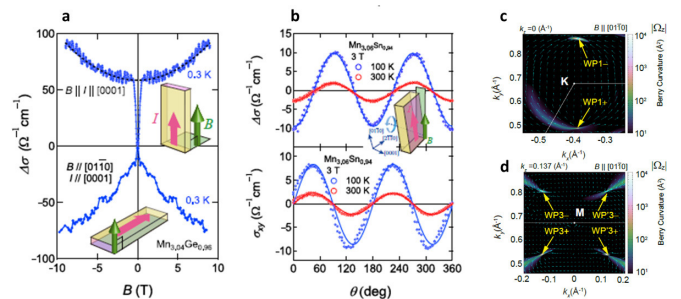


Fig. 1. (a) The magnetoconductivity as a function of the magnetic field B for the parallel and perpendicular configurations with the current $I \parallel [0001]$ measured at 0.3 K in Mn_3Ge . The dashed line is a fit to the quadratic magnetic field dependence. (b) Angle dependence of the longitudinal magnetoconductivity (top) and the planar Hall effect (PHE) (bottom) in $\text{Mn}_{3.06}\text{Sn}_{0.94}$ obtained at 300 and 100 K under $B = 3\text{T}$. (c, d) Contour plots of the calculated Berry-curvature spectrum $|\Omega_z|$ in the k_x - k_y -plane under $B \parallel [01-10]$ at $k_z = 0$ (\AA^{-1}) (c) and at $k_z = 0.137$ (\AA^{-1}) (d). The arrows indicate the Berry curvature induced by the pairs of Weyl points WP1 and WP3 (WP3) near the Fermi level.

further verified that the angular dependence of the magneto-conductivity and the planar Hall signal observed in Mn_3Sn agree well with the theoretical forms for the chiral anomaly (Fig. 1b), another transport evidence for magnetic Weyl fermions.

Moreover, we compare our results on the anomalous Hall and Nernst effects with the first-principles calculations that consider the substantial bandwidth renormalization and quasiparticle damping due to the strong electronic correlation in Mn_3X systems (Fig. 1c, d). The calculated transverse thermoelectric coefficients well reproduce the overall temperature dependence of the experimental data, suggesting that the large Berry curvature stemming from the Weyl nodes leads to significantly enhanced AHE and ANE in the absence of net magnetization.

Strongly correlated topological states have become a central focus for quantum materials research, and Mn_3X ($X = Sn, Ge$) is widely considered a textbook example of this kind. Our findings provide concrete evidence for the presence of Weyl fermions in both materials, which may trigger further exploration of their rich physics and useful properties emerging from the interplay between magnetism and band topology.

References

- [1] T. Jungwirth *et al.*, Nat. Nanotechnol. **11**, 231 (2016).
- [2] S. Nakatsuji *et al.*, Nature **527**, 212 (2015).
- [3] M. Ikhlas, T. Tomita *et al.*, Nat. Phys. **13**, 1085 (2017).
- [4] K. Kuroda *et al.*, Nat. Mater. **16**, 1090 (2017).
- [5] T. Chen, T. Tomita, S. Minami, M. Fu *et al.*, Nat. Comm. **12**, 572 (2021).

Authors

T. Chen, T. Tomita, S. Minami, M. Fu, T. Koretsune^a, M. Kitatani, I. Muhammad, D. Nishio-Hamane, R. Ishii, F. Ishii^b, R. Arita^{c,d}, and S. Nakatsuji
^aTohoku University
^bKanazawa University
^cRIKEN CEMS
^dThe University of Tokyo

Giant Effective Damping of Octupole Oscillation in a Chiral Antiferromagnet Mn_3Sn

Miwa, Nakatsuji, and Otani Groups

Understanding of spin dynamics forms the basis of spintronic application. For the ultrafast THz control of staggered moments in antiferromagnets, the time-resolved observation of spin dynamics is essential for developing the associated technology. However, such observation has been limited to insulators to date. Recently, the metallic antiferromagnets Mn_3X have attracted significant attention for its strong response (e.g. anomalous Hall effect) comparable to ferromagnets owing to the hidden ferroic order, which configures large Berry curvature originated from Weyl points in a momentum space. Such ferroic order can be characterized by cluster magnetic octupoles based on neighbouring magnetic moments, and thus it is highly important to clarify the dynamics of cluster octupole for designing the spintronic application. In this research, we conduct time-resolved observation of spin-dynamics in a chiral antiferromagnet Mn_3Sn .

Bulk single-crystal $D0_{19}$ - Mn_3Sn has been employed. Mn_3Sn has the hexagonal Ni_3Sn -type crystal structure consisting of an $ABAB$ stacking of the kagome lattice of

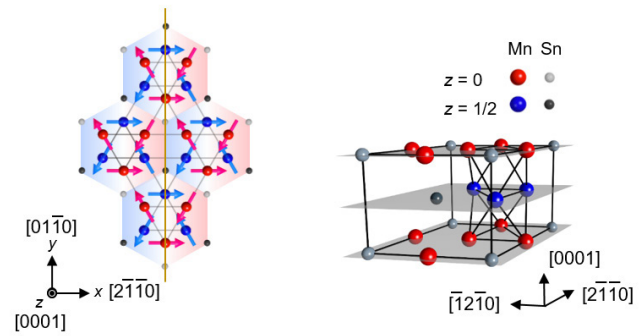


Fig. 1. (a) Spin and crystal structures of Mn_3Sn . Different colors are used to denote Mn and Sn atoms in the $z = 0$ and $z = 1/2$ planes. The inverse triangular spin-structure can be viewed as a ferroic ordering of cluster magnetic octupole, which possesses the same symmetry as the spin-magnetization (e.g. as indicated by a mirror plane (orange line)).

Mn atoms along the $[0001]$ axis. Red (blue) circles in Fig. 1 indicate Mn atoms in A - (B -) plane of the kagome lattice. An inverse triangular spin structure is stabilized by exchange and Dzyaloshinskii-Moriya interactions [1,2]. The inverse triangular spin structure is made of a ferroic ordering of cluster magnetic octupoles [3].

Figure 2(a) shows typical TR-MOKE results, where a magnetic field of 2 T was applied normal to the surface. First, a pump light induces rapid decrease in the polar MOKE intensity of a probe light, similar to ultrafast demagnetization observed in ferromagnetic metals [4]. Consecutively, the MOKE intensity start to recover with delay time more than 0.3 ps, exhibiting a small but clear oscillation during the recovery. To further characterize the oscillating component, a non-oscillating component was estimated as a background (black solid curve) and subtracted from the raw data. The lower panel of Fig. 1(b) shows the TR-MOKE signals after subtracting the background. Figure 1(c) also shows typical TR-MOKE results (upper panel) and the analysis for the oscillating component (lower panel) in a relatively long-time range. From the fits in the lower panel of Figs. 1(b) (orange curve) and 1(c) (blue curve), oscillation frequencies (ω_I, ω_{II}) are determined as a function of an external magnetic field, namely, $\omega_I = 0.86$ THz and $\omega_{II} = 18$ GHz. The oscillating behaviour is most significant when the magnetic field is normal to the Mn_3Sn surface. Because

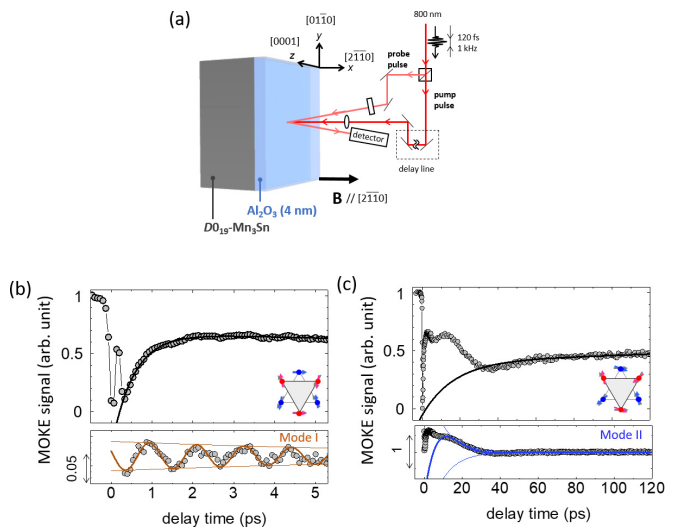


Fig. 2. (a) Schematic diagram of the time-resolved polar MOKE measurements (TR-MOKE). (b), (c) TR-MOKE signals of Mn_3Sn under a magnetic field of 2 T in the $[2-1-10]$ direction. Backgrounds, indicated by black curves in upper panels, were subtracted from the raw data and plotted in the lower panels.

TR-MOKE signal is proportional to the surface normal polarization of the cluster magnetic octupoles, the oscillating Kerr signal should come from a change of size of the cluster magnetic octupole order.

Two oscillation modes I and II are found through the analyses shown in Figs. 1(b) and 1(c), which should come from the dynamics of the cluster magnetic octupoles. The mode I and II are assigned to the optical and collective-precession-like modes. From Fig. 1(c), we find that the dynamics of the cluster octupole in Mn_3Sn is enhanced by exchange interaction, and it is feasible to conduct an ultrafast switching at < 10 ps, a hundred times faster than the case of spin-magnetization in a ferromagnet. Moreover, our theoretical analysis with the aforementioned experimental results shows that the Néel type domain wall velocity in Mn_3Sn can be estimated as > 10 km/s, which is greater than the recently reported value (~ 2 km/s) for the ferrimagnetic systems in the vicinity of the angular momentum compensation temperature [5]. Significantly, our study provides the first demonstration of the time-resolved observation of the spin-wave oscillation in an antiferromagnetic metal.

References

- [1] S. Nakatsuji, N. Kiyohara, and T. Higo, *Nature* **527**, 212 (2015).
- [2] S. Tomiyoshi and Y. Yamaguchi, *J. Phys. Soc. Jpn.* **51**, 2478 (1982).
- [3] M.-T. Suzuki, T. Koretsune, and M. Ochi, *Phys. Rev. B* **95**, 094406 (2017).
- [4] E. Beauprepaire *et al.*, *Phys. Rev. Lett.* **76**, 4250 (1996).
- [5] K.-J. Kim *et al.*, *Nat. Mater.* **16**, 1187 (2017).

Authors

S. Miwa, S. Iihama^a, T. Nomoto^b, T. Tomita, T. Higo, M. Ikhlas, S. Sakamoto, Y. Otani, S. Mizukami^a, R. Arita^b, and S. Nakatsuji^a
^aTohoku University
^bThe University of Tokyo

Low Gilbert Damping in Epitaxial Thin Films of the Nodal-Line Semimetal $D0_3$ - Fe_3Ga

Miwa and Nakatsuji Groups

$D0_3$ -ordered Fe_3Ga [Fig. 1(a)] is a nodal-line semimetal and shows a giant anomalous Nernst effect (ANE). The origin of the ANE was attributed to the large density of states (DOS) and the large Berry curvature near the Fermi level. The large Berry curvature emerges as a result of spin-orbit-coupling-induced gap opening along the nodal lines consisting of nearly flat valence and conduction bands touching each other. This peculiar band structure may be useful for spintronics device application because a gate voltage may effectively modulate Berry-curvature-associated responses as well as magnetic anisotropy. In this regard, it is important to characterize the magnetization dynamics of $D0_3$ - Fe_3Ga . For such a purpose, we fabricated epitaxial thin films of $D0_3$ - Fe_3Ga and bcc-Fe and performed ferromagnetic resonance (FMR) measurements to evaluate their Gilbert damping constants.

50-nm-thick $D0_3$ - Fe_3Ga and Fe thin films were grown by dc magnetron sputtering and molecular beam epitaxy, respectively. We confirmed that the $D0_3$ - Fe_3Ga layer was grown epitaxially by performing high-energy electron diffraction and x-ray diffraction measurements. We conducted FMR measurements using a vector network analyzer and a coplanar waveguide. We employed a field-modulation technique [2], which measures the magnetic-field (H) deriva-

tive of the transmission coefficient ΔS_{21} , to minimize field-independent background signals.

Figure 1(b) shows typical FMR spectra of the Fe_3Ga thin film taken with magnetic fields applied along the [001] direction. Here, a FMR spectrum refers to ΔS_{21} as a function of magnetic field at a fixed frequency. From the FMR spectra, we deduced the peak positions and peak widths, which are shown in Figs. 1(c) and 1(d), respectively. We fitted the Kittel formula to the FMR peak positions, and the fits are shown by solid curves in Fig. 1(c). We found that the in-plane cubic anisotropy $H_{4//}$ of Fe_3Ga favors the magnetization along the [110] direction ($H_{4//} \sim -15$ mT), while those of Fe and disordered Fe-Ga alloys favor the [100] direction ($H_{4//} \sim +60$ mT for Fe and $H_{4//} \sim +75$ -100 mT for the Fe-Ga alloys [3]). This magnetic-anisotropy change indicates that the $D0_3$ atomic ordering significantly alters the electronic band structure of Fe-Ga alloys and induces the giant ANE as a result.

The FMR peak widths of the Fe and Fe_3Ga thin films [Fig. 1(d)] showed linear behavior, the slope of which corresponds to the Gilbert damping constant. The linear fits yielded the Gilbert damping constants of $\alpha = 0.0023 \pm 0.0002$ for Fe and $\alpha = 0.0060 \pm 0.0002$ for $D0_3$ - Fe_3Ga . These values are somewhat consistent with what is expected from the theoretical DOSs, indicating that Ga atoms do not significantly increase the spin-orbit coupling strength. Although the Gilbert damping constant of $D0_3$ - Fe_3Ga is larger than that of bcc-Fe, it is still low compared to typical ferromagnets such as CoFeB ($\alpha \sim 0.004$ -0.006) [4] and Permalloy ($\alpha \sim 0.007$) [5]. In other words, the nodal lines near the Fermi level do not hinder the magnetization dynamics much. The low Gilbert damping may be useful for spintronics device applications because one may be able to efficiently manipulate the magnetization direction by exploiting the peculiar band structure of $D0_3$ - Fe_3Ga .

In summary, we have investigated the magnetization dynamics of the epitaxial thin films of the nodal-line semimetal $D0_3$ - Fe_3Ga by ferromagnetic resonance measurements. We have deduced the intrinsic Gilbert damping constant of $D0_3$ - Fe_3Ga to be $(6.0 \pm 0.2) \times 10^{-3}$, which is

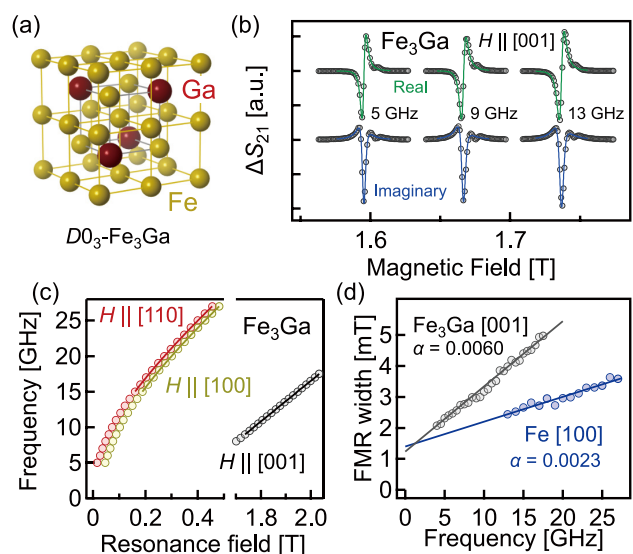


Fig. 1. (a) Crystal structure of $D0_3$ - Fe_3Ga . (b) Typical Ferromagnetic resonance (FMR) spectra of $D0_3$ - Fe_3Ga . (c) Resonance frequency plotted against resonance magnetic fields. The solid curves are the fits using the Kittel formula. (d) FMR peak widths of $D0_3$ - Fe_3Ga and bcc-Fe. The solid lines represent the linear fits, the slope of which represents the intrinsic Gilbert damping constant.

larger than the Fe Gilbert damping constant of $(2.3 \pm 0.2) \times 10^{-3}$ but as low as other typical ferromagnets. The low Gilbert damping and the peculiar band structure with a large Berry curvature make $D0_3\text{-Fe}_3\text{Ga}$ attractive as a building block of spintronics devices.

References

- [1] A. Sakai, S. Minami, T. Koretsune, T. Chen, T. Higo, Y. Wang, T. Nomoto, M. Hirayama, S. Miwa, D. Nishio-Hamane, F. Ishii, R. Arita, and S. Nakatsuji, *Nature* **581**, 53 (2020).
- [2] S. Tamaru, S. Tsunegi, H. Kubota, and S. Yuasa, *Rev. Sci. Instrum.* **89**, 053901 (2018).
- [3] S. Budhathoki, A. Sapkota, K. M. Law, B. Nepal, S. Ranjit, S. K. C. T. Mewes, and A. J. Hauser, *J. Magn. Magn. Mater.* **496**, 165906 (2020).
- [4] A. Conca, J. Greser, T. Sebastian, S. Klingler, B. Obry, B. Leven, and B. Hillebrands, *J. Appl. Phys.* **113**, 213909 (2013).
- [5] Y. Zhao, Q. Song, S.-H. Yang, T. Su, W. Yuan, S. S. P. Parkin, J. Shi, and W. Han, *Sci. Rep.* **6**, 22890 (2016).

Authors

S. Sakamoto, T. Higo, S. Tamaru^a, H. Kubota^a, K. Yakushiji^a, S. Nakatsuji, and S. Miwa
^aNational Institute of Advanced Industrial Science (AIST)

Textbook Renormalization Group Prescription in Tensor-Network Language

Kawashima Group

Kadanoff's block-spin method gives a simple physical picture for the general RG transformations. Combined with Migdal's bond-moving trick, it serves as the first approximation that allows us direct estimation of the critical exponents, though the accuracy may not be satisfactory in many cases. However, it is not obvious how we can systematically improve on it so that eventually we can obtain, at least in principle, estimates as accurate as we like. Modern tensor-network (TN)-based methods, such as tensor renormalization group (TRG), tensor network renormalization (TNR), loop-TNR, high-order TRG (HOTRG), etc, opened up new possibilities for the RG transformations. Generalizing the conventional real-space RG (RSRG) transformations, they are more versatile and, more importantly, systematically improvable. The free energy, the energy, the magnetization, or any other locally defined order parameters can be computed by one of those methods. As for the estimation of the scaling dimensions, the CFT-based transfer-matrix method based on the conformal-field theory has been widely used for two-dimensional classical systems. For higher dimensions, however, the only method generally applicable

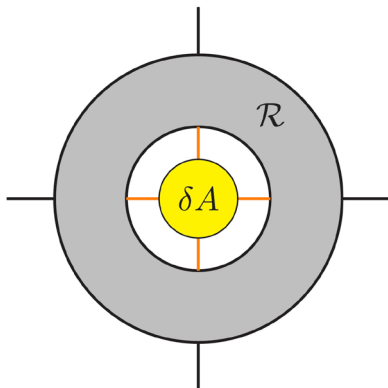


Fig. 1. Schematic diagram of the linearized tensor RG equation "R". In the proposed method, it can be generated using automatic differentiation once the coarse graining is implemented.

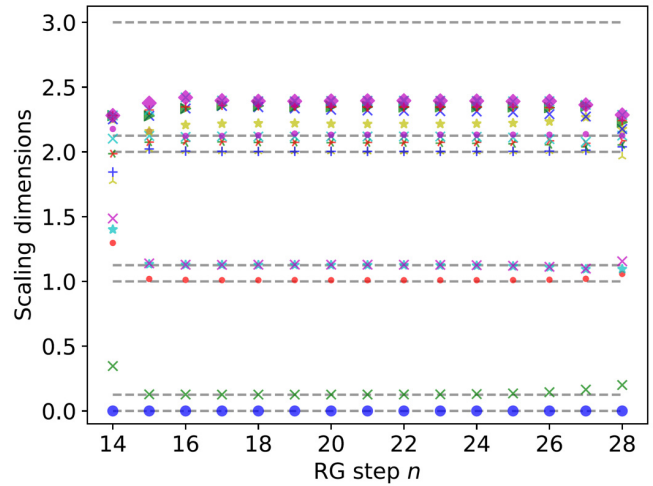


Fig. 2. The scaling dimensions of the 2D Ising model obtained directly from the linearized RG plotted against the number of RG steps applied at the critical point. The flat region represents the fixed point values.

was to estimate the correlation functions and apply the finite-size scaling to them. This indirect method may be good for obtaining one or two scaling dimensions, but it is obviously not a systematic way for obtaining a series of scaling dimensions.

Conceptually, it is straight-forward to construct a method for obtaining the series of scaling dimensions from any RSRG method. Simply we can expand the renormalized tensor with respect to the preceding tensor, i.e., the tensor at one RG step before the current one (Fig. 1). At the fixed point, the linear term would produce the scaling dimensions as its eigenvalues. This is exactly what we learn from textbooks for obtaining the scaling dimensions, in many cases with the Migdal-Kadanoff (MK) approximation as an example. In the MK approximation for the Ising model, we have only two independent fields, and it is impossible to obtain more than two scaling dimensions, whereas in the general TN-based method, we have as many fields as we like and, accordingly, we can in principle obtain many scaling dimensions systematically from the same calculation. However, it has been hard to carry out this straight-forward textbook program in practice because of the influence of the short-range entanglement.

In the paper [1], we adopted the graph-independent local truncation (GILT) method to eliminate the short-range entanglement. This made it possible to fully exploit the RG interpretation of various tensor-network-based methods and show a way to carry out the above-mentioned textbook RG prescription in the TN language: identify a fixed point, linearize the RG equation around this fixed point, and diagonalize it to obtain scaling dimensions. For the RSRG, we used HOTRG though it is not the only possible choice. As shown in Fig. 2, our benchmark calculation on the 2D classical Ising model shows that the proposed method works equally well compared with the above-mentioned CFT-based transfer matrix. The advantage of the present scheme is its potential applications to 3D systems, where the CFT-based method is inapplicable.

Reference

- [1] X. Lyu, R. G. Xu, and N. Kawashima, *Phys. Rev. Research* **3**, 023048 (2021)

Authors

X. Lyu, R. G. Xu^a, and N. Kawashima
^aThe University of Tokyo

Weak Ferromagnetism and Possible Non-Fermi Liquid Behavior in Itinerant Electronic Material Co₃SnC

Uwatoko Group

In Fermi-liquid (FL) theory, the quasiparticle (QP) approximation and the generalized Boltzmann equation can describe the collective behaviors of strongly correlated multi-electron systems. For magnetic materials, strong magnetic correlations usually induce large changes in the QP-QP interactions, which make the QPs behave abnormally. Especially, when approaching the magnetic quantum critical point (QCP), various pronounced deviations from the Landau FL behaviors appear, e.g., non-Fermi liquid (NFL) and strong enhancement of the QP effective mass. On these issues, many correlated electronic materials including the heavy fermion (HF) systems have been studied through tuning the magnetic orders by strengthening the hybridizations between the 4f and conduction electrons and/or enhancing the magnetic correlations via external parameters. These studies are helpful to reveal the intrinsic characteristics of the competing electronic orders near QCPs.

Cobalt-contained materials are such alternatives to explore exotic QCPs owing to the various spin states of cobalt ions and their strong response to the external stimuli. Especially for those materials with both localized and itinerant electrons, the varieties of magnetic transition and phase diagram are more interesting. Metallic perovskite $M_3M'X$ (M is transition metals; M' is the main group elements; X is C, N) is such an example with diversified crystal structures and magnetic phase transitions. But the intrinsic magnetic interaction in $M_3M'X$ is controversial although various classical models were proposed. One possible reason for the absence of the universal theoretical model is that the system is not limited to the simple localized and/or itinerant interactions. Some reports have argued that these materials are close to the boundary of the localized and itinerant ferromagnetism and thus can be taken as an excellent platform to study the crossover between them. Among them, $Co_3M'X$ could be a good example to clarify these issues considering its unstable magnetic ground state and

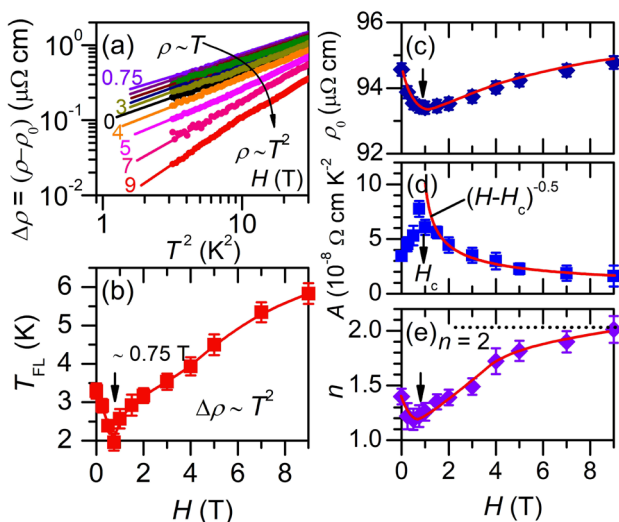


Fig. 1. (a) $\Delta\rho(T)$ vs. T^2 in a log-log scale; the arrow shows the crossover from T - to T^2 -dependence. (b) Field-dependence of T_{FL} ; the arrow shows the critical field; field dependence of the parameters: (c) ρ_0 ; (d) A and the exponential fitting results by the $(H-H_c)^{-0.5}$ (the red solid line); (e) n ; the arrows in (c)-(e) indicate the change tendency and guides to the eye.

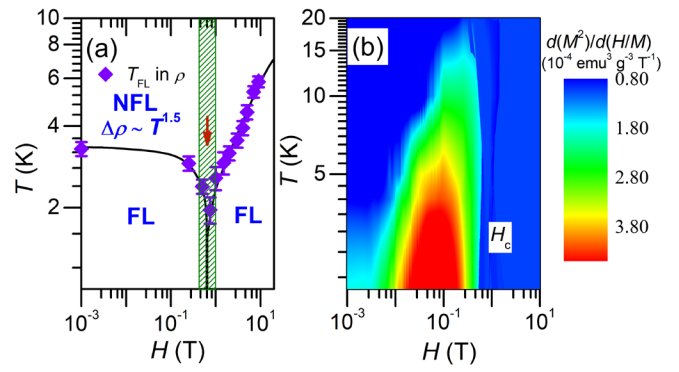


Fig. 2. Phase diagram and field-dependence of characteristic parameters for Co_3SnC : (a) T_{FL} ; (b) the color shows its change tendency of $d(M^2)/d(H/M)$ vs. H which is proportional to the magnitude of magnetic fluctuations.

the abnormal quantum behaviors are expected by applying non-thermodynamic parameters.

In this study, weak ferromagnetism and NFL behaviors were observed in Co_3SnC via measurements of magnetic properties, electrical transport and specific heat under magnetic fields. Magnetic measurements suggest that it undergoes a paramagnetic to itinerant ferromagnetic phase transition with NFL behaviors including the power-law temperature dependence of resistivity, the $-T\log T$ -dependent upturn in specific heat, and the $T^{4/3}$ -dependence of inverse susceptibility. With increasing the magnetic fields, the temperature coefficient of T^2 -term in resistivity follows a $(H-H_c)^{-0.5}$ -divergence upon approaching the critical field H_c , apart from the $1/(H-H_c)$ -dependence with the whole Fermi surface under the singular scattering. The exponent n in the temperature dependence of resistivity shows an increase from $n = 1.0$ to 2.0 with increasing the field above H_c as the evidence for the field-induced crossover from NFL to FL behavior; the relative mass enhancement factor $\lambda(H)/\lambda(0)$ reduce to nearly 60% at 9.0 T, indicating the gradual suppression of magnetic fluctuations and electron-electron scattering. The results indicate that Co_3SnC is a good candidate for exploring itinerant quantum magnetic QCP.

Reference

[1] B. S. Wang, Y. Uwatoko, J. -G. Cheng, and Y. P. Sun, Phys. Rev. B. **102**, 085153 (2020)

Authors

B. S. Wang^a, Y. Uwatoko, J.-G. Cheng^a and Y. P. Sun^{b,c}

^aInstitute of Physics, CAS

^bHigh Magnetic Field Laboratory, CAS

^cInstitute of Solid State Physics, CAS

Pattern Formation Induced by Mechanochemical Coupling of Reaction-Diffusion and Membrane Deformation

Noguchi Group

Shapes of biological membranes are dynamically regulated in living cells. Although membrane shape deformation by proteins at thermal equilibrium has been extensively studied, nonequilibrium dynamics have been much less explored. Recently, chemical reaction propagation has been experimentally observed in plasma membranes. Thus, it is important to understand how the reaction-diffusion dynamics are modified on deformable curved membranes.

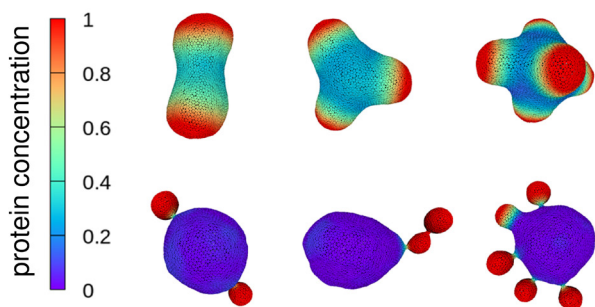


Fig. 1. Snapshots of vesicles with Turing patterns. Top panel: multi-spindle shapes. Bottom panel: budded vesicles. Color indicates the concentration of the curvature-inducing protein.

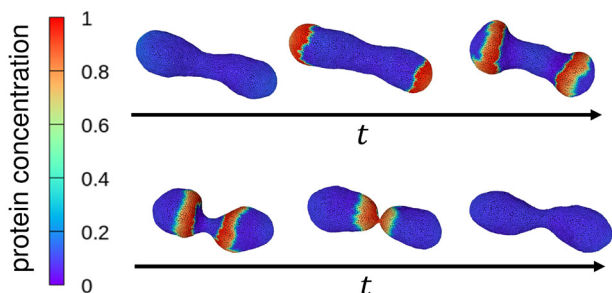


Fig. 2. Sequential snapshots of a shape-oscillation vesicle. Budding repeatedly occurs, accompanied by the propagation wave. Color indicates the concentration of the curvature-inducing protein.

In this study, we present nonequilibrium pattern formation on vesicles induced by mechanochemical feedback between membrane deformation and chemical reactions, using dynamically triangulated membrane simulations combined with a modified Brusselator model that is one of the simplest reaction-diffusion models. Two proteins (curvature-inducing and regulatory proteins) bind to the membrane. We found that membrane deformation changes stable patterns relative to those that occur on a non-deformable curved surface, as determined by linear stability analysis [1]. Temporal oscillation of the protein concentration can be changed into Turing pattern (stable spatial patterns). Budding and multi-spindle shapes are also induced by Turing patterns as shown in Fig. 1.

We also found that the propagating wave patterns change into non-propagating patterns and spiral wave patterns due to the mechanochemical effects [2]. Moreover, the wave speed is positively or negatively correlated with the local membrane curvature depending on the spontaneous curvature and bending rigidity. In addition, self-oscillation of the vesicle shape occurs, associated with the reaction-diffusion waves of curvature-inducing proteins as shown in Fig. 2. This agrees with the experimental observation of GUVs with a reconstituted Min system, which plays a key role in the cell division of *Escherichia coli*. Our results demonstrate the importance of mechanochemical feedback in pattern formation on deforming membranes.

References

- [1] N. Tamemoto and H. Noguchi, *Sci. Rep.* **10**, 19582 (2020).
 [2] N. Tamemoto and H. Noguchi, *Soft Matter* **17**, 6589 (2021).

Authors

N. Tamemoto and H. Noguchi

Structures and Dynamics of Hydrogen Cluster Materials $\text{Li}_5\text{MoH}_{11}$ and $\text{Li}_6\text{NbH}_{11}$

Yamamuro Group

In the current research field of batteries, there are strong demands for high-performance hydrogen storage materials and ionic (H^+ , Li^+ , etc.) conductors. Recently, a series of novel materials $\text{Li}_5\text{MoH}_{11}$, $\text{Li}_5\text{WH}_{11}$, $\text{Li}_6\text{NbH}_{11}$, $\text{Li}_6\text{TaH}_{11}$ which contain unusual ninefold hydrogen-coordinated clusters MH_9 ($\text{M} = \text{Mo}, \text{W}, \text{Nb}, \text{Ta}$), whose structure is shown in the inset of Fig. 1, were synthesized by Orimo group in Tohoku University [1]. These are of interest since they have high hydrogen density and possible high Li ionic conductivity. The dynamics of MH_9 cluster may play important roles in determining the physical properties of the materials. We have performed the neutron powder diffraction (NPD) and quasielastic neutron scattering (QENS) experiments of $\text{Li}_5\text{MoH}_{11}$ and $\text{Li}_6\text{NbH}_{11}$.

Both samples were synthesized from solid-state reactions under high pressure (ca. 5 GPa) and high temperature (ca. 700 K). Owing to these difficulties, the sample amounts of $\text{Li}_5\text{MoH}_{11}$ and $\text{Li}_6\text{NbH}_{11}$ were 33 mg and 20 mg, respectively. The NPD and QENS measurements were conducted using high intensity total diffractometer NOVA (BL21) and biomolecular dynamic spectrometer DNA (BL02) in MLF, J-PARC, respectively. The DNA data were collected with both high and low energy resolution modes.

From the Rietveld analyses for the NPD data at room temperature, we have checked the purity of the samples ($\text{Li}_5\text{MoH}_{11}$: 75 %, $\text{Li}_6\text{NbH}_{11}$: 57 %) and confirmed that the MH_9 clusters are orientationally disordered. Figure 1 shows the intermediate scattering functions of $\text{Li}_5\text{MoH}_{11}$. Similar data were obtained also in $\text{Li}_6\text{NbH}_{11}$. Relaxation phenomena were observed in a wide temperatures range between 150 K and 300 K. It is quite unusual that the relaxation occurs in a wide time range over 3 orders of magnitude as shown in the data at 300 K. Therefore, the data were fitted with not an exponential but Kohlraush-Williams-Watts (KWW) function

$$I(Q, t) = a(Q) + b(Q) \exp[-(t/\tau_{\text{KWW}})^\beta],$$

where Q is magnitude of a scattering vector, t is a time, τ_{KWW} is a relaxation time, β is a non-exponential parameter, and $a(Q)$ and $b(Q)$ are elastic and relaxation components, respectively. The β parameter ($0 < \beta < 1$) reflects the width

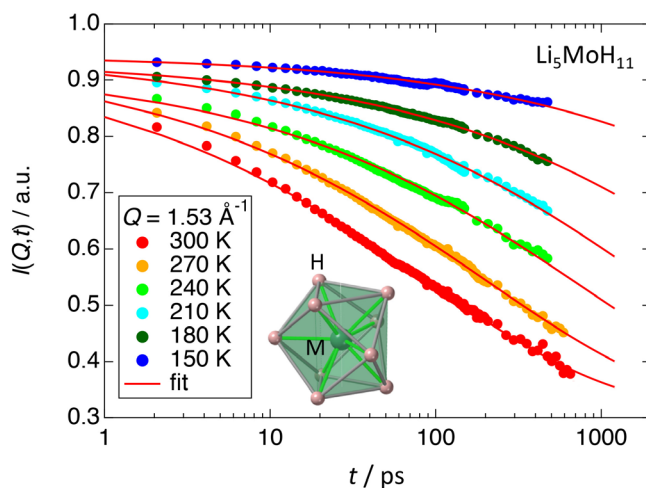


Fig. 1. Intermediate scattering functions ($Q = 1.53 \text{ \AA}^{-1}$) of $\text{Li}_5\text{MoH}_{11}$ measured at several temperatures between 150 K and 300 K. The solid curves are fitting curves to the KWW functions with $\beta = 0.38$. The inset shows the structure of the MH_9 cluster.

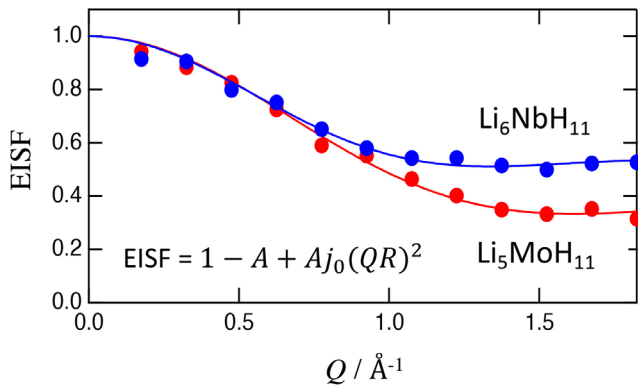


Fig. 2. Elastic Incoherent Structure Factor (EISF) obtained at 300 K for $\text{Li}_5\text{MoH}_{11}$ and $\text{Li}_6\text{NbH}_{11}$. The solid curves are the fitting curves to the equation in the figure.

of the relaxation time distribution; no distribution at $\beta = 1$. The fittings were satisfactory as shown by solid curves in Fig. 1. The determined β were 0.38 for $\text{Li}_5\text{MoH}_{11}$ and 0.33 for $\text{Li}_6\text{NbH}_{11}$, indicating that the distribution of the relaxation time is very wide; cf. β is around 0.5 for glass forming liquids. The activation energies obtained from the temperature dependence of the relaxation times were 15 kJmol^{-1} for $\text{Li}_5\text{MoH}_{11}$ and 27 kJmol^{-1} for $\text{Li}_6\text{NbH}_{11}$. The magnitude of the activation energy may depend on the ionic valence and size (M-H distance) of the hydrogen cluster (MoH_9^{3-} : 1.76 \AA , NbH_9^{4-} : 1.86 \AA).

Figure 2 shows the Q dependence of EISF (Elastic Incoherent Scattering Factor) which is defined by $\text{EISF} = a(Q)/[a(Q) + b(Q)]$. As shown by the solid curves in Fig. 2, EISF was well fitted by

$$\text{EISF} = 1 - A + Aj_0^2(QR),$$

where $j_0(QR)$ is a 0th order sphere Bessel function with a radius R . This indicates that MH_9 clusters are spherically rotating at 300 K, which is consistent with the structural information. The rotational states of the MH_9 clusters are now investigated with a first-principle MD simulation technique. We guess that the wide distribution of the relaxation time is associated with the positional disorder of Li ions conducting in the crystals.

This work is financially supported by JSPS KAKENHI No. JP 18H05513 and JP18H05518.

Reference

[1] S. Takagi, Y. Iijima, T. Sato, H. Saitoh, K. Ikeda, T. Otomo, K. Miwa, T. Ikeshoji, and S. Orimo, *Sci. Rep.* **7**, 44253 (2017).

Authors

Y. Ohmasa, H. Akiba, S. Takagi^a, S. Orimo^a, H. Saito^b, T. Yamada^c, Y. Kawakita^d, K. Ikeda^e, T. Otomo^c and O. Yamamuro

^aTohoku University

^bQST

^cCROSS

^dJAEA

^eKEK

Magnetic Order in the Chemically Substituted Frustrated Antiferromagnet CsCrF_4

Masuda Group

In geometrically frustrated magnets, macroscopically degenerated ground-states in low-energy regime can be solved by small perturbations. This tells us that magnetic states at low temperatures highlights small effects such as

magnetic anisotropy, exchange randomness, and site dilution. These thus play key roles in determining ground states in frustrated magnets. The equilateral triangular spin tube antiferromagnet CsCrF_4 [1,2] is a candidate for realizing a ground state sensitive to small perturbations. Magnetic Cr^{3+} ions having $S = 3/2$ form triangular spin tubes along the crystallographic c axis, as illustrated in Fig. 1. The tubes couple magnetically with one another and form the kagome-triangular lattice in the ab plane [3]. Neutron powder diffraction study conducted by our group identified long-range magnetic order below 2.8 K [4]. The magnetic moments form a quasi- 120° structure in the ab plane. It is unique that the 120° structure propagates antiferromagnetically along the a and c axes with a magnetic propagation vector $\mathbf{k}_{\text{mag}} = (1/2, 0, 1/2)$. Discussion of ground states in the kagome-triangular lattice model suggested that the ground state of CsCrF_4 is close to the boundary on the magnetic phase diagram in the kagome-triangular lattice model [4]. This proposes that small perturbations may induce various types of magnetic states in CsCrF_4 .

To introduce small perturbations into CsCrF_4 , we investigate chemical substitution effect. A magnetic Fe-substituted $\text{CsCr}_{1-x}\text{Fe}_x\text{F}_4$ showed long-range magnetic order and enhancement of magnetic anisotropy [5]. In a nonmagnetic Al-substituted $\text{CsCr}_{1-x}\text{Al}_x\text{F}_4$, a weak feature of magnetic ordering was observed [5]. Hereby, we report chemical substitution effects on the magnetic ground state in CsCrF_4 [6].

We carried out neutron powder diffraction experiments on $\text{CsCr}_{0.94}\text{Fe}_{0.06}\text{F}_4$ and $\text{CsCr}_{0.98}\text{Al}_{0.02}\text{F}_4$. In both compounds, magnetic Bragg peaks indicative of the long-range magnetic order are clearly observed, as shown in Fig. 2. Most strikingly, the magnetic peaks in $\text{CsCr}_{0.94}\text{Fe}_{0.06}\text{F}_4$ are indexed by a propagation vector $\mathbf{k}_{\text{mag}} = (0, 0, 1/2)$, which is different symmetry from $\mathbf{k}_{\text{mag}} = (1/2, 0, 1/2)$ in the parent CsCrF_4 . Magnetic structure analysis identifies that the 120° structure does not alternate in the ab plane, whereas the intratube structure is the same as in CsCrF_4 . Based on the Goodenough-Kanamori rule on superexchange interactions [7,8], it is predicted that ferromagnetic (antiferromagnetic) interactions between the Cr^{3+} ions via the F ions turn into antiferromagnetic (ferromagnetic) interactions by the Fe^{3+} ion substitution, namely bond substitution. The identified magnetic structure, thus, means that the bond substitution by the magnetic Fe^{3+} ion modifies the intertube structure, but the intratube structure is intact.

On the contrary, in $\text{CsCr}_{0.98}\text{Al}_{0.02}\text{F}_4$ the observed magnetic peaks are indexed by the same propagation vector as in the parent CsCrF_4 . Analyzing the magnetic structure,

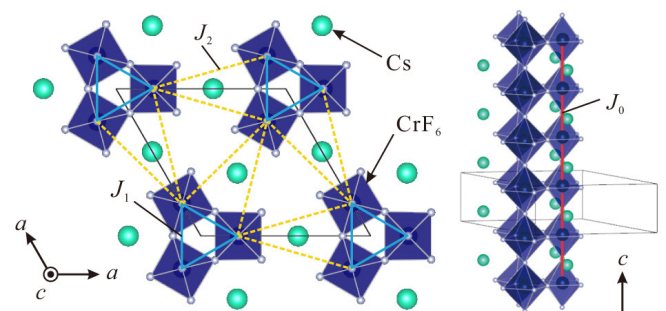


Fig. 1. Schematic view of the crystal structure of CsCrF_4 . Red lines indicate the nearest-neighbor interaction along the c axis. Blue and yellow lines indicate the nearest- and second-neighbor interactions in the ab plane.

Zero-Energy Excitation in the Classical Kagome Antiferromagnet $\text{NaBa}_2\text{Mn}_3\text{F}_{11}$

Masuda Group

Localization of spin-wave excitations, so-called *zero-energy mode*, is one of the unique phenomena in geometrically frustrated magnets [1]. Largely degenerate ground states allow a continuous rearrangement of spins with no energy cost, generating a dispersionless mode in a spin-wave excitation spectrum. The classical kagome antiferromagnet is a prototypical model for the dispersionless mode in the spin-wave excitations. It has an infinite degeneracy of 120° structures in the ground state. This degeneracy allows a continuous change of the spin arrangement with no energy cost, as illustrated in Fig. 1(a).

In real kagome antiferromagnets, the macroscopic degeneracy of the 120° structures is solved by some types of magnetic anisotropy such as the Dzyaloshinskii-Moriya interaction, single-ion anisotropy, and magnetic dipole-dipole interaction. Then, the zero-energy mode becomes visible as an excited state lifted by those anisotropies. Although the zero-energy mode is one of the most characteristic phenomena in frustrated kagome antiferromagnets, it has been reported only in $\text{KFe}_3(\text{OH})_6(\text{SO}_4)_2$ [2]. Therefore, further study in different materials is highly desirable.

Our target material, a classical kagome antiferromagnet $\text{NaBa}_2\text{Mn}_3\text{F}_{11}$ [3], is a promising candidate exhibiting the zero-energy mode. Mn^{2+} ions having spin $S = 5/2$ are responsible for magnetic properties. Neutron powder diffraction demonstrated that antiferromagnetic order below $T_N = 2$ K forms the 120° structure selected by the magnetic dipolar interaction [4], as shown in Fig. 1(a). According to theoretical studies, the zero-energy mode in the classical kagome antiferromagnet with the magnetic dipolar interaction is predicted to emerge at its lowest excited state [5], as shown in Fig. 1(b). Hereby, we report the zero-energy mode excitation in $\text{NaBa}_2\text{Mn}_3\text{F}_{11}$ through a combination of inelastic neutron scattering technique and linear spin-wave calculations [6].

Figures 2(a)-2(d) show a temperature variation of the inelastic neutron scattering spectra for a powder sample of $\text{NaBa}_2\text{Mn}_3\text{F}_{11}$. Magnetic diffuse scattering indicative of short-range correlation is observed at 30 K in the paramagnetic phase [Fig. 2(d)]. The diffuse scattering is suppressed with decreasing temperature, and the spectrum splits into two parts: strong intensity at 0.2 meV and weak intensity at 1.5 meV [Figs. 2(a)-2(c)]. In the magnetic ordered state at 1.5 K, spin-wave excitations having a magnetic anisotropy

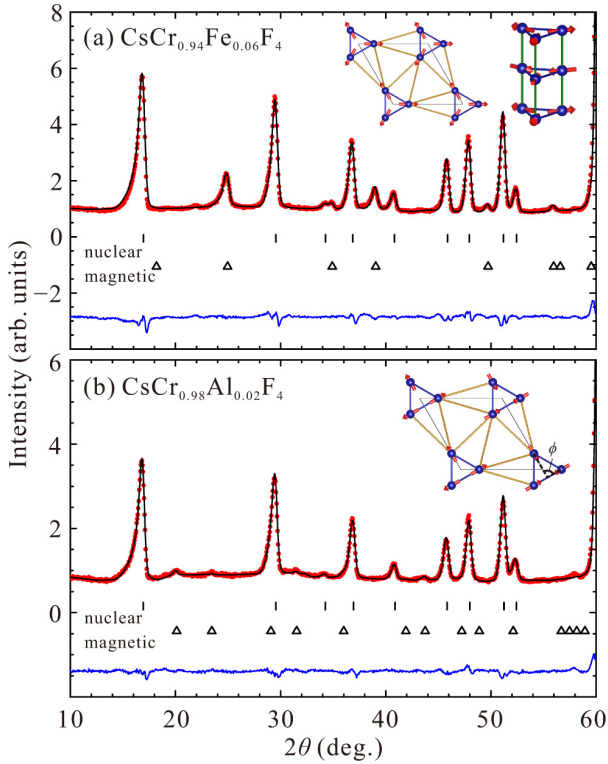


Fig. 2. Neutron diffraction profiles for (a) $\text{CsCr}_{0.94}\text{Fe}_{0.06}\text{F}_4$ and (b) $\text{CsCr}_{0.98}\text{Al}_{0.02}\text{F}_4$ at 1.5 K. Red circles and black curves show the experimental data and simulations, respectively. Vertical bars and triangles indicate the position of the nuclear and magnetic Bragg peaks. Blue curves show the difference between the data and simulations. Insets are the determined magnetic structures.

we find that the spin configuration in $\text{CsCr}_{0.98}\text{Al}_{0.02}$ is not changed drastically, even though a relative angle between three spins in the 120° structure deviates more from 120° than that in CsCrF_4 . Since substituting the Cr^{3+} ion with the Al^{3+} ion creates a spin vacancy, trigonal symmetry of the 120° structure is locally broken. However, the spin vacancy only produces a small effect on the ground state of CsCrF_4 , and therefore the quasi- 120° structure is still realized globally in $\text{CsCr}_{0.98}\text{Al}_{0.02}\text{F}_4$.

In conclusion, we have studied magnetic orders in magnetic Fe- and nonmagnetic Al-substituted CsCrF_4 through the neutron powder diffraction experiment. The magnetic structure analysis reveals that the Fe-substituted sample exhibits a 120° structure having $\mathbf{k}_{\text{mag}} = (0, 0, 1/2)$, and the Al-substituted one has a quasi- 120° structure having $\mathbf{k}_{\text{mag}} = (1/2, 0, 1/2)$. Importantly, the magnetic structure in $\text{CsCr}_{0.94}\text{Fe}_{0.06}\text{F}_4$ differs from that in the parent CsCrF_4 . This result concludes that the ground state in CsCrF_4 is more sensitive to magnetic substitution rather than nonmagnetic one on the Cr site.

References

- [1] H. Manaka *et al.*, J. Phys. Soc. Jpn. **78**, 093701 (2009).
- [2] H. Manaka *et al.*, J. Phys. Soc. Jpn. **80**, 084714 (2011).
- [3] K. Seki and K. Okunishi, Phys. Rev. B **91**, 224403 (2015).
- [4] M. Hagihala *et al.*, npj Quantum Mater. **4**, 13 (2019).
- [5] H. Manaka *et al.*, J. Phys. Soc. Jpn. **88**, 114703 (2019).
- [6] S. Hayashida, M. Hagihala, M. Avdeev, Y. Miura, H. Manaka, and T. Masuda, Phys. Rev. B **102**, 174440 (2020).
- [7] J. B. Goodenough, Phys. Rev. **100**, 564 (1955).
- [8] J. Kanamori, J. Phys. Chem. Solids **10**, 87 (1959).

Authors

S. Hayashida, M. Hagihala^a, M. Avdeev^b, Y. Miura^c, H. Manaka^d, and T. Masuda

^aHigh Energy Accelerator Research Organization (KEK)

^bAustralian Nuclear Science and Technology Organisation (ANSTO)

^cSuzuka National College of Technology

^dKagoshima University

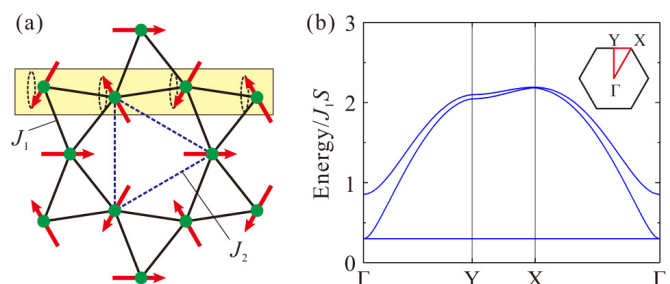


Fig. 1. (a) Magnetic structure having $\mathbf{k} = \mathbf{0}$ of $\text{NaBa}_2\text{Mn}_3\text{F}_{11}$. The red arrows represent directions of spins. Dashed loops illustrate the zero-energy mode as described in the text. Solid and dashed lines are the nearest-neighbor and second-neighbor paths, respectively. (b) Spin-wave excitation having the nearest-neighbor exchange interaction J_1 and magnetic dipole-dipole interaction $J_{\text{MDD}} = J_1/100$. The energy is normalized by the magnitude of J_1 and spin S .

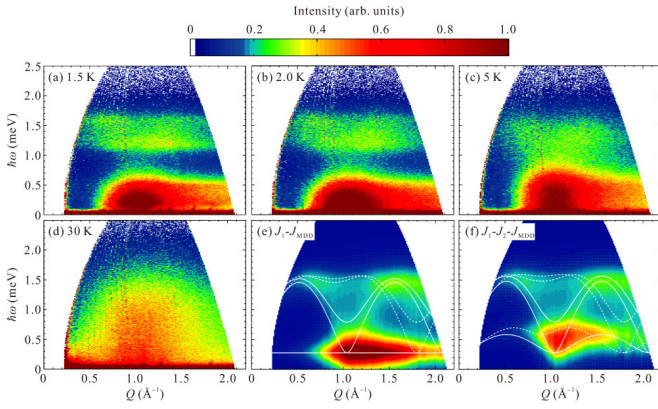


Fig. 2. Inelastic neutron scattering spectra of $\text{NaBa}_2\text{Mn}_3\text{F}_{11}$ at (a) 1.5 K, (b) 2.0 K, (c) 5 K and (d) 30 K. The incident neutron energy is $E_i = 3.1$ meV. Calculated spin-wave spectra with (e) $J_1 = 0.28$ meV, $J_2 = 0$, and $J_{\text{MDD}} = 4.9$ μeV and with (f) $J_1 = 0.27$ meV, $J_2 = J_1/10$, and $J_{\text{MDD}} = 4.9$ μeV . Solid and dashed curves in (e) and (f) are spin-wave dispersions along $[1\ 0\ 0]$ and $[1\ 1\ 0]$ directions, respectively.

gap of 0.21 meV is observed, as shown in Fig. 2(a). Notably, the excitation at 0.21 meV does not shift on varying wave number Q . This suggests that the excitation is a dispersionless zero-energy mode lifted by the magnetic dipolar interaction.

To identify if the observed dispersionless mode indeed originate from the magnetic dipolar interaction, we simulated the spin-wave excitation spectra in the linear spin-wave theory with considering the nearest-neighbor exchange interaction J_1 , the second neighbor exchange interaction J_2 , and the nearest-neighbor magnetic dipolar interactions J_{MDD} . Figures 2(e) and 2(f) show powder-averaged spin-wave spectra in J_1 - J_{MDD} and J_1 - J_2 - J_{MDD} models, respectively. The calculated spectra semi-qualitatively reproduce the low-energy strong excitation and high-energy weak excitation. Importantly, the calculated spectrum shows that the second-neighbor interaction J_2 makes the zero-energy excitation dispersive (Fig. 2(f)), because further neighboring interactions suppress the continuous rearrangement of the spins with no energy cost. This means that the observed dispersionless excitation at 0.2 meV indicates that J_2 is negligible in $\text{NaBa}_2\text{Mn}_3\text{F}_{11}$.

The most remarkable finding is that the energy position of the dispersionless mode is reproduced solely by the magnetic dipolar interaction. We note that the magnetic dipolar interaction is ubiquitous in every real magnet even though the qualitative behavior of most kagome antiferromagnet can be explained by models including only the nearest-neighbor interaction. Therefore, we come to the conclusion that the observed dispersionless excitation in $\text{NaBa}_2\text{Mn}_3\text{F}_{11}$ is the ideal zero-energy mode in the realistic classical kagome antiferromagnet.

In summary, we discovered a dispersionless zero energy mode in the classical kagome antiferromagnet $\text{NaBa}_2\text{Mn}_3\text{F}_{11}$ by the inelastic neutron scattering technique. The calculations based on the linear spin-wave theory reveal that the excitation is described by the zero-energy mode lifted solely by the magnetic dipole-dipole interactions. $\text{NaBa}_2\text{Mn}_3\text{F}_{11}$ is a unique classical kagome antiferromagnet exhibiting a truly dispersionless lifted zero-energy excitation.

References

- [1] A. B. Harris, C. Kallin, and A. J. Berlinsky, Phys. Rev. B **45**, 2899 (1992).
- [2] K. Matan *et al.*, Phys. Rev. Lett. **96**, 247201 (2006).
- [3] H. Ishikawa *et al.*, J. Phys. Soc. Jpn. **83**, 043703 (2014).
- [4] S. Hayashida *et al.*, Phys. Rev. B **97**, 054411 (2018).

[5] M. Maksymenko, R. Moessner, and K. Shtengel, Phys. Rev. B **96**, 134411 (2017).

[6] S. Hayashida, H. Ishikawa, Y. Okamoto, T. Okubo, Z. Hiroi, G. J. Nilsen, H. Mutka, and T. Masuda, Phys. Rev. B **101**, 214409 (2020).

Authors

S. Hayashida, H. Ishikawa, Y. Okamoto^a, T. Okubo^b, Z. Hiroi, G. J. Nilsen^c, H. Mutka^d, and T. Masuda

^aNagoya University

^bThe University of Tokyo

^cISIS Neutron and Muon Source

^dInstitute Laue Langevin

Spin Density Wave Induced by Bound Two-Magnon in $S = 1/2$ Frustrated Chain Compound $\text{NaCuMoO}_4(\text{OH})$

Masuda Group

Frustrated magnetism has attracted great attention because of nontrivial phases induced by the lift of macroscopic degeneracy. One of the interesting examples is found in $S = 1/2$ one-dimensional spin system with nearest-neighbor ferromagnetic and next-nearest-neighbor antiferromagnetic interactions [1]. A theory predicts that a bound two-magnon in high magnetic field induces exotic phases characterized by the spin-density-wave (SDW) and spin multipole correlations in the frustrated ferromagnetic chain [2]. So far, these states have not been fully investigated by spectroscopic method because of high saturation field and/or difficulty of obtaining a large single crystal for existing model compounds. $\text{NaCuMoO}_4(\text{OH})$ is an experimental realization of the system having decent energy scale, saturation field of 26 T [3] which is available on the pulse magnet for neutron scattering [4]. The synthesis of a single crystal

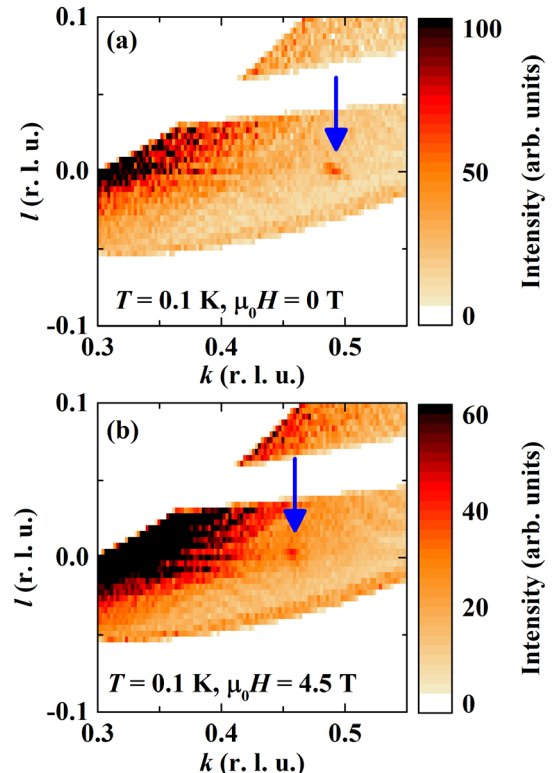


Fig. 1. Contour maps of neutron intensities in the $(0kl)$ plane around the reciprocal lattice point $(0, \delta, 0)$ at 0.1 K under the magnetic field of (a) 0 and (b) 4.5 T.

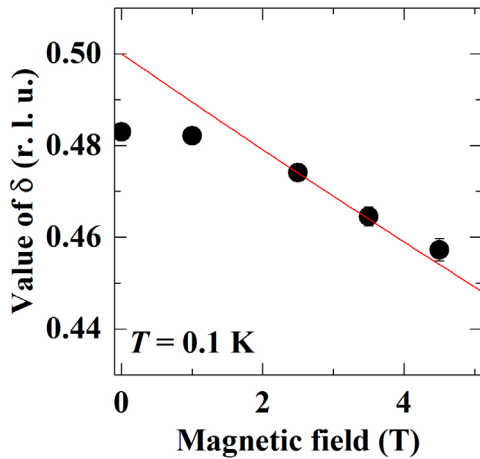


Fig. 2. Value of δ as a function of field

was reported [5]. The NMR and heat capacity study suggest a magnetic transition at H_c of 1.5 - 1.8 T [3]. For the full identification of the magnetic states in zero and finite fields neutron diffraction technique is indispensable. We hereby report the magnetic structure analysis by using the time-of-flight neutron diffractometer SENJU installed at J-PARC [6] on a single crystal NaCuMoO₄(OH).

Figure 1(a) and 1(b) shows the contour maps of neutron intensities in the $(0k)$ plane around the reciprocal lattice point $(0, \delta, 0)$ at 0.1 K under the magnetic field of (a) 0 and (b) 4.5 T. We found that the peak indicated by the blue arrow in Fig. 1(a) appear at $(0, \delta, 0)$ ($\delta \sim 0.48$) below the transition temperature of 0.6 K. It means that the peak comes from the magnetic origin. We further found peaks at $(1\delta 1)$ and $(0\delta 2)$. Magnetic structure analysis reveals that the proper-screw structure with the ferromagnetic interchain coupling with the propagation vector of $(0, \delta, 0)$ is realized at zero field. Furthermore, we found that the magnetic peak at $(0\delta 0)$ was shifted to smaller k direction by applying a magnetic field as shown in Fig. 1(b). This behavior suggests that the field induces SDW state, in which the density correlation of bound magnon is developed and its incommensurability is represented in terms of magnetization. In Fig. 2 the value of δ is independent of the field below H_c , and it decreases with increasing the field above H_c . The negative slope of the line above H_c indicated by red line is consistent with the theoretical prediction for the SDW₂ state [7]. The result demonstrates that the bound two-magnon leads to the SDW state in high magnetic field in the compound.

References

- [1] S. Furukawa, M. Sato, and S. Onoda, Phys. Rev. Lett. **105**, 257205 (2010).
- [2] T. Hikihara, L. Kecke, T. Momoi, and A. Furusaki, Phys. Rev. B **78**, 144404 (2008).
- [3] K. Nawa, Y. Okamoto, A. Matsuo, K. Kindo, Y. Kitahara, S. Yoshida, S. Ikeda, S. Hara, T. Sakurai, S. Okubo, H. Ohta, and Z. Hiroi, J. Phys. Soc. Jpn. **83**, 103702 (2014).
- [4] H. Nojiri, S. Yoshii, M. Yasui, K. Okada, M. Matsuda, J. -S. Jung, T. Kimura, L. Santodonato, G. E. Granroth, K. A. Ross, J. P. Carlo, and B. D. Gaulin, Phys. Rev. Lett. **106**, 237202 (2011).
- [5] K. Nawa, Y. Okamoto, and Z. Hiroi, J. Phys.: Conf. Ser. **828**, 012005 (2017).
- [6] T. Ohhara, R. Kiyonagi, K. Oikawa, K. Kaneko, T. Kawasaki, I. Tamura, A. Nakao, T. Hanashima, K. Munakata, T. Moyoshi, T. Kuroda, H. Kimura, T. Sakakura, C.-H. Lee, M. Takahashi, K.-i. Ohshima, T. Kiyotani, Y. Noda, and M. Arai, J. Appl. Cryst. **49**, 120 (2016).
- [7] M. Sato, T. Momoi, and A. Furusaki, Phys. Rev. B **79**, 060406(R) (2009).

Authors

S. Asai, T. Oyama, K. Nawa^a, A. Nakao^b, K. Munakata^b, K. Kuwahara^c, M. Hagihala^d, S. Itoh^d, Z. Hiroi, and T. Masuda

^aInstitute of Multidisciplinary Research for Advanced Materials, Tohoku University
^bResearch Center for Neutron Science and Technology, Comprehensive Research Organization for Science and Society
^cInstitute of Quantum Beam Science, Ibaraki University
^dHigh Energy Accelerator Research Organization

Neutron Resonance Spin Echo Measurements on the Magnetic Skyrmion Lattice State in MnSi

Nakajima Group

Magnetic skyrmions are vortex-like spin objects, which can be regarded as topological defects composed of magnetic moments in a magnetic material [1]. They were discovered in a small phase pocket in the vicinity of the critical temperature in chiral cubic magnets; previous small-angle neutron scattering (SANS) [2] and Lorentz transmission electron microscopy [3] measurements have revealed that the magnetic vortices are arranged to form a triangular lattice on a plane perpendicular to an applied magnetic field. It is also reported that the magnetic skyrmions can be driven by flowing an electric current [4]. These observations show that magnetic skyrmions behave like particles once they are formed, while it remains unclear how the particle character emerges upon the phase transition from the paramagnetic (PM) phase to the skyrmion lattice (SkL) phase.

In the present study, we investigate the PM-to-SkL transition in an archetypal skyrmion compound MnSi by means of neutron spin echo (NSE) spectroscopy [5], which is suited for probing diffusive dynamics with the time scales of the order of pico- to submicroseconds. Actually, spin fluctuations in MnSi were studied by means of polarimetric and ferromagnetic NSE measurements [6], in which the Larmor precession of polarized neutron spin is utilized for detecting very small changes in neutron velocity upon quasi-elastic scattering processes. However, neither the polarimetric nor ferromagnetic NSE is suited for the SkL phase. The former is limited to zero-field measurements. Although the latter is applicable for in-field measurements, the non-collinear

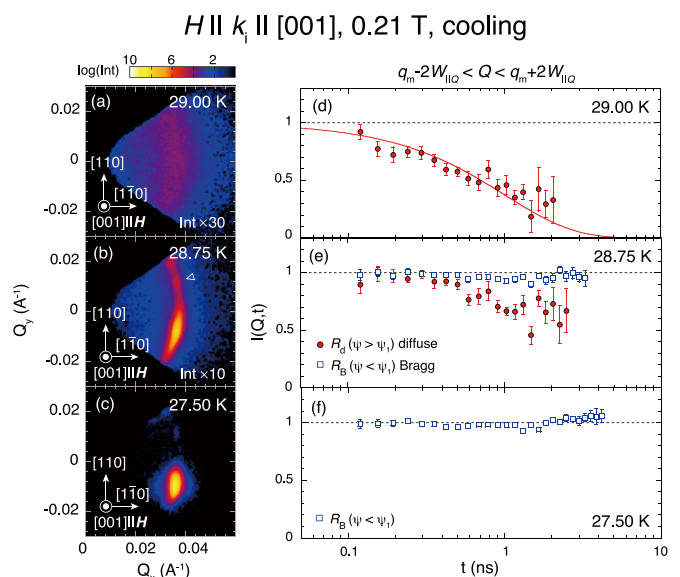


Fig. 1. [(a)-(c)] Intensities of scattered neutrons projected on the Q_x - Q_y plane measured at (a) 29.00, (b) 28.75, and (c) 27.50 K. on cooling. [(d)-(f)] $I(Q,t)$ profiles at each temperature.

Dynamics Fracture Behaviors of Slide-Ring Gels

Mayumi Group

Tough hydrogels have been attracting a lot of interest because of their potential application for biomaterials. To improve the mechanical strength of hydrogels, various chemical design of polymer networks have been proposed in the last two decades. One of the promising strategies to toughen gels is to introduce weak “sacrificial” crosslinks into polymer networks [1]. The sacrificial bonds in tough polymer gels are broken under deformation, and a part of input mechanical energy is dissipated, which leads to the large fracture energy of the dissipative gels. A problem of the dissipative tough polymer gels is their low mechanical recoverability. When reversible bonds (e.g. hydrogen bonds, ionic bonds, etc.) are utilized as sacrificial bonds, the broken sacrificial bonds can be recovered, but it takes a relatively long time (at least minutes) for complete recovery. For the applications as implant biomaterials such as artificial ligaments and prosthetic joints, the mechanical instant recoverability is needed because they should show constant mechanical responses under repeated deformations at a high frequency (e.g. 1 Hz).

Another tough polymer gel is slide-ring (SR) gel, in which polymer chains are cross-linked by ring molecules (Fig.1) [2]. The sliding of the movable cross-links composed of rings homogenizes network structure and reduces stress concentration in polymer networks, which results in high deformability and softness of SR gels. We have been investigating toughening mechanism of SR gels composed of polyethylene glycol (PEG) and cyclodextrin (CD). For conventional polymer gels cross-linked by fixed covalent bonds, the fracture energy is dominated by the strand length between cross-links. In the case of SR gels, the sliding of the cross-links enlarges the strand length and enhances the fracture toughness [3].

A unique feature of SR gels is their high mechanical recoverability. SR gels show no mechanical hysteresis under repeated stretching. This suggests that the sliding movement of the cross-links is faster than breaking/reforming dynamics of the reversible sacrificial cross-links. We systematically investigated the crack propagation behavior of SR gels at

spin arrangement of the SkL leads to mixing of spin-flip and non-spin-flip scatterings, which depolarizes the neutron spins. We thus employ neutron resonance spin echo technique, specifically the modulation-of-intensity-with-zero-effort (MIEZE) method, in which the intermediate spin correlation function $I(Q,t) = S(Q,t)/S(Q,0)$, where $S(Q,t)$ is the temporally Fourier transformed dynamical structure factor, is obtained not from the final neutron spin polarization after experienced the precessions mentioned above, but from beating patterns appearing in intensities of scattered neutrons as a function of time. Since the MIEZE signals are independent of the spin state of scattered neutrons, this technique is suited for measuring magnetic scattering in a magnetic field [7].

In Figs. 1(a)-1(c), we show typical SANS patterns measured in a magnetic field of 0.21 T at the VIN ROSE instrument in the materials and life science experiment facility in J-PARC. We observed a ring-like diffuse scattering pattern at 29 K, which is slightly above the critical temperature of 28.8 K (Fig. 1(a)). This indicates that a short-range isotropic spin correlation is developing in the sample. As the temperature is lowered, a Bragg peak emerges and coexists with the ring-like diffuse scattering (Fig. 1(b)). Finally, the diffuse scattering completely disappears and only the Bragg peak remains at 27.5 K (Fig. 1(c)). We obtained $I(Q,t)$ profiles of the diffuse and Bragg scattering components as shown in Figs. 1(d)-1(f). The $I(Q,t)$ profile at 29 K shows a decay, which is well described by a single-exponential decay function, revealing that the magnetic moments involved in the diffuse scattering are fluctuating with a characteristic time of 1 ns. By contrast, no temporal decay of the spin correlation is found at 27.5 K (Fig. 1(f)). At the intermediate temperature where the Bragg and diffuse scattering coexist, the $I(Q,t)$ profile for the diffuse component still shows a decay, while that for the Bragg peak is approaching unity. This demonstrates that the isotropic spin fluctuations with short-range spin correlations coexists with static SkL domains near the boundary between the PM and SkL phases. We also analyzed the $I(Q,t)$ values as a function of azimuthal angle, and concluded that an aggregation of the magnetic skyrmions upon cooling leads to orientational disorder of the small SkL domains. This picture is consistent with the particle-like character of the magnetic skyrmions. The present results also show that the MIEZE-type NSE at VIN ROSE is a powerful tool to study spin dynamics of magnetic skyrmion systems, for which measuring spin dynamics in low- Q regions in a magnetic field is essential.

References

- [1] N. Nagaosa and Y. Tokura, Nat. Nanotechnol. **8**, 899 (2013).
- [2] S. Muhlbauer *et al.*, Science **323**, 915 (2009).
- [3] X. Z. Yu *et al.*, Nature **465**, 901 (2010).
- [4] X. Z. Yu *et al.*, Nat. Mater. **10**, 106 (2011).
- [5] T. Nakajima *et al.*, Phys. Rev. Research **2**, 043393 (2020).
- [6] C. Pappas *et al.*, Phys. Rev. Lett. **102**, 197202 (2009).
- [7] J. Kindervater *et al.*, Phys. Rev. X **9**, 041059 (2019).

Authors

T. Nakajima, T. Oda^a, M. Hino^a, H. Endo^b, K. Ohishi^c, K. Kakurai^{c,d}, A. Kikkawa^d, Y. Taguchi^d, Y. Tokura^{d,e}, and T. Arima^{d,e}
^aKyoto University.
^bIMSS, High Energy Accelerator Research Organization.
^cComprehensive Research Organization for Science and Society (CROSS).
^dRIKEN Center for Emergent Matter Science (CEMS)
^eThe University of Tokyo.

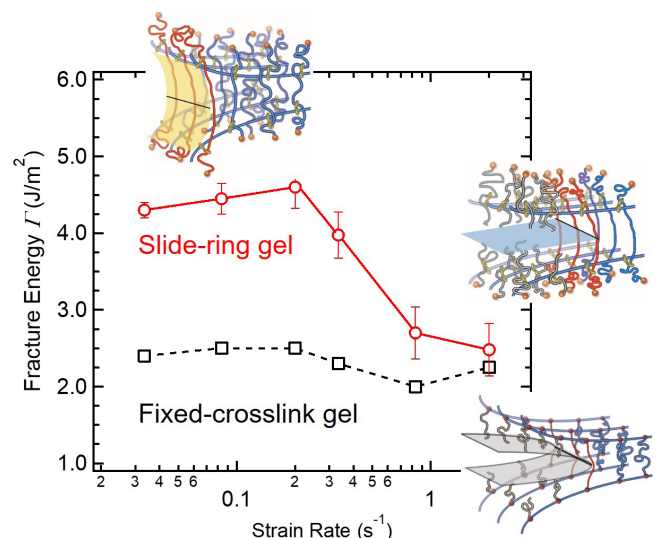


Fig. 1. Strain rate dependence of fracture energy of slide-ring and fixed cross-link gels.

various strain rates to evaluate the sliding dynamics of the movable cross-links [4]. At a certain strain rate and crack propagation velocity, a drastic decrease of the fracture energy was observed (Fig.1). For lower strain rates and crack propagation velocities, the slide-ring cross-links have enough time to slide along the polymer axes, which leads to the enhanced fracture energy. At fast fracture, however, the sliding of cross-links cannot catch up with the network deformation, and the fracture energy decreases to the same level as that of a fixed cross-link gel. From the critical crack propagation velocity at the transition point, we estimated the time scale of the sliding dynamics to be micro-seconds. This result is consistent with the diffusion coefficient of the sliding dynamics for CDs on PEG axis evaluated by a full atomistic molecular dynamics simulation [5]. The fast sliding motion of the cross-links is the origin of the high mechanical recoverability of SR gels under repeated deformations. SR gels exhibits high toughness and mechanical recoverability, which are needed for implant biomaterials and elastomer actuators for soft robots.

References

- [1] J. Y. Sun, X. Zhao, W. K. Illeperuma, O. Chaudhuri, K. H. Oh, D. J. Mooney, J. J. Vlassak, and Z. Suo, *Nature* **489**, 133 (2012).
- [2] K. Ito, *Polym. J.* **39**, 489 (2007).
- [3] C. Liu, H. Kadono, K. Mayumi, K. Kato, H. Yokoyama, and K. Ito, *ACS Macro Lett.* **6**, 1409 (2017).
- [4] C. Liu, H. Yokoyama, K. Mayumi, and K. Ito, *Mech. Mater.* **156**, 103784 (2021).
- [5] Y. Yasuda, Y. Hidaka, K. Mayumi, T. Yamada, K. Fujimoto, S. Okazaki, H. Yokoyama, and K. Ito, *J. Am. Chem. Soc.* **141**, 9655 (2019).

Authors

K. Mayumi, C. Liu, K. Ito^a

^aThe University of Tokyo

Charge-Fluctuation-Mediated Superconductivity in Organic Complexes

Kindo, Kohama, and Tokunaga Groups

Electron pairing in unconventional superconductors is driven by quantum fluctuations of electronic degrees of freedom. For various unconventional superconductors, such as high- T_c cuprates and heavy-fermion systems, their magnetic degrees of freedom often play an essential role in the pairing mechanisms. Although charge degrees of freedom can also mediate the Cooper-pair formation as exotic pairings, experimental investigation of the charge-fluctuation-mediated superconductivity has been insufficient for detailed discussion because only a few materials show superconductivity with pure charge instability.

The β'' -type organic charge-transfer complexes are known as the candidates showing superconductivity mediated by charge fluctuations. As shown in Fig. 1, the organic molecules in the β'' -type structure are uniformly arranged. Since the valence of each molecule is +0.5, the energy band of the electronic system is 1/4-filled. In this case, it is known that charge density exhibits inhomogeneous distribution in neighboring sites to reduce the intersite Coulomb repulsion when electron correlations are strong. Therefore, it is expected that this charge instability can trigger a superconducting transition. In the present research, we investigated the low-temperature electronic states of some β'' -type materials, β'' -(BEDT-TTF)₄[(H₃O)M(C₂O₄)₃]G (M=metal ions, G=guest molecules), using various

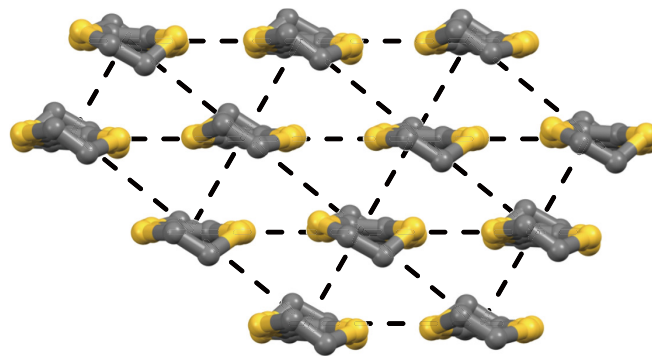


Fig. 1. Molecular arrangement of organic molecules in the conducting plane of the β'' -type organic materials. The dashed lines show predominant transfer integrals between the molecules, forming the distorted triangular lattice.

measurements and unveiled that the superconductivity in this compound is possibly mediated by charge fluctuations [1,2].

Figure 2 shows the high-magnetic-field quantum oscillations in magnetoresistance $\Delta R/R$ of β'' -(BEDT-TTF)₄[(H₃O)Ga(C₂O₄)₃]PhNO₂ at various temperatures. As shown by the dashed envelopes, the amplitude of the oscillations is modulated below 8 K. Detailed analyses with the Lifshitz-Kosevich formula indicate that a transition occurs at 8 K, leading to a split of the Fermi pocket and an enhancement of the effective mass. This transition is observed in ultrasonic properties whereas a low-temperature x-ray diffraction measurement detects no significant anomaly at the temperature. Also, this transition has no magnetic field dependence. As orbital degrees of freedom are quenched in the present material, these results mean that a local lattice modulation is induced by charge disproportionation. Just below this transition temperature, this compound shows a transition from the charge disproportionation to the superconducting state at $T_c \sim 7$ K. By replacement of the guest molecules, T_c is reduced with a decline of the charge disproportionation. This tendency implies that the charge fluctuations enhanced in this compound govern the pairing of the superconductivity.

Besides, we performed heat capacity measurements to determine the gap symmetry of the superconductivity. The temperature, magnetic field, and field-angle dependence of the heat capacity indicates that the gap function is aniso-

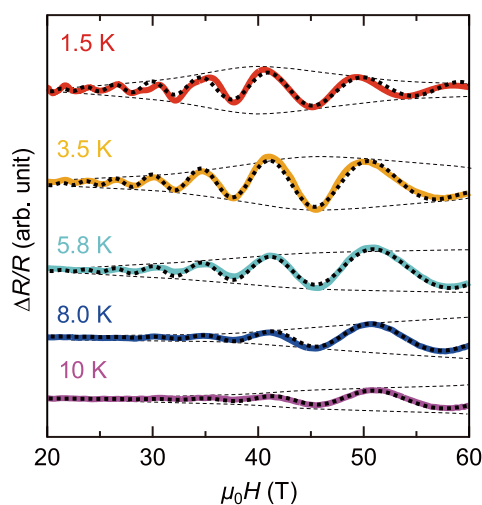


Fig. 2. High-magnetic-field Shubnikov-de Haas oscillations of β'' -(BEDT-TTF)₄[(H₃O)Ga(C₂O₄)₃]PhNO₂ shown as $\Delta R/R$. The dotted curves on the data are fits to a two-component Lifshitz-Kosevich formula. The dashed envelopes are guides for the eye to emphasize the amplitude change.

tropic and has no node on the Fermi surface, distinct from that of nodal *d*-wave symmetry arising from antiferromagnetic spin fluctuations observed in many unconventional superconductors. This full-gapped nature suggests that intersite repulsion, leading to the charge disproportionation, works as an attractive force for the on-site Cooper pairing.

These results indicate that the present superconductivity is formed by the charge fluctuations, and also, elucidate the detailed features of the charge-fluctuation-mediated superconductivity.

References

- [1] S. Imajo, H. Akutsu, A. Akutsu-Sato, A. L. Morritt, L. Martin, and Y. Nakazawa, *Phys. Rev. Res.* **1**, 033184 (2019).
 [2] S. Imajo, H. Akutsu, R. Kurihara, T. Yajima, Y. Kohama, M. Tokunaga, K. Kindo, and Y. Nakazawa, *Phys. Rev. Lett.* **125**, 177002 (2020).

Authors

S. Imajo, R. Kurihara, Y. Kohama, M. Tokunaga, and K. Kindo

Magnetic-Field-Induced Insulator-Metal Transition in a Strongly Correlated Insulator $V_{1-x}W_xO_2$ at 500 T

Y. H. Matsuda and Takeyama Groups

The magnetic ground state of most of strongly correlated insulators is antiferromagnetic ordered state. Roles of electron spins in realizing the insulating nature in correlated systems is well understood in the single-band Hubbard model; the magnetic energy determined by the exchange interaction J is much smaller than the Coulomb energy U , and thus the electrical insulating nature is essentially insensitive to the magnetic state. In some of actual materials, however, spin degree of freedom couples to crystal lattice through the orbital degree of freedom and results in nontrivial electronic states. Actually, in some of the strongly correlated insulators, the ground state exhibits spin-singlet state instead of the antiferromagnetic state. One of the most studied correlated insulators with the singlet ground state is VO_2 that undergoes a very sharp metal-insulator transition at 340 K. It has been debated for more than 60 years whether

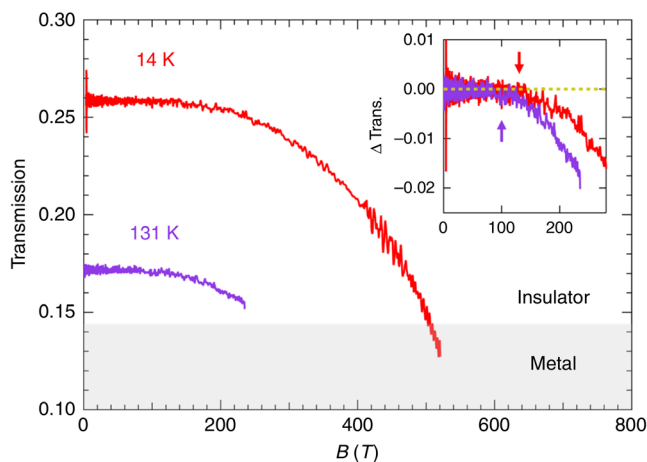


Fig. 1. Magnetic-field dependence of the optical transmission at 14 and 131 K. The transmission is plotted before the breaking point of the destructive measurement. The shaded area indicates transmission lower than that in the high-temperature metallic phase at 291 K. Inset: transmission change Δ Trans. as a function of the magnetic field. The dashed yellow line corresponds to Δ Trans.= 0. The red and purple arrow indicate the field positions (B^*) where Δ Trans. deviates from zero.

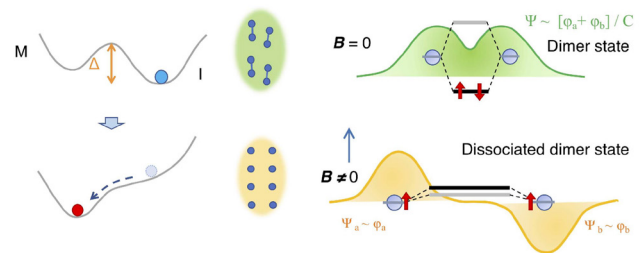


Fig. 2. Schematic of the magnetic-field-induced insulator-metal (IM) transition. The left side shows that the potential barrier Δ is lowered by the Zeeman energy. The middle part schematically shows the collapse of the V-V dimers. The right part shows that applying a magnetic field induces the dissociation of the dimer owing to the destabilization of formation of the bonding state Ψ of the molecular orbital, where ϕ_a and ϕ_b are the wave functions of the independent vanadium ions.

the electron correlation or the structural instability is more essential driving force behind the transition.

In the present work, we have demonstrated that a tungsten (W)-doped VO_2 undergoes insulator-metal (IM) transition by applying a ultrahigh magnetic field of 500 T. The field is produced by the electromagnetic flux compression 1000-T generator at the ISSP [1]. Figure 1 shows the magneto-transmission of a $V_{0.94}W_{0.06}O_2$ thin film at $1.977 \mu\text{m}$ [2]. A reduction of the transmission with magnetic field when the field is greater than 100 T is a direct evidence of the field induced metallization. One of the most probable explanation for the field-induced IM transition is that the singlet-dimer state is suppressed by such a ultrahigh magnetic field, and which results in breaking of structural V-V dimers as well. The molecular orbital occupied by two electrons with different spin directions is collapsed by forced alignment of the two spins by the strong magnetic field of 500 T. The discovered spin-controlled IM transition suggests that the principal driving force to the insulating state at a low temperature is structural instability (formation of dimers) rather than the electron correlation.

From another view point, the observed collapse of the V-V dimer is a similar phenomenon with the so-called the chemical catastrophe where a chemical bond is destroyed by the Zeeman effect of a super-strong magnetic field greater than 10^6 T in the cosmic space [3]. An energy to collapse the molecular orbital of the V-V dimer is scaled down by 3-4 orders of magnitude in a solid compared to a normal molecule, which enable us to observe the chemical catastrophe in a solid. Figure 2 is a schematic of the field-induced IM transition of W-doped VO_2 ; the V-V dimers are dissociated by forced alignment of spins in a 500-T-field [2].

References

- [1] D. Nakamura, Akihiko Ikeda, H. Sawabe, Y. H. Matsuda, and S. Takeyama, *Rev. Sci. Instrum.* **89**, 095106 (2018).
 [2] Y. H. Matsuda, D. Nakamura, A. Ikeda, S. Takeyama, Y. Suga, H. Nakahara, and Y. Muraoka, *Nat. Commun.* **11** 3591 (2020).
 [3] M. Date, *Australian Journal of Physics* **48**, 187 (1995).

Authors

Y. H. Matsuda, D. Nakamura, A. Ikeda, S. Takeyama, Y. Suga^a, H. Nakahara^a, and Y. Muraoka^a
^aOkayama University

Capacitive Detection of Physical Quantities in Pulsed Magnetic Fields

Tokunaga Group

Capacitance is known as a physical quantity that can be measured with high precision. We have developed a system to precisely measure various physical quantities that change in pulsed high magnetic fields using high-speed capacitance measurements [1].

First, we measured magnetostriction. We attach a pair of electrode plates on top of a sample and on the probe with keeping a small gap between them. We can detect small change in the sample length through the change in the capacitance of this setup. Using this method, we observed magnetostriction in a Heusler alloy caused by a significant magneto-volume effect [2]. The entropy change associated with this magneto-volume effect is regarded as the origin of the giant inverse magneto-caloric effect observed in this class of materials [2,3]. Therefore, quantitative evaluation of the structural change can be essential to understand the magnetocaloric effect. In non-magnetic metals, magnetostriction can be used to detect the field-induced changes in band filling. Utilizing this technique, we achieved thermodynamic evidence of complete valley polarization in elemental bismuth in the ultra-quantum limit state [4].

Capacitance measurements are also valuable for studying multiferroic materials in which magnetic order correlates with the dielectric property. If the change in magnetic symmetry makes the crystal polar, we can detect it through electric polarization measurements. On the other hand, the change is hardly discernible in the polarization if the spin order does not break global inversion symmetry, such as in the antiferroelectric state. Our capacitive measurement of dielectric constants enabled to detect this kind of change in symmetry at high magnetic fields. Figures 1 show the magnetization and dielectric constant of single crystals of

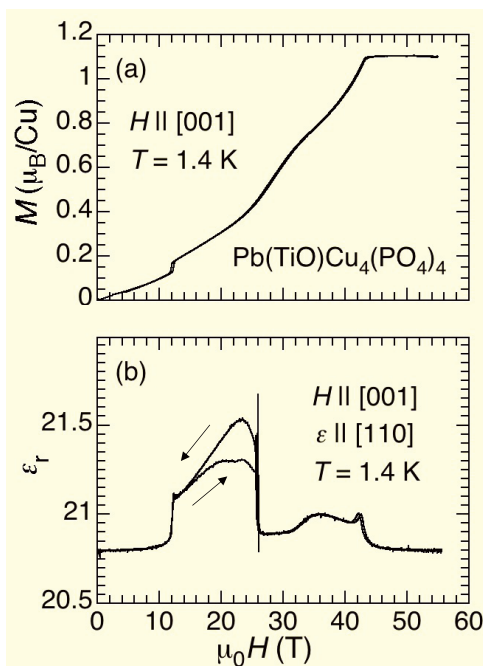


Fig. 1. Field dependence of (a) magnetization and (b) real part of the relative dielectric constant of $\text{Pb}(\text{TiO})\text{Cu}_4(\text{PO}_4)_4$. Successive transitions of cluster spin multipole order show up as multiple anomalies in both physical quantities. Broad hump structure in magnetization around 26 T becomes prominent in the dielectric constant measured using the capacitance method.

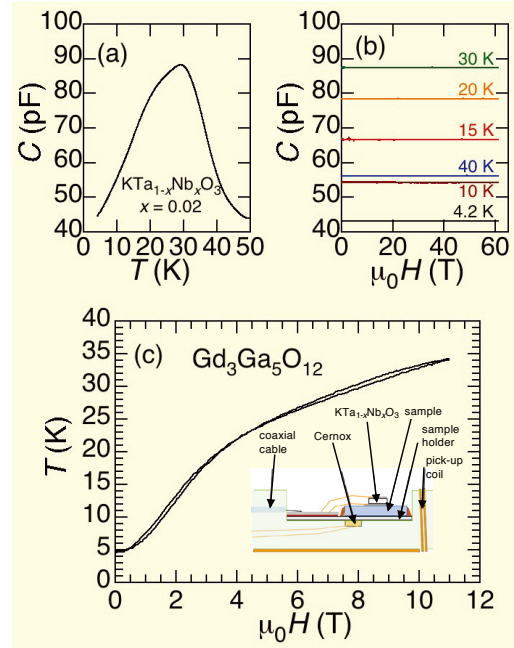


Fig. 2. (a) Temperature variation of the capacitance of $\text{KTa}_{1-x}\text{Nb}_x\text{O}_3$ at zero magnetic field. (b) Magnetic field dependence of the capacitance of $\text{KTa}_{1-x}\text{Nb}_x\text{O}_3$ at various temperatures. These two results indicate that this material can be used as a capacitance thermometer insensitive to a magnetic field. (c) Magnetocaloric effects in $\text{Gd}_3\text{Ga}_5\text{O}_{12}$ measured using this capacitance thermometer. The inset shows schematics of the experimental setup. Our fast capacitance measurements enable to evaluate the magnetocaloric effect in this material in a pulsed magnetic field.

$\text{Pb}(\text{TiO})\text{Cu}_4(\text{PO}_4)_4$. In contrast to the broad hump structure in the magnetization curve, dielectric constant shows a steep change around 26 T with field hysteresis, which unambiguously indicates the change in magnetic symmetry at this field. This technique provides us with a novel tool to identify the symmetry of magnetic phases emerging in high magnetic fields.

By measuring dielectric constants of some non-magnetic materials attached to a sample, we can evaluate the temperature change of a sample in magnetic fields: the so-called magneto-caloric effect. We show an example of the measurements of the magneto-caloric effect using $\text{KTa}_{1-x}\text{Nb}_x\text{O}_3$ ($x = 0.02$) as a capacitance thermometer, whose dielectric constant has a temperature dependence as shown in Fig. 2(a). We have previously developed a similar system to measure the magneto-caloric effect using a thin-film resistance thermometer [5]. Although this method works effectively, we have to calibrate the effect of magnetoresistance in the thermometer in advance at each temperature. On the other hand, in the present capacitance thermometer, the capacitance is almost insensitive to the applied magnetic field, as shown in Fig. 2(b). Using this thermometer, we can successfully measure the magneto-caloric effect of a magnetic refrigerant $\text{Gd}_3\text{Ga}_5\text{O}_{12}$ in a pulsed magnetic field (Fig. 2(c)). Due to the non-magnetic nature of this thermometer, we can also measure magnetocaloric effects simultaneously with magnetization. Such simultaneous measurements will enable us to precisely determine the field-temperature phase diagram of all the kind of magnetic materials and to discuss more precise thermodynamics.

High precision measurements of capacitance improve evaluation of the structure, symmetry, and entropy changes of the sample in pulsed magnetic fields. We expect that such a technological innovation will open up new horizons in science at high magnetic fields.

References

- [1] A. Miyake *et al.*, Rev. Sci. Instrum. **91**, 105103 (2020).
- [2] T. Kihara *et al.*, Phys. Rev. Mater. **5**, 034416 (2021).
- [3] T. Kihara *et al.*, Phys. Rev. B **90**, 214409 (2014).
- [4] A. Iwasa *et al.*, Sci. Rep. **9**, 1672 (2019).
- [5] T. Kihara *et al.*, Rev. Sci. Instrum. **84**, 074901 (2013).

Authors

A. Miyake^a, H. Mitamura, S. Kawachi, K. Kimura^a, T. Kimura^a, T. Kihara^b, M. Tachibana^c, and M. Tokunaga

^aThe University of Tokyo

^bIMR, Tohoku University

^cNational Institute for Material Science

Generation of Long Pulsed-Magnetic Fields by Using Electric-Double-Layer-Capacitors

Kohama Group

The generation of pulsed magnetic fields was first achieved by Pyotr L. Kapitsa approximately a century ago. After his pioneering work, various power supplies were tested for pulsed field generation. The most common power supply for generating a pulsed magnetic field is the high-voltage and high-speed capacitor bank. However, such a capacitor bank has small value of capacitance ($C = 1 - 100$ mF) and consequently restricts the available range of pulsed duration up to ~ 0.1 s. The short pulse duration makes it difficult to put pulsed magnets to widespread use. Developing an alternative power supply for generating pulsed high magnetic fields is a demanding task in high magnetic field science.

In this study, we have reported a power supply based on an electric-double-layer-capacitor (EDLC) which is composed of a series connection of 336 EDLC cells [1]. This system has a total capacitance of 10.7 F and can store the energy of 3.87 MJ with the charged voltage of 860 V. We find that the EDLC based power supply can generate high magnetic field up to 30 T with pulse duration of ~ 1 s. Because of the low-cost and compact design of developed EDLC based power supply, our system can be used in many research and industrial fields.

Figure 1a and b show the pulsed field profiles generated by our EDLC system. The arrows in Fig. 1 indicate the timing of the closing an energy bifurcation thyristor, which leads to an intentional reduction of the pulsed current. Due to the large capacitance of EDLC bank, we could observe the overdamped-like waveform for the setup A (Fig. 1a), which has long pulse duration of \sim a few seconds. The peak values of the fields (currents) are 16.2 T and 23.9 T (5.91 kA and 4.39 kA) for setup A and setup B (Fig.1b). The peaks of the fields shift to later times with decreasing charged voltage and indicate the strong influence of Joule heating on the pulsed field profile. Indeed, the calculated temperature of the pulsed magnet as shown in the right axes in Fig. 1(b) clearly shows the large Joule heating effect. In the paper, we have also reported how the pulsed field profile is influenced by the capacitance, internal resistance, coil resistance, charged voltage, coil inductance (not shown in this material) and found that a suitable choice of the coil design could increase accessible field strength up to 30 T and enhance pulsed duration up to a few seconds.

In summary, we have developed the EDLC based power supply which is cost-effective and compact discharge system and can generate strong magnetic fields with long duration. These systems can be used for many research fields such as nuclear magnetic resonance and neutron scattering experiments, which typically require long accumulation times to achieve good signal/noise ratios. In addition, we have confirmed that the generated pulsed field profile is well described by a series-connected RLC model with taking Joule heating into account. Finally, we note that connecting several EDLC units in parallel and series can generate a strong pulsed field of more than 30 T with a long time duration of a few seconds.

Reference

- [1] K. Matsui, T. Kanda, Y. Ihara, K. Kindo, and Y. Kohama, Rev. Sci. Instrum. **92**, 024711 (2021).

Authors

K. Matsui, T. Kanda, Y. Ihara^a, K. Kindo, and Y. Kohama
^aHokkaido University

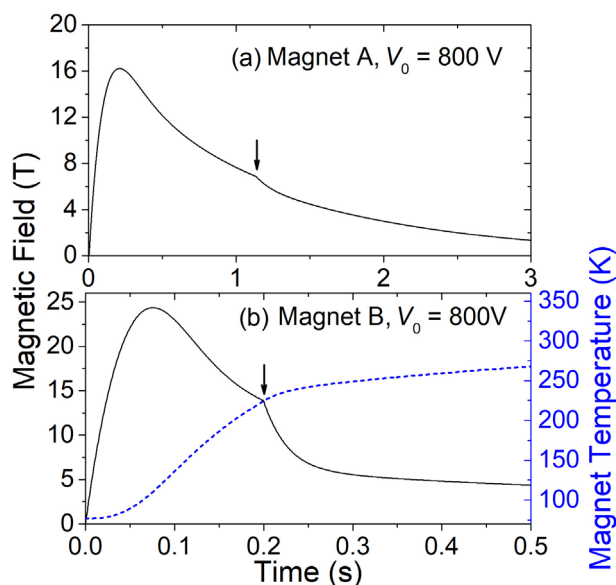


Fig. 1. Pulsed Field Profile generated by the EDLC based power supply. (a) Magnetic field profile generated with low-impedance pulsed magnet. (b) Magnetic field profile generated with high-impedance pulsed magnet. The right axis represents the calculated magnet temperature.

Observation of the Quantum Shift of a Backward Rescattering Caustic by Carrier-Envelope Phase Mapping

Itatani Group

When an atom or molecule is exposed to linearly-polarized intense optical fields, an electron wavepacket is freed from the atom, accelerated by the field, then collides with the parent ion. This process, recollision, is the fundamental of attosecond science. When recollision becomes recombination, the ionizing atoms emits a high energy photon (high harmonic generation). Meanwhile, it is well known that a part of recolliding events becomes elastic scattering. Especially the backward rescattering leads to the generation of high-energy electrons with a drift kinetic energy up to $10U_p$, where U_p is the ponderomotive potential. Recent theoretical progress of the adiabatic theory of rescattering gives an analytical formula for photoelectron momentum distributions (PEMDs) near the $10U_p$ cutoff which is scaled by the cutoff energy. Although the theoretical treatment of rescattering is fully quantum mechanical and straightfor-

ward, the experimental verification has been very difficult because it is not easy to realize systematic experiments to extract well-defined single rescattering events with multi-cycle laser pulses.

We hereby used intense few-cycle pulses in infrared to measure the backward PEMDs with controlled carrier-envelope phases (CEPs). The extremely short duration of the optical pulse allows to extract the single rescattering events of the three highest energies, and the CEP control enables to systematically change the maximum intensity in the focused volume without affecting the other parameters such as spatial distribution of the field intensity. Figure 1 shows the CEP dependent PEMDs with a pulse energy of 210 μJ . Dashed and solid curves represent classical and quantum caustics. The CEP dependent PEMD assures the one-to-one correspondence of the electron momentum at the instance of rescattering and the CEP, which we call the CEP mapping method. From this CEP mapping, we successfully determined the field intensity and the pulse duration to be $2.6 \times 10^{13} \text{ W/cm}^2$ and 13.8 fs, respectively. Using these parameters, the observed PEMDs are deconvolved to three PEMDs that correspond to the rescattering events of different intensities within a single optical pulse, as shown in Fig. 2.

The laser parameters, elastic scattering differential cross sections, and tunnel ionization rate of the target are encoded in PDMDs. Such information can be extracted from the

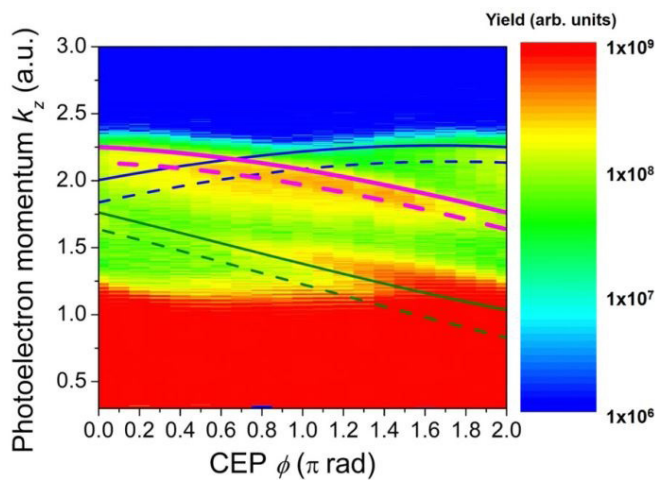


Fig. 1. Measured PEMDs as a function of CEP at a pulse energy of 190 μJ . Dashed and solid curves represent classical and quantum caustics at the intensity of $2.6 \times 10^{13} \text{ W/cm}^2$ and pulse duration of 13.8 fs.

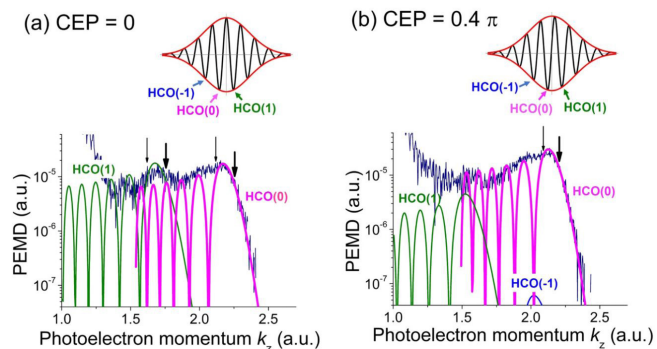


Fig. 2. Measured PEMDs at CEP=0 and 0.4π at an estimated intensity of $2.6 \times 10^{13} \text{ W/cm}^2$ and a pulse duration of 13.8 fs. The thick red, thin blue, and thin green curves show calculated PEMDs corresponding to a half cycle of the electric field as depicted in the top figures. Thin and thick arrows indicate the classical and quantum caustics, respectively.

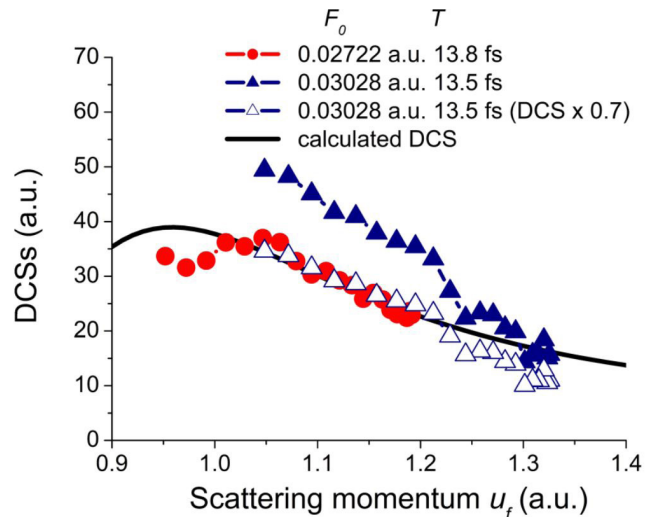


Fig. 3. Extracted DCSs of Xe^+ for estimated field amplitudes of 0.02722 (circle) and 0.03028 a. u. (closed triangle) as a function of the rescattering momentum. The black curve represents calculated DCSs.

observed PEMDs based on the adiabatic theory. Based on the quantitative agreement of the observed cutoff behavior of PEMDs with the adiabatic theory, elastic scattering cross section as a function of scattering momenta is successfully determined as shown in Fig. 3.

In summary, we experimentally and theoretically explored the rescattering PEMDs of a Xe atoms near the cutoff using CEP-stable few-cycle pulses [1]. The observed PEMDs are well reproduced by the analytical formula of the adiabatic theory including the quantum shift of the caustics. The results not only demonstrate the fact that the CEP mapping method with the adiabatic rescattering theory allows to extract well-defined elastic scattering, but also opens an opportunity to use rescattering to observe novel electron states such as vortex electrons [2].

References

- [1] T. Mizuno, N. Ishii, T. Kanai, P. Rosenberger, D. Zietlow, M. F. Kling, O. Tolstikhin, T. Morishita, and J. Itatani, *Phs. Rev. A* **103**, 043121 (2021).
- [2] O. I. Tolstikhin and T. Morishita, *Phys. Rev. A* **99**, 063415 (2019).

Authors

T. Mizuno, N. Ishii, T. Kanai, P. Rosenberger^a, D. Zietlow^a, M. F. Kling^{a, b}, O. Tolstikhin^c, T. Morishita^d, and J. Itatani^a
^aLudwig-Maximilians-Universität München
^bMax Planck Institute for Quantum Optics
^cMoscow Institute of Physics and Technology
^dThe University of Electro-Communications

Observation of Small Fermi Pockets in a Copper Oxide High- T_c Superconductor

Kondo and Kohama Groups

High-temperature superconductivity is one of the most significant discoveries in physics in the latter half of the 20th century. Since the discovery of high-temperature superconductivity in 1986, their physical properties have been intensively studied from various aspects. However, a unified understanding of the mechanism for high-temperature superconductivity has not yet been established. The most basic and important issue relevant to it is the relationship between antiferromagnetic state forming Mott insulator and high-temperature superconductivity induced by carrier doping.

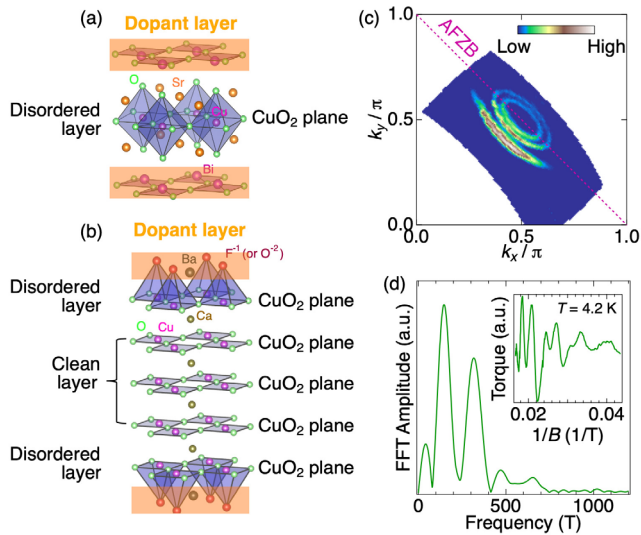


Fig. 1. (a) Crystal structure of single-layer cuprate superconductor ($\text{Bi}_2\text{Sr}_2\text{CuO}_{6+\delta}$ is presented as an example). (b) Crystal structure of 5-layer cuprate superconductor, $\text{Ba}_2\text{Ca}_4\text{Cu}_5\text{O}_{10}(\text{F},\text{O})_2$, we have focused on in this study. (c) Fermi surfaces of $\text{Ba}_2\text{Ca}_4\text{Cu}_5\text{O}_{10}(\text{F},\text{O})_2$ observed by laser-ARPES. (d) Quantum oscillation measurements for the same compound.

In this study, we focused on a multi-layered cuprate high- T_c superconductor (Fig. 1b) with a clean superconducting plane (CuO_2 layer) that is structurally flat and has charges uniformly distributed along the plane. Here we perform laser-based angle-resolved photoelectron spectroscopy (ARPES) with high energy resolution and quantum oscillation measurement at a strong magnetic field and present the first observation of small Fermi pockets formed in the close vicinity of the Mott insulating phase. Furthermore, we find the coexistence of antiferromagnetism and high-temperature superconductivity in the same CuO_2 sheet.

Superconductivity of cuprate superconductors occurs via carrier doping to the CuO_2 layers from the dopant layers sandwiching them. The main target in previous studies was for structurally simple compounds with one or two CuO_2 planes per unit cell (Fig. 1a). While these have the advantage to be easy in synthesizing, it has been pointed out that the direct contact of the dopant layers to the superconducting layers causes structural distortion and non-uniform charge distribution along the CuO_2 plane, leading to disordered electronic states. To solve this problem, we selected a multilayer system with five CuO_2 planes per unit cell, $\text{Ba}_2\text{Ca}_4\text{Cu}_5\text{O}_{10}(\text{F},\text{O})_2$, for a study (Fig. 1b).

This compound has inner CuO_2 planes that can avoid direct contact to the dopant layers. These inner CuO_2 planes are structurally flat, and at the same time, protected by the outer CuO_2 plane from the dopant layers causing the effects of spatially non-uniform carrier doping and defects. Therefore, this multilayered system gives us an excellent opportunity to study an extremely clean superconducting layer that is close to the ideal case treated in theoretical studies.

By performing high-resolution laser-ARPES and quantum oscillation measurements for the clean superconducting layers (Fig. 1c), we successfully observed small Fermi pockets, which had been theoretically expected yet elusive for more than 30 years of research for cuprates. The spectra of Fermi pockets are much sharper in energy than that of Fermi arc, indicating that the pockets we observed indeed come from the inner CuO_2 plane protected from the random potential induced by dopant layers. Moreover, we have confirmed the existence of d -wave superconducting gap

around the Fermi pockets, providing spectroscopic evidence for the coexistence between antiferromagnetism and superconductivity in the same CuO_2 sheet.

Our results are expected to facilitate the experimental and theoretical research pursuing the mechanism of high-temperature superconductivity in cuprates. In particular, these will contribute to solving the long-standing puzzle of the Fermi arc phenomena and urge the need for revisiting the Mott physics leading to the electron pairing in cuprates, which, up to now, has been based mainly on the research on single- and double-layered compounds with inhomogeneous electronic states.

References

[1] S. Kunisada *et al.*, *Science* **369**, 833 (2020).

Authors

S. Kunisada, S. Isono^a, Y. Kohama, S. Sakai^b, C. Bareille, S. Sakuragi, R. Noguchi, K. Kurokawa, K. Kuroda, Y. Ishida, S. Adachi^c, R. Sekine^a, T.K. Kim^d, C. Cacho^d, S. Shin, T. Tohyama^a, K. Tokiwa^a and T. Kondo

^aTokyo University of Science

^bRIKEN Center for Emergent Matter Science (CEMS)

^cMANA, National Institute of Material Science

^dDiamond Light Source

Higher-Order Topological Insulator Built from van der Waals Stacking of Bismuth-Halide Chains

Kondo Group

A Z_2 weak topological insulator (WTI) state can be formed in a material with stacked quantum spin Hall insulators (QSHIs), where the topological surface states appear only on side surfaces by accumulating helical edge states of QSHIs [1]. Similarly, a higher-order topological insulator (HOTI) is expected to be built from stacking QSHIs so that 1D helical hinge states are formed by accumulating the edge states. Utilizing symmetry-based indicators, the HOTI phases have been predicted in materials which were previously regarded as trivial insulators [2]. So far, only bulk bismuth has been experimentally shown to be in the HOTI phase [3]. However, bismuth is a semimetal, whose bulk cannot become insulating by carrier doping. Therefore, the experimental realization of a HOTI in an insulating material has been awaited.

In this study, we propose that quasi-1D bismuth halides offer a novel platform to investigate various topological phases that depend on the stacking sequences of Bi_4X_4 (where X is I or Br) chains. A WTI state has been observed in $\beta\text{-Bi}_4\text{I}_4$ with single-layered chains per unit cell, while a normal insulator state has been obtained in $\alpha\text{-Bi}_4\text{I}_4$, which takes a double-layered structure (Fig. 1) [1]. Although Bi_4Br_4 also consists of double layers, each layer is alternately rotated by 180 degrees, leading to the prediction of a HOTI phase due to the slight shift of the inversion center in the unit cell. Based on this, we present angle-resolved photoemission spectroscopy (ARPES) results showing that Bi_4Br_4 is a HOTI for the first time as a real 3D material [4].

An advantage of employing quasi-1D materials lies in the formation of a number of steps aligned parallel to the chain direction on the cleavage surface. Figure 2(a) shows a photographic image of ribbon-like Bi_4Br_4 crystals used in the experiments. While the cleaved surface is relatively rough, as shown in Fig. 2(b), Grazing incidence Small-angle X-ray

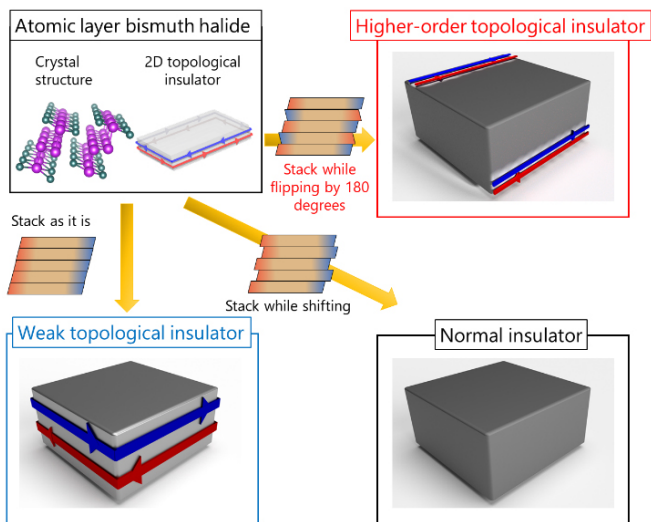


Fig. 1. Schematic of the various topological properties realized by stacking quasi-1D bismuth halide chains.

Scattering (GISAXS) measurements has revealed that the surface consists only of the top (001) surface and the side (100) surface. This result indicates that a huge number of hinges between the two planes are exposed on the cleaved surface, offering the possibility of detecting the topological hinge states by ARPES measurements.

Figure 2(c) presents the ARPES result of Bi_4Br_4 taken by high-resolution laser-ARPES. The strong photoemission signals observed at ~ 0.6 eV below the Fermi level (E_F) are assigned to the bulk valence band. Interestingly, we also observed metallic in-gap states with Dirac-like dispersions around E_F (bottom panel of Fig. 2(c)). This is further confirmed in the momentum distribution curves at the

energy of the roughly estimated Dirac point (middle panel of Fig. 2(c)). The in-gap states are found to form a quasi-1D intensity distribution in the Fermi surface mapping. These observations are in stark contrast to the case for a trivial insulator $\alpha\text{-Bi}_4\text{I}_4$, where no indication for in-gap states is found in ARPES image or the corresponding momentum distribution curve (Fig. 2(d)). Therefore, the 1D Dirac state in Bi_4Br_4 is attributed to the topological states, demonstrating the realization of the HOTI phase in Bi_4Br_4 . Our comprehensive study on bismuth halides also shows that the difference in chain stacking is the origin of the different band topologies among Bi_4Br_4 , $\alpha\text{-Bi}_4\text{I}_4$, and $\beta\text{-Bi}_4\text{I}_4$. The quasi-1D HOTI state we have verified in this study will bring the new capability of designing and engineering functional materials utilizing the stacking-dependence of the topological phases.

References

- [1] R. Noguchi *et al.*, Nature **566**, 518 (2019).
- [2] F. Tang, H. C. Po, A. Vishwanath, and X. Wan, Nat. Phys. **15**, 470 (2019).
- [3] F. Schindler *et al.*, Nat. Phys. **14**, 918 (2018).
- [4] R. Noguchi *et al.*, Nat. Mater. (2021). <https://doi.org/10.1038/s41563-020-00871-7>

Authors

R. Noguchi, M. Kobayashi^a, Z. Jiang^b, K. Kuroda, T. Takahashi^a, Z. Xu^b, D. Lee^b, M. Hirayama^c, M. Ochi^d, T. Shirasawa^d, P. Zhang, C. Lin, C. Bareille, S. Sakuragi, H. Tanaka, S. Kunişada, K. Kurokawa, K. Yaji, A. Harasawa, V. Kandyba^e, A. Giampietri^f, A. Barinov^g, T. K. Kim^g, C. Cacho^g, M. Hashimoto^h, D. Lu^h, S. Shin, R. Arita^{g,i}, K. Lai^b, T. Sasagawa^a, and T. Kondo

^aTokyo Institute of Technology

^bUniversity of Texas at Austin

^cRIKEN Center for Emergent Matter Science (CEMS)

^dOsaka University

^eNational Metrology Institute of Japan, National Institute of Advanced Industrial Science and Technology

^fElettra Synchrotron Trieste

^gDiamond Light Source

^hStanford Synchrotron Radiation Lightsource, SLAC National Accelerator Laboratory

ⁱThe University of Tokyo

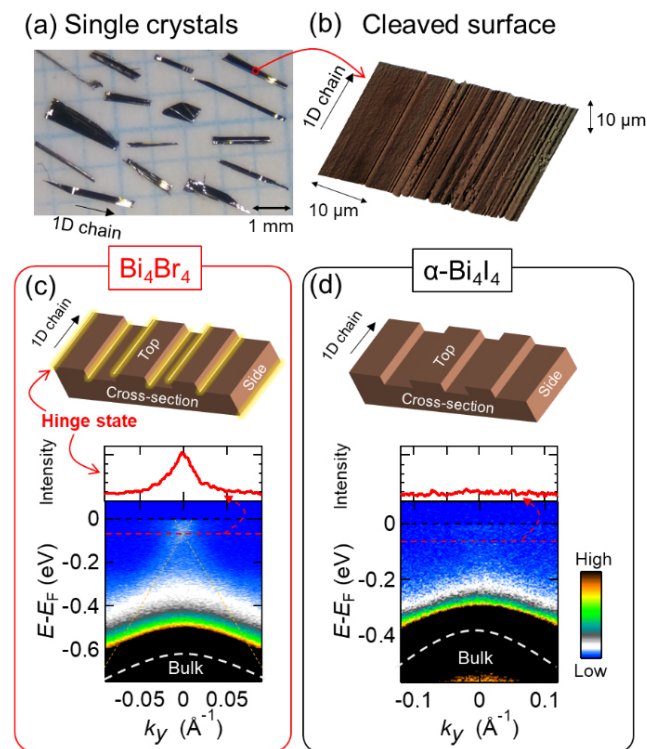


Fig. 2 (a) Photograph of Bi_4Br_4 crystals. (b) Laser microscope image of a cleaved surface. (c) ARPES band map of Bi_4Br_4 around the Γ point (bottom) and the corresponding momentum distribution curve at $E-E_F = -60$ meV (middle). Schematic of the cleaved surface of Bi_4Br_4 with topological hinge states (top). (d) Similar results to (c), but for $\alpha\text{-Bi}_4\text{I}_4$.

Observation and Control of the Weak Topological Insulator State in ZrTe_5

Kondo Group

A quantum spin Hall insulator hosts topological states at the one-dimensional (1D) edge, along which backscattering by nonmagnetic impurities is strictly prohibited. Its 3D analogue, a weak topological insulator (WTI), possesses similar quasi-1D topological states confined at side surfaces. The enhanced confinement could provide a route for dissipationless current and better advantages for applications relative to strong topological insulators (STIs) [1]. However, the topological side surface is usually not cleavable and is thus hard to observe.

ZrTe_5 was predicted to be a WTI candidate at the early stage of exploring WTIs [2]. This compound exhibits very high mobility, thus it has been regarded as a promising platform for devices. Nonetheless, the topological property of ZrTe_5 has not been experimentally identified to date because the observation of band structure on the side surface has not been successful so far. All the previous surface-sensitive studies were carried out on the top surface, which only confirms the lack of surface states; whether or not this material is topological, therefore, has not been determined beyond speculation. Another difficulty for this study is that

ZrTe₅ is in proximity to multiple topological phases, whereas this feature could bring an attractive functionality of controlling bulk topology by fine-tuning a physical parameter.

In this study, we visualize the topological states of ZrTe₅ by spin- and angle- resolved photoemission spectroscopy (ARPES): a quasi-1D band with spin-momentum locking was revealed on the side surface. We further demonstrate that the bulk band gap is controlled by external strain, realizing a more stable WTI state or an ideal Dirac semimetal (DS) state. The highly directional spin-current and the tunable band gap in ZrTe₅ will provide an excellent platform for applications [3].

ZrTe₅ has a quasi-1D crystal structure. In principle, it should be possible to cleave both top and side surfaces. Along the lattice *b* direction, the layers are stacked by van der Waals forces, and a clean surface can be easily obtained by cleavage. Instead, Te-Te bonding exists between adjacent layers along the lattice *c* direction, causing much more difficulty in cleaving the side *a-b* surface. In this work, we successfully cleaved the side *a-b* surface with a top post and silver epoxy. The problem, however, is that the cleaved areas are very small and inhomogeneous. With a synchrotron-based nano-ARPES (spot size < 1 μm), we took real space maps of photoemission intensity on several samples, as sketched in Fig. 1(a). It is found that the typical dimension of cleaved areas is around or smaller than 50 μm (Fig. 1(b)).

In *k*-space, a quasi-1D Fermi surface is exhibited by plotting ARPES intensities about the Fermi level, which shows no dispersion along lattice *b* direction (Fig. 1(d)). Along the lattice *a* direction, the band shows a hole-like dispersion (Fig. 1(c)). With different photon energies (74 eV and 7 eV), we did not find any change for this band, which support its surface origin (no *k_z* dispersion). For the topological surface state, spin polarization is expected. To confirm this, we have used spin-resolved ARPES to check

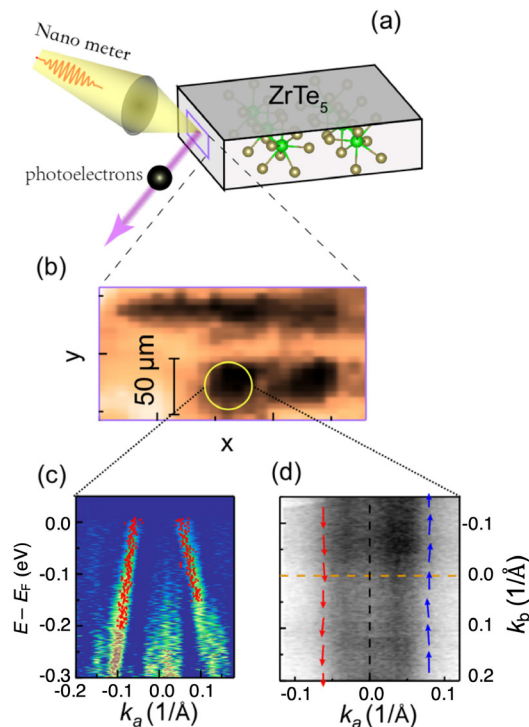


Fig. 1. ARPES measurements with nano-ARPES on the side surface. (a) Schematic of the experimental setup. (b) Real space intensity mapping with nano-ARPES. The signal is clear only within an area of 50 μm. (c) Band structure along the chain direction. The hole-like band is one of the topological surface band. (d) Fermi surface of the surface band in (c). Its spin-texture is indicated by red and blue arrows.

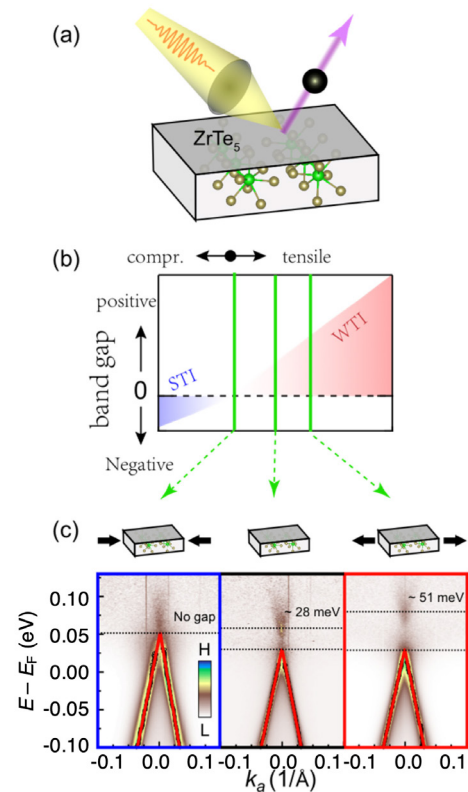


Fig. 2. ARPES measurements with laser-ARPES on the top surface with strain. (a) Schematic of the experimental setup. (b) Topological phase diagram of ZrTe₅ with different strain along chain direction. (c) Band structure observed from the top surface with different strain.

the spin texture of the surface band. A clear spin polarization is detected along the lattice *b* direction. In contrast, the spin polarization is almost zero along the lattice *a* and *c* directions, as indicated by red and blue arrows in Fig. 1(d). Therefore, the band is spin-polarized along the *b*-direction with spin-momentum locking, consistent with the spin-texture of WTIs with a quasi-1D dispersion.

On the top surface (Fig. 2(a)), we observe a small bulk gap (~ 28 meV), as shown in the middle panel of Fig. 2(c), which indicates that the WTI state in ZrTe₅ is protected only marginally from external perturbations. Theoretical calculations proposed that the band gap changes with external strain. Thus, we further designed a strain device and checked the strain dependence of band structure in ZrTe₅. Both compressive strain and tensile strain are applied along the chain direction of ZrTe₅. The band structures under different strains are displayed in Fig. 2(c). The sample with no strain shows a band gap of ~28 meV. With tensile strain, the band gap is enlarged to ~ 51 meV. In contrast, we could reduce the band gap by compressive strain, even realizing a Dirac semimetal state with no band gap. In Fig. 2(b), we summarized the topological phases of ZrTe₅ with different strains.

Our results demonstrate the existence and tunability of the WTI states in ZrTe₅. The spin-momentum locked quasi-1D surface states and the strain-tunable bulk gap make ZrTe₅ an ideal platform for 2D devices and spin engineering.

Reference

- [1] R. Noguchi *et al.*, Nature, **566**, 518 (2019).
- [2] H. Weng, X. Dai, and Z. Fang, Phys. Rev. X **4**, 011002 (2014).
- [3] P. Zhang *et al.*, Nature Commun. **12**, 406 (2021).

Authors

P. Zhang, R. Noguchi, K. Kuroda, C. Lin, K. Kawaguchi, K. Yaji^a, A. Harasawa, M. Lippmaa, S. Nie^b, H. Weng^c, V. Kandyba^d, A. Giampietrid, A. Barinov^d, Q. Li^e, G.D. Gu^e, S. Shin^f, and T. Kondo

^aNational Institute for Materials Science
^bStanford University
^cChinese Academy of Sciences
^dElettra - Sincrotrone Trieste
^eBrookhaven National Laboratory
^fThe University of Tokyo

Bose-Einstein Condensation Superconductivity Induced by Disappearance of the Nematic State

Okazaki Group

The crossover from the superconductivity of the Bardeen-Cooper-Schrieffer (BCS) regime to the Bose-Einstein condensation (BEC) regime holds a key to understanding the nature of pairing and condensation of fermions. Figure 1a shows a canonical phase diagram of BCS-BEC crossover. Weak-coupling Bardeen-Cooper-Schrieffer (BCS) pairing and strong-coupling Bose-Einstein condensation (BEC) are connected continuously through the BCS-BEC crossover regime. This regime holds a key to understanding the nature of pairing and condensation of particles. In the weak-coupling BCS regime, the dispersion of the Bogoliubov quasiparticle (BQP) shows the characteristic back-bending near k_F , which is downward convex around $k = 0$ in the case of a hole band below E_F , as shown in Fig. 1b, where k is the crystal momentum of electrons. On the other hand, in the strong-coupling BEC regime, the dispersion with a minimum

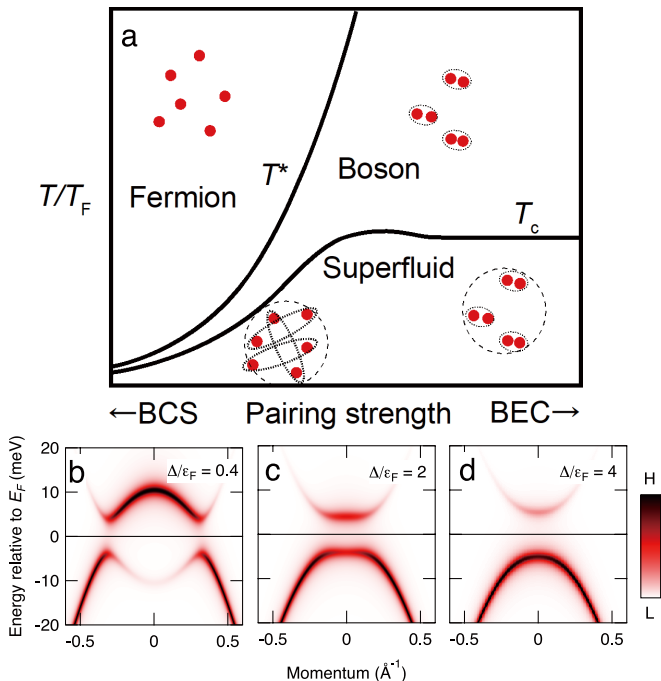


Fig. 1. Phase diagram of the BCS-BEC crossover and BQP band dispersions. (a) Canonical phase diagram of BCS-BEC crossover. T_c and T^* are condensation and pairing temperatures, respectively. As the pairing strength increases, T^* and T_c become separate, and a pseudogap is expected at $T^* > T > T_c$. (b)-(d) BQP band dispersions in the BCS regime, the crossover regime, and the BEC regime, respectively. The dispersion is downward convex around $k = 0$ for the BCS regime, becomes flat in the crossover regime, and then becomes upward convex in the BEC regime, because of the chemical potential shift. Δ/ϵ_F is referred to as a measure of the pairing strength for single-band superconductors.

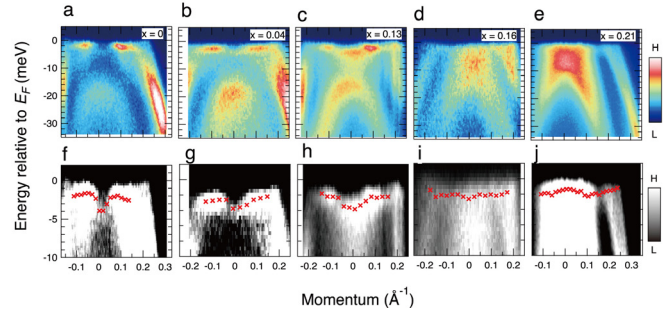


Fig. 2. ARPES intensity plots of $\text{FeSe}_{1-x}\text{S}_x$ along the Γ -M direction measured in the SC state. (a)-(e) ARPES intensity plots of $x = 0, 0.04, 0.13, 0.16,$ and 0.21 along the Γ -M direction taken at 2 K with s-polarized incident light. (f)-(j) Enlarged plots of (a)-(e) around E_F . The red markers represent the BQP band dispersions determined from the energy distribution curves.

gap at $k = 0$ is expected, which is upward convex around $k = 0$ in the case of a hole band below E_F , as shown in Fig. 1d. In the crossover regime, the BQP dispersion is intermediate between two extreme cases and the flat dispersion appears. In the crossover regime, a pseudogap is also expected to open at a temperature higher than T_c as a result of preformed bosonic pairs, as shown in Fig. 1a. Here, we provide systematic evidence for the BCS-BEC crossover in iron-based superconductors $\text{FeSe}_{1-x}\text{S}_x$ from laser-excited angle-resolved photoemission spectroscopy, and show that the system enters the BEC regime with $x = 0.21$, where the nematic state that breaks the orbital degeneracy is fully suppressed.

Figures 2a-2e show the ARPES intensity plots of $\text{FeSe}_{1-x}\text{S}_x$ (where $x = 0, 0.04, 0.13, 0.16,$ and 0.21) taken in the SC state with s-polarized light. To see the BQP band dispersions more clearly, we show enlarged plots around E_F in Figs. 2f-2j. We have plotted the BQP band dispersions determined from the energy distribution curves (EDCs) of each composition as indicated by red markers. From these plots, we can see that the BQP band dispersion, which is downward convex at $x = 0$, systematically changes and becomes flat at $x = 0.16$; it then, eventually, becomes upward convex at $x = 0.21$. This systematic change is consistent with that expected from the chemical potential shift in the BCS-BEC crossover, as shown in Figs. 1b-1d, and thus strongly suggests that $\text{FeSe}_{1-x}\text{S}_x$ is tuned from the BCS-BEC crossover regime ($x = 0$) to the BEC regime ($x = 0.21$). To obtain complete evidence for the BCS-BEC crossover, we have investigated the existence of a pseudogap, and found that the pseudogap appears at $T^* \sim 15$ K for $x = 0.21$. Thus, from the BQP band and the existence of the pseudogap, we have concluded that BEC superconductivity is realized for $x = 0.21$. We have also investigated the substitution dependence of Δ/ϵ_F , where Δ and ϵ_F are the SC gap and the Fermi energy, respectively, and from the obtained substitution dependence, we have also concluded that the multiband nature is important for the realization of BEC superconductivity in this system, and that it is induced by the suppression of electronic nematicity.

Reference

[1] T. Hashimoto, Y. Ota, A. Tsuzuki, T. Nagashima, A. Fukushima, S. Kasahara, Y. Matsuda, K. Matsuura, Y. Mizukami, T. Shibauchi, S. Shin, and K. Okazaki, *Sci. Adv.* **6**, eabb9052 (2020).

Authors

T. Hashimoto, Y. Ota, A. Tsuzuki, T. Nagashima, A. Fukushima, S. Kasahara^a, Y. Matsuda^a, K. Matsuura^b, Y. Mizukami^b, T. Shibauchi^b, S. Shin^b, and K. Okazaki
^aKyoto University
^bThe University of Tokyo

Joint Research Highlights

Quadrupole Orders in Pr-Based Compounds with fcc Lattice Structure

H. Tsunetsugu, T. Ishitobi, and K. Hattori

Recently, physical properties of electric quadrupoles in PrMgNi_4 were studied experimentally and their antiferro ordering has been discussed [1]. Praseodymium ions constitute a frustrated structure of fcc lattice, and little had been known for its ordered quadrupolar pattern. Studying this issue theoretically, we have identified various ordered patterns and determined the phase diagram [2].

A non-Kramers doublet is the ground state of Pr^{3+} ion in a crystal field with cubic symmetry, and two components of electric quadrupole are active therein: O_{20} and O_{22} with symmetry z^2 and x^2-y^2 , respectively. Despite the same number of degrees of freedom, ordering of those quadrupoles may show different features from those in easy-plane magnets due to two reasons. First, while magnetic moments are axial vectors, electric quadrupoles are second-rank tensors, and therefore their effective interactions have a different form. We have determined its minimal form with two parameters J and K corresponding to isotropic and anisotropic couplings. The second reason is the presence of a third order Z_3 anisotropy which time-reversal symmetry prohibits for magnetic moments. This is induced by a hybridization of a singlet excited state, and its excitation energy Δ is another control parameter of this system.

We have employed a mean field approach with a four-site unit and determined the phase diagram at zero and finite temperatures. In the limit of $\Delta \rightarrow \infty$, the Z_3 anisotropy vanishes and three ordered phases appear at low temperatures depending on the ratio of J and K : O_{20} ferro, O_{20} antiferro, and O_{22} antiferro. For $\Delta < \infty$, the Z_3 anisotropy takes effects and this leads to a phase diagram with rich

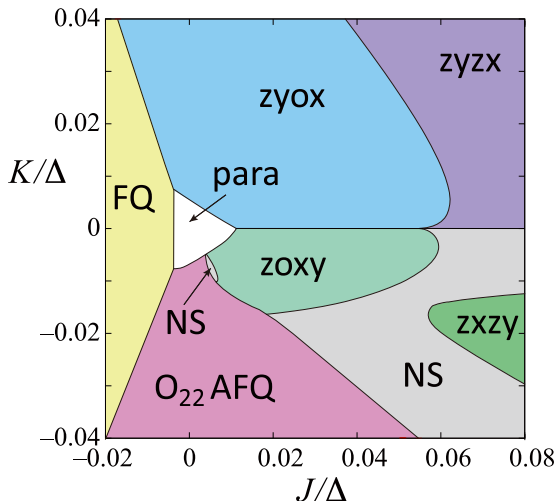


Fig. 1. Phase diagram of the J - K - Δ model for electric quadrupoles on the fcc lattice at temperature $T = 0.1\Delta$. See Ref.2 for details of ordered phases.

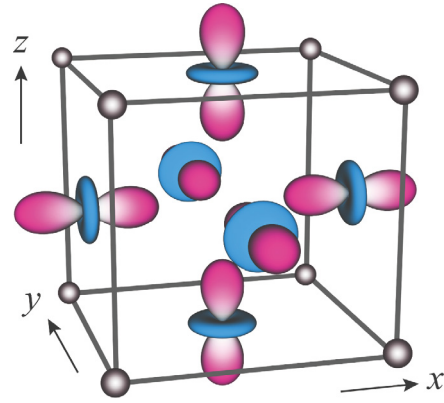


Fig. 2. Structure of electric quadrupoles in the $zyox$ phase. Quadrupoles are not ordered on the corner sites.

structure. Related to induced canting of O_{22} components, the most important result is the instability of the two-site antiferro orders to more complex four-site structures. It is also interesting that two of the new phases ($zyox$ and $zoxz$) exhibit a partial order in which one sublattice remains disordered and quadrupole is polarized as x^2 , y^2 , and z^2 in each of the other three sublattices. They are a triple- q order in which three components with different polarizations and wave vectors are coupled by the Z_3 anisotropy, and we have confirmed their stability by a phenomenological Landau theory. Thus, we have established the basic picture of the phase structure for quadrupole orders, and hope that this encourages further experimental studies as well as more advanced theoretical analysis on this issue.

References

- [1] Y. Kusanose *et al.*, J. Phys. Soc. Jpn. **88**, 083703 (2019); Y. Kusanose *et al.*, JPS Conf. Proc. **30**, 011160 (2020).
- [2] H. Tsunetsugu, T. Ishitobi, and K. Hattori, J. Phys. Soc. Jpn. **90**, 043701 (2021).

Authors

H. Tsunetsugu, T. Ishitobi^a, and K. Hattori^a
^aTokyo Metropolitan University

Microscopic Theory of the Spin Hall Magnetoresistance

M. Matsuo and T. Kato

Magnetoresistance is one of the fundamental phenomena in the research field of spintronics. Recently, a novel type of magnetoresistance called spin Hall magnetoresistance (SMR) has been observed in a bilayer system composed of a normal metal (NM) and a ferromagnetic insulator (FI) [1]. SMR is explained by the combination of charge-spin conversions in NM and loss of spins at the NM/FI interface [1,2] (see Fig. 1 (a)). When an in-plane charge current is applied to the

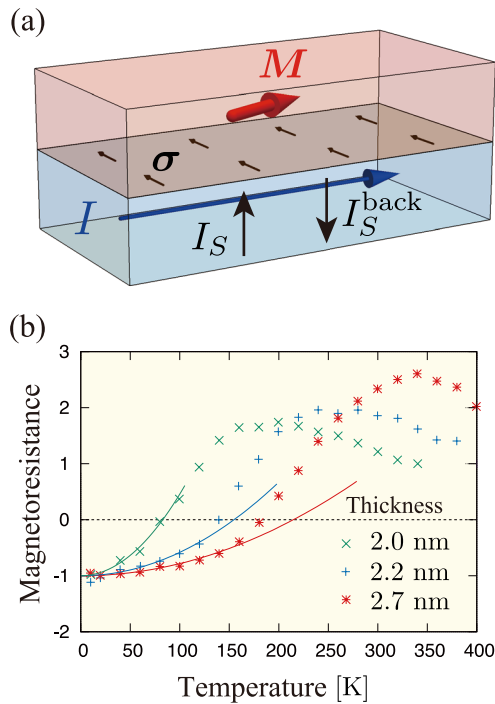


Fig. 1. (a) Schematic diagram of the normal-metal(NM)/ferromagnetic-insulator(FI) bilayer system for the spin Hall magnetoresistance (SMR) measurement. (b) Experimental data of SMR measured in Pt/NiO/YIG bilayer systems. The data is normalized as -1 at zero temperature using the extrapolated value by the fitting.

NM layer with a large spin-orbit interaction, spin accumulation is caused near the NM/FI interface by the spin Hall effect. The amount of spin accumulation is affected by the orientation of FI magnetization because it changes the rate of spin loss at the interface. A backward spin current owing to spin diffusion is converted into the charge current again by the inverse spin Hall effect and induces longitudinal magnetoresistance, which depends on the orientation of FI magnetization. Recently, SMR has been reported for the bilayer system composed of NM and an antiferromagnetic insulator (AFI) [3], where the orientation of the Néel vector of AFI has been changed by the orientation of magnetization of FI using the NM/AFI/FI trilayer structure.

SMR can be described theoretically by combining the spin diffusion theory with the boundary condition at the interface in terms of the spin-mixing conductance [2]. However, in this theory, the spin-mixing conductance at the interface is a phenomenological parameter that has to be determined experimentally; therefore, its temperature dependence cannot be predicted. Furthermore, the magnetization-orientation dependence of the spin-mixing conductance is assumed phenomenologically by its definition. This semiclassical description of SMR seems to be insufficient for studying quantum features of magnetic insulators such as the effect of thermally excited magnons.

In our work, we constructed a microscopic theory of SMR and derived a general formula of a spin conductance at the interface for both NM/FI and NM/AFI bilayer systems in terms of spin susceptibilities. We clarified that the spin current is composed of static and dynamic parts. The static part of spin current originates from spin flip owing to an effective magnetic field induced by an interfacial exchange coupling. This part is almost independent of the temperature, and takes a maximum when the magnetization (or the Néel vector) is perpendicular to accumulated spins in a normal metal, which is consistent with intuitive discussions in previous experimental studies. However, the dynamic part,

which is induced by creation or annihilation of magnons, depends on the temperature, and has opposite magnetization dependence, i.e., takes a maximum when the magnetization (or the Néel vector) is parallel to accumulated spins in a normal metal. The dynamic part becomes larger when the amplitude of the localized spin, S_0 , is smaller. This indicates that the sign of SMR changes at a specific temperature if S_0 is sufficiently small. In Fig. 1 (b), we show the measured temperature dependence of SMR in Pt/NiO/YIG bilayer systems [3]. The sign of SMR changes at 80, 140, and 180 K for NiO thickness of 2.0, 2.2, and 2.7 nm. In addition, we show the fitted curve in the figure using quadratic temperature dependence that is predicted by our theory. This fitting indicates that the quadratic temperature dependence explains well the experimental data at low temperatures. We also derived the Onsager relation between spin conductance and thermal spin-current noise.

This study has been performed as a joint study with Mamoru Matsuo, who was a visiting professor of ISSP in the academic year 2016.

References

- [1] H. Nakayama *et al.*, Phys. Rev. Lett. **110**, 206601 (2013).
- [2] Y. T. Chen *et al.*, Phys. Rev. B **87**, 144411 (2013).
- [3] D. Hou *et al.*, Phys. Rev. Lett. **118**, 147202 (2017).
- [4] T. Kato, Y. Ohnuma, and M. Matsuo, Phys. Rev. B **102**, 094437 (2020).

Authors

T. Kato, Y. Ohnuma^a, and M. Matsuo^a
^aKavli Institute for Theoretical Sciences

Controlling Magnetic Anisotropy of Nano-Size Islands by Alloying

Y. Hasegawa and W. C. Lin

Atomically-thin Fe and Co layers and nano-size island structures formed on the Cu(111) substrate usually exhibit magnetization in the in-plane and out-of-plane directions, respectively. The preferred magnetization directions is due to magnetic anisotropy, and controlling the energy barrier due to the anisotropy are fundamentally important for preserving the magnetization direction and switching it from one of the preferred directions to the other for magnetic storage/recording and spintronics devices.

The magnetic anisotropy basically originates from the spin-orbit interaction, and in the case of the $3d$ magnetic elements, the magnetic anisotropic energy (MAE) is described with its perturbation. MAE is, therefore, closely related with the occupation/un-occupation of $3d$ valence bands near the Fermi energy. In the present study using spin-polarized scanning tunneling microscopy (SP-STM) we investigated how the anisotropy and MAE of the $3d$ magnetic islands can be controlled by adjusting the valence occupation, that is, by alloying the two elements: Fe and Co, which exhibit the contrasting anisotropic behaviors [1].

Figure 1 shows one of the $\text{Co}_{50}\text{Fe}_{50}$ islands pseudo-morphically grown on the Cu(111) substrate. The thickness of the triangular island is 2 monolayer, and the white bar in the STM image corresponds to 10 nm. Spin-polarized tunneling conductance spectra taken at the marked site with a Fe-coated W tip exhibits a strong peak at the sample bias voltage of -0.3 V (-0.3 eV below the Fermi level). The peak just below the Fermi level has been assigned to $3d$

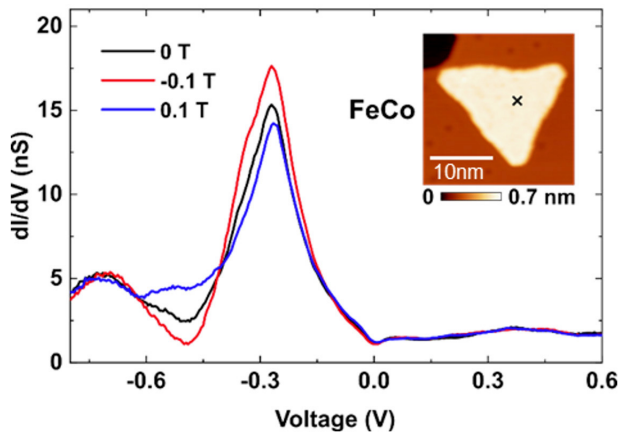


Fig. 1. Spin-polarized tunneling spectra taken at the marked site of a $\text{Co}_{50}\text{Fe}_{50}$ island structure presented in the inset STM image. Spectra taken under magnetic fields of 0 T and ± 1 T applied in the perpendicular direction to the island are presented. A Fe-coated W tip was used as a spin-polarized probe.

minority states of pure Co and the alloy islands. The peak height varies depending on the magnetic field applied in the perpendicular direction. Since the Fe layer coating the probe tip is in-plane magnetized, the applied magnetic field tilts the probe magnetization toward the field direction. The reduction in the -0.3 V peak height, that is, tunneling from the minority states, by a positive (upward) magnetic field indicates upward magnetization of the alloy island. The magnetic field dependence of the tunneling conductance is also found around -0.5 V. The states there are majority ones as they react to the applied field in the manner opposite to the minority ones.

The magnetic response of the tunneling conductance spectra indicates that the alloy island exhibits perpendicular magnetic anisotropy (PMA). In order to make it clear we swept the applied magnetic field and measured the tunneling conductance at -0.3 V. The obtained result is shown in Fig. 2. Gradual increase (decrease) with the increment (decrement) of the magnetic field is due to the tilt of the probe magnetization by the applied field. Then sudden drops observed around ± 0.12 T are due to the flip of the magnetization of the alloyed island from anti-parallel to parallel directions to the applied field. From the positions the drops, we can measure switching magnetic field or coercivity, which are closely related with the energy barrier between the two PMA configurations.

The PMA energy depends on the size of the islands; basically proportional to the area or the number of the composing atoms. We measured the switching field on

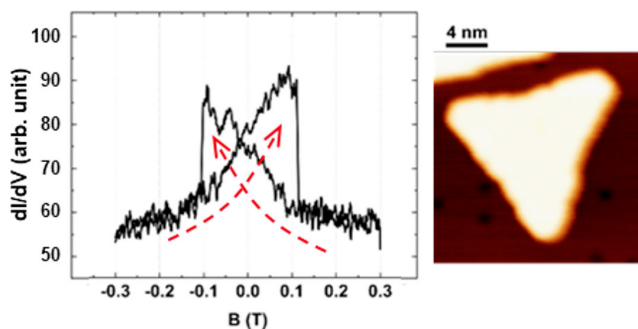


Fig. 2. Tunneling conductance at the sample bias voltage of -0.3 V taken at the center of the CoFe alloy island presented in the right STM image during a sweep of the applied perpendicular magnetic field. The sweeping directions are marked with red dashed arrows. Sudden drops of the tunneling conductance indicate switching of magnetization of the island.

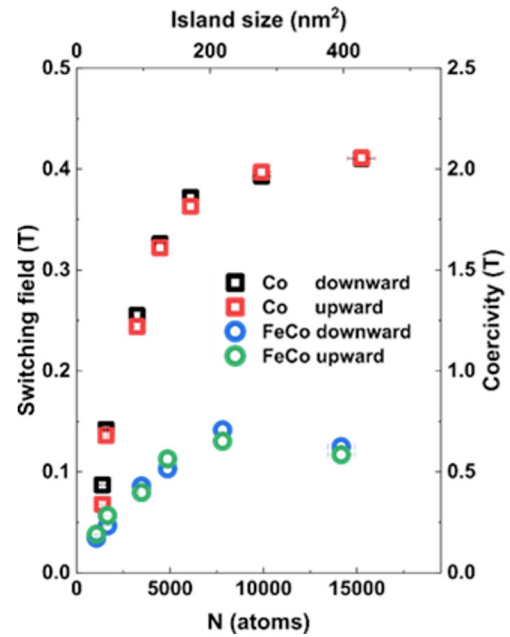


Fig. 3. Plot of switching magnetic field as a function of the number of the constituent atoms for both pure Co and CoFe islands. Coercivity (right vertical axis) was estimated from the switching fields taken with an antiferromagnetic tip, whose stray field is negligible.

various sizes of the alloy islands, and the results are summarized in Fig. 3 and compared with those taken on pure Co islands. One can clearly find that the switching field of the alloy islands is significantly reduced from pure Co islands by a factor of 3-4. For both Co and CoFe alloy islands, the switching field gradually increases with the size of the islands or the number of the composing atoms, but around 8000 atoms it exhibits saturation or even reduction with the island size. The peculiar behavior of the switching field is explained with a crossover of two magnetization reverse processes; for small islands the magnetization flips at a time whereas large islands are reversed through a process of domain wall nucleation and propagation. It should be noted here that since a ferromagnetic tip is used stray field from the tip significantly reduces the switching field; through the comparison with the switching field measured with an antiferromagnetic Co-coated tip, which directly provides coercivity, we estimated coercivity of our samples as depicted in the right axis of Fig. 3. Nevertheless, the results presented in Fig. 3 clearly indicate that the switching field is significantly reduced by the alloying, and suggest that the crossover same as pure Co islands also occur on the alloy islands.

Reference

[1] H.-H. Yang, C.-C. Hsu, W.-C. Lin, and Y. Hasegawa, *Phys. Rev. B* *104*, 035422 (2021).

Authors

H.-H. Yang, C.-C. Hsu^a, W.-C. Lin^a, and Y. Hasegawa
^aNational Taiwan Normal University

Free-Standing Oxide Thin Film Membranes

R. Takahashi and M. Lippmaa

A fundamental parameter that determines the physical properties of crystalline materials is the lattice parameter, which is generally determined by the chemical composition

and the lattice type of a crystal. Options for tuning materials properties or electronic phases by changing the lattice parameters is generally limited to the use of thermal expansion, the application of mechanical pressure, or ionic substitutions — also known as chemical pressure. Thin films offer an additional option of using epitaxial strain for lattice parameter control, since nanometer-scale films grown on single-crystal substrates tend to assume the same in-plane lattice parameter as the substrate material. Even in mechanically hard materials, such as oxides, epitaxial tensile or compressive strains of several percent can be routinely obtained. Larger strain states, however, are difficult to obtain without mechanical failure of a crystal. Likewise, it can be difficult to fabricate entirely strain free thin films. An interesting technique that can be used to apply very high local or long-range strain fields on thin layers is the use of free-standing thin films. In our recent work, we have developed a new oxide thin film lift-off process based on the use of lattice-matched BaO sacrificial layers to grow thin films that can be released from a substrate and transferred to a secondary carrier [1]. The technique can be used to extend the achievable range of mechanical strain in oxide materials and is the basis for constructing novel vibrational energy harvesting devices.

The process of fabricating free-standing BaTiO₃ films is illustrated in Fig. 1. A sacrificial BaO layer is first grown on a SrTiO₃ substrate. The BaO layer is nearly lattice matched with titanate lattices and can be grown epitaxially on the substrate surface. The membrane material, in this case BaTiO₃, is grown on top of the sacrificial BaO layer. The heterostructure is then removed from the thin film growth chamber and attached with an adhesive layer to a flexible secondary carrier, such as a glass sheet or even a polymer backing. When the whole structure is immersed in water, the BaO layer dissolves, detaching the single-crystal substrate from the membrane layer, as illustrated in Fig. 1c, which shows the detached membrane on a secondary flexible carrier and the detached substrate. In principle, the substrate can be recycled for growing another thin film.

One interesting application of the membrane process is the development of piezoelectric energy converters for harvesting vibrational energy. The use of a membrane device is beneficial because the piezoelectric film, such as BaTiO₃, can be grown epitaxially under optimal growth conditions on a high-quality single crystal substrate, yielding the highest piezoelectric coefficient. However, the bulk substrate prevents the application of large strains on the film, as is required for low-frequency vibrational energy harvesting. Much higher strains can be achieved in a membrane device where the piezoelectric film is detached from the substrate and sandwiched between flexible conducting electrodes,

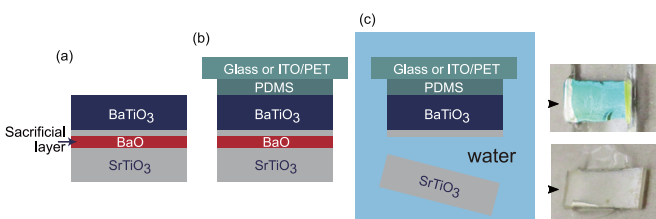


Fig. 1. Free-standing oxide thin film membrane fabrication process: (a) growth of a sacrificial BaO layer and the functional membrane layer, (b) attaching the heterostructure with a poly-dimethylpolysiloxane (PDMS) adhesive layer to a indium tin oxide-coated polyethylene terephthalate (PET) carrier, and (c) removing the substrate by dissolving the BaO layer in water.

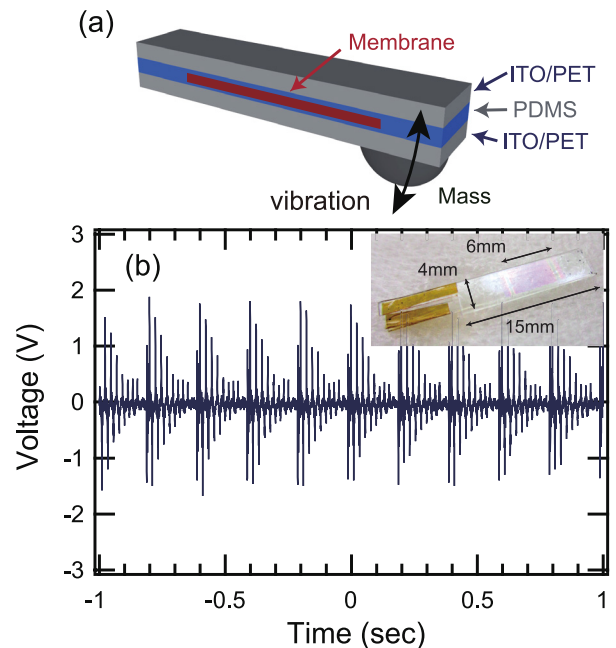


Fig. 2. Construction of a vibrational energy harvesting device consisting of a BaTiO₃ membrane embedded between two ITO/PET electrodes (a). The actual test device is shown in the inset of (b). The voltage signal obtained by vibrating the test device at 5 Hz is shown in (b).

as illustrated in Fig. 2a. An energy harvester device can be constructed by supporting a flexible membrane cantilever from one end and attaching a test mass on the free end. When mechanical vibration is applied, a periodic current can be generated in an external circuit, powering, for example, a low-power environmental sensor device. The output signal of a test cantilever using a BaTiO₃ film is shown in Fig. 2b.

The demonstration of the process used a BaTiO₃ film, but the technique itself is applicable to any material that can be grown epitaxially on the sacrificial BaO layer. For energy harvesting devices, a flexible backing is generally required to maintain the integrity of a millimeter-scale membrane.

An obvious use of the technique is to fabricate films that are truly strain free and for this reason, the technique has much broader potential applications than flexible piezoelectric energy conversion devices.

Reference

[1] R. Takahashi and M. Lippmaa, ACS Appl. Mater. Interfaces 12, 25042 (2020).

Authors

R. Takahashi^a, and M. Lippmaa
^aNihon University

Lasing Dynamics in Perovskite Microcavities

S. Chen and H. Akiyama

Perovskite materials have shown remarkable progress in both the field of solar cell and light emitting devices, for solar cell, conversion efficiencies more than 25% have been achieved, and for light emitting devices, perovskite-based vertical cavity surface emitting lasers (VCSEL) and distributed feedback (DFB) lasers have been fabricated, and very fascinating single-mode lasing properties have been demonstrated, however, the detailed lasing mechanism is still unclear.

We have fabricated various kinds of CsPbBr_3 perovskite microcavities with a low-temperature liquid-phase growth method, such as microplate, microrods, and microcubes, as shown in Figure 1, with a size from several tens to 200 micrometers. A clear substrate dependence of the morphologies of the perovskite microstructures in this growth method has been observed [1]. With the excitation of a femtosecond laser beam from a Ti: sapphire ultrafast laser system, all the microcavities show lasing behavior under elevated excitation densities, the higher carrier density more that Mott density at lasing threshold indicates the lasing behavior in these perovskite microcavities should be mainly related to electron-hole plasma rather exciton.

The lasing dynamics of the microcavities were further studied with time-resolved photoluminescence system. Figure 2 shows the spectrally and temporally resolved lasing images recorded by a streak camera. With increasing excitation fluences, two importance features have been observed, one is the redshift of the dominant lasing spectra to the low energy side due to the band gap renormalization (BGR) effect, another one is the blueshift of each lasing mode to higher energy side due to the reduction of the refractive index caused by the high injection carrier density. At a certain excitation density, for example $180 \mu\text{J}/\text{cm}^2$, we can see a redshift of each mode to low energy side with time going on after excitation, which indicates a recovery of index in microcavity, and the blueshift of the total lasing spectra with time going on indicates a recovery of BGR, therefore the lasing dynamics is merged with the transient BGR effect and the transient change of refractive index in perovskite microcavities, detailed explanations can be found in the published paper [2].

We also fabricated CsPbBr_3 perovskite nanocrystals with a ligand-assisted recrystallization method, and sandwiched the perovskite nanocrystals with two high-reflectivity distributed Bragg reflectors (DBRs) to form a VCSEL device [3]. The lasing performances of the perovskite nanocrystal

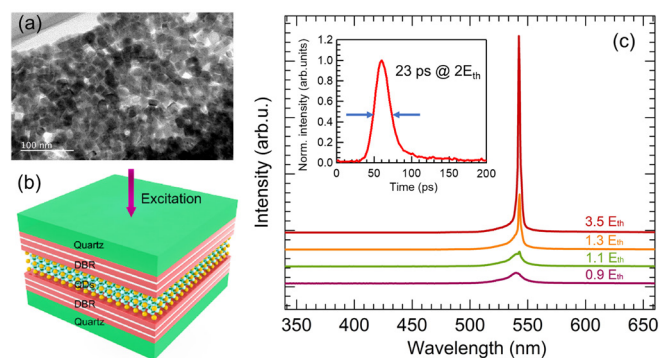


Fig. 2. (a) TEM image of CsPbBr_3 perovskite nanocrystals with an average size around 12 nm. (b) Schematic of the CsPbBr_3 nanocrystal based VCSEL, where the CsPbBr_3 nanocrystals are sandwiched with two high-reflectivity DBRs. (c) Emission spectra of the VCSEL with different excitation densities. The inset shows a waveform of the output pulse with a pulse width of 23 ps from the VCSEL with an excitation density 2 times of the threshold.

based VCSEL have been characterized with femtosecond pulse excitations, and single-mode lasing of the VCSEL has been observed. The threshold excitation density was around $8 \mu\text{J}/\text{cm}^2$. The cavity quality factor Q of the VCSEL is estimated to be around 1425. With the excitation power over 2 times of the threshold, the output pulse width of the perovskite based VCSEL is measured to be around 23 ps, demonstrating a potential application in short pulse generation of perovskite based VCSELs. Investigations on the carrier dynamics in the VCSEL is still in progress.

References

- [1]. G. Weng, J. Yan, S. Chen, C. Zhao, H. Zhang, J. Tian, Y. Liu, X. Hu, J. Tao, S. Chen, Z. Zhu, H. Akiyama, and J. Chu, *Photonics Res.* **9**, 54 (2021).
- [2]. G. Weng, J. Tian, S. Chen, J. Yan, H. Zhang, Y. Liu, C. Zhao, X. Hu, X. Luo, J. Tao, S. Chen, Z. Zhu, and J. Chu, *H. Akiyama, ACS Photonics* **8**, 787 (2021).
- [3] C. Zhao, J. Tao, J. Tian, Y. Bai, G. Weng, H. Liu, Y. Liu, J. Yan, S. Chen, Y. Pan, X. Hu, S. Q. Chen, H. Akiyama, L. Wang, and J. Chu, *Chemical Engineering Journal*, 2020, in press, <https://doi.org/10.1016/j.cej.2020.127660>

Authors

S. Chen^a and H. Akiyama
^aEast China Normal University

Second Hydrogen-Ordered Phase of Ice VI: Ice XIX

R. Yamane, K. Komatsu, and Y. Uwatoko

Ice exhibits extraordinary structural variety in its polymorphic structures. To date, more than 20 crystalline and amorphous phases of ice have been reported.

The existence of a new form of diversity in ice polymorphism has recently been debated in both experimental and theoretical studies, questioning whether hydrogen-disordered ice can transform into multiple hydrogen-ordered phases, contrary to the known one-to-one correspondence between disordered ice and its ordered phase. Recent experiments on a high-pressure hydrogen-disordered phase, ice VI, revealed an unknown hydrogen-ordered form besides the known ordered phase, ice XV. However, due to experimental difficulties under the high-pressure condition, the intriguing manner of hydrogen ordering in ice VI has been investigated only using decompressed sample to ambient pressure. Also,

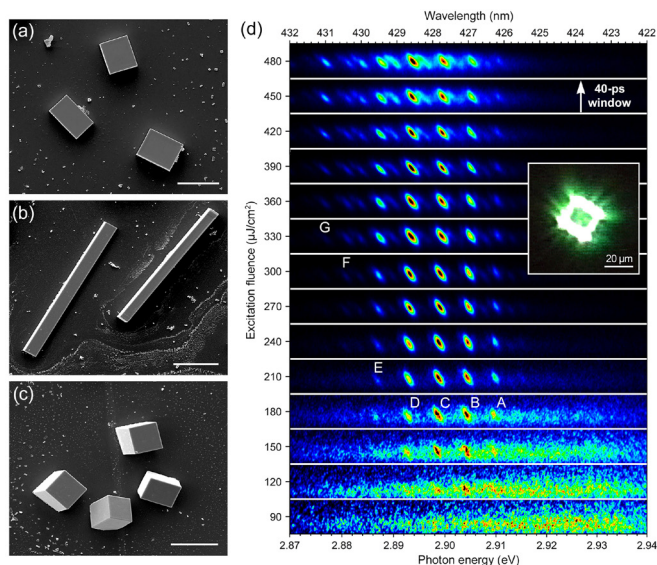


Fig. 1. SEM micrograph of CsPbBr_3 single-crystal microcavities on substrates of (a) single-crystal Si, (b) sapphire, and (c) amorphous quartz. Streak-camera images (d) of the emissions from microplate with various excitation densities. In the vertical dimension, a time range of 40 ps for each slice is shown. The distinct lasing modes are labeled as Mode A (with the highest photon energy) to Mode G (with the lowest photon energy) above the threshold. In each slice, a redshift to low energy with time for each mode is clearly demonstrated. Inset is a lasing image of a microplate under the excitation of femtosecond laser beam, showing a whispering-gallery mode (WGM) lasing.

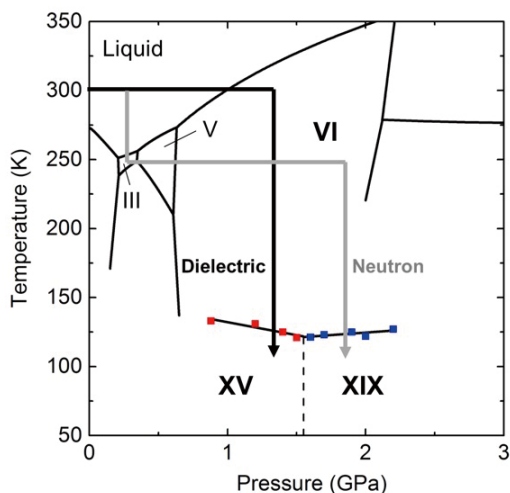


Fig. 1. Representative experimental paths of dielectric and neutron diffraction experiments described in the phase diagram of ice obtained herein. Phase boundaries among ice VI, ice XV, and ice XIX are described by black solid lines, based on dielectric experiments (red and blue squares correspond to phase transition temperatures from ice VI to ice XV and XIX, respectively). The dotted line shows the provisional phase boundary between ice XV and ice XIX.

no previous study reports direct experimental evidence for the multiplicity of hydrogen-ordered phase of ice VI. We report a second hydrogen-ordered phase for ice VI, ice XIX, unambiguously demonstrated by in-situ dielectric and neutron diffraction measurements under high pressure originally developed by our group [1]. Based on a newly obtained phase diagram of ice VI, XV and XIX (Fig. 1), we revealed that ice XIX is thermodynamically stabilized by pressure compared to ice XV.

To investigate hydrogen ordering of ice VI in its stable pressure region, comprehensive dielectric experiments were first carried out in the pressure range 0.88–2.2 GPa, using a newly developed pressure cell. Ice VI was initially obtained at room temperature and its dielectric properties were determined in both cooling and heating runs in the temperature range 100–150 K. Neutron diffraction experiments were conducted at 1.6 and 2.2 GPa, in which ice XIX appears as hydrogen-ordered phase of ice VI based on the dielectric experiments, using Mito-system at J-PARC [2]. Both cooling and heating runs were conducted at each pressure in the temperature range 80–150 K.

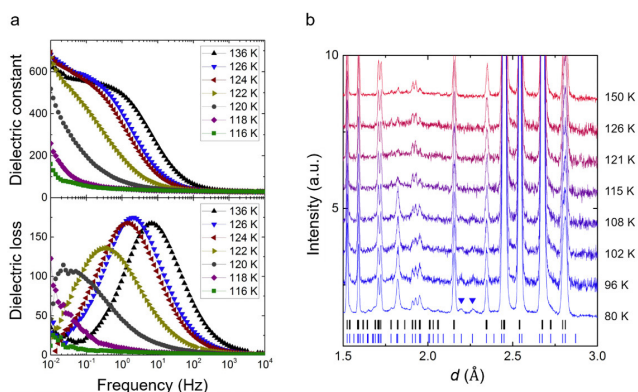


Fig. 2. a Dielectric constant and dielectric loss of HCl-doped ice VI and its hydrogen-ordered phase (ice XIX) obtained at 1.9 GPa upon cooling. b Neutron diffraction patterns of ice VI and XIX obtained at 1.6 GPa in the cooling run. Only an expanded area showing new peaks of ice XIX is displayed. The blue and black ticks represent all the peak positions expected from the unit cells of ice XIX and ice XV, respectively. Blue triangles indicate new peaks at 2.20 Å and 2.26 Å, which do not appear from the unit cell of ice XV.

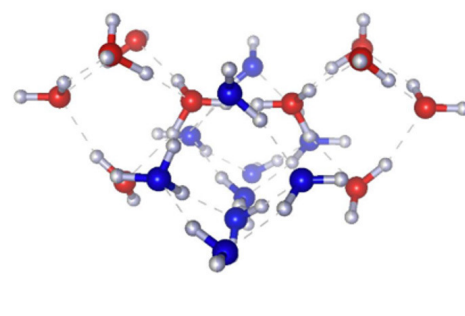


Fig. 3. Proposed crystal structure of ice XIX based on *Pcc2* structure model.

Phase transitions from ice VI to its hydrogen-ordered phases were observed at around 120–130 K, along with sudden weakening of the dielectric response of ice VI with decreasing temperature (Fig. 2a). The reason for this weakening is that hydrogen ordering of ice suppresses reorientation of water molecules which induces the dielectric response of ice. The transition from ice VI to ice XIX was also observed in the neutron diffraction experiments, as appearance of new peaks due to symmetry lowering (Fig. 2b). Some of the new peaks, e.g. those at 2.20 Å and 2.26 Å (indicated by blue triangles in Fig. 2b), cannot be explained by the structure of ice XV. This is unambiguous evidence that ice VI has a hydrogen-ordered phase distinct from ice XV, and we named this unknown phase as ice XIX.

Based on the phase boundary of ice VI and its hydrogen-ordered phases, ice VI contracts upon hydrogen ordering, which thermodynamically stabilizes ice XIX in the higher-pressure region compared to ice XV because of its smaller volume than ice XV.

In addition, from our structural analysis, two structural models, whose space groups are *P4̄* and *Pcc2*, are the most plausible for the crystal structure of ice XIX (the *Pcc2* structural model is shown in Fig. 3). It should be noted that the proposed structure models intrinsically include hydrogen atoms whose site occupancy is 50 %; in other words, the models exhibit that ice XIX is partially ordered state. This indicates a possibility that there exists another fully hydrogen-ordered phase of ice VI instead of the partially hydrogen-ordered ice XIX considering the third law of thermodynamics. Considering the suggested space group of ice XV, *P1̄* or *Pmmn*, centrosymmetry of hydrogen configurations is the most significant difference in hydrogen configuration between ice XIX and ice XV. Such symmetry difference would induce intriguing difference of physical properties between ice XIX and XV in terms of such as optic and dielectric.

References

- [1] R. Yamane, K. Komatsu, J. Gouchi, Y. Uwatoko, S. Machida, T. Hattori, H. Ito, and H. Kagi, *Nat. Commun.* **12**, 1129 (2021).
- [2] K. Komatsu, M. Moriyama, T. Koizumi, K. Nakayama, H. Kagi, J. Abe, and S. Harjo, *High Press. Res.* **33**, 208 (2013).

Authors

R. Yamane^a, K. Komatsu^b, J. Gouchi, Y. Uwatoko, S. Machida^c, T. Hattori^d, H. Ito^b, and H. Kagi^b

^aTohoku University

^bThe University of Tokyo

^cNeutron Science and Technology Center, CROSS

^dJ-PARC Center, Japan Atomic Energy Agency

Fabrication of a Compact Cubic-Anvil Pressure cell

N. Fujiwara and Y. Uwatoko

We have succeeded in fabricating the smallest cubic-anvil pressure cell (CAPC) to date. This miniaturization allowed us to investigate physical properties at high pressures of over 4 GPa under a magnetic field [1, 2].

In strongly correlated electron systems, one of the most intriguing topics is the quantum phase transition. Unlike a conventional thermally induced phase transition, this phase transition is driven via quantum fluctuations at zero temperature, leading to an unconventional ground state even at finite temperatures. Pressure is a representative parameter as well as carrier doping in this phase transition. At low pressures below 3-4 GPa, a piston-cylinder pressure cell (PCPC) has been most widely used for various experiments because of its large sample space. However, this pressure cell is unavailable at high pressures above 4 GPa. The CAPC marks high hydrostaticity among pressure cells available at pressures above 4 GPa. Conventionally, the CAPC has not been suitable for measurements that require a magnetic field due to its large body size. In fact, the CPAC has been used mainly for resistivity or alternating-current susceptibility and recently for neutron-scattering measurements at zero field [3].

We have fabricated the smallest PCAC to date using $\phi 60$ NiCrAl guide blocks and investigated pressure homogeneity from ^{63}Cu nuclear-quadrupole-resonance (NQR) linewidth of Cu_2O . The NQR frequency is proportional to the electric field gradient at a ^{63}Cu site and the spectral shape is sensitive to local disorder or inhomogeneity. Therefore, the NQR measurements are available for investigating hydrostaticity inside the pressure cell.

Figure 1(a) shows a sectional view of the CAPC, and Fig. 1(b) shows a bird's-eye view of three WC anvils mounted on the $\phi 60$ NiCrAl guide block. The four WC anvils are fitted in the NiCrAl sliding blocks covered with Teflon sheets. The four anvils move toward the 6.0-mm pyrophyllite cube without friction when the load is imposed on the NiCrAl guide blocks. The cube is made of lower and upper pyrophyllite gaskets and contains a $\phi 3.0$ Teflon capsule (see the inset of Fig. 2(a)). A single coil wound around Cu_2O power samples is inserted into the Teflon capsule filled

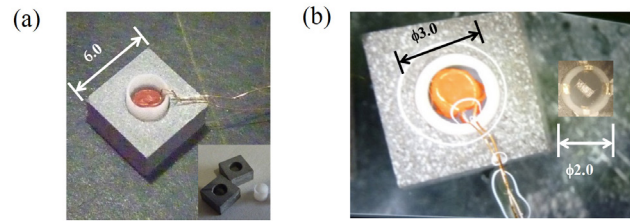


Fig. 2. (a) Bird's-eye view of a $\phi 3.0$ Teflon capsule mounted on a pyrophyllite gasket. A nuclear-quadrupole-resonance (NQR) coil wrapped around powder samples of Cu_2O is inserted into the capsule. The inset shows upper and lower gaskets and a Teflon capsule. (b) Overview of the $\phi 3.0$ Teflon capsule on the gasket. The inset shows the $\phi 2.0$ Teflon capsule used for the resistivity measurements.

with pressure transmitting media, the mixture of fluorinate FC-70 and FC-77 (see Fig. 2(a)). An overview of the $\phi 3.0$ Teflon capsule on the gasket is shown in Fig. 2(b). The Teflon capsule has a $\phi 2.5 \times 1.5$ mm sample space and is significantly larger than that used for conventional resistivity measurements (see the inset of Fig. 2(b)).

Figure 3(a) shows the ^{63}Cu -NQR spectra of Cu_2O measured at room temperature with a conventional spectrometer and the $\phi 60$ CAPC. The spectra were obtained using the fast Fourier transform of the spin-echo signal. Figure 3(b) shows the pressure dependence of the NQR linewidth. The linewidth for the CAPC is compared with that for the PCPC. The NQR spectra for the PCPC exhibited double-peaks structure above 2 GPa [1], and the data below 2 GPa were plotted in Fig. 3(b). The linewidth for the PCPC increases with increasing pressure above 0.8 GPa where the mixture of the FC-70 and FC-77 begins to freeze, whereas that for the CAPC saturates at high pressures above 4 GPa. The pressure homogeneity for the CAPC is better than that for the PCPC in a high-pressure regime. This result suggests that pressure application from multiple directions suppress the inhomogeneity much more effectively than uniaxial pressure application.

In conclusion, we have fabricated a CAPC having a diameter of 60 mm, the smallest cubic-anvil cell to date, which allowed us to measure physical properties under a magnetic field utilizing a superconducting magnet with a large-bore sample space greater than 100 mm. In this pressure cell, a large sample space having $\phi 2.5 \times 1.5$ mm was secured. This pressure cell would open a new avenue for the quest for novel pressure-induced phenomena in strongly correlated systems.

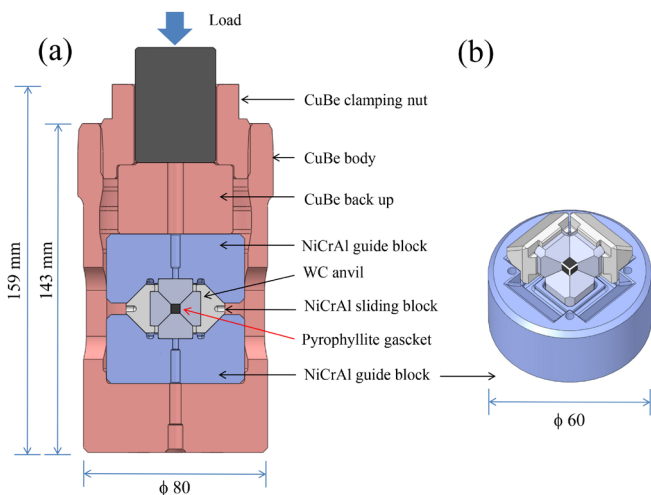


Fig. 1. (a) Sectional view of a cubic anvil pressure cell (CAPC) with $\phi 60$ NiCrAl guide blocks. (b) A bird's-eye view of three WC anvils and a pyrophyllite cube mounted on the lower NiCrAl guide block.

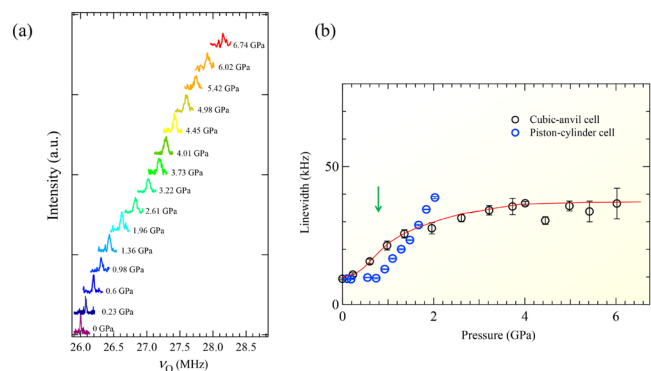


Fig. 3. (a) ^{63}Cu -NQR spectra of Cu_2O measured with the CAPC at room temperature. (b) Half width at half maximum of the NQR spectra measured using the CAPC (black open circles) and NiCrAl piston-cylinder pressure cell (blue open circles). The curve is a guide for the eye.

References

- [1] S. Nakagawa, J. Gochi, T. Kuwayama, S. Nagasaki, T. Takahashi, J. Cheng, Y. Uwatoko, and N. Fujiwara, *Rev. Sci. Instru.* **91** 073907 (2020).
 [2] N. Fujiwara and Y. Uwatoko, *Butsuri* **76** 295 (2021).
 [3] S. E. Dissanayake, M. Matsuda, K. Munakata, H. Kagi, J. Gouchi, and Y. Uwatoko, *J. Phys.: Condens. Matter* **31** 384001 (2019).

Authors

N. Fujiwara^a and Y. Uwatoko
^aKyoto University

Magnetolectric Effect in the Antiferromagnetic Ordered State of Ce₃TiBi₅ with Ce zig-zag Chains

M. Shinozaki, G. Motoyama, and Y. Uwatoko

Some magnetoelectric effects, including the Edelstein effect, often occur in the materials without some inversion symmetry. Materials exhibiting such cross-correlation are expected as various new functional materials. Recently, a new magnetoelectric effect is attracting attention in the metallic antiferromagnetic compound, in which the spatial inversion symmetry is broken at the magnetic site. This new cross-correlation is understood as a phenomenon that appears as a result of the realization of odd parity multipole [1, 2].

We discovered a new antiferromagnetic heavy fermion compound Ce₃TiBi₅ in which the local inversion symmetry at cerium site is broken (Figs. 1(a) and (b)). The crystal structure of Ce₃TiBi₅ is *P6₃/mcm*, and the global inversion symmetry is maintained. Therefore, the current-induced magnetization phenomenon in the sense of the Edelstein effect does not occur. Ce₃TiBi₅ has only one cerium site, and the cerium forms zigzag chains along the *c*-axis. The antiferromagnetic ordering temperature of T_N is 5.0 K, electrical resistivity, magnetic susceptibility, and specific heat show a

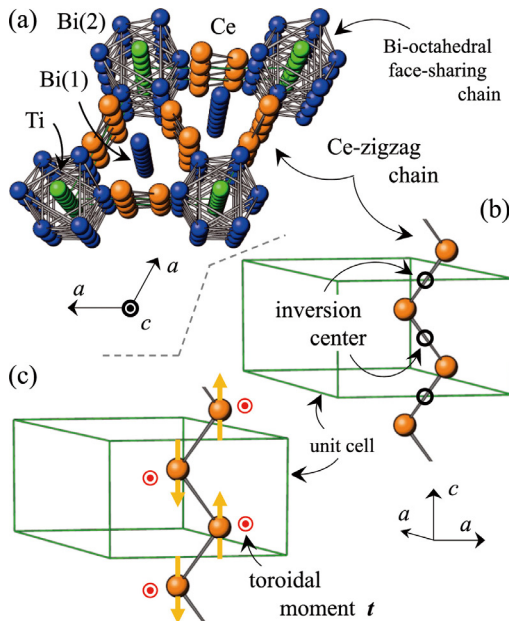


Fig. 1. (a) Top view of the crystal structure of Ce₃TiBi₅. (b) Schematic side view of the crystal structure, where only Ce ions on a front side are drawn for clarity. Green line denotes a unit cell. Black circles indicate the position of the inversion center. (c) Magnetic structure on the Ce-zigzag chain, where the unit cell does not change even at the ordered state. Orange arrows on the Ce ions indicate the expected magnetic moments below T_N . The red mark denotes a toroidal moment on a Ce ion at the ordered state, which is a candidate as a realized odd multipole state on Ce₃TiBi₅.

distinct anomaly, respectively. Some odd parity multipoles are expected in the antiferromagnetic state, although the magnetic structure has not yet been determined (Fig. 1(c)).

We performed the magnetization measurements with applying several constant electric currents parallel to the *c*-axis of Ce₃TiBi₅ at around T_N using commercial magnetometer of MPMS. In this measurement, slight static magnetic field was applied to determine the sample position. Current-induced magnetization (M_{ME}) was obtained from subtracting magnetization induced by applying slight static magnetic field and zero electric current as blank magnetization.

We have succeeded in measuring the current-induced magnetization only on the antiferromagnetic state [3, 4]. Figure 2(a) shows the temperature (T) dependence of M_{ME} on Ce₃TiBi₅. It is found that $M_{ME}(T)$ starts to appear just below T_N with decreasing T , although it is almost independent of temperature and is approximately zero above T_N . This T dependence was also observed at several electrical current (i), and then we show plots of M_{ME} versus i at 3.0 K in Fig. 2(b) to discuss the i dependence of the magnitude of M_{ME} . M_{ME} shows the linear i dependence, which suggests that M_{ME} on Ce₃TiBi₅ linearly increases with an increase in the electric field.

Next, T dependence of M_{ME} at several magnetic field (H) is shown in Fig. 2(c). $M_{ME}(T)$ exhibits an identical curve despite a difference in the magnitude of H . The magnitude of M_{ME} at each magnetic field and $T = 3.0$ K was decided from the $M_{ME}(T)$ at several magnetic fields ($5 \leq H \leq 40$ Oe) and is plotted in Fig. 2(d). The magnitude of M_{ME} is independent of H in this field range, which indicates that M_{ME} has a similar value even in zero magnetic field.

The current-induced magnetization was observed only below the antiferromagnetic transition temperature of 5.0 K. This current-induced magnetization exhibits linear dependence with respect to the DC electric current and demonstrates little dependence on the magnetic field, i.e., the behavior persists even in zero magnetic field. Based on these

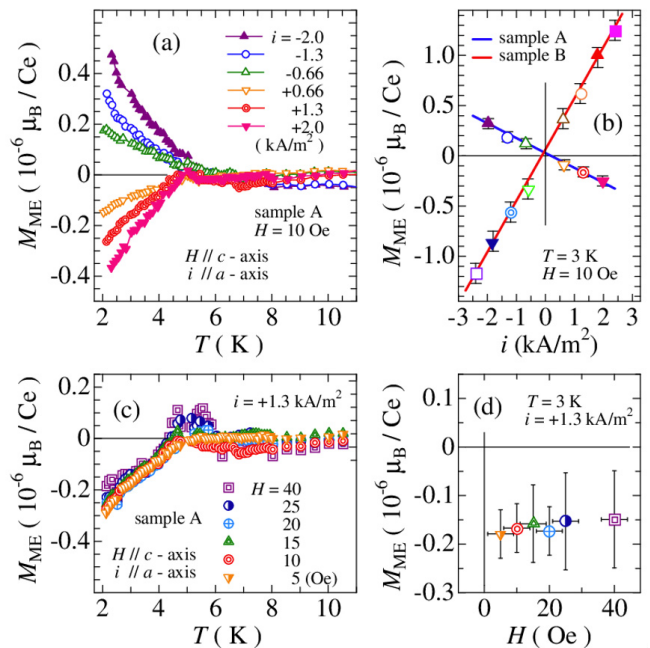


Fig. 2. (a) Comparison of the T dependence of the M_{ME} between several i for sample A. (b) i dependences of M_{ME} at 3 K for samples A and B. (c) Comparison of the T dependence of M_{ME} between different H . (d) H dependence of M_{ME} at 3 K.

results, we suggest that the current-induced magnetization originated from the magnetoelectric effect of the odd multipole state on the Ce-zigzag chain structure. Meanwhile, the sign and magnitude of the slope of i dependence of M_{ME} has large sample dependence as shown in Fig. 2(b). We consider the sample dependence to be explained by the imbalance of the domain structure of the AFM state. However, we do not know what kind of domain structure is realized in the antiferromagnetic state. We are conducting experiments with an interest in the consistency between the realized odd parity multipole state on Ce_3TiBi_5 and the current-induced magnetization measurements with various geometry.

References

- [1] S. Hayami, H. Kusunose, and Y. Motome, Phys. Rev. B **90**, 024432 (2014).
- [2] H. Saito, K. Uenishi, N. Miura, C. Tabata, H. Hidaka, T. Yanagisawa, and H. Amitsuka, J. Phys. Soc. Jpn. **87**, 033702 (2018).
- [3] M. Shinozaki, G. Motoyama, M. Tsubouchi, M. Sezaki, J. Gouchi, S. Nishigori, T. Mutou, A. Yamaguchi, K. Fujiwara, K. Miyoshi, and Y. Uwatoko, J. Phys. Soc. Jpn. **89**, 033703 (2020).
- [4] H. Saito, H. Amitsuka, G. Motoyama, and M. Shinozaki, Solid State Physics 55, 611 (2020).

Authors

M. Shinozaki^a, G. Motoyama^a, J. Gouchi, S. Nishigori^a, T. Mutou^a, A. Yamaguchi^b, K. Fujiwara^a, K. Miyoshi^a, and Y. Uwatoko

^aShimane University
^bUniversity of Hyogo

High Precision Study of the Anderson Transition

T. Ohtsuki and K. Slevin

More than six decades have passed since Anderson's seminal paper on localization. During the subsequent decades, there have been numerous important discoveries including weak localization, universal conductance fluctuations, and the scaling theory of localization. Since the proposal of the scaling theory, determining the critical behavior of the localization-delocalization transition, which is usually referred to as the Anderson transition (AT), has continued to attract considerable attention.

One of the most widely used approaches to study the AT quantitatively is to calculate the Lyapunov exponents (LE's) and to analyze them using finite size scaling. Large scale computations using the supercomputer System B at ISSP have enabled us to calculate LE's with high precisions for very large system sizes. We consider a system of size $L_x \times L \times L$, which we divide into layers of an $L \times L$ square. The transfer matrix M relates the wave functions on the 1st layer to L_x th layer, and the LE's are the eigenvalues of the matrix $\Omega = \lim_{L_x \rightarrow \infty} \ln(M^\dagger M)/2L_x$. From the smallest positive LE, γ , we define a quantity $\Gamma = \gamma L$.

The conventional method requires the simulation of a single very long sample. While this method has been employed very successfully in numerous simulations over the preceding decades [1], the calculations are inherently serial and do not allow us to take advantage of massively parallel computing. We devised an alternative method to simulate an ensemble of much shorter samples and take an ensemble average, allowing us to make full use of System B.

We have analyzed the LE's using finite size scaling, and estimated the critical exponent for the divergence of the correlation length, $\nu = 1.572$ [1.566,1.577] for three dimensional (3D) Anderson model of localization [1,2],

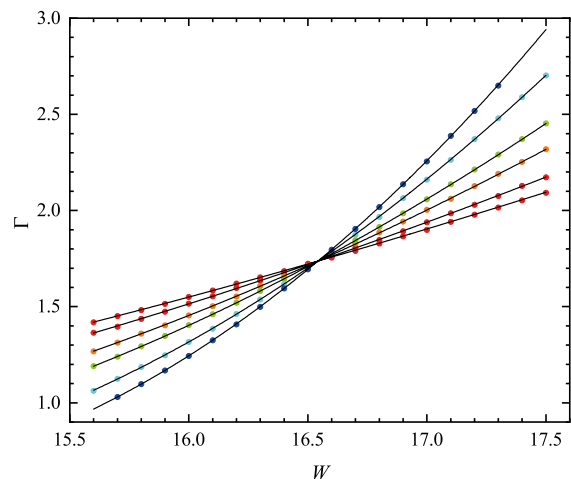


Fig. 1. Γ as a function of the disorder strength W in the 3D Anderson model of localization for various cross section size $L = 12, 18, 24, 32, 48$ and 64 . $L = 96$ is underway using new System B.

$H = \sum_i \varepsilon_i |i\rangle\langle i| - \sum_{\langle i,j \rangle} |i\rangle\langle j|$, where ε_i is the onsite random potential distributed uniformly in $[-W/2, W/2]$. We fit the W and L dependence of Γ using finite size scaling (Fig. 1).

The critical exponent changes when a magnetic field is applied. This can be realized by inserting Peierls phase in the nearest neighbor transfer. We obtain $\nu = 1.443$ [1.437,1.449] which is distinctly different from the case without a magnetic field [3].

At the critical point, the wave functions exhibit multifractality, hence the local density of states fluctuates significantly. If we consider dilute magnetic impurities, the Kondo temperature T_K varies from one magnetic impurity to another due to the large fluctuations of wave functions (Fig. 2). We have calculated the local density of states at the critical point using the kernel polynomial method and calculated the Kondo temperature distribution [4]. The massively parallel calculations on System B enabled us to reach the small T_K needed to check the analytic prediction.

In addition to the cases of Anderson's model of localization with and without magnetic fields, depending on whether we have spin-rotation symmetry, chiral symmetry as well as particle-hole symmetry, we have 10 symmetry classes for random quantum systems. In recent years, the non-Hermitian systems with randomness, which are classified into 38 symmetry classes, are attracting renewed interests. We have studied the critical behaviors of AT with chiral

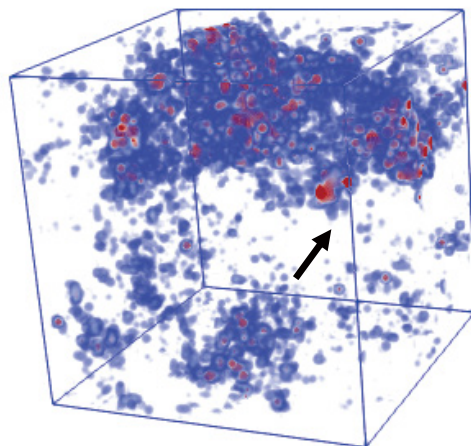


Fig. 2. Schematic of a magnetic impurity and a multifractal wave function.

and/or particle-hole symmetries [5], and most of the critical exponents for the AT in 3D are now determined. In addition, we have verified that the transfer matrix method and the finite size scaling work for non-Hermitian systems. We are now studying the localization-delocalization transition for non-Hermitian systems [6,7] and determining the critical exponents, which might explain the critical behavior of light localization.

References

- [1] K. Slevin and T. Ohtsuki, New J. Phys. **16**, 015012 (2014).
- [2] K. Slevin and T. Ohtsuki, J. Phys. Soc. Jpn. **87**, 094703 (2018).
- [3] K. Slevin and T. Ohtsuki, J. Phys. Soc. Jpn. **85**, 104712 (2016).
- [4] K. Slevin, S. Kettemann, and T. Ohtsuki, Eur. Phys. J. B **92**, 281 (2019).
- [5] X. Luo, B. Xu, T. Ohtsuki, and R. Shindou, Phys. Rev. B **101**, 020202 (2020).
- [6] X. Luo, T. Ohtsuki, and R. Shindou, Phys. Rev. Lett. **126**, 090402 (2021).
- [7] X. Luo, Z. Xiao, K. Kawabata, T. Ohtsuki, and R. Shindou, arXiv:2105.02514.

Authors

T. Ohtsuki^a and K. Slevin^b

^aSophia University

^bOsaka University

Spin Waves in the Two-Dimensional Honeycomb Lattice XXZ-Type van der Waals Antiferromagnet CoPS₃

C. Kim, J. G. Park and T. Masuda

The recent introduction of magnetic van der Waals (vdW) materials has opened new and novel opportunities to examine the low-dimensional magnetism in real materials. In particular, *TMPS*₃ (*TM* = Mn, Fe, Co, Ni) family has attracted special interests in the community as a class of antiferromagnetic 2D vdW materials. The crystal structure of *TMPS*₃ is a monoclinic structure with a *C* 2/*m* space group, where a weak vdW force couples honeycomb layers with edge-shared *TMS*₆ octahedra on the *ab*-plane along the *c*-axis. Since magnetic structure and exchange interactions in *TMPS*₃ depend on the *TM* elements, they provide an excellent playground to validate spin dynamics theory in low dimensions experimentally.

CoPS₃ has been less studied among them due to the difficulty in synthesizing high-purity samples [1]. Therefore, the magnetic Hamiltonian of CoPS₃ has been unknown so far and needs investigation. CoPS₃ has antiferromagnetic phase transition at $T_N = 122$ K with zig-zag magnetic order. The spins are aligned along the *a* axis with a small canting to the *c* axis. The magnetic susceptibility shows a difference between $H \parallel ab$ and $H \parallel c$ in the paramagnetic state, which implies XY-like anisotropy [1].

Moreover, Co²⁺ magnetic systems have recently drawn significant attention because Co compounds may host Kitaev interactions [2]. A spin-orbital entangled state is an essential ingredient to realize the Kitaev interactions, which can be verified by measuring spin excitations. Typically, a spin-orbital exciton, the crystal field excitation between $J_{\text{eff}} = 1/2$ to $3/2$ state, is strong evidence of a spin-orbital entangled state. Most cobalt compounds have such excitation at 20~30meV, proportional to the strength of spin-orbit coupling of cobalt [3].

In this study [4], we examined such a possibility using inelastic neutron scattering at the time-of-flight

spectrometer of HRC at J-PARC. Our temperature-dependent measurements show that CoPS₃ does not show the spin-orbital exciton expected near 30 meV at high temperature in stark contrast with initial expectations. Figure 1 shows the temperature dependence of magnetic excitations. Above $T_N = 122$ K, there is no sign of excitations near 30 meV. This can only be interpreted as evidence for the ground state of CoPS₃ being an $S = 3/2$ state, not the spin-orbital entangled $J_{\text{eff}} = 1/2$ state. Figure 2 shows the spin-wave spectrum of CoPS₃ with incident neutron energy $E_i = 71$ meV. The measured spin-wave spectrum shows two magnon branches over 40 meV with a massive 13 meV spin gap. Also, the spin-wave spectrum shows extra gap-like features at 24~27 meV. Based on the former analysis about temperature dependence of magnetic excitations, we use magnetic Hamiltonian with $S = 3/2$ system to explain the spin-waves of CoPS₃. This magnon was well-fitted using an anisotropic Heisenberg (XXZ) model with a reasonable anisotropy coefficient $\alpha \equiv J_z/J_x = 0.6$ and strong easy-axis single-ion anisotropy $K = 2.4$ meV along the *a*

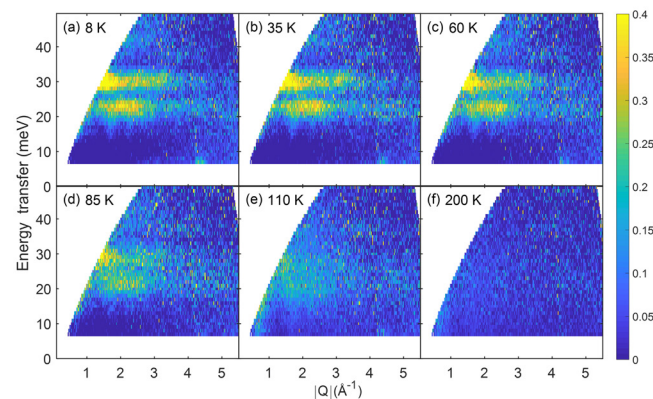


Fig. 1. (a-f) Magnon spectra of CoPS₃ at different temperatures with $E_i = 71.3$ meV.

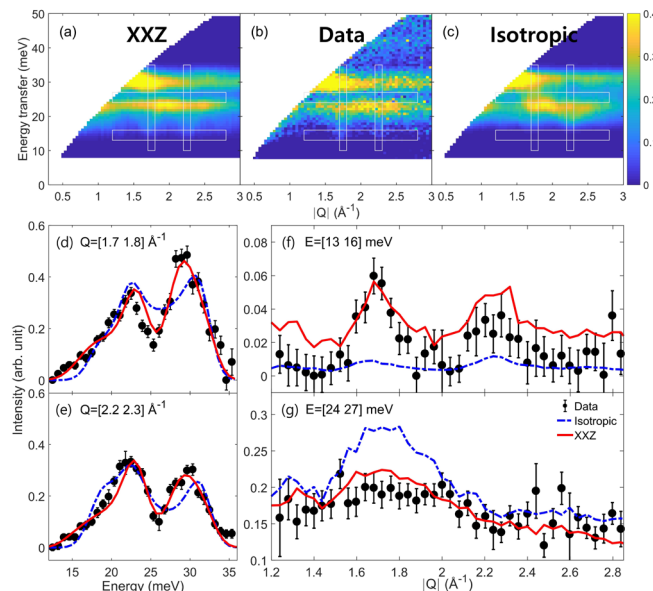


Fig. 2. The experimental INS data of CoPS₃ measured at $T = 8$ K with $E_i = 71.3$ meV is shown in (b). (a), (c) The best-fit magnon spectra with the XXZ model and the isotropic Heisenberg model. An instrumental energy resolution of 3 meV was used to convolute the theoretical results shown in (a) and (c). Horizontal and vertical white boxes denote the integration range for the constant-*E* and constant-*Q* cuts in (d-g), respectively. (d), (e) Constant-*Q* cut at the momentum range of $Q = [1.7\ 1.8]$ and $Q = [2.2\ 2.3]$ Å⁻¹ for the measured data with the best-fit simulations. (f), (g) Constant-*E* cut with the energy range of $E = [13\ 16]$ and $E = [24\ 27]$ meV

axis. The magnetic structure from our magnetic Hamiltonian also consistent with the reported magnetic structure. In summary, our experiment and theoretical analysis suggest CoPS₃ as another exciting platform to study anisotropic XXZ-type spin Hamiltonian in the honeycomb antiferromagnet. Moreover, it provides an excellent playground for future investigation of low-dimensional magnetism with magnetic van der Waals materials.

References

- [1] A. R. Wildes *et al.*, *J. Phys.: Condens. Matter* **29**, 455801 (2017).
- [2] H. Liu *et al.*, *Phys. Rev. B* **97**, 014407 (2018).
- [3] K. Tomiyasu *et al.*, *Phys. Rev. B* **84**, 054405 (2011).
- [4] C. Kim *et al.*, *Phys. Rev. B* **102**, 184429 (2020).

Authors

C. Kim^a, J. Jeong^a, P. Park^a, T. Masuda, S. Asai, S. Itoh^b, H. S. Kim^c, A. Wildes^d, and J. G. Park^a
^aSeoul National University
^bKEK
^cKangwon National University
^dInstitut Laue-Langevin

Quantum Spin Liquid State in a Square-Kagome Antiferromagnet

M. Fujihala, K. Morita, and T. Masuda

New insight into the spin behavior in an exotic state of matter puts us closer to next-generation spintronic devices. The quantum spin liquid (QSL) state is an exotic state of magnet where the spin of electrons, which generally exhibits order at low temperatures, remains disordered. Observation of a QSL state is one of the most important goals in condensed-matter physics. However, the QSL state in two-dimensional (2D) systems has not been clearly observed in real materials owing to the presence of site-mixing disorder or deviations from ideal models. The lack of a suitable model material exhibiting the QSL hinders observations of the QSL state in the 2D spin-1/2 systems.

Square-kagome lattice (SKL) magnet is known as the highly frustrated 2D system. There is a possibility that the QSL ground states are realized in the antiferromagnetic $S = 1/2$ Heisenberg model on SKL [1]. However, the lack of a model compound for the SKL system has obstructed a deeper understanding of its spin state. Motivated by the present status on the study of the SKL system, we

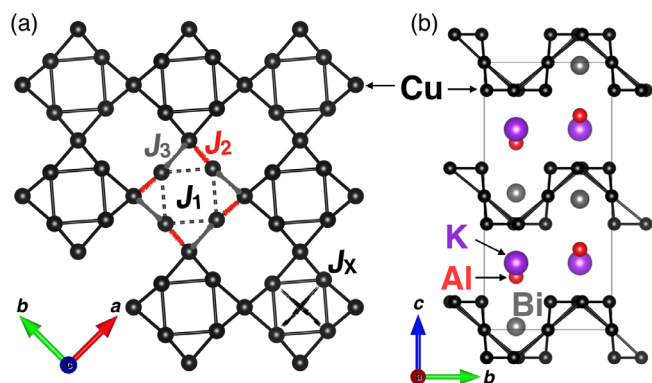


Fig. 1. (a) Crystal structure of $\text{KCu}_6\text{AlBiO}_4(\text{SO}_4)_5\text{Cl}$. Square-kagome lattice consisting of the Cu^{2+} ions with nearest-neighbor exchange couplings J_1 , J_2 , J_3 and next-nearest-neighbor exchange coupling J_x . (b) Crystal structure of $\text{KCu}_6\text{AlBiO}_4(\text{SO}_4)_5\text{Cl}$ featuring a large inter-layer spacing.

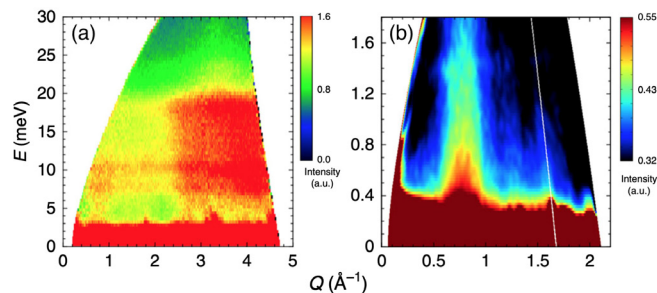


Fig. 2. (a) INS spectra at 5 K observed using HRC with an incident neutron energy of 45.95 meV. (b) INS spectra at 0.3 K observed using AMATERAS with incident neutron energy of 3.14 meV.

searched for compounds with the SKL containing Cu^{2+} spins, and synthesized the first compound of a SKL antiferromagnet, $\text{KCu}_6\text{AlBiO}_4(\text{SO}_4)_5\text{Cl}$, successfully [2]. As shown in Fig. 1(a), the SKL in the crystal structure of $\text{KCu}_6\text{AlBiO}_4(\text{SO}_4)_5\text{Cl}$ comprises the Cu^{2+} ions. In each SK unit, the square is enclosed by four scalene triangles. From this crystal structure, it is recognized that $\text{KCu}_6\text{AlBiO}_4(\text{SO}_4)_5\text{Cl}$ has three types of first neighbor interactions, J_1 , J_2 and J_3 , as shown in Fig. 1(a). By comprehensive experimental studies via magnetic susceptibility, magnetization, heat capacity, and muon spin relaxation, we confirm that the absence of magnetic long-range order down to 58mK, roughly three orders of magnitude lower than the NN interactions.

The quantum statistics of quasiparticle excitations depend on the type of QSL, in particular, the nature of their excitation. To grasp the whole picture of the spin excitation, we performed the inelastic neutron scattering (INS) experiments using the high-resolution chopper spectrometer HRC and cold-neutron disk chopper spectrometer AMATERAS installed in the MLF at J-PARC. As shown in Fig. 2(a), flat signals at around $E = 10$ and 7 meV are observed at 5 K. The signal due to magnetic excitation is generally enhanced at low- Q values, whereas phonon excitation is dominant at high- Q . The signals at around 10 and 7 meV increase with decreasing with Q , indicating that it comes from magnetic excitation. As shown in Fig. 2(b), streak-like excitation at $Q = 0.8, 1.25,$ and 1.58 \AA^{-1} is clearly visible down to the elastic line, and its intensity increases continuously without signature of energy gap at least within the instrumental resolution. These INS data are consistent with a gapless continuum of spinon excitations. From the above, the flat signals at 10 and 7 meV probably indicate a van Hove singularity of spinon continuum edges at this energy.

Our experimental results strongly suggest the formation of a gapless QSL in $\text{KCu}_6\text{AlBiO}_4(\text{SO}_4)_5\text{Cl}$ at very low temperature close to the ground state; however, they are inconsistent with the theoretical studies based on the J_1 - J_2 - J_3 SKL Heisenberg model. We calculate the dynamical spin structure factor $S(\mathbf{q}, \omega)$ in the SKL model with various values of the parameters, but we could not reproduce the INS experimental results. Therefore, in order to realize the QSL state in the SKL, we must impose an additional condition such as longer-range exchange interactions. Further experimental and theoretical study would reveal the conditions inducing the QSL state in SKL antiferromagnets.

References

- [1] K. Morita *et al.*, *J. Phys. Soc. Jpn.* **87**, 043704 (2018).
- [2] M. Fujihala *et al.*, *Nat. Commun.* **11**, 3429 (2020).

Authors

M. Fujihala^a, K. Morita^a, R. A. Mole^b, S. Mitsuda^a, T. Tohyama^a, S.

Two-step Magnetic Anomaly in the High Field Magnetization Process in $\text{Yb}_{1+x}\text{In}_{1-x}\text{Cu}_4$

S. Yamanaka, A. Matsuo, and C. Michioka

The intermetallic compound YbInCu_4 exhibits a first-order valence transition at 42 K under ambient pressure; Ytterbium ions have trivalent local moments in the high-temperature phase, and they become a mixed-valence state of an average valence of 2.9 in the low-temperature phase [1, 2]. In addition, a magnetic field-induced valence transition also occurs below 42 K with the transition field of ~ 30 T [3, 4]. To clarify the mechanism of the valence transition, substitution effects in Yb or In site have been extensively studied [3, 5]. Although this system was originally discovered as a solid solution RCu_2 without site-ordering, there are few reports on the substitution of In site by Yb itself on YbInCu_4 . In this study, the magnetic and transport properties of $\text{Yb}_{1+x}\text{In}_{1-x}\text{Cu}_4$ are investigated using polycrystalline samples synthesized by the arc melting method, and the magnetic phase diagram in $\text{Yb}_{1+x}\text{In}_{1-x}\text{Cu}_4$ is investigated.

Figure 1 shows the temperature dependence of the magnetic susceptibility χ of $\text{Yb}_{1+x}\text{In}_{1-x}\text{Cu}_4$ measured in a magnetic field of 1 T. In a parent material, $\text{Yb}_{1.01}\text{In}_{0.99}\text{Cu}_4$, χ rapidly decreases below 42 K due to decrease in the effective valence of Yb ion from trivalent, which is consistent with the previous report [1]. The sharp magnetic anomaly accompanied by the valence transition in $\text{Yb}_{1.01}\text{In}_{0.99}\text{Cu}_4$ seems to change to a broad shape and shift to a higher temperature with increasing x . In all compositions, χ s obey the Curie-Weiss law above 150 K, and the values of the effective magnetic moment estimated from Curie-Weiss fits roughly agree with the calculated value for free Yb^{3+} ion, $4.54 \mu_B$. This fact confirms that the valence state of Yb ions in the high-temperature phase is trivalent.

Figure 2 shows the temperature dependence of the

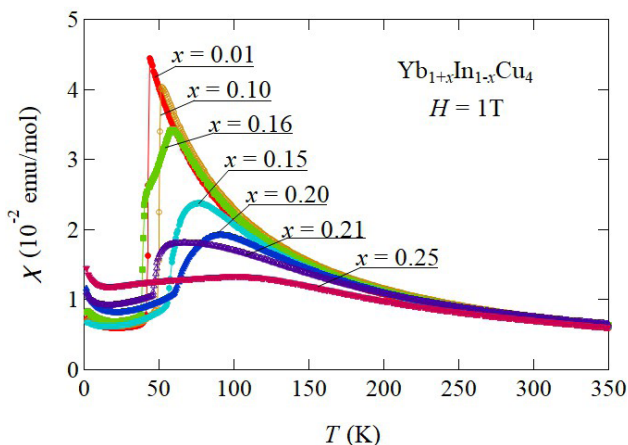


Fig. 1. Temperature dependence of the magnetic susceptibility χ of $\text{Yb}_{1+x}\text{In}_{1-x}\text{Cu}_4$ measured in a field of 1 T.

electrical resistivity ρ of $\text{Yb}_{1+x}\text{In}_{1-x}\text{Cu}_4$. In all compositions, ρ rapidly decreases below the valence transition temperature due to decrease in magnetic scattering accompanied by decrease in the localized moment of Yb^{3+} . The valence transition temperature seems to shift to higher temperature with increasing x , consistent with behaviors of χ . For $x = 0.21$ and $x = 0.25$, ρ reaches a minimum value at approximately 40 K and then increases with decreasing temperature. These behaviors are typical in a metallic state with an impurity-Kondo-effect in which ρ shows $-\ln T$ dependence. It is natural to think that in the Yb-rich phase such as $x = 0.21$ or 0.25, all the Yb ions could not behave homogeneously and a part of Yb ions remain trivalent with an impurity moment.

Figure 3 shows the magnetization curve of $\text{Yb}_{1+x}\text{In}_{1-x}\text{Cu}_4$ measured at 4.2 K up to 72 T. For $x = 0.16, 0.15$, and 0.20, two-step magnetic anomalies are observed in the high field magnetization process. If this originates from phase separation, three or more steps would frequently appear. However, no such a behavior was observed in the results of more than 20 samples. In addition, the magnetization value for $x = 0.16, 0.15$, and 0.20 reaches $2 \mu_B$ after the first step and reaches $4 \mu_B$ after the second step. The fact that the similar behavior was observed in all three compounds suggests that the magnetic moments of the plateaux may be meaningful. Although the changes in the magnetic transition field by substitutions in YbInCu_4 have been reported, their magnetic transitions are all one step. The present observation of a successive phase transition in this system is the first time. The temperature dependences of χ and ρ do not show a behavior corresponding to the two-step anomaly. An intermediate phase is induced only by the magnetic field. The degen-

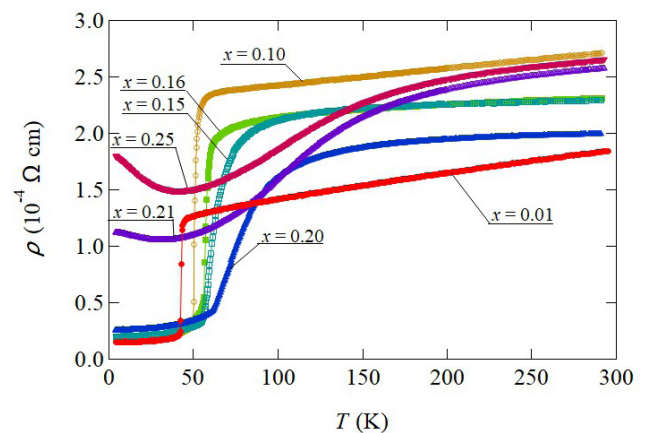


Fig. 2. Temperature dependence of the electrical resistivity ρ of $\text{Yb}_{1+x}\text{In}_{1-x}\text{Cu}_4$.

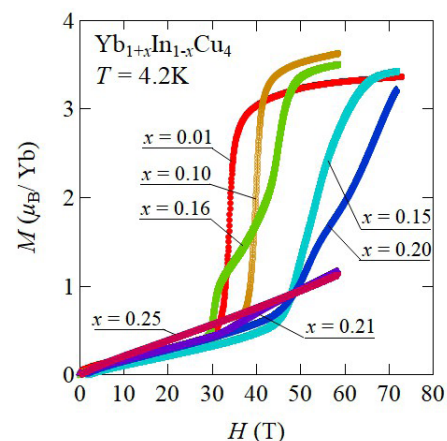


Fig. 3 Magnetization curves M - H of $\text{Yb}_{1+x}\text{In}_{1-x}\text{Cu}_4$ measured at 4.2 K up to 72 T.

erated ground state of Yb^{3+} ($^2F_{7/2}$) is split by the crystal electric field (CEF) effects, and each state has a different saturation magnetization. In $x = 0.16, 0.15,$ and $0.20,$ the lower transition field induces the trivalent state however the magnetic moment is limited by CEF. Subsequently in the higher transition field, the Zeeman-energy exceeds CEF and induces a full saturation magnetization of Yb^{3+} of $4 \mu_B$. For $x = 0.01$ and $0.10,$ the magnetization reaches about $4 \mu_B$ in a one-step transition without an intermediate phase. This is probably because CEF of small substituted compounds is smaller than the magnetic transition field which induces the trivalent state.

In conclusion, we discovered the successive magnetic transition in the magnetization process in $\text{Yb}_{1+x}\text{In}_{1-x}\text{Cu}_4$ ($x = 0.15, 0.16,$ and 0.20) and proposed that it originates from competition and corporation of the Zeeman energy, CEF effect and magnetic interactions.

This study was selected for the 22nd distinguished paper award sponsored by Japan Society of Powder and Powder Metallurgy.

References

- [1] I. Felner and I. Nowik, *Phys. Rev. B* **33**, 617 (1986).
- [2] B. Kindler, D. Finsterbusch, R. Graf, F. Ritter, W. Assmus, and B. Lüthi, *Phys. Rev. B* **50**, 704 (1994).
- [3] K. Yoshimura, T. Nitta, M. Mekata, T. Shimizu, T. Sakakibara, T. Goto, and G. Kido, *Phys. Rev. Lett.* **60**, 851 (1988).
- [4] T. Shimizu, K. Yoshimura, T. Nitta, T. Sakakibara, T. Goto, and M. Mekata, *J. Phys. Soc. Jpn.* **57**, 405 (1988).
- [5] J. He, N. Tsujii, M. Nakanishi, K. Yoshimura, and K. Kosuge, *J. Alloys Compd.* **240**, 261 (1996).

Authors

S. Yamanaka^a, T. Nakahigashi^a, C. Michioka^a, H. Ueda^a, A. Matsuo, K. Kindo, and K. Yoshimura^a
^aKyoto University

Origin of Inverse Magnetocaloric Effects in Ni-Mn-based Heusler Alloys

T. Kihara, X. Xu, and M. Tokunaga

The development of heat-exchange systems using the magnetocaloric effect is a topic where material science can solve energy problems. The magnetocaloric effect has long been used to realize ultra-low temperature using the adiabatic demagnetization procedure. This effect was recently expected for heat exchangers with higher efficiency than conventional gas-compression/expansion systems [1]. However, most of the materials that exhibit significant magnetocaloric effect contain heavy rare-earth elements, so that the high cost of the materials hinders their practical use. We have studied thermodynamic properties of Heusler alloys without rare-earth elements to realize the giant magnetocaloric effect involving the entropy of the lattice and electronic systems [2-5].

Ni-Mn-based Heusler alloys have attracted considerable attention as magnetic shape memory alloys [6]. In our previous work on Ni-Co-Mn-In alloys, we directly observed prominent negative magnetocaloric effects at the field-induced phase transitions from paramagnetic martensite to ferromagnetic austenite phase. From the systematic high-field studies of magnetocaloric effect, magnetization, heat capacity, and microscopy, we concluded that this effect originated from the increase of lattice entropy associated with the structural phase transition [2].

In the present study, we measured the magnetization,

magnetocaloric effect, and magnetostriction of Ni-Co-Mn-Ga alloys in pulsed high magnetic fields up to 56 T [4, 5]. As shown in Fig. 1(a), metamagnetic transitions similar to those in the Ni-Co-Mn-In alloy were observed in this material. Magnetostriction measured on a polycrystalline sample using the capacitance method [7] showed a significant lattice distortion associated with this transition [Fig. 1(b)], suggesting that this magnetic transition is accompanied by a structural phase transition from the martensite to the austenite phase.

The change in the sample temperature at the magnetic field-induced phase transition shows a negative magnetocaloric effect, as shown in Fig. 2. In contrast to the Ni-Co-Mn-In alloy, the negative magnetocaloric effect shows up even after completing the field-induced magnetic and structural transition. The experimental results of heat capacity and theoretical results of first-principles calculation show that the electronic specific heat coefficient increases significantly at the transition to the austenite phase: the entropy of the electron system plays an essential role in the magnetocaloric effect of this system. The increase in lattice and electronic entropy associated with the magnetic field-induced phase transition dominates over the decrease in the spin entropy change, which shows up as a negative magnetocaloric effect that decreases the sample temperature in a magnetic field. If we can incorporate these entropy changes in the same sign, we expect magnetocaloric effects beyond the limit of the spin system. Microscopic discussion in the present study will pave the way for this giant magnetocaloric effect.

Most of the previous studies on magnetocaloric materials have focused on their properties in the magnetic field region below 5 T. In the future society where hydrogen energy and high-temperature superconducting cables are put to practical use. In this situation, large-scale application of the magneto-

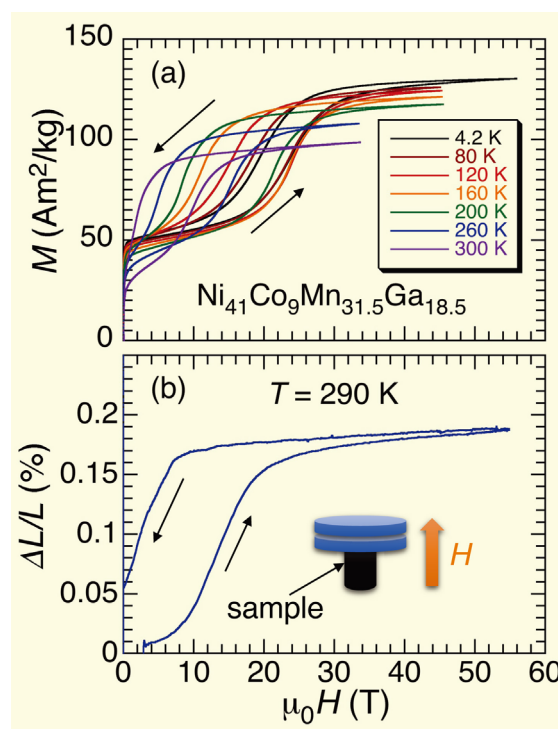


Fig. 1. (a) Field-dependence of magnetization in a polycrystal of $\text{Ni}_{41}\text{Co}_9\text{Mn}_{31.5}\text{Ga}_{18.5}$ at several temperatures. Steep increase in magnetization indicates emergence of metamagnetic transitions. (b) Longitudinal magnetostriction of $\text{Ni}_{41}\text{Co}_9\text{Mn}_{31.5}\text{Ga}_{18.5}$ measured at 290 K. The inset shows schematics of the capacitance method. Prominent increase of the sample length corresponds to the structural transition from the martensite to the austenite phase simultaneously with the metamagnetic transition.

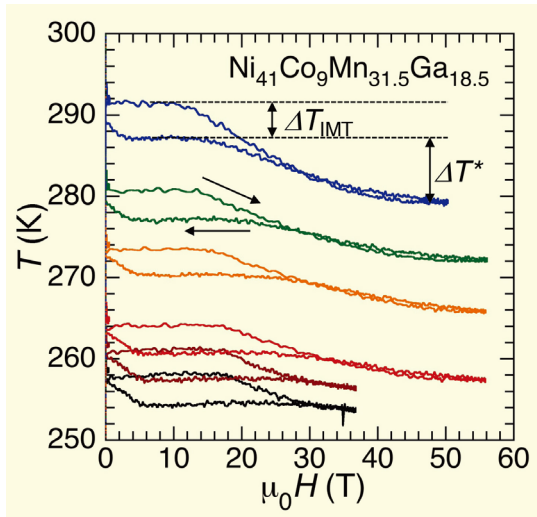


Fig. 2. Magnetocaloric effect of $\text{Ni}_{41}\text{Co}_9\text{Mn}_{31.5}\text{Ga}_{18.5}$ studied in adiabatic magnetization process realized in pulsed magnetic fields. Instantaneous change in sample temperature is detected using a thin-film resistive thermometer attached to the sample. In addition to steep reduction of temperature at the metamagnetic transition (ΔT_{IMT}), further negative magnetocaloric effect is observed at higher fields (ΔT^*).

caloric effects using large superconducting magnets, such as gas liquefaction projects, will also be important. The evaluation of the magnetocaloric effects in Heusler alloys at high magnetic fields provides an essential hint for solving energy problems in near future.

References

- [1] K. A. Gschneidner Jr., V. K. Pecharsky, and A. O. Tsokol, Rep. Prog. Phys. **68**, 1479 (2005).
- [2] T. Kihara *et al.*, Phys. Rev. B **90**, 214409 (2014).
- [3] X. Xu *et al.*, MATEC Web of Conf. **33**, 01004 (2015).
- [4] T. Kihara *et al.*, Scr. Mater. **181**, 25 (2020).
- [5] T. Kihara *et al.*, Phys. Rev. Mater. **5**, 034416 (2021).
- [6] R. Kainuma *et al.*, Nature **439**, 957 (2006).
- [7] A. Miyake *et al.*, Rev. Sci. Instrum. **91**, 105103 (2020).

Authors

T. Kihara^a, T. Roy^a, X. Xu^a, A. Miyake, M. Tsujikawa^a, H. Mitamura, M. Tokunaga, Y. Adachi^b, T. Eto^c, and T. Kanomata^d

^aTohoku University

^bYamagata University

^cKurume Institute of Technology

^dTohoku Gakuin University

Observation of In-Plane Magnetic Field Induced Phase Transitions in FeSe

J. S. Kim, Y. Kohama, and J. M. Ok

In conventional superconductors, spin polarization can destroy superconductivity when Zeeman energy surpasses the binding energy of Cooper pairs, known as the Pauli paramagnetic limit. Beyond the Pauli limit, exotic superconducting phases, often coexisting with complex magnetic orders, have been observed in some unconventional superconductors. Even in these cases, however, field-induced spin imbalance is usually at most a few %. So far, realization of the highly spin-imbalanced superconductivity and possible field-induced exotic phases have been remained elusive, partly due to the lack of the suitable material candidates.

FeSe is a promising candidate hosting a strongly spin imbalanced state at high magnetic fields. The observed in-plane upper critical field of FeSe is $H_{c2}^{ab} \approx 25$ T, well above the conventional BCS value of the Pauli limiting

field $H_P \approx 15.6$ T ($H_P = 1.84 T_c$), and the Zeeman energy at H_{c2} becomes comparable with the superconducting gap Δ_{SC} ($\mu_B H_{c2} \sim \Delta_{SC}$). In addition, high-quality FeSe single crystals are found to be in the clean limit with a much longer mean free path l than the superconducting coherence length ξ ($l \gg \xi$). More importantly, FeSe is in the so-called BCS-BEC (Bose-Einstein condensate) crossover regime ($\Delta_{SC} \sim E_F$) with exceptionally small Fermi energies. The spin imbalance reaches up to $\sim 40\%$ for one of the Fermi surfaces (FSs) at $H_{c2}^{ab} \approx 25$ T, much larger than the typical value of a few % in other superconductors. Therefore, FeSe can be a model system to study whether, and if so how, competing magnetic or superconducting instabilities trigger exotic field-induced phases in multiband superconductors with a large spin imbalance.

In this work, using torque magnetometry, specific heat, and magnetocaloric measurements, we identified successive anomalies with increasing in-plane magnetic field, below H_{c2} at low temperatures and in the clean limit. The signatures of unusual phase transitions below H_{c2}^{ab} and below $T^* \approx 2$ K are observed in the field-dependent torque magnetometry $\tau(H)$. The torque magnetometry in superconductors usually exhibits a typical saw-tooth shaped curve of the field derivative $\tau(H)$, $d\tau/dH$ due to vortex pinning. In FeSe, however, we observed two additional anomalies at $H_1 \sim 15$ T and $H_2 \sim 22$ T, well below the irreversible field H_{irr} at which the hysteresis in $\tau(H)$ starts to develop (Fig. 1a and 1b). The transition fields H_1 and H_2 follow the distinct dependence on temperature or field angle from those of $H_{\text{irr}} \approx H_{c2}$ (Figs. 1a and 1c). Upon increasing temperature or the tilting angle of the magnetic field (θ) from $H \parallel ab$, H_{irr} systematically decreases, similar to H_{c2} . In contrast, the anomalies are pronounced only at low temperatures below T^* and near $H \parallel ab$ with $\theta \leq 15^\circ$. Also, the transition fields H_1 and H_2 remain almost the same with variation of temperature or field angle (Figs. 2a and 2b). The anomalies seen in torque magnetometry are further confirmed by magnetocaloric and specific heat measurements [1]. These findings clearly evidence the presence of field-induced phases near the in-plane magnetic fields below H_{c2}^{ab} .

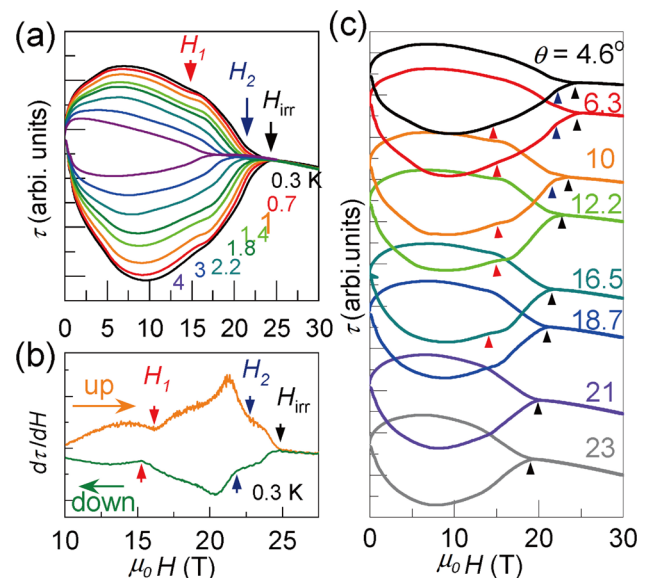


Fig. 1. (a) Magnetic field dependent torque $\tau(H)$ close to $H \parallel ab$ at various temperatures. The irreversibility field at $H_{\text{irr}} \sim 25$ T and anomalies at $H_1 \sim 15$ T and $H_2 \sim 22$ T are indicated by black, red and blue arrows, respectively. (b) The field-derivative curve $d\tau(H)/dH$ showing clear anomalies at H_1 and H_2 . (c) Magnetic field dependent torque $\tau(H)$ at various field angles.

AuthorsJ. M. Ok^a, C. I. Kwon^a, J. S. You^a, S. K. Park^a, K.-S. Kim^a, J. S. Kim^a, Y. Kohama, K. Kindo, J.-H. Kim^b, Y. J. Jo^b, E. S. Choi^c, W. Kang^d, E. G. Moon^e, and A. Gurevich^f^aPohang University of Science and Technology^bKyungpook National University^cNational High Magnetic Field Laboratory^dEwha Womans University^eKorea Academy Institute of Science and Technology^fOld Dominion University

Hydrogen-Bonded Structure of Water Responsible for Ion Selective Permeability of Self-Assembled Liquid Crystalline Polymer Membranes

T. Kato and Y. Harada

Liquid crystals (LC) are appealing for nanofiltration membranes with uniform subnanopores which enable efficient and thermally stable filtration and ion selectivity [1]. Many principles of water filtration are intuitive: particles bigger than the pore size cannot pass through a membrane, and electrostatic interactions between ions, water molecules and the membrane can aid the process. However, the permeability of these LC membranes is higher for larger, dianionic SO_4^{2-} ions than it is for monoanionic, smaller Cl^- ions, which could not be explained using the common filtration principles, which implies the presence of another driving force for ion selectivity. One of such possibility is the structure of the water surrounding the ions

Here we investigated the hydrogen-bonded configuration of water molecules in the subnanopores of a bicontinuous cubic LC membrane formed by in-situ polymerization of compound 1 (Fig. 1a), and how it affects the permeation of dianionic SO_4^{2-} and monoanionic Cl^- [2]. We used high-resolution X-ray emission spectroscopy (XES) [3] to learn

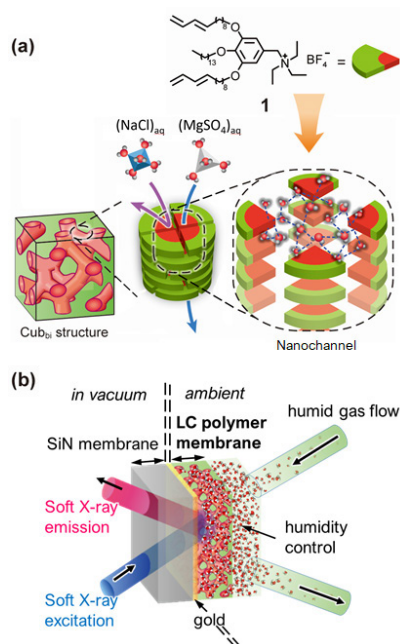


Fig. 1. (a) Molecular structure of an LC monomer (**1**). The monomers were self-assembled to form a bicontinuous cubic (Cub_{Bi}) LC structure through which ions are selectively transported. (b) Schematic image of soft X-ray emission detection from water in the LC membrane.

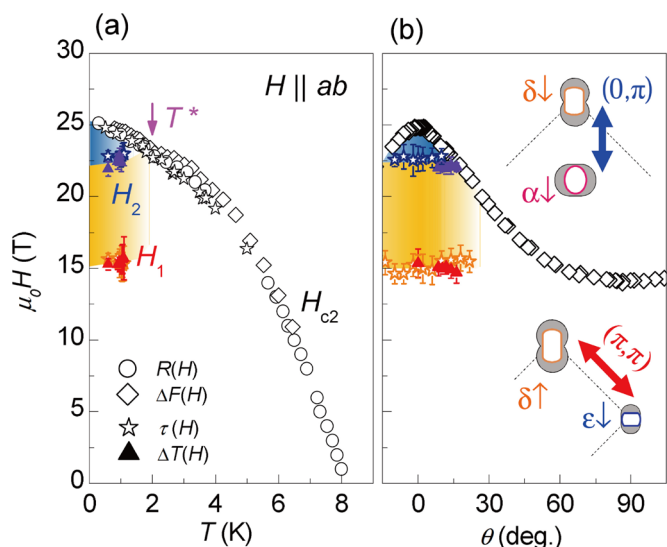


Fig. 2. (a,b) Magnetic phase diagram of FeSe for $H \parallel ab$ as a function of temperature (a) and field orientation (θ) with respect to the ab plane (b). The upper critical field $H_{c2}^{ab}(T)$ (open symbols) are determined by resistivity (black open circle), TDO frequency (black open diamond), and torque magnetometry (black open star) measurements, while the field-induced phase transitions at H_1 and H_2 are obtained by torque magnetometry (colored open star) and the magnetocaloric effect (colored solid triangle). The inset shows schematics of the possible nesting effect via $q = (0, \pi)$ or (π, π) between the spin-split Fermi surfaces (FSs) with anisotropic superconducting gap (gray shade). Near H_1 , the nesting effect is expected between two FSs with opposite spins via a SDW momentum $q = (\pi, \pi)$ (bottom), while the nesting with $q = (0, \pi)$ is expected near H_2 between two FSs with the same spins (top).

One possible candidate for the high field anomalies is then the FFLO phase. In this case, the Cooper-pair state ($k \uparrow, -k+q \downarrow$) is formed with a momentum mismatch (q) between the spin-split FSs. In multiband superconductors, each FS has its own FFLO instability with a different modulation length q_i^{-1} (i , band index), and these instabilities compete with each other, inducing the multiple FFLO orders at different magnetic fields. Alternatively, the spin-density wave (SDW) phase of field-induced quasiparticles can be another promising candidate. When the superconductivity is suppressed by Pauli pair breaking near the superconducting gap nodes or minima, the SDW order can be triggered by the nesting effect by field-induced quasiparticles. Due to an exceptionally small E_F , the Zeeman effect results in the spin-split FSs much different in size, which significantly affects the nesting condition in FeSe. We found that the nesting via $q = (\pi, \pi)$ nicely matches the two different FSs with opposite spins at $H \sim 16$ T, and with the same spins at $H \sim 22$ T (Fig. 2b), in good agreement with the observed transition fields, H_1 and H_2 . The incipient spin fluctuations and strong coupling between the field-induced quasiparticles may allow the coexisting phase with the SDW and superconductivity.

In the current stage, the detailed nature of the field-induced phase transitions, including possible coexistence of the SDW and the FFLO orders, remains to be clarified. Nevertheless, these observations clearly demonstrate that FeSe offers a unique system, in which field-induced phase transitions occur in the superconducting state. This poses a challenge to our understanding on the complex interplay between anisotropic superconducting order, incipient magnetic instabilities, and the multi-band effect in the largely spin-imbalanced superconducting systems.

Reference

[1] J. M. Ok, C. I. Kwon, Y. Kohama, J. S. You, S. K. Park, J. Kim, Y. J. Jo, E. S. Choi, K. Kindo, W. Kang, K.-S. Kim, E. G. Moon, A.

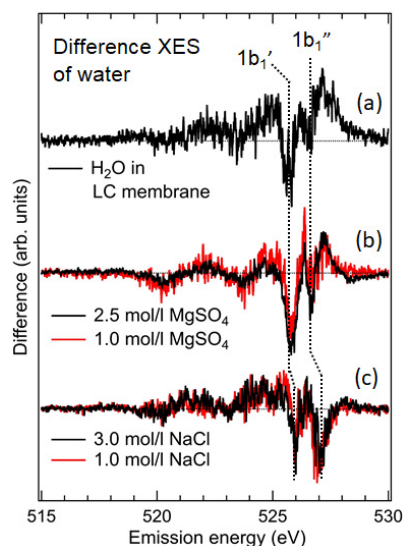


Fig. 2. Valence electronic structure of H₂O in (a) the LC membrane, (b) 1.0 mol/l and 2.5 mol/l MgSO₄, (c) 1.0 mol/l and 3.0 mol/l NaCl aqueous solutions.

how water arranges itself in the subnanopores.

XES spectra of pure liquid H₂O absorbed in the LC membrane and hydrating water of permeating solutes, MgSO₄ and NaCl were collected at the SPring-8 BL07LSU HORNET station using a high-resolution XES spectrometer [4]. A custom-made ambient pressure cell was used to expose the LC membrane to humidity-controlled moisture and nitrogen as a carrier gas. (Fig. 1b). To explore the origin of the selective ion permeation ($73\pm 5\%$ for MgSO₄ and $30\pm 6\%$ for NaCl), hydrogen-bonded structures of H₂O in the LC membrane were compared with those in the MgSO₄ and NaCl hydrations. Spectra of water within the subnanopores (Fig. 2a) revealed that its hydrogen-bonded network, when confined, loses some structural features characteristic of bulk water in favor of new structural features. Very similar structural features are observed in the spectra of the hydration shell of SO₄²⁻ (Fig. 2b) but not in that of Cl⁻ (Fig. 2c). We interpret this as the reason for the greater membrane permeability of SO₄²⁻ than that of Cl⁻. In the near future computational studies might help understand the exact structure of the hydrogen-bonded network within the subnanopores. The nature of hydrogen-bonded networks becomes an additional parameter that should be considered and controlled to obtain highly efficient water filtrations.

References

- [1] (a) T. Kato *et al.*, Nat. Rev. Mater. **2**, 17001 (2017); (b) T. Ichikawa *et al.*, J. Am. Chem. Soc. **134**, 2634 (2012). (c) M. Henmi *et al.*, Adv. Mater. **24**, 2238 (2012). (d) T. Sakamoto *et al.*, Adv. Sci. **5**, 1700405 (2018). (e) K. Hamaguchi *et al.*, ACS Macro Lett. **8**, 24 (2019). (f) M. Gupta *et al.*, ACS Macro Lett. **8**, 1303 (2019).
- [2] R. Watanabe, T. Sakamoto, K. Yamazoe, J. Miyawaki, T. Kato, and Y. Harada, Angew. Chem. Int. Ed. **59**, 23461 (2020).
- [3] T. Fransson *et al.*, Chem. Rev. **116**, 7551 (2016).
- [4] Y. Harada *et al.*, Rev. Sci. Instrum. **83**, 013116 (2012).

Authors

R. Watanabe^a, T. Sakamoto^a, K. Yamazoe, J. Miyawaki, T. Kato^a, and Y. Harada

Progress of Facilities

Supercomputer Center

The Supercomputer Center (SCC) is a part of the Materials Design and Characterization Laboratory (MDCL) of ISSP. Its mission is to serve the whole community of computational condensed-matter physics of Japan, providing it with high performance computing environment. In particular, the SCC selectively promotes and supports large-scale computations. For this purpose, the SCC invites proposals for supercomputer-aided research projects and hosts the Steering Committee, as mentioned below, that evaluates the proposals.

The ISSP supercomputer system consists of two subsystems: System B, which was replaced recently (Oct. 2020), is intended for larger total computational power and has more nodes with relatively loose connections whereas System C is intended for higher communication speed among nodes. System B (ohtaka) consists of 1680 CPU nodes of Dell PowerEdge C6525 and 8 FAT nodes of Dell PowerEdge R940 with total theoretical performance of 6.881 PFLOPS. System C (enaga) consists of 252 nodes of HPE SGI 8600 with 0.77 PFLOPS. Replacement of the System C is scheduled in April 2022.

In addition to the hardware administration, the SCC puts increasing effort on the software support. Since 2015, the SCC has been conducting “Project for advancement of software usability in materials science (PASUMS)”. In this project, for enhancing the usability of the ISSP supercomputer system, we conduct several software-advancement activities: developing new application software that runs efficiently on the ISSP supercomputer system, adding new functions to existing codes, help releasing private codes for public use, creating/improving manuals for public codes, etc. Three target programs were selected in fiscal year 2020: (1) PHYSBO (proposal made by R. Tamura

(NIMS)), (2) 2DMAT (proposal made by T. Hoshi (Tottori Univ.)), and (3) MateriApps Installer (proposal made by S. Todo (Univ. of Tokyo)). In 2021, we also started the data repository service.

All staff members of university faculties or public research institutes in Japan are invited to propose research projects (called User Program). The proposals are evaluated by the Steering Committee of SCC. Pre-reviewing is done by the Supercomputer Project Advisory Committee. In fiscal year 2020, totally 387 projects were approved including the ones under the framework of Supercomputing Consortium for Computational Materials Science (SCCMS), which specially supports FUGAKU and other major projects in computational materials science. The total points applied and approved are listed on Table. 1 below.

The research projects are roughly classified into the following three (the number of projects approved, not including SCCMS):

- First-Principles Calculation of Materials Properties (189)
- Strongly Correlated Quantum Systems (40)
- Cooperative Phenomena in Complex, Macroscopic Systems (137)

In all the three categories, most proposals involve both methodology and applications. The results of the projects are reported in 'Activity Report 2020' of the SCC. Every year 3-4 projects are selected for “invited papers” and published at the beginning of the Activity Report. In the Activity Report 2020, the following three invited papers are included:

1. “High precision study of the Anderson transition”, Tomi OHTSUKI (Sophia U.) and Keith SLEVIN (Osaka U.)
2. “Some Recent Developments in ab initio Thermodynamics of Ion Disorder in Solids”, Shusuke KASAMATSU (Yamagata U.)

First semester (Apr.-Sep.)									Second semester (Oct.-Mar.)								
Class	Max Points		Application	Number of Projects	Total Points												
	System B	System C			Applied		Approved										
					System B	System C	System B	System C									
A	100	50	any time	8	0.8k	0.4k	0.8k	0.4k	A	100	50	any time	10	1.0k	0.4k	1.0k	0.4k
B	500	100	twice a year	61	28.4k	4.0k	22.8k	3.9k	B	1k	100	twice a year	57	46.6k	3.2k	22.0k	2.0k
C	5k	1k	twice a year	115	446.5k	80.1k	239.8k	42.4k	C	8k	1k	twice a year	96	595.8k	59.0k	226.0k	22.3k
D	10k	1k	any time	3	22.5k	2.0k	15.0k	2.0k	D	10k	1k	any time	0	0k	0k	0k	0k
E	15k	3k	twice a year	9	127.4k	27.0k	88.5k	21.4k	E	25k	3k	twice a year	7	175.0k	18.0k	87.0k	8.4k
S	-	-	twice a year	0	0	0	0	0	S	-	-	twice a year	0	0	0	0	0
SCCMS				11	23.7k	4.6k	23.7k	4.6k	SCCMS				10	50.0k	4.5k	50.0k	4.5k
Total				207	649.3k	118.0k	390.6k	74.6k	Total				180	868.3k	85.0k	386.0k	37.5k

Table 1. Research projects approved in 2020

The maximum points allotted to the project of each class are the sum of the points for the two systems. Computation of one node for 24 hours corresponds to one point for the CPU nodes of System B and System C. The FAT nodes require four points for a 1-node 24-hours use.

3. “Large-Scale Molecular Dynamics Simulations of Karman Vortex and Sound Wave: Cavitation and Polymer Effects”, Yuta ASANO (ISSP), Hiroshi WATANABE(Keio Univ.) and Hiroshi NOGUCHI (ISSP)

Neutron Science Laboratory

The Neutron Science Laboratory (NSL) has been playing a central role in neutron scattering activities in Japan since 1961 by performing its own research programs as well as providing a strong General User Program (GUP) for the university-owned various neutron scattering spectrometers installed at the JRR-3 (20 MW) operated by Japan Atomic Energy Agency (JAEA) in Tokai, Ibaraki (Fig. 1). In 2003, the Neutron Scattering Laboratory was reorganized as the Neutron Science Laboratory to further promote the neutron science with use of the instruments in JRR-3. Under GUP supported by NSL, 12 university-group-owned spectrometers in the JRR-3 reactor are available for a wide scope of researches on material science. The submitted proposals were about 300 and the visiting users reached over 6000 person-day in FY2010. In 2009, NSL and Neutron Science Division (KENS), High Energy Accelerator Research Organization (KEK) built a chopper spectrometer, High Resolution Chopper Spectrometer, HRC, at the beam line BL12 of MLF/J-PARC (Materials and Life Science Experimental Facility, J-PARC) (Fig. 2). HRC covers wide energy transfer ($100 \mu\text{eV} < \hbar\omega < 0.5 \text{ eV}$) and momentum transfer ($0.03 \text{ \AA}^{-1} < Q < 30 \text{ \AA}^{-1}$) ranges, and therefore becomes complementary to the existing inelastic spectrometers at JRR-3. HRC has accepted general users through the J-PARC proposal system since FY2011.

Triple axis spectrometers, HRC, a four-circle diffractometer, and a high resolution powder diffractometer are utilized for a conventional solid state physics and a variety of research fields on hard-condensed matter, while in the field of soft-condensed matter science, researches are mostly carried out by using a small angle neutron scattering (SANS-U) and/or neutron spin echo (iNSE) instruments. The upgraded time-of-flight (TOF) inelastic scattering spectrometer, AGNES, is available both for hard- and soft-matter science. Our GUP has produced 2068 publications and 285 dissertations until April 30, 2021. Their lists for the last 10 years are given in Activity Report on Neutron Scattering Research which is available in ISSP and NSL web pages.

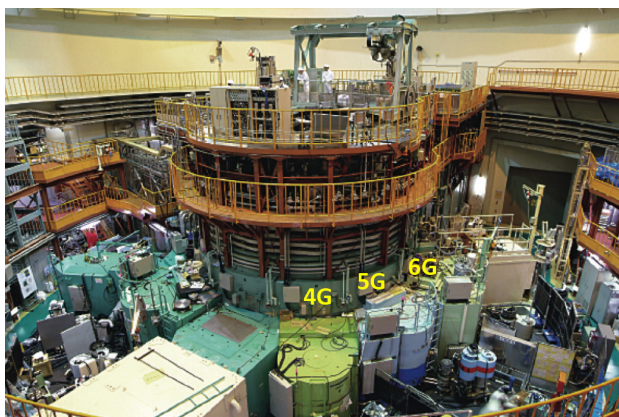


Fig. 1. Reactor hall of JRR-3. Three triple axis spectrometers are shown in the photo.

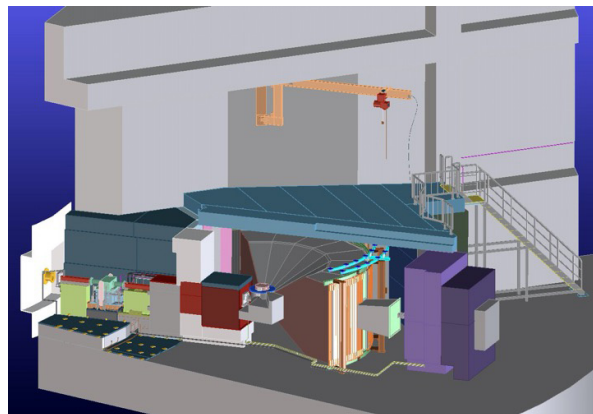


Fig. 2. Schematic view of HRC.

Since the Great East Japan Earthquake on March 11, 2011, JRR-3 had been closed mainly from safety issues. Hence, our domestic activity was only on HRC. To take up a recent research highlight, well-defined spin wave was successfully measured in the pressure-induced magnetic phase in CsFeCl_3 [1]. Collaboration between HRC and CTAX, which is mentioned below, has clarified the hybridization of phase and amplitude modes near a quantum critical point [2]. Another progress on HRC was that a superconducting magnet up to 5 T became available. Field dependence of spin-wave spectra in 2D antiferromagnet $\text{Ba}_2\text{MnGe}_2\text{O}_7$ was measured. From FY2012 to FY2020, NSL has managed User-Program Supports for Overseas Experiments. 398 people (for 297 proposals) have performed their experiments in various foreign facilities and published 114 papers. The lists for this program are also available in Activity Report on Neutron Scattering Research mentioned above.

As for international cooperative programs, NSL operates the U.S.-Japan Cooperative Program on neutron scattering, providing further research opportunities to material scientists who utilize the neutron scattering technique for their research interests. In 2010, relocation of the U.S.-Japan triple-axis spectrometer, CTAX, was completed, and it is now open to users. NSL has another agreement with Australian Centre for Neutron Scattering (ANSTO), which was the main foreign facility for the User-Program Supports for Overseas Experiments.

It is really good news that JRR-3 has restarted in February 2021 after long shutdown and the normal GUP will come back from July 2021. During the shutdown period, we had been concentrating our efforts on upgrading the instruments and neutron beam circumstances. Specific actions taken include: the installation of focusing collimation systems, such as focusing monochromator and focusing analyzer, and material lens; and the introduction of polarization optics together with the installation of non-magnetization neutron shield. The neutron guides in the Guide Hall have also been upgraded by replacing the existing ones with super-mirror guides. These upgrades should result in increase in neutron beam flux several times. The sample environments such as cryostat and pressure cells have also been upgraded. We are looking forward to restarting science activities in JRR-3.

- [1] S. Hayashida *et al.*, Phys. Rev. B **97**, 140405(R) (2018).
- [2] S. Hayashida *et al.*, Sci. Adv. **5**, eaaw5639 (2019).

International MegaGauss Science Laboratory

The objective of this laboratory (Fig. 1) is to study the physical properties of solid-state materials (such as metals, semiconductors, insulators, superconductors, and magnetic materials) in a high magnetic field of 100 T or even higher. Such a high magnetic field can control material phases and functions. Our pulsed magnets, at moment, can generate up to 87 Tesla (T) by non-destructive manner, and up to 1200 T by destructive manner. The world record indoor magnetic field 1200 T was achieved in 2018. The laboratory is open for scientists in domestic as well as from overseas. Lots of fruitful results have come out not only from the collaborative researches but also from our in-house activities.



Fig. 1. The building C of the IMGSL.

Our interests cover the study on quantum phase transitions (QPT) induced by high magnetic fields. Field-induced QPT has been explored in various materials such as quantum spin systems, strongly correlated electron systems and other magnetic materials. One of our ultimate goals is to provide the joint-research users with a 100 T millisecond-long pulse using a non-destructive magnet, and to offer versatile high-precision physical measurements. Measurable physical quantities or properties are magneto-optical spectra, magnetization, magnetostriction, electrical transport, specific heat, nuclear magnetic resonance, and ultrasound propagation. They can be carried out with sufficiently high accuracy. Another ultimate goal is to extend the magnetic field region and discover novel phenomena happening only in extremely strong magnetic fields exceeding 100 T. Recent technical developments allow us to even measure magnetostriction and ultrasound propagation in the destructive magnetic fields over 100 T, that can directly reach potential structural changes in the ultrahigh magnetic fields. Recent discovery of magnetic field induced insulator-metal transitions of strongly correlated materials in 500 T would open new direction of the megagauss field research, namely exploration of field-induced novel phases in materials with strong interactions comparable to thermal energy of a room temperature.

A 210 MJ flywheel generator (Fig. 2), which is the world largest DC power supply (recorded in the Guinness Book of World Records) was installed in the DC flywheel generator station at our laboratory, and used as an energy source of super-long pulse magnets. The magnet technologies are intensively devoted to the quasi-steady long pulse magnet

	Alias	Type	B_{\max}	Pulse width Bore	Power source	Applications	Others
Building C Room 101-113	ElectroMagnetic Flux Compression	Destructive	1200 T	$3\mu\text{s}$ (100-1200T) 10 mm	5 MJ, 50 kV 2 MJ, 50 kV	Magneto-Optical Magnetization	5 K – room temperature
	Horizontal Single-turn Coil	Destructive	300 T 200 T	$6\mu\text{s}$ 5 mm 10 mm	0.2 MJ, 50 kV	Magneto-Optical measurements Magnetization	5 K – room temperature
	Vertical Single-turn Coil	Destructive	300 T 200 T	$8\mu\text{s}$ 5 mm 10 mm	0.2 MJ, 40 kV	Magneto-Optical Magnetization	2 K – room temperature
Building C Room 114-120	Mid-pulse Magnet	Non-destructive	60 T 70 T	40 ms 18 mm 40 ms 10 mm	0.9 MJ, 10 kV	Magneto-Optical measurements Magnetization Magneto-Transport Hall resistance Polarization Magneto-Striction Magneto-Imaging Torque Magneto- Calorimetry Heat Capacity	Independent Experiment in 5 site Lowest temperature 0.1 K
Building C Room 121	PPMS	Steady	14 T			Resistance Heat Capacity	Down to 0.3 K
	MPMS	Steady	7 T			Magnetization	
Building K	Short-Pulse Magnet	Non-destructive	87 T (2-stage pulse) 85 T	5 ms 10 mm 5 ms 18 mm	0.5 MJ, 20 kV	Magnetization Magneto-Transport	2 K – room temperature
	Long-Pulse Magnet	Non-destructive	43.5 T	1 s 30 mm	210 MJ, 2.7 kV	Resistance Magneto-Calorimetry	2 K – room temperature

Table 1. Available Pulse Magnets, Specifications



Fig. 2. Upper: The K-building for the flywheel generator (left hand side) and a long pulse magnet station (right hand side). Lower: The flywheel giant DC generator which is 350 ton in weight and 5 m high (bottom). The generator, capable of a 51 MW output power with the 210 MJ energy storage, is planned to energize the long pulse magnet generating 100 T without destruction.

(an order of 1-10 sec) energized by the giant DC power supply. The giant DC power source will also be used for the giant outer-magnet coil to realize a 100 T nondestructive magnet by inserting a conventional pulse magnet coil in its center bore. Recently, the super-long pulsed magnet has been intensively used to investigate thermal properties such as specific heat and magnetocaloric effects.

Magnetic fields exceeding 100 T can be obtained with only destruction of a magnet coil. The ultrahigh magnetic fields are obtained in a microsecond time scale. The project, financed by the ministry of education, culture, sports, science and technology aiming to generate 1000 T with the electromagnetic flux compression (EMFC) system (Fig. 3), has been completed. Our experimental techniques using the destructive magnetic fields have intensively been developed. The system which is unique to ISSP in the world scale is comprised of a power source of 5 MJ main condenser bank and 2 MJ condenser bank. Two magnet stations are constructed and both are energized from each power source. Both systems are fed with another 2 MJ condenser bank used for a seed-field coil of which magnetic flux is to be compressed. The 2 MJ EMFC system can generate 450 T. The 5 MJ system is used for generation of

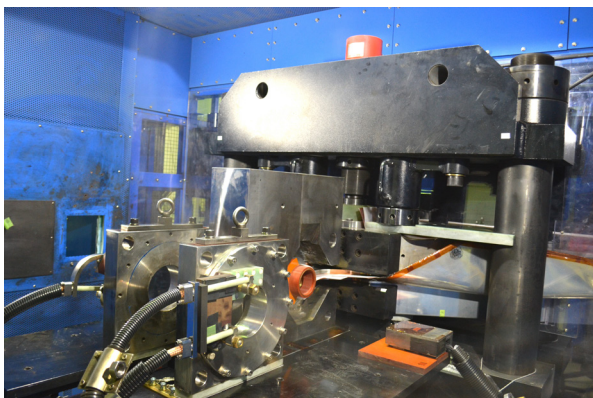


Fig. 3. A view of the coil setup of the electromagnetic flux compression inside of an anti-explosive house. The world strongest indoor magnetic field 1200 T was achieved in 2018.

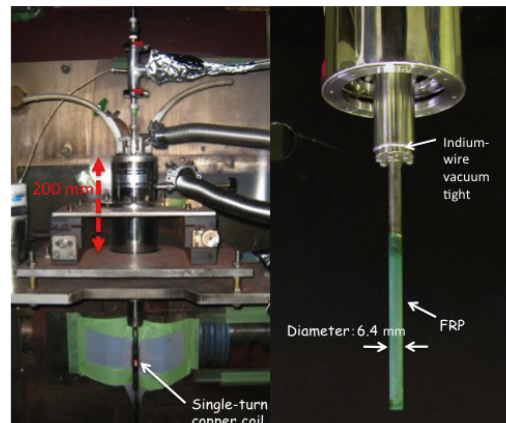


Fig. 4. Schematic picture of the V-type single-turn coil equipped with a 40 kV, 200 kJ fast capacitor bank system. The liquid-helium-bath cryostat with a plastic tail is also shown.

1000 T-class magnetic field. For the research in magnetic field range of 100 - 300 T, we have two single-turn coil (STC) systems that have a fast-capacitor bank system of 200 kJ for each. One is the horizontal type (H-type) and the other is a vertical type (V-type, Fig. 4). Various kinds of laser spectroscopy experiments such as the cyclotron resonance and the Faraday rotation are possible using the H-type STC, while a stable low temperature condition of 2 K is available for the V-type STC.

Center of Computational Materials Science

With the advancement of hardware and software technologies, large-scale numerical calculations have been making important contributions to materials science and will have even greater impact on the field in the near future. CCMS is a specialized research center established in 2011 for promoting computer-aided materials science with massively parallel computers, such as the Fugaku supercomputer, which has been recently developed in Kobe as the core of a billion-dollar national project. Activities of CCMS are divided into the following three categories: (1) highly efficient and large-scale use of the Fugaku supercomputer and its application to grand-challenge problems in computational materials science, (2) activities as the center for the community of computational condensed matter physics and materials science, and (3) computational physics research aiming to solve rare-element problems.



Fig. 1. Group photo in the CDMSI symposium

For the first category, each group in CCMS is carrying out various individual research projects in its own expertise to efficiently utilize large-scale parallel computers. For example, the Ozaki group has been developing efficient and accurate methods and software packages to extend the applicability of DFT to more realistic systems, and investigated the structural and electronic properties of various 2D materials in successful collaboration with experimental groups and industrial companies. There are other activities such as development of Tensor Network (TN) based numerical methods and Markov-chain Monte Carlo methods by the Kawashima group and the Todo group.

As for the activities in the second category, apart from major annual conferences and formal international meetings as shown in Fig. 1, the CCMS/CDMSI hosted, and also provided a series of lectures and training sessions at Kashiwa. For example, training sessions "Kashiwa Hands-On" for getting accustomed to various application programs, such as OpenMX, HΦ, mVMC, AkaiKKR, and MateriApps LIVE!, as shown in Fig. 2, have been held monthly. Each session is designed for 5-10 trainees and takes 4-5 hours. We also coordinate the use of the computational resources available to our community, and support community members through various activities such as administrating the website "MateriApps" for information on application software in computational science as shown in Fig. 3.

For the third category, the Akai team and the Fukushima group are working on the development of new permanent magnet materials. In order to meet the ever-increasing demands for new permanent magnet materials that are used for high performance permanent magnets, CCMS is theoretically investigating the various magnetic properties, such as saturation magnetization, Curie temperature, and magnetic

anisotropy, of iron-based magnetic materials, including rare-earth magnet materials, $R_2(\text{Fe,Co})_{14}\text{B}$, $R_2(\text{Fe,Co})_{17}$, and $R\text{Fe}_{11.5}\text{Ti}_{0.5}$ ($R = \text{La, Ce, \dots, Lu, Y}$) on the basis of first-principles calculations.

These activities are supported by funds for various governmental projects including Element Strategy Initiative and the Program for Promoting Researches on the Supercomputer Fugaku.

The following is the selected list of meetings organized by CCMS in recent years:

- 2019/10/8-2019/10/10 The 3rd Innovation Camp for Computational Materials Science (3rd ICCMS), Takinoyu Hotel, Yamagata.
- 2019/12/6 TIA-Kakehashi Poster Workshop 2019 The University of Tokyo Kashiwa Campus Station Satellite, Kashiwa
- 2019/12/13 Element Strategy Initiative Advisory Council (ESIAC) 2019, TKP Garden city, Yokohama.
- 2020/2/3-2020/2/4 4th Element Strategy Symposium: New Developments in Industry-Academia Research Collaboration, Ito Hall, Tokyo.
- 2020/2/25 PCoMS Skill improvement training for graduate students & postdocs ISSP, Kashiwa.
- 2020/6/19-2020/6/23 Matching Workshop for industries & graduate students/ postdocs, Online.
- 2020/12/21-2020/12/22 Joint Research Meeting of ISSP Supercomputer Joint Use and CCMS Annual Activity Report 2020, Online.

In addition to the events listed above, we organize regular hands-on program for various application, such as Open MX and HΦ.



Fig. 2. Software in the CCMS community

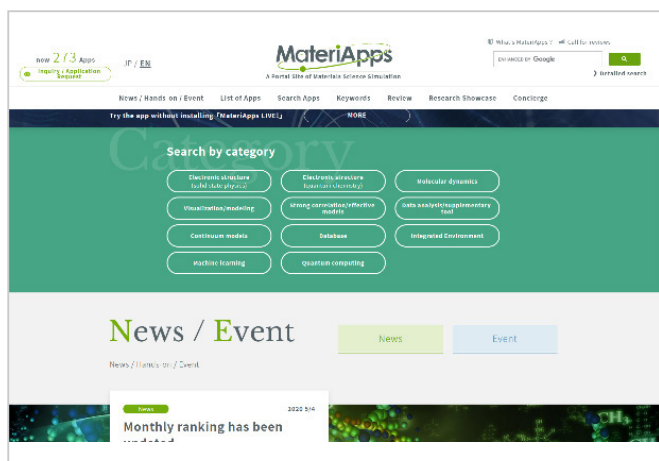


Fig. 3. MateriApps Website

Laser and Synchrotron Research Center (LASOR Center)

Laser and synchrotron research center (LASOR Center) was established in October 2012 to push the frontiers of the photon and materials science. LASOR has 10 groups in 2019, which is the biggest division in ISSP. Most of the research activities on the development of new lasers with an extreme performance and the application to materials science are studied in specially designed buildings D and E with large clean rooms and the isolated floor from the vibrations in Kashiwa Campus. On the other hand, the experiments utilizing the synchrotron radiation are performed at beamline BL07LSU in SPring-8 (Hyogo).

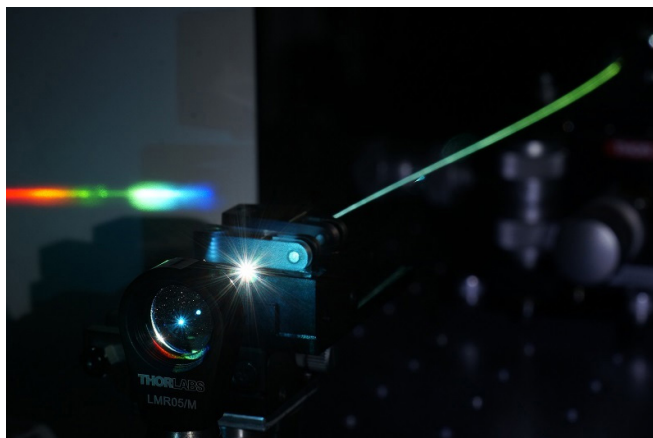


Fig. 1. Optical frequency comb

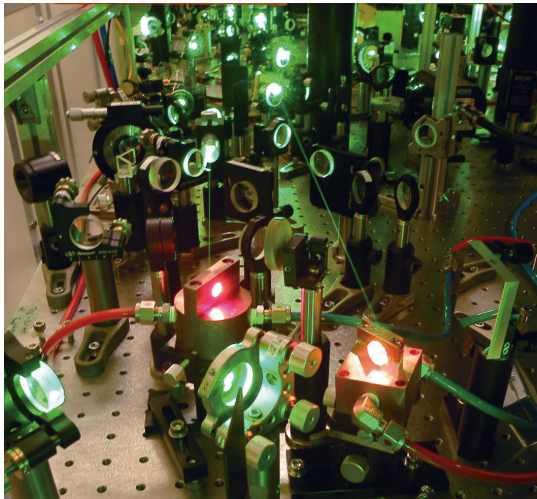


Fig. 2. Close look of a high-peak-power ultrashort-pulse laser

The development of novel laser-based light sources in the vacuum-ultraviolet to soft-X-ray regions innovated materials investigations as represented by the highest-energy-resolution photoemission, ultrafast time-domain, and ultrafast non-linear spectroscopies. Materials science research powered by lasers thus has entered a new era. The ultra-short and high-power lasers are more and more attractive light source for both basic science and industry. The state-of-the-art laser source and spectroscopy are intensively explored.

Another stream pursued at ISSP is the synchrotron-based research. The drastic advance in brilliance of the synchrotron radiation has also opened a new field of its own in photon science. The soft-X-ray beam-line in SPring-8 (BL07LSU) was implemented with the longest undulator in the world: The end stations illuminated by the brilliant soft-X-rays are used to output innovative achievements based on high-resolution spectroscopy data. In 2018, Japanese government has made a statement to construct a new synchrotron facility in Tohoku. LASOR has decided to subjectively contribute to this facility from the design to the operation.

Lasers and synchrotrons have developed independently; now both light sources cover a wide photon-energy range with an overlap in the vacuum-ultraviolet to soft-X-ray regions. Foreseeing their common interests in research fields and technologies, ISSP integrated the two streams, namely the extreme lasers and synchrotron radiations, into the common platform. Through the mutual interactions between the forefronts of lasers and synchrotrons, LASOR will be the center of innovations in light and materials science, with

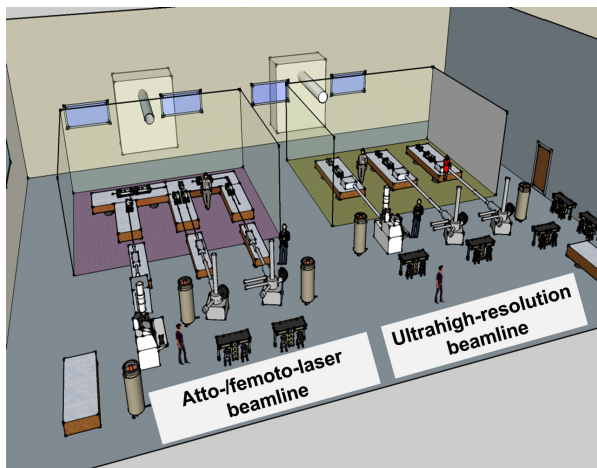


Fig. 3. Design of E building for extreme VUV- and SX-lasers and new spectroscopy.

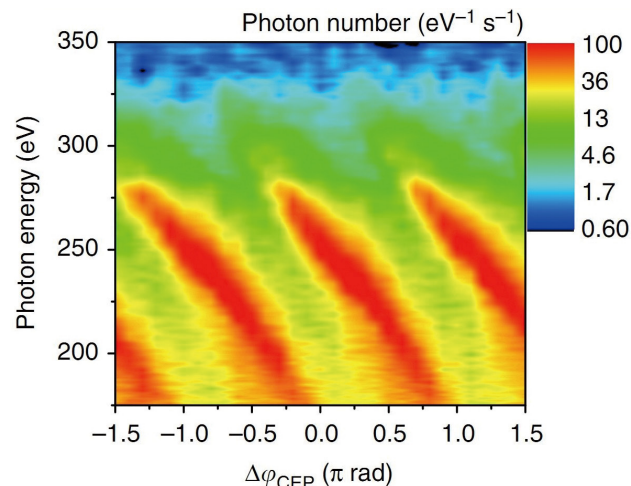


Fig. 4. Phase-dependence of high harmonic spectra in soft X rays.

the aid of world-wide joint research and close collaborations with other divisions in ISSP such as New Materials Science, Nanoscale Science, and Condensed Matter Theory.

The mission of LASOR is to cultivate and propel the following three scientific fields:

1. Laser Science,
2. Synchrotron radiation Science,
3. Extreme Spectroscopy,

• **Laser science group**

We were committed to continuing to developed various state-of-the-art laser systems such as high-power solid-state or gas lasers, high-intensity lasers, ultra-short pulse lasers down to attosecond time scale (Peta Hz linewidth), ultra-stable lasers with 1-Hz linewidth, optical frequency combs, mid-infrared lasers, THz light source, and semiconductor lasers.

High-power and ultrashort pulse laser technology has progressed for this 10 years. It opened two directions of research. One is a coherent extreme ultraviolet light source realized by a high-harmonic generation (HHG) scheme. The average power of HHG became high enough to use it for a photoemission spectroscopy. The photon energies of 7 eV to 60 eV are now available. They can be either very narrow band width or ultrashort pulse. The other is an industrial science such as a laser processing. Pulse duration variable, 100-W average power, femtosecond laser is now available in LASOR for any collaborative research including companies.

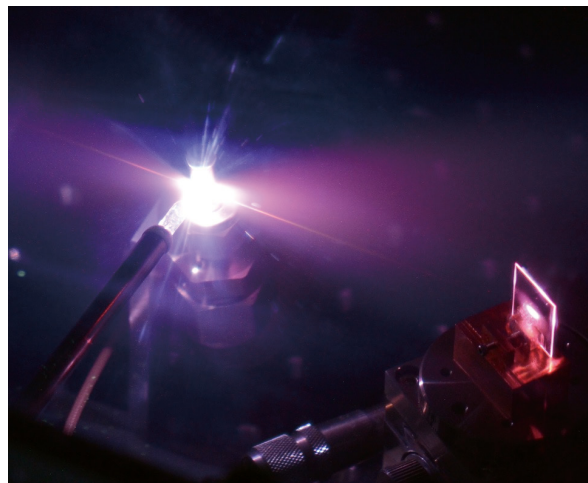


Fig. 5. 10-MHz high harmonic generation in an enhancement cavity.

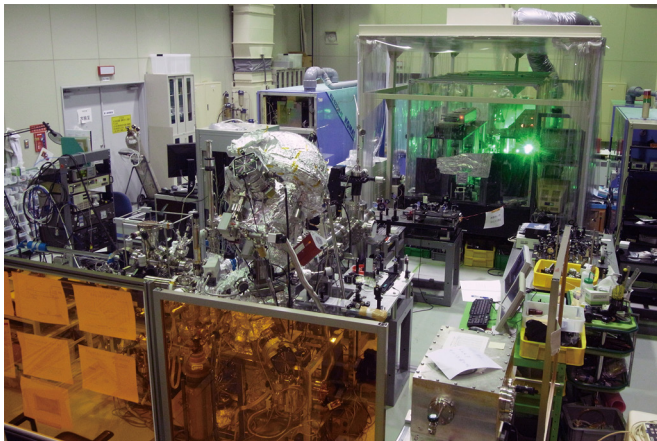


Fig. 6. Pump-probe photoemission system using 60-eV laser

We also aim to develop novel laser spectroscopy and coherent non-linear optical physics, enabled via emerging lasers and optical science/technology, and extensively study basic light-matter physics, optical materials science, and applied photonics. Such researches include ultrafast spectroscopy for excited state dynamics, terahertz magnetic-field spectroscopy for spin dynamics, quantitative micro-spectroscopy on semiconductor lasers and nano-structure photonics devices, such as quantum wire lasers, gain-switch semiconductor laser, multi-junction solar cells, and bio-luminescent systems.

• Synchrotron radiation science group

By inheriting and developing the synchrotron techniques cultivated for more than 20 years, we continuously develop world cutting-edge spectroscopies such as time-resolved photoemission/diffraction, ultrahigh resolution soft X-ray emission, 3D (depth + 2D microscopy) nano ESCA and X-ray magneto-optical effect and provide these techniques both for basic material science and for applied science, which contributes to the device applications in collaboration with outside researchers. In order to pioneer new spectroscopies for the next-generation light sources, we upgrade fast polarization switching of the undulator light source in cooperation with SPring-8. In addition, we promote frontier works on the use of X-ray free electron lasers, SACLA with high spatial and temporal coherence comparable to optical lasers in collaboration with scientists of laser light sources and spectroscopies.

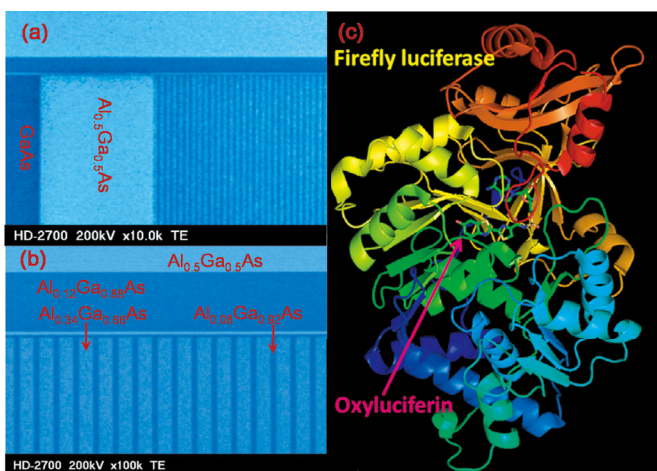


Fig. 7. Photonics devices under study: (left panel) semiconductor quantum wires and (right panel) firefly-bioluminescence system consisting of light emitter (oxyluciferin) and enzyme (luciferase)

• Extreme spectroscopy group

The advent of laser-based light sources in the soft-X-ray region is opening a new stage in the field that has been cultivated by the synchrotron radiations. One of the milestones is to develop a laser-based light source of ~ 7 eV for the sub-meV-resolution photoemission spectroscopy. In this five years, available photon energy became 11 eV with help of Yb-fiber laser technology. It has high photon flux (10^{14} photons/sec) with sub picosecond time resolution. Laser-based spin-resolved ARPES was realized in LASOR. This technology would open brand-new spectroscopy. High-harmonic generation based photoemission spectroscopy in the 20-60 eV region is another direction to be pursued. Time-domain spectroscopy in the femtosecond region was achieved. Combined with the picosecond time-domain spectroscopy utilizing the pulsed light delivered from synchrotrons, we investigate the electronic structures and dynamics of matter in bulk, on surface, and into the nano-scale. The ultimate objective is to expand the soft-X-ray operando methodologies by lasers. Diffractions, magneto-optical effects, and inelastic scatterings now done at synchrotrons will be performed by lasers, to access the real-time dynamics of chemical reactions and phase transitions down to the femtoseconds.

State-of-the-art laser based organism spectroscopy is a new direction in LASOR. ISSP research area is shifting from simple material and science to complex one including living body and functional material with excited state physics.

Synchrotron Radiation Laboratory

The Synchrotron Radiation Laboratory (SRL) was established in 1975 as a research division dedicated to solid state physics using synchrotron radiation (SR). Currently, SRL is composed of two research sites, the Harima branch and the E-building of the Institute for Solid State Physics.

• Brilliant soft X-ray beamline at Harima branch

In 2006, the SRL staffs have joined the Materials Research Division of the Synchrotron Radiation Research Organization (SRRO) of the University of Tokyo and they have played an essential role in constructing a new high brilliant soft X-ray beamline, BL07LSU, in SPring-8. The

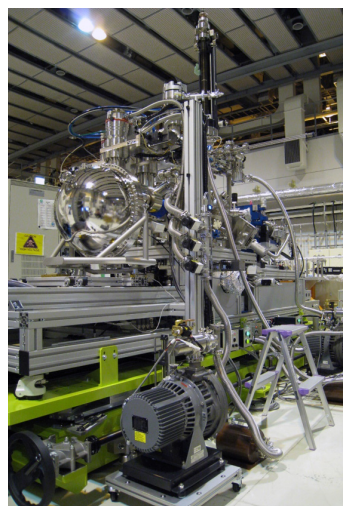


Fig. 1. Ambient pressure photoemission

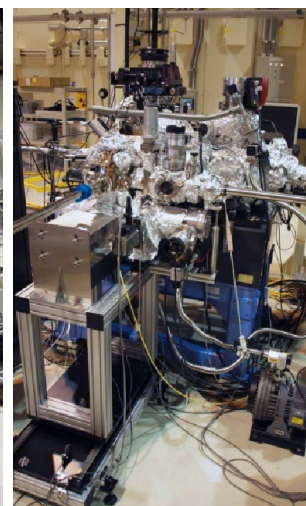


Fig. 2. 3D nano-ESCA station

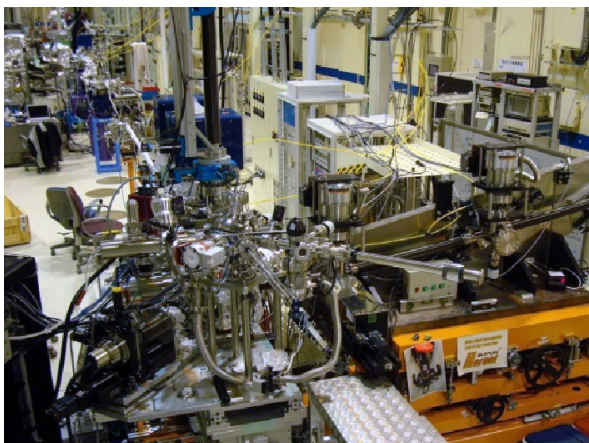


Fig. 3. Soft X-ray emission station

light source is the polarization-controlled 25-m long soft X-ray undulator with electromagnetic phase shifters that allow fast switching of the circularly (left, right) and linearly (vertical, horizontal) polarized photons.

The monochromator is equipped with a varied line-spacing plain grating, which covers the photon energy range from 250 eV to 2 keV. At the downstream of the beamline, a lot of experimental stations have been developed for frontier spectroscopy researches: three endstations, i.e. ambient pressure photoemission (Fig. 1), three-dimensional (3D) nano-ESCA (Fig. 2), high resolution soft X-ray emission spectroscopy (XES) (Fig. 3) stations are regularly maintained by the SRL staffs and open for public use, and at free-port station many novel spectroscopic tools have been developed and installed such as soft X-ray resonant magneto-optical Kerr effect (XMOKE) and so on. The beamline construction was completed in 2009 and SRL established the Harima branch laboratory in SPring-8. At SPring-8 BL07LSU, each end-station has achieved high performance: the time-resolved soft X-ray spectroscopy (TR-SX) station equipped with a two-dimensional angle-resolved time-of-flight (ARTOF) analyzer has established the laser-pump and SR-probe method with the time-resolution of 50 ps which corresponds to the SR pulse-width. This apparatus was moved to E-building in the 2020 summer to realize better temporal resolution using the fsec high harmonic laser pulse of 11 eV; the 3D nano-ESCA station reaches the spatial resolution of 70 nm; the XES station provides spectra with the energy resolution around 70 meV at 400 eV and enables real ambient pressure experiments. Soft X-ray resonant MOKE station has been developed to make novel magneto-optical experiment using fast-switching of the polarization-

controlled 25-m long soft X-ray undulator. In 2020, 24 user groups made their experiments during the SPring-8 operation time. The number is slightly decreased compared with the usual annual operation because of the COVID-19 problem. The official beamtime was cut off in April and May and replaced by the beamtime in the latter half of 2020.

• High-resolution Laser SARPES at E-building

High-resolution Laser Spin- and Angle-Resolved Photoemission Spectroscopy (SARPES) is a powerful technique to investigate the spin-dependent electronic states in solids. In FY2014, LASOR and SRL staffs constructed a new SARPES apparatus (Fig. 4), which was designed to provide high-energy and -angular resolutions and high efficiency of spin detection using a laser light at E-building. The achieved energy resolution of 1.7 meV in SARPES spectra is the highest in the world at present. From FY2015, the new SARPES system has been opened to outside users.

The Laser-SARPES system consists of an analysis chamber, a carousel chamber connected to a load-lock chamber, and a molecular beam epitaxy chamber, which are kept ultra-high vacuum (UHV) environment and are connected to UHV gate valves. The electrons are excited with 6.994-eV photons, yielded by 6th harmonic of a Nd:YVO₄ quasi-continuous wave laser with a repetition rate of 120 MHz, and 10.7 eV photons, driven by the third harmonic radiation at 347 nm of an Yb: fiber chirped pulse amplifier laser, which was developed by Kobayashi's lab in LASOR. The hemispherical electron analyzer is a custom-made Scienta Omicron DA30-L, modified for installing the spin detectors. The spectrometer is equipped with two high-efficient spin detectors associating very low energy electron diffraction are orthogonally placed each other, which allows us to analyze the three-dimensional spin polarization of electrons. At the exit of the hemispherical analyzer, a multi-channel plate and a CCD camera are also installed, which enables us to perform the angle-resolved photoelectron spectroscopy with two-dimensional (energy-momentum) detection. The laser-SARPES with 7-eV laser can provide both high-resolution spin-integrated and spin-resolved photoemission spectra in various types of solids, such as spin-orbit coupled materials and ferromagnetic materials. In addition, using the 10.7-eV makes it possible to follow their ultrafast spin dynamics in the time domain by pump-probe scheme.

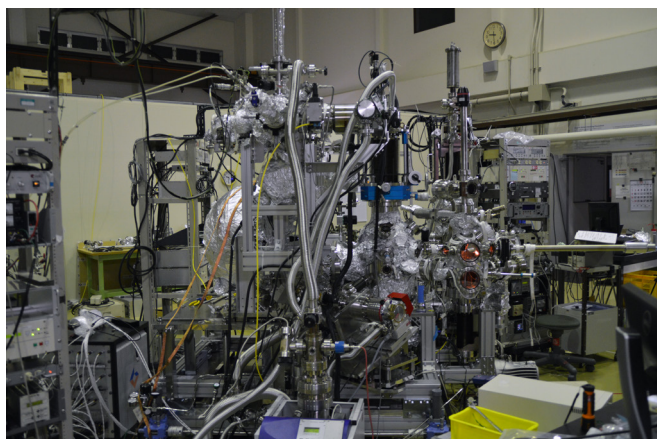


Fig. 4. Laser-SARPES system at E-building

Conferences and Workshops

Frontiers of Quantum Computational Science

July 9-10, 2020

H. Shinaoka, T. Okubo, J. Otsuki, N. Kawashima, S. Todo, T. Misawa, and S. Morita

Various numerical methods such as dynamical mean-field approximation, variational Monte Carlo, and tensor network methods have been developed for solving quantum many-body problems. In addition, there are many attempts to quantitatively predict the properties of strongly correlated materials by integrating these elaborate many-body methods and first-principles methods. In recent years, new approaches using machine learning, quantum computers, and quantum chemical methods have emerged for solving many-body problems. There is a need for an opportunity for researchers in different fields to meet, exchange information, and have extensive discussions. The Institute of Solid State Physics has been playing an essential role as a center for computational condensed matter physics. Thus, it is of great significance for the future development of computational condensed matter physics to hold a short-term workshop with experts in these different fields.

In line with the workshop theme, we invited young researchers in quantum computing, machine learning, information theory, and in first-principles and model calculations on quantum many-body systems. The final program consisted of 20 oral talks (including 11 invited talks) and 15 poster talks. The number of registered participants was 180, and more than 150 attended both days, with a maximum of 120 simultaneous participants in real-time. Although the workshop was held online using Webex and Slack due to the COVID-19 pandemic, there were extensive discussions between participants in oral and poster talks.



Present Status of Neutron Scattering Research and the Future Prospect after the Restart of JRR-3

July 27-29, 2020

T. Masuda, T. Nakajima, O. Yamamuro, M. Fujita, T. Sato, T. Osakabe, M. Sugiyama, and M. Hino

Neutron Science Laboratory (NSL) operates collaboration research using research reactor JRR-3 and has been leading neutron scattering science. JRR-3, however, has suspended its operation since the Great East Japan Earthquake in 2011. Owing to the strong and patient demand from the neutron science community, JRR-3 has finally restarted in February 2021 after the long aseismic reinforcing work. In prior to the restart, NSL held the ISSP regular workshop for the neutron users to discuss the frontier of the research related to neutron science, for the instrumental scientists to propose possible research plan after the restart, and for both to discuss new institution of collaboration research constructed under the latest safety standard. Because of the COVID19 the workshop was held using ZOOM, and 115 scientists including those from abroad participated. 15 presentations on solid state physics and 15 presentations on material science and soft matter were made followed by active discussions. 5 presentation on the new institution of the collaboration research were made on the last day. NSL director Yamamuro proposed the revised plan of Instrumentation and Research Team for the update and maintenance of spectrometers and the promotion of the science for the instrumental scientists as well as the revised proposal format of the general user program meeting the latest safety standard. In spite of the first ZOOM workshop for NSL it finished a success.

Recent Developments and Future Prospects of Quantum Materials Research

September 24, 28, 29, 2020
Y. Otani, M. Yamashita, and Z. Hiroi

Condensed matter physics has evolved significantly through the discovery of new substances, phenomena and concepts. Especially in the strongly correlated electron system field where simple one-particle approximation breaks down, close cooperation of synthesis, measurement, and theory, which bear these three elements, is important. In recent years, quantum materials that have developed strongly correlated electron systems have been attracting attention, and the Institute for Solid State Physics, University of Tokyo has established a quantum materials research group with the aim of breaking through research through the fusion of fields. Furthermore, the experimental group of the Material Design and Characterization Laboratory, which has been responsible for material development, and the Research Division of the Condensed Matter Physics, which has been mainly responsible for measurement, are strongly collaborating with the Quantum Materials Research Group to develop active research.

Based on the above situation, this ISSP workshop focused on material development in quantum materials research and experimental research using various measurement methods, and aimed to give an overview of the current state of recent research and discuss future research prospects. The event was co-sponsored by the Quantum Materials Research Group, the Research Division of the Condensed Matter Physics, and the Material Design and Characterization Laboratory.

The workshop was held in the morning of three days in the form of presentation at Zoom, and a total of 18 researchers gave lectures in the program. Pre-registration reached 171 people, with 120-130 participants daily throughout the three days. The speakers introduced recent research on quantum materials and expressed their opinions on future prospects, and there were many questions and comments from the participants, and lively discussions took place. Although it was held in an unusual format using Zoom, it was as meaningful an opportunity as the conventional workshop. It was also an opportunity to think about the future of the research at the Institute for Solid State Physics.

Computational Materials Science —New Perspectives2020—

December 21- 22, 2020
O. Sugino, T. Ozaki, N. Kawashima, H. Noguchi, T. Fukushima,
Y. Higuchi, S. Morita, J. Haruyama, M. Kawamura, M. Fukuda, and K. Ido

This workshop was organized for the computational condensed matter research community, especially for the users of the ISSP supercomputers, to exchange the most recent information on the computational condensed matter research and on the high-performance computation of related research areas. This was held as a series of annual workshop of ISSP supercomputer that has been held every year. However, the workshop has been postponed from April to December due to the state of emergency caused by COVID-19 and has been held at ONLINE. The registered people were 135. The selected topics include the target of the Fugaku supercomputer project, the emergent data-driven material research, and “Project for advancement of software usability in materials science (PASUMS)” that developed the ab-Initio Configuration Sampling tool kit (abICS) to solve the replica exchange Monte Carlo (RXMC) sampling coupled directly with local structural relaxation and energy calculation using DFT codes in 2019. In addition to 19 invited talks, 26 poster presentations, and a special lecture for data-repository were given by Prof. Miho Funamori. In the poster presentation, short talk presentations and discussions using an online bulletin board and zoom break-out room have been set. The posters were evaluated by invited speakers and the organizers; three posters were selected and given the poster award.



Present and Future of Data Science in Condensed Matter Physics

February 22 and 24, 2021

K. Yoshimi, T. Ozaki, O. Sugino, H. Noguchi, T. Fukushima, K. Ido, M. Fukuda, R. Tamura, and N. Kawashima

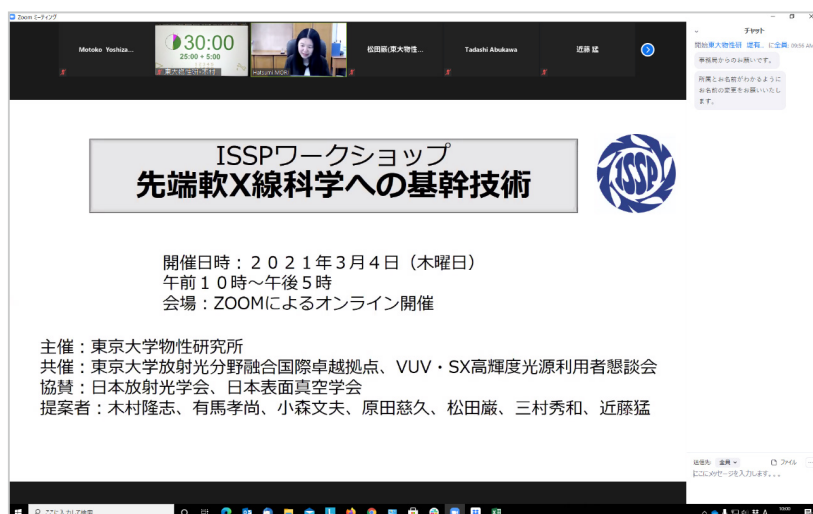
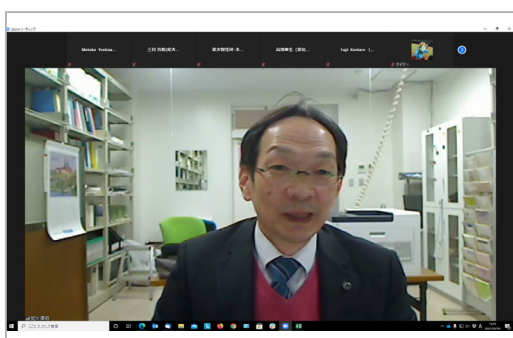
Recently, researchers are becoming more enthusiastic in application of data-scientific methods to condensed matter physics, with the hope for developing a new scheme for numerical simulation, improvement of quality of theoretical predictions, and acceleration in search and development of new materials. From these activities, problems arise concerning how we manage ever-increasing data and make them more usable in the new schemes. We intended this workshop to be an opportunity for the participants to share experience in application of data-scientific methods to condensed matter physics and biochemistry, as well as data-base construction and its maintenance. We had 209 registrations and recorded 150 maximum simultaneous participants on the first day and 120 for the second. The first day was dedicated to the application of machine learning in physics and biochemistry whereas the second day was for data-repositories and data-bases. Concerning application of the machine learning, Sugino (ISSP) gave a presentation on machine learning for basic aspects of the theoretical condensed matter physics, i.e., the numerical estimation of the Kohn-Sham exchange-correlation potential. Ozaki (ISSP), Fukushima (ISSP) and Chikyo (NIMS) presented their works on the comprehensive high-throughput calculation and/or construction of material data-bases. Terayama (Yokohama City U.) discussed the 3D structural study of protein molecules aided by the machine learning, and Inoue (ISSP) talked about function prediction of amino-acid sequences. As for data-repositories and data-bases, Katsura (NIMS) talked about the construction of the data-base from the graphic information of research papers, and its applications. Taura (U Tokyo) presented the current state of the starting project on "mdx". Kobayashi (ISSP)'s talk was about laser manufacturing as a potential target of data-accumulation and machine-learning. Miyake (AIST) presented their recent result on the data assimilation method based on both numerical and experimental data in search of new magnetic materials. Upon these results, we also held a panel discussion to further discuss what new framework is to be created for the data management and how we should proceed in its applications, with panellers being Kobayashi (ISSP), Tamura (U Tokyo and NIMS), Katsura (NIMS) and Shoji (TOYOTA) and the mediator Yoshimi (ISSP).

Core Technology Toward the Frontier Soft X-Ray Science

March 4, 2021

T. Kimura, T. Arima, F. Komori, Y. Harada, I. Matsuda, H. Mimura, and T Kondo

The workshop was organized on March 4 by the Institute for Solid State Physics (ISSP) and Synchrotron Radiation Research Organization of the University of Tokyo (UTokyo-SRRO) and User Community VUV-SX High-Brilliance Light Sources. The workshop was held online using ZOOM, and about 140 participants from a wide range of fields, including universities, companies and research institutes, attended. In this workshop, eight researchers were invited to give talks on the latest trends in soft X-ray science and to discuss the new direction that will emerge from the next-generation synchrotron radiation facility in Sendai. The next-generation synchrotron radiation facility is expected to improve the coherence and intensity of X-rays. In each lecture, various research results on imaging and spectroscopic techniques were reported, ranging from basic beamline technologies to applied measurements, which can use the features of the new facility. The newly-organized general discussion session (Moderator: Professor Abukawa from Tohoku University) provided an opportunity for in-depth questions and answers about the contents of each lecture. In the last session, Director Harada presented the prospects and direction of the SOR facility towards the operation start of the new synchrotron radiation facility in 2023.



ISSPワークショップ
先端軟X線科学への基幹技術

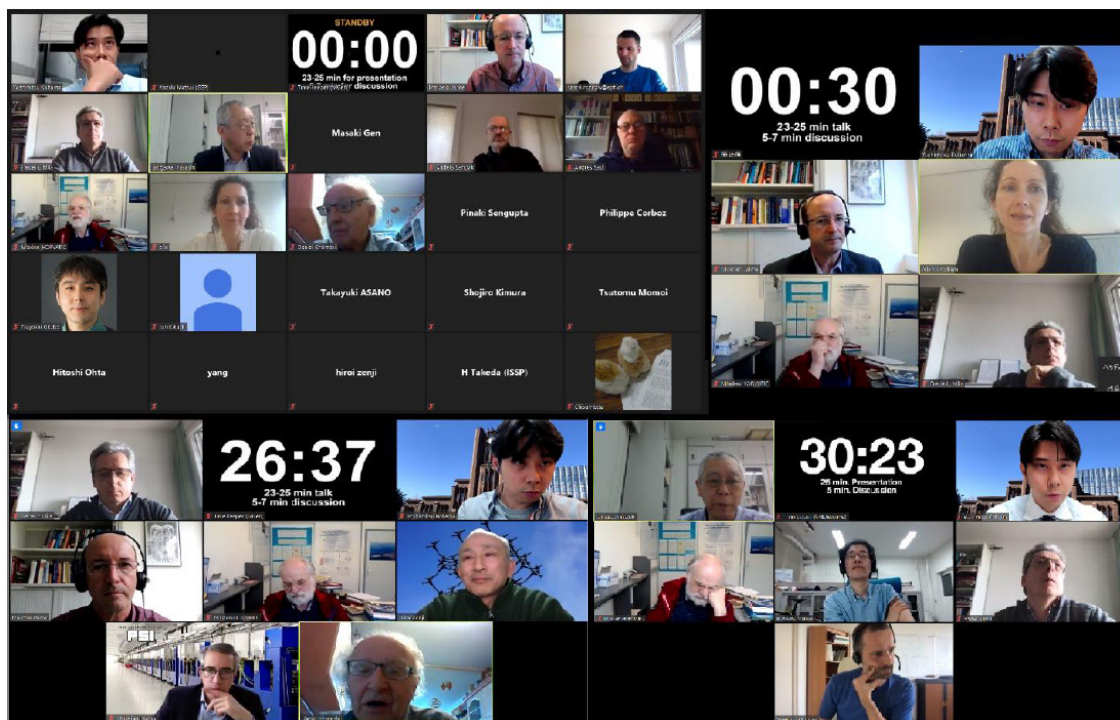
開催日時：2021年3月4日（木曜日）
午前10時～午後5時
会場：ZOOMによるオンライン開催

主催：東京大学物性研究所
共催：東京大学放射光分野融合国際卓越拠点、VUV・SX高輝度光源利用者懇談会
協賛：日本放射光学会、日本表面真空学会
提案者：木村隆志、有馬孝尚、小森文夫、原田慈久、松田蔵、三村秀和、近藤猛

The International Workshop on Quantum Magnets in Extreme Conditions

March 22-26, 2021
Y. Kohama, F. Mila, and M. Jaime

This workshop was held as an online virtual conference due to the COVID-19 pandemic. The main focus of this workshop was the fascinating emergent physical properties of solid-state quantum magnets in both theoretical and experimental research fields. The workshop was free of charge and started from 21:00 pm to 24:00 pm in JST (13:00 pm - 16:00 pm in CET and 8:00 am - 11:00 am in EDT) to encourage the participation of international students and upcoming international researchers. The total number of registrations was 438. The numbers of participants on Monday, Tuesday, Wednesday, Thursday, and Friday were 320, 234, 221, 179, and 151, respectively (the total number of participants was 1105). The 25 talks were given by the invited speakers who are leading scientists in their field of research. It should be noted that the second international workshop on Quantum Magnets in Extreme Conditions is tentatively scheduled in 2023 as a hybrid conference. We hope that the next workshop can give us a chance to share novel ideas and to exchange the forthcoming results in this exciting research field.



Subjects of Joint Research

令和2年度 共同利用課題一覧（前期） / Joint Research List (2020 First Term)

嘱託研究員 / Commission Researcher

No.	課題名	氏名	所属	Title	Name	Organization
担当所員：森 初果						
1	自己組織化二分子膜における電子-プロトン相関物性の探究	加藤 浩之	大阪大学	大学院理学研究科	Study of electron -proton correlated properties in self-assembled bilayers	Hiroyuki Kato Osaka University
担当所員：長谷川 幸雄						
2	極低温走査トンネル顕微鏡を用いた鉄カルコゲナイド超伝導体 FeSeTe の研究	吉田 靖雄	金沢大学	理工学域	Low-temperature STM study on iron-chalcogenide superconductor FeSeTe	Yasuo Yoshida Kanazawa University
3	走査トンネル顕微鏡による局所強磁性共鳴法の開発	安 東秀	北陸先端科学技術大学院大学	先端科学技術研究科	Development of local ferromagnetic resonance in scanning tunneling microscopy	Toshu An Japan Advanced Institute of Science and Technology
4	走査トンネル顕微鏡による Fe 系超伝導薄膜の評価	シルビア ハインドル	東京工業大学	科学技術創成研究院	Investigation of Fe-based superconducting thin films by scanning tunneling microscopy	Silvia Haindl Tokyo Institute of Technology
担当所員：リップマー ミック						
5	Materials Foundry のための材料開発システムの構築に向けた薄膜合成装置の開発	高橋 竜太	日本大学	工学部	Development of Films Deposition System for High-throughput Material Exploration	Ryota Takahashi Nihon University
担当所員：川島 直輝						
6	二次元物質構造解析むけ実験データ解析の高度化	星 健夫	鳥取大学	大学院工学研究科	Advancement of the experimental data analysis for 2D material structure	Takeo Hoshi Tottori University
担当所員：上床 美也						

No.	課題名	氏名	所属		Title	Name	Organization
7	希釈冷凍機温度で使用可能な 10GPa 級超高压発生装置の開発	松林 和幸	電気通信大学	大学院情報理工学研究科	Development of 10GPa class high pressure apparatus for low temperature	Kazuyuki Matsubayashi	The University of Electro-Communications
8	高压下量子振動観測システムの開発	摂待 力生	新潟大学	理学部	Development of quantum oscillation under high pressure	Rikio Settai	Niigata University
9	酸化物試料の作製と高压下物性測定	川中 浩史	産業技術総合研究所	電子光技術研究部門	Sample preparation and high pressure experiments	Hirofumi Kawanaka	National Institute of Advanced Industrial Science and Technology
10	有機伝導体の圧力効果	村田 惠三	大阪経済法科大学	21 世紀社会研究所	Effect of pressure on the organic conductor	Keizo Murata	Osaka University of economics and Law
11	3d 遷移化合物に関する圧力効果	鹿又 武	東北学院大学	工学総合研究所	Effect of pressure on the 3d transition compounds	Takeshi Kanomata	Tohoku Gakuin University
12	擬一次元有機物質の圧力下物性研究	糸井 充穂	日本大学	医学部	Study on pressure induced superconductivity of quasi organic conductor	Miho Itoi	Nihon University
13	多重極限関連圧力装置の調整	高橋 博樹	日本大学	文理学部	Adjustment of Cubic Anvil apparatus	Hiroki Takahashi	Nihon University
14	高压下 X 線回折法の開発	江藤 徹二郎	久留米工業大学	工学部	Development of High Pressure X-ray diffraction measurements	Tetsujiro Eto	Kurume Institute of Technology
15	極低温下の磁気特性	鳥塚 潔	日本工業大学	共通教育学群	Development of magnetic measurement method	Kiyoshi Torizuka	Nippon Institute of Technology
16	圧力下 NMR 測定法に関する開発	藤原 直樹	京都大学	大学院人間・環境学研究科	Development of NMR measurement method under high pressure	Kyoto University	Naoki Fujiwara
17	希土類 122 化合物における圧力効果	繁岡 透	山口大学	大学院理工学研究科	Pressure effect of rare earth 122 compounds	Toru Shigeoka	Yamaguchi University
18	低温用マルチアンビル装置の開発	辺土 正人	琉球大学	理学部	Development of multi-anvil apparatus for low temperature	Masato Hedou	University of Ryukyus
19	磁性体の圧力効果	巨海 玄道	久留米工業大学	工学部	Effect of pressure on the Magnetic Materials	Gendo Oomi	Kurume Institute of Technology
20	DAC を用いた物性測定方法の開発	狩野 みか	日本工業大学	共通教育学群	Development of physical property measurement method using DAC	Mika Kano	Nippon Institute of Technology
担当：中性子科学研究施設							
21	4G における共同利用推進	佐藤 卓	東北大学	多元物質科学研究所	Research and Support of General-Use at 4G	Taku Sato	Tohoku University
22	”	奥山 大輔	東北大学	多元物質科学研究所	”	Daisuke Okuyama	Tohoku University

No.	課題名	氏名	所属		Title	Name	Organization
23	”	那波 和宏	東北大学	多元物質科学研究所	”	Kazuhiro Nawa	Tohoku University
24	6G、T1-1 における共同利用推進	岩佐 和晃	茨城大学	フロンティア応用原子科学研究センター	Research and Support of General-Use at 6G and T1-1	Kazuaki Iwasa	Ibaraki University
25	T1-1、T1-3 における共同利用推進	大山 研司	茨城大学	大学院理工学研究科	Research and Support of General-Use at T1-1 and T1-3	Kenji Ohoyama	Ibaraki University
26	T1-1 における共同利用推進	桑原 慶太郎	茨城大学	大学院理工学研究科	Research and Support of General-Use at T1-1	Keitaro Kuwahara	Ibaraki University
27	”	横山 淳	茨城大学	理学部	”	Makoto Yokoyama	Ibaraki University
28	”	伊賀 文俊	茨城大学	大学院理工学研究科	”	Fumitoshi Iga	Ibaraki University
29	T1-2、T1-3、6G における共同利用推進	藤田 全基	東北大学	金属材料研究所	Research and Support of General-Use at T1-2, T1-3 and 6G	Masaki Fujita	Tohoku University
30	”	南部 雄亮	東北大学	金属材料研究所	”	Yusuke Nambu	Tohoku University
31	”	池田 陽一	東北大学	金属材料研究所	”	Yoichi Ikeda	Tohoku University
32	”	谷口 貴紀	東北大学	金属材料研究所	”	Takanori Taniguchi	Tohoku University
33	T2-2、T1-3 における共同利用推進	木村 宏之	東北大学	多元物質科学研究所	Research and Support of General-Use at T2-2 and T1-3	Hiroyuki Kimura	Tohoku University
34	”	坂倉 輝俊	東北大学	多元物質科学研究所	”	Terutoshi Sakakura	Tohoku University
35	”	山本 孟	東北大学	多元物質科学研究所	”	Hajime Yamamoto	Tohoku University
36	C1-2 における共同利用推進	杉山 正明	京都大学	複合原子力科学研究所	Research and Support of General-Use at C1-2	Masaaki Sugiyama	Kyoto University
37	C1-2、C2-3-1 における共同利用推進	井上 倫太郎	京都大学	複合原子力科学研究所	Research and Support of General-Use at C1-2 and C2-3-1	Rintaro Inoue	Kyoto University
38	”	守島 健	京都大学	複合原子力科学研究所	”	Ken Morishima	Kyoto University
39	C3-1-2、C2-3-1 における共同利用推進	日野 正裕	京都大学	複合原子力科学研究所	Research and Support of General-Use at C3-1-2 and C2-3-1	Masahiro Hino	Kyoto University

No.	課題名	氏名	所属		Title	Name	Organization
40	C3-1-2 における共同利用推進	田崎 誠司	京都大学	大学院工学研究科	Research and Support of General-Use at C3-1-2	Seiji Tasaki	Kyoto University
41	”	小田 達郎	京都大学	複合原子力科学研究所	”	Tatsuro Oda	Kyoto University
42	”	北口 雅暁	名古屋大学	大学院理学研究科	”	Masaaki Kitaguchi	Nagoya University
43	C1-2、C2-3-1 における共同利用推進	中川 慎太郎	東京大学	生産技術研究所	Research and Support of General-Use at C1-2 and C2-3-1	Shintaro Nakagawa	The University of Tokyo
担当所員：徳永 将史							
44	パルス強磁場用断熱消磁冷却システムの開発	野口 悟	大阪府立大学	大学院理学系研究科	Development of adiabatic demagnetization cooling system for pulsed fields	Satoru Noguchi	Osaka Prefecture University
担当所員：近藤 猛							
45	有機化合物の光電子分光	金井 要	東京理科大学	理工学部	Photoemission study on organic compounds	Kaname Kanai	Tokyo University of Science
46	トポロジカル絶縁体の電子状態の解明	木村 昭夫	広島大学	大学院理学研究科	Electronic-structure study of topological insulators	Akio Kimura	Hiroshima University
47	光電子分光法を用いた各種分子性結晶の電子状態の研究及び装置の低温化	木須 孝幸	大阪大学	基礎工学研究科	Research on electron state of molecular crystals using photoemission spectroscopy	Takayuki Kisu	Osaka University
48	トポロジカル超伝導体の探索	坂野 昌人	東京大学	大学院工学系研究科	Research for topological insulators	Masato Sakano	The University of Tokyo
49	高分解能光電子分光による強相関物質の研究	横谷 尚睦	岡山大学	異分野基礎科学研究所	Ultra-high resolution study on strongly correlated materials	Takayoshi Yokota	Okayama University
担当所員：岡崎 浩三							
50	鉄系超伝導体のレーザー光電子分光	下志万 貴博	理化学研究所	創発物性科学研究センター	Laser-ARPES on Fe superconductor	Takahiro Shimojima	RIKEN
51	60-eV レーザーを用いた時間分解光電子分光の開発	石坂 香子	東京大学	大学院工学系研究科	The development of time-resolved photoemission using 60eV laser	Kyoko Ishizaka	The University of Tokyo
52	固体中のマヨラナ粒子の研究	松田 祐司	京都大学	大学院理学研究科	Study of Majorana Fermion in Solids by Laser Photoemission Spectroscopy	Yuji Matsuda	Kyoto University
53	”	佐藤 昌利	京都大学	基礎物理学研究所	”	Masatoshi Sato	Kyoto University

No.	課題名	氏名	所属		Title	Name	Organization
54	レーザー励起光電子顕微鏡を使った抵抗変化メモリ材料の研究	木下 健太郎	東京理科大学	理学部	Study on Materials for Resistive Switching Memories using laser-PEEM	Kentaro Kinoshita	The University of Tokyo
55	収差補正型光電子顕微鏡の建設と利用研究	小嗣 真人	東京理科大学	基礎工学部	Construction and utilization research of aberration correction photoelectron emission microscopy	Masato Kotsugi	Tokyo University of Science
56	FeSe 超伝導体における BCS-BES クロスオーバーの研究	紺谷 浩	名古屋大学	大学院理学研究科	Study of BCS-BES crossover in FeSe superconductors	Hiroshi Kontani	Nagoya University
57	時間分解光電子分光を用いた強相関物質の研究	溝川 貴司	早稲田大学	理工学術院	Time-resolved photoemission study on strongly-correlated materials	Takashi Mizokawa	Waseda University
58	時間分解光電子分光や超高分解能光電子分光を用いた超伝導体や強相関物質の研究	吉田 鉄平	京都大学	総合人間学部 / 人間・環境学研究科	Laser ARPES study on superconductors and strongly-correlated materials	Teppey Yoshida	Kyoto University
59	超高分解能レーザー光電子分光による高温超伝導体の研究	チャン ウェイル	上智大学	機能創造理工学	Study of high-Tc superconductors by high-resolution laser ARPES	Weilu Zhang	Sophia University
60	テラヘルツ光源を用いた光誘起絶縁体-金属転移の研究	久保田 雄也	放射光科学研究センター	XFEL 研究開発部門	Investigation of the photo-induced insulator-to-metal transition by terahertz optics	Yuya Kubota	JASRI
担当所員：原田 慈久							
61	軟 X 線発光・共鳴非弾性散乱分光の磁気円・線二色性測定システムの構築	菅 滋正	大阪大学	産業科学研究所	Construction of a noble system for circular and linear dichroism in soft X-ray emission and RIXS spectroscopy	Shigemasa Suga	Osaka University
62	軟 X 線吸収 / 発光分光法によるリチウムイオン電池電極材料の電子物性研究	細野 英司	産業技術総合研究所	省エネルギー研究部門	Study on the electronic property of electrode materials for Li-ion batteries by soft X-ray absorption/emission spectroscopy	Eiji Hosono	AIST
63	”	朝倉 大輔	産業技術総合研究所	”	”	Daisuke Asakura	AIST
64	高分解能光電子分光による酸化バナジウムの研究	藤原 秀紀	大阪大学	大学院基礎工学研究科	Study on vanadium oxides by high resolution Photoemission	Hidenori Fujiwara	Osaka University
65	省エネ・創エネ・蓄電デバイスのオペランド分光	尾嶋 正治	東京大学	大学院工学系研究科	Operando nano-spectroscopy for energy efficient, power generation and energy storage devices	Masaharu Oshima	The University of Tokyo
66	原子レベルで制御されたモデル有機分子表面上の界面水の電子状態観測	林 智広	東京工業大学	物理工学院	Analysis of the electronic structure of the interfacial water formed on model organic surfaces	Tomohiro Hayashi	Tokyo Institute of Technology
67	三次元 nanoESCA による実デバイスのオペランド電子状態解析	永村 直佳	物質・材料研究機構	”	Operando analysis of the electronic structure of actual device by 3DnanoESCA	Naoka Nagamura	National Institute for Materials Science
68	時間分解光電子顕微分光実験の開発	木下 豊彦	高輝度光科学研究センター	”	Technical development of time-resolved photoemission microscopy measurement	Toyohiko Kinoshita	JASRI
担当所員：松田 巖							

No.	課題名	氏名	所属		Title	Name	Organization
69	スピン分解光電子分光の測定技術開発	木村 真一	大阪大学	大学院生命機能研究科	Technical development of spin-resolved photoemission spectroscopy measurement	Shin-ichi Kimura	Osaka University
70	時間分解磁気光学実験の技術開発	小嗣 真人	東京理科大学	基礎工学部	Technical development of time-resolved magneto-optical experiment	Masato Kotsugi	Tokyo University of Science
71	超高速磁化応答による磁性波動関数の制御	小林 正起	東京大学	大学院工学系研究科	Regulation of magnetic wave functions by ultrafast magnetization response	Masaki Kobayashi	The University of Tokyo
72	コヒーレント共鳴軟 X 線散乱による磁気ドメイン構造の観測	山崎 裕一	物質・材料研究機構	統合型材料開発・情報基盤部門	Observation of magnetic domain structure for ferromagnetic thin films by means of resonant soft x-ray scattering	Yuichi Yamasaki	NIMS
73	遷移金属化合物の時間分解 X 線分光と回折	和達 大樹	兵庫県立大学	大学院物質理学研究科	Time-resolved x-ray spectroscopy and diffraction of transition-metal-compounds	Hiyoki Wadachi	University of Hyogo
74	雰囲気光電子分光装置の高度化	山本 達	東北大学	多元物質科学研究所	Updates of the NAP-XPS machine	Susumu Yamamoto	Tohoku University
75	偏光制御型軟 X 線分光装置の開発	平田 靖透	防衛大学校	応用物理学科	Development of a system for the polarization-controlled soft X-ray spectroscopy	Yasuyuki Hirata	National Defense Academy

一般研究員 / General Researcher

No.	課題名	氏名	所属		Title	Name	Organization
担当所員：瀧川 仁							
1	正三角スピン有機トリラジカルの核磁気共鳴による磁気誘電現象の解明	細越 裕子	大阪府立大学	大学院理学系研究科	NMR study on the magnetodielectric properties of organic equilateral triangular spin system	Yuko Hosokoshi	Osaka Prefecture University
担当所員：榊原 俊郎							
2	重い電子系超伝導体の対称性の決定	町田 一成	立命館大学	理工学部	Determination of pairing symmetry in heavy Fermion superconductors	Kazushige Machida	Ritsumeikan University
3	トポロジカル超伝導のネマチック相研究	孫 悦	青山学院大学	理工学部	Study of the nematic phase of topological superconductors	Yue Sun	Aoyama Gakuin University
4	”	宮沢 貴磨	青山学院大学	理工学部	”	Miyazawa Takamaro	Aoyama Gakuin University
5	空間反転対称性の破れた重い電子系物質 CeIrSi ₃ のフェルミ面転移	木村 憲彰	東北大学	大学院理学研究科	Fermi surface reconstruction in noncentrosymmetric heavy fermion compound CeIrSi ₃	Noriaki Kimura	Tohoku University
6	重い電子系化合物における量子臨界現象	横山 淳	茨城大学	大学院理工学研究科	Quantum critical behavior in heavy-fermion compounds	Makoto Yokoyama	Ibaraki University

No.	課題名	氏名	所属		Title	Name	Organization
7	”	ラフマント	茨城大学	大学院理工学研究科	”	Rahmanto	Ibaraki University
8	新奇ウラン系スピン三重項超伝導体における極低温精密磁化・熱膨張測定	清水 悠晴	東北大学	金属材料研究所	Novel spin-triplet uranium superconductors studied by precise magnetization and thermal-expansion measurements	Yusei Shimizu	Tohoku University
9	有機ラジカルから成るフラストレート系の低温物性測定	山口 博則	大阪府立大学	大学院理学系研究科	Low-temperature physical properties of frustrated spin systems composed of organic radicals	Hironori Yamaguchi	Osaka Prefecture University
10	磁場方位制御下における Sr ₂ RuO ₄ の極低温磁歪測定	橘高 俊一郎	中央大学	理工学部	Low-temperature magnetostriction measurement on Sr ₂ RuO ₄ under precise control of field orientation	Shunichiro Kittaka	Chuo University
11	”	河野 洋平	中央大学	理工学部	”	Yohei Kono	Chuo University
12	遍歴電子メタ磁性系及びフラストレーション系の極低温比熱測定	齋藤 明子	物質・材料研究機構	液体水素材料研究センター	Investigation of Itinerant-electron Metamagnetism and Geometrically-frustrated Spin-systems by Low-temperature Specific-heat Measurements	Akiko T. Saito	National Institute for Materials Science
担当所員：山下 穰							
13	三角格子反強磁性体の低温比熱測定	柄木 良友	琉球大学	教育学部	Low temperature specific heat measurements of triangular antiferromagnets.	Yoshitomo Karaki	University of the Ryukyus
14	YbRh ₂ Si ₂ の超低温における dHvA 効果測定	宍戸 寛明	大阪府立大学	大学院工学研究科	dHvA effect measurements on YbRh ₂ Si ₂ at ultra-low temperatures	Hiroaki Shishido	Osaka Prefecture University
15	熱輸送測定による量子常誘電・常磁性状態の研究	下澤 雅明	大阪大学	大学院基礎工学研究科	Studies of quantum disordered states of electric and magnetic dipoles by thermal transport measurements	Masaaki Shiozawa	Osaka University
担当所員：勝本 信吾							
16	量子ホール効果のための高移動度半導体試料作製と超低温での測定	福田 昭	兵庫医科大学	物理学教室	Development of the high mobility semiconductor samples for the quantum Hall state and their measurements in very low temperature	Akira Fukuda	Hyogo College of Medicine
17	二次元銅酸化物のホール測定と MPMS による磁化の測定	神戸 士郎	山形大学	大学院理工学研究科	Hall coefficient measurement of 2D cuprates and measurement of magnetic property by MPMS II	Shiro Kambe	Yamagata University
18	”	島袋 義仁	山形大学	大学院理工学研究科	”	Yoshihito Shimabukuro	Yamagata University
19	ナノセンシングデバイスの研究	米谷 玲皇	東京大学	大学院新領域創成科学研究科	Research on nanosensing device	Reo Kometani	The University of Tokyo
20	”	黎 学思	東京大学	大学院新領域創成科学研究科	”	Xuesi Li	The University of Tokyo
21	”	齊藤 正樹	東京大学	大学院新領域創成科学研究科	”	Masaki Saito	The University of Tokyo

No.	課題名	氏名	所属		Title	Name	Organization
22	”	橋本 将	東京大学	大学院新領域創成科学研究科	”	Sho Hashimoto	The University of Tokyo
23	”	田中 駿太郎	東京大学	大学院新領域創成科学研究科	”	Shuntaro Tanaka	The University of Tokyo
24	Ti/MoS ₂ 界面における超伝導状態の研究	石黒 亮輔	日本女子大学	理学部	Study of superconductivity at a Ti/MoS ₂ interface	Ryosuke Ishiguro	Japan Women's University
25	”	浜本 あや	日本女子大学	理学部	”	Aya Hamamoto	Japan Women's University
26	酸化チタンナノシート上グラフェンの量子輸送	原 正大	熊本大学	大学院先端科学研究部	Quantum transport in a graphene on a titanium oxide nanosheet	Masahiro Hara	Kumamoto University
27	”	志手 大輝	熊本大学	大学院自然科学教育部	”	Daiki Shite	Kumamoto University
28	微細素子化した強相関物質における電流誘起された電子相の開拓 2	成田 秀樹	京都大学	大学院理学研究科	Investigation of electric current induced electronic phase in a microfabricated strongly correlated materials 2	Hideki Narita	Kyoto University
担当所員：小森 文夫							
29	特異なスピン状態を持つ希土類及び遷移金属化合物表面及び吸着磁性原子電子状態とスピン状態の STS 解析	菅 滋正	大阪大学	産業科学研究所	Scanning Tunneling Spectroscopy of surfaces of exotic rare earth and transition metal compounds and adsorbed magnetic atoms	Shigemasa Suga	Osaka University
30	窒素を飽和吸着させた Cu(001) 面における構造緩和 (2)	山田 正理	中央大学	理工学部	Structural relaxation on a Cu(001) surface saturated with adsorbed nitrogen (2)	Masamichi Yamaada	Chuo University
31	微傾斜 Si(111) $\sqrt{3} \times \sqrt{3}$ -B 基板上に成長した Bi(110) 超薄膜の電子状態	中辻 寛	東京工業大学	物質理工学院	Electronic structure of Bi(110) thin films grown on vicinal Si(111) $\sqrt{3} \times \sqrt{3}$ -B substrates	Kan Nakatsuji	Tokyo Institute of Technology
32	”	中村 玲雄	東京工業大学	物質理工学院	”	Leo Nakamura	Tokyo Institut of Technology
33	酸素サーファクタントを用いた Fe 薄膜の成長過程と電子状態	中辻 寛	東京工業大学	物質理工学院	Oxygen surfactant assisted growth of Fe thin-films and their electronic states	Kan Nakatsuji	Tokyo Institute of Technology
34	”	木村 彰博	東京工業大学	物質理工学院	”	Akihiro Kimura	Tokyo Institute of Technology
35	真空転写法により形成したツイストグラフェンの電子状態評価	田中 悟	九州大学	大学院工学研究院	Evaluation of electronic structures of twisted graphene fabricated by vacuum transfer technique	Satoru Tanaka	Kyushu University
36	”	今村 均	九州大学	大学院工学府	”	Hitoshi Imamura	Kyushu University
37	SiC ナノ周期表面上に転写したグラフェンの電子状態の観察	田中 悟	九州大学	大学院工学研究院	Evaluation of electronic structures of graphene transferred on SiC periodic nanosurfaces	Satoru Tanaka	Kyushu University

No.	課題名	氏名	所属		Title	Name	Organization
38	”	魚谷 亮介	九州大学	大学院工学府	”	Ryosuke Uotani	Kyushu University
39	強相関トポロジカル絶縁体の極低温・強磁場STM観察	宮町 俊生	電気通信大学	情報理工学研究科	Low-temperature/High-magnetic field STM of strongly correlated topological insulators	Toshio Miyamachi	The University of Electro-Communications
担当所員：長谷川 幸雄							
40	走査トンネル顕微鏡を用いた重い電子系 Eu 化合物の電子状態測定	志賀 雅亘	九州大学	大学院工学府	Electronic density of state measurement of Eu-heavy fermion system using STM technique	Masanobu Shiga	Kyushu University
41	IV 族二次元材料及びそのヘテロ構造の低温走査トンネル顕微鏡観察	高村 由起子	北陸先端科学技術大学院大学	マテリアルサイエンス系	STM investigation of group IV 2D materials and their heterostructures	Yukiko Takamura	JAIST
42	原子層物質 $\sqrt{7} \times \sqrt{3}$ -Inの超伝導に対する界面の影響	平山 博之	東京工業大学	理学院	Interface effect on the superconductivity of the $\sqrt{7} \times \sqrt{3}$ -In atomic layer material	Hiroyuki Hirayama	Tokyo Institute of Technology
43	”	荻野 嵩大	東京工業大学	理学院	”	Takahiro Ogino	Tokyo Institute of Technology
担当所員：リップマー ミック							
44	機械学習を導入した高効率薄膜作製手法の開発	大久保 勇男	物質・材料研究機構	機能性材料研究拠点	High-throughput thin film growth combined with a machine learning approach	Isao Ohkubo	National Institute for Materials Science
担当所員：吉信 淳							
45	遷移金属酸化物ナノシート表面への欠陥導入による外来分子吸着の制御	野内 亮	大阪府立大学	大学院工学研究科	Control of molecular adsorption on transition metal oxide nanosheet films by introduction of surface defects	Ryo Nouchi	Osaka Prefecture University
46	有機金属構造体薄膜-超伝導体界面の構築	塚原 規志	群馬工業高等専門学校	電子メディア工学科	Building up the interface between a metal-organic framework film and a superconductor	Noriyuki Tsukahara	National Institute of Technology (KOSEN), Gunma College
担当所員：秋山 英文							
47	エルビウムデルタドープ GaAs の発光特性評価	矢口 裕之	埼玉大学	大学院理工学研究科	Luminescence properties of Er delta-doped GaAs	Hiroyuki Yaguchi	Saitama University
48	”	高宮 健吾	埼玉大学	総合技術支援センター	”	Kengo Takamiya	Saitama University
49	”	清水 椋平	埼玉大学	大学院理工学研究科	”	Ryohei Shimizu	Saitama University
50	Si 基板上に直接成長させた GaN の成長条件が光学特性に及ぼす影響	小柴 俊	香川大学	創造工学部	Influence of growth conditions of GaN on Si substrate on optical properties	Shyun Koshiba	Kagawa University

No.	課題名	氏名	所属		Title	Name	Organization
51	”	石川 由依	香川大学	工学部	”	Yui Ishikawa	Kagawa University
52	希薄磁性半導体 GaGdAs を用いたスピン LED の発光の増強と円偏光度制御	宮川 勇人	香川大学	創造工学部	Intensity enhancement and circular polarization control of spin-polarized light-emitting diodes using diluted magnetic semiconductor	Hayato Miyagawa	Kagawa University
53	”	森 健	香川大学	工学部	”	Takeshi Mori	Kagawa University
担当所員：大谷 義近、中辻 知							
54	希土類金属間化合物の強磁場低温物性研究	海老原 孝雄	静岡大学	学術院理学領域	Physical properties in rare earth intermetallic compounds at high magnetic fields in low temperature	Takao Ebihara	Shizuoka University
55	”	ジュマエダ・ジャトミカ	静岡大学	大学院自然科学教育部	”	Jumaeda Jatmika	Shizuoka University
担当所員：大谷 義近							
56	微細素子化した強相関物質における電流誘起された電子相の開拓	成田 秀樹	京都大学	大学院理学研究科	Investigation of electric current induced electronic phase in a microfabricated strongly correlated materials	Hideki Narita	Kyoto University
担当所員：廣井 善二							
57	固体基板上に作製された強磁性 CoPt 規則相の磁化測定	山浦 淳一	東京工業大学	元素戦略研究センター	Magnetization measurement of ferromagnetic CoPt ordered phases fabricated on solid substrates	Junichi Yamaura	Tokyo Institute of Technology
58	”	真島 豊	東京工業大学	科学技術創成研究院	”	Yutaka Majima	Tokyo Institute of Technology
59	”	遠山 諒	東京工業大学	物質理工学院	”	Ryo Toyama	Tokyo Institute of Technology
60	新しい Jeff=0 スピン軌道結合モット絶縁体の磁気特性に関する研究	原口 祐哉	東京農工大学	大学院工学研究科	Investigation of magnetism in the novel Jeff=0 spin orbit coupled Mott insulators	Yuya Haraguchi	University of Agriculture and Technology
61	希土類 4f 電子数制御による新規体積変化アクチュエーター材料の創製	横山 泰範	名古屋大学	大学院工学研究科	Development of novel volume-change-driven actuator materials by control of rare earth 4f electron number	Yasunori Yokoyama	Nagoya University
62	”	竹中 康司	名古屋大学	大学院工学研究科	”	Koshi Takenaka	Nagoya University
63	”	長谷川 遙加	名古屋大学	大学院工学研究科	”	Haruka Hasegawa	Nagoya University
64	”	渋谷 隼矢	名古屋大学	大学院工学研究科	”	Junya Shibutani	Nagoya University

No.	課題名	氏名	所属	Title	Name	Organization
担当所員：川島 直輝						
65	テンソルネットワーク中のエンタングルメント最適化法の開発	原田 健自	京都大学	大学院情報学研究科	Development of entanglement optimization method in tensor networks	Kenji Harada Kyoto University
66	蜂の巣格子拡張 Kitaev- Γ 模型の基底状態相図 2	鈴木 隆史	兵庫県立大学	大学院工学研究科	Ground-state phase diagram of the extended Kitaev- Γ model on a honeycomb lattice 2	Takafumi Suzuki University of Hyogo
担当所員：上床 美也						
67	六方晶 $\text{Hf}_{1-x}\text{Ta}_x\text{Fe}_2\text{By}$ の磁気熱量効果	松本 圭介	愛媛大学	大学院理工学研究科	Magnetocaloric effect in $\text{Hf}_{1-x}\text{Ta}_x\text{Fe}_2\text{By}$	Keisuke Matsumoto Ehime University
68	”	高畦 恋	愛媛大学	大学院理工学研究科	”	Ren Takaaze Ehime University
69	希土類三元系合金 $\text{Ho}_{1-x}\text{Er}_x\text{CuSi}$ の比熱	松本 圭介	愛媛大学	大学院理工学研究科	Specific heat study of $\text{Ho}_{1-x}\text{Er}_x\text{CuSi}$	Keisuke Matsumoto Ehime University
70	”	小林 将己	愛媛大学	大学院理工学研究科	”	Masaki Kobayashi Ehime University
71	擬三元化合物 $\text{Ce}_{1-x}\text{La}_x\text{NiC}_2$ の結晶育成と物質評価 3	繁岡 透	山口大学	大学院創成科学研究科	Crystal growth and characterization of pseudo-ternary compounds $\text{Ce}_{1-x}\text{La}_x\text{NiC}_2$	Toru Shigeoka Yamaguchi University
72	”	内間 清晴	沖縄キリスト教短期大学	英語科	”	Kiyoharu Uchima Okinawa Christian Junior College
73	擬三元化合物 $\text{CeNi}_{1-x}\text{Pd}_x\text{C}_2$ の結晶育成と物質評価	繁岡 透	山口大学	大学院創成科学研究科	Crystal growth and characterization of pseudo-ternary compounds $\text{CeNi}_{1-x}\text{Pd}_x\text{C}_2$	Toru Shigeoka Yamaguchi University
74	”	内間 清晴	沖縄キリスト教短期大学	英語科	”	Kiyoharu Uchima Okinawa Christian Junior College
75	YbH_{2+x} の磁性と伝導	中村 修	岡山理科大学	研究・社会連携センター	Magnetic and transport properties in YbH_{2+x}	Osamu Nakamura Okayama University of Science
76	多型化合物 RIr_2Si_2 (R = 希土類) の磁気特性 6	内間 清晴	沖縄キリスト教短期大学	英語科	Magnetic characteristics of polymorphic compounds RIr_2Si_2 (R=Rare earth) ₆	Kiyoharu Uchima Okinawa Christian Junior College
77	”	繁岡 透	山口大学	大学院創成科学研究科	”	Toru Shigeoka Yamaguchi University
78	ハーフメタルホイスラー合金の磁気体積効果に関する研究	重田 出	鹿児島大学	大学院理工学研究科	Study on the magneto-volume effect of half-metallic Heusler alloys	Iduru Shigeta Kagoshima University
79	”	辻川 聡一朗	鹿児島大学	理学部	”	Soichiro Tsujikawa Kagoshima University

No.	課題名	氏名	所属		Title	Name	Organization
80	三角格子反強磁性体の低温磁性	柄木 良友	琉球大学	教育学部	Low temperature magnetism of triangular antiferromagnets	Yoshitomo Karaki	University of the Ryukyus
81	Ho _{1-x} La _x Rh ₂ Si ₂ 単結晶の磁場中比熱測定 (2)	藤原 哲也	山口大学	大学院創成科学研究科	Specific heat measurement under magnetic field of Ho _{1-x} La _x Rh ₂ Si ₂ single crystal II	Tetsuya Fujiwara	Yamaguchi University
82	”	西崎 裕哉	山口大学	大学院創成科学研究科	”	Yuya Nishizaki	Yamaguchi University
83	混晶系 HoRh _{2-x} Pd ₂ Si ₂ の磁化測定	藤原 哲也	山口大学	大学院創成科学研究科	Magnetization measurements of pseudo-ternary system HoRh _{2-x} Pd ₂ Si ₂	Tetsuya Fujiwara	Yamaguchi University
84	”	金子 達哉	山口大学	理学部	”	Tatsuya Kaneko	Yamaguchi University
85	HoRh ₂ Si ₂ の Pd 置換系化合物の単結晶育成	藤原 哲也	山口大学	大学院創成科学研究科	Single crystal growth of Co substituted HoRh _{2-x} Pd _x Si ₂ compounds	Tetsuya Fujiwara	Yamaguchi University
86	”	杉田 静留	山口大学	理学部	”	Shizuru Sugita	Yamaguchi University
87	EuMn ₂ Ge ₂ 単結晶の磁場中比熱測定 (2)	藤原 哲也	山口大学	大学院創成科学研究科	Specific heat measurement under magnetic field of EuMn ₂ Ge ₂ single crystal II	Tetsuya Fujiwara	Yamaguchi University
88	”	小林 遼平	山口大学	理学部	”	Ryohei Kobayashi	Yamaguchi University
89	Ta ₂ NiSe ₅ の Ta,Ni サイト置換物質における高圧力下電気抵抗測定	広瀬 雄介	新潟大学	理学部	Electrical resistivity measurement under pressure of Ta/Ni site substituted Ta ₂ NiSe ₅	Yusuke Hirose	Niigata University
90	”	佐野 純佳	新潟大学	大学院自然科学研究科	”	Sumika Sano	Niigata University
91	磁気転移を示す Ce 化合物の高圧力下電気抵抗測定	広瀬 雄介	新潟大学	理学部	Electrical resistivity measurement under pressure magnetic Ce compound	Yusuke Hirose	Niigata University
92	”	山田 峻輔	新潟大学	大学院自然科学研究科	”	Shunsuke Yamada	Niigata University
93	高圧下における (Fe _{1-x} Zn _x) ₂ Mo ₃ O ₈ の電気磁気特性	赤星 大介	東邦大学	理学部	Magnetoelectric properties of (Fe _{1-x} Zn _x) ₂ Mo ₃ O ₈ under high pressures	Daisuke Akahoshi	Toho University
94	MnCo _{1-x} Ge 合金の磁気特性に関する研究 (3)	江藤 徹二郎	久留米工業大学	共通教育科	Study of magnetic properties in MnCo _{1-x} Ge alloys(3)	Tetsujiro Eto	Kurume Institute of Technology
95	有機伝導体物性に与える高圧力媒体の分子形状の効果	村田 惠三	大阪経済法科大学	21世紀社会総合研究センター	Effect of Molecular Shape of the High Pressure Medium to the Properties of Organic Conductors.	Keizo Murata	Osaka University of Economics and Law
96	鉄系超伝導体 FeSe _{1-x} Te _x の高圧下電子相図の研究	芝内 孝禎	東京大学	大学院新領域創成科学研究科	Studies on electrical phase diagrams under high pressure in FeSe _{1-x} Te _x	Takasada Shibauchi	The University of Tokyo

No.	課題名	氏名	所属		Title	Name	Organization
97	”	橋本 颯一郎	東京大学	大学院新領域創成科学研究科	”	Kenichiro Hashimoto	The University of Tokyo
98	”	向笠 清隆	東京大学	大学院新領域創成科学研究科	”	Kiyotaka Mukasa	The University of Tokyo
99	Cu ₂ MnAl 合金への磁場中熱処理効果	三井 好古	鹿児島大学	大学院理工学研究科	In-field annealing effects on the Cu ₂ MnAl alloys	Yoshifuru Mitsui	Kagoshima University
100	”	中川 駿	鹿児島大学	大学院理工学研究科	”	Shun Nakagawa	Kagoshima University
101	Sm ₂ Fe ₁₇ N ₃ 化合物の磁場中相成長	三井 好古	鹿児島大学	大学院理工学研究科	In-field phase growth of Sm ₂ Fe ₁₇ N ₃ compounds	Yoshifuru Mitsui	Kagoshima University
102	”	高橋 巡季	鹿児島大学	大学院理工学研究科	”	Junki Takahashi	Kagoshima University
103	Yb(Co _{1-x} Ni _x) ₂ Zn ₂₀ の極低温磁化測定	阿曾 尚文	琉球大学	理学部	Low-temperature magnetization measurements in Yb(Co _{1-x} Ni _x) ₂ Zn ₂₀	Naofumi Aso	University of the Ryukyus
104	”	金城 龍廣	琉球大学	理学部	”	Tatsuhiko Kinjo	University of the Ryukyus
105	圧力誘起価数転移の探索と高圧下輸送特性	辺土 正人	琉球大学	理学部	Searching of pressure-induced valence transition and transport properties under high pressure	Masato Hedo	University of the Ryukyus
106	”	仲間 隆男	琉球大学	理学部	”	Takao Nakama	University of the Ryukyus
107	磁場で制御した Sm ₂ Fe ₁₇ H ₃ の磁気特性	小山 佳一	鹿児島大学	大学院理工学研究科	Magnetic properties of Sm ₂ Fe ₁₇ H ₃ prepared under magnetic fields	Keiichi Koyama	Kagoshima University
108	”	尾上 昌平	鹿児島大学	大学院理工学研究科	”	Masahira Onoue	Kagoshima University
109	高圧下電気抵抗測定による新規分子導体 β'-(BEST) ₂ CuCl ₂ の温度圧力相図の決定と超伝導相の探索	小林 拓矢	埼玉大学	大学院理工学研究科	Determination of pressure-temperature phase diagram of new molecular conductor β'-(BEST) ₂ CuCl ₂ and search for superconducting phase by measuring electrical resistivity under high pressures	Takuya Kobayashi	Saitama University
110	”	谷口 弘三	埼玉大学	大学院理工学研究科	”	Hiromi Taniguchi	Saitama University
111	”	伊藤 有咲	埼玉大学	大学院理工学研究科	”	Arisa Ito	Saitama University
112	”	菅原 佳哉	埼玉大学	理学部	”	Yoshiya Sugawara	Saitama University
113	鉄セレン系化合物における圧力効果と置換効果	久田 旭彦	徳島大学	大学院社会産業理工学研究部	Effect of pressure and substitution in iron-selenide compounds	Akihiko Hisada	Tokushima University

No.	課題名	氏名	所属		Title	Name	Organization
114	”	森野 瑛介	徳島大学	理工学部	”	Eisuke Morino	Tokushima University
115	反強磁性ホイスラー合金 Ru ₂ MnZ (Z= Ge, Sn, Sb) のネール温度の圧力効果	安達 義也	山形大学	大学院理工学研究科	Pressure effect of the Neel temperature for the antiferromagnetic Heusler alloys Ru ₂ MnZ (Z= Ge, Sn, Sb)	Yoshiya Adachi	Yamagata University
116	”	渡辺 健	山形大学	大学院理工学研究科	”	Ken Watanabe	Yamagata University
117	ウラン化合物の磁性の圧力効果	本多 史憲	東北大学	金属材料研究所	Effect of Pressure on the magnetism of uranium compounds	Fuminori Honda	Tohoku University
118	Ni ₂ MnZ (Z= In, Sn, Sb) 強磁性ホイスラー合金の磁化の圧力効果	安達 義也	山形大学	大学院理工学研究科	Pressure effect of the magnetization for the ferromagnetic Heusler alloys Ni ₂ MnZ (Z= In, Sn, Sb)	Yoshiya Adachi	Yamagata University
119	”	吉田 圭吾	山形大学	大学院理工学研究科	”	Keigo Yoshida	Yamagata University
120	重い電子系強磁性体の圧力下 dHvA 効果	摂待 力生	新潟大学	理学部	de Haas-van Alphen effect in heavy fermion ferromagnet compound under pressure	Rikio Settai	Niigata University
121	”	三橋 大貴	新潟大学	理学部	”	Daiki Mitsuhashi	Niigata University
122	Ce ₂ RuGe の圧力下電気抵抗測定	摂待 力生	新潟大学	理学部	Electrical resistivity measurement of Ce ₂ RuGe under pressure	Rikio Settai	Niigata University
123	”	池田 悠	新潟大学	理学部	”	Yu Ikeda	Niigata University
124	金属絶縁体転移を持つ Cu(Ir _{1-x} Rh _x) ₂ S ₄ の高圧下磁性	伊藤 昌和	鹿児島大学	総合科学域総合教育学系	Magnetic properties of Cu(Ir _{1-x} Rh _x) ₂ S ₄ with the metal-insulator transition in high pressure	Masakazu Ito	Kagoshima University
125	”	鹿島 頌太	鹿児島大学	大学院理工学研究科	”	Shota Kashima	Kagoshima University
126	”	今村 有助	鹿児島大学	大学院理工学研究科	”	Yusuke Imamura	Kagoshima University
127	ハニカム格子を含むアクチノイド化合物の高圧物性	芳賀 芳範	日本原子力研究開発機構	先端基礎研究センター	High-pressure physical properties of uranium compound having honeycomb structure	Yoshinori Haga	Japan Atomic Energy Agency
128	S置換した FeSe の低温 NMR 測定	藤原 直樹	京都大学	大学院人間・環境学研究科	Low-temperature NMR study on S-substituted FeSe	Naoki Fujiwara	Kyoto University
129	”	桑山 昂典	京都大学	大学院人間・環境学研究科	”	Takanori Kuwayama	Kyoto University
130	”	中村 昂矢	京都大学	大学院人間・環境学研究科	”	Kouya Nakamura	Kyoto University

No.	課題名	氏名	所属	Title	Name	Organization
担当所員：尾崎 泰助						
131	実験と計算の協奏による二次元材料の構造・電子状態解析及び制御	アントワヌ フロランス	北陸先端科学技術大学院大学	マテリアルサイエンス系	Analysis and control of crystal and electronic structures of 2D materials through concerted collaboration of experiment and theory	Antoine Fleurence JAIST
132	〃	新田 寛和	北陸先端科学技術大学院大学	先端科学技術研究科	〃	Hirokazu Nitta JAIST
担当所員：益田 隆嗣						
133	空間反転対称性の破れた超伝導体の結晶性評価	古川 はづき	お茶の水女子大学	基幹研究院 自然科学系	Evaluation of single crystal quality of non-centrosymmetric superconductors	Hazuki Furukawa Ochanomizu University
134	中性子回折研究用単結晶試料の結晶性評価	阿曾 尚文	琉球大学	理学部	Crystal quality evaluation of single crystals for neutron diffraction	Naofumi Aso University of the Ryukyus
135	多縮重度系の (Y,Yb)T ₂ Zn ₂₀ (T = 遷移金属元素) における不純物近藤効果の熱力学的検証	池田 陽一	東北大学	金属材料研究所	Thermodynamical verification of the impurity-Kondo effect on a multiplet system (Y,Yb)T ₂ Zn ₂₀ (T = transition-metal elements)	Yoichi Ikeda Tohoku University
担当所員：金道 浩一						
136	歪みの少ないカゴメ格子チタンフッ化物の磁性	植田 浩明	京都大学	大学院理学研究科	Magnetism of kagome lattice titanium fluorides with small distortion	Hiroaki Ueda Kyoto University
137	〃	林 真弘	京都大学	大学院理学研究科	〃	Masahiro Hayashi Kyoto University
138	積層化合物 T _x MX ₂ を基軸とした擬二次元磁性体の強磁場磁化測定	道岡 千城	京都大学	大学院理学研究科	High-field magnetization measurements of quasi-two-dimensional magnets based on layered compounds T _x MX ₂ (T = 3d-transition metal, M = Ta, Nb, X = S, Se)	Chishiro Michioka Kyoto University
139	〃	森山 広大	京都大学	大学院理学研究科	〃	Kodai Moriyama Kyoto University
140	〃	山中 俊介	京都大学	大学院理学研究科	〃	Shunsuke Yamanaka Kyoro University
141	〃	奈良 建佑	京都大学	大学院理学研究科	〃	Nara Kensuke Kyoto University
142	ルテニウムダブルペロブスカイト酸化物におけるスピン軌道励起子磁性の探索	原口 祐哉	東京農工大学	大学院工学研究科	Search for a spin-orbit excitonic magnetism in ruthenium double perovskite oxides	Yuya Haraguchi University of Agriculture and Technology
143	〃	八東 波椰斗	東京農工大学	工学部	〃	Hayato Yatsuzuka Tokyo University of Agriculture and Technology
144	重い電子系化合物が示す非従来型超伝導と磁性の相関	横山 淳	茨城大学	大学院理工学研究科	Interplay between unconventional superconductivity and magnetism in heavy-fermion compounds	Makoto Yokoyama Ibaraki University

No.	課題名	氏名	所属		Title	Name	Organization
145	”	ラフマント	茨城大学	大学院理工学研究科	”	Rahmanto	Ibaraki University
146	Bi-2212 単結晶における修正コーラー則の検証	渡辺 孝夫	弘前大学	大学院理工学研究科	Investigation of the modified Kohler' s rule on Bi-2212 single crystals	Takao Watanabe	Hirosaki University
147	”	原田 圭市	弘前大学	大学院理工学研究科	”	Keiichi Harada	Hirosaki University
148	”	藤井 武則	東京大学	低温センター	”	Takenori Fujii	University of Tokyo
149	dimer-Mott 系有機導体における磁場中金属-絶縁体転移	杉浦 栞理	東北大学	金属材料研究所	Field induced M-I transition in dimer-Mott type organic conductors	Shiori Sugiura	Tohoku University
150	幾何学的フラストレート磁性体の強磁場磁化測定	菊池 彦光	福井大学	学術研究院工学系部門	Magnetization measurements of the frustrated magnets	Hikomitsu Kikuchi	University of Fukui
151	強いスピン軌道相互作用を持つ超伝導体における量子振動測定	芝内 孝禎	東京大学	大学院新領域創成科学研究科	Quantum oscillation measurements on superconductors with strong spin-orbit interaction	Takasada Shibauchi	The University of Tokyo
152	”	橋本 颯一郎	東京大学	大学院新領域創成科学研究科	”	Kenichiro Hashimoto	The University of Tokyo
153	”	水上 雄太	東京大学	大学院新領域創成科学研究科	”	Yuta Mizukami	The University of Tokyo
154	”	石田 浩祐	東京大学	大学院新領域創成科学研究科	”	Kousuke Ishida	The University of Tokyo
155	”	向笠 清隆	東京大学	大学院新領域創成科学研究科	”	Kiyotaka Mukasa	The University of Tokyo
156	”	石原 滉大	東京大学	大学院新領域創成科学研究科	”	Kota Ishihara	The University of Tokyo
157	新奇ウラン系スピン三重項超伝導体及び関連物質の強磁場物性	清水 悠晴	東北大学	金属材料研究所	High-magnetic field effects on novel spin-triplet uranium superconductors and related compounds	Yusei Shimizu	Tohoku University
158	topological Kondo insulator $\text{SmB}_6, \text{YbB}_{12}$ の磁化特性と比熱	伊賀 文俊	茨城大学	理学部	Magnetic and thermal properties of topological Kondo insulator SmB_6 and YbB_{12}	Fumitoshi Iga	Ibaraki University
159	”	松浦 航	茨城大学	大学院理工学研究科	”	Wataru Matsuura	Ibaraki university
160	高圧合成新規希土類 Ce および Pr_{12} ホウ化物の強磁場中の磁化と比熱	伊賀 文俊	茨城大学	理学部	Magnetic and thermal properties in high magnetic fields of Ce- and Pr- dodeca-borides produced by high pressure synthesis	Fumitoshi Iga	Ibaraki University
161	”	山田 貴大	茨城大学	大学院理工学研究科	”	Takahiro Yamada	Ibaraki University

No.	課題名	氏名	所属		Title	Name	Organization
162	金属絶縁体転移を持つ Cu(Ir _{1-x} Rh _x) ₂ S ₄ の高磁場電気抵抗	伊藤 昌和	鹿児島大学	総合科学域総合教育学系	High magnetic field electric resistivity of Cu(Ir _{1-x} Rh _x) ₂ S ₄ with the metal-insulator transition	Masakazu Ito	Kagoshima University
163	〃	鹿島 頌太	鹿児島大学	大学院理工学研究科	〃	Shota Kashima	Kagoshima University
164	〃	今村 有助	鹿児島大学	大学院理工学研究科	〃	Yusuke Imamura	Kagoshima University
165	遍歴三角格子反強磁性体 GdGaI の強磁場磁化過程	大熊 隆太郎	沖縄科学技術大学院大学	量子物質科学ユニット	High-field magnetization study of itinerant triangular lattice antiferromagnet GdGaI	Ryutaro Okuma	Okinawa Institute of Science and Technology
担当所員：徳永 将史							
166	重い電子系における強磁場中の電子状態研究	海老原 孝雄	静岡大学	大学院理学領域	Electronic states at high magnetic fields in Heavy Fermion systems	Takao Ebihara	Shizuoka University
167	〃	丸山 博史	静岡大学	大学院総合科学技術研究科	〃	Hiroshi Maruyama	Shizuoka University
168	磁気光学顕微鏡による超伝導体中の量子渦の実空間非平衡ダイナミクス観測手法の確立	黒川 穂高	東京大学	大学院総合文化研究科	Observing the real-space nonequilibrium dynamics of vortices in superconductor with a magneto-optical microscope	Hodaka Kurokawa	University of Tokyo
169	(Al _x M _{2-x})GeO ₅ (M=Cr, V, Fe) の強磁場磁化測定	香取 浩子	東京農工大学	大学院工学研究科	High-field magnetization measurements of (Al _x M _{2-x})GeO ₅ (M=Cr, V, Fe)	Hiroko Katori	Tokyo University of Agriculture and Technology
170	〃	柿本 和勇	東京農工大学	工学府	〃	Kazuo Kakimoto	Tokyo University of Agriculture and Technology
171	〃	早川 隆史	東京農工大学	工学部	〃	Takashi Hayakawa	Tokyo University of Agriculture and Technology
172	多層ディラック電子系 BaMnBi ₂ における量子振動現象の研究	酒井 英明	大阪大学	大学院理学研究科	Study of quantum oscillation phenomena in BaMnBi ₂	Hideaki Sakai	Osaka University
173	〃	近藤 雅起	大阪大学	大学院理学研究科	〃	Masaki Kondo	Osaka University
174	〃	阪口 駿也	大阪大学	理学部	〃	Shunya Sakaguchi	Osaka University
175	正四角台塔反強磁性体の強磁場電気磁気特性の測定	木村 健太	東京大学	大学院新領域創成科学研究科	High-field magnetoelectric properties in square-cupola-based antiferromagnets	Kenta Kimura	The University of Tokyo
176	トラス型フェルミ面を持つラッシュバ型半導体の量子極限伝導特性の研究	村川 寛	大阪大学	大学院理学研究科	High field study for quantum limit transport properties of torus Fermi surface in Rashba semiconductor	Hiroshi Murakawa	Osaka university
177	マンガン (III) スピントクロスオーバー錯体における磁気熱量効果	木原 工	東北大学	金属材料研究所	Magnetocaloric effect in manganese(III) spin-crossover complex	Takumi Kihara	Tohoku University

No.	課題名	氏名	所属		Title	Name	Organization
178	ハニカム格子を含むアクチノイド化合物の強磁場物性	芳賀 芳範	日本原子力研究開発機構	先端基礎研究センター	High-field physical properties of uranium compounds having honeycomb lattice	Yoshinori Haga	Japan Atomic Energy Agency
179	ウラン重い電子系超伝導体・磁性体における強磁場物性測定	清水 悠晴	東北大学	金属材料研究所	High-field properties for uranium heavy-fermion superconductors and magnetic materials	Yusei Shimizu	Tohoku University
180	強磁場磁化過程測定によるペロブスカイト PbMnO ₃ の電荷分布解明	東 正樹	東京工業大学	フロンティア材料研究所	Clarification of charge distribution in perovskite PbMnO ₃ by high-field magnetization measurement	Masaki Azuma	Tokyo Institute of technology
181	近藤絶縁体 YbIr ₃ Si ₇ の高磁場相における量子振動の検証	佐藤 雄貴	京都大学	大学院理学研究科	Quantum oscillation in High field phase of Kondo insulator YbIr ₃ Si ₇	Sato Yuki	Kyoto University
担当所員：松田 康弘							
182	近藤半導体 (Yb,R)B ₁₂ 、および新規高圧合成物質のワンターンコイル 120T 強磁場磁化と伝導	伊賀 文俊	茨城大学	理学部	Magnetization and transport properties by using one-turn coil in a 120 T pulse magnet of Kondo insulator (Yb,R)B ₁₂ and novel rare-earth borides produced by high-pressure synthesis	Fumitoshi Iga	Ibaraki University
183	”	竹森 氷馬	茨城大学	大学院理工学研究科	”	Hyoma Takamori	ibaraki university
担当所員：小濱 芳允							
184	正四角台塔反強磁性体 Pb(TiO)Cu ₄ (PO ₄) ₄ における強磁場中での電気磁気光学効果の研究	木村 健太	東京大学	大学院新領域創成科学研究科	Optical magnetoelectric effect of the square-cupola-based antiferromagnet Pb(TiO)Cu ₄ (PO ₄) ₄ in a high magnetic field	Kenta Kimura	The University of Tokyo
185	微視的プローブによる強磁場誘起電子相の探索とその周辺ダイナミクス観測	井原 慶彦	北海道大学	大学院理学研究科	NMR study for magnetic field induced electronic state and their dynamics	Yoshihiko Ihara	Hokkaido University
186	”	福岡 脩平	北海道大学	大学院理学研究科	”	Shuhei Fukuoka	Hokkaido University
担当所員：小林 洋平							
187	次世代レーザーとレーザー加工の基礎技術研究	吉富 大	産業技術総合研究所	電子光技術研究部門	Basic research on next generation laser systems and laser machining technology	Dai Yoshitomi	Nat. Inst. of Advanced Industrial Science and Technology
188	”	高田 英行	産業技術総合研究所	電子光技術研究部門	”	Hideyuki Takada	National Institute of Advanced Industrial Science and Technology
189	”	奈良崎 愛子	産業技術総合研究所	電子光技術研究部門	”	Aiko Narazaki	National Institute of Advanced Industrial Science and Technology
190	”	鳥塚 健二	産業技術総合研究所	電子光技術研究部門	”	Kenji Torizuka	National Institute of Advanced Industrial Science and Technology
191	”	田中 真人	産業技術総合研究所	分析計測標準研究部門	”	Masahito Tanaka	National Institute of Advanced Industrial Science and Technology

No.	課題名	氏名	所属		Title	Name	Organization
192	”	小川 博嗣	産業技術総合研究所	分析計測標準研究部門	”	Hiroshi Ogawa	National Institute of Advanced Industrial Science and Technology
193	”	佐藤 大輔	産業技術総合研究所	分析計測標準研究部門	”	Daisuke Satoh	National Institute of Advanced Industrial Science and Technology
194	”	澁谷 達則	産業技術総合研究所	分析計測標準研究部門	”	Tatsunori Shibuya	National Institute of Advanced Industrial Science and Technology
195	”	黒田 隆之助	産業技術総合研究所	先端オペランド計測技術オープンイノベーションラボラトリ	”	Ryunosuke Kuroda	National Institute of Advanced Industrial Science and Technology
196	”	盛合 靖章	産業技術総合研究所	先端オペランド計測技術オープンイノベーションラボラトリ	”	Yasuaki Moriai	National Institute of Advanced Industrial Science and Technology
197	”	寺澤 英知	産業技術総合研究所	先端オペランド計測技術オープンイノベーションラボラトリ	”	Eichi Terasawa	National Institute of Advanced Industrial Science and Technology
198	”	牛窪 大樹	産業技術総合研究所	先端オペランド計測技術オープンイノベーションラボラトリ	”	Daiki Ushikubo	National Institute of Advanced Industrial Science and Technology
199	青色半導体レーザー用ファイバ型光コンバイナの開発	藤本 靖	千葉工業大学	工学部	Development on fiber power combiner for GaN semiconductor lasers	Yasushi Fujimoto	Chiba Institute of Technology (CIT)
200	ワイドバンドギャップ半導体への赤外パルスレーザー加工	富田 卓朗	徳島大学	大学院社会産業理工学研究部	Infrared pulsed laser processing on wide bandgap semiconductors	Takuro Tomita	Tokushima University
201	”	岡田 達也	徳島大学	大学院社会産業理工学研究部	”	Tatsuya Okada	Tokushima University
202	短波長パルスレーザーによる CFRP 加工	森山 匡洋	東京大学	大学院理学系研究科附属フotonサイエンス研究機構	CFRP processing with short wavelength pulsed laser	Masahiro Moriyama	The University of Tokyo
203	分光分析によるレーザー加工プロセス解明に関する研究	山口 誠	秋田大学	大学院理工学研究科	Study on laser modification by using optical spectroscopic measurements	Makoto Yamaguchi	Akita University
担当所員：原田 慈久							
204	トポロジカル絶縁体 Bi/ 垂直磁化膜 MnGa 界面におけるゾーン境界における Fermi 面の観測	小林 正起	東京大学	大学院工学系研究科	Observation of the Fermi surface of the interface state between topological insulator Bi and perpendicular magnet MnGa	Masaki Kobayashi	The University of Tokyo
担当所員：板谷 治郎							
205	時間分解非線形分光法を用いたハライド薄膜のコヒーレントフォノンの検出	牧野 哲征	福井大学	学術研究院工学系部門	Coherent phonons of oxyhalide thin films studied by time-resolved nonlinear spectroscopy	Takayuki Makino	University of Fukui
206	”	山口 拓真	福井大学	大学院工学研究科	”	Takuma Yamaguchi	University of Fukui

No.	課題名	氏名	所属		Title	Name	Organization
207	”	鈴木 健	福井大学	大学院工学研究科	”	Ken Suzuki	University of Fukui
担当所員：近藤 猛							
208	レーザー角度分解光電子分光を用いた新規ファンデルワールス磁性化合物 GdGaI の微細電子状態観測	山神 光平	沖縄科学技術大学院大学	量子物質科学ユニット	Electronic states of new van der Waals magnetic compound GdGaI studied by laser angle-resolved photoemission spectroscopy	Kohei Yamagami	Okinawa Institute of Science and Technology
担当所員：岡崎 浩三							
209	高分解能レーザー励起光電子顕微鏡を用いた鉄系超伝導体の電子ネマティック状態の実空間観察 II	橋本 颯一郎	東京大学	大学院新領域創成科学研究科	Real-space observation of electronic nematicity in iron-based superconductors by using a high-resolution laser photoemission electron microscope II	Kenichiro Hashimoto	The University of Tokyo
210	”	水上 雄太	東京大学	大学院新領域創成科学研究科	”	Yuta Mizukami	The University of Tokyo
211	”	石田 浩祐	東京大学	大学院新領域創成科学研究科	”	Kousuke Ishida	The University of Tokyo
212	”	影山 遙一	立命館大学	理工学部	”	Yoichi Kageyama	Ritsumeikan University
213	励起子絶縁体 Ta ₂ NiSe ₅ 及びモット絶縁体 Ca ₂ RuO ₄ における光誘起絶縁体-金属転移の研究	久保田 雄也	放射光科学研究センター	XFEL 研究開発部門	Investigation of the photo-induced insulator-to-metal transition in an excitonic insulator Ta ₂ NiSe ₅ and a Mott insulator Ca ₂ RuO ₄	Yuya Kubota	Japan Synchrotron Radiation Research Institute (JASRI)
214	励起子絶縁体における光誘起半金属相の研究	溝川 貴司	早稲田大学	理工学術院先進理工学部	Photoinduced semimetallic phases in excitonic insulators	Takashi Mizokawa	Waseda University
215	T' 構造をもつ銅酸化物高温超伝導体の角度分解光電子分光による研究	チャン ウェイル	上智大学	機能創造理工学	Photoemission spectroscopy of electron-doped T' -cuprate superconductors	Zhang Weilu	Sophia University
216	時間分解角度分解光電子分光による電荷密度波物質 VTe ₂ のトポロジカル表面状態の観測	三石 夏樹	東京大学	大学院工学系研究科	Observation of topological surface states in charge density wave material VTe ₂ by time- and angle-resolved photoemission spectroscopy	Natsuki Mitsuishi	The University of Tokyo
一般研究員・大阪大学 先端強磁場科学研究センター / General Researcher・Center for Advanced High Magnetic Field Science Osaka University							
No.	課題名	氏名	所属		Title	Name	Organization
1	Fe-Ni 系合金におけるマルテンサイト変態の時間依存性	福田 隆	大阪大学	大学院工学研究科	Time dependence of martensitic transformation in Fe-Ni based alloys	Takashi Fukuda	Osaka University
2	磁気力の半径方向成分によるタンパク質結晶の磁気浮上と熱物性値計測	牧 祥	大阪大谷大学	薬学部	Magnetic levitation and thermal property measurement of protein crystallization by the use of the radial component of magnetic force	Syou Maki	Osaka Ohtani University
3	均一粒径クロミック化合物における強磁場物性	浅野 貴行	福井大学	学術研究院工学系部門	Magnetic properties under high magnetic field in chromic compounds with a uniform particle size	Takayuki Asano	University of Fukui

No.	課題名	氏名	所属		Title	Name	Organization
4	”	西首 時夫	福井大学	大学院工学研究科	”	Tokio Nishikubi	University of Fukui
5	量子スピン系の電場励起 ESR と方向二色性	木村 尚次郎	東北大学	金属材料研究所	Electric dipole spin resonance and directional dichroism of the quantum spin systems	Shojiro Kimura	Tohoku University
6	ホイスラー合金 Ni_2MnX ($X = In, Al, Sn, Sb$) 系の磁化・超磁歪ならびに高速磁場応答性の研究	左近 拓男	龍谷大学	理工学部	Research on time dependences of magnetstriction of Ni_2MnX ($X = In, Al, Sn, Sb$) type and Pd_2MnSn type Heusler alloys	Takuo Sakon	Ryukoku University
7	層状反強磁性体 $EuIn_2As_2$ の磁気特性の解明	酒井 英明	大阪大学	大学院理学研究科	Study of the magnetic properties for layered antiferromagnet $EuIn_2As_2$	Hideaki Sakai	Osaka University
8	”	近藤 雅起	大阪大学	大学院理学研究科	”	Masaki Kondo	Osaka University
9	”	真栄城 竜生	大阪大学	大学院理学研究科	”	Ryusei Maeshiro	Osaka University
10	”	阪口 駿也	大阪大学	理学部	”	Shunya Sakaguchi	Osaka University
11	希土類ワイル物質の強磁場下輸送特性の研究	村川 寛	大阪大学	大学院理学研究科	High-magnetic-field studies of the rare-earth Weyl materials	Hiroshi Murakawa	Osaka University
12	”	中岡 優大	大阪大学	大学院理学研究科	”	Yudai Nakaoka	Osaka University
13	パルス強磁場を用いた圧力下 ESR 装置における渦電流軽減の検討	櫻井 敬博	神戸大学	研究基盤センター	Investigation of eddy current reduction in high pressure ESR system using pulsed high magnetic field	Takahiro Sakurai	Kobe University
14	正四角台塔反強磁性体の強磁場 ESR	木村 健太	東京大学	大学院新領域創成科学研究科	High-field ESR measurements of square-cupola-based antiferromagnets	Kenta Kimura	The University of Tokyo
15	$CaBa(Co_{1-x}Fe_x)_4O_7$ ($0 \leq x \leq 1$) 単結晶試料の強磁場下での磁化・電気分極・ESR 測定	桑原 英樹	上智大学	理工学部	Magnetization, electric polarization, and ESR measurements for $CaBa(Co_{1-x}Fe_x)_4O_7$ ($0 \leq x \leq 1$) single crystals in pulsed high magnetic fields	Hideki Kuwahara	Sophia University
16	”	白崎 巧	上智大学	理工学部	”	Takumi Shirasaki	Sophia University
17	ハルデン磁性体のバルクエッジ相関に関する研究	柏木 隆成	筑波大学	数理物質系	Study of bulk-edge interaction of Haldane magnets	Takanari Kashiwagi	Univ. of Tsukuba
18	強いスピン-軌道相互作用を活かした酸化物スピントロニクス	松野 丈夫	大阪大学	大学院理学研究科	Oxide spintronics utilizing strong spin-orbit coupling	Jobu Matsuno	Osaka University
19	カルボン酸、スルホン酸を架橋配位子とした金属錯体の構造と磁性に関する研究	本多 善太郎	埼玉大学	大学院理工学研究科	Crystal structures and magnetic properties of carboxylate, sulfonate-bridged transition metal complexes	Zentaro Honda	Saitama University
20	バックルドハニカム格子反強磁性体 $Cs_3Fe_2Cl_9$ の強磁場下 ESR 測定	吉田 紘行	北海道大学	大学院理学研究科	High-field ESR measurements on buckled honeycomb lattice antiferromagnets $Cs_3Fe_2Cl_9$	Hiroyuki Yoshida	Hokkaido University

No.	課題名	氏名	所属		Title	Name	Organization
21	SmB ₆ /SrB ₆ /CaB ₆ 人工超格子の強磁場中ホール効果測定	宍戸 寛明	大阪府立大学	大学院工学研究科	Hall resistance measurements for SmB ₆ /SrB ₆ /CaB ₆ superlattices under high magnetic field	Hiroaki Shishido	Osaka Prefecture University
22	三角格子磁性体の強磁場 ESR	南部 雄亮	東北大学	金属材料研究所	ESR measurements under high magnetic fields on a triangular magnet	Yusuke Nambu	Tohoku University
23	フェルダジル系塩から成る量子スピン系の強磁場磁性	山口 博則	大阪府立大学	大学院理学系研究科	High-field magnetic properties of quantum spin systems composed of verdazyl-based salts	Hironori Yamaguchi	Osaka Prefecture University
24	ナノ構造を導入した希土類系高温超伝導薄膜における強磁場中臨界電流密度に関する研究	土屋 雄司	名古屋大学	工学部	Study on the critical current density in high-magnetic field in RE-based cuprate superconductors with nano-structure	Yuji Tsuchiya	Nagoya University
25	ディラック電子系 NiTe ₂ と Pd 置換系の磁化測定による量子振動の研究	宮坂 茂樹	大阪大学	大学院理学研究科	Quantum oscillation in Dirac fermion system, NiTe ₂ and Pd-doping systems via magnetization measurement	Shigeki Miyasaka	Osaka University
26	微視的プローブによる強磁場誘起電子相の探索とその周辺ダイナミクス観測	井原 慶彦	北海道大学	大学院理学研究科	NMR study for magnetic field induced electronic state and their dynamics	Yoshihiko Ihara	Hokkaido University
27	〃	福岡 脩平	北海道大学	大学院理学研究科	〃	Shuheki Fukuoka	Hokkaido University

物質合成・評価設備 G クラス / Materials Synthesis and Characterization G Class Researcher

No.	課題名	氏名	所属		Title	Name	Organization
1	FZ 法での四ほう酸ストロンチウム (SrB ₄ O ₇) 結晶の育成と評価	小松 隆一	山口大学	大学院理工学研究科	Growth and characterization of strontium tetraborate crystal by the floating zone method	Ryuichi Komatsu	Yamaguchi University
2	超臨界メタノール条件下でのエステル交換反応に固体触媒が与える影響	秋月 信	東京大学	大学院新領域創成科学研究科	The effect of solid catalysts on the ester exchange reaction in supercritical methanol	Makoto Akizuki	The University of Tokyo
3	〃	張 瑞子	東京大学	大学院新領域創成科学研究科	〃	Zhang Ruizi	The University of Tokyo
4	高温高圧水における析出炭素の除去による固体触媒再生の検討	秋月 信	東京大学	大学院新領域創成科学研究科	Examination of solid catalyst regeneration by removing precipitated carbon in sub- and supercritical water	Makoto Akizuki	The University of Tokyo
5	〃	チン ブンセイ	東京大学	大学院新領域創成科学研究科	〃	Chen Wenjing	The university of Tokyo
6	高温高圧条件下の水 - メタノール溶媒が固体触媒反応に及ぼす影響	秋月 信	東京大学	大学院新領域創成科学研究科	Investigation of the effect of hot compressed methanol-water mixed solvent on solid catalyzed reactions	Makoto Akizuki	The University of Tokyo
7	〃	島田 綾子	東京大学	大学院新領域創成科学研究科	〃	Ayako Shimada	The university of Tokyo
8	単結晶 CaMn _{1-x} Sb _x O ₃ の誘電特性および磁気特性の研究	谷口 晴香	岩手大学	理工学部	Study of dielectric and magnetic properties of single crystalline CaMn _{1-x} Sb _x O ₃	Haruka Taniguchi	Iwate University

No.	課題名	氏名	所属		Title	Name	Organization
9	数値計算を用いた泥岩中の化学的浸透現象に伴う歪についての検討	廣田 翔伍	東京大学	大学院新領域創成科学研究科	Numerical investigation of rock deformation caused by chemical osmosis in mudstones	Shogo Hirota	The University of Tokyo
10	黒鉛層間金属微粒子の TEM 観察	白井 誠之	岩手大学	理工学部	TEM observation of metal particles intercalated between graphite layers	Masayuki Shirai	Iwate University
11	〃	袖野 美果	岩手大学	大学院総合科学研究科	〃	Mika Sodeno	Iwate University
12	新規希土類磁石の構造解析	齋藤 哲治	千葉工業大学	工学部	Study of new rare-earth magnets	Tetsuji Saito	Chiba Institute of Technology
13	ナノ構造材料を用いたクリーンエネルギーデバイス開発	細野 英司	産業技術総合研究所	省エネルギー研究部門	Development of clean energy devices by using nanostructured materials	Eiji Hosono	National Institute of Advanced Industrial Science and Technology
14	〃	太田 道広	産業技術総合研究所	省エネルギー研究部門	〃	Michihiro Ohta	National Institute of Advanced Industrial Science and Technology
15	〃	プリヤンカ ジュド	産業技術総合研究所	省エネルギー研究部門	〃	Priyanka Jood	National Institute of Advanced Industrial Science and Technology
16	マイクロミキサを用いた機能性無機ナノ粒子の連続合成	陶 究	産業技術総合研究所	化学プロセス研究部門	Continuous synthesis of functional inorganic nanoparticles using a micromixer	Sue Kiwamu	National Institute of Advanced Industrial Science and Technology
17	高圧下におけるオリビン高圧相間の同位体分配実験	佐野 亜沙美	日本原子力研究開発機構	J-PARC センター	Isotope partitioning experiment on olivine and its high pressure polymorph	Asami Sano	JAEA
18	misfit 単結晶の構造観察	小林 夏野	岡山大学	異分野基礎科学研究所	Observation of local structure on misfit single crystal	Kaya Kobayashi	Okayama University
19	(Pr, Nd, Sm) _{0.5} Sr _{0.5} FeO ₃ の高温における磁性と熱電特性に関する研究	中津川 博	横浜国立大学	大学院工学研究院	Magnetism and thermoelectric properties at high temperature in (Pr, Nd, Sm) _{0.5} Sr _{0.5} FeO ₃	Hiroshi Nakatsugawa	Yokohama National University
20	Kitaev相互作用をもつ三角格子磁性体の磁気特性評価	原口 祐哉	東京農工大学	大学院工学研究院	Investigation of magnetism of triangular lattice magnets with Kitaev interaction	Yuya Haraguchi	Tokyo University of Agriculture and Technology
21	〃	大野田 豪宏	東京農工大学	大学院工学研究院	〃	Takehiro Ohnoda	Tokyo University of Agriculture and Technology
22	ペロブスカイト型 Ni 酸化物における Ni 価数と磁性との関係	香取 浩子	東京農工大学	大学院工学研究院	Relationship between Ni valence and magnetism in perovskite-type Ni oxides	Hiroko Katori	Tokyo University of Agriculture and Technology
23	〃	柿本 和勇	東京農工大学	工学府	〃	Kazuo Kakimoto	Tokyo University of Agriculture and Technology
24	〃	早川 隆史	東京農工大学	工学部	〃	Takashi Hayakawa	Tokyo University of Agriculture and Technology
25	ハーフメタルホイスラー合金の遍歴電子強磁性体のスピンゆらぎ理論による解析に関する研究	重田 出	鹿児島大学	大学院理工学研究科	Study on analysis of half-metallic Heusler alloys by the spin fluctuation theory of itinerant electron ferromagnets	Iduru Shigeta	Kagoshima University

No.	課題名	氏名	所属		Title	Name	Organization
26	”	横山 喬亮	鹿児島大学	理学部	”	Takaaki Yokoyama	Kagoshima University
27	準結晶・近似結晶の磁性に関する研究 IV	鈴木 慎太郎	東京理科大学	基礎工学部	Magnetism of quasicrystal and approximants IV	Shintaro Suzuki	Tokyo University of Science
28	有機伝導体の磁化測定によるモット物理の研究	宮川 和也	東京大学	大学院工学系研究科	Study of Mott physics by magnetization measurements of organic conductors	Kazuya Miyagawa	The University of Tokyo
29	ホイスラー化合物での反強磁性の研究	廣井 政彦	鹿児島大学	大学院理工学研究科	Study on antiferromagnetism in Heusler compounds	Masahiko Hiroi	Kagoshima University
30	”	赤石 幸起	鹿児島大学	理学部	”	Kouki Akaishi	Kagoshima University
31	κ 型有機導体における交流磁化率測定によるモット型超伝導-反強磁性絶縁体相境界の研究	谷口 弘三	埼玉大学	大学院理工学研究科	Studies on Mott-type superconductor-antiferromagnetic insulator phase boundary by AC susceptibility measurements in k-type organic conductors	Hiromi Taniguchi	Saitama University
32	”	高橋 啓太	埼玉大学	理学部	”	Keita Takahashi	Saitama University
33	重希土類元素を含む充填スクッテルダイト化合物の新物質探索	関根 ちひろ	室蘭工業大学	大学院工学研究科	Search for new filled-skutterudite compounds including heavy rare-earth metal	Chihiro Sekine	Muroran Institute of Technology
34	”	上野 公輔	室蘭工業大学	大学院工学研究科	”	Kosuke Ueno	Muroran Institute of Technology
35	酸窒化物蛍光体の超高压力合成と結晶構造、発光特性評価	佐々木 拓也	名古屋大学	大学院工学研究科	High-pressure synthesis, crystal structure, and photoluminescence properties of oxynitride phosphors	Takuya Sasaki	Nagoya University
36	”	近藤 信介	名古屋大学	大学院工学研究科	”	Shinsuke Kondo	Nagoya University
37	圧力誘起構造相転移を利用した酸窒化物蛍光体の合成と発光制御	佐々木 拓也	名古屋大学	大学院工学研究科	High-pressure synthesis and photoluminescence control of oxide-system phosphors by pressure-induced structural phase transition	Takuya Sasaki	Nagoya University
38	”	立岩 一晃	名古屋大学	工学部	”	Kazuaki Tateiwa	Nagoya University
39	新規金属間化合物の高圧合成と物性	丹羽 健	名古屋大学	大学院工学研究科	High-pressure synthesis and physical properties of novel intermetallic compounds	Ken Niwa	Nagoya University
40	”	高野 航一	名古屋大学	大学院工学研究科	”	Koichi Takano	Nagoya University
41	塩化アンモニウムおよび直接窒化による遷移金属窒化物の高圧合成	丹羽 健	名古屋大学	大学院工学研究科	High-pressure synthesis of transition metal nitrides via nitridation of using ammonium chloride or molecular nitrogen	Ken Niwa	Nagoya University
42	”	浅野 秀斗	名古屋大学	大学院工学研究科	”	Shuto Asano	Nagoya University

No.	課題名	氏名	所属		Title	Name	Organization
43	高圧下における TaN ナノワイヤー結晶の合成	ニコ アレキサンダー ガイダ	名古屋大学	工学部	Synthesis of TaN nanowire crystals under high pressure	Nico Alexander Gaida	Nagoya University
44	高圧下でのアミノ酸のペプチド化反応と不斉増幅	鍵 裕之	東京大学	大学院理学系研究科	Peptide formation and chiral amplification of amino acids under high pressure	Hiroyuki Kagi	The University of Tokyo
45	〃	織田 翔太郎	東京大学	大学院理学系研究科	〃	Shotaro Oda	The University of Tokyo
46	高温高圧中性子回折測定を用いた鉄-ニッケル合金中の水素原子のサイト依存性の解明	飯塚 理子	東京大学	大学院理学系研究科地殻化学実験施設	Neutron diffraction measurements on hydrogenated iron-nickel alloy at high-PT conditions	Riko Iizuka	The University of Tokyo
47	〃	市東 力	東京大学	大学院理学系研究科	〃	Chikara Shito	The University of Tokyo
48	高温高圧下における下部マントル鉱物への窒素の取り込みに関する研究	福山 鴻	東京大学	大学院理学系研究科 地殻化学実験施設	The study on nitrogen incorporation into the lower-mantle minerals under high pressure and high temperature	Ko Fukuyama	The University of Tokyo
49	ペロブスカイト関連化合物の高圧合成	稲熊 宜之	学習院大学	理学部	High-pressure synthesis of perovskite-related compounds	Yoshiyuki Inaguma	Gakushuin University
50	〃	植田 紘一郎	学習院大学	理学部	〃	Koichiro Ueda	Gakushuin University
51	〃	和泉 一成	学習院大学	大学院自然科学研究科	〃	Kazunari Izumi	Gakushuin University
52	高温高圧水中でのバイオマス変換に使用するマイクロポーラス材料の安定性向上	大島 義人	東京大学	大学院新領域創成科学研究科	Improving stability of microporous materials for biomass upgrading in sub- and supercritical water	Yoshito Oshima	The University of Tokyo
53	〃	アピバンボリラク チャン ウィット	東京大学	大学院新領域創成科学研究科	〃	Apibanboriak Chanwit	The University of Tokyo
54	高脂質含有バイオマスの超臨界水ガス化における水素生産のための2段階接触分解装置と改質装置の開発	布浦 鉄兵	東京大学	環境安全研究センター	Development of a two-stage catalytic cracker and reformer for hydrogen production in supercritical water gasification of biomass with high lipid content	Tepei Nunoura	The University of Tokyo
55	〃	ダイアン グバタンガ	東京大学	大学院新領域創成科学研究科	〃	Diane Gubatanga	The University of Tokyo
56	加圧熱水処理によるコーヒー滓からの吸着材製造	布浦 鉄兵	東京大学	環境安全研究センター	Coffee-based adsorbents production via hydrothermal carbonization	Tepei Nunoura	The University of Tokyo
57	〃	秦 世明	東京大学	大学院新領域創成科学研究科	〃	Qin Shiming	The University of Tokyo
58	超臨界二酸化炭素、塩水、岩石間の相互作用が起きる場の基礎的理解	秋月 信	東京大学	大学院新領域創成科学研究科	Research on fundamentals of interaction between supercritical carbon dioxide, brine and rock	Makoto Akizuki	The University of Tokyo
59	〃	外野 圭太	東京大学	大学院新領域創成科学研究科	〃	Keita Hokano	The University of Tokyo

No.	課題名	氏名	所属		Title	Name	Organization
60	プロトン伝導性固体電解質膜の異相接合界面における輸送現象の研究	大友 順一郎	東京大学	大学院新領域創成科学研究科	Study of the transport phenomenon at proton conductor' s heterojunction	Junichiro Otomo	The University of Tokyo
61	”	中根 健太	東京大学	工学部	”	Nakane Kenta	The University of Tokyo
62	プロトン伝導性固体電解質薄膜を用いた低温作動燃料電池・電解合成セルの開発	大友 順一郎	東京大学	大学院新領域創成科学研究科	Development of low-temperature solid oxide fuel cells and electrolysis cells using proton-conducting solid electrolyte thin films	Junichiro Otomo	The University of Tokyo
63	”	松尾 拓紀	東京大学	大学院新領域創成科学研究科	”	Hiroki Matsuo	The University of Tokyo
64	カルシウムループ法によるメタンガスプロセスの開発	大友 順一郎	東京大学	大学院新領域創成科学研究科	Development of Ca looping process for production of methane	Junichiro Otomo	The University of Tokyo
65	”	李 智漢	東京大学	大学院新領域創成科学研究科	”	Lee Jihan	The University of Tokyo
66	中温域でのアンモニア電解合成における赤外分光法を用いた反応機構解明	大友 順一郎	東京大学	大学院新領域創成科学研究科	Elucidation of reaction mechanism of ammonia electrosynthesis at intermediate temperature with infrared spectroscopy	Junichiro Otomo	The University of Tokyo
67	”	秋山 大樹	東京大学	大学院新領域創成科学研究科	”	Daiki Akiyama	The University of Tokyo
68	ケミカルループ燃焼法における酸素放出型キャリアの構造制御	大友 順一郎	東京大学	大学院新領域創成科学研究科	Structure control of oxygen carrier materials in chemical looping systems	Junichiro Otomo	The University of Tokyo
69	”	山村 泰平	東京大学	大学院新領域創成科学研究科	”	Taihei Yamamura	The University of Tokyo
70	アンモニア電解合成の反応器設計	大友 順一郎	東京大学	大学院新領域創成科学研究科	Reactor design for ammonia electrosynthesis	Junichiro Otomo	The University of Tokyo
71	”	福田 一峻	東京大学	大学院新領域創成科学研究科	”	Kazutaka Fukuda	The University of Tokyo
72	混合電解質を用いたセルによる輸送特性制御と電解合成への応用	大友 順一郎	東京大学	大学院新領域創成科学研究科	Transport property control by mixed electrolyte cell and its application to electrosynthesis	Junichiro Otomo	The University of Tokyo
73	”	田島 星也	東京大学	大学院新領域創成科学研究科	”	Seiya Tajima	The University of Tokyo
74	CSD 法によるプロトン伝導性電解質薄膜の低温合成およびセル性能評価	大友 順一郎	東京大学	大学院新領域創成科学研究科	Low temperature synthesis of electrolyte thin film by CSD method and evaluation of cell performance	Junichiro Otomo	The University of Tokyo
75	”	戸田 亮輔	東京大学	大学院新領域創成科学研究科	”	Ryousuke Toda	The University of Tokyo
76	燃料電池の電解質・電極の異相界面の解析と燃料電池の性能向上	大友 順一郎	東京大学	大学院新領域創成科学研究科	Analysis of heterogeneous interface of electrolyte and electrode, and improvement of SOFC	Junichiro Otomo	The University of Tokyo

No.	課題名	氏名	所属		Title	Name	Organization
77	”	黄 睿	東京大学	大学院新領域創成科学研究科	”	Huang Rui	The University of Tokyo
78	イオン及び電子伝導特性の制御による SOEC 性能の改善	大友 順一郎	東京大学	大学院新領域創成科学研究科	Improvement of solid-oxide electrolysis cells performance by controlling ionic and electronic transport properties	Junichiro Otomo	The University of Tokyo
79	”	オルティスコラレスフリアンアンドレス	東京大学	大学院新領域創成科学研究科	”	Ortiz Corrales Julian Andres	The University of Tokyo
80	イオン-電子混合伝導体の異相界面の作製と輸送現象の解明	大友 順一郎	東京大学	大学院新領域創成科学研究科	Formation of heterojunction of mixed ionic electronic conductors and clarification of its transport phenomena	Junichiro Otomo	The University of Tokyo
81	”	甚野 幸一	東京大学	大学院新領域創成科学研究科	”	Koichi Jinno	The University of Tokyo
82	メソポーラスマテリアルに担持した金属触媒のキャラクタリゼーション	佐々木 岳彦	東京大学	大学院新領域創成科学研究科	Characterization of metal catalysts loaded on mesoporous materials	Takehiko Sasaki	The University of Tokyo
83	廃プラスチックの炭化による二酸化炭素回収および貯留	布浦 鉄兵	東京大学	環境安全研究センター	Carbon capture through carbonization of plastic waste	Teppey Nunoura	The University of Tokyo
84	”	ジェニファーチャーウィーファン	東京大学	大学院新領域創成科学研究科	”	Jennifer Chia Wee Fern	The University of Tokyo
85	二価の鉄イオンを含む六方晶フェライトの化学組成と磁気特性	植田 浩明	京都大学	大学院理学研究科	Chemical compositions and magnetic properties of hexaferrites with ferrous ion	Hiroaki Ueda	Kyoto university
86	”	奥津 陽太	京都大学	大学院理学研究科	”	Yota Okutsu	Kyoto University
87	新規パイロクロア格子反強磁性体の磁気的性質	岡本 佳比古	名古屋大学	大学院工学研究科	Magnetic properties of a novel pyrochlore lattice antiferromagnet	Yoshihiko Okamoto	Nagoya University
88	新規遷移金属窒化物の超高压合成と結晶育成および物性	長谷川 正	名古屋大学	大学院工学研究科	High pressure synthesis, crystal growth and physical properties of novel transition metal nitrides	Masashi Hasegawa	Nagoya University
89	”	野田 航希	名古屋大学	工学部	”	Koki Noda	Nagoya University
90	サマリウム系希土類オルソフェライト単結晶成長とテラヘルツ帯スピン分光	中嶋 誠	大阪大学	レーザー科学研究所	Single crystal growth for Samarium rare-earth orthoferrite and ultrafast terahertz spin control	Makoto Nakajima	Osaka University
91	”	北原 英明	大阪大学	レーザー科学研究所	”	Hideaki Kitahara	Osaka University
92	”	小池 遥平	大阪大学	レーザー科学研究所	”	Yohei Koike	Osaka University
93	”	凌 子祺	大阪大学	レーザー科学研究所	”	Ling Ziqi	Osaka University

No.	課題名	氏名	所属		Title	Name	Organization
94	”	遠矢 雄浩	大阪大学	レーザー科学研究所	”	Toya Kazuhiro	Osaka university
95	フェロイック物質に係る物質開発・新規な物性現象の探求	木村 剛	東京大学	大学院新領域創成科学研究科	Exploration of novel ferroic materials and phenomena	Tsuyoshi Kimura	The University of Tokyo
96	”	木村 健太	東京大学	大学院新領域創成科学研究科	”	Kenta Kimura	The University of Tokyo
97	”	三澤 龍介	東京大学	大学院新領域創成科学研究科	”	Ryusuke Misawa	The University of Tokyo
98	”	林田 健志	東京大学	大学院新領域創成科学研究科	”	Takeshi Hayashida	The University of Tokyo
99	”	八木 直輝	東京大学	大学院新領域創成科学研究科	”	Naoki Yagi	The University of Tokyo
100	”	姜 山	東京大学	大学院新領域創成科学研究科	”	Kang San	The University of Tokyo
101	”	林 悠生	東京大学	大学院新領域創成科学研究科	”	Yuki Hayashi	The University of Tokyo
102	”	大島 貴彦	東京大学	大学院新領域創成科学研究科	”	Takahiko Oshima	The University of Tokyo
103	回転対称性の破れを伴う超伝導体・磁性体に関する研究	水上 雄太	東京大学	大学院新領域創成科学研究科	Studies on superconductors and magnetic materials with rotational symmetry breaking	Yuta Mizukami	The University of Tokyo
104	”	石田 浩祐	東京大学	大学院新領域創成科学研究科	”	Kousuke Ishida	The University of Tokyo
105	”	向笠 清隆	東京大学	大学院新領域創成科学研究科	”	Kiyotaka Mukasa	The University of Tokyo
106	”	田中 桜平	東京大学	大学院新領域創成科学研究科	”	Ohei Tanaka	The University of Tokyo
107	”	石原 滉大	東京大学	大学院新領域創成科学研究科	”	Kota Ishihara	The University of Tokyo
108	”	斎藤 三樹彦	東京大学	大学院新領域創成科学研究科	”	Mikihiko Saito	The University of Tokyo
109	”	原澤 龍平	東京大学	工学部	”	Ryuhei Harasawa	The University of Tokyo
110	外場制御可能な磁気超構造を有する物質の開発	有馬 孝尚	東京大学	大学院新領域創成科学研究科	Exploration of materials hosting controllable magnetic superstructure	Takahisa Arima	The University of Tokyo

No.	課題名	氏名	所属		Title	Name	Organization
111	”	徳永 祐介	東京大学	大学院新領域創成科学研究科	”	Yusuke Tokunaga	The University of Tokyo
112	”	阿部 伸行	東京大学	大学院新領域創成科学研究科	”	Nobuyuki Abe	The University of Tokyo
113	”	近江 毅志	東京大学	大学院新領域創成科学研究科	”	Omi Tsuyoshi	The University of Tokyo
114	”	荒木 勇介	東京大学	大学院新領域創成科学研究科	”	Araki Yusuke	The University of Tokyo
115	”	佐藤 樹	東京大学	大学院新領域創成科学研究科	”	Tatsuki Sato	The University of Tokyo
116	”	渡辺 義人	東京大学	大学院新領域創成科学研究科	”	Yoshito Watanabe	The University of Tokyo
117	”	蘇 丹	東京大学	大学院新領域創成科学研究科	”	Su Dan	The University of Tokyo
118	”	柳内 晃	東京大学	大学院新領域創成科学研究科	”	Hikaru Yagiuchi	The University of Tokyo
119	”	磯貝 レオナ	東京大学	大学院新領域創成科学研究科	”	Leona Isogai	The University of Tokyo
120	”	吉田 健斗	東京大学	大学院新領域創成科学研究科	”	Kento Yoshida	The University of Tokyo
121	バナジウムカルコゲナイドにおける柔粘性結晶状態の研究	片山 尚幸	名古屋大学	大学院工学研究科	Study of plastic crystal state in vanadium chalcogenides	Naoyuki Katayama	Nagoya University
122	”	小島 慶太	名古屋大学	大学院応用物理学専攻	”	Keita Kojima	Nagoya University
123	バルク材料に負の圧力をかける新しい圧力技術の開発	片山 尚幸	名古屋大学	大学院工学研究科	Development of novel pressure technique which enables to apply negative pressure on bulk materials	Naoyuki Katayama	Nagoya University
124	”	塩見 学	名古屋大学	工学部	”	Manabu Shiomi	Nagoya University
125	3次元トポロジカル絶縁体薄膜とグラフェンによるヘテロ構造デバイスの物性	田邊 洋一	岡山理科大学	理学部	Physical properties of 3D topological insulator thin film / graphene heterostructure device	Yoichi Tanabe	Okayama University of Science
126	高温高圧中性子回折測定を用いた鉄-ニッケル合金中の水素原子のサイト依存性の解明	森 悠一郎	東京大学	大学院理学系研究科	Neutron diffraction measurements on hydrogenated iron-nickel alloy at high-PT conditions	Yuichiro Mori	The University of Tokyo
127	外場制御可能な磁気超構造を有する物質の開発	柳田 真佑	東京大学	大学院新領域創成科学研究科	Exploration of materials hosting controllable magnetic superstructure	Shinsuke Yanagida	The University of Tokyo

No.	課題名	氏名	所属		Title	Name	Organization
128	”	車地 崇	東京大学	大学院新領域創成科学研究科	”	Takashi Kurumaji	The University of Tokyo

物質合成・評価設備 U クラス / Materials Synthesis and Characterization U Class Researcher

No.	課題名	氏名	所属		Title	Name	Organization
1	プラズマ風洞による宇宙往還機熱防護システムの動的酸化に関する研究	田中 聖也	東京大学	大学院工学系研究科	Investigation on dynamic oxidation of thermal protection system using plasma wind tunnel	Seiya Tanaka	The University of Tokyo
2	スピングラス物質の合成	古府 麻衣子	日本原子力研究開発機構	J-PARC センター	Synthesis of spin glass materials	Maiko Kofu	Japan Atomic Energy Agency

長期留学研究員 / Long Term Young Researcher

No.	課題名	氏名	所属		Title	Name	Organization
1	発光量絶対値測定系を用いたイクオリンの発光量子収率の測定	小野 稜平	群馬大学	理工学府	Measurement of luminescence quantum yield of aequorin using calibrated total-photon flux spectrometer	Ryohei Ono	Gunma University
2	銅と有機分子界面におけるバンド状態の巨大スピン分裂の直接観測	下澤 皁介	東京理科大学	大学院理工学研究科	Direct observation of giant spin splitting band on organic molecules/cooper interface.	Kousuke Shimozawa	Tokyo University of Science
3	金属と有機分子界面におけるラシュバ分裂の増大	小久保 裕太	東京理科大学	理工学部	Enhancement of Rashba splitting on molecule/metal interface	yuta Kokubo	Tokyo University of Science

令和2年度 共同利用課題一覧 (後期) / Joint Research List (2020 Latter Term)

嘱託研究員 / Commission Researcher

No.	課題名	氏名	所属	Title	Name	Organization
担当所員：小森 文夫						
1	レーザースピン角度分解光分光による表面電子状態の研究	矢治 光一郎	物質・材料研究機構	先端材料解析研究拠点	SARPES studies of atomic layer materials at surfaces	Koichiro Yaji National Institute for Materials Science
担当所員：上床 美也						
2	低温用マルチアンビル装置の開発	辺土 正人	琉球大学	理学部	Development of multi-anvil apparatus for low temperature	Masato Hedo University of Ryukyus
3	希土類 122 化合物における圧力効果	繁岡 透	山口大学	大学院理工学研究科	Pressure effect of rare earth 122 compounds	Toru Shigeoka Yamaguchi University
4	圧力下 NMR 測定法に関する開発	藤原 直樹	京都大学	大学院人間・環境学研究科	Development of NMR measurement method under high pressure	Naoki Fujiwara Kyoto University
5	極低温下の磁気特性	鳥塚 潔	日本工業大学	共通教育学群	Development of magnetic measurement method	Kiyoshi Torizuka Nippon Institute of Technology
6	有機伝導体の圧力効果	村田 恵三	大阪経済法科大学		Effect of pressure on the organic conductor	Keizo Murata Osaka University of Economics and Law
7	酸化物試料の作製と高圧下物性測定	川中 浩史	産業技術総合研究所	電子光技術研究部門	Sample preparation and high pressure experiments	Hirofumi Kawanaka National Institute of Advanced Industrial Science and Technology
8	高圧下量子振動観測システム	摂待 力生	新潟大学	理学部	Development of quantum oscillation under high pressure	Rikio Settai Niigata University
9	希釈冷凍機温度で使用可能な 10GPa 級超高压発生装置の開発	松林 和幸	電気通信大学	大学院情報理工学研究科	Development of 10GPa class high pressure apparatus for low temperature	Kazuyuki Matsubayashi The University of Electro-Communications
10	DAC を用いた物性測定方法の開発	狩野 みか	日本工業大学	共通教育学群	Development of physical property measurement method using DAC	Mika Kano Nippon Institute of Technology
11	3 d 遷移化合物に関する圧力効果	鹿又 武	東北学院大学	工学総合研究所	Effect of pressure on the 3d transition compounds	Kanomata Takeshi Tohoku Gakuin University
12	擬一次元有機物質の圧力下物性研究	糸井 充穂	日本大学	医学部	Study on pressure induced superconductivity of quasi organic conductor	Miho Itoi Nihon University
13	多重極限関連圧力装置の調整	高橋 博樹	日本大学	文理学部	Adjustment of Cubic Anvil apparatus	Hiroki Takahashi Nihon University

No.	課題名	氏名	所属		Title	Name	Organization
14	高圧下 X 線回折法の開発	江藤 徹二郎	久留米工業大学	工学部	Development of High Pressure X-ray diffraction measurements	Tetsujiro Eto	Kurume Institute of Technology
15	中性子回折用圧力発生装置の開発	宗像 孝司	総合科学研究機構	中性子科学センター	Development of high pressure apparatus for neutron diffraction	Koji Munakata	CROSS
担当所員：山室 修							
16	4G における共同利用推進	佐藤 卓	東北大学	多元物質科学研究所	Research and Support of General-Use at 4G	Taku J Sato	Tohoku University
17	”	奥山 大輔	東北大学	多元物質科学研究所	”	Daisuke Okuyama	Tohoku University
18	”	那波 和宏	東北大学	多元物質科学研究所	”	Kazuhiro Nawa	Tohoku University
19	6G、T1-1 における共同利用推進	岩佐 和晃	茨城大学	フロンティア応用原子科学研究センター	Research and Support of General-Use at 6G and T1-1	Kazuaki Iwasa	Ibaraki University
20	T1-1、T1-3 における共同利用推進	大山 研司	茨城大学	大学院理工学研究科	Research and Support of General-Use at T1-1 and T1-3	Kenji Ohoyama	Ibaraki University
21	T1-1 における共同利用推進	桑原 慶太郎	茨城大学	大学院理工学研究科	Research and Support of General-Use at T1-1	Keitaro Kuwahara	Ibaraki University
22	”	横山 淳	茨城大学	理学部	”	Makoto Yokoyama	Ibaraki University
23	”	伊賀 文俊	茨城大学	大学院理工学研究科	”	Fumitoshi Iga	Ibaraki University
24	T1-2、T1-3、6G における共同利用推進	藤田 全基	東北大学	金属材料研究所	Research and Support of General-Use at T1-2, T1-3 and 6G	Masaki Fujita	Tohoku University
25	”	南部 雄亮	東北大学	金属材料研究所	”	Yusuke Nambu	Tohoku University
26	”	池田 陽一	東北大学	金属材料研究所	”	Yoichi Ikeda	Tohoku University
27	”	谷口 貴紀	東北大学	金属材料研究所	”	Takanori Taniguchi	Tohoku University
28	T2-2、T1-3 における共同利用推進	木村 宏之	東北大学	多元物質科学研究所	Research and Support of General-Use at T1-2 and T1-3	Hiroyuki Kimura	Tohoku University
29	”	坂倉 輝俊	東北大学	多元物質科学研究所	”	Terutoshi Sakakura	Tohoku University

No.	課題名	氏名	所属		Title	Name	Organization
30	”	山本 孟	東北大学	多元物質科学研究所	”	Hajime Yamamoto	Tohoku University
31	C1-2 における共同利用推進	杉山 正明	京都大学	複合原子力科学研究所	Research and Support of General-Use at C1-2	Masaaki Sugiyama	Kyoto University
32	C1-2、C2-3-1 における共同利用推進	井上 倫太郎	京都大学	複合原子力科学研究所	Research and Support of General-Use at C1-2 and C2-3-1	Rintaro Inoue	Kyoto University
33	”	守島 健	京都大学	複合原子力科学研究所	”	Ken Morishima	Kyoto University
34	C3-1-2、C2-3-1 における共同利用推進	日野 正裕	京都大学	複合原子力科学研究所	Research and Support of General-Use at C2-1-2 and C2-3-1	Masahiro Hino	Kyoto University
35	C3-1-2 における共同利用推進	田崎 誠司	京都大学	複合原子力科学研究所	Research and Support of General-Use at C3-1-2	Seiji Tasaki	Kyoto University
36	”	小田 達郎	京都大学	複合原子力科学研究所	”	Tatsuro Oda	Kyoto University
37	”	北口 雅暁	名古屋大学	大学院理学研究科	”	Masaaki Kitaguchi	Nagoya University
38	C1-2、C2-3-1 における共同利用推進	中川 慎太郎	東京大学	生産技術研究所	Research and Support of General-Use at C1-2 and C2-3-1	Shintaro Nakagawa	The University of Tokyo
担当所員：近藤 猛							
39	光電子分光法を用いた各種分子性結晶の電子状態の研究及び装置の低温化	木須 孝幸	大阪大学	大学院基礎工学研究科	Research on electron state of molecular crystals using photoemission spectroscopy	Takayuki Kisu	Osaka University
40	トポロジカル絶縁体の電子状態の解明	木村 昭夫	広島大学	大学院理学研究科	Electronic-structure study of topological insulators	Akio Kimura	Hiroshima University
41	トポロジカル超伝導体の探索	坂野 昌人	東京大学	大学院工学系研究科	Research for topological insulators	Masato Sakano	The University of Tokyo
42	有機化合物の光電子分光	金井 要	東京理科大学	理工学部	Photoemission study on organic compounds	Kaname Kanai	Tokyo University of Science
43	高分解能光電子分光による強相関物質の研究	横谷 尚睦	岡山大学	異分野基礎科学研究所	Ultra-high resolution study on strongly correlated materials	Takayoshi Yokoya	Okayama University
担当所員：岡崎 浩三							
44	固体中のマヨラナ粒子の研究	松田 祐司	京都大学	大学院理学研究科	Study of Majorana Fermion in Solids by Laser Photoemission Spectroscopy	Yuji Matsuda	Kyoto University

No.	課題名	氏名	所属		Title	Name	Organization
45	〃	佐藤 昌利	京都大学	基礎物理学研究所	〃	Masatoshi Sato	Kyoto University
46	60-eV レーザーを用いた時間分解光電子分光の開発	石坂 香子	東京大学	大学院工学系研究科	The development of time-resolved photoemission using 60eV laser	Kyoko Ishizaka	The University of Tokyo
47	収差補正型光電子顕微鏡の建設と利用研究	小嗣 真人	東京理科大学	基礎工学部	Construction and utilization research of aberration correction photoelectron emission microscopy	Masato Kotsugi	Tokyo University of Science
48	FeSe 超伝導体における BCS-BES クロスオーバーの研究	紺谷 浩	名古屋大学	大学院理学研究科	Study of BCS-BES crossover in FeSe superconductors	Hiroshi Kontani	Nagoya University
49	時間分解光電子分光を用いた強相関物質の研究	溝川 貴司	早稲田大学	理工学術院	Time-resolved photoemission study on strongly-correlated materials	Takashi Mizokawa	Waseda University
50	時間分解光電子分光や超高分解能光電子分光を用いた超伝導体や強相関物質の研究	吉田 鉄平	京都大学	大学院人間・環境学研究科	Laser ARPES study on superconductors and strongly-correlated materials	Tepei Yoshida	Kyoto University
51	鉄系超伝導体のレーザー光電子分光	下志万 貴博	理化学研究所	創発物性科学研究センター	Laser-ARPES on Fe superconductor	Takahiro Shimojima	RIKEN
52	超高分解能レーザー光電子分光による高温超伝導体の研究	チャン ウェイル	上智大学	大学院機能創造理工学科	Study of high T_c superconductors by high-resolution laser ARPES	Weilu Zhang	Sophia University
担当所員：原田 慈久							
53	軟 X 線発光・共鳴非弾性散乱分光の磁気円・線二色性測定システムの構築	菅 滋正	大阪大学	産業科学研究所	Construction of a noble system for circular and linear dichroism in soft X-ray emission and RIXS spectroscopy	Shigemasa Suga	Osaka University
54	軟 X 線吸収 / 発光分光法によるリチウムイオン電池電極材料の電子物性研究	細野 英司	産業技術総合研究所	省エネルギー研究部門	Study on the electronic property of electrode materials for Li-ion batteries by soft X-ray absorption/emission spectroscopy	Eiji Hosono	National Institute of Advanced Industrial Science and Technology
55	〃	朝倉 大輔	産業技術総合研究所	省エネルギー研究部門	〃	Daisuke Asakura	National Institute of Advanced Industrial Science and Technology
56	高分解能光電子分光による酸化バナジウムの研究	藤原 秀紀	大阪大学	大学院基礎工学研究科	Study on vanadium oxides by high resolution Photoemission	Hidenori Fujiwara	Osaka University
57	省エネ・創エネ・蓄電デバイスのオペランド分光	尾嶋 正治	東京大学	大学院工学系研究科	Operando nano-spectroscopy for energy efficient, power generation and energy storage devices	Masaharu Oshima	The University of Tokyo
58	原子レベルで制御されたモデル有機分子表面上の界面水の電子状態観測	林 智広	東京工業大学	物質理工学院	Analysis of the electronic structure of the interfacial water formed on model organic surfaces	Tomohiro Hayashi	Tokyo Institute of Technology
59	時間分解光電子顕微分光実験の技術開発	木下 豊彦	高輝度光科学研究センター	分光・イメージング推進室	Technical development of time-resolved photoemission microscopy measurement	Toyohiko Kinoshita	JASRI
60	三次元 nanoESCA による実デバイスのオペランド電子状態解析	永村 直佳	物質・材料研究機構	先端材料解析研究拠点	Operando analysis of the electronic structure of actual device by 3DnanoESCA	Naoka Nagamura	National Institute for Materials Science

No.	課題名	氏名	所属	Title		Name	Organization
担当所員：松田 巖							
61	不均一触媒反応のオペランド光電子測定	小坂谷 貴典	自然科学研究機構	分子科学研究所	Operendo photoelectron spectroscopy of heterogeneous catalysts	Takanori Koitaya	National Institute of Natural Sciences
62	単原子層シートの原子・電子構造のダイナミクス研究	虻川 匡	東北大学	多元物質科学研究所	Dynamics in atomic and electronic structures of monatomic sheets	Tadashi Abukawa	Tohoku University
63	雰囲気光電子分光装置の高度化	山本 達	東北大学	多元物質科学研究所	Updates of the NAP-XPS machine	Susumu Yamamoto	Tohoku University
64	偏光制御型軟 X 線分光装置の開発	平田 靖透	防衛大学校	応用物理学科	Development of a system for the polarization-controlled soft X-ray spectroscopy	Yasuyuki Hirata	National Defence Academy
65	遷移金属化合物の時間分解 X 線分光と回析	和達 大樹	兵庫県立大学	大学院物理学研究科	Time-resolved x-ray spectroscopy and diffraction of transition-metal-compounds	Hiroki Wadachi	University of Hyogo
66	超高速磁化応答による磁性波動関数の制御	小林 正起	東京大学	大学院工学系研究科	Regulation of magnetic wave functions by ultrafast magnetization response	Masaki Kobayashi	The University of Tokyo
67	時間分解磁気光学実験の技術開発	小嗣 真人	東京理科大学	基礎工学部	Technical development of time-resolved magneto-optical experiment	Masato Kotsugi	Tokyo University of Science

一般研究員 / General Researcher

No.	課題名	氏名	所属	Title		Name	Organization
担当所員：瀧川 仁							
1	正三角スピン系有機トリラジカルの窒素核磁気共鳴による磁気誘電現象の解明	細越 裕子	大阪府立大学	大学院理学系研究科	NMR study on the magnetodielectric properties of organic equilateral triangular spin system	Yuko Hosokoshi	Osaka Prefecture University
担当所員：榎原 俊郎							
2	新規超伝導体 UTe ₂ の対関数の対称性の研究	町田 一成	立命館大学	理工学部	Investigation on new superconductor UTe ₂	Kazunari Machida	Ritsumeikan University
3	量子スピンアイス物質における量子モノポールの実験的検出	町田 洋	学習院大学	理学部物理学科	Experimental detection of quantum monopole in quantum spin ice systems	Yo Machida	Gakushuin University
4	”	上原 大毅	学習院大学	大学院自然科学研究科	”	Taiki Uehara	Gakushuin University
5	高度なスピン配列制御が作り出す多彩な量子状態の低温物性	山口 博則	大阪府立大学	大学院理学系研究科	Low temperature physical properties of various quantum states formed by advance spin alignment control	Hironori Yamaguchi	Osaka Prefecture University

No.	課題名	氏名	所属		Title	Name	Organization
6	重い電子化合物 YbCu ₄ Au の極低温比熱測定	谷口 貴紀	東北大学	金属材料研究所	The specific heat measurement with a dilution refrigerator in the heavy fermion compound YbCu ₄ Au	Takanori Taniguchi	Tohoku University
7	大型単結晶試料を用いた Sr ₂ RuO ₄ の磁場方位制御下における極低温磁化測定	橋高 俊一郎	中央大学	理工学部	Low-temperature magnetization measurement on a large single crystal of Sr ₂ RuO ₄ under a precise control of field orientation	Shunichiro Kittaka	Chuo University
8	〃	河野 洋平	中央大学	理工学部	〃	Yohei Kono	Chuo University
9	ファラデー力磁力計による単サイトで発現するメタ磁性の解明	池田 陽一	東北大学	金属材料研究所	Clarification of the metamagnetism occurring in isolated magnetic Yb ions with a Faraday force magnetometer	Yoichi Ikeda	Tohoku University
10	〃	北澤 崇文	東北大学	大学院理学研究科	〃	Takafumi Kitazawa	Tohoku University
11	ウラン・トリウム非従来型超伝導体・磁性体の磁化・熱膨張測定	清水 悠晴	東北大学	金属材料研究所	Magnetization and magnetosriction measurements of uranium-thorium based unconventional superconductors	Yusei Shimizu	Tohoku University
12	新規金属有機カゴメ格子磁性体のスピン液体状態の研究	山口 明	兵庫県立大学	大学院物質理学研究科	Study of spin liquid state in a novel metal-organic kagome antiferromagnet	Akira Yamaguchi	University of Hyogo
13	〃	松下 琢	名古屋大学	大学院理学研究科	〃	Taku Matsushita	Nagoya University
14	〃	丸本 涼太	名古屋大学	理学研究科	〃	Ryota Marumoto	Nagoya University
15	〃	帳 中岳	東海国立大学機構名古屋大学	物質科学国際研究センター	〃	Zhongyue Zhang	Nagoya University
16	空間反転対称性の破れた重い電子系物質 CeIrSi ₃ のフェルミ面転移	呉 易簡	東北大学	大学院理学研究科	Fermi surface reconstruction in noncentrosymmetric heavy fermion compound CeIrSi ₃	Wu Yijian	Tohoku University
担当所員：山下 穰							
17	YbRh ₂ Si ₂ の超低温における磁気トルク測定	宍戸 寛明	大阪府立大学	大学院工学研究科	Magnetic torque measurements on YbRh ₂ Si ₂ at ultra-low temperatures	Hiroaki Shishido	Osaka Prefecture University
担当所員：勝本 信吾							
18	二次元銅酸化物のホール測定と MPMS による磁化の測定 III	神戸 士郎	山形大学	大学院理工学研究科	Hall coefficient measurement of 2D cuprates and measurement of magnetic property by MPMS III	Shiro Kambe	Yamagata University
19	酸化チタンナノシート上グラフェンの量子輸送	原 正大	熊本大学	大学院先端科学研究部	Quantum transport in a graphene on a titanium oxide nanosheet	Masahiro Hara	Kumamoto University
20	金属とファンデルワールス結晶と接合界面における界面状態の研究	石黒 亮輔	日本女子大学	理学部	Study of Interface States at Junction between Metals and van der Waals Crystals	Ryosuke Ishiguro	Japan Women's University

No.	課題名	氏名	所属		Title	Name	Organization
21	〃	浜本 あや	日本女子大学	大学院理学研究科	〃	Aya Hamamoto	Japan Women's University
22	量子ホール効果のための高移動度半導体試料作製と超低温での測定	福田 昭	兵庫医科大学	物理学教室	Development of the high mobility semiconductor samples for the quantum Hall state and their measurements in very low temperature	Akira Fukuda	Hyogo College of Medicine
担当所員：小森 文夫							
23	真空転写法により形成したツイスト2層グラフェンの電子状態評価	田中 悟	九州大学	大学院工学研究院	Evaluation of electronic structures of twisted bilayer graphene fabricated by a vacuum transfer technique	Satoru Tanaka	Kyushu University
24	〃	ビシコフスキー アントン	九州大学	大学院工学研究院	〃	Visikovskiy Anton	Kyushu University
25	〃	今村 均	九州大学	大学院工学研究院	〃	Hitoshi Imamura	Kyushu University
26	SiC ナノ周期表面上に転写したグラフェンの電子状態の観察	田中 悟	九州大学	大学院工学研究院	Evaluation of electronic structures of graphene transferred on SiC periodic nanosurfaces	Satoru Tanaka	Kyushu University
27	〃	魚谷 亮介	九州大学	大学院工学研究院	〃	Ryosuke Uotani	Kyushu University
28	酸素サーファクタントを用いた Fe 薄膜の成長過程と電子状態	中辻 寛	東京工業大学	物質理工学院	Oxygen surfactant assisted growth of Fe thin-films and their electronic states	Kan Nakatsuji	Tokyo Institute of Technology
29	微傾斜 Si(111) $\sqrt{3} \times \sqrt{3}$ -B 基板上に成長した Bi(110) 超薄膜の電子状態	中辻 寛	東京工業大学	物質理工学院	Electronic structure of Bi(110) thin films grown on vicinal Si(111) $\sqrt{3} \times \sqrt{3}$ -B substrates	Kan Nakatsuji	Tokyo Institute of Technology
30	Si(110) ₃ × 2-Bi 表面の原子構造	中辻 寛	東京工業大学	物質理工学院	Atomic structure of Si(110) ₃ × 2-Bi surface	Kan Nakatsuji	Tokyo Institute of Technology
31	特異なスピン状態を持つ希土類及び遷移金属化合物表面及び吸着磁性原子電子状態とスピン状態の STS 解析	菅 滋正	大阪大学	産業科学研究所	Scanning tunneling spectroscopy of surfaces of exotic rare earth and transition metal compounds and adsorbed magnetic atoms	Shigemasa Suga	Osaka University
32	窒素を吸着させた Cu(001) 面における構造緩和	山田 正理	中央大学	理工学部	Structural relaxation on a Cu(001) surface with adsorbed nitrogen	Masamichi Yamada	Chuo University
担当所員：リップマー ミック							
33	機械学習を活用した高効率薄膜作製手法の高度化	大久保 勇男	物質・材料研究機構	国際ナノアーキテクトゥクス研究拠点	Development of an efficient thin film growth technique using a machine learning approach	Isao Ohkubo	National Institute for Materials Science
34	無機材料薄膜合成	大口 裕之	芝浦工業大学	工学部	Film growth of inorganic materials	Hiroyuki Oguchi	Shibaura Institute of Technology
担当所員：秋山 英文							

No.	課題名	氏名	所属		Title	Name	Organization
35	多波長励起フォトルミネッセンス測定による GaPN 混晶および GaPAsN 混晶のアップコンバージョン発光に関する研究	矢口 裕之	埼玉大学	大学院理工学研究科	Multiple wavelength excited photoluminescence measurements of up-conversion luminescence from GaPN and GaPAsN alloys	Hiroyuki Yaguchi	Saitama University
36	”	高宮 健吾	埼玉大学	総合技術支援センター	”	Kengo Takamiya	Saitama University
37	”	相良 鋼	埼玉大学	大学院理工学研究科	”	Hagane Sagara	Saitama University
担当所員：中辻 知、大谷 義近							
38	希土類金属間化合物の強磁場低温物性研究	海老原 孝雄	静岡大学	学術院理学領域	Physical properties in rare earth intermetallic compounds at high magnetic fields in low temperature	Takao Ebihara	Shizuoka University
39	”	丸山 博史	静岡大学	大学院総合科学技術研究科	”	Hiroshi Maruyama	Shizuoka University
40	”	ジュマエダ・ジャトミカ	静岡大学	自然科学教育部	”	Jumaeda Jatmika	Shizuoka University
担当所員：廣井 善二							
41	Si 基板上垂直配向 L10 規則化 CoPt の磁化測定	山浦 淳一	東京工業大学	元素戦略研究センター	Magnetization measurement of perpendicular oriented L10-ordered CoPt on Si substrates	Junichi Yamaura	Tokyo Institute of Technology
42	”	真島 豊	東京工業大学	科学技術創成研究院	”	Yutaka Majima	Tokyo Institute of Technology
43	”	遠山 諒	東京工業大学	物質理工学院	”	Ryo Toyama	Tokyo Institute of Technology
44	新しい三角格子クラスター Mott 絶縁体における量子スピン液体相の探索	原口 祐哉	東京農工大学	大学院工学研究院	Search for quantum spin liquid phase in a new triangular lattice cluster Mott insulator	Yuya Haraguchi	University of Agriculture and Technology
45	交流磁化率測定による有機超伝導体の相分離の研究	谷口 弘三	埼玉大学	大学院理工学研究科	Study on phase separation phenomena in organic superconductor by ac susceptibility measurements	Hiromi Taniguchi	Saitama University
46	”	高橋 啓太	埼玉大学	大学院理工学研究科	”	Keita Takahashi	Saitama University
担当所員：上床 美也							
47	YbH _{2+x} の磁性と伝導	中村 修	岡山理科大学	研究・社会連携センター	Magnetic and transport properties in YbH _{2+x}	Osamu Nakamura	Okayama University of Science
48	MnCo _{1-x} Ge 合金の磁気特性に関する研究 (4)	江藤 徹二郎	久留米工業大学	共通教育科	Study of magnetic properties in MnCo _{1-x} Ge alloys(4)	Tetsujiro Eto	Kurume Institute of Technology

No.	課題名	氏名	所属		Title	Name	Organization
49	圧力誘起価数転移によって発生する Yb モーメントの磁気秩序についての検証 (2)	藤原 哲也	山口大学	大学院創成科学研究科	Evidence for the magnetic ordering of Yb moment accompanied by the valence transition II	Tetsuya Fujiwara	Yamaguchi University
50	”	金子 達哉	山口大学	大学院創成科学研究科	”	Tatsuya Kaneko	Yamaguchi University
51	TmRh ₂ Si ₂ 化合物の単結晶育成 (2)	藤原 哲也	山口大学	大学院創成科学研究科	Single crystal growth of TmRh ₂ Si ₂ compound II	Tetsuya Fujiwara	Yamaguchi University
52	”	西崎 裕哉	山口大学	大学院創成科学研究科	”	Yuya Nishizaki	Yamaguchi University
53	HoRh ₂ Si ₂ の Pd 置換系化合物の単結晶育成 (2)	藤原 哲也	山口大学	大学院創成科学研究科	Single crystal growth of Co substituted HoRh _{2-x} Pd _x Si ₂ compounds II	Tetsuya Fujiwara	Yamaguchi University
54	”	小林 遼平	山口大学	大学院創成科学研究科	”	Ryohei Kobayashi	Yamaguchi University
55	EuMn ₂ Ge ₂ 単結晶の磁場中比熱測定 (3)	藤原 哲也	山口大学	大学院創成科学研究科	Specific heat measurement under magnetic field of EuMn ₂ Ge ₂ single crystal III	Tetsuya Fujiwara	Yamaguchi University
56	”	杉田 静留	山口大学	大学院創成科学研究科	”	Shizuru Sugita	Yamaguchi University
57	重い電子化合物 YbCu ₄ Au の極低温高压測定	谷口 貴紀	東北大学	金属材料研究所	The ultra-low temperature and high-pressure measurement in the heavy fermion compound YbCu ₄ Au	Takanori Taniguchi	Tohoku University
58	”	高濱 元史	東北大学	大学院理学研究科	”	Motofumi Takahama	Tohoku University
59	有機伝導体物性に与える高圧力媒体の分子形状の効果 # 2	村田 恵三	大阪経済法科大学	21世紀社会総合研究センター	Effect of Molecular Shape of the High Pressure Medium to the Properties of Organic Conductors #2	Keizo Murata	Osaka University of Economics and Law
60	スピン三重項超伝導体 UTe ₂ の磁性と超伝導の圧力効果	本多 史憲	東北大学	金属材料研究所	Effect of Pressure on the magnetism and superconductivity of a spin triplet superconductor UTe ₂	Fuminori Honda	Tohoku University
61	”	清水 悠晴	東北大学	金属材料研究所	”	Yusei Shimizu	Tohoku University
62	ウラン化合物の磁性の圧力効果	本多 史憲	東北大学	金属材料研究所	Effect of Pressure on the magnetism of uranium compounds	Fuminori Honda	Tohoku University
63	”	小泉 堯嗣	東北大学	大学院工学研究科	”	Takatsugu Koizumi	Tohoku University
64	ハーフメタルホイスラー合金の磁気体積効果に関する研究	重田 出	鹿児島大学	大学院理工学研究科	Study on the magneto-volume effect of half-metallic Heusler alloys	Iduru Shigeta	Kagoshima University
65	”	辻川 聡一朗	鹿児島大学	大学院理工学研究科	”	Soichiro Tsujikawa	Kagoshima University

No.	課題名	氏名	所属		Title	Name	Organization
66	HfTe ₃ の高圧力下電気抵抗率の測定	加瀬 直樹	東京理科大学	理学部応用物理学科	High pressure study of the single crystal of HfTe ₃	Naoki Kase	Tokyo University of Science
67	磁気冷凍材料候補物質 EuS の圧力下磁化測定	脇倉 和平	室蘭工業大学	希土類材料研究センター	Pressure effects on the magnetic and magnetocaloric properties of EuS	Kazuhei Wakiya	Muroran Institute of Technology
68	”	西村 肇	室蘭工業大学	大学院工学研究科	”	Hajime Nishimura	Muroran Institute of Technology
69	中性子回折用小型圧力セルの開発	宗像 孝司	総合科学研究機構	中性子科学センター	Development of compact pressure cell for neutron diffraction	Koji Munakata	CROSS
70	スピネル Fe _{1-x} Cu _x Cr ₂ S ₄ の高圧下磁性	伊藤 昌和	鹿児島大学	総合科学域総合教育学系	Magnetic properties of spinel Fe _{1-x} Cu _x Cr ₂ S ₄ in high pressure	Masakazu Ito	Kagoshima University
71	Sm ₂ Fe ₁₇ -N ₂ 気相 - 固相反応において窒素ガス圧力が磁気特性に及ぼす効果	尾上 昌平	鹿児島大学	研究推進機構研究支援センター	Effect of nitrogen gas pressure on the magnetic properties of Sm ₂ Fe ₁₇ N _x	Masahira Onoue	Kagoshima University
72	”	高橋 巡季	鹿児島大学	大学院理工学研究科	”	Junki Takahashi	Kagoshima University
73	磁場中熱処理により分解した Cu-Mn-Al 合金の磁気特性	三井 好古	鹿児島大学	大学院理工学研究科	Magnetic properties of Cu-Mn-Al alloys decomposed by in-magnetic-field annealing	Yoshifuru Mitsui	Kagoshima University
74	”	中川 駿	鹿児島大学	大学院理工学研究科	”	Shun Nakagawa	Kagoshima University
75	圧力下 NMR 測定法に関する開発	藤原 直樹	京都大学	大学院人間・環境学研究科	Development of NMR measurements under pressure	Naoki Fujiwara	Kyoto University
76	”	中村 昂矢	京都大学	大学院人間・環境学研究科	”	Kouta Nakamura	Kyoto University
77	”	桑山 昂典	京都大学	大学院人間・環境学研究科	”	Takanori Kuwayama	Kyoto University
78	”	猪股 和也	京都大学	大学院人間・環境学研究科	”	Kazuya Inomata	Kyoto University
79	ウラン化合物の磁性の圧力効果	モーリヤ アルビン	東北大学	金属材料研究所	Effect of Pressure on the magnetism of uranium compounds	Arvind Maurya	Tohoku University
担当所員：益田 隆嗣							
80	(Ce _{1-x} La _x) ₅ Ga ₂ Ge 単結晶試料の極低温比熱測定	小林 理気	琉球大学	理学部	Specific heat measurement at very low temperature on (Ce _{1-x} La _x) ₅ Ga ₂ Ge systems	Riki Kobayashi	University of the Ryukyus
81	”	岡部 孝俊	琉球大学	大学院理工学研究科	”	Takatoshi Okabe	University of the Ryukyus

No.	課題名	氏名	所属		Title	Name	Organization
82	CeTe _{1-x} Ge _x 単結晶試料の高エネルギー X 線ラウエ装置による結晶方位同定	小林 理気	琉球大学	理学部	Alignment of CeTe _{1-x} Ge _x single crystals by high-energy X-ray Laue diffraction	Riki Kobayashi	University of the Ryukyus
83	”	岩田 由規	琉球大学	大学院理工学研究科	”	Yuki Iwata	University of the Ryukyus
84	Ce ₅ (Si _{1-x} Ge _x) ₃ 単結晶試料の極低温比熱測定	小林 理気	琉球大学	理学部	Specific heat measurement at very low temperature on Ce ₅ (Si _{1-x} Ge _x) ₃ systems	Riki Kobayashi	University of the Ryukyus
85	”	藤井 岳	琉球大学	大学院理工学研究科	”	Gaku Fujii	University of the Ryukyus
担当所員：金道 浩一							
86	新しいコバルト系キタエフ-ハイゼンベルグ型磁性体における磁場誘起相転移の探索	原口 祐哉	東京農工大学	大学院工学研究院	Search for field-induced phase transitions in new cobalt-based Kitaev-Heisenberg-type magnets	Yuya Haraguchi	University of Agriculture and Technology
87	”	吉田 悠澄	東京農工大学	工学府	”	Yuto Yoshida	Tokyo University of Agriculture and Technology
88	パルス強磁場磁化測定による Yb 希薄系における単サイトメタ磁性の全貌の観測	池田 陽一	東北大学	金属材料研究所	Observation of the whole picture of single-site metamagnetism in a diluted Yb system by a pulsed high magnetic field magnetization measurement	Yoichi Ikeda	Tohoku University
89	”	北澤 崇文	東北大学	大学院理学研究科	”	Takafumi Kitazawa	Tohoku University
90	幾何学的フラストレート磁性体の強磁場磁化測定	菊池 彦光	福井大学	学術研究院	Magnetization measurements of the frustrated magnets	Hikomitsu Kikuchi	University of Fukui
91	比熱および電気抵抗測定による Yb 希薄系における縮重度の大きな不純物近藤効果の検証	池田 陽一	東北大学	金属材料研究所	Verification of the highly degenerated impurity Kondo effect in diluted Yb systems by specific heat and electrical resistivity measurements	Yoichi Ikeda	Tohoku University
92	”	北澤 崇文	東北大学	大学院理学研究科	”	Takafumi Kitazawa	Tohoku University
93	Bi-2212 単結晶における修正コーラー則の検証 (II)	渡辺 孝夫	弘前大学	大学院理工学研究科	Investigation of the modified Kohler' s rule on Bi-2212 single crystals(II)	Takao Watanabe	Hirosaki University
94	”	藤井 武則	東京大学	低温センター	”	Takenori Fujii	The University of Tokyo
95	”	原田 圭市	弘前大学	大学院理工学研究科	”	Keiichi Harada	Hirosaki University
96	ウラン系磁性体・常磁性体における強磁場領域履歴メタ磁性の探索	清水 悠晴	東北大学	金属材料研究所	Study of itinerant metamagnetism in uranium-based magnetic and paramagnetic systems	Yusei Shimizu	Tohoku University
97	スピネル Fe _{1-x} Cu _x Cr ₂ S ₄ の高磁場電気抵抗	伊藤 昌和	鹿児島大学	総合科学域総合教育学系	High magnetic field electric resistivity of spinel Fe _{1-x} Cu _x Cr ₂ S ₄	Masakazu Ito	Kagoshima University

No.	課題名	氏名	所属		Title	Name	Organization
98	α -RuBr ₃ の磁場配向試料の作製と強磁場磁化過程の測定	今井 良宗	東北大学	大学院理学研究科	Preparation of magnetically oriented α -RuBr ₃ and high-field magnetization measurements	Yoshinori Imai	Tohoku University
99	有機ラジカル系が創る新規スピンモデルの低温物性	山口 博則	大阪府立大学	理学系研究科	Low temperature physical properties of new spin models formed by organic radicals	Hironori Yamaguchi	Osaka Prefecture University
100	有機ビラジカルによる強磁性フラストレート磁性体の強磁場磁化測定	細越 裕子	大阪府立大学	大学院理学系研究科	High-field magnetization study of ferromagnetic frustrated lattice made of organic biradicals	Yuko Hosokoshi	Osaka Prefecture University
担当所員：徳永 将史							
101	重い電子系における強磁場中の電子状態研究	海老原 孝雄	静岡大学	学術院理学領域	Electronic states at high magnetic fields in Heavy Fermion systems	Takao Ebihara	Shizuoka University
102	”	丸山 博史	静岡大学	大学院総合科学技術研究科	”	Hiroshi Maruyama	Shizuoka University
103	”	ジュマエダ・ジャトミカ	静岡大学	自然科学教育部	”	Jumaeda Jatmika	Shizuoka University
104	カイヤナイト M ₂ GeO ₅ (M=Cr, V) の磁性	香取 浩子	東京農工大学	大学院工学研究科	Magnetism of Kyanite M ₂ GeO ₅ (M=Cr and V)	Hiroko Katori	Tokyo University of Agriculture and Technology
105	”	柿本 和勇	東京農工大学	工学府	”	Kazuo Kakimoto	Tokyo University of Agriculture and Technology
106	トラス型フェルミ面を持つラッシュバ型半導体の量子極限伝導特性の研究	村川 寛	大阪大学	大学院理学研究科	High field study for quantum limit transport properties of torus Fermi surface in Rashba semiconductor	Hiroshi Murakawa	Osaka University
107	元素置換した BaMnX ₂ 単結晶における強磁場輸送現象の研究	酒井 英明	大阪大学	大学院理学研究科	Study of high-field transport phenomena in chemically-substituted BaMnX ₂ single crystals	Hideaki Sakai	Osaka University
108	”	近藤 雅起	大阪大学	大学院理学研究科	”	Masaki Kondo	Osaka University
109	”	阪口 駿也	大阪大学	大学院理学研究科	”	Shunya Sakaguchi	Osaka University
110	新規超伝導体 UTe ₂ の電子状態の圧力効果の研究	本多 史憲	東北大学	金属材料研究所	Study of exotic electronic properties of a new superconductor UTe ₂ under high pressure	Fuminori Honda	Tohoku University
111	ウラン系化合物における新奇フラストレーション系磁性体の探索	清水 悠晴	東北大学	金属材料研究所	Exploration of novel frustrated magnetic system in uranium compounds	Yusei Shimizu	Tohoku University
112	Sr ₂ CoGe ₂ O ₇ の強磁場磁気熱量効果	赤木 暢	神戸大学	分子フォトサイエンス研究センター	High-field magnetocaloric effect in Sr ₂ CoGe ₂ O ₇	Mitsuru Akaki	Kobe University
113	正四角台塔反強磁性体 Ba(TiO)Cu ₄ (PO ₄) ₄ におけるパルス磁場中誘電率測定	木村 健太	東京大学	大学院新領域創成科学研究科	Dielectric constant measurements of square cupola antiferromagnet Ba(TiO)Cu ₄ (PO ₄) ₄	Kanta Kimura	The University of Tokyo

No.	課題名	氏名	所属		Title	Name	Organization
114	反強磁性金属 α -Mn のパルス強磁場下磁化過程の解明	秋葉 和人	岡山大学	大学院自然科学研究科	Magnetization process of antiferromagnetic metal α -Mn in pulsed magnetic field	Kazuto Akiba	Okayama University
担当所員：松田 康弘							
115	量子カゴメ反強磁性体 $\text{CaCu}_3(\text{OH})_6\text{Cl}_2 \cdot 0.6\text{H}_2\text{O}$ の強磁場磁化測定	吉田 紘行	北海道大学	大学院理学研究院	High-field magnetization measurements on quantum kagome antiferromagnet $\text{CaCu}_3(\text{OH})_6\text{Cl}_2 \cdot 0.6\text{H}_2\text{O}$	Hiroyuki Yoshida	Hokkaido University
担当所員：小濱 芳允							
116	正四角台塔反強磁性体 $\text{Pb}(\text{TiO})\text{Cu}_4(\text{PO}_4)_4$ における強磁場中での電気磁気光学効果の研究	木村 健太	東京大学	大学院新領域創成科学研究科	Optical magnetoelectric effect of the square-cupola-based antiferromagnet $\text{Pb}(\text{TiO})\text{Cu}_4(\text{PO}_4)_4$ in a high magnetic field	Kenta Kimura	The University of Tokyo
117	クロムスピネル酸化物におけるスピンネマティック相の探索	木村 尚次郎	東北大学	金属材料研究所	Explorations of the spin nematic phase in the chromium spinel oxide	Shojiro Kimura	Tohoku University
118	有機スピン液体候補物質の超強磁場下物性測定	宮川 和也	東京大学	大学院工学系研究科	Physical property measurement of organic spin liquid candidate material under ultra high field	Kazuya Miyagawa	The University of Tokyo
119	リフレクトメーターを用いた超強磁場下での電気抵抗測定の開発	東京工業大学	元素戦略研究センター	研究員	Development of electrical resistance measurement by reflectometer under ultra-high magnetic field	Shiro Kawachi	Tokyo Institute of Technology
担当所員：小林 洋平							
120	次世代レーザーとレーザー加工の基礎技術研究	吉富 大	産業技術総合研究所	電子光基礎技術研究部門	Basic research on next generation laser systems and laser machining technology	Dai Yoshitomi	Advanced Industrial Science and Technology
121	”	鳥塚 健二	産業技術総合研究所	電子光基礎技術研究部門	”	Kenji Torizuka	Advanced Industrial Science and Technology
122	”	高田 英行	産業技術総合研究所	電子光基礎技術研究部門	”	Hideyuki Takada	Advanced Industrial Science and Technology
123	”	奈良崎 愛子	産業技術総合研究所	電子光基礎技術研究部門	”	Aiko Narazaki	Advanced Industrial Science and Technology
124	”	田中 真人	産業技術総合研究所	分析計測標準研究部門	”	Masahito Tanaka	Advanced Industrial Science and Technology
125	”	小川 博嗣	産業技術総合研究所	分析計測標準研究部門	”	Hiroshi Ogawa	Advanced Industrial Science and Technology
126	”	佐藤 大輔	産業技術総合研究所	分析計測標準研究部門	”	Daisuke Satoh	Advanced Industrial Science and Technology
127	”	澁谷 達則	産業技術総合研究所	分析計測標準研究部門	”	Tatsunori Shibuya	Advanced Industrial Science and Technology

No.	課題名	氏名	所属		Title	Name	Organization
128	”	黒田 隆之助	産業技術総合研究所	先端オペランド計測技術オープンイノベーションラボラトリ	”	Ryunosuke Kuroda	Advanced Industrial Science and Technology
129	”	盛合 靖章	産業技術総合研究所	先端オペランド計測技術オープンイノベーションラボラトリ	”	Yasuaki Moriai	Advanced Industrial Science and Technology
130	”	寺澤 英知	産業技術総合研究所	先端オペランド計測技術オープンイノベーションラボラトリ	”	Eichi Terasawa	Advanced Industrial Science and Technology
131	”	牛窪 大樹	産業技術総合研究所	先端オペランド計測技術オープンイノベーションラボラトリ	”	Daiki Ushikubo	Advanced Industrial Science and Technology
132	短波長パルスレーザーによる CFRP 加工	森山 匡洋	東京大学	大学院理学系研究科付属フotonサイエンス研究機構	CFRP processing with short wavelength pulsed laser	Masahiro Moriyama	The University of Tokyo
133	Yb モードロックファイバーレーザーに同期した Er モードロックファイバーレーザーの開発	田中 耕一郎	京都大学	大学院理学研究科	Development of Er mode-locked fiber-laser system synchronized with Yb mode-locked fiber-laser	Koichiro Tanaka	Kyoto University
134	”	北條 真之	京都大学	大学院理学研究科	”	Masayuki Hojo	Kyoto University
135	”	高橋 伸弥	京都大学	大学院理学研究科	”	Shinya Takahashi	Kyoto University
136	”	内田 健人	京都大学	大学院理学研究科	”	Kento Uchida	Kyoto University
137	青色半導体レーザー用ファイバ型光コンバイナの開発	藤本 靖	千葉工業大学	工学部 電気電子工学科	Development on fiber power combiner for GaN semiconductor lasers	Yasushi Fujimoto	Chiba Institute of Technology (CIT)
138	半導体におけるフェムト秒レーザー加工に表面粗さが与える影響	富田 卓朗	徳島大学	徳島大学	Influence of surface roughness on femtosecond laser processing of semiconductors	Takuro Tomita	Tokushima University
139	”	坂東 賢哉	徳島大学	大学院創成科学研究科	”	Kenya Bando	Tokushima University
140	フェムト秒レーザー加工における固体材料の構造変化に関する研究	山口 誠	秋田大学	大学院理工学研究科	Study on structural change of solid materials in femtosecond laser processing	Makoto Yamaguchi	Akita University
141	”	岡田 達也	徳島大学	大学院 社会産業理工学研究部	”	Tatsuya Okada	Tokushima University
担当所員：板谷 治郎							
142	時間分解非線形分光法を用いた酸化物薄膜のコヒーレントフォノンの励起エネルギー依存性	牧野 哲征	福井大学	学術研究院工学系部門	Excitation energy dependence of coherent phonons in oxide thin films studied by time-resolved nonlinear spectroscopy	Takayuki Makino	University of Fukui
143	”	山口 拓真	福井大学	大学院工学研究科	”	Takuma Yamaguchi	University of Fukui

No.	課題名	氏名	所属		Title	Name	Organization
144	”	鈴木 健	福井大学	大学院工学研究科	”	Ken Suzuki	University of Fukui
担当所員：岡崎 浩三							
145	励起子絶縁体 Ta ₂ NiSe ₅ 及びモット絶縁体 Ca ₂ RuO ₄ における光誘起絶縁体-金属転移の研究	久保田 雄也	理化学研究所	放射光科学研究センター	Investigation of the photo-induced insulator-to-metal transition in an excitonic insulator Ta ₂ NiSe ₅ and a Mott insulator Ca ₂ RuO ₄	Yuya Kubota	RIKEN SPring-8 Center
146	励起子絶縁体における超高速電荷ダイナミクス	溝川 貴司	早稲田大学	理工学術院 先進理工学部	Ultrafast charge dynamics in excitonic insulators	Takashi Mizokawa	Waseda University
147	時間分解光電子分光法を用いた SmS における光誘起相転移ダイナミクスの研究	渡邊 浩	大阪大学	大学院生命機能研究科	Photo-induced phase transition dynamics on the SmS by TrARPES	Hiroshi Watanabe	Osaka University
148	T' 構造をもつ銅酸化物高温超伝導体の角度分解光電子分光による研究	チャン ウェイル	上智大学	機能創造理工学系	Photoemission spectroscopy of electron-doped T'-cuprate superconductors	Zhang Weilu	Sophia University
担当所員：近藤 猛							
149	He _x -Au(100) 再構成表面上グラフェンのスピ分解角度分解光電子分光	伊藤 孝寛	名古屋大学	シンクロトロン光研究センター	Spin- and angle-resolved photoemission study of Graphene on He _x -Au(100) reconstructed surface	Takahiro Ito	Nagoya University
150	”	古田 貫志	名古屋大学	大学院工学研究科	”	Kanji Furuta	Nagoya University
151	”	細谷 知輝	名古屋大学	大学院工学研究科	”	Tomoki Hosoya	Nagoya University
152	”	松永 和也	名古屋大学	大学院工学研究科	”	Kazuya Matsunaga	Nagoya University
153	”	山本 凌	名古屋大学	大学院工学研究科	”	Ryo Yamamoto	Nagoya University
154	トポロジカル絶縁体 Bi/ 垂直磁化膜 MnGa ヘテロ構造における Bi 膜厚に依存したトポロジカル表面状態	小林 正起	東京大学	大学院工学系研究科	Thickness-dependence of topological surface in topological insulator Bi/perpendicular ferromagnet MnGa heterostructure	Masaki Kobayashi	The University of Tokyo
一般研究員・大阪大学 先端強磁場科学研究センター / General Researcher・Center for Advanced High Magnetic Field Science Osaka University							
No.	課題名	氏名	所属		Title	Name	Organization
1	頂点及び辺共有した四面体を有する低次元物質の強磁場物性	浅野 貴行	福井大学	学術研究院工学系部門	High-field properties of low-dimensional materials with corner- and edge-sharing tetrahedron	Takayuki Asano	University of Fukui
2	”	西首 時夫	福井大学	大学院工学研究科	”	Tokio Nishikubi	University of Fukui

No.	課題名	氏名	所属		Title	Name	Organization
3	磁気力の半径方向成分によるタンパク質結晶の磁気浮上と熱物性値計測	牧 祥	岡山理科大学	フロンティア理工学研究所	Magnetic levitation and thermal property measurement of protein crystals by the radial component of magnetic force	Syou Maki	Okayama University of Science
4	有機ラジカル系から成る量子スピン系の強磁場磁性	山口 博則	大阪府立大学	大学院理学系研究科	High-field magnetic properties of quantum spin systems composed of organic radicals	Hironori Yamaguchi	Osaka Prefecture University
5	希土類ワイル物質の強磁場下輸送特性の研究	村川 寛	大阪大学	大学院理学研究科	High-magnetic-field studies of the rare-earth Weyl materials	Hiroshi Murakawa	Osaka university
6	強いスピン-軌道相互作用を活かした酸化物スピントロニクス	松野 丈夫	大阪大学	大学院理学研究科	Oxide spintronics utilizing strong spin-orbit coupling	Matsuno Jobu	Osaka University
7	新規低次元遷移金属配位高分子の構造とその量子磁性の解明	本多 善太郎	埼玉大学	大学院理工学研究科	Crystal structures and quantum-magnetism of novel low-dimensional transition metal coordination polymers	Zentaro Honda	Saitama University
8	量子スピン系の電場励起 ESR と方向二色性	木村 尚次郎	東北大学	金属材料研究所	Electric dipole spin resonance and directional dichroism of the quantum spin systems	Shojiro Kimura	Tohoku University
9	層状強磁性体 CrGeTe ₃ の磁気特性におけるキャリアドーブ効果の解明	酒井 英明	大阪大学	大学院理学研究科	Study of the magnetic properties for carrier-doped layered ferromagnet CrGeTe ₃	Hideaki Sakai	Osaka University
10	〃	近藤 雅起	大阪大学	大学院理学研究科	〃	Masaki Kondo	Graduate School of Science Osaka University
11	〃	真栄城 竜生	大阪大学	大学院理学研究科	〃	Maeshiro Ryusei	Osaka University
12	〃	阪口 駿也	大阪大学	大学院理学研究科	〃	Shunya Sakaguchi	Osaka University
13	パルス強磁場用極低温実験装置の開発	野口 悟	大阪府立大学	大学院理学系研究科	Development of the cryostat for pulsed high magnetic field	Satoru Noguchi	Osaka Prefecture University
14	〃	中川 豪	大阪府立大学	大学院理学系研究科	〃	Takeshi Nakagawa	Osaka Prefecture University
15	正四角台塔反強磁性体の強磁場 ESR	木村 健太	東京大学	大学院新領域創成科学研究科	High-field ESR measurements of square-cupola-based antiferromagnets	Kenta Kimura	The University of Tokyo
16	〃	赤木 暢	神戸大学	分子フォトサイエンス研究センター	〃	Mitsuru Akaki	Kobe University
17	高温超伝導体のパルス強磁場下電流電圧特性	掛谷 一弘	京都大学	大学院工学研究科	Current-voltage characteristics in high-Tc superconductors under pulsed high magnetic fields	Itsuhiro Kakeya	Kyoto University
18	REFe ₂ O ₄ の磁化測定 (RE=Tm, Lu)	掛谷 一弘	京都大学	大学院工学研究科	Magnetization measurement in REFe ₂ O ₄ (RE=Tm, Lu)	Itsuhiro Kakeya	Kyoto University
19	〃	田中 勝久	京都大学	大学院工学研究科	〃	Katsuhisa Tanaka	Kyoto University

No.	課題名	氏名	所属		Title	Name	Organization
20	三角格子反強磁性体 CuFeO ₂ の圧力下強磁場磁化過程	赤木 暢	神戸大学	分子フォトサイエンス研究センター	High-field magnetization under high-pressure in triangular antiferromagnet CuFeO ₂	Mitsuru Akaki	Kobe University
21	パルス強磁場を用いた圧力下 ESR 装置の開発	櫻井 敬博	神戸大学	研究基盤センター	Development of high-pressure ESR system using pulse high magnetic field	Takahiro Sakurai	Kobe University
22	”	赤木 暢	神戸大学	分子フォトサイエンス研究センター	”	Mitsuru Akaki	Kobe University
23	CaBa(Co _{1-x} Fe _x) ₄ O ₇ (0 ≤ x ≤ 1) 単結晶試料の強磁場下での磁化・電気分極・ESR 測定	桑原 英樹	上智大学	理工学部	Magnetization, electric polarization, and ESR measurements for CaBa(Co _{1-x} Fe _x) ₄ O ₇ (0 ≤ x ≤ 1) single crystals in pulsed high magnetic fields	Hideki Kuwahara	Sophia University
24	”	赤木 暢	神戸大学	分子フォトサイエンス研究センター	”	Mitsuru Akaki	Kobe University
25	”	白崎 巧	上智大学	大学院理工学研究科	”	Takumi Shirasaki	Sophia University
26	パルス強磁場によるマルテンサイト変態の時間依存性に関する研究	寺井 智之	大阪大学	大学院工学研究科	Research for time dependence of martensitic transformation by using pulse magnet	Tomoyuki Terai	Osaka University
27	三角格子反強磁性体の強磁場 ESR	南部 雄亮	東北大学	金属材料研究所	Electron spin resonance under high magnetic fields on a triangular antiferromagnet	Yusuke Nambu	Tohoku University
28	”	唐 一飛	東北大学	大学院理学研究科	”	Yifei Tang	Tohoku University
29	ホイスラー合金 Ni ₂ MnX (X = Al, Sb) および Pd ₂ MnSn の磁化・磁歪の高速磁場応答性の研究	左近 拓男	龍谷大学	先端理工学部	Research on time dependences of magnetstriction of Ni ₂ MnX (X = Al, Sb) type and Pd ₂ MnSn type Heusler alloys	Takuo Sakon	Ryukoku University
30	ナノ構造を導入した希土類系高温超伝導薄膜における強磁場中臨界電流密度に関する研究	土屋 雄司	名古屋大学	工学部電気工学専攻	Study on the critical current density in high-magnetic field in RE-based cuprate superconductors with nano-structure	Yuji Tsuchiya	Nagoya University

物質合成・評価設備 G クラス / Materials Synthesis and Characterization G Class Researcher

No.	課題名	氏名	所属		Title	Name	Organization
1	超臨界水中の固体触媒の劣化挙動解明と再生	秋月 信	東京大学	大学院新領域創成科学研究科	Elucidation and regeneration of solid catalyst deterioration behavior in supercritical water	Makoto Akizuki	The University of Tokyo
2	”	チン ブンセイ	東京大学	大学院新領域創成科学研究科	”	Chen Wenjing	The University of Tokyo
3	新規希土類磁石の構造解析	齋藤 哲治	千葉工業大学	工学部	Study of new rare-earth magnets	Tetsuji Saito	Chiba Institute of Technology
4	超臨界二酸化炭素、塩水、岩石間の相互作用が起きる場の基礎的理解	秋月 信	東京大学	大学院新領域創成科学研究科	Research on the fundamentals of the interaction among supercritical carbon dioxide, brine, and rock	Makoto Akizuki	The University of Tokyo

No.	課題名	氏名	所属		Title	Name	Organization
5	”	外野 圭太	東京大学	大学院新領域創成科学研究科	”	Keita Hokano	The University of Tokyo
6	材料形態制御によるクリーンエネルギーデバイス開発	細野 英司	産業技術総合研究所	ゼロエミッション国際共同研究センター	Development of clean energy devices by morphology control of materials	Eiji Hosono	National Institute of Advanced Industrial Science and Technology
7	”	太田 道広	産業技術総合研究所	ゼロエミッション国際共同研究センター	”	Michihiro Ohta	National Institute of Advanced Industrial Science and Technology
8	”	プリヤンカ ジュド	産業技術総合研究所	ゼロエミッション国際共同研究センター	”	Priyanka Jood	National Institute of Advanced Industrial Science and Technology
9	”	三石 雄悟	産業技術総合研究所	ゼロエミッション国際共同研究センター	”	Yugo Miseki	National Institute of Advanced Industrial Science and Technology
10	$\text{Nd}_{1-x}\text{Ca}_x\text{FeO}_3$ ($0.1 \leq x \leq 0.9$) の高温における磁性と熱電特性に関する研究	中津川 博	横浜国立大学	大学院 工学研究院	Magnetism and thermoelectric properties at high temperature in $\text{Nd}_{1-x}\text{Ca}_x\text{FeO}_3$ ($0.1 \leq x \leq 0.9$)	Hiroshi Nakatsugawa	Yokohama National University
11	層間チューニングされたハニカム格子イリジウム酸化物の物性解明	原口 祐哉	東京農工大学	大学院工学研究院	Study of physical properties on interlayer-tuned honeycomb lattice iridium oxides	Yuya Haraguchi	Tokyo University of Agriculture and Technology
12	”	有海 大樹	東京農工大学	大学院工学府	”	Hiroki Arikai	Tokyo University of Agriculture and Technology
13	新しい Pr_4+ 系キタエフ-ハイゼンベルグ型磁性体の探索と磁性	香取 浩子	東京農工大学	大学院工学研究院	Search and magnetism of new Pr_4+ Kitaev-Heisenberg type magnets	Hiroko Katori	Tokyo University of Agriculture and Technology
14	”	小日置 隆	東京農工大学	大学院工学府	”	Yutaka Kobiki	Tokyo University of Agriculture and Technology
15	ハーフメタルホイスラー合金の遍歴電子強磁性体のスピンゆらぎ理論による解析に関する研究	重田 出	鹿児島大学	大学院理工学研究科	Study on analysis of half-metallic Heusler alloys by the spin fluctuation theory of itinerant electron ferromagnets	Iduru Shigeta	Kagoshima University
16	”	横山 喬亮	鹿児島大学	大学院理工学研究科	”	Takaaki Yokoyama	Kagoshima University
17	ホイスラー化合物での反強磁性の研究	廣井 政彦	鹿児島大学	大学院理工学研究科	Study on antiferromagnetism in Heusler compounds	Masahiko Hiroi	Kagoshima University
18	”	赤石 幸起	鹿児島大学	大学院理工学研究科	”	Kouki Akaishi	Kagoshima University
19	有機伝導体の磁化測定によるモットおよびディラック物理の研究	宮川 和也	東京大学	大学院工学系研究科	Study of Mott and Dirac physics in organic conductors by magnetization measurements	Kazuya Miyagawa	The University of Tokyo
20	新規遷移金属珪化物の超高压合成	丹羽 健	名古屋大学	大学院工学研究科	High-pressure synthesis and novel transition metal silicide	Ken Niwa	Nagoya University
21	”	高野 航一	名古屋大学	大学院工学研究科	”	Koichi Takano	Nagoya University

No.	課題名	氏名	所属		Title	Name	Organization
22	様々な窒素源を用いた前期遷移金属窒化物の高圧合成	丹羽 健	名古屋大学	大学院工学研究科	High-pressure synthesis of early transition metal nitrides using various nitrogen source	Ken Niwa	Nagoya University
23	”	浅野 秀斗	名古屋大学	大学院工学研究科	”	Shuto Asano	Nagoya University
24	アルミン酸塩 $AeAl_2O_4$ を母体とした新規蛍光体の高圧合成と評価	佐々木 拓也	名古屋大学	大学院工学研究科	High-pressure synthesis and characterization of aluminate phosphors with $AeAl_2O_4$ as a host structure	Takuya Sasaki	Nagoya University
25	”	近藤 信介	名古屋大学	大学院工学研究科	”	Shinsuke Kondo	Nagoya University
26	高温高圧下におけるアルミノ珪酸塩蛍光体の創製	佐々木 拓也	名古屋大学	大学院工学研究科	High-pressure synthesis of aluminosilicate phosphors under high pressure and high temperature	Takuya Sasaki	Nagoya University
27	”	立岩 一晃	名古屋大学	大学院工学研究科	”	Kazuaki Tateiwa	Nagoya University
28	ハロゲン化アンモニウムを用いた新規遷移金属窒化物の高圧合成	佐々木 拓也	名古屋大学	大学院工学研究科	High-pressure synthesis of transition-metal nitrides using ammonium halide	Takuya Sasaki	Nagoya University
29	”	野田 航希	名古屋大学	大学院工学研究科	”	Koki Noda	Nagoya University
30	マグネシウムシリサイドの相関係	ニコ アレキサンダー ガイダ	名古屋大学	工学部	Phase relations in magnesium silicide	Nico Alexander Gaida	Nagoya University
31	多極子転移を示す充填スクッテルダイト化合物の新物質探索	関根 ちひろ	室蘭工業大学	大学院工学研究科	Search for new filled-skutterudite compounds exhibit multipole ordering	Chihiro Sekine	Muroran Institute of Technology
32	”	上野 公輔	室蘭工業大学	大学院工学研究科	”	Kosuke Ueno	Muroran Institute of Technology
33	超臨界水を用いた金属酸化物微粒子の合成	秋月 信	東京大学	大学院新領域創成科学研究科	Synthesis of metal oxide nanoparticles using supercritical water	Makoto Akizuki	The University of Tokyo
34	”	シュソウコン	東京大学	大学院新領域創成科学研究科	”	Zhenghui Zhu	The University of Tokyo
35	超臨界水熱合成法を利用した複合金属酸化物微粒子のその場有機修飾技術の研究	秋月 信	東京大学	大学院新領域創成科学研究科	In-situ organic modification of composite metal oxide particles using supercritical hydrothermal method	Makoto Akizuki	The University of Tokyo
36	”	李 雪	東京大学	大学院新領域創成科学研究科	”	Xue Li	The University of Tokyo
37	高温高圧水中でのバイオマス変換に使用するマイクロポーラス材料の安定性向上	大島 義人	東京大学	大学院新領域創成科学研究科	Improving stability of microporous materials for biomass upgrading in sub- and supercritical water	Yoshito Oshima	The University of Tokyo
38	”	アピバンボリラク チャン ウィット	東京大学	大学院新領域創成科学研究科	”	Apibanboriak Chanwit	The University of Tokyo

No.	課題名	氏名	所属		Title	Name	Organization
39	メソポーラスマテリアル・グラフェンオキシドに担持した金属触媒のキャラクタリゼーション	佐々木 岳彦	東京大学	大学院新領域創成科学研究科	Characterization of metal catalysts supported on mesoporous materials and graphene oxide	Takehiko Sasaki	The University of Tokyo
40	一次元テルル化物における超伝導	岡本 佳比古	名古屋大学	大学院工学研究科	Superconductivity in one-dimensional tellurides	Yoshihiko Okamoto	Nagoya University
41	新規遷移金属窒化物関連物質の超高压合成と結晶化学および物性	長谷川 正	名古屋大学	大学院工学研究科	High pressure synthesis, crystal chemistry and physical properties of novel transition metal nitrides and related compounds	Masashi Hasegawa	Nagoya University
42	”	張 仲景	名古屋大学	大学院工学研究科	”	Chang Chung Ching	Nagoya University
43	サマリウム系希土類オルソフェライト単結晶成長とテラヘルツ波による磁化制御	中嶋 誠	大阪大学	レーザー科学研究所	Single crystal growth for Samarium rare-earth orthoferrite and ultrafast control of magnetization by terahertz pulses	Makoto Nakajima	Osaka University
44	”	マグ ウサラ バリン カトリ ン ベンダン	大阪大学	レーザー科学研究所	”	Pendang Valynn Katrine Magsara	Osaka University
45	”	小池 遥平	大阪大学	レーザー科学研究所	”	Yohei Koike	Osaka University
46	新規フェロイック物質開発・物性開拓に関する研究	木村 剛	東京大学	大学院新領域創成科学研究科	Investigation of new ferroic materials and phenomena	Tsuyoshi Kimura	The University of Tokyo
47	”	木村 健太	東京大学	大学院新領域創成科学研究科	”	Kenta Kimura	The University of Tokyo
48	”	林田 健志	東京大学	大学院新領域創成科学研究科	”	Takeshi Hayashida	The University of Tokyo
49	”	三澤 龍介	東京大学	大学院新領域創成科学研究科物質系専攻	”	Ryusuke Misawa	The University of Tokyo
50	”	姜 山	東京大学	大学院新領域創成科学研究科	”	kang san	The University of Tokyo
51	”	八木 直輝	東京大学	大学院新領域創成科学研究科	”	Naoki Yagi	The University of Tokyo
52	”	大島 貴彦	東京大学	大学院新領域創成科学研究科	”	Takahiko Oshima	The University of Tokyo
53	”	林 悠生	東京大学	大学院新領域創成科学研究科	”	Yuki Hayashi	The University of Tokyo
54	外場制御可能な磁気超構造を有する物質の開発	有馬 孝尚	東京大学	大学院新領域創成科学研究科	Exploration of materials hosting controllable magnetic superstructure	Taka-hisa Arima	The University of Tokyo
55	”	徳永 祐介	東京大学	大学院新領域創成科学研究科	”	Yusuke Tokunaga	The University of Tokyo

No.	課題名	氏名	所属		Title	Name	Organization
56	”	近江 毅志	東京大学	大学院新領域創成科学研究科	”	Tsuyoshi Omi	The University of Tokyo
57	”	佐藤 樹	東京大学	大学院新領域創成科学研究科	”	Tatuki Sato	The University of Tokyo
58	”	荒木 勇介	東京大学	大学院新領域創成科学研究科	”	Yusuke Araki	The University of Tokyo
59	”	海本 祐真	東京大学	大学院新領域創成科学研究科	”	Yuma Umimoto	The University of Tokyo
60	”	渡辺 義人	東京大学	大学院新領域創成科学研究科	”	Yoshito Watanabe	The University of Tokyo
61	”	蘇丹	東京大学	大学院新領域創成科学研究科	”	Su Dan	The University of Tokyo
62	”	柳内 晃	東京大学	大学院新領域創成科学研究科	”	Hikaru Yagiuchi	The University of Tokyo
63	”	磯貝 レオナ	東京大学	大学院新領域創成科学研究科	”	Leona Isogai	The University of Tokyo
64	”	吉田 健斗	東京大学	大学院新領域創成科学研究科	”	Kento Yoshida	The University of Tokyo
65	”	柳田 真佑	東京大学	大学院新領域創成科学研究科	”	Shinsuke Yanagida	The University of Tokyo
66	バナジウムカルコゲナイドにおける柔粘性結晶のダイナミクス	片山 尚幸	名古屋大学	大学院工学研究科	Study of lattice dynamics at the plastic crystal state in vanadium chalcogenides	Naoyuki Katayama	Nagoya University
67	”	小島 慶太	名古屋大学	大学院応用物理学専攻	”	Keita Kojima	Nagoya University
68	バルク材料への負の圧力印可を可能とする新しい圧力技術の開発	片山 尚幸	名古屋大学	大学院工学研究科	Development of novel pressure technique which enables to apply negative pressure on bulk materials	Naoyuki Katayama	Nagoya University
69	”	塩見 学	名古屋大学	工学部	”	Manabu Shiomi	Nagoya University
70	外場制御可能な磁気超構造を有する物質の開発	車地 崇	東京大学	大学院新領域創成科学研究科	Exploration of materials hosting controllable magnetic superstructure	Takashi Kurumaji	The University of Tokyo

物質合成・評価設備 U クラス / Materials Synthesis and Characterization U Class Researcher

No.	課題名	氏名	所属		Title	Name	Organization
1	超臨界水を用いた rGO/NiFe ₂ O ₄ ナノコンポジットの合成の検討	布浦 鉄兵	東京大学	環境安全研究センター	Study on rGO/NiFe ₂ O ₄ nanocomposite synthesis in supercritical water	Teppey Nunoura	The University of Tokyo
2	〃	ヨウ ジョンミ	東京大学	大学院新領域創成科学研究科	〃	Yang Jiongmei	The University of Tokyo
3	高温高压下中性子回折測定による鉄-ケイ素系での水素原子のサイト決定と溶存量の測定	鍵 裕之	東京大学	大学院理学系研究科	Solubility and site occupancy of hydrogen in Fe-Si system using in-situ neutron diffraction measurement under high pressure and high temperature conditions	Hiroyuki Kagi	The University of Tokyo
4	〃	市東 力	東京大学	大学院理学系研究科	〃	Chikara Shito	The University of Tokyo
5	〃	森 悠一郎	東京大学	大学院理学系研究科	〃	Yuichiro Mori	The University of Tokyo
6	高脂質含有バイオマスの超臨界水ガス化における水素生産のための2段階接触分解装置と改質装	布浦 鉄兵	東京大学	環境安全研究センター	Development of a two-stage catalytic cracker and reformer for hydrogen production in supercritical water gasification of biomass with high lipid content	Teppey Nunoura	The University of Tokyo
7	〃	ダイアン グバタンガ	東京大学	新領域創成科学研究科	〃	Diane Gubatanga	The University of Tokyo
8	地上ガンマ線望遠鏡の焦点面検出器の開発	奥村 暁	名古屋大学	宇宙地球環境研究所	Development of the focal plane instrument of a ground-based gamma-ray telescope	Akira Okumura	Nagoya University
9	〃	黒田 裕介	名古屋大学	大学院理学研究科	〃	Yusuke Kuroda	Nagoya University
10	〃	芳賀 純也	名古屋大学	大学院理学研究科	〃	Junya Haga	Nagoya University
11	MOF を鋳型とした極細無機ナノワイヤーの創製	北尾 岳史	東京大学	大学院新領域創成科学研究科	Synthesis of ultrathin inorganic nanowire templated by MOFs	Takashi Kitao	The University of Tokyo
12	α -RuI ₃ の高压合成	今井 良宗	東北大学	大学院理学研究科	High pressure synthesis of α -RuI ₃	Yoshinori Imai	Tohoku University
13	〃	藤原 秀行	東北大学	大学院理学研究科	〃	Hideyuki Fujihara	Tohoku University
14	レアメタルフリー磁性材料 L10-FeCo の磁気特性の解析	小嗣 真人	東京理科大学	基礎工学部	Analysis of magnetic properties of rare-metal-free super magnet "L10-FeCo"	Masato Kotsugi	Tokyo University of science
15	〃	熊谷 卓也	東京理科大学	基礎工学部	〃	Takuya Kumagai	Tokyo University of science
16	〃	宮下 拓也	東京理科大学	基礎工学部	〃	Takuya Miyashita	Tokyo University of science

No.	課題名	氏名	所属		Title	Name	Organization
17	”	中尾 太一	東京理科大学	基礎工学部	”	Taichi Nakao	Tokyo University of science
18	”	齋藤 彪我	東京理科大学	基礎工学部	”	Hyuga Saito	Tokyo University of science
19	”	宇田 浩一	東京理科大学	基礎工学部	”	Koichi Uda	Tokyo University of science
20	新規トポロジカル超伝導体の物質合成と物性評価	水上 雄太	東京大学	大学院新領域創成科学研究科	Synthesis and characterization of novel topological superconductors	Yuta Mizukami	The University of Tokyo
21	”	向笠 清隆	東京大学	大学院新領域創成科学研究科	”	Kiyotaka Mukasa	The University of Tokyo
22	”	石原 滉大	東京大学	大学院新領域創成科学研究科	”	Kota Ishihara	The University of Tokyo

長期留学研究員 / Long Term Young Researcher

No.	課題名	氏名	所属		Title	Name	Organization
1	発光量絶対値測定系を用いたイクオリンの発光量子収率の測定	小野 稜平	群馬大学	理工学府	Measurement of luminescence quantum yield of aequorin using calibrated total-photon flux spectrometer	Ryohei Ono	Gunma University
2	銅と有機分子界面におけるバンド状態の巨大スピン分裂の直接観測	下澤 皐介	東京理科大学	大学院理工学研究科	Direct observation of giant spin splitting band on organic molecules/cooper interface	Kousuke Shimozawa	Tokyo University of Science
3	金属と有機分子界面におけるラッシュバ分裂の増大	小久保 裕太	東京理科大学	理工学部	Enhancement of Rashba splitting on molecule/metal interface	yuta Kokubo	Tokyo University of Science

令和2年度 中性子科学研究施設 共同利用課題一覧 / Joint Research List of Neutron Scattering Researcher 2020

No.	課題名	氏名	所属	Title	Name	Organization
・申請装置 4G: GPTAS						
1	GPTAS (汎用3軸中性子分光器) IRT 課題	佐藤 卓	東北大学	多元物質科学研究所	IRT project of GPTAS	Taku J Sato Tohoku University
2	磁性準結晶中の隠れた磁気秩序の探索	佐藤 卓	東北大学	多元物質科学研究所	Hidden magnetic order in magnetic quasicrystals	Taku J Sato Tohoku University
3	量子スカーミオン励起の探索	佐藤 卓	東北大学	多元物質科学研究所	Quantum magnetic-skyrmion excitation	Taku J Sato Tohoku University
4	ハニカムおよびジグザグ格子上の非相反磁気励起の探索	佐藤 卓	東北大学	多元物質科学研究所	Nonreciprocal quasiparticles in honeycomb and/or zigzag magnets	Taku J Sato Tohoku University
5	a-Cu ₂ V ₂ O ₇ の非相反マグノンに対する bc 面内磁場効果	佐藤 卓	東北大学	多元物質科学研究所	Effect of in-plane magnetic field for the nonreciprocal magnon in a-Cu ₂ V ₂ O ₇	Taku J Sato Tohoku University
6	Sr ₂ RuO ₄ の非弾性散乱	古川 はづき	お茶の水女子大学	基幹研究院 自然科学系	Inelastic neutron scattering experiments on Sr ₂ RuO ₄	Hazuki Furukawa Ochanomizu University
7	強磁性超伝導体における磁性と超伝導の研究	古川 はづき	お茶の水女子大学	基幹研究院 自然科学系	A study of magnetic state in ferromagnetic superconductors	Hazuki Furukawa Ochanomizu University
8	空間反転対称性の破れた超伝導体の非弾性散乱	古川 はづき	お茶の水女子大学	基幹研究院 自然科学系	Inelastic neutron scattering experiments on non-centrosymmetric superconductors	Hazuki Furukawa Ochanomizu University
9	YbT ₂ Zn ₂₀ (T=遷移金属) の結晶場状態の決定	池田 陽一	東北大学	金属物理学研究所	Determination of crystalline electric field level scheme of YbT ₂ Zn ₂₀ (T=transition metal)	Yoichi Ikeda Tohoku University
10	リチウム鉄フェライトにおける非相反マグノン	那波 和宏	東北大学	多元物質科学研究所	Nonreciprocal magnons in noncentrosymmetric Lithium Ferrite	Kazuhiro Nawa Tohoku University
11	量子スピン鎖におけるスピノンラッシュバ分裂	那波 和宏	東北大学	多元物質科学研究所	Spinon Rashba splitting on the quantum spin chain	Kazuhiro Nawa Tohoku University
12	反強磁性体 CeNiC ₂ の磁気構造	郷地 順	東京大学	物性研究所	Magnetic structure of antiferromagnetic compound CeNiC ₂	Jun Gouchi The University of Tokyo
13	強誘電体の相転移機構 (変位型及び秩序-無秩序型) に関する統一的理解の確立	重松 宏武	山口大学	教育学部	Establishment of the unified explanation about the phase transition mechanism (displacive and order-disorder)	Hirotake Shigematsu Yamaguchi University
14	スピニアイスにおけるトポロジカル相転移	門脇 広明	東京都立大学	理工学研究科物理学専攻	Topological phase transition in spin ice	Hiroaki Kadowaki Tokyo Metropolitan University
15	電気磁気交差相関現象を示す重い電子系反強磁性体 Ce ₃ TiBi ₅ の磁気構造	阿曾 尚文	琉球大学	理学部物質地球科学科	Magnetic structure in a heavy fermion antiferromagnet Ce ₃ TiBi ₅ exhibiting electromagnetic cross-correlation phenomenon	Naofumi Aso University of the Ryukyus

No.	課題名	氏名	所属		Title	Name	Organization
16	価数揺動希土類化合物における電荷・フォノン結合現象の検証	筒井 智嗣	高輝度光科学研究センター	放射光利用研究基盤センター	Investigation of valence-phonon coupling in valence fluctuation compounds	Satoshi Tsutsui	Japan Synchrotron Radiation Research Institute
・申請装置 5G: PONTA							
17	PONTA (高性能偏極中性子散乱装置) IRT 課題	中島 多朗	東京大学	物性研究所	IRT project of PONTA	Taro Nakajima	The University of Tokyo
18	MnO 酸化物の磁気相転移とスピncurrentに関する研究	古川 はづき	お茶の水女子大学	基幹研究院 自然科学系	Contribution of magnetism on spin current in MnO	Hazuki Furukawa	Ochanomizu University
19	偏極中性子回折による NaBH ₄ 水溶液中の二水素結合の解析	吉田 亨次	福岡大学	理学部	Dihydrogen Bonding in Aqueous NaBH ₄ Solutions by Polarized Neutron Diffraction	Koji Yoshida	Fukuoka University
20	YbT ₂ Zn ₂₀ (T= 遷移金属) の結晶場状態の決定	池田 陽一	東北大学	金属物理学研究所	Determination of crystalline electric field level scheme of YbT ₂ Zn ₂₀ (T=transition metal)	Yoichi Ikeda	Tohoku University
21	重水素化 CPL-1 に吸着された酸素分子の高エネルギー磁気励起	浅井 晋一郎	東京大学	物性研究所	High-Energy Magnetic Excitation in Oxygen Molecule Adsorbed in deuterated CPL-1	Shinichiro Asai	The University of Tokyo
22	Cu ₂ (4-F-bza) ₄ (2-mpyz) に吸着された酸素分子の磁気励起	浅井 晋一郎	東京大学	物性研究所	Magnetic Excitation in Oxygen Molecule Adsorbed in Nanoporous Metal Complex Cu ₂ (4-F-bza) ₄ (2-mpyz)	Shinichiro Asai	The University of Tokyo
23	スピン状態クロスオーバーが起こるダブルペロブスカイト型コバルト酸化物 Sr ₂ CoNbO ₆ の中性子非弾性散乱研究	浅井 晋一郎	東京大学	物性研究所	Inelastic neutron scattering study for double perovskite cobalt oxide Sr ₂ CoNbO ₆	Shinichiro Asai	The University of Tokyo
24	メイプルリーフ格子物質 MgMn ₃ O ₇ ・3D ₂ O の粉末中性子回折実験	浅井 晋一郎	東京大学	物性研究所	Neutron Diffraction study of Maple Leaf Compound MgMn ₃ O ₇ ・3D ₂ O	Shinichiro Asai	The University of Tokyo
25	メイプルリーフ格子物質 MgMn ₃ O ₇ ・3D ₂ O の中性子非弾性散乱	浅井 晋一郎	東京大学	物性研究所	Inelastic Neutron Scattering of Maple Leaf Compound MgMn ₃ O ₇ ・3D ₂ O	Shinichiro Asai	The University of Tokyo
26	鉄系超伝導体のスピン揺動	李 哲虎	産業技術総合研究所	省エネルギー研究部門	Spin fluctuations of iron-based superconductors	Chul-Ho Lee	National Institute of Advanced Industrial Science and Technology
27	低次元反強磁性体 Ni ₂ V ₂ O ₇ の磁場温度相図の決定	長谷 正司	物質・材料研究機構	中性子散乱グループ	Determination of the magnetic phase diagram of the low dimensional antiferromagnet Ni ₂ V ₂ O ₇	Masashi Hase	National Institute for Materials Science
28	磁気冷凍材料 R ₃ RuO ₇ (R = Nd, Tb) の磁気構造の決定	長谷 正司	物質・材料研究機構	中性子散乱グループ	Determination of the magnetic structures of the magnetic refrigeration materials R ₃ RuO ₇ (R = Nd, Tb)	Masashi Hase	National Institute for Materials Science
・申請装置 6G: TOPAN							
29	TOPAN (東北大理: 3軸型偏極中性子分光器) IRT 課題	藤田 全基	東北大学	金属材料研究所	IRT project of TOPAN	Masaki Fujita	Tohoku University
30	偏極中性子非弾性散乱による Tb ₃ Fe ₅ O ₁₂ におけるマグノン極性の測定	南部 雄亮	東北大学	金属材料研究所	Magnon polarization in Tb ₃ Fe ₅ O ₁₂	Yusuke Nambu	Tohoku University

No.	課題名	氏名	所属		Title	Name	Organization
31	Possible Z2 vortex in the two-dimensional triangular antiferromagnet FeGa ₂ S ₄	南部 雄亮	東北大学	金属材料研究所	Possible Z2 vortex in the two-dimensional triangular antiferromagnet FeGa ₂ S ₄	Yusuke Nambu	Tohoku University
32	近藤半金属におけるワイルフェルミオンの磁気状態	岩佐 和晃	茨城大学	フロンティア応用原子科学研究センター	Magnetic states of Weyl fermion in Kondo semimetals	Kazuaki Iwasa	Ibaraki University
33	YbT ₂ Zn ₂₀ (T=遷移金属)の結晶場状態の決定	池田 陽一	東北大学	金属物理学研究所	Determination of crystalline electric field level scheme of YbT ₂ Zn ₂₀ (T=transition metal)	Yoichi Ikeda	Tohoku University
34	T'構造銅酸化物 Pr _{2-x} Ca _x CuO ₄ における磁気相関と超伝導の研究	藤田 全基	東北大学	金属材料研究所	Study of spin correlations and superconductivity in T'-structured cuprate oxide Pr _{2-x} Ca _x CuO ₄	Masaki Fujita	Tohoku University
・申請装置 CI-1: HER							
35	HER (高エネルギー分解能3軸型中性子分光器) IRT 課題	益田 隆嗣	東京大学	物性研究所	IRT project of HER	Takatsugu Masuda	The University of Tokyo
36	量子スカーミオン励起の探索	佐藤 卓	東北大学	多元物質科学研究所	Quantum magnetic-skyrmion excitation	Taku J Sato	Tohoku University
37	ハニカムおよびジグザグ格子上の非相反磁気励起の探索	佐藤 卓	東北大学	多元物質科学研究所	Nonreciprocal quasiparticles in honeycomb and/or zigzag magnets	Taku J Sato	Tohoku University
38	a-Cu ₂ V ₂ O ₇ の非相反マグノンに対するbc面内磁場効果	佐藤 卓	東北大学	多元物質科学研究所	Effect of in-plane magnetic field for the nonreciprocal magnon in a-Cu ₂ V ₂ O ₇	Taku J Sato	Tohoku University
39	(Ni,Mn)TiO ₃ のメモリー効果	古川 はづき	お茶の水女子大学	基幹研究院 自然科学系	Memory effect on spinglass system (Ni,Mn)TiO ₃	Hazuki Furukawa	Ochanomizu University
40	Ce(Co,Rh)In ₅ の磁性と超伝導発現機構の関係	古川 はづき	お茶の水女子大学	基幹研究院 自然科学系	Magnetism and Superconductivity in Ce(Co,Rh)In ₅	Hazuki Furukawa	Ochanomizu University
41	近藤半金属におけるワイルフェルミオンの磁気状態	岩佐 和晃	茨城大学	フロンティア応用原子科学研究センター	Magnetic states of Weyl fermion in Kondo semimetals	Kazuaki Iwasa	Ibaraki University
42	T'構造銅酸化物 Pr _{2-x} Ca _x CuO ₄ における磁気相関と超伝導の研究	藤田 全基	東北大学	金属材料研究所	Study of spin correlations and superconductivity in T'-structured cuprate oxide Pr _{2-x} Ca _x CuO ₄	Masaki Fujita	Tohoku University
43	量子スピン液体の研究	門脇 広明	東京都立大学	理工学研究科物理学専攻	Quantum spin liquid	Hiroaki Kadowaki	Tokyo Metropolitan University
44	CeNiSnはtopological Kondo insulatorなのか?	門脇 広明	東京都立大学	理工学研究科物理学専攻	Is CeNiSn topological Kondo insulator ?	Hiroaki Kadowaki	Tokyo Metropolitan University
・申請装置 CI-2: SANS-U							
45	SANS-U (二次元位置測定小角散乱装置) IRT 課題	Li Xiang	東京大学	物性研究所	IRT project of SANS-U	Xiang Li	The University of Tokyo

No.	課題名	氏名	所属		Title	Name	Organization
46	フェージゲルの伸張下での構造評価	Li Xiang	東京大学	物性研究所	Simultaneous tensile test and SANS measurements of novel hybrid gels from polymer and M13 phage	Xiang Li	The University of Tokyo
47	高均一ゲルの伸張下での空間相関の探求	Li Xiang	東京大学	物性研究所	Investigation of spatial correlation of highly homogeneous gels under elongation	Xiang Li	The University of Tokyo
48	重水素化ラベリングを用いた均一ゲルの構造解析	Li Xiang	東京大学	物性研究所	Structure analysis of homogeneous gel with assistance of deuteration labeling	Xiang Li	The University of Tokyo
49	選択的ドメイン重水素化と中性子小角散乱によるマルチドメインタンパク質のドメイン運動の解明	井上 倫太郎	京都大学	複合原子力科学研究所	Elucidation of domain motions in multi-domain protein through selective deuteration-assisted small-angle neutron scattering.	Rintaro Inoue	Kyoto University
50	磁性準結晶中の隠れた磁気秩序の探索	佐藤 卓	東北大学	多元物質科学研究所	Hidden magnetic order in magnetic quasicrystals	Taku J Sato	Tohoku University
51	反転対称性を持つ R _{Ga} 2 における磁気スキルミオンの探索	南部 雄亮	東北大学	金属材料研究所	Search for magnetic skyrmion in R _{Ga} 2 with inversion symmetry	Yusuke Nambu	Tohoku University
52	中性子小角散乱実験による Sr ₂ RuO ₄ の異常金属状態の研究	古川 はづき	お茶の水女子大学	基幹研究院 自然科学系	Anomalous vortex state in Sr ₂ RuO ₄ studied by SANS experiments	Hazuki Furukawa	Ochanomizu University
53	空間反転対称性の破れた超伝導体のヘリカル磁束格子の観測	古川 はづき	お茶の水女子大学	基幹研究院 自然科学系	Herical vortex phase on non-centrosymmetric superconductors	Hazuki Furukawa	Ochanomizu University
54	強磁性超伝導体における自発的磁束格子構造の研究	古川 はづき	お茶の水女子大学	基幹研究院 自然科学系	Spontaneous vortex phase in ferromagnetic superconductors	Hazuki Furukawa	Ochanomizu University
55	MnSi における変動電流下の磁気スキルミオン格子変形の周波数依存性	奥山 大輔	東北大学	多元物質科学研究所	Frequency dependence of the magnetic skyrmion deformation in MnSi under an alternative electric current flow	Daisuke Okuyama	Tohoku University
56	マイクロエマルションの角層浸透機構	櫻木 美菜	崇城大学	工学部ナノサイエンス学科	The penetration mechanism of microemulsions into the stratum corneum	Mina Sakuragi	Sojo UnIversity
57	レゾルシナレン系カプセルの正多面体構造における溶媒依存性	藤井 翔太	北九州市立大学	環境技術研究所	Solvent dependence of resorcinarene-based capsules on their platonic structures and catalytic ability	Shota Fujii	The University of Kitakyushu
58	中性子散乱法によるブロックポリマー/リン脂質ハイブリッドバシクル中のナノドメインの構造解析	西村 智貴	京都大学	工学研究科	Nanodomain formation in oligopeptide-block-poly(propylene oxide)/phospholipid hybrid vesicles: A contrast-matching SANS study	Tomoki Nishimura	Kyoto University
59	イミダゾリウム系イオン液体中におけるエタノールクラスターの形成	高椋 利幸	佐賀大学	理工学部	Formation of Ethanol Clusters in Imidazolium-based Ionic Liquids	Toshiyuki Takamuku	Saga University
60	セグメントラベルを活用した中性子小角散乱によるマルチドメイン蛋白質の溶液構造解析	中川 洋	日本原子力研究開発機構	階層構造研究グループ	Analysis of solution structure of segment labelled multi-domain protein by SANS	Hiroshi Nakagawa	Japan Atomic Energy Agency
・申請装置 C2-3-1: iNSE							
61	iNSE (中性子スピンエコー分光器)IRT 課題	Li Xiang	東京大学	物性研究所	IRT project of iNSE	Xiang Li	The University of Tokyo

No.	課題名	氏名	所属		Title	Name	Organization
62	MnSi におけるスキルミオンのダイナミクス	左右田 稔	お茶の水女子大学	基幹研究院自然科学系	Dynamics of skyrmion in MnSi	Minoru Soda	Ochanomizu University
63	セグメントラベルによるマルチドメイン蛋白質の動的構造と機能発現との関係性の解析	中川 洋	日本原子力研究開発機構	階層構造研究グループ	Analysis of relationship between structural dynamics and function of segment labelled multi-domain protein	Hiroshi Nakagawa	Japan Atomic Energy Agency
・申請装置 C3-1-1: AGNES							
64	AGNES (高分解能パルス冷中性子分光器) IRT 課題	山室 修	東京大学	物性研究所	IRT project of AGNES	Osamu Yamamuro	The University of Tokyo
65	新規水素クラスター物質 Li ₅ MoH ₁₁ の速いダイナミクス	山室 修	東京大学	物性研究所	Fast dynamics of novel hydrogen cluster material Li ₅ MoH ₁₁	Osamu Yamamuro	The University of Tokyo
66	新規水素クラスター物質 Li ₅ MoH ₁₁ の遅いダイナミクス	山室 修	東京大学	物性研究所	Slow dynamics of novel hydrogen cluster material Li ₅ MoH ₁₁	Osamu Yamamuro	The University of Tokyo
67	アルキルアンモニウム系プロトン性イオン液体の速いダイナミクス	山室 修	東京大学	物性研究所	Fast dynamics of alkylammonium based protic ionic liquids	Osamu Yamamuro	The University of Tokyo
68	アルキルアンモニウム系プロトン性イオン液体の遅いダイナミクス	山室 修	東京大学	物性研究所	Slow dynamics of alkylammonium based protic ionic liquids	Osamu Yamamuro	The University of Tokyo
・申請装置 C3-1-2: MINE1							
69	MINE1 (京大複合研: 多層膜中性子干渉計・反射率計) IRT 課題	日野 正裕	京都大学	複合原子力科学研究所	MINE1 (Multilayer neutron interferometer and reflectmeter)	Masahiro Hino	Kyoto University
70	MINE2 (京大複合研: 多層膜中性子干渉計・反射率計) IRT 課題	日野 正裕	京都大学	複合原子力科学研究所	MINE2 (Multilayer neutron interferometer and reflectmeter)	Masahiro Hino	Kyoto University
71	高分子 / 水界面における生体分子の吸着状態の解析	松野 寿生	九州大学	大学院工学研究院	Analyses of adsorbed biomolecules at the polymer/water interface	Hisao Matsuno	Kyushu University
・申請装置 T1-1: HQR							
72	HQR(高分解能中性子散乱装置)IRT 課題	大山 研司	茨城大学	理工学研究科	IRT project of HQR	Kenji Ohoyama	Ibaraki University
73	重い電子超伝導体 CeNiGe ₃ の秩序変数の圧力依存性	池田 陽一	東北大学	金属物理学研究所	Pressure dependence of the order parameter in CeNiGe ₃	Yoichi Ikeda	Tohoku University
74	Rb ₂ MoO ₄ における多形転移とソフトフォノン	重松 宏武	山口大学	教育学部	Polymorph Transition and Soft Phonon in Rb ₂ MoO ₄	Hirotake Shigematsu	Yamaguchi University
75	強誘電体の相転移機構 (変位型及び秩序-無秩序型) に関する統一的理解の確立	重松 宏武	山口大学	教育学部	Establishment of the unified explanation about the phase transition mechanism (displacive and orderdisorder)	Hirotake Shigematsu	Yamaguchi University

No.	課題名	氏名	所属	Title	Name	Organization
・申請装置 T1-2: AKANE						
76	AKANE (東北大金研:三軸型中性子分光器) IRT 課題	藤田 全基	東北大学	金属材料研究所	IRT project of AKANE	Masaki Fujita Tohoku University
77	重い電子超伝導体 CeNiGe ₃ の秩序変数の圧力依存性	池田 陽一	東北大学	金属物理学研究所	Pressure dependence of the order parameter in CeNiGe ₃	Yoichi Ikeda Tohoku University
78	T' 構造銅酸化物 Pr _{2-x} Ca _x CuO ₄ における磁気相関と超伝導の研究	藤田 全基	東北大学	金属材料研究所	Study of spin correlations and superconductivity in T'-structured cuprate oxide Pr _{2-x} Ca _x CuO ₄	Masaki Fujita Tohoku University
79	鉄系超伝導体のスピン揺動	李 哲虎	産業技術総合研究所	省エネルギー研究部門	Spin fluctuations of iron-based superconductors	Chul-Ho Lee National Institute of Advanced Industrial Science and Technology
・申請装置 T1-3 HERMES						
80	HERMES (東北大金研:中性子粉末回折装置) IRT 課題	南部 雄亮	東北大学	金属材料研究所	IRT project of HERMES	Yusuke Nambu Tohoku University
81	キタエフ候補物質 RuX ₃ (X = Br, I) の結晶構造と磁気構造	佐藤 卓	東北大学	多元物質科学研究所	Crystal and magnetic structure of the possible Kitaev-candidates RuX ₃ (X = Br, I)	Taku J Sato Tohoku University
82	Ce(Te _{1-x} Ge _x) ₃ (x=0.33) の磁気構造解析	小林 理気	琉球大学	理学部	Determination of magnetic structure in Ce(Te _{1-x} Ge _x) ₃ (x=0.33)	Riki Kobayashi University of the Ryukyus
83	近藤半金属におけるワイルフェルミオンの磁気状態	岩佐 和晃	茨城大学	フロンティア応用原子科学研究センター	Magnetic states of Weyl fermion in Kondo semimetals	Kazuaki Iwasa Ibaraki University
84	EuTGe ₃ (T=Rh, Ir) におけるらせん磁気構造の探索	松村 武	広島大学	大学院先端物質科学研究科	Search for a helimagnetic structure of noncentrosymmetric EuTGe ₃ (T=Rh, Ir)	Takeshi Matsumura Hiroshima University
85	T' 構造銅酸化物の超伝導発現と結晶構造の関係	藤田 全基	東北大学	金属材料研究所	Relation between superconducting mechanism and crystal structure in T' cuprate oxide	Masaki Fujita Tohoku University
86	電気磁気交差相関現象を示す重い電子系反強磁性体 Ce ₃ TiBi ₅ の磁気構造	阿曾 尚文	琉球大学	理学部物質地球科学科	Magnetic structure in a heavy fermion antiferromagnet Ce ₃ TiBi ₅ exhibiting electromagnetic cross-correlation phenomenon	Naofumi Aso University of the Ryukyus
87	量子臨界点近傍にある YbCo ₂ Zn ₂₀ の置換系試料の結晶構造と磁気構造	阿曾 尚文	琉球大学	理学部物質地球科学科	Crystal and magnetic structures in doped systems of YbCo ₂ Zn ₂₀ in vicinity of a quantum critical point	Naofumi Aso University of the Ryukyus
・申請装置 T2-2: FONDER						
88	FONDER (中性子 4 軸回折装置) IRT 課題	木村 宏之	東北大学	多元物質科学研究所	IRT proposal for FONDER (Neutron 4-circle diffractometer)	Hiroyuki Kimura Tohoku University
89	塑性歪みを加えた Pt ₃ Fe 反強磁性体における強磁性の発現機構	小林 悟	岩手大学	理工学部	Mechanism of ferromagnetism in plastically deformed Pt ₃ Fe antiferromagnet	Satoru Kobayashi Iwate University

No.	課題名	氏名	所属		Title	Name	Organization
90	有機ラジカル分子 $C_{20}H_{14}Cl_3N_4$ の磁気秩序	左右田 稔	お茶の水女子大学	基幹研究院自然科学系	Magnetic Ordering in Organic Radical Compound $C_{20}H_{14}Cl_3N_4$	Minoru Soda	Ochanomizu University
91	マルチフェロイック $Tb_{0.5}Gd_{0.5}Mn_2O_5$ における磁気構造と強誘電性の研究	木村 宏之	東北大学	多元物質科学研究所	Magnetic structure and its relevance to the ferroelectricity in multiferroic $Tb_{0.5}Gd_{0.5}Mn_2O_5$	Hiroyuki Kimura	Tohoku University
92	T'-type Pr_2CuO_4 における結晶構造の還元効果	木村 宏之	東北大学	多元物質科学研究所	Oxygen reduction effect on the crystal structure in the T'-structure of Pr_2CuO_{4+y}	Hiroyuki Kimura	Tohoku University
93	ジグザグ三角鎖磁性体 $Fe_2O(SeO_3)_2$ の磁気構造	那波 和宏	東北大学	多元物質科学研究所	Magnetic structure of the saw-tooth chain magnet $Fe_2O(SeO_3)_2$	Kazuhiro Nawa	Tohoku University
94	typeIII 型反強磁性体 Pt-Mn における整合-非整合磁気相転移	高橋 美和子	筑波大学	数理物資系	Commensurate-Incommensurate Magnetic Phase Transition in Type-III Anti-ferromagnet Pt-Mn	Miwako Takahashi	Tsukuba University
・申請装置 Accessory							
95	アクセサリ- IRT 課題	上床 美也	東京大学	物性研究所	IRT project of Accessory	Yoshiya Uwatoko	The University of Tokyo

令和2年度 軌道放射物性研究施設 共同利用課題一覧 / Joint Research List of Synchrotron Radiation Researcher 2020

播磨分室 BL07LSU / Harima Branch BL07LSU

No.	課題名	氏名	所属		Title	Name	Organization
1	軟 X 線発光分光測定を用いた生体適合性ポリマーブラシ誘導体に閉じ込められた水分子の電子状態解析	赤田 圭史	東京大学	物性研究所	Analysis of electronic states in water molecules confined in biocompatible polymer brush derivatives using soft X-ray emission spectroscopy	Keishi Akada	The University of Tokyo
2	固体電気化学デバイスのオペランド軟 X 線発光分光	朝倉 大輔	産業技術総合研究所	省エネルギー研究部門	Operando soft X-ray emission spectroscopy of solid-state electrochemical devices	Daisuke Asakura	National Institute of Advanced Industrial Science and Technology
3	磁場中共鳴非弾性軟 X 線散乱 (SX-RIXS) による Co ₂ FeSi ホイスラー合金バルク単結晶の電子状態研究	梅津 理恵	東北大学	金属材料研究所	Electronic state of bulk-single crystal Co ₂ FeSi Heusler alloy probed by resonant inelastic soft X-ray scattering (SX-RIXS) in magnetic field	Rie Umetsu	Tohoku University
4	高分解能軟 X 線分光を用いた層状遷移金属酸化物における高度蓄電機能と電子状態の相関解析	大久保 將史	東京大学	工学系研究科	Study on key electronic factors of layered oxides for high performance charge storage using high-resolution soft x-ray spectroscopy	Masashi Okubo	The University of Tokyo
5	レドックスフロー電池における触媒活性点のオペランド電子状態解析	大平 昭博	産業技術総合研究所	省エネルギー研究部門	Operando analysis of electronic structure of catalytic active sites in redox flow batteries	Akihiro Oohira	National Institute of Advanced Industrial Science and Technology
6	酸素透過時における混合導電性酸化物表面の時間分解軟 X 線光電子分光測定	籠宮 功	名古屋工業大学		Time-resolved soft X-ray core-level spectroscopy on surfaces in mixed conductive oxides during oxygen permeation	Isao Kagomiya	Nagoya Insutitute of Technology
7	酸素透過時における混合伝導体表面の軟 X 線雰囲気光電子分光実験	籠宮 功	名古屋工業大学		Ambient pressure X-ray photoelectron spectroscopy on surfaces in mixed conductive oxides during oxygen permeation	Isao Kagomiya	Nagoya Insutitute of Technology
8	X 線吸収分光および発光分光による有機膜と水分子の相互作用の評価	倉橋 直也	東京大学	物性研究所	Analysis of interaction between organic film and water molecule by x-ray absorption and emission spectroscopy.	Naoya Kurahashi	The University of Tokyo
9	高分子電解質中の水分子の状態解析研究	倉橋 直也	東京大学	物性研究所	State analysis study of water molecules in polymer electrolyte	Naoya Kurahashi	The University of Tokyo
10	オペランド光電子分光によるプラチナー酸化パラジウムモデル触媒を用いたメタン転換反応メカニズムの解明	小坂谷 貴典	分子科学研究所	物質分子科学研究領域	Elucidation of the mechanism of methane conversion reaction on Pt-PdO model catalysts by operando AP-XPS	Takanori Koitaya	Institute for Molecular Science
11	オペランド光電子分光測定によるパラジウム合金系触媒におけるメタン酸化カップリング反応の直接観測	小坂谷 貴典	分子科学研究所	物質分子科学研究領域	Direct observation of methane oxidative coupling on palladium alloy catalysts by operando AP-XPS	Takanori Koitaya	Institute for Molecular Science
12	p 型 Mn ドープ強磁性半導体における p-d 交換相互作用の起源解明	小林 正起	東京大学	大学院工学系研究科	Unveiling the origin of the p-d exchange interaction in p-type Mn-doped ferromagnetic semiconductors	Masaki Kobayashi	The University of Tokyo
13	単結晶ナノワイヤ正極を用いる二次電池の顕微光電子マッピングとオペランド測定	張 文雄	東京大学	物性研究所	XPS mapping and operando measurements of LIB using single crystalline nanowires as cathodes	Wenxiong Zhang	The University of Tokyo
14	雰囲気 X 線光電子分光による Pd 系合金ナノ粒子表面 CO ₂ 水素化反応過程の解明	唐 佳藝	兵庫県立大学	工学研究科	Ambient-pressure XPS studies of CO ₂ hydrogenation on Pd-based alloy nanoparticle catalysts	Jiayi Tang	University of Hyogo
15	磁性ファンデアワールス・ヘテロ構造における磁気近接効果の起源の解明	中野 匡規	東京大学	大学院工学系研究科	Elucidation of the origin of the magnetic proximity effect at the magnetic van der Waals heterostructures	Masaki Nakano	The University of Tokyo

No.	課題名	氏名	所属		Title	Name	Organization
16	磁性ファンデアワールス・ヘテロ構造におけるフェロバレー状態の観測	中野 匡規	東京大学	大学院工学系研究科	Observation of a ferrovalley state in the magnetic van der Waals heterostructures	Masaki Nakano	The University of Tokyo
17	小角軟 X 線非弾性散乱による Mg 合金中 LPSO 構造形成メカニズムの解明	西堀 麻衣子	九州大学	大学院総合理工学研究院	Investigation of LPSO-structure formation mechanism by small angle inelastic X-ray scattering	Maiko Nishibori	Kyushu University
18	軟 X 線吸収・発光分光解析による生体親和性高分子界面における中間水の定量評価	西村 慎之介	九州大学	先端物質化学研究所	Quantitative evaluation of the interfacial intermediate water on biocompatible polymers by soft X-ray absorption and emission spectroscopies	Shinnosuke Nishimura	Kyushu University
19	軟 X 線発光分光を用いた界面水分子の電子状態解析で加速する体外式膜型人工肺 (ECMO) 配管内壁コーティング材料の改良【コロナ関連課題】	原田 慈久	東京大学	物性研究所	Improvement of inner-wall coating material for ECMO accelerated by electronic structure analysis of interfacial water using soft X-ray emission spectroscopy [coronavirus-related proposal]	Yoshihisa Harada	The University of Tokyo
20	軟 X 線発光分光を用いた界面水分子の電子状態解析で加速する体外式膜型人工肺 (ECMO) 配管内壁コーティング材料の改良 (II)【コロナ関連課題】	原田 慈久	東京大学	物性研究所	Improvement of inner-wall coating material for ECMO accelerated by electronic structure analysis of interfacial water using soft X-ray emission spectroscopy (II) [coronavirus-related proposal]	Yoshihisa Harada	The University of Tokyo
21	高速偏光スイッチングを利用した磁気光学測定による磁性金属薄膜の複素誘電率の決定	平田 靖透	防衛大学校		Determination of the complex permittivity of thin films of magnetic metal by magneto-optical measurement using fast polarization switching	Yasuyuki Hirata	National Defense Academy
22	Li 脱挿入による Li-rich/Li-poor ₂ 相ドメイン壁の移動のオペランド顕微光電子マッピング解析	細野 英司	産業技術総合研究所	省エネルギー研究部門	Operando/Micro-XPS mapping analysis for domain wall migration by two-phase reaction between Li-rich and Li-poor phases due to Li insertion and extraction	Eiji Hosono	National Institute of Advanced Industrial Science and Technology
23	共鳴非弾性軟 X 線回折によるサイズ弁別電子状態解析	宮脇 淳	東京大学	物性研究所	Size-Selective Electronic State Probed by Resonant Inelastic Soft X-ray Diffraction	Jun Miyawaki	The University of Tokyo
24	温度応答性高分子が構造変化する分子機構と水の役割	山添 康介	東京大学	物性研究所	Molecular mechanism of conformation change of temperature-responsive polymer and the role of water	Kosuke Yamazoe	The University of Tokyo
25	軟 X 線オペランド計測の高度化が拓く次世代触媒科学	山本 達	東京大学	物性研究所	Next Generation Catalysis Science Opened by Sophistication of Operando Soft X-ray Spectroscopies	Susumu Yamamoto	The University of Tokyo
26	雰囲気光電子分光で探る遷移金属錯体への水素脱着に伴う化学物性	吉信 淳	東京大学	大学院新領域創成科学研究科	The transformation of chemical properties of transition metal complex induced by hydrogen: AP-XPS study	Jun Yoshinobu	The University of Tokyo

柏キャンパス E 棟 / Laser and Synchrotron Research Laboratory in Kashiwa

No.	課題名	氏名	所属		Title	Name	Organization
1	レーザー角度分解光電子分光を用いた新規ファンデルワールス磁性化合物 GdGa ₃ の微細電子状態観測	岡田 佳憲	沖縄科学技術大学	量子物質科学	Laser-excited angle resolved photoemission study on the electronic structure for van der Waals magnetic compound GdGa ₃	Yoshinori Okada	Okinawa Institute of Science and Technology
2	銅と有機分子界面におけるバンド状態の巨大スピン分裂の直接観測	金井 要	東京理科大学	大学院理工学研究科	Direct observation of giant spin splitting band on organic molecules/copper interface	Kaname Kanai	Tokyo University of Science
3	SARPES を用いた疑一次元超伝導体 TaSe ₃ におけるトポロジカル表面状態の観察	近藤 猛	東京大学	物性研究所	SARPES study on topological surfaces states of TaSe ₃ superconductor	Takeshi Kondo	The University of Tokyo
4	SARPES を用いた CDW 物質における ワイル半金属相の研究	近藤 猛	東京大学	物性研究所	SARPES study of a new Weyl semimetal of the CDW compounds	Takeshi Kondo	The University of Tokyo

No.	課題名	氏名	所属		Title	Name	Organization
5	Ga 単結晶表面の角度分解光電子分光	矢治 光一郎	物質材料研究機構	先端材料解析研究拠点	ARPES study of gallium single crystal surface	Koichiro Yaji	National Institute for Materials Science
6	擬一次元物質におけるトポロジカル状態のスピンテクスチャーの研究	Ye Mao	Chinese Academy of Sciences		Study on the spin texture of the topological states in quasi-one-dimensional material	Mao Ye	Chinese Academy of Sciences
7	トポロジカル絶縁体 Bi/ 垂直磁化膜 MnGa ヘテロ構造における Bi 膜厚に依存したトポロジカル表面状態	小林 正起	東京大学	大学院工学系研究科	Thickness-dependence of topological surface in topological insulator Bi/perpendicular ferromagnet MnGa heterostructure	Masaki Kobayashi	The University of Tokyo
8	擬一次元ビスマスハライドのトポロジカル表面状態とバンドギャップ制御	近藤 猛	東京大学	物性研究所	Topological surface state and band-gap control in quasi-1D Bi-Halides	Takeshi Kondo	The University of Tokyo
9	Hex-Au(100) 再構成表面上グラフェンのスピン分解角度分解光電子分光	伊藤 孝寛	名古屋大学	シンクロトロン光科学研究センター	Spin- and angle-resolved photoemission study of Graphene on Hex-Au(100) reconstructed surface	Takahiro Ito	Nagoya University

令和2年度 スーパーコンピュータ共同利用課題一覧 / Joint Research List of Supercomputer System 2020

No.	課題名	氏名	所属	Title	Name	Organization
1. 第一原理計算 / First-Principles Calculation of Materials Properties						
1	高機能スピントロニクス磁性材料の電子構造解析および電気磁気効果解析	小田 竜樹	金沢大学理工研究域数物科学系	Analyses on electronic structure and magnetoelectric effect in high-performance spintronics and magnetic materials	Tatsuki Oda	Kanazawa University
2	電気化学界面のシミュレーション	杉野 修	東京大学物性研究所	Simulation of electrochemical interfaces	Osamu Sugino	The University of Tokyo
3	水素の計算物質科学	杉野 修	東京大学物性研究所	Computational hydrogenomics	Osamu Sugino	The University of Tokyo
4	量子論による半導体界面形成機構と電子物性の解明	押山 淳	名古屋大学未来材料・システム研究所	Mechanisms of Semiconductor Interface Formation and its Electronic Properties based on Quantum Theory	Atsushi Oshiyama	Institute of Materials and Systems for Sustainability
5	量子論による半導体界面形成機構と電子物性の解明	押山 淳	名古屋大学未来材料・システム研究所	Mechanisms of Semiconductor Interface Formation and its Electronic Properties based on Quantum Theory	Atsushi Oshiyama	Institute of Materials and Systems for Sustainability
6	表面、界面、欠陥等の複雑構造における原子構造と原子ダイナミクスに関する解析	渡邊 聡	東京大学大学院工学系研究科マテリアル工学専攻	Analyses related to atomic structures and atom dynamics at complex structures such as surfaces, interfaces and defects	Satoshi Watanabe	The University of Tokyo
7	第一原理電子状態・輸送特性計算コード RSPACE の開発とデバイスシミュレーション	小野 倫也	神戸大学大学院工学研究科電気電子工学専攻	Development of first-principles electronic-structure and transport calculation code RSPACE and simulations for device	Tomoya Ono	Kobe University
8	第一原理電子状態・輸送特性計算コード RSPACE の開発とデバイスシミュレーション	小野 倫也	神戸大学大学院工学研究科電気電子工学専攻	Development of first-principles electronic-structure and transport calculation code RSPACE and simulations for device	Tomoya Ono	Kobe University
9	高圧力下における共有結合性液体・ガラスの構造と電子状態の第一原理計算	下條 冬樹	熊本大学大学院自然科学研究科	First-Principles Molecular-Dynamics Study of Structural and Electronic Properties of Covalent Liquids and Glasses under Pressure	Fuyuki Shimojo	Kumamoto University
10	高機能スピントロニクス磁性材料の電子構造解析および電気磁気効果解析	小田 竜樹	金沢大学理工研究域数物科学系	Analyses on electronic structure and magnetoelectric effect in high-performance spintronics and magnetic materials	Tatsuki Oda	Kanazawa University
11	CeO ₂ (100) でのメタンの酸化反応	横 哲	東北大学材料科学高等研究所	Oxidative reaction of CH ₄ on CeO ₂ (100)	Akira Yoko	Tohoku University
12	パワー半導体における界面欠陥構造の特定とその低減法の提案：第一原理計算からのアプローチ	松下 雄一郎	東京工業大学	Identification of interface-state defects in power semiconductors: Approach from ab-initio calculations	Yu-ichiro Matsushita	Tokyo Institute of Technology
13	量子シミュレーションによる動的不均一触媒理論	森川 良忠	大阪大学 大学院工学研究科 精密科学・応用物理学専攻	Quantum simulations on dynamical heterogeneous catalysts	Yoshitada Morikawa	Osaka University
14	ベリ一位相法による金属強磁性体の異常ホール係数の第一原理計算	石井 史之	金沢大学ナノマテリアル研究所	First-principles calculation of anomalous Hall coefficient in metallic ferromagnet by using Berry phase approach	Fumiyuki Ishii	Kanazawa University
15	パワー半導体における界面欠陥構造の特定とその低減法の提案：第一原理計算からのアプローチ	松下 雄一郎	東京工業大学	Identification of interface-state defects in power semiconductors: Approach from ab-initio calculations	Yu-ichiro Matsushita	Tokyo Institute of Technology

No.	課題名	氏名	所属	Title	Name	Organization
16	氷惑星および氷衛星内部における 氷物質の熱力学特性	小松 勇	自然科学研究機構アストロバイオロジーセンター&国立天文台	Thermodynamic properties of icy materials in the interior of planets and satellites	Yu Komatsu	National Institutes of Natural Sciences AstroBiology Center & National Astronomical Observatory of Japan
17	電子の長距離量子輸送シミュレーションに向けた第一原理アルゴリズムの開発と応用	江上 喜幸	北海道大学大学院工学研究院	Development and application of first-principles algorithms for long-range electron transport simulation	Yoshiyuki Egami	Hokkaido University
18	第一原理計算を用いたクラスレート化合物の熱電特性解析	大西 正人	東京大学機械工学専攻	Analysis of Thermoelectric Properties of Clathrate Compounds with Ab Initio Calculations	Masato Ohnishi	The University of Tokyo
19	表面、界面、欠陥等の複雑構造における原子構造と原子ダイナミクスに関する解析	渡邊 聡	東京大学大学院工学系研究科マテリアル工学専攻	Analyses related to atomic structures and atom dynamics at complex structures such as surfaces, interfaces and defects	Satoshi Watanabe	The University of Tokyo
20	原子層エッチングプロセスにおける表面反応解析	浜口 智志	大阪大学工学研究科	Analyses of Surface Reactions in Atomic Layer Etching Processes	Satoshi Hamaguchi	Osaka University
21	水素を含む固体の先端計算による水素機能予測	常行 真司	東京大学大学院理学系研究科物理学専攻	Prediction of hydrogen function by advanced calculation of solids containing hydrogen	Shinji Tsuneyuki	The University of Tokyo
22	密度汎関数法と溶液理論を用いた電気化学反応の解析 2	春山 潤	東京大学物性研究所	Electrochemical reaction analysis using density functional calculation + implicit solvation model2	Jun Haruyama	The University of Tokyo
23	並列計算を用いた計算物質科学とデータ駆動科学の融合	星 健夫	鳥取大学大学院工学研究科機械宇宙工学専攻応用数理工学講座	Fusion of computational material science and data-driven science with parallel computation	Takeo Hoshi	Tottori University
24	GaN 中の不純物・らせん転位複合体の原子構造と電子構造の第一原理計算による研究	白石 賢二	名古屋大学 未来材料・システム研究所	First Principles Studies on Atomic and Electronic Structures of Impurity-screw dislocation complexes in Gan	Kenji Shiraishi	Nagoya University
25	燃料電池電極触媒及び水素透過膜の省貴金属化	坂口 紀史	北海道大学大学院工学研究院 附属エネルギー・マテリアル融合領域研究センター	Reduction of Rare Metals in Fuel Cell Catalysts and Hydrogen Permeable Membrane	Norihito Sakaguchi	Hokkaido University
26	高圧力下における共有結合性液体・ガラスの構造と電子状態の第一原理 計算	下條 冬樹	熊本大学大学院自然科学研究科	First-Principles Molecular-Dynamics Study of Structural and Electronic Properties of Covalent Liquids and Glasses under Pressure	Fuyuki Shimojo	Kumamoto University
27	大規模第一原理電子輸送シミュレーションに向けたアルゴリズム開発と応用	江上 喜幸	北海道大学大学院工学研究院	Development and application of algorithms for large-scale first-principles electron-transport simulation	Yoshiyuki Egami	Hokkaido University
28	遷移金属合金の磁気熱量効果	小口 多美夫	大阪大学産業科学研究所	Magnetocaloric Effect of Transition-Metal Alloys	Tamio Oguchi	Osaka University
29	量子シミュレーションによる動的不均一触媒理論	森川 良忠	大阪大学 大学院工学研究科 精密科学・応用物理学専攻	Quantum simulations on dynamical heterogeneous catalysts	Yoshitada Morikawa	Osaka University
30	マルチフィジックスシミュレーションによる半導体気相成長の解明	白石 賢二	名古屋大学 未来材料・システム研究所	Theoretical Studies on Semiconductor MOVPE Growth Based on Multi-Physics Simulation	Kenji Shiraishi	Nagoya University
31	表面および界面構造探索手法の開発	山下 智樹	長岡技術科学大学	Development of surface and interface structure prediction methods	Tomoki Yamashita	Nagaoka University of Technology
32	群論に基づくバンド計算	斎藤 峯雄	金沢大学理工研究域数物科学系	Band structure calculation based on the group theory	Mineo Saito	Kanazawa University

No.	課題名	氏名	所属	Title	Name	Organization
33	全電子混合基底法プログラムの改良と応用	大野 かおる	横浜国立大学大学院工学研究院	Improvement and application of all-electron mixed basis program	Kaoru Ohno	Yokohama National University
34	ギ酸分解触媒及び酸素吸蔵材料の省貴金属化	國貞 雄治	北海道大学大学院工学研究院 附属エネルギー・マテリアル融合領域研究センター	Reduction of Rare Metals in Formic Acid Decomposition Catalysts and Oxygen Storage Materials	Yuji Kunisada	Hokkaido University
35	第一原理計算における Pt(100) 薄膜の強磁性発現に関する研究	佐藤 徹哉	慶應義塾大学理工学部	Study of ferromagnetism in Pt(100) thin films by first-principles calculation	Tetsuya Sato	Keio University
36	結晶構造予測のためのデータ同化手法の開発と水素を含む化合物への応用	常行 真司	東京大学大学院理学系研究科物理学専攻	Development of data assimilation method for crystal structure prediction and its application to hydrogen-containing compounds	Shinji Tsuneyuki	The University of Tokyo
37	「厳密」な第一原理 GW+Bethe-Salpeter 法の開発	野口 良史	静岡大学工学部	Development of Exact First-Principles GW+Bethe-Salpeter Method	Yoshifumi Noguchi	Shizuoka University
38	双極子近似を超えた光・分子相互作用のための第一原理計算手法の開発と応用	岩佐 豪	北海道大学	Development and applications of first principles methods for light-matter interactions beyond the dipole approximation	Takeshi Iwasa	Hokkaido University
39	フォノンの磁性への影響の理論解析	合田 義弘	東京工業大学物質理工学院材料系	Theoretical analysis of influences of phonons on magnetism	Yoshihiro Gohda	Tokyo Institute of Technology
40	Ga 添加型永久磁石界面に対する第一原理的研究	立津 慶幸	名城大学	First-principles study on grain boundaries in Ga-doped permanent magnets	Yasutomi Tatetsu	Meio University
41	プロトン伝導性酸塩基複合体中の局所構造と分子運動の解析	堀 優太	筑波大学計算科学研究センター	The analysis of the local structures and molecular dynamics in proton-conduction acid-base composites	Yuta Hori	University of Tsukuba
42	低次元ペロブスカイトにおける励起子自己捕獲現象の第一原理計算	レービガーハンネス	横浜国立大学 大学院工学研究院 物理工学コース	First principles theory of exciton self-trapping in low-dimensional perovskites	Hannes Raebiger	Yokohama National University
43	統計物理・第一原理計算連携シミュレーションによる蓄電固体界面の熱力学解析	笠松 秀輔	山形大学学術研究院	Thermodynamic analysis of charge-storing interfaces based on direct coupling of statistical physics and first-principles calculation	Shusuke Kasamatsu	Yamagata University
44	自己組織化単分子膜を用いた PbS 量子ドット系のフォノンエンジニアリング	邵 成	東京大学機械工学塩見研究室	Phonon engineering in PbS quantum dot ligand system	Cheng Shao	The University of Tokyo
45	第一原理計算・統計物理・機械学習の連携による不規則物質系の物性予測	笠松 秀輔	山形大学学術研究院	Analysis of disordered materials using a combination of first-principles calculations, statistical physics, and machine learning	Shusuke Kasamatsu	Yamagata University
46	密度汎関数法と溶液理論を用いた電気化学反応の解析 2-2	春山 潤	東京大学物性研究所	Electrochemical reaction analysis using density functional calculation + implicit solvation model 2-2	Jun Haruyama	The University of Tokyo
47	金属/半導体界面のギャップ状態制御の物理：第一原理計算による研究 II	中山 隆史	千葉大学理学部物理学科	First-principles study on physics of gap-state control at metal/semiconductor interfaces II	Takashi Nakayama	Chiba University
48	反転中心の破れた反強磁性体の第一原理電子状態計算	山内 邦彦	京都大学学際融合教育研究推進センター	First-principles electronic structure calculations of non-centrosymmetric antiferromagnets	Kunihiko Yamauchi	Kyoto University
49	金属-絶縁体界面における結合した電子-フォノン輸送	邵 成	東京大学機械工学塩見研究室	Coupled electron-phonon transport at metal-insulator interface	Cheng Shao	The University of Tokyo

No.	課題名	氏名	所属	Title	Name	Organization
50	第一原理計算における Pt(100) 薄膜の強磁性発現に関する研究	佐藤 徹哉	慶應義塾大学理工学部	Study of ferromagnetism in Pt(100) thin films by first-principles calculation	Tetsuya Sato	Keio University
51	原子層エッチングプロセスにおける表面反応解析	浜口 智志	大阪大学工学研究科	Analyses of Surface Reactions in Atomic Layer Etching Processes	Satoshi Hamaguchi	Osaka University
52	分子・金属界面の第一原理計算	濱田 幾太郎	大阪大学工学研究科精密科学・応用物理専攻	First-principles study of molecule/metal interfaces	Ikutaro Hamada	Osaka University
53	高分子系有機半導体の電子状態・界面準位の第一原理的研究	柳澤 将	琉球大学理学部物質地球科学科物理系	First-principles theoretical study on the electronic structure and interface gap states of organic semiconductor polymers	Susumu Yanagisawa	University of the Ryukyus
54	人工ニューラルネットワーク力場構築のための効率的な学習データ生成法の模索 II	島村 孝平	熊本大学大学院先端科学研究部	Study of Efficient Training Data Generation Method for Constructing Artificial Neural Network Force Field II	Kohei Shimamura	Kumamoto University
55	第一原理計算による新規二次電池材料の解析	山田 淳夫	東京大学工学系研究科	First principles analyses on novel materials for secondary batteries	Atsuo Yamada	The University of Tokyo
56	保存則を満たす GW+Bethe-Salpeter 法の開発	野口 良史	静岡大学工学部	Development of GW+Bethe-Salpeter method	Yoshifumi Noguchi	Shizuoka University
57	原子層面内ヘテロ構造・積層構造におけるスピン偏極・擬スピン偏極の生成	明楽 浩史	北海道大学大学院工学研究院	Generation of spin and pseudospin polarizations in atomic-layer inplane heterostructures and stacked structures	Hiroshi Akera	Hokkaido University
58	ナノ構造の量子伝導の第一原理計算	小林 伸彦	筑波大学 数理物質系 物理工学域	First-principles study of quantum transport in nanostructures	Nobuhiko Kobayashi	University of Tsukuba
59	氷惑星および氷衛星内部における 水物質の熱力学特性	小松 勇	自然科学研究機構アストロバイオロジーセンター&国立天文台	Thermodynamic properties of icy materials in the interior of planets and satellites	Yu Komatsu	National Institutes of Natural Sciences AstroBiology Center & National Astronomical Observatory of Japan
60	多元系液体鉄合金の超高压下における構造と輸送特性	大村 訓史	広島工業大学 工学部	Structural and transport properties of multi-component liquid Fe mixtures under high pressure	Satoshi Ohmura	Hiroshima Institute of Technology
61	ハイブリッド汎関数による水/酸化チタン界面構造の第一原理シミュレーション	大戸 達彦	大阪大学大学院基礎工学研究科	First-principles molecular dynamics study of water/TiO ₂ interfaces using hybrid functionals	Tatsuhiko Ohto	Osaka University
62	量子化学計算を用いた高性能フッ素ポリマーエレクトレットの開発	鈴木 雄二	東京大学大学院工学系研究科機械工学専攻	Development of High-performance Polymer Electret Using Quantum Chemical Analysis	Yuji Suzuki	The University of Tokyo
63	第一原理計算による水素化物の準安定固体相および超伝導の探索 II	明石 遼介	東京大学大学院理学系研究科物理学専攻	First principles exploration of the metastable phases of hydrides and their superconductivity II	Ryosuke Akashi	The University of Tokyo
64	溶媒中の人工網膜分子の物性：第一原理分子動力学シミュレーション	大村 訓史	広島工業大学 工学部	Effects of solvents on properties of artificial-retina molecule: ab initio molecular dynamics simulations	Satoshi Ohmura	Hiroshima Institute of Technology
65	第一原理計算による水素化物の準安定固体相および超伝導の探索	明石 遼介	東京大学大学院理学系研究科物理学専攻	First principles exploration of the metastable phases of hydrides and their superconductivity	Ryosuke Akashi	The University of Tokyo
66	フォノン及び電子フォノン相互作用の第一原理精密解析	南谷 英美	分子科学研究所	Ab-initio analysis of phonon and electron-phonon interaction	Emi Minamitani	Institute for Molecular Science

No.	課題名	氏名	所属	Title	Name	Organization
67	二次元物質および表面合金の第一原理計算	石井 史之	金沢大学ナノマテリアル研究所	First-Principles Calculations of Two-Dimensional Materials and Surface Alloys	Fumiyuki Ishii	Kanazawa University
68	永久磁石内部の異相界面に対する第一原理的研究	立津 慶幸	名城大学	First-principles study on grain boundaries with multiple subphases in permanent magnets	Yasutomi Tatetsu	Meio University
69	Na-Mg-F 系超高压相における秩序無秩序転移	梅本 幸一郎	東京工業大学地球生命研究所	Order-disorder transition in ultrahigh-pressure phase of the Na-Mg-F system	Koichiro Umemoto	Tokyo Institute of Technology
70	DFT 計算による非接触原子間力顕微鏡のエネルギー散逸チャンネルで捉えた原子変位機構の解明	新井 豊子	金沢大学	DFT calculation of atomic displacement captured by energy dissipation channel of noncontact atomic force microscope	Toyoko Arai	Kanazawa University
71	シリコン結晶マトリックスにナノ粒子アレイを導入することによる2経路フォノン干渉共鳴誘導ストップバンド	胡 世謙	東京大学機械工学塩見研究室	Two-Path Phonon-Interference Resonance Induces a Stop-Band in Silicon Crystal Matrix by Embedded Nanoparticles Array	Shiqian Hu	The University of Tokyo
72	高分子系有機半導体の電子状態・界面準位の第一原理的研究	柳澤 将	琉球大学理学部物質地球科学科物理系	First-principles investigation on the electronic properties of polymer organic semiconductors	Susumu Yanagisawa	University of the Ryukyus
73	第一原理計算に基づく金属/半導体界面のギャップ状態制御の物理 III: 電場下・合金界面への展開	中山 隆史	千葉大学理学部物理学科	First-principles study on physics of gap-state control at metal/semiconductor interfaces III: effects of electric field and alloy interface	Takashi Nakayama	Chiba University
74	反転中心の破れた反強磁性体の第一原理電子状態計算	山内 邦彦	京都大学学際融合教育研究推進センター	First-principles electronic structure calculations of non-centrosymmetric antiferromagnets	Kunihiko Yamauchi	Kyoto University
75	第一原理計算による高温水中の多価アルコールの反応過程の研究	佐々木 岳彦	東京大学 大学院新領域創成科学研究科	Reaction processes of polyalcohols in high temperature water by First Principles Calculations	Takehiko Sasaki	The University of Tokyo
76	ギ酸分解触媒及び酸素吸蔵材料の省貴金属化	國貞 雄治	北海道大学大学院工学研究院 附属エネルギー・マテリアル融合領域研究センター	Reduction of Rare Metals in Formic Acid Decomposition Catalysts and Oxygen Storage Materials	Yuji Kunisada	Hokkaido University
77	固体光吸収の第一原理計算	篠原 康	東京大学工学系研究科附属光量子科学研究センター	First-principles calculations for light absorption of crystalline solids	Yasushi Shinohara	The University of Tokyo
78	原子層面内ヘテロ構造・積層構造におけるスピン偏極・擬スピン偏極の生成	明楽 浩史	北海道大学大学院工学研究院	Generation of spin and pseudospin polarizations in atomic-layer inplane heterostructures and stacked structures	Hiroshi Akera	Hokkaido University
79	第一原理計算を用いた永久磁石内の様々な相・相界面に対する交換結合定数計算および界面磁気特性の解明	寺澤 麻子	高度情報科学技術研究機構	First-principles calculation of exchange coupling constants and investigation of interface magnetism for various phases and their interfaces of permanent magnets	Asako Terasawa	Research Organization for Information Science and Technology
80	ナノ構造の量子伝導の第一原理計算	小林 伸彦	筑波大学 数理物質系 物理工学域	First-principles study of quantum transport in nanostructures	Nobuhiko Kobayashi	University of Tsukuba
81	フォノン及び電子フォノン相互作用の第一原理精密解析	南谷 英美	分子科学研究所	Ab-initio analysis of phonon and electron-phonon interaction	Emi Minamitani	Institute for Molecular Science
82	第一原理計算を用いたクラスレート化合物の熱電特性解析	大西 正人	東京大学機械工学専攻	Analysis of Thermoelectric Properties of Clathrate Compounds with Ab Initio Calculations	Masato Ohnishi	The University of Tokyo
83	Sb 系テラヘルツトランジスタのための歪バンド構造設計	藤代 博記	東京理科大学	Strained Band-Structure Engineering for Antimonide-Based Terahertz Transistors	Hiroki Fujishiro	Tokyo University of Science

No.	課題名	氏名	所属	Title	Name	Organization
84	ナノ界面・分子構造の最適特性設計のための第一原理 / 機械学習連成計算	鶴田 健二	岡山大学大学院自然科学研究科	Hybrid Ab-Initio/Machine-Learning Optimization of Nano Interfaces and Molecular Structures	Kenji Tsuruta	Okayama University
85	第一原理分子動力学法に基づくガラスの静的構造に関する研究	高良 明英	熊本大学技術部	Ab initio molecular dynamics study on static structure of glass materials	Akihide Koura	Kumamoto University
86	酸化物界面の安定構造探索および偏析現象の解明	幾原 雄一	東京大学大学院工学系研究科総合研究機構	Study of atomic structure and segregation behavior in oxide interface	Yuichi Ikuhara	The University of Tokyo
87	第一原理分子動力学法に基づくガラスの静的構造に関する研究	高良 明英	熊本大学技術部	Ab initio molecular dynamics study on static structure of glass materials	Akihide Koura	Kumamoto University
88	熱力学状態図作成のための第一原理計算：交換相関汎関数依存性	中村 和磨	九州工業大学	Ab initio calculation for thermodynamic phase diagram: Investigation on exchange-correlation functional dependence	Kazuma Nakamura	Kyushu Institute of Technology
89	van der Waals 密度汎関数法による金(110)表面に吸着した銅フタロシアニンの理論的研究	濱本 雄治	大阪大学 大学院工学研究科 物理学系専攻	van der Waals density functional study of Cu phthalocyanine adsorbed on the Au(110) surface	Yuji Hamamoto	Osaka University
90	イリジウム酸化物 $\text{Ca}_5\text{Ir}_3\text{O}_{12}$ の第一原理フォノン計算	中村 和磨	九州工業大学	Ab initio phonon calculation for $\text{Ca}_5\text{OIr}_3\text{O}_{12}$	Kazuma Nakamura	Kyushu Institute of Technology
91	van der Waals 密度汎関数法による金(110)表面に吸着した銅フタロシアニンの理論的研究	濱本 雄治	大阪大学 大学院工学研究科 物理学系専攻	van der Waals density functional study of Cu phtyalocyanine adsorbed on the Au(110) surface	Yuji Hamamoto	Osaka University
92	第一原理計算による高温水中のソルビトールの環化脱水反応の研究	佐々木 岳彦	東京大学 大学院新領域創成科学研究科	Study on cyclodehydration of sorbitol in hot water by First Principles calculations	Takehiko Sasaki	The University of Tokyo
93	超並列計算を用いた計算物質科学とデータ駆動科学の融合	星 健夫	鳥取大学大学院工学研究科機械宇宙工学専攻応用数理工学講座	Fusion of computational material science and data-driven science with massively parallel computation	Takeo Hoshi	Tottori University
94	群論に基づくバンド計算	斎藤 峯雄	金沢大学理工研究域数物科学系	Band structure calculation based on the group theory	Mineo Saito	Kanazawa University
95	照射損傷と格子間原子との相互作用の研究	大澤 一人	九州大学応用力学研究所	Study of interaction between radiation damage and interstitial atom	Kazuhito Ohsawa	Kyushu University
96	ダブルペロブスカイト型光触媒の電子構造に関する研究	西館 数芽	岩手大学理工学部	Investigation on the electronic structure of photo-catalytic double-perovskite	Kazume Nishidate	IWATE University
97	燃料電池電極触媒及び水素透過膜の省貴金属化	坂口 紀史	北海道大学大学院工学研究院 附属エネルギー・マテリアル融合領域研究センター	Reduction of Rare Metals in Fuel Cell Catalysts and Hydrogen Permeable Membrane	Norihito Sakaguchi	Hokkaido University
98	第一原理分子動力学法による異種界面原子構造の解析	幾原 雄一	東京大学大学院工学系研究科総合研究機構	Analysis of hetero-interface by ab-initio molecular dynamics simulations	Yuichi Ikuhara	The University of Tokyo
99	KKR グリーン関数法を用いたハイスループット材料計算手法の開発	福島 鉄也	東京大学物性研究所	High-throughput screening calculations by KKR Green's function method	Tetsuya Fukushima	The University of Tokyo
100	機械学習を用いた高性能フッ素ポリマーエレクトレットの開発	鈴木 雄二	東京大学大学院工学系研究科機械工学専攻	Development of High-performance Polymer Electret with the Aid of Machine Learning	Yuji Suzuki	The University of Tokyo

No.	課題名	氏名	所属	Title	Name	Organization
101	二次元複合材料におけるフォノン熱伝導の研究	胡 世謙	東京大学機械工学塩見研究室	Study of Phonon Thermal Conduction in Two-dimensional (2D) Composite Materials	Shiqian Hu	The University of Tokyo
102	絶縁体非線形光吸収の第一原理計算	篠原 康	東京大学工学系研究科附属量子科学研究センター	First-principles calculations for nonlinear light absorption of insulators	Yasushi Shinohara	The University of Tokyo
103	グラフェンへのドーピングと分子吸着	藤本 義隆	東京工業大学大学院理工学研究科物性物理学専攻	Doping and molecular adsorption of graphene	Yoshitaka Fujimoto	Tokyo Institute of Technology
104	Na フラックス GaN 成長における融液構造および融液物性の解析	河村 貴宏	三重大学大学院工学研究科	First-principles analysis of melt structure and property in Na flux GaN growth	Takahiro Kawamura	Mie University
105	KKR グリーン関数法による磁性不規則合金のデータベース構築	福島 鉄也	東京大学物性研究所	Construction of magnetic materials database by KKR Green's function method	Tetsuya Fukushima	The University of Tokyo
106	乱れた構造を伴う希土類磁石材料の磁気特性	赤井 久純	東京大学物性研究所	Magnetic properties of rare earth magnetic materials with structural dis- order	Hisazumi Akai	The University of Tokyo
107	不純物ドーピングによる ϵ 型と κ 型の Ga_2O_3 の光学的バンドギャップ制御	首藤 健一	横浜国立大学・工学部	Optical gaps of metastable Ga_2O_3 structures modulated by impurity dope	Ken-ichi Shudo	Yokohama Nat'l Univ.
108	第一原理計算による有機強誘電体・圧電体の物性予測	石橋 章司	産業技術総合研究所	Prediction of properties of organic ferroelectrics and piezoelectrics by first-principles calculation	Shoji Ishibashi	National Institute of Advanced Industrial Science and Technology
109	合金触媒の原子構造と電子構造に関する第一原理計算	野澤 和生	鹿児島大学理学部物理科学科	First-principles study of atomic and electronic structures of intermetallic compound catalysts	Kazuki Nozawa	Kagoshima University
110	純水による Si 単結晶の触媒表面基準エッチングのメカニズム解明	BUI VANPHO	大阪大学大学院工学研究科	Study on removal mechanism in catalyst referred etching of single crystalline Si with pure water	Vanpho Bui	Osaka University
111	スピン流 - 電流変換物質における電界効果の第一原理計算	山口 直也	金沢大学ナノマテリアル研究所	First-principles Calculation of Electric Field Effects in Spin-to-charge Conversion Materials	Naoya Yamaguchi	Kanazawa University
112	シリサイド薄膜系の原子構造と電子状態	服部 賢	奈良先端科学技術大学院大学物質創成科学研究科	Atomic structure and electronic states for silicide films	Ken Hattori	Nara Institute of Science and Technology
113	環境調和型シリサイド SrSi_2 の熱電性能への不純物添加効果の理論的研究	飯田 努	東京理科大学	A theoretical study on the effect of impurity doping on the thermoelectric performance of environmental friendly silicide SrSi_2	Tsutomu Iida	Tokyo University of Science
114	半導体表面界面における構造的素励起の研究	影島 博之	島根大学大学院自然科学研究科	Study on structural elementary excitations at semiconductor surfaces and interfaces	Hiroyuki Kageshima	Shimane University
115	人工ニューラルネットワーク力場構築のための効率的な学習データ生成法の模索	島村 孝平	熊本大学大学院先端科学研究部	Study of Efficient Training Data Generation Method for Constructing Artificial Neural Network Force Field	Kohei Shimamura	Kumamoto University
116	パワー半導体デバイスのリーク電流と貫通転位における電子状態	原嶋 庸介	名古屋大学未来材料・システム研究所	Leakage current on power semiconductor devices and an electronic structure on a threading dislocation	Yosuke Harashima	Nagoya University
117	量子古典混合アルゴリズムを用いた結晶系の第一原理計算	水上 渉	大阪大学 先導的学際研究機構	First principles calculations of crystals with quantum classical hybrid algorithms	Wataru Mizukami	Osaka University

No.	課題名	氏名	所属	Title	Name	Organization
118	Sb系テラヘルツトランジスタのための歪バンド構造設計	藤代 博記	東京理科大学	Strained Band-Structure Engineering for Antimonide-Based Terahertz Transistors	Hiroki Fujishiro	Tokyo University of Science
119	不純物ドーピングによる Ga ₂ O ₃ および GaN の光学的バンドギャップ制御	首藤 健一	横浜国立大学・工学部	Optical gaps of metastable Ga ₂ O ₃ and GaN with impurity doping effect	Ken-ichi Shudo	Yokohama Nat'l Univ.
120	量子古典混合アルゴリズムを用いた第一原理計算のノイズを考慮したシミュレーション	水上 渉	大阪大学 先導的学際研究機構	Noisy simulations of first-principles calculations using quantum classical hybrid algorithms	Wataru Mizukami	Osaka University
121	乱れた構造を伴う希土類磁石材料の磁気特性	赤井 久純	東京大学物性研究所	Magnetic properties of rare earth magnetic materials with structural disorder	Hisazumi Akai	The University of Tokyo
122	ポストポストペロブスカイト転移における Al 不純物の影響についての第一原理研究	梅本 幸一郎	東京工業大学地球生命研究所	First principles study of effect of Al impurity on the post-post-perovskite transitions	Koichiro Umemoto	Tokyo Institute of Technology
123	新たなナノスケール表面界面の電子物性の理論的研究	小林 功佳	お茶の水女子大学理学部物理学科	Theoretical study on electronic properties of new nanoscale surfaces and interfaces	Katsuyoshi Kobayashi	Ochanomizu University
124	微小グラフェンシートの STM 観測で得られる特異な輝点列の起源の解明	有馬 健太	大阪大学 大学院 工学研究科	Origin of specific dot patterns on small graphene sheets observed by STM	Kenta Arima	Osaka University
125	対称性指標を用いた網羅的なトポロジカル物質探索	渡邊 悠樹	東京大学工学系研究科物理工学専攻	Comprehensive material search based on symmetry indicators	Haruki Watanabe	The University of Tokyo
126	固体表面・界面、微粒子の新規電子物性の探索と実現	稲岡 毅	琉球大学理学部	Search and realization of novel electronic properties of solid surfaces and interfaces and of small particles	Takeshi Inaoka	University of the Ryukyus
127	磁性分子複合体・結晶・界面系の原子・磁気構造の解析と外部電場・磁場効果の調査	小幡 正雄	金沢大学理工研究域	Analysis on atomic and magnetic structure in magnetic molecular complex, crystal and interface and investigation of external electric and magnetic field effect	Masao Obata	Kanazawa University
128	希土類セスキオキシドにおける電子格子相互作用の計算	牧野 哲征	福井大学学術研究院工学系部門	Electron-phonon interaction calculation in rare-earth sesquioxides	Takayuki Makino	University of Fukui
129	密度汎関数理論と線形応答理論の枠組みにおけるゼーベック係数計算手法の開発	高 成柱	東京工業大学物質理工学院	Development of Seebeck coefficient calculation method in the framework of density functional theory and linear response theory	Sonju Kou	Tokyo Institute of Technology
130	強相関電子系における多極子秩序と超伝導	池田 浩章	立命館大学理工学部物理科学科	Multipole orders and superconductivity in strongly correlated electron systems	Hiroaki Ikeda	Ritsumeikan University
131	半導体デバイス中のキャリアダイナミクスの機械学習モデルに関する研究	村口 正和	北海道科学大学	Study on machine learning model of carrier dynamics in semiconductor devices	Masakazu Muraguchi	Hokkaido University of Science
132	原子層物質形成反応の解析と物性予測	島田 敏宏	北海道大学 大学院工学研究院	Analysis of reaction and prediction of properties of atomic layer materials	Toshihiro Shimada	Hokkaido University
133	酸化チタン界面における光触媒反応メカニズムの理論的解析	城塚 達也	茨城大学	Theoretical Analysis of Photocatalytic Reaction Mechanism at Titanium Dioxide Interfaces	Tatsuya Joutsuka	Ibaraki University
134	PMT 基底関数法を用いた第一原理多体有効モデル構築	榑原 寛史	鳥取大学大学院工学研究科	First-principles derivation of a many-body effective model based on PMT basis	Hirofumi Sakakibara	Tottori University

No.	課題名	氏名	所属	Title	Name	Organization
135	機械学習と第一原理計算による赤外およびラマンスペクトルの予測方法の検証	平塚 将起	工学院大学機械工学科	Estimation of Infrared and Raman spectra using ab initio calculation and machine learning	Masaki Hiratsuka	Kogakuin University
136	LCPAO 法を用いた一様電場下にある絶縁体・半導体バルクにおけるバンド分散の第一原理的解析	山口 直也	金沢大学ナノマテリアル研究所	First-principles Analysis of Band Dispersion in Bulk Insulators/Semiconductors Under Finite Electric Fields by Using the LCPAO Method	Naoya Yamaguchi	Kanazawa University
137	プロトン伝導性有機結晶中の水素結合構造の解析	堀 優太	筑波大学計算科学研究センター	The analysis of the hydrogen-bonding structures in proton-conduction organic crystals	Yuta Hori	University of Tsukuba
138	第一原理計算と機械学習を用いた固体中の塑性波伝播の分子動力学シミュレーション	三澤 賢明	岡山大学大学院自然科学研究科	Molecular Dynamics Simulation on Plastic-Wave Propagation in Solid Materials Based on First-Principles Calculation and Machine Learning	Masaaki Misawa	Okayama University
139	対称性指標を用いた網羅的なトポロジカル物質探索	渡邊 悠樹	東京大学工学系研究科物理工学専攻	Comprehensive material search based on symmetry indicators	Haruki Watanabe	The University of Tokyo
140	2次元物質の周期表に基づく動的に安定な合金の新しい探索法	小野 頌太	岐阜大学	A new method for exploring dynamically stable alloys from the periodic table of 2D materials	Shota Ono	Gifu University
141	有機・無機材料界面における自己秩序化現象の機構解明	折本 裕一	九州大学大学院総合理工学研究院物質科学部門	Elucidation of the mechanism of self-ordering phenomena at the interface between organic and inorganic materials	Yuuichi Orimoto	Kyushu University
142	第一原理 KKR 計算を用いた磁気特性の評価	櫻井 誠大	東京大学物性研究所	First-principles KKR calculations for evaluating magnetic properties	Masahiro Sakurai	The University of Tokyo
143	低温で酸素移動が生じる金属酸化物の第一原理計算	横 哲	東北大学材料科学高等研究所	First-principles calculation for low-temperature oxygen transfer in metal oxide	Akira Yoko	Tohoku University
144	高温高圧における分子結晶の炭化反応と電子状態	島田 敏宏	北海道大学 大学院工学研究院	Carbonization reaction and electronic structures of molecular crystals under high temperature high pressure conditions	Toshihiro Shimada	Hokkaido University
145	新しい基底関数法 PMT を用いた第一原理多体有効模型構築	榊原 寛史	鳥取大学大学院工学研究科	First-principles derivation of a many-body effective model based on a new basis PMT	Hirofumi Sakakibara	Tottori University
146	有機物水溶液の電子状態	高橋 修	広島大学大学院理学研究科	Electronic state of organic compounds in aqueous solution	Osamu Takahashi	Hiroshima University
147	第一原理計算と機械学習を用いた非平衡過程に関する分子動力学的研究	三澤 賢明	岡山大学大学院自然科学研究科	Molecular dynamics study on non-equilibrium processes using first-principles calculation and machine leaning	Masaaki Misawa	Okayama University
148	触媒インフォマティクスに向けた複合酸化物の表面物性計算	日沼 洋陽	東京工業大学科学技術創成研究院	Calculation of multication oxide surface properties for catalyst informatics	Yoyo Hinuma	Tokyo Institute of Technology
149	遷移金属合金の磁気熱量効果	小口 多美夫	大阪大学産業科学研究科	Magnetocaloric Effect of Transition-Metal Alloys	Tamio Oguchi	Osaka University
150	電気伝導度の温度依存性とゼーベック係数の第一原理計算	真砂 啓	大阪大学基礎工学部	First principles calculations of thermal dependence of conductivity and Seebeck coefficient	Akira Masago	Osaka University
151	物質表面における電子場の局所量解析	福田 将大	東京大学物性研究所	Analysis of local quantities of electron field in material surface	Masahiro Fukuda	The University of Tokyo

No.	課題名	氏名	所属	Title	Name	Organization
152	低圧化学気相成長法による金属膜の高速成長の第一原理計算	城塚 達也	茨城大学	Ab Initio Calculation of High-Rate Deposition of Metal Film by Low-Pressure Chemical Vapor Deposition	Tatsuya Joutsuka	Ibaraki University
153	液晶における電子輸送機構のモデル化と解明	大野 玲	東京工業大学	Modeling and elucidation of electron transport mechanism in liquid crystals	Akira Ohno	Tokyo Institute of Technology
154	金属ドーブによるセリウム酸化物の格子歪現と酸素貯蔵能向上に関する第一原理計算	横 哲	東北大学材料科学高等研究所	First-principles calculation of oxygen storage capacity and structural distortion of metal doped cerium oxide	Akira Yoko	Tohoku University
155	触媒インフォマティクスに向けた合成可能な表面探索	日沼 洋陽	東京工業大学科学技術創成研究院	Search of accessible surfaces for catalyst informatics	Yoyo Hinuma	Tokyo Institute of Technology
156	合金触媒の原子構造と電子構造に関する第一原理計算	野澤 和生	鹿児島大学理学部物理科学科	First-principles study of atomic and electronic structures of intermetallic compound catalysts	Kazuki Nozawa	Kagoshima University
157	磁性分子複合体・結晶・界面系の原子・磁気と原子構造の解析と外部電磁場効果の調査	小幡 正雄	金沢大学理工研究域	Analysis on atomic and magnetic structure in magnetic molecular complex, crystal and interface and investigation of external electromagnetic field effect	Masao Obata	Kanazawa University
158	波数空間分解光電子分光を用いた分子結晶表面の解析手法の確立	二木 かおり	千葉大学	Establishment of molecular crystal surface analysis technique using wave number space resolved photoelectron spectroscopy	Kaori Niki	Chiba University
159	純水による Si 単結晶の触媒表面基準エッチングのメカニズム解明	BUI VANPHO	大阪大学大学院工学研究科	Study on removal mechanism of single crystalline Si planarized by catalyst referred etching in pure water	Vanpho Bui	Osaka University
160	ダブルペロブスカイト型光触媒の電子構造に関する研究	西館 数芽	岩手大学理工学部	Investigation on the electronic structure of photo-catalytic double-perovskite	Kazume Nishidate	IWATE University
161	ドライエッチング工程におけるフロロカーボン誘電膜の第一原理計算	レービガーハンネス	横浜国立大学 大学院工学研究院 物理工学コース	First principles calculation of fluorocarbon layer in dry etching process	Hannes Raebiger	Yokohama National University
162	デラフォサイト型銅酸化物における定常電場印加下での電子構造計算	牧野 哲征	福井大学学術研究院工学系部門	Electronic structure calculation under presence of static electric field in delafossite-type cuprates	Takayuki Makino	University of Fukui
163	固体表面・界面、微粒子の新規電子物性の探索と実現	稲岡 毅	琉球大学理学部	Search and realization of novel electronic properties of solid surfaces and interfaces and of small particles	Takeshi Inaoka	University of the Ryukyus
164	酸化物における電場印加下でのフォノン分散および状態密度の計算	牧野 哲征	福井大学学術研究院工学系部門	Calculation of phonon dispersion and density of states under electric field in oxides	Takayuki Makino	University of Fukui
165	強相関系酸化物反強磁性体における電子構造の計算	牧野 哲征	福井大学学術研究院工学系部門	Calculation of electronic states in strongly-electron-correlated antiferromagnetic oxides	Takayuki Makino	University of Fukui
166	強相関電子系における多極子秩序と超伝導	池田 浩章	立命館大学理工学部物理科学科	Multipole orders and superconductivity in strongly correlated electron systems	Hiroaki Ikeda	Ritsumeikan University
167	第一原理計算に基づくマグネシウム合金の欠陥場の解析	松中 大介	信州大学工学部機械システム工学科	First-principles Study of Defects of Magnesium Alloys	Matsunaka Daisuke	Shinshu University
168	新たなナノスケール表面界面の電子物性の理論的研究	小林 功佳	お茶の水女子大学理学部物理学科	Theoretical study on electronic properties of new nanoscale surfaces and interfaces	Katsuyoshi Kobayashi	Ochanomizu University

No.	課題名	氏名	所属	Title	Name	Organization
169	第一原理計算に基づくマグネシウム合金の欠陥場の解析	松中 大介	信州大学工学部機械システム工学科	First-principles Study of Defects of Magnesium Alloys	Matsunaka Daisuke	Shinshu University
170	ナノ界面・分子構造の最適特性設計のための第一原理/機械学習連成計算	鶴田 健二	岡山大学大学院自然科学研究科	Hybrid Ab-Initio/Machine-Learning Optimization of Nano Interfaces and Molecular Structures	Kenji Tsuruta	Okayama University
171	異なる幅を持つグラフェンナノリボンのフェルミレベル近傍電子状態の解析	有馬 健太	大阪大学 大学院 工学研究科	Analysis of electronic structures around the Fermi level of graphene nanoribbons with different widths	Kenta Arima	Osaka University
172	照射損傷と格子間原子との相互作用の研究	大澤 一人	九州大学応用力学研究所	Study of interaction between radiation damage and interstitial atom	Kazuhito Ohsawa	Kyushu University
173	半導体表面界面における構造的素励起の研究	影島 博之	島根大学大学院自然科学研究科	Study on structural elementary excitations at semiconductor surfaces and interfaces	Hiroyuki Kageshima	Shimane University
174	低圧化学気相成長法による金属膜の高速成長の第一原理計算	城塚 達也	茨城大学	Ab Initio Calculation of High-Rate Deposition of Metal Films by Low-Pressure Chemical Vapor Deposition	Tatsuya Joutsuka	Ibaraki University
175	酸化チタン界面における光触媒反応メカニズムの理論的解析	城塚 達也	茨城大学	Theoretical Analysis of Photocatalytic Reaction Mechanism at Titanium Dioxide Interfaces	Tatsuya Joutsuka	Ibaraki University
176	金属表面上の吸着フタロシアニン分子間相互作用	有賀 哲也	京都大学理学研究科化学専攻	Interaction among phthalocyanine molecules adsorbed on metal surfaces	Aruga Tetsuya	Kyoto University
177	窒化ガリウム p-n ダイオードの不純物と貫通転位複合体の電子状態計算	原嶋 庸介	名古屋大学未来材料・システム研究所	First-principles study on complexes of impurity and dislocation in GaN p-n diodes	Yosuke Harashima	Nagoya University
178	第一原理計算による有機強誘電体・圧電体の物性予測	石橋 章司	産業技術総合研究所	Prediction of properties of organic ferroelectrics and piezoelectrics by first-principles calculation	Shoji Ishibashi	National Institute of Advanced Industrial Science and Technology
179	ビスマステルル/強磁性金属界面の電子状態とスピン構造の解明	千葉 貴裕	福島工業高等専門学校	Band structure and spin texture of Bi-Te/ferromagnetic-metal interface	Takahiro Chiba	Fukushima College
180	反強磁性 Cr の電子状態に対する N 添加効果の解析	小田 洋平	福島工業高等専門学校	Analysis of N-doping effect on electronic structure in antiferromagnetic Cr	Yohei Kota	Fukushima College
181	π 電子系有機分子/金属界面の電子状態と分子間相互作用	有賀 哲也	京都大学理学研究科化学専攻	Electronic structure and interaction at the interface of π -electron organic molecules and metals	Aruga Tetsuya	Kyoto University
182	グラフェンにおける金属インターカレーション構造のバンド計算	秋山 了太	東京大学理学系研究科物理学専攻	Band calculation in metal-intercalated graphene	Ryota Akiyama	The University of Tokyo
183	Pb 系トポロジカル絶縁体のバルク絶縁性向上のためのドーパント探索	徳本 有紀	東京大学生産技術研究所	Exploring dopants to improve bulk-insulation of Pb-based topological insulators	Yuki Tokumoto	The University of Tokyo
184	Quantum ESPRESSO の性能測定	吉澤 香奈子	高度情報科学技術研究機構	Performance measurement of Quantum ESPRESSO	Kanako Yoshizawa	Research Organization for Information Science & Technology
185	第一原理計算による光熱変換原理の解明	江目 宏樹	山形大学	Study of the principle of photothermal conversion by ab initio calculations	Hiroki Gonome	Yamagata University

No.	課題名	氏名	所属	Title	Name	Organization
186	α -Al ₂ O ₃ における荷電欠陥の第一原理計算	石川 亮	東京大学総合研究機構	First-principles calculation on charged defects in α -Al ₂ O ₃	Ryo Ishikawa	The University of Tokyo
187	表面および界面構造探索手法の開発	山下 智樹	長岡技術科学大学	Development of surface and interface structure prediction methods	Tomoki Yamashita	Nagaoka University of Technology
188	シリサイド薄膜系の原子構造と電子状態	服部 賢	奈良先端科学技術大学院大学物質創成科学研究科	Atomic structure and electronic states for silicide films	Ken Hattori	Nara Institute of Science and Technology
189	分子接合の第一原理伝導計算	大戸 達彦	大阪大学大学院基礎工学研究科	First-principles transport calculations for molecular junctions	Tatsuhiko Ohto	Osaka University
2. 強相関 / Strongly Correlated Quantum Systems						
190	高精度第一原理強相関電子状態計算手法による高温超伝導体の網羅的研究	今田 正俊	早稲田大学理工学術院	Exhaustive Studies on High Temperature Superconductors by Highly Accurate ab initio Scheme for Strongly Correlated Electron Systems	Masatoshi Imada	Waseda University
191	準粒子干渉実験データの機械学習による銅酸化物高温超伝導の解析	今田 正俊	早稲田大学理工学術院	Machine learning analyses on quasi-particle interference data of cuprate high-temperature superconductors	Masatoshi Imada	Waseda University
192	量子スピン液体物質の高精度第一原理有効ハミルトニアンによる数値解析	山地 洋平	東京大学大学院工学系研究科物理工学専攻	Numerical studies of quantum spin liquid candidates by highly accurate ab initio effective hamiltonians	Youhei Yamaji	The University of Tokyo
193	Pd(dmit) ₂ 系分子性導体に対する第一原理低エネルギー有効Hamiltonianの系統的解析	三澤 貴宏	東京大学物性研究所	Systematic analysis of ab initio low-energy effective Hamiltonians for Pd(dmit) ₂ molecular conductors	Takahiro Misawa	The University of Tokyo
194	量子相互情報量による量子スピン液体の数値的研究	山地 洋平	東京大学大学院工学系研究科物理工学専攻	Numerical studies of quantum spin liquids by quantum mutual information	Youhei Yamaji	The University of Tokyo
195	強相関系の磁性・トポロジカル相形成と輸送現象	川上 則雄	京都大学大学院理学研究科物理学宇宙物理学専攻	Magnetism, topological phase formation and transport phenomena in strongly correlated systems	Norio Kawakami	Kyoto University
196	スピン軌道結合の強い相関電子系の理論的研究	求 幸年	東京大学大学院工学系研究科	Theoretical study of correlated electron systems with strong spin-orbit coupling	Yukitoshi Motome	The University of Tokyo
197	ニッケル酸化物超伝導体と銅酸化物超伝導体の比較	野村 悠祐	理化学研究所 創発物性科学研究センター	Comparison between nickelate and cuprate superconductors	Yusuke Nomura	RIKEN
198	スピン軌道結合の強い相関電子系の理論的研究	求 幸年	東京大学大学院工学系研究科	Theoretical study of correlated electron systems with strong spin-orbit coupling	Yukitoshi Motome	The University of Tokyo
199	強相関系の相形成と輸送現象	川上 則雄	京都大学大学院理学研究科物理学宇宙物理学専攻	Study of phase formation and transport phenomena in strongly correlated quantum systems	Norio Kawakami	Kyoto University
200	軌道間相互作用が増強するスピン揺らぎ媒介超伝導に関する研究	黒木 和彦	大阪大学	Study on spin-fluctuation-mediated superconductivity enhanced by interorbital interactions	Kazuhiko Kuroki	Osaka University
201	ニッケル酸化物超伝導体に対する強相関第一原理計算	野村 悠祐	理化学研究所 創発物性科学研究センター	Ab initio calculation for strongly-correlated nickelate superconductor	Yusuke Nomura	RIKEN

No.	課題名	氏名	所属	Title	Name	Organization
202	銅酸化物における特異な電子状態による超伝導増強機構に関する研究	黒木 和彦	大阪大学	Study on the enhanced superconductivity in cuprates with peculiar electronic structures	Kazuhiko Kuroki	Osaka University
203	ボンド依存した異方的相互作用をもつ系における多重 Q 磁気秩序相の探索	速水 賢	東京大学大学院工学系研究科	Search for multiple- Q magnetic orders in systems with bond-dependent anisotropic interactions	Satoru Hayami	The University of Tokyo
204	非エルミートポロジカル系におけるバルクエッジ対応	吉田 恒也	筑波大学 数理物質系	Bulk-edge correspondence for non-Hermitian topological systems	Tsuneya Yoshida	University of Tsukuba
205	非エルミートポロジカル系における強相関効果	吉田 恒也	筑波大学 数理物質系	Correlation effects on non-Hermitian topological states	Tsuneya Yoshida	University of Tsukuba
206	希土類永久磁石のための Ce 磁性化合物の最適化設計	松本 宗久	高エネルギー加速器研究機構 物質構造科学研究所	Optimal design of Ce-based magnetic compounds for rare-earth permanent magnets	Munehisa Matsumoto	Institute of Materials Structure Science, High Energy Accelerator Research Organization (KEK)
207	時間依存密度行列繰り込み群法によるモット絶縁体の光学伝導度のスペクトル形状解析	遠山 貴己	東京理科大学理学部応用物理学科	Time-dependent DMRG study of spectral shape in the optical conductivity of Mott insulators	Takami Tohyama	Tokyo University of Science
208	強相関電子系で発現する量子スピン液体の解析	井戸 康太	東京大学物性研究所	Numerical analyses on quantum spin liquids in strongly correlated electron systems	Kota Ido	The University of Tokyo
209	2チャンネル近藤状態とフェルミ液体状態の間に現れる量子臨界点の研究	堀田 貴嗣	東京都立大学理学研究科物理学専攻	Research of Quantum Critical Points Emerging between Two-Channel Kondo and Fermi-Liquid States	Takashi Hotta	Tokyo Metropolitan University
210	Kitaev量子スピン液体に対する乱れの効果	那須 譲治	横浜国立大学	Disorder effect on Kitaev quantum spin liquids	Joji Nasu	Yokohama National University
211	遍歴電子系における正方格子型スキルミオン結晶探索	速水 賢	東京大学大学院工学系研究科	Search for square-lattice skyrmion crystal in itinerant electron systems	Satoru Hayami	The University of Tokyo
212	2次元格子モデルにおける電荷グラス相の探索の理論	堀田 知佐	東京大学総合文化研究科	Exploring charge glass phase in two-dimensional lattice models	Chisa Hotta	The University of Tokyo
213	時間依存密度行列繰り込み群法による二次元ハバード模型の光学伝導度のスペクトル形状解析	遠山 貴己	東京理科大学理学部応用物理学科	Time-dependent DMRG study of spectral shape in the optical conductivity of two-dimensional Hubbard model	Takami Tohyama	Tokyo University of Science
214	有機ディラック電子系 α -(BETS) $_2$ I $_3$ における隠れた秩序状態	小林 晃人	名古屋大学 大学院理学研究科	Hidden Ordered State in Organic Dirac Electron System α -(BETS) $_2$ I $_3$	Akito Kobayashi	Nagoya University
215	統合型動的平均場近似ソフトウェア DCore の開発と応用	品岡 寛	埼玉大学理学部物理学科	Development and application of DFT+DMFT software DCore	Hiroshi Shinaoka	Saitama University
216	光誘起非平衡ダイナミクスにおける不均一効果	石原 純夫	東北大学大学院理学研究科	Inhomogeneous effect in light induced nonequilibrium state	Sumio Ishihara	Tohoku University
217	有機ディラック電子系 α -(BETS) $_2$ I $_3$ の低温相における隠れた秩序状態	小林 晃人	名古屋大学 大学院理学研究科	Hidden Order in Low Temperature Phase of Organic Dirac Electron System α -(BETS) $_2$ I $_3$	Akito Kobayashi	Nagoya University
218	量子化学計算を用いた固体の電子状態計算の開発	西口 和孝	大阪大学大学院理学研究科物理学専攻	Development of electronic structure calculation for solids with quantum chemistry calculations	Kazutaka Nishiguchi	Osaka University

No.	課題名	氏名	所属	Title	Name	Organization
219	2次元格子モデルにおける電荷ガラス相の探索の理論その2	堀田 知佐	東京大学総合文化研究科	Exploring charge glass phase in two-dimensional lattice models	Chisa Hotta	The University of Tokyo
220	強相関電子系における新規量子現象の研究	柳沢 孝	産業技術総合研究所	Study of new quantum phenomena in correlated electron systems	Takashi Yanagisawa	National Institute of Advanced Industrial Science and Technology
221	モンテカルロ法および第一原理計算による強相関電子系の数値的研究	柳沢 孝	産業技術総合研究所	Numerical study of strongly correlated electron systems	Takashi Yanagisawa	National Institute of Advanced Industrial Science and Technology
222	有機電荷秩序相における電界誘起金属-絶縁体転移の解明	酒井 正俊	千葉大学大学院工学研究院電気電子	Field-induced metal-insulator transition in organic charge order phase	Masatoshi Sakai	Chiba University
223	ポスト-ハートレー-フォック法を用いた固体の電子状態計算の開発	西口 和孝	大阪大学大学院理学研究科物理学専攻	Development of electronic structure calculation for solids with post-Hartree-Fock	Kazutaka Nishiguchi	Osaka University
224	ファンデルワールス希土類化合物における置換可能元素のスクリーニング	小林 理気	琉球大学	Screening of substitutable element in van der Waals coupling rare-earth compounds	Riki Kobayashi	University of the Ryukyus
225	相関電子系における非平衡ダイナミクスの数値的研究	石原 純夫	東北大学大学院理学研究科	Numerical study of nonequilibrium dynamics in correlated electron systems	Sumio Ishihara	Tohoku University
226	変分モンテカルロ法による銅酸化物高温超伝導体のストライプ秩序と超伝導の解析	渡部 洋	立命館大学	Study for stripe order and superconductivity in high- T_c cuprates by variational Monte Carlo method	Hiroshi Watanabe	Ritsumeikan University
227	希土類金属化合物における置換可能非磁性元素のスクリーニングII	小林 理気	琉球大学	Screening of substitutable non-magnetic element in rare-earth inter-metallic compounds II	Riki Kobayashi	University of the Ryukyus
228	ハバードモデルによる、強相関電子系での超伝導状態、および磁性状態の研究。	山田 篤志	千葉大学理学研究科	Studies of the superconductivity and magnetic states in the strongly correlated electron systems using Hubbard models.	Atsushi Yamada	Chiba University
229	有機電荷秩序相における電子状態の余剰キャリア依存性	酒井 正俊	千葉大学大学院工学研究院電気電子	Excess carrier dependent electronic state in organic charge order phase	Masatoshi Sakai	Chiba University
3. 巨視系の協同現象 / Cooperative Phenomena in Complex, Macroscopic Systems						
230	複雑流体中におけるキャビテーションの分子動力学シミュレーション	浅野 優太	東京大学物性研究所	Molecular dynamics simulation of cavitation in complex fluids	Yuta Asano	The University of Tokyo
231	テンソルネットワーク法によるKitaev関連モデルの計算	川島 直輝	東京大学物性研究所	Tensor-network study of Kitaev models	Naoki Kawashima	The University of Tokyo
232	全原子・粗視化力場によるソフトマターの分子シミュレーション	篠田 渉	名古屋大学大学院工学研究科	Molecular Simulation of Soft Materials using All-Atom and Coarse-Grained Force Field	Wataru Shinoda	Nagoya University
233	テンソルネットワーク法によるKitaev関連モデルの計算	川島 直輝	東京大学物性研究所	Tensor-network study of Kitaev models	Naoki Kawashima	The University of Tokyo
234	複雑流体中のキャビテーションの分子動力学シミュレーション	浅野 優太	東京大学物性研究所	Molecular dynamics simulation of cavitation in complex fluids	Yuta Asano	The University of Tokyo

No.	課題名	氏名	所属	Title	Name	Organization
235	全原子・粗視化力場によるソフトマターの分子シミュレーション	篠田 渉	名古屋大学大学院工学研究科	Molecular Simulation of Soft Materials using All-Atom and Coarse-Grained Force Field	Wataru Shinoda	Nagoya University
236	無秩序キタエフ模型の大規模並列計算によるO(N) 解法	藤本 聡	大阪大学基礎工学研究科	O(N) solution to the disordered Kitaev model using the large-scale parallel computing	Satoshi Fujimoto	Osaka University
237	環状鎖と線状鎖の混合系における二軸伸張流下のストレスオーバーシュート現象の確認	萩田 克美	防衛大学校応用科学群応用物理学科	Confirmation of stress-overshoot phenomena under biaxial elongational flow of ring-linear mixtures	Katsumi Hagita	National Defense Academy
238	分子動力学シミュレーションによるタンパク質集合体の離合集散の研究	奥村 久士	自然科学研究機構生命創成探究センター	Molecular dynamics simulations for assembly and disassembly of protein aggregates	Hisashi Okumura	Institute for Molecular Science
239	不純物の乱れから生じる隠れたSU(2) 対称反強磁性スピンの巨大磁気応答	諏訪 秀磨	東京大学大学院理学系研究科物理学専攻	Giant magnetic response of hidden SU(2) symmetric antiferromagnets induced by impurity disorder	Hidemaro Suwa	The University of Tokyo
240	有限温度フラストレート磁性体の物性解明	大久保 毅	東京大学大学院理学系研究科 物理学専攻	Finite temperature properties of frustrated spin systems	Tsuyoshi Okubo	The University of Tokyo
241	生体膜の構造形成	野口 博司	東京大学物性研究所	Structure formation of biomembrane	Hiroshi Noguchi	The University of Tokyo
242	マテリアルズ・インフォマティクスを用いた熱機能材料探索	塩見 淳一郎	東京大学工学系研究科	Development of Thermal Functional Materials Using Materials Informatics	Junichiro Shiomi	The University of Tokyo
243	蛋白質物性に強く関与するソフトモードの効率的サンプリングシミュレーション	北尾 彰朗	東京工業大学生命理工学院	Efficient sampling simulation of the soft modes significantly contribute to protein properties	Akio Kitao	The University of Tokyo
244	マルチスケール流動シミュレーション用プラットフォームを用いた流体-弾性体連成シミュレーション	川勝 年洋	東北大学大学院理学研究科物理学専攻	Fluid-elastomer hybrid simulations using multiscale simulation platform	Toshihiro Kawakatsu	Tohoku University
245	数値的手法によるトポロジカル相とバルクエッジ対応の研究：古典力学系から量子系まで	初貝 安弘	筑波大学大学院数理物質科学研究科物理学専攻	Numerical study of bulk-edge correspondence and topological phases: From quantum to classical mechanics	Yasuhiro Hatsugai	University of Tsukuba
246	新奇なランダムトポロジカル系の量子相転移	大槻 東巳	上智大学理工学部	Quantum phase transitions in novel disordered topological systems	Tomi Ohtsuki	Sophia University
247	新奇なランダム系の量子相転移	大槻 東巳	上智大学理工学部	Quantum phase transitions in novel disordered systems	Tomi Ohtsuki	Sophia University
248	生体膜の構造形成	野口 博司	東京大学物性研究所	Structure formation of biomembrane	Hiroshi Noguchi	The University of Tokyo
249	量子多体系におけるトポロジカルな秩序と量子ダイナミクス	藤堂 眞治	東京大学大学院理学系研究科物理学専攻	Topological Order and Quantum Dynamics in Quantum Many-body Systems	Syngé Todo	The University of Tokyo
250	マテリアルズ・インフォマティクスを用いた熱機能材料探索	塩見 淳一郎	東京大学工学系研究科	Development of Thermal Functional Materials Using Materials Informatics	Junichiro Shiomi	The University of Tokyo
251	拡張 Kitaev 模型におけるスピン動的構造因子	井戸 康太	東京大学物性研究所	Spin dynamical structure factor in extended Kitaev model	Kota Ido	The University of Tokyo

No.	課題名	氏名	所属	Title	Name	Organization
252	有限温度フラストレート磁性体の物性解明	大久保 毅	東京大学大学院理学系研究科 物理学専攻	Finite temperature properties of frustrated spin systems	Tsuyoshi Okubo	The University of Tokyo
253	フラストレート磁性体における新奇秩序	川村 光	公益財団法人豊田理化学研究所	Novel order in frustrated magnets	Hikaru Kawamura	Toyota Physical and Chemical Research Institute
254	拡張動的平均場理論による第一原理データと実験測定結果の自己無撞着解析	松本 宗久	高エネルギー加速器研究機構 物質構造科学研究所	Self-consistent analysis between ab initio data and experimental measurement results via extended dynamical mean field theory	Munehisa Matsumoto	Institute of Materials Structure Science, High Energy Accelerator Research Organization (KEK)
255	蛋白質物性に強く関与するソフトモードの効率的サンプリングシミュレーション	北尾 彰朗	東京工業大学生命理工学院	Efficient sampling simulation of the soft modes significantly contribute to protein properties	Akio Kitao	The University of Tokyo
256	拡張アンサンブル法による複雑系の研究	岡本 祐幸	名古屋大学大学院理学研究科	Study on complex systems by generalized-ensemble algorithms	Yuko Okamoto	Nagoya University
257	汎関数くりこみ群を用いたKitaevスピン液体の動力学的研究	加藤 雄介	東京大学総合文化研究科広域科学専攻 関連基礎科学系	Dynamics of Kitaev spin liquid via functional renormalization group method	Yusuke Kato	The University of Tokyo
258	両親媒性分子凝集体の大変形プロセス	樋口 祐次	東京大学物性研究所	Large deformation process of amphiphilic molecular aggregate	Yuji Higuchi	The University of Tokyo
259	2次元反強磁性体の巨大磁気応答における不純物効果	諏訪 秀磨	東京大学大学院理学系研究科物理学専攻	Impurity effect on giant magnetic response of a two-dimensional antiferromagnet	Hidemaro Suwa	The University of Tokyo
260	物質科学における並列ベイズ計算	福島 孝治	東京大学大学院総合文化研究科	Parallel Bayesian computation in material science	Koji Hukushima	The University of Tokyo
261	準結晶電子系における非平衡ダイナミクスの数値解析	古賀 昌久	東京工業大学	Numerical analysis for nonequilibrium dynamics in electronic systems on quasicrystals	Akihisa Koga	Tokyo Institute of Technology
262	蜂の巣格子拡張Kitaevモデルの基底状態相図 2	鈴木 隆史	兵庫県立大学 大学院工学研究科	Ground state phase diagram of extended Kitaev model II	Takafumi Suzuki	University of Hyogo
263	実験理論データ統合による最適化磁性材料設計	松本 宗久	高エネルギー加速器研究機構 物質構造科学研究所	Optimal design of magnetic materials via data integration between experiments and theory	Munehisa Matsumoto	Institute of Materials Structure Science, High Energy Accelerator Research Organization (KEK)
264	粗視化シミュレーションによる両親媒性分子の凝集プロセス	樋口 祐次	東京大学物性研究所	Self-assemble process of amphiphilic molecules by coarse-grained molecular dynamics simulation	Yuji Higuchi	The University of Tokyo
265	汎関数くりこみ群によるKitaevハイゼンベルグの動力学的研究	加藤 雄介	東京大学総合文化研究科広域科学専攻 関連基礎科学系	Functional renormalization group approach for dynamics of Kitaev-Heisenberg model	Yusuke Kato	The University of Tokyo
266	新型コロナウイルス感染症の治療薬開発に向けたタンパク質デザイン	新井 宗仁	東京大学大学院総合文化研究科	Protein design toward the development of therapeutic drugs for COVID-19	Munehito Arai	The University of Tokyo
267	フラストレート磁性体における新奇秩序	川村 光	公益財団法人豊田理化学研究所	Novel order in frustrated magnets	Hikaru Kawamura	Toyota Physical and Chemical Research Institute
268	量子多体系におけるトポロジカルな秩序と量子ダイナミクス	藤堂 眞治	東京大学大学院理学系研究科物理学専攻	Topological Order and Quantum Dynamics in Quantum Many-body Systems	Syngé Todo	The University of Tokyo

No.	課題名	氏名	所属	Title	Name	Organization
269	ポリマー材料の巨大熱物性データベースの機械学習支援開発	Liao Yuxuan	東京大学機械工学専攻	Machine-learning-assisted Development of Giant Thermal-Property Database for Polymer Materials	Yuxuan Liao	The University of Tokyo
270	非平衡定常系の大域的な熱力学関数	中川 尚子	茨城大学理学部	Global thermodynamic functions extended to nonequilibrium steady states	Naoko Nakagawa	Ibaraki University
271	S=2 反強磁性鎖における対称性に守られたトポロジカル相	坂井 徹	兵庫県立大学大学院物質理学研究科	Symmetry Protected Topological Phase of the S=2 antiferromagnetic chain	Toru Sakai	University of Hyogo
272	量子スピン系の低エネルギー状態に関する数値的研究	中野 博生	兵庫県立大学大学院物質理学研究科	Numerical study on low-energy states of quantum spin systems	Hiroki Nakano	University of Hyogo
273	フラストレーション系に現れる相転移と臨界現象の動的スケール解析	尾関 之康	電気通信大学情報理工学研究所	Dynamical scaling analysis for phase transitions and critical phenomena in frustrated systems	Yukiyasu Ozeki	The University of Electro-Communications
274	圧力下における Sr および Ag をドーピングした Bi ₂ Se ₃	Jeschke Harald	岡山大学異分野基礎科学研究所	Sr and Ag doped Bi ₂ Se ₃ under pressure	Harald Jeschke	Okayama University
275	高分子流体・固体のマルチスケールシミュレーション	村島 隆浩	東北大学大学院理学研究科	Multiscale simulation of polymeric fluids and solids	Takahiro Murashima	Tohoku University
276	マルチスケール流動シミュレーション用プラットフォームを用いた複雑流動の解析	川勝 年洋	東北大学大学院理学研究科物理学専攻	Analyses on complex fluids using multiscale simulation platform	Toshihiro Kawakatsu	Tohoku University
277	拡張アンサンブル法による複雑系の研究	岡本 祐幸	名古屋大学大学院理学研究科	Study on complex systems by generalized-ensemble algorithms	Yuko Okamoto	Nagoya University
278	磁場誘起スピンネマティック液体の数値対角化による研究	坂井 徹	兵庫県立大学大学院物質理学研究科	Numerical Diagonalization Study on the Field-Induced Spin Nematic Liquid	Toru Sakai	University of Hyogo
279	Numerical study of spin-nematic order in the S=1/2 J ₁ J ₂ K-Heisenberg model on the square lattice	ゴウケ マティアス	沖縄科学技術大学院大学	Numerical study of spin-nematic order in the S=1/2 J ₁ J ₂ K-Heisenberg model on the square lattice	Matthias Gohlke	Okinawa Institute of Science and Technology Graduate University
280	カゴメ格子上的 J ₁ -J ₂ 反強磁性体の古典モンテカルロ計算	品岡 寛	埼玉大学理学部物理学科	Classical Monte Carlo study of J ₁ -J ₂ Heisenberg antiferromagnet on the kagome lattice	Hiroshi Shinaoka	Saitama University
281	ポリマー材料の巨大熱物性データベースの機械学習支援開発	Liao Yuxuan	東京大学機械工学専攻	Machine-learning-assisted Development of Giant Thermal-Property Database for Polymer Materials	Yuxuan Liao	The University of Tokyo
282	擬1次元 Cr ニクタイトにおける超伝導の理論研究	Jeschke Harald	岡山大学異分野基礎科学研究所	Theory for Superconductivity in quasi-one-dimensional Cr-based pnictides	Harald Jeschke	Okayama University
283	産業や医療に有用な新規タンパク質の合理的設計	新井 宗仁	東京大学大学院総合文化研究科	Computational rational design of novel proteins for industrial and pharmaceutical applications	Munehito Arai	The University of Tokyo
284	フラストレートした量子磁性体に対する熱ゆらぎの効果	下川 統久朗	沖縄科学技術大学院大学	Thermal effects on quantum frustrated magnetisms	Tokuro Shimokawa	Okinawa Institute of Science and Technology Graduate University
285	フラストレーション系に現れる相転移と臨界現象の動的スケール解析 II	尾関 之康	電気通信大学情報理工学研究所	Dynamical scaling analysis for phase transitions and critical phenomena in frustrated systems II	Yukiyasu Ozeki	The University of Electro-Communications

No.	課題名	氏名	所属	Title	Name	Organization
286	蜂の巣格子上拡張Kitaevモデルの基底状態相図	鈴木 隆史	兵庫県立大学 大学院工学研究科	Ground-state phase diagram of extended Kitaev model on a honeycomb lattice	Takafumi Suzuki	University of Hyogo
287	準結晶系における新規秩序相と非平衡現象の探索	古賀 昌久	東京工業大学	Study of new ordered phase and nonequilibrium phenomena in quasicrystals	Akihisa Koga	Tokyo Institute of Technology
288	全原子分子動力学シミュレーションによる実在系バイオポリマーの力学的特性及び熱的特性発現の分子機構の解明	岡崎 進	東京大学大学院新領域創成科学研究科物質系専攻	Investigation of the molecular origins of the mechanical and thermal properties of realistic bio-polymers using all-atomistic molecular dynamics	Susumu Okazaki	The University of Tokyo
289	フラストレートした量子磁性体に対する熱ゆらぎの効果	下川 統久朗	沖縄科学技術大学院大学	Thermal effects on quantum frustrated magnetisms	Tokuro Shimokawa	Okinawa Institute of Science and Technology Graduate University
290	テンソルくりこみ群によるスピングラス研究	福島 孝治	東京大学大学院総合文化研究科	Tensor renormalization-group study of spin glasses	Koji Hukushima	The University of Tokyo
291	相転移キネティクスとポリアモルフィズム	淵崎 員弘	愛媛大学理工学研究科	Kinetics of phase transition and polyamorphism	Kazuhiro Fuchizaki	Ehime University
292	エンタングルメント最適化法の開発	原田 健自	京都大学大学院情報学研究科	Development of entanglement optimization method	Kenji Harada	Kyoto University
293	エンタングルメント最適化法の開発	原田 健自	京都大学大学院情報学研究科	Development of entanglement optimization method	Kenji Harada	Kyoto University
294	天然構造が極めて類似したタンパク質における熱変性の理論研究	吉留 崇	東北大学大学院工学研究科	A theoretical study for thermal unfolding of proteins with quite similar native structure	Takashi Yoshidome	Tohoku University
295	液体 BaTiO ₃ の分子動力学シミュレーション	橋本 保	産業技術総合研究所	Molecular dynamics simulation of liquid BaTiO ₃	Tamotsu Hashimoto	National Institute of Advanced Industrial Science and Technology (AIST)
296	量子スピン系の低エネルギー状態に関する数値的研究	中野 博生	兵庫県立大学大学院物質理学研究科	Numerical study on low-energy states of quantum spin systems	Hiroki Nakano	University of Hyogo
297	遠隔系間に光誘起されるフォノン量子もつれ状態のダイナミクス	石田 邦夫	宇都宮大学大学院工学研究科	Dynamics of phonon entanglement creation between remote electron-phonon systems	Kunio Ishida	Utsunomiya University
298	テンソルネットワーク法を用いた相転移・臨界現象の解明	森田 悟史	東京大学物性研究所	Study of phase transitions and critical phenomena by tensor network methods	Satoshi Morita	The University of Tokyo
299	拡張準古典方程式を用いた熱ホール効果の磁場依存性	北 孝文	北海道大学理学部物理学科	Magnetic field dependence of the thermal Hall effect based on the augmented quasiclassical equations	Takafumi Kita	Hokkaido University
300	フラストレート磁性体における多重q秩序状態のスピン伝導・熱伝導	青山 和司	大阪大学大学院理学研究科宇宙地球専攻	Transport properties of multiple-q states in frustrated magnets	Kazushi Aoyama	Osaka University
301	相転移キネティクスとポリアモルフィズム	淵崎 員弘	愛媛大学理工学研究科	Kinetics of phase transition and polyamorphism	Kazuhiro Fuchizaki	Ehime University
302	水と水溶液の大規模メタダイナミクスシミュレーション	灘 浩樹	産業技術総合研究所環境創生研究部門	Large-scale metadynamics simulations for water and aqueous solutions	Hiroki Nada	National Institute for Advanced Industrial Science and Technology

No.	課題名	氏名	所属	Title	Name	Organization
303	テンソルくりこみ群による相転移・臨界現象の解明	森田 悟史	東京大学物性研究所	Study of phase transitions and critical phenomena by tensor renormalization group	Satoshi Morita	The University of Tokyo
304	誤差付き有効モデル推定	田村 亮	国立研究開発法人 物質・材料研究機構	Effective model estimation with error bars	Ryo Tamura	National Institute for Materials Science
305	液膜破壊を伴う流動現象の分子動力学計算	渡辺 宙志	慶応義塾大学理工学部	Molecular Dynamics Study of Crown Formation During the Splash	Hiroshi Watanabe	Keio University
306	過飽和炭酸カルシウム水溶液に現れる多様なクラスター構造のメタダイナミクスシミュレーション解析	灘 浩樹	産業技術総合研究所環境創生研究部門	Metadynamics Simulation Analysis of Various Cluster Structures Appearing in Calcium Carbonate Supersaturated Solution	Hiroki Nada	National Institute for Advanced Industrial Science and Technology
307	結晶粒界・異相界面におけるフォノン散乱機構の系統的解析	藤井 進	ファインセラミックスセンターナノ構造研究所	Systematic Investigation on Phonon Transport at Nanoscale Interfaces	Susumu Fujii	Japan Fine Ceramics Center
308	非平衡分子動力学シミュレーションによるアミロイド線維破壊の研究	奥村 久士	自然科学研究機構生命創成探究センター	Disruption of amyloid fibril by nonequilibrium molecular dynamics simulations	Hisashi Okumura	Institute for Molecular Science
309	ハニカム格子上の多スピン交換模型における磁性	安田 千寿	琉球大学理学部	Magnetism in the multiple-spin exchange model on the honeycomb lattice	Chitoshi Yasuda	University of the Ryukyus
310	テンソルネットワーク法によるスピンの大きい量子系の相転移の研究	金子 隆威	近畿大学	Tensor-network study of phase transitions in large spin systems	Ryui Kaneko	Kinki University
311	ニューラルネットワークによる開放量子ダイナミクスの数値手法開発	吉岡 信行	理化学研究所	Developing numerical tool for open quantum dynamics based on neural networks	Nobuyuki Yoshioka	RIKEN
312	機械学習を用いたコード最適化の並列化の検討	渡辺 宙志	慶応義塾大学理工学部	Code Optimization using Machine Learning on Parallel Computer	Hiroshi Watanabe	Keio University
313	メゾスコピック素子における断熱ポンピングの理論	加藤 岳生	東京大学物性研究所	Theory of Adiabatic Pumping in Mesoscopic Devices	Takeo Kato	The University of Tokyo
314	金属のフェムト秒赤外発光の統一理解	小野 頌太	岐阜大学	Unified understanding of the femtosecond infrared luminescence for metals	Shota Ono	Gifu University
315	ハニカム格子上の多スピン交換模型における磁性	安田 千寿	琉球大学理学部	Magnetism in the multiple-spin exchange model on the honeycomb lattice	Chitoshi Yasuda	University of the Ryukyus
316	Z_2 渦トポロジカル転移のテンソル繰り込みによる研究	押川 正毅	東京大学物性研究所	An exploration of the topological phase transition driven by Z_2 vortex with Tensor Network Renormalization	Masaki Oshikawa	The University of Tokyo
317	双極子相互作用が存在する磁性薄膜における非平衡状態の磁気構造	小松 尚登	物質・材料研究機構	Magnetic structures under the non-equilibrium state of the magnetic thin films with the dipolar interaction	Hisato Komatsu	National Institute for Materials Science
318	磁性体における相転移に伴うスピン伝導	青山 和司	大阪大学大学院理学研究科宇宙地球専攻	Spin transport near a phase transition in magnets	Kazushi Aoyama	Osaka University
319	イジングマシンにおける新規アルゴリズム構築	田中 宗	慶応義塾大学理工学部物理情報工学科	Building Algorithms for Ising Machines	Shu Tanaka	Keio University

No.	課題名	氏名	所属	Title	Name	Organization
320	遠隔系間に光誘起されるフォノン量子もつれ状態のダイナミクス	石田 邦夫	宇都宮大学大学院工学研究科	Dynamics of phonon entanglement creation between remote electron-phonon systems	Kunio Ishida	Utsunomiya University
321	ペーストの流れの記憶の多様性	中原 明生	日本大学理工学部 一般教育教室 (物理)	Diversity in memory effects of flow in paste	Akio Nakahara	Nihon University
322	近藤量子ドットを介した断熱電荷ポンピングの数値計算	加藤 岳生	東京大学物性研究所	Numerical Study of Adiabatic Charge Pumping through Kondo Quantum Dots	Takeo Kato	The University of Tokyo
323	量子パイロクロア磁性体の磁気励起研究	佐藤 卓	東北大学多元物質科学研究所	Magnetic excitations in the quantum pyrochlore magnet	Taku Sato	Tohoku University
324	厳密対角化と TPQ 法による量子パイロクロア磁性体の研究	門脇 広明	首都大学東京 理工学研究科 物理学専攻	Exact diagonalization and TPQ of quantum pyrochlore model	Hiroaki Kadowaki	Tokyo Metropolitan University
325	スパース推定による広域 X 線吸収微細構造計測の解析手法の確立	熊添 博之	熊本大学パルスパワー科学研究所	Establishment of new analysis method for extend X-ray absorption fine structure with sparse modeling	Hiroyuki Kumazoe	Kumamoto University
326	高分子流体・固体のマルチスケールシミュレーション	村島 隆浩	東北大学大学院理学研究科	Multiscale simulation of polymeric fluids and solids	Takahiro Murashima	Tohoku University
327	1次元フラストレート量子スピン系の数値的研究	飛田 和男	埼玉大学大学院理工学研究科物質科学部門	Numerical Study of One Dimensional Frustrated Quantum Spin Systems	Kazuo Hida	Saitama University
328	質量保存型反応拡散系の粗大化ダイナミクス	舘野 道雄	東京大学 大学院総合文化研究科	Coarsening mechanism in mass-conserved reaction diffusion systems	Michio Tateno	The University of Tokyo
329	コロイド粒子系に関する分子シミュレーション	寺尾 貴道	岐阜大学工学部	Molecular simulation of colloidal particles	Takamichi Terao	Gifu University
330	高密度剛体球系における非平衡相転移と遅い緩和	磯部 雅晴	名古屋工業大学	Nonequilibrium phase transition and slow dynamics in the dense hard sphere systems	Masaharu Isobe	Nagoya Institute of Technology
331	非平衡環境と接した定常状態の普遍的性質の解明	白井 達彦	早稲田大学基幹理工学部	Universal properties of non-equilibrium steady states	Tatsuhiko Shirai	Waseda University
332	ソフトマテリアルの秩序構造とそのダイナミクス, 光学的性質の計算	福田 順一	九州大学 大学院理学研究院	Calculation of ordered structures, dynamics and optical properties of soft materials	Jun-ichi Fukuda	Kyushu University
333	厳密対角化による量子パイロクロア磁性体の研究	門脇 広明	首都大学東京 理工学研究科 物理学専攻	Exact diagonalization of quantum pyrochlore model	Hiroaki Kadowaki	Tokyo Metropolitan University
334	空間構造をもつ一次元量子スピン系の数値的研究	利根川 孝	神戸大学大学院理学研究科	Numerical Study of the One-Dimensional Quantum Spin Systems with Spatial Structures	Takashi Tonegawa	Kobe University
335	非平衡定常系の大域的な熱力学関数	中川 尚子	茨城大学理学部	Global thermodynamic functions extended to nonequilibrium steady states	Naoko Nakagawa	Ibaraki University
336	ケージドルシフェリン化合物およびその共役酸・塩基の電子励起状態	樋山 みやび	群馬大学	Theoretical study for caged compound and its conjugate acid/bases	Miyabi Hiyama	Gunma University

No.	課題名	氏名	所属	Title	Name	Organization
337	ソフトマテリアルの秩序構造とそのダイナミクス, 光学的性質の計算	福田 順一	九州大学 大学院理学研究院	Calculation of ordered structures, dynamics and optical properties of soft materials	Jun-ichi Fukuda	Kyushu University
338	Z ₂ 渦トポロジカル転移のテンソル繰り込みによる研究	押川 正毅	東京大学物性研究所	An exploration of the topological phase transition driven by Z ₂ vortices with Tensor Network Renormalization	Masaki Oshikawa	The University of Tokyo
339	超構造によるバンドエンジニアリングとその応用	苅宿 俊風	物材機構	Superstructure based band engineering and its application	Toshikaze Kariyado	NIMS
340	コロイド粒子系に関する分子シミュレーション	寺尾 貴道	岐阜大学工学部	Molecular simulation of colloidal particles	Takamichi Terao	Gifu University
341	Kitaev スピン液体のスピンゼーベック効果の数値計算	山田 昌彦	大阪大学基礎工学研究科	Numerical simulation of the spin Seebeck effect in Kitaev spin liquids	Masahiko Yamada	Osaka University
342	摩擦の物理	松川 宏	青山学院大学理工学部	Physics of Friction	Hiroshi Matsukawa	Aoyama Gakuin University
343	空間構造をもつ一次元量子スピン系の数値的研究	利根川 孝	神戸大学大学院理学研究科	Numerical Study of the One-Dimensional Quantum Spin Systems with Spatial Structures	Takashi Tonegawa	Kobe University
344	Phase field 法による多細胞シミュレーション	館野 道雄	東京大学 大学院総合文化研究科	Multicellular simulation by phase field method	Michio Tateno	The University of Tokyo
345	球体カゴメ系 (W ₇₂ V ₃₀) の状態密度, 動的構造因子の計算	福元 好志	東京理科大学	Exact diagonalization calculations of density of states and dynamical structure factor for the spherical-kagome spin-system {W ₇₂ V ₃₀ }	Fukumoto Yoshiyuki	Tokyo University of Science
346	サイト変調された揺らぎを用いたアニーリング技術の創出	白井 達彦	早稲田大学基幹理工学部	Quantum annealing with inhomogeneous fluctuations	Tatsuhiko Shirai	Waseda University
347	二次元物質の積層を中心とした超構造による新奇物性探索	苅宿 俊風	物材機構	Study of superstructure induced novel phenomena: stacking of atomically thin materials	Toshikaze Kariyado	NIMS
348	タンパク質動的プロセス解析法: 低温電子顕微鏡実験と分子シミュレーションの統合	吉留 崇	東北大学大学院工学研究科	A Method for Analyzing Protein Dynamics: A Hybrid of Cryo-Electron Microscopy Experiment and Molecular Simulation	Takashi Yoshidome	Tohoku University
349	量子アニーリング機械を目指した近接相互作用量子ビット系のパルス操作による全結合実装方式の検討	棚本 哲史	帝京大学	All to all connections in two dimensional qubit array with two-body interactions aiming at quantum annealing machine	Tetsufumi Tanamoto	Teikyo University
350	金属のフェムト秒赤外発光の統一理解 II	小野 頌太	岐阜大学	Unified understanding of the femtosecond infrared luminescence for metals: II	Shota Ono	Gifu University
351	1次元フラストレート量子スピン系の数値的研究	飛田 和男	埼玉大学大学院理工学研究科物質科学部門	Numerical Study of One Dimensional Frustrated Quantum Spin Systems	Kazuo Hida	Saitama University
352	空間反転対称な遍歴磁性体における多重ヘリカルスピン密度波	内田 尚志	北海道科学大学	Multiple helical spin density waves in inversion-symmetric itinerant magnets	Takashi Uchida	Hokkaido University of Science
353	球体カゴメ系 (W ₇₂ V ₃₀) の磁気的性質へのランダムネスの効果	福元 好志	東京理科大学	Effects of exchange randomness on magnetic properties of a spherical-kagome spin-system {W ₇₂ V ₃₀ }	Fukumoto Yoshiyuki	Tokyo University of Science

No.	課題名	氏名	所属	Title	Name	Organization
354	駆動力に対する込み合い細胞運動の応答理論の構築	松下 勝義	大阪大学理学研究科	Construction of Response Theory for Motion of Crowding Cells	Katsuyoshi Matsushita	Osaka University
355	X線結晶構造解析における2波近似理論の破れの研究	沖津 康平	東京大学 大学院工学系研究科	Study on bankruptcy of the two-beam approximation in X-ray crystal structure analysis	Kouhei Okitsu	School of Engineering, The University of Tokyo
356	時間反転対称性の破れた超伝導体接合の数値解析法の研究	田沼 慶忠	秋田大学大学院理工学研究科	Study on numerical analysis method of superconducting junctions with broken time reversal symmetry states	Yasunari Tanuma	Akita University
357	量子パイロクロア磁性体の磁気励起研究	佐藤 卓	東北大学多元物質科学研究所	Magnetic excitations in the quantum pyrochlore magnet	Taku Sato	Tohoku University
358	温度勾配のある系の非平衡定常状態の分子動力学計算	羽田野 直道	東京大学生産技術研究所	Molecular Dynamics Calculation of Non-equilibrium Steady State in Systems with Temperature Gradient	Naomichi Hatano	The University of Tokyo
359	タンパク質中の不均一な熱輸送物性の解析	倭 剛久	名古屋大学	Non-uniform thermal transport properties in proteins	Takahisa Yamato	Nagoya University
360	ホタル生物発光関連分子の吸収/蛍光スペクトル解析	樋山 みやび	群馬大学	Theoretical analysis for photo absorption- and emission spectra for firefly bioluminescence related molecules	Miyabi Hiyama	Gunma University
361	固有値ソルバの統一的インターフェース Rokko の開発と量子スピン系への応用	坂下 達哉	玉川大学	Development of integrated interface of eigensolvers Rokko and application to quantum spin systems	Tatsuya Sakashita	Tamagawa University
362	DNAの引っ張りシミュレーションによる巻き戻し機構の解明	水口 朋子	京都工芸繊維大学	DNA unwinding mechanism studied by steered molecular dynamics simulations	Tomoko Mizuguchi	Kyoto Institute of Technology
363	集団運動での細胞込み合い状況下での多体効果	松下 勝義	大阪大学理学研究科	Many body effects in the collective motion of crowding cells	Katsuyoshi Matsushita	Graduate School of Science, Osaka University
364	固有値ソルバの統一的インターフェース Rokko の開発と量子スピン系への応用	坂下 達哉	玉川大学	Development of integrated interface of eigensolvers Rokko and application to quantum spin systems	Tatsuya Sakashita	Tamagawa University
365	二次元遍歴磁性体における多重Q状態	内田 尚志	北海道科学大学	Multiple-Q states in two-dimensional itinerant magnets	Takashi Uchida	Hokkaido University of Science

令和2年度 スーパーコンピュータ計算物質科学スパコン共用事業課題一覧
/ Supercomputing Consortium for Computational Materials Science Project List of Supercomputer System 2020

前期 / The first half term							
No.	課題名	氏名	所属		Title	Name	Organization
1	低次元過冷却液体における粘弾性緩和の大規模分子動力学計算	芝 隼人	東京大学	情報基盤センタ	Large-scale molecular dynamics simulation of viscoelastic relaxation in a two-dimensional supercooled liquid	Hayato Shiba	The University of Tokyo
2	物質設計に向けた Wannier 関数データベースの作成	吉見 一慶	東京大学	物性研究所	Creating a Wannier function database toward material design	Kazuyoshi Yoshimi	The University of Tokyo
3	鉄系超伝導体関連物質の系統的な低エネルギー有効モデル導出・解析	三澤 貴宏	東京大学	物性研究所	Systematic derivation and analysis of low-energy effective models for iron based superconductors and related materials	Takahiro Misawa	The University of Tokyo
4	大規模 GW/BSE 法による有機薄膜太陽電池の光電変換過程の解析	藤田 貴敏	分子科学研究所		Investigation of charge photogeneration process in organic thin film solar cells by large-scale GW/Bethe-Salpeter equation method	Takatoshi Fujita	Institute for Molecular Science
5	二次電池材料の電子論	小口 多美夫	大阪大学	産業科学研究所	Electron Theory on Secondary-Battery Materials	Tamio Oguchi	Osaka University
6	貴金属フリーの汎用元素ナノ触媒に向けた第一原理計算	武次 徹也	北海道大学	大学院理学研究院	Ab initio study toward abundant element nanocatalysts with less precious metals	Tetsuya Taketsugu	Hokkaido University
7	大規模計算とデータ駆動手法による高性能永久磁石の開発	三宅 隆	産業技術総合研究所		Development of high-performance permanent magnets by large-scale simulation and data-driven approach	Takashi Miyake	National Institute of Advanced Industrial Science and Technology
8	ナトリウムイオン電池用水系電解液のイオン輸送機構の理論的解析	山田 淳夫	東京大学	大学院工学系研究科	Theoretical analysis on ion conduction mechanism in aqueous electrolytes for sodium-ion battery	Atsuo Yamada	The University of Tokyo
9	量子ビーム実験と第一原理計算の融合による磁性材料の最適化	小野 寛太	高エネルギー加速器研究機構		Optimized design of magnetic materials based on the integration between quantum beam experiment and first-principles calculation	Kanta Ono	High Energy Accelerator Research Organization
10	3次元量子スピン液体の追究	今田 正俊	早稲田大学 / 豊田理化学研究所		Studies on quantum spin liquids in three dimensions	Masatoshi Imada	Waseda University/Toyota Physical and Chemical Research Institute
11	省エネルギー次世代半導体デバイス開発のための量子論マルチシミュレーション	押山 淳	名古屋大学	未来材料・システム研究所	Quantum-theory-based multiscale simulation for next-generation power devices	Atsushi Oshiyama	Nagoya University
後期 / The second half term							
12	メソスケール全原子分子動力学フレームワーク開発	芝 隼人	東京大学	情報基盤センタ	Development of all atom molecular simulation framework on a mesoscale	Hayato Shiba	The University of Tokyo
13	フラグメント分割型 GW/BSE 法による有機太陽電池の電荷分離過程の解析	藤田 貴敏	分子科学研究所		Computational Investigation of Charge Photogeneration in Organic Solar Cells by Fragment-Based GW/BSE Method	Takatoshi Fujita	Institute for Molecular Science

14	ハイドレートメルト電解液の特異なイオン輸送機構の理論的解析	山田 淳夫	東京大学	大学院工学系研究科	Theoretical Analysis of Unusual Ion Transport Mechanism in Hydrate Melt Electrolyte	Atsuo Yamada	The University of Tokyo
15	機械学習による超伝導機構の解析	今田 正俊	早稲田大学 / 豊田理化学研究所		Analyses on Superconducting Mechanism by Machine Learning	Masatoshi Imada	Waseda University/Toyota Physical and Chemical Research Institute
16	省エネルギー次世代半導体デバイス開発のための量子論マルチシミュレーション	押山 淳	名古屋大学	未来材料・システム研究所	Quantum-theory-based multiscale simulation for next-generation power devices	Atsushi Oshiyama	Nagoya University
17	全原子分子動力学シミュレーションを用いた chain-increment 法によるポリマーブレンド相溶性評価	松林 伸幸	大阪大学	大学院基礎工学研究科	Evaluation of the polymer blend miscibility by using chain-increment method with all-atom molecular dynamics simulation	Nobuyuki Matubayasi	Osaka University
18	磁性材料の第一原理計算	合田 義弘	東京工業大学	物質理工学院	First-principles study of magnetic materials	Yoshihiro Gohda	Tokyo Institute of Technology
19	遷移金属酸化物材料の機能性	杉野 修	東京大学	物性研究所	Functionality of transition metal oxides	Osamu Sugino	The University of Tokyo
20	大規模数値計算による高性能永久磁石の開発	福島 鉄也	東京大学	物性研究所	Large-scale simulation for permanent magnets	Tetsuya Fukushima	The University of Tokyo
21	全固体ナトリウム金属電池創成のための新規塩化物固体電解質材料の探索	中山 将伸	名古屋工業大学		Novel chloride solid electrolytes for all solid-state sodium metal battery	Masanobu Nakayama	Nagoya Institute of Technology

Publications

Division of Condensed Matter Science

Takigawa group

We have been performing nuclear magnetic resonance experiments on various quantum spin systems and strongly correlated electron systems to explore novel quantum phases with exotic ordering and fluctuation phenomena. The major achievements in the year 2020 include: (1) development of systematic methods to identify symmetries of ordered phases with electronic multipoles from the angle dependence of the NMR Knight shift and their application to ^{111}Cd -NMR measurements in the spin-orbit coupled metallic pyrochlore compound $\text{Cd}_2\text{Re}_2\text{O}_7$, (2) quantitative determination of magnetic-field-induced dipolar and octupolar moments in the low-temperature ordered phases of the $5d$ double-perovskite oxide $\text{Ba}_2\text{MgReO}_6$ based on the ^{17}O NMR experiments. In this material, strong spin-orbit coupling combined with the cubic crystal field generates a quartet ground state with $J_{\text{eff}} = 3/2$, providing ideal platform to explore multipolar order of t_{2g} electron systems.

1. *Field-Orientation Effect on Ferro-Quadrupole Order in $\text{PrTi}_2\text{Al}_{20}$: S. Kittaka, T. Taniguchi, K. Hattori, S. Nakamura, T. Sakakibara, M. Takigawa, M. Tsujimoto, A. Sakai, Y. Matsumoto and S. Nakatsuji, *J. Phys. Soc. Jpn.* **89**, 043701(1-4) (2020).
2. Regular-triangle trimer and charge order preserving the Anderson condition in the pyrochlore structure of CsW_2O_6 : Y. Okamoto, H. Amano, N. Katayama, H. Sawa, K. Niki, R. Mitoka, H. Harima, T. Hasegawa, N. Ogita, Y. Tanaka, M. Takigawa, Y. Yokoyama, K. Takehana, Y. Imanaka, Y. Nakamura, H. Kishida and K. Takenaka, *Nat Commun* **11**, 3144-1-8 (2020).
3. *Pressure-induced phase transition in the J_1 - J_2 square lattice antiferromagnet $\text{RbMoOPO}_4\text{Cl}$: H. Takeda, T. Yamauchi, M. Takigawa, H. Ishikawa and Z. Hiroi, *Phys. Rev. B* **103**, 104406 (2021).
4. * $\text{PrTi}_2\text{Al}_{20}$ における強四極子秩序変数の磁場によるスイッチング - 磁場に依存する四極子間相互作用について -: 谷口 貴紀, 服部 一匡, 橋高 俊一郎, 瀧川 仁, *固体物理* **55**, 245-264 (2020).

Sakakibara group

We investigated the magnetic phase transitions of the cubic chiral magnet EuPtSi by means of high-precision magnetization measurements and established the magnetic phase diagrams. The incommensurate-commensurate transition in the helical state with a tiny change in the propagation vectors was detected exclusively by the magnetization along the [111] direction. The transition temperature T_N^* shifted to lower temperature with increasing $H // [111]$. The ground-state magnetizations of the helical state for $H // [100]$ and $[111]$ were examined at temperatures below 100 mK. We found evidence that the q vectors pinned to the lattice at low fields were depinned by increasing fields above 10 kOe and gradually rotated towards the field directions. Metastable skyrmion phase can be created at 60 mK by slowly cooling in a field. We obtained the ground-state magnetization of the skyrmion lattice state, showing a sharp tilted plateau structure. The transitions from the skyrmion phase to the conical phase by changing fields were perfectly discontinuous at 60 mK possibly because of the supercooled dynamics.

1. ^{105}Pd NMR and NQR study of the cubic heavy fermion system $\text{Ce}_3\text{Pd}_{20}\text{Si}_6$: I. Jakovac, M. Horvatic, E. F. Schwier, A. Prokofiev, S. Paschen, H. Mitamura, T. Sakakibara and M. S. Grbic, *J. Phys.: Condens. Matter* **32**, 245601(1-7) (2020).
2. *Field-Orientation Effect on Ferro-Quadrupole Order in $\text{PrTi}_2\text{Al}_{20}$: S. Kittaka, T. Taniguchi, K. Hattori, S. Nakamura, T. Sakakibara, M. Takigawa, M. Tsujimoto, A. Sakai, Y. Matsumoto and S. Nakatsuji, *J. Phys. Soc. Jpn.* **89**, 043701(1-4) (2020).
3. †Heavy Fermion State of YbNi_2Si_3 without Local Inversion Symmetry: S. Nakamura, K. Hyodo, Y. Matsumoto, Y. Haga, H. Sato, S. Ueda, K. Mimura, K. Saiki, K. Iso, M. Yamashita, S. Kittaka, T. Sakakibara and S. Ohara, *J. Phys. Soc. Jpn.* **89**, 024705(1-5) (2020).
4. *Kitaev Spin Liquid Candidate Os_xCl_3 Comprised of Honeycomb Nano-Domains: K. Kataoka, D. Hirai, T. Yajima, D. Nishio-Hamane, R. Ishii, K.-Y. Choi, D. Wulferding, P. Lemmens, S. Kittaka, T. Sakakibara, H. Ishikawa, A. Matsuo, K. Kindo and Z. Hiroi, *J. Phys. Soc. Jpn.* **89**, 114709(1-9) (2020).

* Joint research among groups within ISSP.

5. †*Emergent spin-1 Haldane gap and ferroelectricity in a frustrated spin- 1/2 ladder: H. Ueda, S. Onoda, Y. Yamaguchi, T. Kimura, D. Yoshizawa, T. Morioka, M. Hagiwara, M. Hagihala, M. Soda, T. Masuda, T. Sakakibara, K. Tomiyasu, S. Ohira-Kawamura, K. Nakajima, R. Kajimoto, M. Nakamura, Y. Inamura, N. Reynolds, M. Frontzek, J. S. White, M. Hase and Y. Yasui, *Phys. Rev. B* **101**, 140408(1-6) (2020).
6. †Fully gapped superconductivity without sign reversal in the topological superconductor PbTaSe₂: Y. Sun, S. Kittaka, T. Sakakibara, K. Machida, R. Sankar, X. Xu, N. Zhou, X. Xing, Z. Shi, S. Pyon and T. Tamegai, *Phys. Rev. B* **102**, 024517(1-7) (2020).
7. †Magnetic properties of a spin-1/2 honeycomb lattice antiferromagnet: Y. Kono, T. Okabe, N. Uemoto, Y. Iwasaki, Y. Hosokoshi, S. Kittaka, T. Sakakibara and H. Yamaguchi, *Phys. Rev. B* **101**, 014437(1-6) (2020).
8. †Magnetic properties of a spin-2 antiferromagnet with metal-radical hybrid spins: Y. Iwasaki, T. Okabe, N. Uemoto, Y. Kono, Y. Hosokoshi, S. Nakamura, S. Kittaka, T. Sakakibara, M. Hagiwara, T. Kawakami and H. Yamaguchi, *Phys. Rev. B* **101**, 174412(1-6) (2020).
9. †Synthesis and Magnetic Properties of M²⁺Ti⁴⁺ Substituted Ba₁₂Fe₂₈Ti₁₅O₈₄: N. Yasuda, S. Kittaka, Y. Kono, T. Sakakibara, K. Kakizaki and K. Kamishima, *J. Magn. Soc. Jpn.* **44**, 2005R004(1-5) (2020).
10. *Magnetization and Thermal Expansion Properties of Quantum Spin Ice Candidate Pr₂Zr₂O₇: N. Tang, A. Sakai, K. Kimura, S. Nakamura, M. Fu, Y. Matsumoto, T. Sakakibara and S. Nakatsuji, *JPS Conf. Proc.* **30**, 011090(1-6) (2020).
11. *Single Crystal Growth and Unique Electronic States of Cubic Chiral EuPtSi and Related Compounds: Y. Ônuki, M. Kakihana, W. Iha, K. Nakaima, D. Aoki, A. Nakamura, F. Honda, M. Nakashima, Y. Amako, J. Gouchi, Y. Uwatoko, S. Nakamura, T. Sakakibara, T. Takeuchi, Y. Haga, H. Ikeda, H. Harima, M. Hedo and T. Nakama, *JPS Conf. Proc.* **29**, 012001(1-9) (2020).
12. *Unique Skyrmion Phases and Conduction Electrons in Cubic Chiral Antiferromagnet EuPtSi and Related Compounds: Y. Ônuki, M. Kakihana, W. Iha, K. Nakaima, D. Aoki, A. Nakamura, F. Honda, M. Nakashima, Y. Amako, J. Gouchi, Y. Uwatoko, S. Nakamura, T. Sakakibara, T. Takeuchi, Y. Haga, H. Ikeda, H. Harima, M. Hedo and T. Nakama, *JPS Conf. Proc.* **30**, 011008(1-11) (2020).
13. *Improved accuracy in high-frequency AC transport measurements in pulsed high magnetic fields: H. Mitamura, R. Watanuki, E. Kampert, T. Förster, A. Matsuo, T. Onimaru, N. Onozaki, Y. Amou, K. Wakiya, K. T. Matsumoto, I. Yamamoto, K. Suzuki, S. Zherlitsyn, J. Wosnitza, M. Tokunaga, K. Kindo and T. Sakakibara, *Review of Scientific Instruments* **91**, 125107/1-25 (2020).
14. Orientation of point nodes and nonunitary triplet pairing tuned by the easy-axis magnetization in UTe₂: S. Kittaka, Y. Shimizu, T. Sakakibara, A. Nakamura, D. Li, Y. Homma, F. Honda, D. Aoki and K. Machida, *Phys. Rev. Research* **2**, 032014(R)(1-6) (2020).
15. †Evidence for nematic superconductivity of topological surface states in PbTaSe₂: T. Le, Y. Sun, H.-K. Jin, L. Che, L. Yin, J. Li, G. Pang, C. Xu, L. Zhao, S. Kittaka, T. Sakakibara, K. Machida, R. Sankar, H. Yuan, G. Chen, X. Xu, S. Li, Y. Zhou and X. Lu, *Science Bulletin* **65**, 1349-1355 (2020).
16. *PrTi₂Al₂₀における強四極子秩序変数の磁場によるスイッチング - 磁場に依存する四極子間相互作用について -: 谷口 貴紀, 服部 一匡, 橘高 俊一郎, 瀧川 仁, *固体物理* **55**, 245-264 (2020).

Mori group

We have successfully developed and unveiled unprecedented functional properties for the molecular materials and systems. The major achievements in 2020 are (1) to establish the molecular design strategy of anhydrous base-acid-type organic proton conductors as an electrolyte of a fuel cell for medium temperatures, (2) to investigate the alkyl-chain-length effect of the transistor properties for anthracene-based organic semiconductors, and (3) to develop the Zn complex with vapochromism induced by intermolecular electron transfer coupled with hydrogen-bond formation.

1. †Anhydrous Purely Organic Solid-State Proton Conductors: Effects of Molecular Dynamics on the Proton Conductivity of Imidazolium Hydrogen Dicarboxylates: Y. Sunairi, S. Dekura, A. Ueda, T. Ida, M. Mizuno and H. Mori, *J. Phys. Soc. Jpn.* **89**, 051008 (2020).
2. 水素科学の最前線、新学術領域研究「ハイドロジェノミクス」の挑戦—高速・局所移動水素と電子とのカップリングによる新発想デバイスの設計：森 初果, までりあ **60**, 165-168 (2020).
3. *A computational examination of the electric-field-induced proton transfer along the interface hydrogen bond between proton donating and accepting self-assembled monolayers: Y. Kanematsu, H. S. Kato, S. Yoshimoto, A. Ueda,

† Joint research with outside partners.

S. Yamamoto, H. Mori, J. Yoshinobu, I. Matsuda and M. Tachikawa, Chem. Phys. Lett. **741**, 137091 (2020).

- *Vapochromism induced by intermolecular electron transfer coupled with hydrogen-bond formation in zinc dithiolene complex: T. Fujino, M. Kawamura, T. Ozaki and H. Mori, J. Mater. Chem. C **8**, 14939-14947 (2020).
- * 水素を活かすセラミックス プロトン-電子カップル型分子性結晶および二分子膜における機能開拓: 森 初果, 加藤 浩之, 藤野 智子, 上田 顕, 吉信 淳, セラミックス **56**, 88-91 (2021).
- Effect of Alkyl Chain Length on Charge Transport Property of Anthracene-Based Organic Semiconductors: D. Zhang, S. Yokomori, R. Kameyama, C. Zhao, A. Ueda, L. Zhang, R. Kumai, Y. Murakami, H. Meng and H. Mori, ACS Appl. Mater. Interfaces **13**, 989 (2021).
- Terahertz-field-induced polar charge order in electronic-type dielectrics: H. Yamakawa, T. Miyamoto, T. Morimoto, N. Takamura, S. Liang, H. Yoshimochi, T. Terashige, N. Kida, M. Suda, H. M. Yamamoto, H. Mori, K. Miyagawa, K. Kanoda and H. Okamoto, Nat Commun **12**, 953 (2021).
- *The Simplest Model for Doped Poly(3,4-ethylenedioxythiophene) (PEDOT): Single-crystalline EDOT Dimer Radical Cation Salts: R. Kameyama, T. Fujino, S. Dekura, M. Kawamura, T. Ozaki and H. Mori, Chem. Eur. J. **27**, 6696 (2021).
- Modulation of the Electronic States and Magnetic Properties of Nickel Catecholdithiolene Complex by Oxidation-coupled Deprotonation: S. Yokomori, S. Dekura, A. Ueda, R. Kumai, Y. Murakami and H. Mori, J. Mater. Chem. C (2021), accepted for publication.

Osada group

The nonlinear anomalous Hall effect (AHE) was realized in organic conductors for the first time. First, using interlayer magnetotransport, we experimentally confirmed that the weak charge ordering (CO) state of a layered organic conductor α -(BEDT-TTF)₂I₃ is a two-dimensional massive Dirac fermion (DF) state with a pair of tilted gapped Dirac cones with finite Berry curvature dipole. Next, we showed that the nonlinear AHE is measurable in the current-carrying state of this massive DF system, where the Berry curvature balance is broken between two Dirac cones due to non-equilibrium distribution. In addition, we proposed the current-field-cooling technique, which enhances the formation of single type of CO domains in experiments. Finally, we performed the transport measurement of α -(BEDT-TTF)₂I₃ in the weak CO state at 1.25GPa, and extracted nonlinear signal from current-reversed data. We successfully observed nonlinear AHE with estimated order and its rectifying characteristics.

- Possible Current-Induced Phenomena and Domain Control in an Organic Dirac Fermion System with Weak Charge Ordering: T. Osada and A. Kiswandhi, J. Phys. Soc. Jpn. **89**, 103701/1-5 (2020).
- Experimental Confirmation of Massive Dirac Fermions in Weak Charge-Ordering State in α -(BEDT-TTF)₂I₃: K. Yoshimura, M. Sato and T. Osada, J. Phys. Soc. Jpn. **90**, 033701/1-5 (2021).
- Possible Nonlinear Anomalous Thermoelectric Effect in Organic Massive Dirac Fermion System: T. Osada and A. Kiswandhi, J. Phys. Soc. Jpn. **90**, 053704/1-5 (2021).
- 黒リン超薄膜の電子構造と物性: 長田 俊人, 「グラフェンから広がる二次元物質の新技术と応用」, 第6章10節, 吾郷浩樹・齋藤理一郎, (エヌ・ティー・エス, 東京, 2020), 437-443.

Yamashita group

We have been studying (1) quantum criticality in heavy-fermion materials by ultralow temperature cryostat, (2) thermal-Hall conductivity of exotic excitations in frustrated magnets and (3) a new technique for the study of strongly-correlated electron systems. In this year, we have performed (1) developments of ultralow-temperature measurements of thermal expansion of CeCoIn₅ and resistivity of YbRh₂Si₂, (2) thermal-Hall measurements of Neel-type skyrmions in GaV₄Se₈, and (3) spintronic superconductor in EuSn₂As₂.

- Thermal-transport studies of kagomé antiferromagnets: M. Yamashita, M. Akazawa, M. Shimozawa, T. Shibauchi, Y. Matsuda, H. Ishikawa, T. Yajima, Z. Hiroi, M. Oda, H. Yoshida, H.-Y. Lee, J. H. Han and N. Kawashima, J. Phys.: Condens. Matter **32**, 074001 (2020).
- †*Heavy Fermion State of YbNi₂Si₃ without Local Inversion Symmetry: S. Nakamura, K. Hyodo, Y. Matsumoto, Y. Haga, H. Sato, S. Ueda, K. Mimura, K. Saiki, K. Iso, M. Yamashita, S. Kittaka, T. Sakakibara and S. Ohara, J. Phys. Soc. Jpn. **89**, 024705(1-5) (2020).
- Presence and absence of itinerant gapless excitations in the quantum spin liquid candidate EtMe₃Sb[Pd(dmit)₂]₂: M. Yamashita, Y. Sato, T. Tominaga, Y. Kasahara, S. Kasahara, H. Cui, R. Kato, T. Shibauchi and Y. Matsuda, Phys.

* Joint research among groups within ISSP.

Rev. B **101**, 140407(R) (2020).

4. *Sample dependence of half-integer quantized thermal Hall effect in the Kitaev spin-liquid candidate α -RuCl₃: M. Yamashita, J. Gouchi, Y. Uwatoko, N. Kurita and H. Tanaka, Phys. Rev. B **102**, 220404(R) (2020).
5. †Ultralow temperature NMR of CeCoIn₅: M. Yamashita, M. Tashiro, K. Saiki, S. Yamada, M. Akazawa, M. Shimozawa, T. Taniguchi, H. Takeda, M. Takigawa and H. Shishido, Phys. Rev. B **102**, 165154 (2020).
6. ヘリウム危機の現状と今後の課題について (解説記事) : 山下 穰, 固体物理 **55**, 215-223 (2020).
7. *Thermal Hall Effects of Spins and Phonons in Kagome Antiferromagnet Cd-Kapellasite: M. Akazawa, M. Shimozawa, S. Kittaka, T. Sakakibara, R. Okuma, Z. Hiroi, H.-Y. Lee, N. Kawashima, J. H. Han and M. Yamashita, Phys. Rev. X **10**, 041059 (2020).
8. *Pressure-induced phase transition in the J_1 - J_2 square lattice antiferromagnet RbMoOPO₄Cl: H. Takeda, T. Yamauchi, M. Takigawa, H. Ishikawa and Z. Hiroi, Phys. Rev. B **103**, 104406 (2021).
9. *Strongly correlated superconductivity in a copper-based metal-organic framework with a perfect kagome lattice: T. Takenaka, K. Ishihara, M. Roppongi, Y. Miao, Y. Mizukami, T. Makita, J. Tsurumi, S. Watanabe, J. Takeya, M. Yamashita, K. Torizuka, Y. Uwatoko, T. Sasaki, X. Huang, W. Xu, D. Zhu, N. Su, J. -G. Cheng, T. Shibauchi and K. Hashimoto, Sci. Adv. **7**, eabf3996(1-8) (2021).

Division of Condensed Matter Theory

Tsunetsugu group

We have studied several topics of strongly correlated systems and nonequilibrium phenomena. Concerning correlated systems, we have investigated the dynamics of domain wall driven by external magnetic or electric field in multiferroic materials, and found its dynamical instability to splitting. We have also reexamined phenomenological Ginzburg-Landau theory for CDW in layered compounds and found new local minima in the free-energy landscape. As for nonequilibrium phenomena, we have analyzed various aspects of high-harmonic generation in solids, including the disorder effect, dynamical point-group symmetries, and relativistic dispersion relation of Dirac semimetals. Regarding periodically-driven (Floquet) systems, we have proposed a new symmetry and derived a general expression for nonequilibrium steady states. In isolated many-body quantum systems, we have investigated conserved quantities that work as dynamical obstructions and prevent ordinary thermalization. Related to the two topics, we studied quantum quench dynamics of strongly correlated electrons in one dimension and found a clogging phenomena where particle current stops but energy current flows.

1. Generalized hydrodynamic approach to charge and energy currents in the one-dimensional Hubbard model: Y. Nozawa and H. Tsunetsugu, Phys. Rev. B **101**, 035121 (2020).
2. *Efficient Terahertz Harmonic Generation with Coherent Acceleration of Electrons in the Dirac Semimetal Cd₃As₂: B. Cheng, N. Kanda, T. N. Ikeda, T. Matsuda, P. Xia, T. Schumann, S. Stemmer, J. Itatani, N. P. Armitage and R. Matsunaga, Phys. Rev. Lett. **124**, 117402 (2020).
3. Explicit Construction of Local Conserved Quantities in the XYZ Spin-1/2 Chain: Y. Nozawa and K. Fukai, Phys. Rev. Lett. **125**, 090602 (2020).
4. Time Crystals Protected by Floquet Dynamical Symmetry in Hubbard Models: K. Chinzei and T. N. Ikeda, Phys. Rev. Lett. **125**, 060601 (2020).
5. Multivalley Free Energy Landscape and the Origin of Stripe and Quasi-Stripe CDW Structures in Monolayer MX₂ Compounds: K. Nakatsugawa, S. Tanda and T. N. Ikeda, Sci. Rep. **10**, 1239 (2020).
6. General description for nonequilibrium steady states in periodically driven dissipative quantum systems: T. N. Ikeda and M. Sato, Science Advances **6**, eabb4019 (2020).
7. Disorder effects on the origin of high-order harmonic generation in solids: K. Chinzei and T. N. Ikeda, Phys. Rev. Research **2**, 013033 (2020).
8. High-order nonlinear optical response of a twisted bilayer graphene: T. N. Ikeda, Phys. Rev. Research **2**, 032015(R) (2020).
9. Noncommutative generalized Gibbs ensemble in isolated integrable quantum systems: K. Fukai, Y. Nozawa, K. Kawahara and T. N. Ikeda, Phys. Rev. Research **2**, 033403 (2020).

† Joint research with outside partners.

10. Dynamics of Composite Domain Walls in Multiferroics in Magnetic Field and Their Instability: K. Kawahara and H. Tsunetsugu, *J. Phys. Soc. Jpn.* **90**, 014703 (2021).
11. Quadrupole Orders on the fcc Lattice: H. Tsunetsugu, T. Ishitobi and K. Hattori, *J. Phys. Soc. Jpn.* **90**, 043701 (2021).
12. Generalized hydrodynamics study of the one-dimensional Hubbard model: Stationary clogging and proportionality of spin, charge, and energy currents: Y. Nozawa and H. Tsunetsugu, *Phys. Rev. B* **103**, 035130 (2021).

Kato group

The main research subject of Kato Lab. is transport properties in mesoscopic devices. We studied (1) optimization of pumping power under adiabatic charge driving, (2) microscopic theory for spin Hall magnetoresistance, (3) Cooper-pair transport through a Josephson junction array, and (4) transport properties through a Kondo quantum dot.

1. Geometrical Optimization of Pumping Power under Adiabatic Parameter Driving: M. Hasegawa and T. Kato, *J. Phys. Soc. Jpn.* **89**, 064706 (2020).
2. Fano-Kondo resonance versus Kondo plateau in an Aharonov-Bohm ring with an embedded quantum dot: M. Eto and R. Sakano, *Phys. Rev. B* **102**, 245402 (2020).
3. Field-induced SU(4) to SU(2) Kondo crossover in a half-filling nanotube dot: Spectral and finite-temperature properties: Y. Teratani, R. Sakano, T. Hata, T. Arakawa, M. Ferrier, K. Kobayashi and A. Oguri, *Phys. Rev. B* **102**, 165106 (2020).
4. Microscopic theory of spin Hall magnetoresistance: T. Kato, Y. Ohnuma and M. Matsuo, *Phys. Rev. B* **102**, 094437 (2020).
5. Fermi Liquid Theory for Nonlinear Transport through a Multilevel Anderson Impurity: Y. Teratani, R. Sakano and A. Oguri, *Phys. Rev. Lett.* **125**, 216801 (2020).
6. Cooper-Pair Tunneling in Small Josephson Junction Arrays Under Radio-Frequency Irradiation: G. M. Kanyolo, K. Takeda, Y. Mizugaki, T. Kato and H. Shimada, *J. Low Temp. Phys.* **201**, 269 (2020).
7. Effects of Tunnel-coupling Asymmetries on Fermi-liquid Transport through an Anderson Impurity: K. Tsutsumi, Y. Teratani, A. Oguri and R. Sakano, *JPS conf. ser.* **30**, 011174(1-6) (2020).
8. †DSQSS: Discrete Space Quantum Systems Solver: Y. Motoyama, K. Yoshimi, A. Masaki-Kato, T. Kato and N. Kawashima, *Computer Physics Communications* **264**, 107944 (2021).
9. 非平衡状態にある近藤効果 (その2) 近藤効果入門 1: 阪野 壘, 小栗 章, *固体物理* **55**, 47-54 (2020).

Division of Nanoscale Science

Katsumoto group

We further advanced the study of flying qubits using spin-polarized quantum Hall edge states. In particular, we improved the beam splitter that splits the electron beam into two channels, and increased the splitting probability from a few percent to 50%, and obtained a beam splitter equivalent to a half mirror in quantum optics. The interferometer using this showed high visibility of over 70%. In the super-normal-super (SNS) junction, the decrease of the superconducting critical current with the positive gate voltage has been unexplained. We have found the phenomenon can be interpreted as the decrease of quantum coherence in the Andreev bound state by the in-plane voltage.

1. Gate-controlled unitary operation on flying spin qubits in quantum Hall edge states: T. Shimizu, T. Nakamura, Y. Hashimoto, A. Endo and S. Katsumoto, *Phys. Rev. B* **102**, 235302 (2020).
2. †Optoelectronic properties of laser-beam-patterned few-layer lateral MoS₂ Schottky junctions: Y. Nagamine, J. Sato, Y. Qian, T. Inoue, T. Nakamura, S. Maruyama, S. Katsumoto and J. Haruyama, *Appl. Phys. Lett.* **117**, 043101 (2020).
3. *Extracting the Chiral Contribution to the Negative Longitudinal Magnetoresistance in Epitaxial Pr₂Ir₂O₇ Thin Films: T. Ohtsuki, Z. Tian, A. Endo, M. Halim, S. Katsumoto, Y. Kohama, K. Kindo, M. Lippmaa and S. Nakatsuji, *JPS Conf. Proc.* **30**, 011181 (1-6) (2020).
4. †Room-temperature quantum spin Hall phase in laser-patterned few-layer 1T'-MoS₂: N. Katsuragawa, M. Nishizawa, T. Nakamura, T. Inoue, S. Pakdel, S. Maruyama, S. Katsumoto, J. J. Palacios and J. Haruyama, *Commun Mater* **1**, 51

* Joint research among groups within ISSP.

(2020).

5. 薄膜材料の電気特性：勝本 信吾，「2020年版薄膜作製応用ハンドブック」，第2章，権田俊一，(NTS出版，東京，2020)，39-79.

Otani group

This year, we have studied the following topics: spin conversion behaviors in bulk, the interfaces and the surfaces, the magnon-phonon or magnon-magnon coupling in ferromagnetic heterostructures, and antiferromagnetic spintronics. I summarize the remarkable achievements this year below. We have established a phenomenological model explaining the contributions of bulk and interfacial spin relaxation. Our study of transverse magnetoresistance in magnetic heterostructure evidenced the spin swapping at the Rashba interface. We have experimentally demonstrated the conversion of acoustically induced spin currents to the charge current using a metal/oxide Rashba interface. This study has also shown significant enhancement of magnon-phonon coupling using the Bragg reflector cavity structure. Besides, our international collaboration showed a large nonlinear ferromagnetic resonance shift due to strong magnon-magnon coupling. We had another collaborative project on skyrmion strings that clarified their detailed propagation dynamics. This year, there are two exciting breakthroughs; Electrical manipulation of a topological antiferromagnetic state and Emergent electromagnetic induction in a helical-spin magnet, both of which appeared in Nature magazine.

1. Underlayer material dependent symmetric and asymmetric behavior of voltage-controlled magnetic anisotropy in CoFeB films: B. Rana, K. Miura, H. Takahashi and Y. Otani, *J. Phys.: Condens. Matter* **32**, 414002 (2020).
2. Electric-field control of interfacial in-plane magnetic anisotropy in CoFeB/MgO junctions: A. Deka, B. Rana, R. Anami, K. Miura, H. Takahashi, Y. Otani and Y. Fukuma, *Phys. Rev. B* **101**, 174405 (2020).
3. Large nonlinear ferromagnetic resonance shift and strong magnon-magnon coupling in Ni₈₀Fe₂₀ nanocross array: K. Adhikari, S. Sahoo, A. K. Mondal, Y. Otani and A. Barman, *Phys. Rev. B* **101**, 054406 (2020).
4. Phenomenological model for the direct and inverse Edelstein effects: H. Isshiki, P. Muduli, J. Kim, K. Kondou and Y. Otani, *Phys. Rev. B* **102**, 184411 (2020).
5. *Effect of sample size on anomalous Nernst effect in chiral antiferromagnetic Mn₃Sn devices: H. Narita, T. Higo, M. Ikhlas, S. Nakatsuji and Y. Otani, *Appl. Phys. Lett.* **116**, 072404 (2020).
6. Enhancement of acoustic spin pumping by acoustic distributed Bragg reflector cavity: Y. Hwang, J. Puebla, M. Xu, A. Lagarrigue, K. Kondou and Y. Otani, *Appl. Phys. Lett.* **116**, 252404 (2020).
7. Evidence for spin swapping from modulation of transverse resistance in magnetic heterostructures with Rashba interface: H. Kim, S. Karube, J. Borge, J. Kim, K. Kondou and Y. Otani, *Appl. Phys. Lett.* **116**, 122403 (2020).
8. *Magneto-optical Kerr effect in a non-collinear antiferromagnet Mn₃Ge: M. Wu, H. Isshiki, T. Chen, T. Higo, S. Nakatsuji and Y. Otani, *Appl. Phys. Lett.* **116**, 132408 (2020).
9. *Electrical manipulation of a topological antiferromagnetic state: H. Tsai, T. Higo, K. Kondou, T. Nomoto, A. Sakai, A. Kobayashi, T. Nakano, K. Yakushiji, R. Arita, S. Miwa, Y. Otani and S. Nakatsuji, *Nature* **580**, 608-613 (2020).
10. Emergent electromagnetic induction in a helical-spin magnet: T. Yokouchi, F. Kagawa, M. Hirschberger, Y. Otani, N. Nagaosa and Y. Tokura, *Nature* **586**, 232 (2020).
11. *Chirality-induced effective magnetic field in a phthalocyanine molecule: S. Miwa, K. Kondou, S. Sakamoto, A. Nihonyanagi, F. Araoka, Y. Otani and D. Miyajima, *Appl. Phys. Express* **13**, 113001 (1-4) (Spotlights 2020) (2020).
12. Acoustic ferromagnetic resonance and spin pumping induced by surface acoustic waves: J. Puebla, M. Xu, B. Rana, K. Yamamoto, S. Maekawa and Y. Otani, *J. Phys. D: Appl. Phys.* **53**, 264002 (2020).
13. *Structural and magnetic properties of Mn₃Ge films with Pt and Ru seed layers: A. Kobayashi, T. Higo, S. Nakatsuji and Y. Otani, *AIP Advances* **10**, 015225(1-6) (2020).
14. Nonlinear Control of Damping Constant by Electric Field in Ultrathin Ferromagnetic Films: B. Rana, C. A. Akosa, K. Miura, H. Takahashi, G. Tatara and Y. Otani, *Phys. Rev. Applied* **14**, 014037 (2020).
15. Nonreciprocal surface acoustic wave propagation via magneto-rotation coupling: M. Xu, K. Yamamoto, J. Puebla, K. Baumgaertl, B. Rana, K. Miura, H. Takahashi, D. Grundler, S. Maekawa and Y. Otani, *Sci. Adv.* **6**, eabb1724 (2020).
16. Voltage controlled on-demand magnonic nanochannels: S. Choudhury, A. K. Chaurasiya, A. K. Mondal, B. Rana, K. Miura, H. Takahashi, Y. Otani and A. Barman, *Sci. Adv.* **6**, eaba5457 (2020).

† Joint research with outside partners.

17. Phase boundary exchange coupling in the mixed magnetic phase regime of a Pd-doped FeRh epilayer: J. R. Massey, K. Matsumoto, M. Strungaru, R. C. Temple, T. Higo, K. Kondou, R. F. L. Evans, G. Burnell, R. W. Chantrell, Y. Otani and C. H. Marrows, *Phys. Rev. Materials* **4**, 024403(1-11) (2020).
18. Propagation dynamics of spin excitations along skyrmion strings: S. Seki, M. Garst, J. Waizner, R. Takagi, N. D. Khanh, Y. Okamura, K. Kondou, F. Kagawa, Y. Otani and Y. Tokura, *Nat Commun* **11**, 256 (2020).
19. *Electrical nucleation, displacement, and detection of antiferromagnetic domain walls in the chiral antiferromagnet Mn₃Sn: S. Sugimoto, Y. Nakatani, Y. Yamane, M. Ikhlas, K. Kondou, M. Kimata, T. Tomita, S. Nakatsuji and Y. Otani, *Commun Phys* **3**, 111 (2020).
20. Creation of magnetic skyrmions by surface acoustic waves: T. Yokouchi, S. Sugimoto, B. Rana, S. Seki, N. Ogawa, S. Kasai and Y. Otani, *Nat. Nanotechnol.* **15**, 361 (2020).
21. Spintronic devices for energy-efficient data storage and energy harvesting: J. Puebla, J. Kim, K. Kondou and Y. Otani, *Commun Mater* **1**, 24 (2020).
22. Nontrivial torque generation by orbital angular momentum injection in ferromagnetic-metal/Cu/Al₂O₃ trilayers: J. Kim, D. Go, H. Tsai, D. Jo, K. Kondou, H.-W. Lee and Y. Otani, *Phys. Rev. B* **103**, L020407 (2021).
23. *Domain structure and domain wall dynamics in topological chiral antiferromagnets from the viewpoint of magnetic octupole: Y. Otani and T. Higo, *Appl. Phys. Lett.* **118**, 040501 (2021).
24. *Omnidirectional Control of Large Electrical Output in a Topological Antiferromagnet: T. Higo, Y. Li, K. Kondou, D. Qu, M. Ikhlas, R. Uesugi, D. Nishio-Hamane, C. L. Chien, Y. Otani and S. Nakatsuji, *Adv. Funct. Mater.* **31**, 2008971-12 (2021).
25. *Spin-orbit torque switching of the antiferromagnetic state in polycrystalline Mn₃Sn/Cu/heavy metal heterostructures: H. Tsai, T. Higo, K. Kondou, A. Kobayashi, T. Nakano, K. Yakushiji, S. Miwa, Y. Otani and S. Nakatsuji, *AIP Advances* **11**, 045110 (1-6) (2021).
26. Strain-induced Megahertz Oscillation and Stable Velocity of an Antiferromagnetic Domain Wall: F. Chen, X. Ge, W. Luo, R. Xing, S. Liang, X. Yang, L. You, R. Xiong, Y. Otani and Y. Zhang, *Phys. Rev. Applied* **15**, 014030 (2021).
27. *Fabrication of polycrystalline Weyl antiferromagnetic Mn₃Sn thin films on various seed layers: T. Nakano, T. Higo, A. Kobayashi, S. Miwa, S. Nakatsuji and K. Yakushiji, *Phys. Rev. Materials* **5**, 054402 (1-9) (2021).
28. Nanochannels for spin-wave manipulation in Ni₈₀Fe₂₀ nanodot arrays: S. Sahoo, S. N. Panda, S. Barman, Y. Otani and A. Barman, *Journal of Magnetism and Magnetic Materials* **522**, 167550 (2021).
29. *Giant Effective Damping of Octupole Oscillation in an Antiferromagnetic Weyl Semimetal: S. Miwa, S. Iihama, T. Nomoto, T. Tomita, T. Higo, M. Ikhlas, S. Sakamoto, Y. Otani, S. Mizukami, R. Arita and S. Nakatsuji, *Small Science* **1**, 2000062 (1-8) (2021).
30. *Large Hall Signal due to Electrical Switching of an Antiferromagnetic Weyl Semimetal State: H. Tsai, T. Higo, K. Kondou, S. Sakamoto, A. Kobayashi, T. Matsuo, S. Miwa, Y. Otani and S. Nakatsuji, *Small Science* **1**, 2000025 (1-9) (2021).

Komori group

Distribution of local lattice distortion due to the hetero atomic overlayer is investigated using scanning tunneling microscopy (STM) on the Cu(111) surface covered by hexagonal Fe₂N atomic layer. We utilize the moiré pattern to reach a higher spatial resolution than simple STM observations. The distortion can be greatly affected by the formation of atomic impurities at the subsurface. Ultrathin films of L1₀-type FeNi are grown using nitrogen-surfactant epitaxy on the Cu(001) substrate. Well-ordered films with little intermixing among Cu, Fe and Ni atoms are realized by optimizing the substrate temperature during the Fe and Ni deposition and the post-annealing temperature. Their ferromagnetic properties are studied by soft X-ray magnetic circular dichroism. An out-of-plane magnetocrystalline anisotropy is large enough for dominating the film shape anisotropy. Electronic structure of 3~4-degree twisted bilayer graphene is investigated using angle-resolved photoemission spectroscopy with synchrotron light. The interface between the two graphene sheets of the present samples is made in a high vacuum. Owing to the strong interlayer interaction, significant band modifications including replica bands are observed at the energy near the Dirac point and crossing points of the Dirac bands. In particular, partial flat bands appear with changes in the Dirac velocity, depending on the twist angles. The observed band structure is consistent with the result of tight-binding calculations.

1. †*Orbital Angular Momentum Induced Spin Polarization of 2D Metallic Bands: T. Kobayashi, Y. Nakata, K. Yaji, T. Shishidou, D. Agterberg, S. Yoshizawa, F. Komori, S. Shin, M. Weinert, T. Uchihashi and K. Sakamoto, *Phys. Rev.*

* Joint research among groups within ISSP.

Lett. **125**, 176401, 1-6 (2020).

2. Sensing surface lattice strain with Kondo resonance of single Co adatom: K. Iwata, T. Miyamachi, E. Minamitani and F. Komori, Appl. Phys. Lett. **116**, 051604, 1-4 (2020).
3. †Twisted bilayer graphene fabricated by direct bonding in a high vacuum: H. Imamura, A. Visikovskiy, R. Uotani, T. Kajiwara, H. Ando, T. Iimori, K. Iwata, T. Miyamachi, K. Nakatsuji, K. Mase, T. Shirasawa, F. Komori and S. Tanaka, Appl. Phys. Express **13**, 075004, 1-5 (2020).
4. *Edge-state correlation accelerates metal-insulator transition in topological semimetal nanofilms: S. Ito, M. Arita, J. Haruyama, B. Feng, W. -C. Chen, H. Namatame, M. Taniguchi, C. -M. Cheng, G. Bian, S. -J. Tang, T. -C. Chiang, O. Sugino, F. Komori and I. Matsuda, Science Advances **6**, eaaz5015 (7 pages) (2020).
5. †*Topological Surface State of Bi₂Se₃ Modified by Adsorption of Organic Donor Molecule Tetrathianaphthacene: T. Kitazawa, K. Yaji, K. Shimosawa, H. Kondo, T. Yamanaka, H. Yaguchi, Y. Ishida, K. Kuroda, A. Harasawa, T. Iwahashi, Y. Ouchi, F. Komori, S. Shin and K. Kanai, Adv. Mater. Interfaces **7**, 2000524, 1-8 (2020).
6. Realizing large out-of-plane magnetic anisotropy in L1₀ FeNi films grown by nitrogen-surfactant epitaxy on Cu(001): K. Kawaguchi, T. Miyamachi, T. Iimori, Y. Takahashi, T. Hattori, T. Yokoyama, M. Kotsugi and F. Komori, Phys. Rev. Materials **4**, 054403, 1-7 (2020).
7. *Fully spin-polarized bulk states in ferroelectric GeTe: J. Krempaský, M. Fanciulli, L. Nicolai, J. Minár, H. Volfová, O. Caha, V. V. Volobuev, J. Sánchez-Barriga, M. Gmitra, K. Yaji, K. Kuroda, S. Shin, F. Komori, G. Springholz and J. Hugo Dil, Phys. Rev. Research **2**, 013107, 1-7 (2020).
8. Hexagonal iron nitride monolayer on Cu(001): Zigzag-line-in-trough alignment: M. Yamada, K. Ienaga, Y. Takahashi, T. Miyamachi and F. Komori, Surface Science **700**, 121679, 1-9 (2020).
9. Subatomic Distortion of Surface Monolayer Lattice Visualized by Moiré Pattern: T. Hattori, N. Kawamura, T. Iimori, T. Miyamachi and F. Komori, Nano Lett. **21**, 2406-2411 (2021).
10. †*Atomic-layer Rashba-type superconductor protected by dynamic spin-momentum locking: S. Yoshizawa, T. Kobayashi, Y. Nakata, K. Yaji, K. Yokota, F. Komori, S. Shin, K. Sakamoto and T. Uchihashi, Nat Commun **12**, 1462 (2021).
11. †Electronic structure of 3 degree-twisted bilayer graphene on 4H-SiC(0001): T. Iimori, A. Visikovskiy, H. Imamura, T. Miyamachi, M. Kitamura, K. Horiba, H. Kumigashira, K. Mase, K. Nakatsuji, S. Tanaka and F. Komori, Phys. Rev. Material **5** (2021), in print.

Hasegawa group

We have investigated monolayer superconducting materials using low temperature scanning tunneling microscopy (STM). In the case of two-dimensional superconductors, it has been known that the superconductivity is directly transformed into insulator by introducing defects or applying magnetic field. Recent transport measurements on superconducting crystalline thin films, however, revealed the presence of metallic phases during the super-insulator transitions. In order to elucidate the phenomena we performed local superconducting gap measurements by STM on atomically-thin well-ordered Pb superconductors under the perpendicular magnetic field. We observed the metallic phase and found by using vicinal substrates to introduce regularly-arranged steps as scatterers that the critical temperature is reduced but the superconducting gap remains the same. Analyzing these peculiar microscopic features will provide a new scenario on the super-insulator transition. We are now developing a new local method to probe spin dynamics of nano-size structures including single atoms/molecules by detecting electron/ferromagnetic resonances based on spin-polarized STM. We have introduced radio-frequency (RF) cables into the STM head and successfully detected response of the RF irradiation in spin-polarized tunneling current. Using spin-polarized STM we have characterized magnetic properties of FeCo alloy island structures and found that the magnetoanisotropy can be significantly reduced by the alloying. We plan to use the alloyed islands as a sample for the resonance detection.

1. Numerical calculation of the potential distribution on the Si(111)-7 × 7 surface for scanning tunneling potentiometry: M. Hamada, H.-H. Yang and Y. Hasegawa, Jpn. J. Appl. Phys. **59**, SN1016 1-6 (2020).
2. Si(111)-7×7 表面上の一次元欠陥における電気伝導評価: 浜田 雅之, 長谷川 幸雄, 表面と真空 **63**, 431-436 (2020).
3. Enhanced critical magnetic field for monoatomic-layer superconductor by Josephson junction steps: F. Oguro, Y. Sato, K. Asakawa, M. Haze and Y. Hasegawa, Phys. Rev. B **103**, 085416 1-7 (2021).

† Joint research with outside partners.

Lippmaa group

We concluded the project on fabricating iridate pyrochlore thin films by solid-state epitaxy. The behavior of iridium and other noble metals in the oxide thin film growth process was studied. In particular, the spontaneous phase separation of noble metals was studied in perovskite and pyrochlore lattices. Several techniques were studied for controlling the sheet carrier density in oxide heterostructures with delta-doping layers. The SrTiO₃ / LaTiO₃ system was used in these experiments. A new sacrificial buffer layer process was developed for fabricating strain-free free-standing oxide thin films.

1. *Growth of Pr₂Ir₂O₇ thin films using solid phase epitaxy: T. Ohtsuki, Z. Tian, M. Halim, S. Nakatsuji and M. Lippmaa, *J. Appl. Phys.* **127**, 035303 (1-9) (2020).
2. Noble metal clustering and nanopillar formation in an oxide matrix: M. Lippmaa, S. Kawasaki, R. Takahashi and T. Yamamoto, *Jpn. J. Appl. Phys.* **59**, 010501 (1-9) (2020).
3. Tuning the carrier density in SrTiO₃/LaTiO₃/SrTiO₃ quantum wells: J. N. Lee, X. Hou, R. Takahashi and M. Lippmaa, *Appl. Phys. Lett.* **116**, 171601 (1-5) (2020).
4. † 水溶性犠牲層を用いた単結晶薄膜分離技術: 高橋 竜太, リップ マーミック, セラミックデータブック **48**, 71-75 (2020).
5. *Extracting the Chiral Contribution to the Negative Longitudinal Magnetoresistance in Epitaxial Pr₂Ir₂O₇ Thin Films: T. Ohtsuki, Z. Tian, A. Endo, M. Halim, S. Katsumoto, Y. Kohama, K. Kindo, M. Lippmaa and S. Nakatsuji, *JPS Conf. Proc.* **30**, 011181 (1-6) (2020).
6. Sacrificial Water-Soluble BaO Layer for Fabricating Free-Standing Piezoelectric Membranes: R. Takahashi and M. Lippmaa, *ACS Appl. Mater. Interfaces* **12**, 25042-25049 (2020).
7. Nanopillar composite electrodes for solar-driven water splitting: M. Lippmaa, S. Kawasaki, R. Takahashi and T. Yamamoto, *MRS Bulletin* **46**, 142-151 (2021).
8. *Observation and control of the weak topological insulator state in ZrTe₅: P. Zhang, R. Noguchi, K. Kuroda, C. Lin, K. Kawaguchi, K. Yaji, A. Harasawa, M. Lippmaa, S. Nie, H. Weng, V. Kandyba, A. Giampietri, A. Barinov, Q. Li, G. D. Gu, S. Shin and T. Kondo, *Nat. Commun.* **12**, 406 (2021).
9. †Realization of closed-loop optimization of epitaxial titanium nitride thin-film growth via machine learning: I. Ohkubo, Z. Hou, J. N. Lee, T. Aizawa, M. Lippmaa, T. Chikyow, K. Tsuda and T. Mori, *Mater. Today Phys.* **16**, 100296 (1-6) (2021).

Functional Materials Group

Yoshinobu group

We conducted several research projects in the fiscal year 2020: (1) The surface chemistry of hydrogen and formic acid on Cu step surfaces and Pd-Cu single atom alloy model catalysts studied by SR-PES, IRAS, HREELS and TPD. (2) The adsorption and desorption of CO₂ on Pt(997) studied by TPD and SR-XPS. (3) The adsorption and desorption of CH₄ on Pt(997) studied by IRAS, TPD and SR-XPS. (4) In-situ SR-XPS study of CVD graphene on a Cu surface. (5) AP-XPS study of Pd deposited MoS₂ under hydrogen pressure. (6) THz field induced second harmonic light modulation on Pt(111).

1. *Emergence of nearly flat bands through a kagome lattice embedded in an epitaxial two-dimensional Ge layer with a bitriangular structure: A. Fleurence, C. -C. Lee, R. Friedlein, Y. Fukaya, S. Yoshimoto, K. Mukai, H. Yamane, N. Kosugi, J. Yoshinobu, T. Ozaki and Y. Yamada-Takamura, *Phys. Rev. B* **102**, 201102 (2020).
2. *Formation of BN-covered silicene on ZrB₂/Si(111) by adsorption of NO and thermal processes: J. Yoshinobu, K. Mukai, H. Ueda, S. Yoshimoto, S. Shimizu, T. Koitaya, H. Noritake, C.-C. Lee, T. Ozaki, A. Fleurence, R. Friedlein and Y. Yamada-Takamura, *J. Chem. Phys.* **153**, 064702 (2020).
3. The roles of step-site and zinc in surface chemistry of formic acid on clean and Zn-modified Cu(111) and Cu(997) surfaces studied by HR-XPS, TPD, and IRAS: Y. Shiozawa, T. Koitaya, K. Mukai, S. Yoshimoto and J. Yoshinobu, *J. Chem. Phys.* **152**, 044703 (2020).
4. *A computational examination of the electric-field-induced proton transfer along the interface hydrogen bond between proton donating and accepting self-assembled monolayers: Y. Kanematsu, H. S. Kato, S. Yoshimoto, A. Ueda, S. Yamamoto, H. Mori, J. Yoshinobu, I. Matsuda and M. Tachikawa, *Chem. Phys. Lett.* **741**, 137091 (2020).
5. †*Atomistic-Level Description of GaN/Water Interface by a Combined Spectroscopic and First-Principles Computa-

* Joint research among groups within ISSP.

tional Approach: M. Sato, Y. Imazeki, T. Takeda, M. Kobayashi, S. Yamamoto, I. Matsuda, J. Yoshinobu, Y. Nakano and M. Sugiyama, *J. Phys. Chem. C* **124**, 12466 (2020).

6. C–H Bond Activation of Methane through Electronic Interaction with Pd(110): T. Koitaya, A. Ishikawa, S. Yoshimoto and J. Yoshinobu, *J. Phys. Chem. C* **125**, 1368 (2021).
7. *水素を活かすセラミックス プロトン電子カップル型分子性結晶および二分子膜における機能開拓: 森 初果, 加藤 浩之, 藤野 智子, 上田 顕, 吉信 淳, *セラミックス* **56**, 88-91 (2021).
8. Role of Intermolecular Interactions in the Catalytic Reaction of Formic Acid on Cu(111): A. Shiotari, S. E. M. Putra, Y. Shiozawa, Y. Hamamoto, K. Inagaki, Y. Morikawa, Y. Sugimoto, J. Yoshinobu and I. Hamada, *Small* **2021**, 2008010 (2021).
9. †*Structure and electronic structure of van der Waals interfaces at a Au(111) surface covered with a well-ordered molecular layer of n-alkanes: H. Mizushima, H. Koike, K. Kuroda, K. Yaji, A. Harasawa, Y. Ishida, M. Nakayama, K. Mase, K. Mukai, T. Kitazawa, T. Kondo, J. Yoshinobu, S. Shin and K. Kanai, *Applied Surface Science* **535**, 147673 (2021).
10. 2020年版薄膜作製応用ハンドブック(権田俊一監修) 第3編第2章第7節「薄膜の表面・界面制御と信頼性」(p.883-p.888): 吉信 淳, (NTS, Tokyo, Japan, 2020).

Akiyama group

In 2020, which is the last year of our NEDO laser project started in 2018, we made development (fab-less production) and characterizations of gain-sitced 1030-1060 nm InGaAs laser diodes (LDs) for short seed-pulse generation below 10 ps, and indeed demonstrated 8 ps pulses generated directly from our developed LDs. We also studied multi-section LDs with strong nonlinearity for short-pulse generation mechanism analysis. Our study in 2020 on novel solar cells included lead-halide Perovskite solar cells, space-use multi-junction solar cells, and textured solar cells. Our study on bio- and chemical-physics has been extended to new luciferin analogs and caged-luciferins.

1. Accurate modeling of electron-hole binding in CuCl. I. Exciton states: S. V. Nair, J. Usukura and E. Tokunaga, *Phys. Rev. B* **102**, 075202 (2020).
2. Accurate modeling of electron-hole binding in CuCl. II. Biexciton wavefunction: J. Usukura, S. V. Nair and E. Tokunaga, *Phys. Rev. B* **102**, 075203 (2020).
3. *In situ* wavelength tuning of quantum-dot single-photon sources integrated on a CMOS-processed silicon waveguide: R. Katsumi, Y. Ota, A. Osada, T. Tajiri, T. Yamaguchi, M. Kakuda, S. Iwamoto, H. Akiyama and Y. Arakawa, *Appl. Phys. Lett.* **116**, 041103 (2020).
4. *Quantum-mechanical hydration plays critical role in the stability of firefly oxyluciferin isomers: State-of-the-art calculations of the excited states: Y. Noguchi, M. Hiyama, M. Shiga, H. Akiyama and O. Sugino, *J. Chem. Phys.* **153**, 201103 (2020).
5. Exciton Localization and Enhancement of the Exciton–LO Phonon Interaction in a CsPbBr₃ Single Crystal: K. Shibata, J. Yan, Y. Hazama, S. Chen and H. Akiyama, *J. Phys. Chem. C* **124**, 18257 (2020).
6. Theoretical Study of the Wavelength Selection for the Photocleavage of Coumarin-caged D-luciferin: J. Usukura, M. Hiyama, M. Kurata, Y. Hazama, X. Qiu, F. M. Winnik, H. Akiyama and N. Koga, *Photochem Photobiol* **96**, 805-814 (2020).
7. Quantitative immunohistochemistry using an antibody-fused bioluminescent protein: K.-Y. Wang, C. Wu, S. Shimajiri, H. Kubota, H. Akiyama and Y. Ohmiya, *BioTechnique* **64**, 302-306 (2020).
8. High performance single-mode vertical cavity surface emitting lasers based on CsPbBr₃ nanocrystals with simplified processing: C. Zhao, J. Tao, J. Tian, G. Weng, H. Liu, Y. Liu, J. Yan, S. Chen, Y. Pan, X. Hu, S. Chen, H. Akiyama and J. Chu, *Chemical Engineering Journal* (**online**), 127660 (2020).
9. Lasing operation in the CsPbBr₃ perovskite micron hemisphere cavity grown by chemical vapor deposition: H. Zhang, C. Zhao, S. Chen, J. Tian, J. Yan, G. Weng, X. Hu, J. Tao, Y. Pan, S. Chen, H. Akiyama and J. Chu, *Chemical Engineering Journal* **389**, 124395 (2020).
10. Absolute electroluminescence imaging with distributed circuit modeling: Excellent for solar-cell defect diagnosis: J. Hong, Y. Wang, Y. Chen, X. Hu, G. Weng, S. Chen, H. Akiyama, Y. Zhang, B. Zhang and J. Chu, *Prog Photovolt Res Appl* **28**, 295 (2020).

† Joint research with outside partners.

11. Modeling and design for low-cost multijunction solar cell via light-trapping rear texture technique: Applied in InGaP/GaAs/InGaAs triple junction: L. Zhu, Y. Hazama, A. Reddy, K. Watanabe, Y. Nakano, M. Sugiyama and H. Akiyama, *Prog Photovolt Res Appl* **28**, 251 (2020).
12. Practical target values of Shockley–Read–Hall recombination rates in state-of-the-art triple-junction solar cells for realizing conversion efficiencies within 1% of the internal radiative limit: T. Nakamura, M. Imaizumi, H. Akiyama and Y. Okada, *Prog Photovolt Res Appl* **28**, 417 (2020).
13. Quantitative study of electron tunneling dynamics in asymmetric coupled InGaN/GaN quantum wells: G. Weng, Y. Liu, S. Chen, T. Ito, X. Hu, C. Zhao, J. Liu, J. Chu and H. Akiyama, *Applied Optics* **59**, 6231–6236 (2020).
14. Importance of Interfacial Passivation in the High Efficiency of Sb₂Se₃ Thin-Film Solar Cells: Numerical Evidence: Y. Chen, Y. Wang, R. Wang, X. Hu, J. Tao, G.-E. Weng, C. Zhao, S. Chen, Z. Zhu, J. Chu and H. Akiyama, *ACS Appl. Energy Mater.* **11**, 10415–10422 (2020).
15. *Direct generation of sub-picosecond pulse via multi-section gain switching: T. Nakamura, T. Ito, H. Nakamae, C. Kim, Y. Hazama, Y. Kobayashi, R. Kuroda and H. Akiyama, *Opt. Lett.* **46**, 1277 (2021).
16. Fabricating over 7%-efficient Sb₂(S,Se)₃ thin-film solar cells by vapor transport deposition using Sb₂Se₃ and Sb₂S₃ mixed powders as the evaporation source: X. Hu, J. Tao, R. Wang, Y. Wang, Y. Pan, G. Weng, X. Luo, S. Chen, Z. Zhu, J. Chu and H. Akiyama, *Journal of Power Sources* **493**, 229737 (2021).
17. Superior single-mode lasing in a self-assembly CsPbX₃ microcavity over an ultrawide pumping wavelength range: G. Weng, J. Yan, S. Chen, C. Zhao, H. Zhang, J. Tian, Y. Liu, X. Hu, J. Tao, S. Chen, Z. Zhu, H. Akiyama and J. Chu, *Photon. Res.* **9**, 54 (2021).
18. Electron–Hole Plasma Lasing Dynamics in CsPbCl_mBr_{3-m} Microplate Lasers: G. Weng, J. Tian, S. Chen, J. Yan, H. Zhang, Y. Liu, C. Zhao, X. Hu, X. Luo, J. Tao, S. Chen, Z. Zhu, J. Chu and H. Akiyama, *ACS Photonics* **8**, 787 (2021).
19. Adaptive automatic solar cell defect detection and classification based on absolute electroluminescence imaging: Y. Wang, L. Li, Y. Sun, J. Xu, Y. Jia, J. Hong, X. Hu, G. Weng, X. Luo, S. Chen, Z. Zhu, J. Chu and H. Akiyama, *Energy* **229**, 120606 (2021).
20. Enhanced Magneto-Optical Kerr Effect of GaAs-Based P-N Junctions in the Terahertz Range: K. Miyagawa, M. Nagai, M. Ashida, C. Kim and H. Akiyama, *J Infrared Milli Terahz Waves* **42**, 325 (2021).

Sugino group

We have studied the density functional theory for molecules and condensed matters either in the ground state or in the excited states. We have also studied energy-materials such as lithium-ion battery, solid-state battery and fuel-cell and bio-materials such as oxyluciferin of firefly. We have also contributed to get theoretical interpretation of experiments. All are based on the first-principles calculations.

1. Hydrogen at Electrochemical Interfaces: O. Sugino, *J. Phys. Soc. Jpn.* **89**, 051013 (2020).
2. †Nuclear quantum effect for hydrogen adsorption on Pt(111): L. Yan, Y. Yamamoto, M. Shiga and O. Sugino, *Phys. Rev. B* **101**, 165414 (2020).
3. *Quantum-mechanical hydration plays critical role in the stability of firefly oxyluciferin isomers: State-of-the-art calculations of the excited states: Y. Noguchi, M. Hiyama, M. Shiga, H. Akiyama and O. Sugino, *J. Chem. Phys.* **153**, 201103 (2020).
4. †Machine learning exchange-correlation potential in time-dependent density-functional theory: Y. Suzuki, R. Nagai and J. Haruyama, *Phys. Rev. A* **101**, 050501 (2020).
5. †Structural Variation in Carbonate Electrolytes by the Addition of Li Salts Studied by X-Ray Total Scattering: K. Kimura, K. Hayashi, H. Kiuchi, M. Morita, J. Haruyama, M. Otani, H. Sakaebe, F. Fujisaki, K. Mori, M. Yonemura, Y. Takabayashi, T. Nakatani, S. Fujinami, T. Fukunaga and E. Matsubara, *Phys. Status Solidi B* **257**, 2000100 (2020).
6. †Dopant arrangements in Y-doped BaZrO₃ under processing conditions and their impact on proton conduction: a large-scale first-principles thermodynamics study: S. Kasamatsu, O. Sugino, T. Ogawa and A. Kuwabara, *J. Mater. Chem. A* **8**, 12674 (2020).
7. *Edge-state correlation accelerates metal-insulator transition in topological semimetal nanofilms: S. Ito, M. Arita, J. Haruyama, B. Feng, W. -C. Chen, H. Namatame, M. Taniguchi, C. -M. Cheng, G. Bian, S. -J. Tang, T. -C. Chiang,

* Joint research among groups within ISSP.

O. Sugino, F. Komori and I. Matsuda, *Science Advances* **6**, eaaz5015 (7 pages) (2020).

- †Surface-state Coulomb repulsion accelerates a metal-insulator transition in topological semimetal nanofilms: S. Ito, M. Arita, J. Haruyama, B. Feng, W. -C. Chen, H. Namatame, M. Taniguchi, C. -M. Cheng, G. Bian, S. -J. Tang, T. -C. Chiang, O. Sugino, F. Komori and I. Matsuda, *Sci. Adv.* **6**, eaaz5015 (2020).
- †Challenge of advanced low temperature fuel cells based on high degree of freedom of group 4 and 5 metal oxides: A. Ishihara, S. Tominaka, S. Mitsushima, H. Imai, O. Sugino and K.-I. Ota, *Current Opinion in Electrochemistry* **21**, 234 (2020).
- †Completing density functional theory by machine learning hidden messages from molecules: R. Nagai, R. Akashi and O. Sugino, *npj Comput Mater* **6**, 43 (2020).
- †Comparative Study on Sulfide and Oxide Electrolyte Interfaces with Cathodes in All-Solid-State Battery via First-Principles Calculations: Y. Okuno, J. Haruyama and Y. Tateyama, *ACS Appl. Energy Mater.* **3**, 11061 (2020).
- †First-Principles Calculation of Copper Oxide Superconductors That Supports the Kamimura-Suwa Model: H. Kamimura, M. Araidai, K. Ishida, S. Matsuno, H. Sakata, K. Shiraiishi, O. Sugino and J.-S. Tsai, *Condensed Matter* **5**, 69 (2020).
- †*Ab initio* construction of the energy density functional for electron systems with the functional-renormalization-group-aided density functional theory: T. Yokota and T. Naito, *Phys. Rev. Research* **3**, L012015 (2021).
- †Advances and challenges for experiment and theory for multi-electron multi-proton transfer at electrified solid-liquid interfaces: K. Sakaushi, T. Komeda, S. Hammes-Schiffer, M. M. Melander and O. Sugino, *Phys. Chem. Chem. Phys.* **22**, 19401-19442 (2021).

Oka group

The Oka group has constructed the theory for detecting Majorana modes in Kitaev's chiral spin liquid using STM setups. In addition, we have done a collaboration with experimentalists on novel transport properties in layered metals, as well as an High harmonics generation measurement in 3D Dirac materials.

- h/e oscillations in interlayer transport of delafossites: C. Putzke, M. D. Bachmann, P. McGuinness, E. Zhakina, V. Sunko, M. Konczykowski, T. Oka, R. Moessner, A. Stern, M. König, S. Khim, A. P. Mackenzie and P. J. W. Moll, *Science* **368**, 1234 (2020).
- Non-perturbative terahertz high-harmonic generation in the three-dimensional Dirac semimetal Cd₃As₂: S. Kovalev, R. M. Dantas, S. Germanskiy, J.-C. Deinert, B. Green, I. Ilyakov, N. Awari, M. Chen, M. Bawatna, J. Ling, F. Xiu, P. H. van Loosdrecht, P. Surówka, T. Oka and Z. Wang, *Nature communications* **11**, 1-6 (2020).
- Scanning Tunneling Microscopy as a Single Majorana Detector of Kitaev's Chiral Spin Liquid: M. Udagawa, S. Takayoshi and T. Oka, *Phys. Rev. Lett.* **126**, 127201 (2021).

Inoue group

In 2020, we revealed a new family of light-driven inward H⁺ pumping rhodopsin, schizorhodopsin (SzR), from Asgard archaea and marine micro-organisms. The mechanism of SzR was investigated by laser flash photolysis and FTIR spectroscopy. As the result, it was revealed that the H⁺ of the retinal is released to the cytoplasmic milieu without being trapped at any amino acid residues in the protein. This is considerably different from that another inward H⁺ pumping rhodopsin, xenorhodopsin. Also, we reported the role of a conserved tryptophan (Trp163) in the gating the mechanism of channelrhodopsin (C1C2). While the mutation of this residue (C1C2 W163F) reduced the channel activity, the H⁺ pump activity was manifested.

- Excitonic Coupling Effect on the Circular Dichroism Spectrum of Sodium-Pumping Rhodopsin KR2: K. J. Fujimoto and K. Inoue, *J. Chem. Phys.* **153**, 045101 (2020).
- Allosteric Communication to the Retinal Chromophore upon Ion Binding in a Light-driven Sodium Ion Pumping Rhodopsin: A. Otomo, M. Mizuno, K. Inoue, H. Kandori and Y. Mizutani, *Biochemistry* **59**, 520-529 (2020).
- Schizorhodopsins: A Novel Family of Rhodopsins from Asgard archaea that Function as Light-Driven Inward H⁺ Pumps: K. Inoue, S. P. Tsunoda, M. Singh, S. Tomida, S. Hososhima, M. Konno, R. Nakamura, H. Watanabe, P. -A. Bulzu, H. L. Banciu, A. -S. Andrei, T. Uchihashi, R. Ghai, O. Bégjà and H. Kandori, *Sci. Adv.* **6**, eaaz2441 (2020).
- Infrared spectroscopic analysis on structural changes around the protonated Schiff base upon retinal isomerization in light-driven sodium pump KR2: S. Tomida, S. Ito, T. Mato, Y. Furutani, K. Inoue and H. Kandori, *Biochimica et*

† Joint research with outside partners.

Biophysica Acta (BBA) - Bioenergetics **1861**, 148190 (2020).

5. Physical disuse contributes to widespread chronic mechanical hyperalgesia, tactile allodynia, and cold allodynia through neurogenic inflammation and spino-parabrachio-amygdaloid pathway activation: Y. Ohmichi, M. Ohmichi, R. Tashima, K. Osuka, K. Fukushige, D. Kanikowska, Y. Fukazawa, H. Yawo, M. Tsuda, M. Naito and T. Nakano, *PAIN* **161**, 1808-1823 (2020).
6. Gate-keeper of ion transport – a highly conserved helix-3 tryptophan in a channelrhodopsin chimera, C1C2/ChRWR: Y. Nagasaka, S. Hososhima, N. Kubo, T. Nagata, H. Kandori, K. Inoue and H. Yawo, *Biophys. Physicobiol.* **17**, 59-69 (2020).
7. Active Learning for Level Set Estimation under Input Uncertainty and Its Extensions: Y. Inatsu, M. Karasuyama, K. Inoue and I. Takeuchi, *Neural Computation* **32**, 2486-2531 (2020).
8. Active Learning of Bayesian Linear Models with High-Dimensional Binary Features by Parameter Confidence-Region Estimation: Y. Inatsu, M. Karasuyama, K. Inoue, H. Kandori and I. Takeuchi, *Neural Computation* **32**, 1998-2031 (2020).
9. Crystal structure of schizorhodopsin reveals mechanism of inward proton pumping: A. Higuchi, W. Shihoya, M. Konno, T. Ikuta, H. Kandori, K. Inoue and O. Nureki, *Proc. Natl. Acad. Sci. USA* **118**, e2016328118 (2021).
10. Exploration of natural red-shifted rhodopsins using a machine learning-based Bayesian experimental design: K. Inoue, M. Karasuyama, R. Nakamura, M. Konno, D. Yamada, K. Mannen, T. Nagata, Y. Inatsu, H. Yawo, K. Yura, O. Bèjà, H. Kandori and I. Takeuchi, *Commun. Biol.* **4**, 362 (2021).
11. TAT Rhodopsin Is an Ultraviolet-Dependent Environmental pH Sensor: C. Kataoka, T. Sugimoto, S. Shigemura, K. Katayama, S. P. Tsunoda, K. Inoue, O. Bèjà and H. Kandori, *Biochemistry*, *acs.biochem.0c00951* (2021), in print.
12. 光で細胞を制御するー多様な微生物型ロドプシンとオプトジェネティクスー: 井上 圭一, *光学* **49**, 2-7 (2020).
13. Shining light on rhodopsin selectivity: How do proteins decide whether to transport H⁺ or Cl⁻? K. Inoue, *J. Biol. Chem.* **295**, 14805-14806 (2020).
14. 光駆動タンパク質ロドプシンの分子機能エンジニアリング: 井上 圭一, *生物工学会誌* **98**, 664-668 (2020).
15. ラットを用いたオプトジェネティクス (光遺伝学): 八尾 寛, 深澤 有吾, 富田 浩史, 五十嵐 敬幸, *日本実験動物協会情報誌 LABIO 21* **80**, 5-8 (2020).
16. A series of commentaries for a symposium entitled “Session 3SDA - Optogenetics: applying photoreceptor for understanding biological phenomena”: S. P. Tsunoda and K. Inoue, *Biophys Rev* **12**, 295 (2020).
17. Expanding horizons of biosciences by light-control: M. Kataoka and T. Nagata, *Biophysics and Physicobiology* (2021), accepted for publication.
18. Application of Optogenetics for Muscle Cells and Stem Cells: T. Asano, D. B. L. Teh and H. Yawo, in: *Optogenetics*, edited by Hiromu Yawo, Hideki Kandori, Amane Koizumi, Ryoichiro Kageyama, (Springer Nature, 2021), 359-375.
19. Diversity, Mechanism, and Optogenetic Application of Light-Driven Ion Pump Rhodopsins: K. Inoue, in: *Optogenetics*, edited by Hiromu Yawo, Hideki Kandori, Amane Koizumi, Ryoichiro Kageyama, (Springer Nature, 2021), 89-126.
20. ロドプシンが拓くタンパク質科学の地平: 井上 圭一, 「未来探究2050 東大30人の知性が読み解く世界」, 東京大学未来ビジョン研究センター, (日本経済新聞出版, 2021), 74-83.

Quantum Materials Group

Oshikawa group

We conducted theoretical studies on a wide range of subjects in quantum many-body problem. In particular, we proposed a novel mechanism of producing *robust* flat band in a network of conducting segments. In particular, in a honeycomb network, the flat band is stable as long as the hopping range is shorter than the segment length and the reflection symmetry of the honeycomb structure is kept. This may be realized in the nearly-commensurate charge density wave (NCCDW) phase of 1T-TaS₂, and could be a factor for the superconductivity observed at low temperatures in the vicinity of the NCCDW phase. We also introduced a new argument based on tilted boundary conditions for the Lieb-Schultz-Mattis (LSM) ingappability. It removes the need of an artificial restriction on system sizes, and elucidates the relation between the LSM ingappability in higher dimensions

* Joint research among groups within ISSP.

and the anomaly in quantum field theory in 1+1 dimensions.

1. †*Particle-Hole Symmetry Breaking in a Spin-Dimer System TiCuCl_3 Observed at 100 T: X. -G. Zhou, Y. Yao, Y. H. Matsuda, A. Ikeda, A. Matsuo, K. Kindo and H. Tanaka, *Phys. Rev. Lett.* **125**, 267207 1-6 (2020).
2. †Stable Flatbands, Topology, and Superconductivity of Magic Honeycomb Networks: J. M. Lee, C. Geng, J. W. Park, M. Oshikawa, S.-S. Lee, H. W. Yeom and G. Y. Cho, *Phys. Rev. Lett.* **124**, 137002 (2020).
3. Generalized Boundary Condition Applied to Lieb-Schultz-Mattis-Type Incommensurabilities and Many-Body Chern Numbers: Y. Yao and M. Oshikawa, *Phys. Rev. X* **10**, 031008 (2020).
4. †Refined symmetry indicators for topological superconductors in all space groups: S. Ono, H. C. Po and H. Watanabe, *Sci. Adv.* **6**, eaaz8367 (1-14) (2020).
5. †Filling-enforced constraint on the quantized Hall conductivity on a periodic lattice: Y.-M. Lu, Y. Ran and M. Oshikawa, *Annals of Physics* **413**, 168060 (2020).
6. †Proof of the Absence of Long-Range Temporal Orders in Gibbs States: H. Watanabe, M. Oshikawa and T. Koma, *J Stat Phys* **178**, 926 (2020).
7. Non-local order parameters and quantum entanglement for fermionic topological field theories: K. Inamura, R. Kobayashi and S. Ryu, *Journal of High Energy Physics* **01**, 121(1-30) (2020).
8. Cyclotron resonance in Kondo insulator: Y. Tada, *Physical Review Research* **2**, 023194 (2020).
9. Quantum criticality of magnetic catalysis in two-dimensional correlated Dirac fermions: Y. Tada, *Physical Review Research* **2**, 033363 (2020).
10. Quantum valence bond ice theory for proton-driven quantum spin-dipole liquids: M. G. Yamada and Y. Tada, *Physical Review Research* **2**, 043077 (2020).
11. †Higher anomalies, higher symmetries, and cobordisms II: Lorentz symmetry extension and enriched bosonic / fermionic quantum gauge theory: Z. Wan, J. Wang and Y. Zheng, *Annals of Mathematical Sciences and Applications* **5**, 171 (2020).
12. †Non-Fermi Liquids in Conducting Two-Dimensional Networks: J. M. Lee, M. Oshikawa and G. Y. Cho, *Phys. Rev. Lett.* **126**, 186601 (2021).
13. †Parafermionization, bosonization, and critical parafermionic theories: Y. Yao and A. Furusaki, *J. High Energ. Phys.* **2021**, 285 (2021).
14. †Twisted boundary condition and Lieb-Schultz-Mattis incommensurability for discrete symmetries: Y. Yao and M. Oshikawa, *Phys. Rev. Lett.* (2021), accepted for publication.

Nakatsuji group

A new era in quantum materials research arises, featuring discoveries of novel topological phases of matter and emergent quasi-particle excitations behaving as elusive elementary particles. Our research activities focus on designing and synthesizing new materials with emergent quantum properties that have never been seen before, then exploring the physics behind such properties with our world-leading measurement facilities. We aim to lead the innovative quest for new quantum materials that bear a far-reaching impact not only on basic science but also on our everyday life in the future. Major research themes: 1. Solid-state analogs of relativistic particles and new quantum phenomena · Weyl fermion and chiral anomaly · Quantum spin ice, magnetic monopole, and emergent photon 2. Room-temperature quantum transport phenomena in topological magnetic materials · Weyl antiferromagnets and their application to spintronic devices · Giant thermal and optical responses driven by the Berry curvature 3. Quantum phase transition in strongly correlated systems · Non-Fermi-liquid behavior and exotic superconductivity in multipolar Kondo materials

1. *Field-Orientation Effect on Ferro-Quadrupole Order in $\text{PrTi}_2\text{Al}_{20}$: S. Kittaka, T. Taniguchi, K. Hattori, S. Nakamura, T. Sakakibara, M. Takigawa, M. Tsujimoto, A. Sakai, Y. Matsumoto and S. Nakatsuji, *J. Phys. Soc. Jpn.* **89**, 043701(1-4) (2020).
2. Unveiling Quadrupolar Kondo Effect in the Heavy Fermion Superconductor $\text{PrV}_2\text{Al}_{20}$: M. Fu, A. Sakai, N. Sogabe, M. Tsujimoto, Y. Matsumoto and S. Nakatsuji, *J. Phys. Soc. Jpn.* **89**, 013704 (2020).
3. *Growth of $\text{Pr}_2\text{Ir}_2\text{O}_7$ thin films using solid phase epitaxy: T. Ohtsuki, Z. Tian, M. Halim, S. Nakatsuji and M. Lippmaa, *J. Appl. Phys.* **127**, 035303 (1-9) (2020).

† Joint research with outside partners.

4. Anomalous transverse response of Co₂MnGa and universality of the room-temperature ratio $\alpha_{ij}^A/\sigma_{ij}^A$ across topological magnets: L. Xu, X. Li, L. Ding, T. Chen, A. Sakai, B. Fauqué, S. Nakatsuji, Z. Zhu and K. Behnia, *Phys. Rev. B* **101**, 180404 (2020).
5. Antichiral spin order, its soft modes, and their hybridization with phonons in the topological semimetal Mn₃Ge: Y. Chen, J. Gaudet, S. Dasgupta, G. G. Marcus, J. Lin, T. Chen, T. Tomita, M. Ikhlas, Y. Zhao, W. C. Chen, M. B. Stone, O. Tchernyshyov, S. Nakatsuji and C. Broholm, *Phys. Rev. B* **102**, 054403 (2020).
6. Strong in-plane anisotropy in the electronic structure of fixed-valence β -LuAlB₄: P. Reiss, J. Baglo, H. Tan, X. Chen, S. Friedemann, K. Kuga, F. Malte Grosche, S. Nakatsuji and M. Sutherland, *Phys. Rev. B* **102**, 081102 (2020).
7. Impact of the lattice on magnetic properties and possible spin nematicity in the S = 1 triangular antiferromagnet NiGa₂S₄: M. E. Valentine, T. Higo, Y. Nambu, D. Chaudhuri, J. Wen, C. Broholm, S. Nakatsuji and N. Drichko, *Phys. Rev. Lett.* **125**, 197201 (2020).
8. Many-Body Resonance in a Correlated Topological Kagome Antiferromagnet: SS. Zhang, JX. Yin, M. Ikhlas, HJ. Tien, R. Wang, N. Shumiya, GQ. Chang, SS. Tsirkin, YG. Shi, CJ. Yi, Z. Guguchia, H. Li, WH. Wang, TR. Chang, ZQ. Wang, YF. Yang, T. Neupert, S. Nakatsuji and MZ. Hasan, *Phys. Rev. Lett.* **125**, 046401 (2020).
9. A tunable stress dilatometer and measurement of the thermal expansion under uniaxial stress of Mn₃Sn: M. Ikhlas, K. R. Shirer, P.-Y. Yang, A. P. Mackenzie, S. Nakatsuji and C. W. Hicks, *Appl. Phys. Lett.* **117**, 233502 (2020).
10. *Effect of sample size on anomalous Nernst effect in chiral antiferromagnetic Mn₃Sn devices: H. Narita, T. Higo, M. Ikhlas, S. Nakatsuji and Y. Otani, *Appl. Phys. Lett.* **116**, 072404 (2020).
11. *Magneto-optical Kerr effect in a non-collinear antiferromagnet Mn₃Ge: M. Wu, H. Isshiki, T. Chen, T. Higo, S. Nakatsuji and Y. Otani, *Appl. Phys. Lett.* **116**, 132408 (2020).
12. Superconducting properties of the ternary boride YRh₄B₄: J. Jatmika, H. Maruyama, M. S. Rahman, A. Sakai, S. Nakatsuji, A. Iyo and T. Ebihara, *Supercond. Sci. Technol.* **33**, 125006 (2020).
13. *Electrical manipulation of a topological antiferromagnetic state: H. Tsai, T. Higo, K. Kondou, T. Nomoto, A. Sakai, A. Kobayashi, T. Nakano, K. Yakushiji, R. Arita, S. Miwa, Y. Otani and S. Nakatsuji, *Nature* **580**, 608-613 (2020).
14. *Iron-based binary ferromagnets for transverse thermoelectric conversion: A. Sakai, S. Minami, T. Koretsune, T. Chen, T. Higo, Y. Wang, T. Nomoto, M. Hirayama, S. Miwa, D. Nishio-Hamane, F. Ishii, R. Arita and S. Nakatsuji, *Nature* **581**, 53-57 (2020).
15. 硬 X 線光電子分光と基礎物性測定により明らかにした価数の量子臨界現象：久我 健太郎，松本 洋介，大川 万里生，中辻 知，*放射光* **33**, 1-8 (2020).
16. Magnetic and transport properties of amorphous, B₂ and L₂₁ Co₂MnGa thin films: Z. Zhu, T. Higo, S. Nakatsuji and Y. Otani, *AIP Advances* **10**, 085020 (2020).
17. *Structural and magnetic properties of Mn₃Ge films with Pt and Ru seed layers: A. Kobayashi, T. Higo, S. Nakatsuji and Y. Otani, *AIP Advances* **10**, 015225(1-6) (2020).
18. *Extracting the Chiral Contribution to the Negative Longitudinal Magnetoresistance in Epitaxial Pr₂Ir₂O₇ Thin Films: T. Ohtsuki, Z. Tian, A. Endo, M. Halim, S. Katsumoto, Y. Kohama, K. Kindo, M. Lippmaa and S. Nakatsuji, *JPS Conf. Proc.* **30**, 011181 (1-6) (2020).
19. *Magnetization and Thermal Expansion Properties of Quantum Spin Ice Candidate Pr₂Zr₂O₇: N. Tang, A. Sakai, K. Kimura, S. Nakamura, M. Fu, Y. Matsumoto, T. Sakakibara and S. Nakatsuji, *JPS Conf. Proc.* **30**, 011090(1-6) (2020).
20. Large Nernst Effect and Thermodynamics Properties in Weyl Antiferromagnet: T. Tomita, M. Ikhlas and S. Nakatsuji, *JPS Conf. Proc* **30**, 011009/1-7 (2020).
21. *Room-temperature terahertz anomalous Hall effect in Weyl antiferromagnet Mn₃Sn thin films: T. Matsuda, N. Kanda, T. Higo, N. P. Armitage, S. Nakatsuji and R. Matsunaga, *Nat Commun* **11**, 909 (2020).
22. *Electrical nucleation, displacement, and detection of antiferromagnetic domain walls in the chiral antiferromagnet Mn₃Sn: S. Sugimoto, Y. Nakatani, Y. Yamane, M. Ikhlas, K. Kondou, M. Kimata, T. Tomita, S. Nakatsuji and Y. Otani, *Commun Phys* **3**, 111 (2020).
23. Sample Quality Dependence of the Magnetic Properties in Non-Collinear Antiferromagnet Mn₃Sn: M. Ikhlas, T. Tomita and S. Nakatsuji, *JPS. Conf. Proc* **30**, 011177 (2020).

* Joint research among groups within ISSP.

24. Crystal structure and magnetic properties of the ferromagnet CoMnSb: H. Nakamura, M. Y. P. Akbar, T. Tomita, A. A. Nugroho and S. Nakatsuji, *JPS Conference Proceedings* **29**, 013004/1-5 (2020).
25. Unconventional free charge in the correlated semimetal Nd₂Ir₂O₇: K. Wang, B. Xu, C. W. Rischau, N. Bachar, B. Michon, J. Teyssier, Y. Qiu, T. Ohtsuki, B. Cheng, N. P. Armitage, S. Nakatsuji and D. van der Marel, *Nat. Phys.* **16**, 1194–1198 (2020).
26. Superconducting properties of the ternary boride YRh₄B₄: J. Jatmika, H. Maruyama, MS. Rahman, A. Sakai, S. Nakatsuji, A. Iyo and T. Ebihara, *SUPERCONDUCTOR SCIENCE & TECHNOLOGY*, **33**, 125006 (2020).
27. *Low Gilbert damping in the nodal-line semimetal D₀₃-Fe₃Ga epitaxial thin film: S. Sakamoto, T. Higo, S. Tamaru, H. Kubota, K. Yakushiji, S. Nakatsuji and S. Miwa, *Phys. Rev. B* **103**, 165122 (1-5) (2021).
28. *Domain structure and domain wall dynamics in topological chiral antiferromagnets from the viewpoint of magnetic octupole: Y. Otani and T. Higo, *Appl. Phys. Lett.* **118**, 040501 (2021).
29. *Omnidirectional Control of Large Electrical Output in a Topological Antiferromagnet: T. Higo, Y. Li, K. Kondou, D. Qu, M. Ikhlas, R. Uesugi, D. Nishio-Hamane, C. L. Chien, Y. Otani and S. Nakatsuji, *Adv. Funct. Mater.* **31**, 2008971-12 (2021).
30. *Spin-orbit torque switching of the antiferromagnetic state in polycrystalline Mn₃Sn/Cu/heavy metal heterostructures: H. Tsai, T. Higo, K. Kondou, A. Kobayashi, T. Nakano, K. Yakushiji, S. Miwa, Y. Otani and S. Nakatsuji, *AIP Advances* **11**, 045110 (1-6) (2021).
31. Anomalous transport due to Weyl fermions in the chiral antiferromagnets Mn₃X, X=Sn, Ge: T. Chen, T. Tomita, S. Minami, M. Fu, T. Koretsune, M. Kitatani, I. Muhammad, D. Nishio-Hamane, R. Ishii, F. Ishii, R. Arita and S. Nakatsuji, *Nat. Commun.* **12**, 572 (2021).
32. Inhomogeneous Kondo-lattice in geometrically frustrated Pr₂Ir₂O₇: M. Kawai, J. Friedman, K. Sherman, M. Gong, I. Giannakis, S. Hajinazar, H. Hu, S. E. Grefe, J. Leshen, Q. Yang, S. Nakatsuji, A. N. Kolmogorov, Q. Si, M. Lawler and P. Aynajian, *Nat. Commun.* **12**, 1377 (2021).
33. *Fabrication of polycrystalline Weyl antiferromagnetic Mn₃Sn thin films on various seed layers: T. Nakano, T. Higo, A. Kobayashi, S. Miwa, S. Nakatsuji and K. Yakushiji, *Phys. Rev. Materials* **5**, 054402 (1-9) (2021).
34. *Giant Effective Damping of Octupole Oscillation in an Antiferromagnetic Weyl Semimetal: S. Miwa, S. Iihama, T. Nomoto, T. Tomita, T. Higo, M. Ikhlas, S. Sakamoto, Y. Otani, S. Mizukami, R. Arita and S. Nakatsuji, *Small Science* **1**, 2000062 (1-8) (2021).
35. *Large Hall Signal due to Electrical Switching of an Antiferromagnetic Weyl Semimetal State: H. Tsai, T. Higo, K. Kondou, S. Sakamoto, A. Kobayashi, T. Matsuo, S. Miwa, Y. Otani and S. Nakatsuji, *Small Science* **1**, 2000025 (1-9) (2021).

Miwa group

We have studied the following topics this year: (1) Spin-torque effect on a chiral antiferromagnet Mn₃Sn, (2) Thin film growth of a line-node ferromagnet Fe₃X, and (3) Chiral molecular spintronics device. In topic (1), we find that it is feasible to control a topological antiferromagnetic state in Mn₃Sn by using an unconventional spin-transfer effect (*Nature* 580, 608). This is a work in collaboration with Nakatsuji and Otani groups. In topic (2), we have succeeded in preparing Fe₃Al and Fe₃Gd thin film by using a molecular beam epitaxy method, which shows giant anomalous Nernst effect as those in a bulk form (*Nature* 581, 53). This is a work in collaboration with Nakatsuji group. In topic (3), we find a chirality-induced effective magnetic field in a phthalocyanine molecule at Fe/MgO interface. Unlike the previous study, our system shows an effective magnetic field in the absence of a bias current in the system (*Appl. Phys. Express* 13, 113001, *Spotlights* 2020).

1. Voltage-controlled magnetic anisotropy in an ultrathin nickel film studied by operando x-ray magnetic circular dichroism spectroscopy: R. Miyakaze, S. Sakamoto, T. Kawabe, T. Tsukahara, Y. Kotani, K. Toyoki, T. Nakamura, M. Goto, Y. Suzuki and S. Miwa, *Phys. Rev. B* **102**, 014419 (1-6) (2020).
2. Investigation of gating effect in Si spin MOSFET: S. Lee, F. Rortais, R. Ohshima, Y. Ando, M. Goto, S. Miwa, Y. Suzuki, H. Koike and M. Shiraishi, *Appl. Phys. Lett.* **116**, 022403 (1-5) (2020).
3. Sizable spin-transfer torque in the Bi/Ni₈₀Fe₂₀ bilayer film: M. Matsushima, S. Miwa, S. Sakamoto, T. Shinjo, R. Ohshima, Y. Ando, Y. Fuseya and M. Shiraishi, *Appl. Phys. Lett.* **117**, 042407 (1-4) (2020).
4. *Electrical manipulation of a topological antiferromagnetic state: H. Tsai, T. Higo, K. Kondou, T. Nomoto, A. Sakai, A. Kobayashi, T. Nakano, K. Yakushiji, R. Arita, S. Miwa, Y. Otani and S. Nakatsuji, *Nature* **580**, 608-613 (2020).

† Joint research with outside partners.

5. *Iron-based binary ferromagnets for transverse thermoelectric conversion: A. Sakai, S. Minami, T. Koretsune, T. Chen, T. Higo, Y. Wang, T. Nomoto, M. Hirayama, S. Miwa, D. Nishio-Hamane, F. Ishii, R. Arita and S. Nakatsuji, *Nature* **581**, 53-57 (2020).
6. Control of Spin–Orbit Torques by Interface Engineering in Topological Insulator Heterostructures: F. Bonell, M. Goto, G. Sauthier, J. F. Sierra, A. I. Figueroa, M. V. Costache, S. Miwa, Y. Suzuki and S. O. Valenzuela, *Nano Lett.* **20**, 5893-5899 (2020).
7. Detection of Spin Transfer from Metal to Molecule by Magnetoresistance Measurement: H. Gamou, K. Shimose, R. Enoki, E. Minamitani, A. Shiotari, Y. Kotani, K. Toyoki, T. Nakamura, Y. Sugimoto, M. Kohda, J. Nitta and S. Miwa, *Nano Lett.* **20**, 75-80 (2020).
8. *Chirality-induced effective magnetic field in a phthalocyanine molecule: S. Miwa, K. Kondou, S. Sakamoto, A. Nihonyanagi, F. Araoka, Y. Otani and D. Miyajima, *Appl. Phys. Express* **13**, 113001 (1-4) (Spotlights 2020) (2020).
9. Over 1% magnetoresistance ratio at room temperature in non-degenerate silicon-based lateral spin valves: H. Koike, S. Lee, R. Ohshima, E. Shigematsu, M. Goto, S. Miwa, Y. Suzuki, T. Sasaki, Y. Ando and M. Shiraishi, *Appl. Phys. Express* **13**, 083002 (1-4) (2020).
10. Enhancement of spin signals by thermal annealing in silicon-based lateral spin valves: N. Yamashita, S. Lee, R. Ohshima, E. Shigematsu, H. Koike, Y. Suzuki, S. Miwa, M. Goto, Y. Ando and M. Shiraishi, *AIP Advances* **10**, 095021 (1-6) (2020).
11. Electrical Control for Extending the Ramsey Spin Coherence Time of Ion-Implanted Nitrogen-Vacancy Centers in Diamond: S. Kobayashi, Y. Matsuzaki, H. Morishita, S. Miwa, Y. Suzuki, M. Fujiwara and N. Mizuoichi, *Phys. Rev. Applied* **14**, 044033 (1-10) (2020).
12. Gate-Tunable Spin XOR Operation in a Silicon-Based Device at Room Temperature: R. Ishihara, Y. Ando, S. Lee, R. Ohshima, M. Goto, S. Miwa, Y. Suzuki, H. Koike and M. Shiraishi, *Phys. Rev. Applied* **13**, 044010 (1-9) (2020).
13. *Low Gilbert damping in the nodal-line semimetal $D0_3$ -Fe₃Ga epitaxial thin film: S. Sakamoto, T. Higo, S. Tamaru, H. Kubota, K. Yakushiji, S. Nakatsuji and S. Miwa, *Phys. Rev. B* **103**, 165122 (1-5) (2021).
14. Physically Unclonable Functions With Voltage-Controlled Magnetic Tunnel Junctions: Y. Tanaka, M. Goto, A. K. Shukla, K. Yoshikawa, H. Nomura, S. Miwa, S. Tomishima and Y. Suzuki, *IEEE Trans. Magn.* **57**, 3400806 (1-6) (2021).
15. *Spin-orbit torque switching of the antiferromagnetic state in polycrystalline Mn₃Sn/Cu/heavy metal heterostructures: H. Tsai, T. Higo, K. Kondou, A. Kobayashi, T. Nakano, K. Yakushiji, S. Miwa, Y. Otani and S. Nakatsuji, *AIP Advances* **11**, 045110 (1-6) (2021).
16. *Fabrication of polycrystalline Weyl antiferromagnetic Mn₃Sn thin films on various seed layers: T. Nakano, T. Higo, A. Kobayashi, S. Miwa, S. Nakatsuji and K. Yakushiji, *Phys. Rev. Materials* **5**, 054402 (1-9) (2021).
17. *Giant Effective Damping of Octupole Oscillation in an Antiferromagnetic Weyl Semimetal: S. Miwa, S. Iihama, T. Nomoto, T. Tomita, T. Higo, M. Ikhlas, S. Sakamoto, Y. Otani, S. Mizukami, R. Arita and S. Nakatsuji, *Small Science* **1**, 2000062 (1-8) (2021).
18. *Large Hall Signal due to Electrical Switching of an Antiferromagnetic Weyl Semimetal State: H. Tsai, T. Higo, K. Kondou, S. Sakamoto, A. Kobayashi, T. Matsuo, S. Miwa, Y. Otani and S. Nakatsuji, *Small Science* **1**, 2000025 (1-9) (2021).
19. 電圧トルク MRAM に向けた新材料探索と磁化反転制御技術開発：野崎 隆行，山本 竜也，三輪 真嗣，鈴木 義茂，湯浅新治，まぐね **15**, 15-23 (2020).
20. 磁気抵抗効果を使ったスピントロニクス現象：三輪 真嗣，電気評論 **105**, 21-28 (2020).

Division of Data-Integrated Materials Science

Fukushima group

We have developed an automatic exhaustive calculation tool which is based on the Korriga-Kohn-Rostoker coherent potential approximation (KKR-CPA) method. Our tool can explore the huge materials space consisting of disordered systems and construct large-scale materials databases. In this year, we implemented new features in our tool. One is the scale-bridging

* Joint research among groups within ISSP.

(multi-scale) simulation technique combining KKR-CPA and Monte Carlo methods for magnetocaloric materials. We applied this method to MnCoGe alloys systems and succeeded in quantitatively evaluating the Curie temperature, magnetic entropy, and isothermal entropy. Another is the calculation technique of electronic structures, magnetic properties, and transport properties at finite temperature. Temperature effects often have a significant influence on the materials properties. To investigate the electronic structures at finite temperature, we need to incorporate the effects of local phonon excitations and spin-wave (magnon) excitations in the framework of the KKR-CPA method. In the KKR Green's function method, the single-site t -matrix is the sum of the coefficients of partial wave expansion at each atomic position and contains information of the single-site scattering effect. We can thus replace the multiple scattering effect by an effective medium potential using CPA. The local phonon excitation and magnon excitation can be treated as the configuration average with respect to the local phonon displacements and local moment disorder (LMD) states, respectively. We performed KKR-CPA calculations of temperature-dependent electronic structures and transport properties of the half-metallic Heusler alloy Co_2MnSi . The electrical resistivity was calculated by the Kubo-Greenwood formula. For Co_2MnSi , due to impurity scattering by the Mn-Co antisite disorder, a rather large residual resistivity exists. Handling the local phonon, magnon, and Mn-Co antisite disorders simultaneously by CPA, we were able to reproduce the experimentally observed temperature-dependent resistivity. Thus, we not only calculated the electronic structures incorporating temperature effects, which are difficult for conventional first-principles approaches, but also estimated the transport properties of the half-metallic Heusler alloy. Our method replicated the experiments and was demonstrated to be effective. Applying this method to other Heusler alloys and superlattices with giant magnetoresistance (GMR) and TMR structures, it will be possible to exploit theoretically-driven materials design of next-generation spintronics.

1. Hole-mediated ferromagnetism in a high-magnetic moment material, Gd-doped GaN: A. Masago, H. Shinya, T. Fukushima, K. Sato and H. Katayama-Yoshida, *J. Phys.: Condens. Matter* **32**, 485803(1-6) (2020).
2. Magnetocaloric effect in MnCoGe alloys studied by first-principles calculations and Monte-Carlo simulation: H. B. Tran, T. Fukushima, Y. Makino and T. Oguchi, *Solid State Commun.* **323**, 114077(1-5) (2020).
3. *First-principles calculations of finite temperature electronic structures and transport properties of Heusler alloy Co_2MnSi : H. Shinya, S. Kou, T. Fukushima, A. Masago, K. Sato, H. Katayama-Yoshida and H. Akai, *Appl. Phys. Lett.* **117**, 042402(1-5) (2020).
4. Tuning structural-transformation temperature toward giantmagnetocaloric effect in MnCoGe alloy: A theoretical study: H. B. Tran, T. Fukushima, K. Sato, Y. Makino and T. Oguchi, *J. Alloys Compd.* **854**, 157063(1-9) (2020).
5. Spin injection through energy-band symmetry matching with high spin polarization in atomically controlled ferromagnet/ferromagnet/ semiconductor structures: M. Yamada, F. Kuroda, M. Tsukahara, S. Yamada, T. Fukushima, K. Sawano, T. Oguchi and K. Hamaya, *NPG Asia Mater.* **12**, 47(1-9) (2020).
6. Valence states and the magnetism of Eu ions in Eu-doped GaN: T. Nunokawa, Y. Fujiwara, Y. Miyata, N. Fujimura, T. Sakurai, H. Ohta, A. Masago, H. Shinya, T. Fukushima, K. Sato and H. Katayama-Yoshida, *J. Appl. Phys.* **127**, 083901(1-7) (2020).
7. High Curie temperature in Eu-doped GaN caused by volume-compensated Ga-vacancy: A. Masago, H. Shinya, T. Fukushima, K. Sato and H. Katayama-Yoshida, *AIP Adv.* **10**, 025216(1-4) (2020).
8. First-principles calculation of electronic density of states and Seebeck coefficient in transition-metal-doped Si-Ge alloys: R. Yamada, A. Masago, T. Fukushima, H. Shinya, T. Q. Nguyen and K. Sato, *Solid State Commun.* **323**, 110227(1-8) (2021).
9. Effect of atomic configuration on magnetic properties and electronic state of CoVMnAl quaternary heusler alloy: R. Y. Umetsu, K. Saito, K. Ono, T. Fukushima, F. Kuroda, T. Oguchi and T. Ishigaki, *J. Alloys Compd.* **855**, 157389(1-9) (2021).
10. Theoretical prediction of large anisotropic magnetocaloric effect in MnP: H. B. Tran, T. Fukushima, H. Momida, K. Sato, Y. Makino and T. Oguchi, *Comput. Mater. Sci.* **188**, 110227(1-8) (2021).
11. Intrinsic defect formation and the effect of transition metal doping on transport properties in a ductile thermoelectric material $\alpha\text{-Ag}_2\text{S}$: a first-principles study: H. N. Nam, R. Yamada, H. Okumura, T. Q. Nguyen, K. Suzuki, H. Shinya, A. Masago, T. Fukushima and K. Sato, *Phys. Chem. Chem. Phys.* (2021), accepted for publication.

† Joint research with outside partners.

Materials Design and Characterization Laboratory

Hiroi group

A new titanium hydride complex $\text{BaCa}_2\text{Ti}_2\text{H}_{14}$ with the 9-fold coordination was discovered. A new spin-orbit-coupled metal candidate PbRe_2O_6 was studied. Kitaev spin liquid candidate Os_xCl_3 comprised of honeycomb nano-domains was investigated. A multipolar order in the spin-orbit-coupled 5d Mott insulator B_2MgReO_6 was studied by high-resolution XRD.

1. *Domain Control by Adjusting Anisotropic Stress in Pyrochlore Oxide $\text{Cd}_2\text{Re}_2\text{O}_7$: S. Tajima, D. Hirai, Y. Kinoshita, M. Tokunaga, K. Akiba, T. C. Kobayashi, H. T. Hirose and Z. Hiroi, *J. Phys. Soc. Jpn.* **89**, 114711 (2020).
2. *Kitaev Spin Liquid Candidate Os_xCl_3 Comprised of Honeycomb Nano-Domains: K. Kataoka, D. Hirai, T. Yajima, D. Nishio-Hamane, R. Ishii, K.-Y. Choi, D. Wulferding, P. Lemmens, S. Kittaka, T. Sakakibara, H. Ishikawa, A. Matsuo, K. Kindo and Z. Hiroi, *J. Phys. Soc. Jpn.* **89**, 114709(1-9) (2020).
3. Variation in Superconducting Symmetry Against Pressure on Noncentrosymmetric Superconductor $\text{Cd}_2\text{Re}_2\text{O}_7$ Revealed by 185/187Re Nuclear Quadrupole Resonance: S. Kitagawa, K. Ishida, T. C. Kobayashi, Y. Matsubayashi, D. Hirai and Z. Hiroi, *J. Phys. Soc. Jpn.* **89**, 053701 (2020).
4. Anomalous changes of electric quadrupole order at low temperatures in the spin-orbit coupled metal $\text{Cd}_2\text{Re}_2\text{O}_7$: S. Uji, S. Sugiura, H. T. Hirose, T. Terashima, Y. Matsubayashi, D. Hirai, Z. Hiroi and T. Hasegawa, *Phys. Rev. B* **102**, 155131 (2020).
5. Antiferromagnetic long-range order in the 5d(1) double-perovskite $\text{Sr}_2\text{MgReO}_6$: S. Gao, D. Hirai, H. Sagayama, H. Ohsumi, Z. Hiroi and T.-H. Arima, *Phys. Rev. B* **101**, 220412 (2020).
6. Coexistence of odd-parity and even-parity order parameters in the multipole order phase of the spin-orbit coupled metal $\text{Cd}_2\text{Re}_2\text{O}_7$: Y. Matsubayashi, K. Sugii, D. Hirai, Z. Hiroi, T. Hasegawa, S. Sugiura, H. T. Hirose, T. Terashima and S. Uji, *Phys. Rev. B* **101**, 205133 (2020).
7. *Helical and collinear spin density wave order in the $S = 1/2$ one-dimensional frustrated chain compound $\text{NaCuMoO}_4(\text{OH})$ investigated by neutron scattering: S. Asai, T. Oyama, K. Nawa, A. Nakao, K. Munakata, K. Kuwahara, M. Hagihala, S. Itoh, Z. Hiroi and T. Masuda, *Phys. Rev. B* **101**, 144437(1-8) (2020).
8. *Zero-energy excitation in the classical kagome antiferromagnet $\text{NaBa}_2\text{Mn}_3\text{F}_{11}$: S. Hayashida, H. Ishikawa, Y. Okamoto, T. Okubo, Z. Hiroi, G. J. Nilsen, H. Mutka and T. Masuda, *Phys. Rev. B* **101**, 214409 (2020).
9. *Anisotropic Triangular Lattice Realized in Rhenium Oxychlorides $\text{A}_3\text{ReO}_5\text{Cl}_2$ ($A = \text{Ba}, \text{Sr}$): D. Hirai, T. Yajima, K. Nawa, M. Kawamura and Z. Hiroi, *Inorg. Chem.* **59**, 10025 (2020).
10. Titanium Hydride Complex $\text{BaCa}_2\text{Ti}_2\text{H}_{14}$ with 9-Fold Coordination: T. Yajima, H. Nakajima, T. Honda, K. Ikeda, T. Otomo, H. Takeda and Z. Hiroi, *Inorg. Chem.* **59**, 4228 (2020).
11. *Spin-orbit-coupled metal candidate PbRe_2O_6 : S. Tajima, D. Hirai, T. Yajima, D. Nishio-Hamane, Y. Matsubayashi and Z. Hiroi, *Journal of Solid State Chemistry* **288**, 121359 (2020).
12. *Thermal Hall Effects of Spins and Phonons in Kagome Antiferromagnet Cd-Kapellasite: M. Akazawa, M. Shimozawa, S. Kittaka, T. Sakakibara, R. Okuma, Z. Hiroi, H.-Y. Lee, N. Kawashima, J. H. Han and M. Yamashita, *Phys. Rev. X* **10**, 041059 (2020).
13. Detection of multipolar orders in the spin-orbit-coupled 5d Mott insulator B_2MgReO_6 : D. Hirai, H. Sagayama, S. Gao, H. Ohsumi, G. Chen, T.-H. Arima and Z. Hiroi, *Phys. Rev. Research* **2**, 022063 (2020).
14. †*Single shot x-ray diffractometry in SACLA with pulsed magnetic fields up to 16 T: A. Ikeda, Y. H. Matsuda, X. Zhou, T. Yajima, Y. Kubota, K. Tono and M. Yabashi, *Phys. Rev. Research* **2**, 043175 1-6 (2020).
15. *Pressure-induced phase transition in the J_1 - J_2 square lattice antiferromagnet $\text{RbMoOPO}_4\text{Cl}$: H. Takeda, T. Yamauchi, M. Takigawa, H. Ishikawa and Z. Hiroi, *Phys. Rev. B* **103**, 104406 (2021).

Kawashima group

We developed highly efficient methods, algorithms, and parallelized programs based on the tensor network (TN) method and applied them to relevant physical problems, which include the following: (1) development of decomposition method of a high-ranked tensor into a ring of smaller low-ranked tensors, (2) development of TN method for boundary phenomena, (3) study of Kitaev spin liquid by TN variational functions, (4) study of spin liquid in frustrated spin systems, (5) TN study of deconfined-critical phenomena, and (6) TN implementation of real-space renormalization group.

* Joint research among groups within ISSP.

1. Frustration-induced supersolid phases of extended Bose–Hubbard model in the hard-core limit: W.-L. Tu, H.-K. Wu and T. Suzuki, *J. Phys.: Condens. Matter* **32**, 455401 (2020).
2. Tensor-Ring Decomposition with Index-Splitting: H.-Y. Lee and N. Kawashima, *J. Phys. Soc. Jpn.* **89**, 054003(1-9) (2020).
3. Abelian and non-Abelian chiral spin liquids in a compact tensor network: H.-Y. Lee, R. Kaneko, T. Okubo and N. Kawashima, *Phys. Rev. B* **101**, 035140 (2020).
4. Boundary conformal spectrum and surface critical behavior of classical spin systems: A tensor network renormalization study: S. Iino, S. Morita and N. Kawashima, *Phys. Rev. B* **101**, 155418 (2020).
5. Construction of variational matrix product states for the Heisenberg spin-1 chain: J. Kim, M. Kim, N. Kawashima, J. H. Han and H.-Y. Lee, *Phys. Rev. B* **102**, 085117(1-8) (2020).
6. Competing quantum phases of hard-core bosons with tilted dipole-dipole interaction: H.-K. Wu and W.-L. Tu, *Phys. Rev. A* **102**, 053306 (2020).
7. *Thermal Hall Effects of Spins and Phonons in Kagome Antiferromagnet Cd-Kapellasite: M. Akazawa, M. Shimozawa, S. Kittaka, T. Sakakibara, R. Okuma, Z. Hiroi, H.-Y. Lee, N. Kawashima, J. H. Han and M. Yamashita, *Phys. Rev. X* **10**, 041059 (2020).
8. Magnetic field induced quantum phases in a tensor network study of Kitaev magnets: H.-Y. Lee, R. Kaneko, L. E. Chern, T. Okubo, Y. Yamaji, N. Kawashima and Y. B. Kim, *Nature Communications* **11**, 1639 (2020).
9. Magnetic field induced competing phases in spin-orbital entangled Kitaev magnets: L. E. Chern, R. Kaneko, H.-Y. Lee and Y. B. Kim, *Phys. Rev. Research* **2**, 013014 (2020).
10. Tensor network wave function of S=1 Kitaev spin liquids: H.-Y. Lee, N. Kawashima and Y. B. Kim, *Phys. Rev. Research* **2**, 033318(1-6) (2020).
11. *分子動力学計算による複雑流体中のカルマン渦の解析: 浅野 優太, 渡辺 宙志, 野口 博司, 分子シミュレーション学会誌 "アンサンブル" **22**, 157-162 (2020).
12. Effective Ruderman–Kittel–Kasuya–Yosida-like Interaction in Diluted Double-exchange Model: Self-learning Monte Carlo Approach: H. Kohshiro and Y. Nagai, *J. Phys. Soc. Jpn.* **90**, 034711 (2021).
13. Continuous phase transition between Neel and valence bond solid phases in a J-Q-like spin ladder system: T. Ogino, R. Kaneko, S. Morita, S. Furukawa and N. Kawashima, *Phys. Rev. B* **103**, 085117 (2021).
14. Global optimization of tensor renormalization group using the corner transfer matrix: S. Morita and N. Kawashima, *Phys. Rev. B* **103**, 045131(1-6) (2021).
15. †DSQSS: Discrete Space Quantum Systems Solver: Y. Motoyama, K. Yoshimi, A. Masaki-Kato, T. Kato and N. Kawashima, *Computer Physics Communications* **264**, 107944 (2021).
16. †*K ω — Open-source library for the shifted Krylov subspace method of the form $(zI - H)x = b$: T. Hoshi, M. Kawamura, K. Yoshimi, Y. Motoyama, T. Misawa, Y. Yamaji, S. Todo, N. Kawashima and T. Sogabe, *Computer Physics Communications* **258**, 107536 (2021).
17. "Data Assimilation Method for Experimental and First-Principles Data: Finite-Temperature Magnetization of $(\text{Nd,Pr,L a,Ce})_2(\text{Fe,Co,Ni})_{14}\text{B}$ ": Y. Harashima, K. Tamai, S. Doi, M. Matsumoto, H. Akai, N. Kawashima, M. Ito, N. Sakuma, A. Kato, T. Shoji and T. Miyake, *Phys. Rev. Materials* **5**, 013806(1-10) (2021).
18. Scaling dimensions from linearized tensor renormalization group transformations: X. Lyu, R. G. Xu and N. Kawashima, *Phys. Rev. Research* **3**, 023048 (2021).
19. Boundary CFT and Tensor Network Approach to Surface Critical Phenomena of the Tricritical 3-State Potts model: S. Iino, *J Stat Phys* **182**, 56 (2021).
20. DSQSS: Discrete Space Quantum Systems Solver: Y. Motoyama, K. Yoshimi, A. Masaki-Kato, T. Kato and N. Kawashima, *Computer Physics Communications* **264**, 107944 (2021), accepted for publication.

Uwatoko group

The effect of pressure on the unique electronic state of the antiferromagnetic (AF) compound EuCu_2Ge_2 has been measured in a wide temperature range from 10 mK to 300 K by electrical resistivity measurements up to 10 GPa. The results exhibit that

† Joint research with outside partners.

critical pressure, ~ 6.5 GPa, coincides with valence transition pressure, corresponding to the quantum criticality of the valence transition. A “palm” cubic-anvil pressure cell (PCAC) having an outer diameter of 60 mm, the smallest cubic-anvil cell to date, was fabricated to physical measurements with superconducting magnet. The PCAC is advantageous because a large sample space and pressure homogeneity are secured even under frozen pressure media environment at high pressures. We investigate the pressure effect on the large anomalous Hall effect (AHE) of $\text{Co}_3\text{Sn}_2\text{S}_2$ up to 12 GPa with a palm cubic anvil cell apparatus and first-principles calculations simulation. We find that both the ferromagnetic transition temperature and the AHE are suppressed monotonically upon the application of high pressure. Combined with theoretical calculations, our results indicate that the distance between Weyl points with opposite chirality in $\text{Co}_3\text{Sn}_2\text{S}_2$ is substantially reduced accompanying the suppression of ferromagnetism by pressure, thus providing an experimental route to tune the AHE of magnetic Weyl semimetals via modifying the nontrivial band topology.

1. Pressure effect on the magnetoresistivity of topological semimetal RhSn: S. Xu, S. Xu, J. Sun, B. Wang, Y. Uwatoko, T. Xia and J. Cheng, *J. Phys.: Condens. Matter* **32**, 355601(1-6) (2020).
2. Magnetoelectric Effect in the Antiferromagnetic Ordered State of Ce_3TiBi_5 with Ce Zig-Zag Chains: M. Shinozaki, G. Motoyama, M. Tsubouchi, M. Sezaki, J. Gouchi, S. Nishigori, T. Mutou, A. Yamaguchi, K. Fujiwara, K. Miyoshi and Y. Uwatoko, *J. Phys. Soc. Jpn.* **89**, 033703(1-5) (2020).
3. Quantum Criticality of Valence Transition for the Unique Electronic State of Antiferromagnetic Compound EuCu_2Ge_2 : J. Gouchi, K. Miyake, W. Iha, M. Hedo, T. Nakama, Y. Ônuki and Y. Uwatoko, *J. Phys. Soc. Jpn.* **89**, 053703(1-5) (2020).
4. Single-Crystal Growth and Physical Properties of EuZn_2Ge_2 : M. Kosaka, S. Michimura, H. Hirabayashi, R. Numakura, R. Iizuka, K. Kuwahara and Y. Uwatoko, *J. Phys. Soc. Jpn.* **89**, 054704(1-8) (2020).
5. Coupled magnetic and structural phase transitions in the antiferromagnetic polar metal $\text{Pb}_2\text{CoOsO}_6$ under pressure: Y. Jiao, Y.-W. Fang, J. Sun, P. Shan, Z. Yu, H. L. Feng, B. Wang, H. Ma, Y. Uwatoko, K. Yamaura, Y. Guo, H. Chen and J. Cheng, *Phys. Rev. B* **102**, 144418(1-7) (2020).
6. High pressure investigation of an organic three-dimensional Dirac semimetal candidate having a diamond lattice: A. Kiswandhi, M. Maesato, S. Tomeno, Y. Yoshida, Y. Shimizu, P. Shahi, J. Gouchi, Y. Uwatoko, G. Saito and H. Kitagawa, *Phys. Rev. B* **101**, 245124(1-7) (2020).
7. *Magnetotransport properties of tellurium under extreme conditions: K. Akiba, K. Kobayashi, T. C. Kobayashi, R. Koezuka, A. Miyake, J. Gouchi, Y. Uwatoko and M. Tokunaga, *Phys. Rev. B* **101**, 245111(1-6) (2020).
8. Physical properties and pressure-induced superconductivity in the single-crystalline band insulator SnO: S. Xu, Y. Zou, J. Sun, Z. Liu, X. Yu, J. Gouchi, Y. Uwatoko, Z. G. Cheng, B. Wang and J. Cheng, *Phys. Rev. B* **101**, 104501(1-8) (2020).
9. Pressure-induced incommensurate antiferromagnetic order in a ferromagnetic B-site ordered double-perovskite $\text{Lu}_2\text{NiMnO}_6$: N. Terada, C. V. Colin, N. Qureshi, T. C. Hansen, K. Matsubayashi, Y. Uwatoko and A. A. Belik, *Phys. Rev. B* **102**, 094412(1-9) (2020).
10. *Sample dependence of half-integer quantized thermal Hall effect in the Kitaev spin-liquid candidate $\alpha\text{-RuCl}_3$: M. Yamashita, J. Gouchi, Y. Uwatoko, N. Kurita and H. Tanaka, *Phys. Rev. B* **102**, 220404(R) (2020).
11. Superconducting phase diagrams of S-doped $2H\text{-TaSe}_2$ under hydrostatic pressure: S. Xu, Z. Liu, P. Yang, K. Chen, J. Sun, J. Dai, Y. Yin, F. Hong, X. Yu, M. Xue, J. Gouchi, Y. Uwatoko, B. Wang and J. Cheng, *Phys. Rev. B* **102**, 184511(1-9) (2020).
12. Weak ferromagnetism and possible non-Fermi-liquid behavior in the itinerant electronic material Co_3SnC : B. Wang, Y. Uwatoko, J. Cheng and Y. Sun, *Phys. Rev. B* **102**, 085153(1-9) (2020).
13. NMR study under pressure on the iron-based superconductor $\text{FeSe}_{1-x}\text{S}_x$ ($x = 0.12$ and 0.23): Relationship between nematicity and AF fluctuations: T. Kuwayama, K. Matsuura, Y. Mizukami, S. Kasahara, Y. Matsuda, T. Shibauchi, Y. Uwatoko and N. Fujiwara, *Mod. Phys. Lett. B* **34**, 2040048(1-6) (2020).
14. Effects of Substituted Elements on Spin Reorientation in $\text{Mn}_{2-x}\text{Fe}_x\text{Sb}_{1-y}\text{Sn}_y$: K. Noguchi, Y. Mitsui, M. Hiroi, R. Y. Umetsu, J. Gouchi, Y. Uwatoko and K. Koyama, *Mater. Trans.* **61**, 1492-1495 (2020).
15. Magnetic Field Effect on Nitrogenation of $\text{Sm}_2\text{Fe}_{17}$: K. Koyama, M. Onoue, R. Kobayashi, Y. Mitsui, R. Y. Umetsu and Y. Uwatoko, *Mater. Trans.* **61**, 1487-1491 (2020).
16. Magnetic Measurements of Narrow-Gap Semiconductor FeSb_2 under High Pressure: T. Deguchi, K. Matsubayashi, Y. Uwatoko, T. Koyama, T. Kohara, H. Nakamura, Y. Mitsui and K. Koyama, *Mater. Trans.* **61**, 1476(1-4) (2020).

* Joint research among groups within ISSP.

17. New phenomena of photo-luminescence and persistent luminescence of a Eu^{2+} , Tb^{3+} codoped $\text{Ca}_6\text{BaP}_4\text{O}_{17}$ phosphor under high hydrostatic pressure: H. Guo, T. Seto, T. Geng, B. Zou, G. Li, Y. Uwatoko, Z. Tang, Z. Li and Y. Wang, *Dalton Trans.* **49**, 8056-2059 (2020).
18. Resistive anisotropy of candidate excitonic insulator Ta_2NiSe_5 under pressure: H. Arima, Y. Naito, K. Kudo, N. Katayama, H. Sawa, M. Nohara, Y. F. Lu, K. Kitagawa, H. Takagi, Y. Uwatoko and K. Matsubayashi, *J. Phys.: Conf. Ser.* **1609**, 012001(1-6) (2020).
19. Pressure-Driven Eu^{2+} -Doped $\text{BaLi}_2\text{Al}_2\text{Si}_2\text{N}_6$: A New Color Tunable Narrow-Band Emission Phosphor for Spectroscopy and Pressure Sensor Applications: Y. Wang, T. Seto, K. Ishigaki, Y. Uwatoko, G. Xiao, B. Zou, G. Li, Z. Tang, Z. Li and Y. Wang, *Adv. Funct. Mater.* **1**, 2001384(1-10) (2020).
20. *Single Crystal Growth and Unique Electronic States of Cubic Chiral EuPtSi and Related Compounds: Y. Ônuki, M. Kakihana, W. Iha, K. Nakaima, D. Aoki, A. Nakamura, F. Honda, M. Nakashima, Y. Amako, J. Gouchi, Y. Uwatoko, S. Nakamura, T. Sakakibara, T. Takeuchi, Y. Haga, H. Ikeda, H. Harima, M. Hedo and T. Nakama, *JPS Conf. Proc.* **29**, 012001(1-9) (2020).
21. *Unique Skyrmion Phases and Conduction Electrons in Cubic Chiral Antiferromagnet EuPtSi and Related Compounds: Y. Ônuki, M. Kakihana, W. Iha, K. Nakaima, D. Aoki, A. Nakamura, F. Honda, M. Nakashima, Y. Amako, J. Gouchi, Y. Uwatoko, S. Nakamura, T. Sakakibara, T. Takeuchi, Y. Haga, H. Ikeda, H. Harima, M. Hedo and T. Nakama, *JPS Conf. Proc.* **30**, 011008(1-11) (2020).
22. Pressure-induced second high- T_c superconducting phase in the organic-ion-intercalated $(\text{CTA})_{0.3}\text{FeSe}$ single crystal: J. P. Sun, M. Z. Shi, B. Lei, S. X. Xu, Y. Uwatoko, X. H. Chen and J. -G. Cheng, *EPL* **130**, 67004(1-5) (2020).
23. Pressure effect on the anomalous Hall effect of ferromagnetic Weyl semimetal $\text{Co}_3\text{Sn}_2\text{S}_2$: Z. Y. Liu, T. Zhang, S. X. Xu, P. T. Yang, Q. Wang, H. C. Lei, Y. Sui, Y. Uwatoko, B. S. Wang, H. M. Weng, J. P. Sun and J. -G. Cheng, *Phys. Rev. Materials* **4**, 044203(1-9) (2020).
24. Fabrication and evaluation via nuclear quadrupole resonance of a palm cubic-anvil pressure cell: S. Nakagawa, J. Gochi, T. Kuwayama, S. Nagasaki, T. Takahashi, J. Cheng, Y. Uwatoko and N. Fujiwara, *Review of Scientific Instruments* **91**, 073907(1-7) (2020).
25. Heat treatment effect on the magnetic properties and martensitic transformations of MnCoGe : K. Noguchi, R. Kobayashi, Y. Mitsui, R. Y. Umetsu, J. Gouchi, Y. Uwatoko and K. Koyama, *Journal of Magnetism and Magnetic Materials* **499**, 166199(1-5) (2020).
26. Magnetic field-induced nitridation of $\text{Sm}_2\text{Fe}_{17}$: M. Onoue, R. Kobayashi, Y. Mitsui, R. Y. Umetsu, Y. Uwatoko and K. Koyama, *Journal of Alloys and Compounds* **835**, 155193(1-7) (2020).
27. Superconducting-Gap Anisotropy of Iron Pnictides Investigated via Combinatorial Microwave Measurements: T. Okada, Y. Imai, K. Kitagawa, K. Matsubayashi, M. Nakajima, A. Iyo, Y. Uwatoko, H. Eisaki and A. Maeda, *Sci Rep* **10**, 7064(1-7) (2020).
28. Quasi-one-dimensional magnetic interactions and conduction electrons in EuCu_5 and EuAu_5 with the characteristic hexagonal structure: S. Matsuda, J. Ota, K. Nakaima, W. Iha, J. Gouchi, Y. Uwatoko, M. Nakashima, Y. Amako, F. Honda, D. Aoki, A. Nakamura, T. Takeuchi, Y. Haga, H. Harima, M. Hedo, T. Nakama and Y. Ônuki, *Philosophical Magazine* **JAN 2020**, 1-14 (2020).
29. Redetermination of the crystal structure of R_5Si_4 ($\text{R} = \text{Pr}, \text{Nd}$) from single-crystal X-ray diffraction data: K. Yokota, R. Watanuki, M. Nakashima, M. Uehara, J. Gouchi, Y. Uwatoko and I. Umehara, *Acta Crystallogr E Cryst Commun* **76**, 510 (2020).
30. Pressure-Induced Metallization and Structural Phase Transition in the Quasi-One-Dimensional TlFeSe_2 : Z.-Y. Liu, Q.-X. Dong, P.-F. Shan, Y.-Y. Wang, J.-H. Dai, R. Jana, K.-Y. Chen, J.-P. Sun, B.-S. Wang, X.-H. Yu, G.-T. Liu, Y. Uwatoko, Y. Sui, H.-X. Yang, G.-F. Chen and J.-G. Cheng, *Chinese Phys. Lett.* **37**, 047102 (2020).
31. Crystallographic and superconducting properties of filled skutterudite $\text{SrOs}_4\text{P}_{12}$: Y. Kawamura, S. Deminami, K. Takeda, T. Kuzuya, L. Salamakha, H. Michor, E. Bauer, J. Gouchi, Y. Uwatoko, T. Kawae and C. Sekine, *Phys. Rev. B* **103**, 085139(1-9) (2021).
32. *Strongly correlated superconductivity in a copper-based metal-organic framework with a perfect kagome lattice: T. Takenaka, K. Ishihara, M. Roppongi, Y. Miao, Y. Mizukami, T. Makita, J. Tsurumi, S. Watanabe, J. Takeya, M. Yamashita, K. Torizuka, Y. Uwatoko, T. Sasaki, X. Huang, W. Xu, D. Zhu, N. Su, J. -G. Cheng, T. Shibauchi and K. Hashimoto, *Sci. Adv.* **7**, eabf3996(1-8) (2021).
33. Author Correction: Experimental evidence for the existence of a second partially-ordered phase of ice VI: R. Yamane,

† Joint research with outside partners.

- K. Komatsu, J. Gouchi, Y. Uwatoko, S. Machida, T. Hattori, H. Ito and H. Kagi, *Nat Commun* **12**, 1800 (2021).
34. Experimental evidence for the existence of a second partially-ordered phase of ice VI: R. Yamane, K. Komatsu, J. Gouchi, Y. Uwatoko, S. Machida, T. Hattori, H. Ito and H. Kagi, *Nat Commun* **12**, 1129(1-6) (2021).
 35. High-pressure phase diagrams of $\text{FeSe}_{1-x}\text{Te}_x$: correlation between suppressed nematicity and enhanced superconductivity: K. Mukasa, K. Matsuura, M. Qiu, M. Saito, Y. Sugimura, K. Ishida, M. Otani, Y. Onishi, Y. Mizukami, K. Hashimoto, J. Gouchi, R. Kumai, Y. Uwatoko and T. Shibauchi, *Nat Commun* **12**, 381(1-7) (2021).
 36. Pressure induced superconducting state in ideal topological insulator BiSbTe_3 : V. K. Gangwar, S. Kumar, M. Singh, L. Ghosh, Y. Zhang, P. Shahi, M. Muntwiler, S. Patil, K. Shimada, Y. Uwatoko, J. Sau, M. Kumar and S. Chatterjee, *Phys. Scr.* **96**, 055802(1-8) (2021).
 37. Internal and External Pressure Effects on Superconductivity in $\text{FeTe}_x\text{Se}_{1-x}$ ($x=0.46, 0.54$) Single Crystals: G. Lingannan, K. Ganesan, S. Mariappan, R. Sankar, Y. Uwatoko and S. Arumugam, *J Supercond Nov Magn* **34**, 725-731 (2021).

Ozaki group

In FY2020, we studied two issues: one is an investigation to unveil structural trends of ternary transition metal nano-particles, and the other is the first-principles calculation of superconducting transition temperature of elemental bulks. (1) As the first issue, we performed first-principles calculations and Monte Carlo sampling to investigate the structures of ternary PdRuM ($M = \text{Pt}, \text{Rh}, \text{or Ir}$) nanoparticles (NPs) with respect to three different spherical shapes. The calculations show that the atomic position is dominant in determining the stability of the ternary NPs. For bare ternary NPs, Pd and Ru atoms favor a location on the vertex sites and the core, respectively, which can be understood by the surface energy of the corresponding slab models. For single-crystalline NPs, the binary shell could be either a solid solution or a segregation alloy depending on composition and morphology. However, polycrystalline Ih NPs only form segregated binary shells surrounding the Ru core. Such configurations tend to minimize the surface lattice to gain more energy from the d orbital of the transition metals. In addition to the bare NPs, we study the oxidized ternary NPs. The results show that the Ru atoms penetrate outwards from the core to the surface reducing the oxidation formation energy. This work clearly demonstrates the structural trends of small ternary NPs, unveiling that the structural trends can be understood by the surface formation energy and the interplay between adsorbent and adsorbing oxygen atoms. (2) As the second issue, we performed systematic calculations to understand the applicability and limitation of Density functional theory for superconductors (SCDFT), which is one of the first-principles methods to compute T_c , and can treat the electron-phonon interaction, electronic Coulomb interaction, and spin fluctuation (SF) fully non-empirically. This method has been applied to mainly the phonon-mediated superconductors. For example, SCDFT is used to reveal the origin of the multi-band superconductivity in MgB_2 , the relationship between the structure and T_c of hydrogen sulfides. We plan to apply this method to a wide variety of materials and accelerate the first-principles exploration of superconductors. For this purpose, we are developing an open-source software Superconducting-Toolkit (SCTK), and release that software on the Web. In this study, we performed a benchmark to the simplest superconductors and non-superconductors, namely 35 elemental metals; we formulated a method to treat SF together with the spin-orbit interaction (SOI) and investigate these two effects on T_c . We believe that this benchmark study will be a milestone for exploring superconductors with high-throughput computations and methodological improvements in the future.

1. Benchmark of density functional theory for superconductors in elemental materials: M. Kawamura, Y. Hizume and T. Ozaki, *Phys. Rev. B* **101**, 134511 (2020).
2. *Emergence of nearly flat bands through a kagome lattice embedded in an epitaxial two-dimensional Ge layer with a bitriangular structure: A. Fleurence, C.-C. Lee, R. Friedlein, Y. Fukaya, S. Yoshimoto, K. Mukai, H. Yamane, N. Kosugi, J. Yoshinobu, T. Ozaki and Y. Yamada-Takamura, *Phys. Rev. B* **102**, 201102 (2020).
3. First-principles study on the stability and electronic structure of monolayer GaSe with trigonal-antiprismatic structure: H. Nitta, T. Yonezawa, A. Fleurence, Y. Yamada-Takamura and T. Ozaki, *Phys. Rev. B* **102**, 235407 (2020).
4. Unfolding optical transition weights of impurity materials for first-principles LCAO electronic structure calculations: Y.-T. Lee, C.-C. Lee, M. Fukuda and T. Ozaki, *Phys. Rev. B* **102**, 075143 (2020).
5. *Formation of BN-covered silicene on $\text{ZrB}_2/\text{Si}(111)$ by adsorption of NO and thermal processes: J. Yoshinobu, K. Mukai, H. Ueda, S. Yoshimoto, S. Shimizu, T. Koitaya, H. Noritake, C.-C. Lee, T. Ozaki, A. Fleurence, R. Friedlein and Y. Yamada-Takamura, *J. Chem. Phys.* **153**, 064702 (2020).
6. *Structural investigation of ternary PdRuM ($M = \text{Pt}, \text{Rh}, \text{or Ir}$) nanoparticles using first-principles calculations: S.-H. Hung, H. Akiba, O. Yamamuro and T. Ozaki, *RSC Adv.* **10**, 16527 (2020).
7. *Electronic structure of a (3×3) -ordered silicon layer on $\text{Al}(111)$: Y. Sato, Y. Fukaya, M. Cameau, A. K. Kundu, D. Shiga, R. Yukawa, K. Horiba, C.-H. Chen, A. Huang, H.-T. Jeng, T. Ozaki, H. Kumigashira, M. Niibe and I.

* Joint research among groups within ISSP.

Matsuda, *Phys. Rev. Materials* **4**, 064005 (2020).

- Neural network atomic potential to investigate the dislocation dynamics in bcc iron: H. Mori and T. Ozaki, *Phys. Rev. Materials* **4**, 040601(R) (2020).
- *Vapochromism induced by intermolecular electron transfer coupled with hydrogen-bond formation in zinc dithiolene complex: T. Fujino, M. Kawamura, T. Ozaki and H. Mori, *J. Mater. Chem. C* **8**, 14939-14947 (2020).
- First-principles adaptive-boost accelerated molecular dynamics simulation with effective boost potential construction methods: a study of Li diffusion in Si crystal: M. Yamamoto, A. Ishii, S. Shinzato, S. Ogata and T. Ozaki, *Japanese Journal of Applied Physics* **59**, 125002 (2020).
- Diverse densest binary sphere packings and phase diagram: R. Koshoji, M. Kawamura, M. Fukuda and T. Ozaki, *Phys. Rev. E* **103**, 023307 (2021).
- †*K ω — Open-source library for the shifted Krylov subspace method of the form $(zI - H)x = b$: T. Hoshi, M. Kawamura, K. Yoshimi, Y. Motoyama, T. Misawa, Y. Yamaji, S. Todo, N. Kawashima and T. Sogabe, *Computer Physics Communications* **258**, 107536 (2021).
- †*RESPACK: An ab initio tool for derivation of effective low-energy model of material: K. Nakamura, Y. Yoshimoto, Y. Nomura, T. Tadano, M. Kawamura, T. Kosugi, K. Yoshimi, T. Misawa and Y. Motoyama, *Computer Physics Communications* **261**, 107781 (2021).
- Structure of one-dimensional monolayer Si nanoribbons on Ag(111): L. Feng, A. Shiotari, K. Yabuoshi, M. Fukuda, T. Ozaki and Y. Sugimoto, *Phys. Rev. Materials* **5**, 034002 (2021).
- *The Simplest Model for Doped Poly(3,4-ethylenedioxythiophene) (PEDOT): Single-crystalline EDOT Dimer Radical Cation Salts: R. Kameyama, T. Fujino, S. Dekura, M. Kawamura, T. Ozaki and H. Mori, *Chem. Eur. J.* **27**, 6696 (2021).

Noguchi group

We have studied (1) Turing patterns on a vesicle by a reaction-diffusion system coupled with mechanochemical feedback, (2) the conformation of ultra-long-chain fatty acid in lipid bilayer, (3) the effects of cavitation on Karman vortex, and (4) sound-wave propagation in a simple fluid. We also proposed (5) a new numerical method to calculate membrane mechanical properties.

- †Conformation of ultra-long-chain fatty acid in lipid bilayer: Molecular dynamics study: K. Kawaguchi, K. M. Nakagawa, S. Nakagawa, H. Shindou, H. Nagao and H. Noguchi, *J. Chem. Phys.* **153**, 165101 (2020).
- †Effects of cavitation on Kármán vortex behind circular-cylinder arrays: A molecular dynamics study: Y. Asano, H. Watanabe and H. Noguchi, *J. Chem. Phys.* **152**, 034501 (2020).
- †Molecular dynamics simulation of soundwave propagation in a simple fluid: Y. Asano, H. Watanabe and H. Noguchi, *J. Chem. Phys.* **153**, 124504 (2020).
- †Virtual bending method to calculate bending rigidity, saddle-splay modulus, and spontaneous curvature of thin fluid membranes: H. Noguchi, *Phys. Rev. E* **102**, 053315 (2020).
- Supramolecular Biocomposite Hydrogels Formed by Cellulose and Host-Guest Polymers Assisted by Calcium Ion Complexes: H. Tsuchiya, G. Sinawang, T.-A. Asoh, M. Osaki, Y. Ikemoto, Y. Higuchi, H. Yamaguchi, A. Harada, H. Uyama and Y. Takashima, *Biomacromolecules* **21**, 3936 (2020).
- Pattern formation in reaction-diffusion system on membrane with mechanochemical feedback: N. Tamemoto and H. Noguchi, *Sci Rep* **10**, 19582 (2020).
- *分子動力学計算による複雑流体中のカルマン渦の解析: 浅野 優太, 渡辺 宙志, 野口 博司, 分子シミュレーション学会誌 "アンサンブル" **22**, 157-162 (2020).
- †Rational Design Principles of Attenuated Cationic Lytic Peptides for Intracellular Delivery of Biomacromolecules: N. Tamemoto, M. Akishiba, K. Sakamoto, K. Kawano, H. Noguchi and S. Futaki, *Mol. Pharmaceutics* **17**, 2175-2185 (2020).
- 高分子材料の破壊に関する粗視化シミュレーション: 樋口 祐次, 分子シミュレーション学会誌 "アンサンブル" **22**, 216-221 (2020).
- Coarse-grained molecular dynamics simulations of void generation and growth processes in the fracture of the lamellar structure of polyethylene: Y. Higuchi, *Phys. Rev. E* **103**, 042502 (2021).

† Joint research with outside partners.

11. Undulation of a moving fluid membrane pushed by filament growth: H. Noguchi and O. Pierre-Louis, *Sci Rep* **11**, 7985 (2021).

Yoshimi group

We have developed and enhanced the usability of programs adopted in the project for advancement of software usability in materials science (PASUMS). Our group's activity of 2020 include development of (1) optimization tools for PHYSics based on Bayesian Optimization (PHYSBO), (2) 2DMAT, and the enhancement of usability for (3) MateriApps Installer. In addition, we have studied (1) derivation and analysis of low-energy effective Hamiltonian of organic conductors using software packages (RESPACK and HΦ) developed in PASUMS and (2) application of sparse modeling in quantum many body problems.

1. †Finite Temperature Properties of Geometrically Charge Frustrated Systems: K. Yoshimi, M. Naka and H. Seo, *J. Phys. Soc. Jpn.* **89**, 034003 (2020).
2. †Sparse Modeling in Quantum Many-Body Problems: J. Otsuki, M. Ohzeki, H. Shinaoka and K. Yoshimi, *J. Phys. Soc. Jpn.* **89**, 012001 (2020).
3. †Transport properties of the organic Dirac electron system α -(BEDT-TSeF)₂I₃: D. Ohki, K. Yoshimi and A. Kobayashi, *Phys. Rev. B* **102**, 235116 (2020).
4. †Electronic correlation and geometrical frustration in molecular solids: A systematic ab initio study of β' -X[Pd(dmit)₂]₂: T. Misawa, K. Yoshimi and T. Tsumuraya, *Phys. Rev. Research* **2**, 032072 (2020).
5. †Sparse sampling and tensor network representation of two-particle Green's functions: H. Shinaoka, D. Geffroy, M. Wallerberger, J. Otsuki, K. Yoshimi, E. Gull and J. Kuneš, *SciPost Phys.* **8**, 012 (2020).
6. †Multiple-magnon excitations shape the spin spectrum of cuprate parent compounds: D. Betto, R. Fumagalli, L. Martignelli, M. Rossi, R. Piombo, K. Yoshimi, D. D. Castro, E. D. Gennaro, A. Sambri, D. Bonn, G. A. Sawatzky, L. Braicovich, N. B. Brookes, J. Lorenzana and G. Ghiringhelli, *Phys. Rev. B* **103**, L140409 (2021).
7. †*DSQSS: Discrete Space Quantum Systems Solver: Y. Motoyama, K. Yoshimi, A. Masaki-Kato, T. Kato and N. Kawashima, *Computer Physics Communications* **264**, 107944 (2021).
8. †*K ω — Open-source library for the shifted Krylov subspace method of the form $(zI - H)x = b$: T. Hoshi, M. Kawamura, K. Yoshimi, Y. Motoyama, T. Misawa, Y. Yamaji, S. Todo, N. Kawashima and T. Sogabe, *Computer Physics Communications* **258**, 107536 (2021).
9. †*RESPACK: An ab initio tool for derivation of effective low-energy model of material: K. Nakamura, Y. Yoshimoto, Y. Nomura, T. Tadano, M. Kawamura, T. Kosugi, K. Yoshimi, T. Misawa and Y. Motoyama, *Computer Physics Communications* **261**, 107781 (2021).

Materials Synthesis and Characterization group

1. Anisotropic Magnetic Field Dependence of Specific Heat in the Cubic Symmetric Quadrupolar Kondo Compound Pr_{0.05}La_{0.95}Pb₃: T. Kawae, M. Koga, Y. Sato, Y. Inagaki, T. Fujiwara, H. S. Suzuki and T. Kitai, *J. Phys. Soc. Jpn.* **89**, 063704 (2020).
2. Kondo-Induced Giant Isotropic Negative Thermal Expansion: D. G. Mazzone, M. Dzero, AM. M. Abeykoon, H. Yamaoka, H. Ishii, N. Hiraoka, J. -P. Rueff, J. M. Ablett, K. Imura, H. S. Suzuki, J. N. Hancock and I. Jarrige, *Phys. Rev. Lett.* **124**, 125701 (2020).
3. *Anisotropic Triangular Lattice Realized in Rhenium Oxychlorides A₃ReO₅Cl₂ (A = Ba, Sr): D. Hirai, T. Yajima, K. Nawa, M. Kawamura and Z. Hiroi, *Inorg. Chem.* **59**, 10025 (2020).
4. *Spin-orbit-coupled metal candidate PbRe₂O₆: S. Tajima, D. Hirai, T. Yajima, D. Nishio-Hamane, Y. Matsubayashi and Z. Hiroi, *Journal of Solid State Chemistry* **288**, 121359 (2020).
5. Magnetic properties of oxides with high concentrations of rare-earth elements R₆AO₁₂ (R = rare-earth element, A = Mo or W): M. Hase, N. Tsujii, H. S. Suzuki, O. Sakai and H. Mamiya, *Journal of Magnetism and Magnetic Materials* **523**, 167539 (2020).
6. *Devil's staircase transition of the electronic structures in CeSb: K. Kuroda, Y. Arai, N. Rezaei, S. Kunisada, S. Sakuragi, M. Alaei, Y. Kinoshita, C. Bareille, R. Noguchi, M. Nakayama, S. Akebi, M. Sakano, K. Kawaguchi, M. Arita, S. Ideta, K. Tanaka, H. Kitazawa, K. Okazaki, M. Tokunaga, Y. Haga, S. Shin, H. S. Suzuki, R. Arita and T. Kondo, *Nat Commun* **11**, 2888/1-9 (2020).

* Joint research among groups within ISSP.

Neutron Science Laboratory

Yamamuro group

Our laboratory is studying chemical physics of complex condensed matters by using neutron scattering, X-ray diffraction, calorimetric, dielectric, and viscoelastic techniques. Our target materials are glasses, liquids, and various disordered systems. The highlight of this year is the inelastic neutron scattering (INS) experiment of vapor-deposited CS₂ glass which was performed on AMATERAS in J-PARC MLF. By combining the results of CS₂ and CCl₄, which was measured in 2018, we have found the general relation between the low-energy excitations and local structures in the glass. The boson peak appears independently of the local structure of the glass, while the dispersive phonon excitations adjacent to the boson peak strongly depends on the quasi-network structure of the glass. Following the quasi-elastic neutron scattering (QENS) of a novel hydrogen-cluster material Li₆NbH₁₁ measured last year, the QENS experiment of Li₅MoH₁₁ was carried out on DNA in J-PARC MLF. Both data demonstrate that the MH₉ cluster is rotating rapidly with widely-distributed relaxation times, which may be caused by the conducting (positionally disordered) Li ions. The correlation between the conducting Li ions and hydrogen clusters was found also in the calorimetric experiment of novel Li conductors containing cage-like ions, Li(CB₉H₁₀) and 0.7Li(CB₉H₁₀)-0.3Li(CB₁₁H₁₂). The synchrotron-radiation X-ray diffraction experiment was conducted in SPring-8 for the glass of a novel metal-organic framework (MOF) material containing CO₂ as guest molecules.

1. Dynamics of Atomic Hydrogen in Palladium Probed by Neutron Spectroscopy: M. Kofu and O. Yamamuro, *J. Phys. Soc. Jpn.* **89**, 051002 (2020).
2. Rational Synthesis for a Noble Metal Carbide: T. Wakisaka, K. Kusada, D. Wu, T. Yamamoto, T. Toriyama, S. Matsumura, H. Akiba, O. Yamamuro, K. Ikeda, T. Otomo, N. Palina, Y. Chen, L. S. R. Kumara, C. Song, O. Sakata, W. Xie, M. Koyama, Y. Kubota, S. Kawaguchi, R. L. Arevalo, S. M. Aspera, E. F. Arguelles, H. Nakanishi and H. Kitagawa, *J. Am. Chem. Soc.* **142**, 1247 (2020).
3. New Insights on the Formation Process and Thermodynamics of the α -Phase PdH(D)_x through Direct Enthalpy Measurement of H(D) Dissolution: S. Dekura, H. Akiba, O. Yamamuro, H. Kobayashi, M. Maesato and H. Kitagawa, *J. Phys. Chem. C* **124**, 8663-8668 (2020).
4. Nanometric Fluctuations of Sound Velocity in Alkali Borate Glasses and Fragility of Respective Melts: S. Kojima, V. N. Novikov, M. Kofu and O. Yamamuro, *Phys. Status Solidi B* **257**, 2000073 (2020).
5. Nanoscale Relaxation in “Water-in-Salt” and “Water-in-Bisalt” Electrolytes: M. A. González, O. Borodin, M. Kofu, K. Shibata, T. Yamada, O. Yamamuro, K. Xu, D. L. Price and M. -L. Sabounji, *J. Phys. Chem. Lett.* **11**, 7279 (2020).
6. *Structural investigation of ternary PdRuM (M = Pt, Rh, or Ir) nanoparticles using first-principles calculations: S.-H. Hung, H. Akiba, O. Yamamuro and T. Ozaki, *RSC Adv.* **10**, 16527 (2020).
7. Quasielastic Neutron Scattering Study on Polymorphism of Glycerol Deuterated Triacylglycerols: Comparison with Saturated, Trans-unsaturated and Cis-unsaturated Triacylglycerols: C. Takechi, T. Kawaguchi, F. Kaneko and O. Yamamuro, *Chem. Lett.* **50**, 435 (2021).
8. ガラス転移温度：山室 修, 「化学便覧基礎編改訂第6版」, 10.15, 日本化学会編, (丸善出版, 2020), 77-81.

Masuda group

The goal of our research is to discover a new quantum phenomenon and to reveal the mechanism of it. In this fiscal year we studied the following topics; Helical and collinear spin density wave order in the $S = 1/2$ one-dimensional frustrated chain compound NaCuMoO₄(OH) investigated by neutron scattering, Magnetic order in the chemically substituted frustrated antiferromagnet CsCrF₄, Zero-energy excitation in the classical kagome antiferromagnet NaBa₂Mn₃F₁₁, Magnetic correlations in YBaCo₄O₇ on kagome and triangular lattices, etc.

1. Analysis of Field-Induced Nonreciprocal Magnon in Noncollinear Magnet and Application to $S = 1$ Triangular Antiferromagnet CsFeCl₃: M. Matsumoto, S. Hayashida and T. Masuda, *J. Phys. Soc. Jpn.* **89**, 034710(1-17) (2020).
2. Horizontal Line Nodes in Sr₂RuO₄ Proved by Spin Resonance: K. Iida, M. Kofu, K. Suzuki, N. Murai, S. Ohira-Kawamura, R. Kajimoto, Y. Inamura, M. Ishikado, S. Hasegawa, T. Masuda, Y. Yoshida, K. Kakurai, K. Machida and S. Lee, *J. Phys. Soc. Jpn.* **89**, 053702(1-5) (2020).
3. Mossbauer Study of Rare-earth Ferroborate NdFe₃(BO₃)₄: S. Nakamura, T. Masuda, K. Ohgushi and T. Katsufuji, *J. Phys. Soc. Jpn.* **89**, 084703(1-6) (2020).
4. †Emergent spin-1 Haldane gap and ferroelectricity in a frustrated spin- 1/2 ladder: H. Ueda, S. Onoda, Y. Yamaguchi, T. Kimura, D. Yoshizawa, T. Morioka, M. Hagiwara, M. Hagiwara, M. Soda, T. Masuda, T. Sakakibara, K. Tomiyasu,

† Joint research with outside partners.

- S. Ohira-Kawamura, K. Nakajima, R. Kajimoto, M. Nakamura, Y. Inamura, N. Reynolds, M. Frontzek, J. S. White, M. Hase and Y. Yasui, *Phys. Rev. B* **101**, 140408(1-6) (2020).
5. *Helical and collinear spin density wave order in the $S = 1/2$ one-dimensional frustrated chain compound $\text{NaCuMoO}_4(\text{OH})$ investigated by neutron scattering: S. Asai, T. Oyama, K. Nawa, A. Nakao, K. Munakata, K. Kuwahara, M. Hagihala, S. Itoh, Z. Hiroi and T. Masuda, *Phys. Rev. B* **101**, 144437(1-8) (2020).
 6. Magnetic correlations in YBaCo_4O_7 on kagome and triangular lattices: M. Soda, S. Itoh, T. Yokoo, G. Ehlers, H. Kawano-Furukawa and T. Masuda, *Phys. Rev. B* **101**, 214444(1-7) (2020).
 7. Magnetic order in the chemically substituted frustrated antiferromagnet CsCrF_4 : S. Hayashida, M. Hagihala, M. Avdeev, Y. Miura, H. Manaka and T. Masuda, *Phys. Rev. B* **102**, 174440(1-6) (2020).
 8. Spin waves in the two-dimensional honeycomb lattice XXZ-type van der Waals antiferromagnet CoPS_3 : C. Kim, J. Jeong, P. Park, T. Masuda, S. Asai, S. Itoh, H.-S. Kim, A. Wildes and J.-G. Park, *Phys. Rev. B* **102**, 184429(1-8) (2020).
 9. *Zero-energy excitation in the classical kagome antiferromagnet $\text{NaBa}_2\text{Mn}_3\text{F}_{11}$: S. Hayashida, H. Ishikawa, Y. Okamoto, T. Okubo, Z. Hiroi, G. J. Nilsen, H. Mutka and T. Masuda, *Phys. Rev. B* **101**, 214409 (2020).
 10. The f-electron State of the Heavy Fermion Superconductor NpPd_5Al_2 and the Isostructural Family: N. Metoki, A. A. Aczel, D. Aoki, S. Chi, J. A. Fernandez-Baca, J.-C. Griveau, M. Hagihala, T. Hong, Y. Haga, K. Ikeuchi, Y. Inamura, K. Kamazawa, R. Kajimoto, H. Kitazawa, T. Masuda, M. Matsuda, M. Nakamura, J. Ohtsuki, D. Pajerowski, H. S. Suzuki, E. Yamamoto and H. Yamauchi, *JPS Conf. Proc.* **30**, 011123(1-6) (2020).
 11. Establishing the carrier scattering phase diagram for ZrNiSn -based half-Heusler thermoelectric materials: Q. Ren, C. Fu, Q. Qiu, S. Dai, Z. Liu, T. Masuda, S. Asai, M. Hagihala, S. Lee, S. Torri, T. Kamiyama, L. He, X. Tong, C. Felser, D. J. Singh, T. Zhu, J. Yang and J. Ma, *Nat Commun* **11**, 3142(1-9) (2020).
 12. †*Gapless spin liquid in a square-kagome lattice antiferromagnet: M. Fujihala, K. Morita, R. Mole, S. Mitsuda, T. Tohyama, S.-I. Yano, D. Yu, S. Sota, T. Kuwai, A. Koda, H. Okabe, H. Lee, S. Itoh, T. Hawaii, T. Masuda, H. Sagayama, A. Matsuo, K. Kindo, S. Ohira-Kawamura and K. Nakajima, *Nat Commun* **11**, 3429 (2020).
 13. Fermionic order by disorder in a van der Waals antiferromagnet: R. Okuma, D. Ueta, S. Kuniyoshi, Y. Fujisawa, B. Smith, C. H. Hsu, Y. Inagaki, W. Si, T. Kawae, H. Lin, F. C. Chuang, T. Masuda, R. Kobayashi and Y. Okada, *Sci Rep* **10**, 15311(8pages) (2020).
 14. Dynamical Studies in Condensed Matter on High Resolution Chopper Spectrometer (HRC) —2nd Phase of HRC Project—: S. Itoh, T. Masuda, T. Yokoo, H. Yoshizawa, M. Soda, S. Asai, Y. Ikeda, S. Ibuka, M. Yoshida, T. Hawaii, H. Saito, D. Kawana, R. Sugiura, T. Asami and Y. Ihata, *JPS Conf. Proc.* **33**, 011058(1-7) (2021).

Nakajima group

Nakajima group has been studying magnetic materials showing cross-correlated phenomena related to topologically-nontrivial magnetic structures. One example is magnetic skyrmion, which is vortex-like spin order behaving like a particle. In this year, we investigated crystallization process of magnetic skyrmions in a chiral magnet MnSi by means of neutron resonance spin-echo spectroscopy in J-PARC. We have been collaborating with scientists in KEK and Kyoto university to develop the resonance-type neutron spin echo spectrometer, and successfully observed spin echo signals revealing that the spin fluctuations near the phase boundary between the paramagnetic and skyrmion lattice phases has a characteristic relaxation time of 1 ns. We also studied rare-earth based skyrmion materials by resonant X-ray magnetic scattering, and also applied polarized small-angle neutron scattering technique to a polar crystal hosting Neel-type magnetic skyrmion lattice.

1. 中性子散乱を用いた磁気スキルミオン研究：中島 多朗，有馬 孝尚，*固体物理* **55**, 265-274 (2020).
2. Crystallization of magnetic skyrmions in MnSi investigated by neutron spin echo spectroscopy: T. Nakajima, T. Oda, M. Hino, H. Endo, K. Ohishi, K. Kakurai, A. Kikkawa, Y. Taguchi, Y. Tokura and T.-H. Arima, *Phys. Rev. Research* **2**, 043393 (2020).
3. Nanometric square skyrmion lattice in a centrosymmetric tetragonal magnet: N. D. Khanh, T. Nakajima, X. Yu, S. Gao, K. Shibata, M. Hirschberger, Y. Yamasaki, H. Sagayama, H. Nakao, L. Peng, K. Nakajima, R. Takagi, T.-H. Arima, Y. Tokura and S. Seki, *Nat. Nanotechnol.* **15**, 444 (2020).
4. Direct Observation of Cycloidal Spin Modulation and Field-induced Transition in Néel-type Skyrmion-hosting VOSe_2O_5 : T. Kurumaji, T. Nakajima, A. Feoktystov, E. Babcock, Z. Salhi, V. Ukleev, T.-H. Arima, K. Kakurai and Y. Tokura, *J. Phys. Soc. Jpn.* **90**, 024705 (2021).

* Joint research among groups within ISSP.

Mayumi group

We have discovered that slide-ring gels, in which polymer chains are cross-linked by ring molecules, show strain-induced crystallization (SIC) under uniaxial stretching. The occurrence of SIC improves significantly the mechanical toughness of slide-ring gels. In addition, the crystalline formation is reversible in response to elongation and retraction, which results in the high mechanical reversibility under cyclic deformations. The novel toughening mechanism of hydrogels by SIC enables the simultaneous improvement of toughness and reversibility required for the applications of hydrogels as biomaterials, such as artificial cartilage and prosthetic joints.

International MegaGauss Science Laboratory

Kindo group

We have examined an Fulde–Ferrell–Larkin–Ovchinnikov phase using some angle-resolved physical property measurements in pulsed magnetic fields, which have unveiled details of pair-breaking effects of the magnetic field on this phase. Magnetism of the $4d$ and $5d$ transition metal double perovskites with strong spin-orbit coupling are investigated up to around 65 T. We discovered the ligand dependent magnetism in Cs_2MX_6 ($M = \text{Nb}, \text{Ta}, X = \text{Cl}, \text{Br}$) and the magnetic field induced phase transition at 50 T in $\text{Ba}_2\text{CaReO}_6$.

1. †Ga Substitution Effect on the Valence Transition of $\text{Eu}_2\text{Pt}_6\text{Al}_{15}$: K. Oyama, A. Mitsuda, H. Wada, Y. Narumi, M. Hagiwara, R. Takahashi, H. Wadati, H. Setoyama and K. Kindo, *J. Phys. Soc. Jpn.* **89**, 114713 (2020).
2. *Kitaev Spin Liquid Candidate Os_xCl_3 Comprised of Honeycomb Nano-Domains: K. Kataoka, D. Hirai, T. Yajima, D. Nishio-Hamane, R. Ishii, K.-Y. Choi, D. Wulferding, P. Lemmens, S. Kittaka, T. Sakakibara, H. Ishikawa, A. Matsuo, K. Kindo and Z. Hiroi, *J. Phys. Soc. Jpn.* **89**, 114709(1-9) (2020).
3. †Multi-Step Magnetic Transitions in EuNiIn_4 : S. Ikeda, K. Kaneko, Y. Tanaka, T. Kawasaki, T. Hanashima, K. Munakata, A. Nakao, R. Kiyonagi, T. Ohhara, K. Mochizuki, A. Kondo, K. Kindo, Y. Homma, M. D. Frontzek and H. Kobayashi, *J. Phys. Soc. Jpn.* **89**, 014707(1-7) (2020).
4. †Vanishment of Metamagnetic Transition in the Metal-to-Insulator Transition Compound BaVS_3 under High Pressure: T. Tahara, T. Kida, Y. Narumi, T. Takeuchi, H. Nakamura, K. Miyake, K. Kindo and M. Hagiwara, *J. Phys. Soc. Jpn.* **89**, 064711(1-5) (2020).
5. †Angle-dependent nontrivial phase in the Weyl semimetal NbAs with anisotropic Fermi surface: M. Komada, H. Murakawa, M. S. Bahramy, T. Kida, K. Yokoi, Y. Narumi, K. Kindo, M. Hagiwara, H. Sakai and N. Hanasaki, *Phys. Rev. B* **101**, 045135(1-6) (2020).
6. †Data-driven determination of the spin Hamiltonian parameters and their uncertainties: The case of the zigzag-chain compound $\text{KCu}_4\text{P}_3\text{O}_{12}$: R. Tamura, K. Hukushima, A. Matsuo, K. Kindo and M. Hase, *Phys. Rev. B* **101**, 224435(1-9) (2020).
7. *Enhanced spin correlations in the Bose-Einstein condensate compound $\text{Sr}_3\text{Cr}_2\text{O}_8$: T. Nomura, Y. Skourski, D. L. Quintero-Castro, A. A. Zvyagin, A. V. Suslov, D. Gorbunov, S. Yasin, J. Wosnitza, K. Kindo, A. T. M. N. Islam, B. Lake, Y. Kohama, S. Zherlitsyn and M. Jaime, *Phys. Rev. B* **102**, 165144 (2020).
8. *Observation of in-plane magnetic field induced phase transitions in FeSe : J. M. Ok, C. I. Kwon, Y. Kohama, J. S. You, S. K. Park, J.-H. Kim, Y. J. Jo, E. S. Choi, K. Kindo, W. Kang, K.-S. Kim, E. G. Moon, A. Gurevich and J. S. Kim, *Phys. Rev. B* **101**, 224509 (2020).
9. *Quantum oscillations and magnetic field induced Fermi surface reconstruction in the charge density wave state of $\text{A}0.9\text{Mo}_6\text{O}_{17}$ ($A = \text{Na}, \text{K}$): H. P. Zhu, M. Yang, J. Z. Ke, H. K. Zuo, T. Peng, J. F. Wang, Y. Liu, X. Xu, Y. Kohama, K. Kindo and M. Greenblatt, *Phys. Rev. B* **102**, 235164 (2020).
10. Thermal and magnetoelastic properties of $\alpha\text{-RuCl}_3$ in the field-induced low-temperature states: R. Schönemann, S. Imajo, F. Weickert, J. Yan, D. G. Mandrus, Y. Takano, E. L. Brosha, P. F. S. Rosa, S. E. Nagler, K. Kindo and M. Jaime, *Phys. Rev. B* **102**, 214432(1-7) (2020).
11. *Anisotropic Fully Gapped Superconductivity Possibly Mediated by Charge Fluctuations in a Nondimeric Organic Complex: S. Imajo, H. Akutsu, R. Kurihara, T. Yajima, Y. Kohama, M. Tokunaga, K. Kindo and Y. Nakazawa, *Phys. Rev. Lett.* **125**, 177002 (2020).
12. †Nonmagnetic Ground States and a Possible Quadrupolar Phase in $4d$ and $5d$ Lacunar Spinel Selenides GaM_4Se_8 ($M =$

† Joint research with outside partners.

- Nb, Ta): H. Ishikawa, T. Yajima, A. Matsuo, Y. Ihara and K. Kindo, *Phys. Rev. Lett.* **124**, 227202(1-6) (2020).
13. †*Particle-Hole Symmetry Breaking in a Spin-Dimer System TlCuCl_3 Observed at 100 T: X. -G. Zhou, Y. Yao, Y. H. Matsuda, A. Ikeda, A. Matsuo, K. Kindo and H. Tanaka, *Phys. Rev. Lett.* **125**, 267207 1-6 (2020).
 14. †*Synthesis, Structure, and Anomalous Magnetic Ordering of the Spin-1/2 Coupled Square Tetramer System $\text{K}(\text{NbO})\text{Cu}_4(\text{PO}_4)_4$: K. Kimura, D. Urushihara, T. Asaka, M. Toyoda, A. Miyake, M. Tokunaga, A. Matsuo, K. Kindo, K. Yamauchi and T. Kimura, *Inorg. Chem.* **59**, 10986-10995 (2020).
 15. *Extracting the Chiral Contribution to the Negative Longitudinal Magnetoresistance in Epitaxial $\text{Pr}_2\text{Ir}_2\text{O}_7$ Thin Films: T. Ohtsuki, Z. Tian, A. Endo, M. Halim, S. Katsumoto, Y. Kohama, K. Kindo, M. Lippmaa and S. Nakatsuji, *JPS Conf. Proc.* **30**, 011181 (1-6) (2020).
 16. Avoided quantum criticality and cluster-glass formation in itinerant ferromagnet $\text{Sr}_{1-x}(\text{La}_{0.5}\text{K}_{0.5})_x\text{RuO}_3$: R. Iwahara, R. Sugawara, *. Rahmanto, Y. Honma, K. Matsuoka, A. Matsuo, K. Kindo, K. Tenya and M. Yokoyama, *Phys. Rev. Materials* **4**, 074404(1-8) (2020).
 17. *Improved accuracy in high-frequency AC transport measurements in pulsed high magnetic fields: H. Mitamura, R. Watanuki, E. Kampert, T. Förster, A. Matsuo, T. Onimaru, N. Onozaki, Y. Amou, K. Wakiya, K. T. Matsumoto, I. Yamamoto, K. Suzuki, S. Zherlitsyn, J. Wosnitzer, M. Tokunaga, K. Kindo and T. Sakakibara, *Review of Scientific Instruments* **91**, 125107/1-25 (2020).
 18. †*Gapless spin liquid in a square-kagome lattice antiferromagnet: M. Fujihala, K. Morita, R. Mole, S. Mitsuda, T. Tohyama, S.-I. Yano, D. Yu, S. Sota, T. Kuwai, A. Koda, H. Okabe, H. Lee, S. Itoh, T. Hawaii, T. Masuda, H. Sagayama, A. Matsuo, K. Kindo, S. Ohira-Kawamura and K. Nakajima, *Nat Commun* **11**, 3429 (2020).
 19. *High-field phase diagram of $\text{Ni}_3\text{V}_2\text{O}_8$ studied by specific heat and magnetocaloric effect measurements: C. Dong, Y. Kohama, Z. Z. He, X. T. Han, K. Sato, A. Matsuo, K. Kindo, M. Yang and J. F. Wang, *J. Phys.: Condens. Matter* **33**, 205402 (2021).
 20. Ligand dependent magnetism of the $J = 3/2$ Mott insulator Cs_2MX_6 ($M = \text{Ta}, \text{Nb}$, $X = \text{Br}, \text{Cl}$): H. Ishikawa, T. Yajima, A. Matsuo and K. Kindo, *J. Phys.: Condens. Matter* **33**, 125802(1-6) (2021).
 21. Magnetization Process in EuCo_2P_2 and EuT_2Ge_2 (T: transition metal): Comparison of Experiment and Theory: T. Takeuchi, T. Tahara, T. Kida, Y. Narumi, M. Hagiwara, K. Kindo, W. Iha, Y. Ashitomi, T. Yara, M. Nakashima, Y. Amako, M. Hedo, T. Nakama and Y. Onuki, *J. Phys. Soc. Jpn.* **90**, 034709(1-15) (2021).
 22. †*Spin Excitations of the $S = 1/2$ One-Dimensional Ising-Like Antiferromagnet $\text{BaCo}_2\text{V}_2\text{O}_8$ in Transverse Magnetic Fields: A. Okutani, H. Onishi, S. Kimura, T. Takeuchi, T. Kida, M. Mori, A. Miyake, M. Tokunaga, K. Kindo and M. Hagiwara, *J. Phys. Soc. Jpn.* **90**, 044704/1-9 (2021).
 23. †*Geometrical Hall effect and momentum-space Berry curvature from spin-reversed band pairs: M. Hirschberger, Y. Nomura, H. Mitamura, A. Miyake, T. Koretsune, Y. Kaneko, L. Spitz, Y. Taguchi, A. Matsuo, K. Kindo, R. Arita, M. Tokunaga and Y. Tokura, *Phys. Rev. B* **103**, L041111(1-6) (2021).
 24. Symmetry change of d-wave superconductivity in κ -type organic superconductors: S. Imajo, K. Kindo and Y. Nakazawa, *Phys. Rev. B* **103**, L060508(1-5) (2021).
 25. *Compact megajoule-class pulsed power supply for generating long-pulsed magnetic fields: K. Matsui, T. Kanda, Y. Ihara, K. Kindo and Y. Kohama, *Review of Scientific Instruments* **92**, 024711 (2021).
 26. *High-resolution calorimetry in pulsed magnetic fields: S. Imajo, C. Dong, A. Matsuo, K. Kindo and Y. Kohama, *Review of Scientific Instruments* **92**, 043901 (2021).

Tokunaga group

In this year, we have developed or improved several measurements in high magnetic fields. Using fast capacitance measurements, we have achieved high-precision measurements of magnetostriction, dielectric constants, and magnetocaloric effects in pulsed-high magnetic fields. We utilize polarizing microscopy to visualize domain structures in CeSb and $\text{Cd}_2\text{Re}_2\text{O}_7$ and study the dynamics of superconducting vortices and field-induced structural transitions in metamagnetic shape memory alloys using a high-speed camera. Utilizing various measurement techniques, we studied magnetic field-induced phase transitions in several heavy fermion and multiferroic materials and magnetotransport properties of topological semimetals. In elemental tellurium, a semiconductor with a chiral crystal structure, our high-field magnetotransport study revealed the existence of metallic states on the as-cleavage surfaces of single crystals.

1. * ^{105}Pd NMR and NQR study of the cubic heavy fermion system $\text{Ce}_3\text{Pd}_{20}\text{Si}_6$: I. Jakovac, M. Horvatic, E. F. Schwier,

* Joint research among groups within ISSP.

- A. Prokofiev, S. Paschen, H. Mitamura, T. Sakakibara and M. S. Grbic, *J. Phys.: Condens. Matter* **32**, 245601(1-7) (2020).
2. *Domain Control by Adjusting Anisotropic Stress in Pyrochlore Oxide $\text{Cd}_2\text{Re}_2\text{O}_7$: S. Tajima, D. Hirai, Y. Kinoshita, M. Tokunaga, K. Akiba, T. C. Kobayashi, H. T. Hirose and Z. Hiroi, *J. Phys. Soc. Jpn.* **89**, 114711 (2020).
 3. †*Bulk quantum Hall effect of spin-valley coupled Dirac fermions in the polar antiferromagnet BaMnSb_2 : H. Sakai, H. Fujimura, S. Sakuragi, M. Ochi, R. Kurihara, A. Miyake, M. Tokunaga, T. Kojima, D. Hashizume, T. Muro, K. Kuroda, T. Kondo, T. Kida, M. Hagiwara, K. Kuroki, M. Kondo, K. Tsuruda, H. Murakawa and N. Hanasaki, *Phys. Rev. B* **101**, 081104/1-7 (2020).
 4. High-field ultrasonic study of quadrupole ordering and crystal symmetry breaking in CeRhIn_5 : R. Kurihara, A. Miyake, M. Tokunaga, Y. Hirose and R. Settai, *Phys. Rev. B* **101**, 155125/1-8 (2020).
 5. †Intriguing behavior of $\text{UCo}_{1-x}\text{Rh}_x\text{Ge}$ ferromagnets in magnetic field along the axis: J. Pospíšil, Y. Haga, A. Miyake, S. Kambe, Y. Tokunaga, M. Tokunaga, E. Yamamoto, P. Proschek, J. Volný and V. Sechovský, *Phys. Rev. B* **102**, 024442/1-13 (2020).
 6. Magnetic phase diagram enriched by chemical substitution in a noncentrosymmetric helimagnet: T. Sato, Y. Araki, A. Miyake, A. Nakao, N. Abe, M. Tokunaga, S. Kimura, Y. Tokunaga and T.-H. Arima, *Phys. Rev. B* **101**, 054414/1-6 (2020).
 7. †Magnetic structures and quadratic magnetoelectric effect in LiNiPO_4 beyond 30 T: E. Fogh, T. Kihara, R. Toft-Petersen, M. Bartkowiak, Y. Narumi, O. Prokhnenko, A. Miyake, M. Tokunaga, K. Oikawa, M. K. Sørensen, J. C. Dyrnum, H. Grimmer, H. Nojiri and N. B. Christensen, *Phys. Rev. B* **101**, 024403/1-12 (2020).
 8. *Magnetotransport properties of tellurium under extreme conditions: K. Akiba, K. Kobayashi, T. C. Kobayashi, R. Koezuka, A. Miyake, J. Gouchi, Y. Uwatoko and M. Tokunaga, *Phys. Rev. B* **101**, 245111(1-6) (2020).
 9. †Metamagnetic transitions and magnetoelectric responses in the chiral polar helimagnet $\text{Ni}_2\text{InSbO}_6$: Y. Araki, T. Sato, Y. Fujima, N. Abe, M. Tokunaga, S. Kimura, D. Morikawa, V. Ukleev, Y. Yamasaki, C. Tabata, H. Nakao, Y. Murakami, H. Sagayama, K. Ohishi, Y. Tokunaga and T. Arima, *Phys. Rev. B* **102**, 054409/1-8 (2020).
 10. †Strong magnetic anisotropy and unusual magnetic field reinforced phase in URhSn with a quasi-kagome structure: Y. Shimizu, A. Miyake, A. Maurya, F. Honda, A. Nakamura, Y. J. Sato, D. Li, Y. Homma, M. Yokoyama, Y. Tokunaga, M. Tokunaga and D. Aoki, *Phys. Rev. B* **102**, 134411/1-11 (2020).
 11. *Anisotropic Fully Gapped Superconductivity Possibly Mediated by Charge Fluctuations in a Nondimeric Organic Complex: S. Imajo, H. Akutsu, R. Kurihara, T. Yajima, Y. Kohama, M. Tokunaga, K. Kindo and Y. Nakazawa, *Phys. Rev. Lett.* **125**, 177002 (2020).
 12. †Dynamic evolution of flux distributions in a pulse-driven superconductor by high-speed magneto-optical imaging: H. Kurokawa, Y. Kinoshita, F. Nabeshima, M. Tokunaga and A. Maeda, *Appl. Phys. Lett.* **116**, 262601/1-5 (2020).
 13. †*Synthesis, Structure, and Anomalous Magnetic Ordering of the Spin-1/2 Coupled Square Tetramer System $\text{K}(\text{NbO})\text{Cu}_4(\text{PO}_4)_4$: K. Kimura, D. Urushihara, T. Asaka, M. Toyoda, A. Miyake, M. Tokunaga, A. Matsuo, K. Kindo, K. Yamauchi and T. Kimura, *Inorg. Chem.* **59**, 10986-10995 (2020).
 14. Anisotropic Quantum Transport through a Single Spin Channel in the Magnetic Semiconductor EuTiO_3 : K. Maruhashi, K. S. Takahashi, M. S. Bahramy, S. Shimizu, R. Kurihara, A. Miyake, M. Tokunaga, Y. Tokura and M. Kawasaki, *Adv. Mater.* **32**, 1908315/1-10 (2020).
 15. †High-Mobility 2D Hole Gas at a SrTiO_3 Interface: L. D. Anh, S. Kaneta, M. Tokunaga, M. Seki, H. Tabata, M. Tanaka and S. Ohya, *Adv. Mater.* **32**, 1906003/1-7 (2020).
 16. Magnetic field induced antiferromagnetic cone structure in multiferroic BiFeO_3 : M. Matsuda, S. E. Dissanayake, T. Hong, Y. Ozaki, T. Ito, M. Tokunaga, X. Z. Liu, M. Bartkowiak and O. Prokhnenko, *Phys. Rev. Materials* **4**, 034412/1-6 (2020).
 17. Capacitive detection of magnetostriction, dielectric constant, and magneto-caloric effects in pulsed magnetic fields: A. Miyake, H. Mitamura, S. Kawachi, K. Kimura, T. Kimura, T. Kihara, M. Tachibana and M. Tokunaga, *Review of Scientific Instruments* **91**, 105103/1-9 (2020).
 18. *Improved accuracy in high-frequency AC transport measurements in pulsed high magnetic fields: H. Mitamura, R. Watanuki, E. Kampert, T. Förster, A. Matsuo, T. Onimaru, N. Onozaki, Y. Amou, K. Wakiya, K. T. Matsumoto, I. Yamamoto, K. Suzuki, S. Zherlitsyn, J. Wosnitza, M. Tokunaga, K. Kindo and T. Sakakibara, *Review of Scientific Instruments* **91**, 125107/1-25 (2020).

† Joint research with outside partners.

19. *Devil's staircase transition of the electronic structures in CeSb: K. Kuroda, Y. Arai, N. Rezaei, S. Kunisada, S. Sakuragi, M. Alaei, Y. Kinoshita, C. Bareille, R. Noguchi, M. Nakayama, S. Akebi, M. Sakano, K. Kawaguchi, M. Arita, S. Ideta, K. Tanaka, H. Kitazawa, K. Okazaki, M. Tokunaga, Y. Haga, S. Shin, H. S. Suzuki, R. Arita and T. Kondo, *Nat Commun* **11**, 2888/1-9 (2020).
20. †High-field magnetization and magnetic phase diagram of metamagnetic shape memory alloys Ni₅₀-Co Mn_{31.5}Ga_{18.5} ($x = 9$ and 9.7): T. Kihara, X. Xu, A. Miyake, Y. Kinoshita, M. Tokunaga, Y. Adachi and T. Kanomata, *Scripta Materialia* **181**, 25-29 (2020).
21. †*Spin Excitations of the $S = 1/2$ One-Dimensional Ising-Like Antiferromagnet BaCo₂V₂O₈ in Transverse Magnetic Fields: A. Okutani, H. Onishi, S. Kimura, T. Takeuchi, T. Kida, M. Mori, A. Miyake, M. Tokunaga, K. Kindo and M. Hagiwara, *J. Phys. Soc. Jpn.* **90**, 044704/1-9 (2021).
22. †*Field-induced valence fluctuations in YbB₁₂: R. Kurihara, A. Miyake, M. Tokunaga, A. Ikeda, Y. H. Matsuda, A. Miyata, D. I. Gorbunov, T. Nomura, S. Zherlitsyn, J. Wosnitza and F. Iga, *Phys. Rev. B* **103**, 115103 1-14 (2021).
23. †*Geometrical Hall effect and momentum-space Berry curvature from spin-reversed band pairs: M. Hirschberger, Y. Nomura, H. Mitamura, A. Miyake, T. Koretsune, Y. Kaneko, L. Spitz, Y. Taguchi, A. Matsuo, K. Kindo, R. Arita, M. Tokunaga and Y. Tokura, *Phys. Rev. B* **103**, L041111(1-6) (2021).
24. †Martensitic Transformation and Metamagnetic Transition in Co-V(Si, Al) Heusler Alloys: K. Nakamura, A. Miyake, X. Xu, T. Omori, M. Tokunaga and R. Kainuma, *Metals* **11**, 226/1-12 (2021).
25. †Observation of inverse magnetocaloric effect in magnetic-field-induced austenite phase of Heusler alloys Ni_{50-x}Co_xMn_{31.5}Ga_{18.5} ($x = 9$ and 9.7): T. Kihara, T. Roy, X. Xu, A. Miyake, M. Tsujikawa, H. Mitamura, M. Tokunaga, Y. Adachi, T. Eto and T. Kanomata, *Phys. Rev. Materials* **5**, 034416_1-13 (2021).
26. †Giant anomalous Hall effect from spin-chirality scattering in a chiral magnet: Y. Fujishiro, N. Kanazawa, R. Kurihara, H. Ishizuka, T. Hori, F. S. Yasin, X. Yu, A. Tsukazaki, M. Ichikawa, M. Kawasaki, N. Nagaosa, M. Tokunaga and Y. Tokura, *Nat Commun* **12**, 317/1-6 (2021).

Y. Matsuda group

The magnetic-field-induced insulator to metal transition in W-doped VO₂ has been discovered in 500 T using the electromagnetic flux compression ultrahigh magnetic field generator, The molecular orbital is destabilized by such a strong magnetic field through the Pauli exclusion principle. This phenomenon can happen with the large spin Zeeman energy and the electron-electron correlation. In magnetic fields as high as 100 -200 T, we have investigated the magnon Bose-Einstein condensation in TiCuCl₃ and spin-state crystallization in LaCoO₃. As for technical achievements, a measurement technique for electric resistivity and a method for boosting magnetic field have been developed. Also, we have proposed a combination of 100 T magnetic fields and an intense x-ray by utilizing the single-turn coil method and the Japanese x-ray free electron laser SACLA. In addition, cyclotron resonance in an InAs quantum well, temperature dependent magnetization process in YbB₁₂, and magnetic properties in Mn₂V₂O₇ have been studied in high magnetic fields.

1. †*Experimental measurements of effective mass in near-surface InAs quantum wells: J. Yuan, M. Hatefipour, B. A. Magill, W. Mayer, M. C. Dartiailh, K. Sardashti, K. S. Wickramasinghe, G. A. Khodaparast, Y. H. Matsuda, Y. Kohama, Z. Yang, S. Thapa, C. J. Stanton and J. Shabani, *Phys. Rev. B* **101**, 205310 1-8 (2020).
2. †*Magnetization plateau observed by ultrahigh-field Faraday rotation in the kagome antiferromagnet herbertsmithite: R. Okuma, D. Nakamura and S. Takeyama, *Phys. Rev. B* **102**, 104429 1-4 (2020).
3. †Pressure and magnetic field effects on ferroelastic and antiferromagnetic orderings in honeycomb-lattice Mn₂V₂O₇: H. C. Wu, D. J. Hsieh, T. W. Yen, P. J. Sun, D. Chandrasekhar Kakarla, J. L. Her, Y. H. Matsuda, C. K. Chang, Y. C. Lai, M. Gooch, L. Z. Deng, K. G. Webber, C. A. Lee, M. M. C. Chou, C. W. Chu and H. D. Yang, *Phys. Rev. B* **102**, 075130 1-8 (2020).
4. †*Quantum limit cyclotron resonance in monolayer epitaxial graphene in magnetic fields up to 560 T: The relativistic electron and hole asymmetry: D. Nakamura, H. Saito, H. Hibino, K. Asano and S. Takeyama, *Phys. Rev. B* **101**, 115420 1-5 (2020).
5. †*Particle-Hole Symmetry Breaking in a Spin-Dimer System TiCuCl₃ Observed at 100 T: X. -G. Zhou, Y. Yao, Y. H. Matsuda, A. Ikeda, A. Matsuo, K. Kindo and H. Tanaka, *Phys. Rev. Lett.* **125**, 267207 1-6 (2020).
6. †Two Spin-State Crystallizations in LaCoO₃: A. Ikeda, Y. H. Matsuda and K. Sato, *Phys. Rev. Lett.* **125**, 177202 1-6 (2020).
7. †The Temperature Dependence of the Magnetization Process of the Kondo Insulator YbB₁₂: Y. H. Matsuda, Y. Kakita

* Joint research among groups within ISSP.

and F. Iga, *Crystals* **10**, 26 1-7 (2020).

- †*Direct measurement of resistivity in destructive pulsed magnetic fields: Y. Kohama, F. Nabeshima, A. Maeda, A. Ikeda and Y. H. Matsuda, *Review of Scientific Instruments* **91**, 033901 1-5 (2020).
- †*Magnetic-field-induced insulator–metal transition in W-doped VO₂ at 500 T: Y. H. Matsuda, D. Nakamura, A. Ikeda, S. Takeyama, Y. Suga, H. Nakahara and Y. Muraoka, *Nat Commun* **11**, 3591 1-7 (2020).
- †*Single shot x-ray diffractometry in SACLA with pulsed magnetic fields up to 16 T: A. Ikeda, Y. H. Matsuda, X. Zhou, T. Yajima, Y. Kubota, K. Tono and M. Yabashi, *Phys. Rev. Research* **2**, 043175 1-6 (2020).
- †*Field-induced valence fluctuations in YbB₁₂: R. Kurihara, A. Miyake, M. Tokunaga, A. Ikeda, Y. H. Matsuda, A. Miyata, D. I. Gorbunov, T. Nomura, S. Zherlitsyn, J. Wosnitza and F. Iga, *Phys. Rev. B* **103**, 115103 1-14 (2021).
- †*Higher magnetic-field generation by a mass-loaded single-turn coil: M. Gen, A. Ikeda, S. Kawachi, T. Shitaokoshi, Y. H. Matsuda, Y. Kohama and T. Nomura, *Review of Scientific Instruments* **92**, 033902 1-5 (2021).

Kohama group

In 2020, we have investigated high-field properties in many different systems, such as CeRhIn₅, SrRuO₃, CuInCr₄S₈, FeSe, Ruby, High-Tc superconductor, and so on. We also developed the resistivity measurement technique for a research in ultra high-magnetic fields above 100 T. The other technical developments including the super-capacitor driven pulsed magnet are underway.

- †Symmetry Lowering on the Field-Induced Commensurate Phase in CeRhIn₅: T. Kanda, K. Arashima, Y. Hirose, R. Settai, K. Matsui, T. Nomura, Y. Kohama and Y. Ihara, *J. Phys. Soc. Jpn.* **89**, 094709 (2020).
- Electronic band structure of (111) SrRuO₃ thin films: An angle-resolved photoemission spectroscopy study: H. Ryu, Y. Ishida, B. Kim, J. R. Kim, W. J. Kim, Y. Kohama, S. Imajo, Z. Yang, W. Kyung, S. Hahn, B. Sohn, I. Song, M. Kim, S. Huh, J. Jung, D. Kim, T. W. Noh, S. Das and C. Kim, *Phys. Rev. B* **102**, 041102 (2020).
- *Enhanced spin correlations in the Bose-Einstein condensate compound Sr₃Cr₂O₈: T. Nomura, Y. Skourski, D. L. Quintero-Castro, A. A. Zvyagin, A. V. Suslov, D. Gorbunov, S. Yasin, J. Wosnitza, K. Kindo, A. T. M. N. Islam, B. Lake, Y. Kohama, S. Zherlitsyn and M. Jaime, *Phys. Rev. B* **102**, 165144 (2020).
- †*Experimental measurements of effective mass in near-surface InAs quantum wells: J. Yuan, M. Hatefipour, B. A. Magill, W. Mayer, M. C. Dartailh, K. Sardashti, K. S. Wickramasinghe, G. A. Khodaparast, Y. H. Matsuda, Y. Kohama, Z. Yang, S. Thapa, C. J. Stanton and J. Shabani, *Phys. Rev. B* **101**, 205310 1-8 (2020).
- Magnetization process of the breathing pyrochlore magnet CuInCr₄S₈ in ultrahigh magnetic fields up to 150 T: M. Gen, Y. Okamoto, M. Mori, K. Takenaka and Y. Kohama, *Phys. Rev. B* **101**, 054434 (2020).
- *Observation of in-plane magnetic field induced phase transitions in FeSe: J. M. Ok, C. I. Kwon, Y. Kohama, J. S. You, S. K. Park, J.-H. Kim, Y. J. Jo, E. S. Choi, K. Kindo, W. Kang, K.-S. Kim, E. G. Moon, A. Gurevich and J. S. Kim, *Phys. Rev. B* **101**, 224509 (2020).
- *Quantum oscillations and magnetic field induced Fermi surface reconstruction in the charge density wave state of A_{0.9}Mo₆O₁₇ (A = Na, K): H. P. Zhu, M. Yang, J. Z. Ke, H. K. Zuo, T. Peng, J. F. Wang, Y. Liu, X. Xu, Y. Kohama, K. Kindo and M. Greenblatt, *Phys. Rev. B* **102**, 235164 (2020).
- *Anisotropic Fully Gapped Superconductivity Possibly Mediated by Charge Fluctuations in a Nondimeric Organic Complex: S. Imajo, H. Akutsu, R. Kurihara, T. Yajima, Y. Kohama, M. Tokunaga, K. Kindo and Y. Nakazawa, *Phys. Rev. Lett.* **125**, 177002 (2020).
- *Observation of small Fermi pockets protected by clean CuO₂ sheets of a high-Tc superconductor: S. Kunisada, S. Isono, Y. Kohama, S. Sakai, C. Bareille, S. Sakuragi, R. Noguchi, K. Kurokawa, K. Kuroda, Y. Ishida, S. Adachi, R. Sekine, T. K. Kim, C. Cacho, S. Shin, T. Tohyama, K. Tokiwa and T. Kondo, *Science* **369**, 833 (2020).
- *Extracting the Chiral Contribution to the Negative Longitudinal Magnetoresistance in Epitaxial Pr₂Ir₂O₇ Thin Films: T. Ohtsuki, Z. Tian, A. Endo, M. Halim, S. Katsumoto, Y. Kohama, K. Kindo, M. Lippmaa and S. Nakatsuji, *JPS Conf. Proc.* **30**, 011181 (1-6) (2020).
- Strain engineering of the magnetic multipole moments and anomalous Hall effect in pyrochlore iridate thin films: W. J. Kim, T. Oh, J. Song, E. K. Ko, Y. Li, J. Mun, B. Kim, J. Son, Z. Yang, Y. Kohama, M. Kim, B.-J. Yang and T. W. Noh, *Sci. Adv.* **6**, eabb1539 (2020).
- †*Direct measurement of resistivity in destructive pulsed magnetic fields: Y. Kohama, F. Nabeshima, A. Maeda,

† Joint research with outside partners.

A. Ikeda and Y. H. Matsuda, *Review of Scientific Instruments* **91**, 033901 1-5 (2020).

13. Angle dependence of H_{c2} with a crossover between the orbital and paramagnetic limits: H. Matsuoka, M. Nakano, T. Shitaokoshi, Y. Wang, Y. Kashiwabara, S. Yoshida, Y. Kohama, T. Ouchi, K. Ishizaka, M. Kawasaki, T. Nojima and Y. Iwasa, *Phys. Rev. Research* **2**, 012064(R) (2020).
14. Crystal-field Paschen-Back effect on ruby in ultrahigh magnetic fields: M. Gen, T. Kanda, T. Shitaokoshi, Y. Kohama and T. Nomura, *Phys. Rev. Research* **2**, 033257 (2020).
15. Van der Waals $\text{SnSe}_{2(1-x)}\text{S}_{2x}$ Alloys: Composition-Dependent Bowing Coefficient and Electron-Phonon Interaction: Z. R. Kudrynskiy, X. Wang, J. Sutcliffe, M. A. Bhuiyan, Y. Fu, Z. Yang, O. Makarovskiy, L. Eaves, A. Solomon, V. T. Maslyuk, Z. D. Kovalyuk, L. Zhang and A. Patanè, *Advanced Functional Materials* **30**, 1908092 (2020).
16. Broad Tunability of Carrier Effective Masses in Two-Dimensional Halide Perovskites: M. Dyksik, H. Duim, X. Zhu, Z. Yang, M. Gen, Y. Kohama, S. Adjokatse, D. K. Maude, M. A. Loi, D. A. Egger, M. Baranowski and P. Plochocka, *ACS Energy Lett.* **5**, 3609 (2020).
17. *High-field phase diagram of $\text{Ni}_3\text{V}_2\text{O}_8$ studied by specific heat and magnetocaloric effect measurements: C. Dong, Y. Kohama, Z. Z. He, X. T. Han, K. Sato, A. Matsuo, K. Kindo, M. Yang and J. F. Wang, *J. Phys.: Condens. Matter* **33**, 205402 (2021).
18. Emergence of Frustrated Short-Range Order above Long-Range Order in the $S = 1/2$ Kagome Antiferromagnet $\text{CaCu}_3(\text{OD})_6\text{Cl}_2 \cdot 0.6\text{D}_2\text{O}$: Y. Ihara, K. Matsui, Y. Kohama, S. Luther, D. Opherden, J. Wosnitzer, H. Kühne and H. K. Yoshida, *J. Phys. Soc. Jpn.* **90**, 023703 (2021).
19. Element-specific field-induced spin reorientation and tetracritical point in MnCr_2S_4 : Sh. Yamamoto, H. Suwa, T. Kihara, T. Nomura, Y. Kotani, T. Nakamura, Y. Skourski, S. Zherlitsyn, L. Prodan, V. Tsurkan, H. Nojiri, A. Loidl and J. Wosnitzer, *Phys. Rev. B* **103**, L020408 (2021).
20. Wide Critical Fluctuations of the Field-Induced Phase Transition in Graphite: C. Marcenat, T. Klein, D. LeBoeuf, A. Jaoui, G. Seyfarth, J. Kacmarcik, Y. Kohama, H. Cercellier, H. Aubin, K. Behnia and B. Fauque, *Phys. Rev. Lett.* **126**, 106801 (2021).
21. *Compact megajoule-class pulsed power supply for generating long-pulsed magnetic fields: K. Matsui, T. Kanda, Y. Ihara, K. Kindo and Y. Kohama, *Review of Scientific Instruments* **92**, 024711 (2021).
22. †*Higher magnetic-field generation by a mass-loaded single-turn coil: M. Gen, A. Ikeda, S. Kawachi, T. Shitaokoshi, Y. H. Matsuda, Y. Kohama and T. Nomura, *Review of Scientific Instruments* **92**, 033902 1-5 (2021).
23. *High-resolution calorimetry in pulsed magnetic fields: S. Imajo, C. Dong, A. Matsuo, K. Kindo and Y. Kohama, *Review of Scientific Instruments* **92**, 043901 (2021).

Center of Computational Materials Science

Akai team

The main objective of is to predict/discover new functionality materials by means of computational materials design (CMD). In particular, new high-performance permanent magnets is one of main targets. Developments of new methods of quantum simulation are also important themes. Our activities include the followings: (1) A method that enabled us to treat low energy collective excitations, phonons and magnons, in the framework of first-principles KKR-CPA was developed and applied to various magnetic systems. The effects of these excitations on magnetization at finite temperature and the Curie temperature of typical magnetic systems, including bcc Fe and permanent-magnet materials $\text{B}_2(\text{Fe}, \text{Co})_{14}\text{B}$, were calculated using low energy effective Hamiltonian obtained by a first-principles KKR-Green's function method where the magnons and phonons were included in a static and local scheme. The effects of these excitations were important in determining the magnetic properties, was concluded; (2) The magnetic Friedel oscillation near the surface of Fe films was detected layer by layer measurement using synchrotron Mössbauer source. The behavior was well reproduced by the hyperfine interactions calculated using the full-potential KKR method and the KKR method combined the optimized effective potential (OEP) method; (3) An efficient method to calculate spin-wave dispersions using the low-energy effective Hamiltonian derived from first-principles calculations was developed and applied to rare-earth based permanent magnet materials including $\text{R}_2(\text{Fe}, \text{Co})_{14}\text{B}$; (4) A search for rare-earth bases permanent magnets materials of better performance at finite temperature were made using massive data obtained as results of first-principles KKR-CPA together with fairly large number of experimental data by a newly developed data assimilation technique. The method developed was proven powerful enough to predict possible candidates for compositions of high-performance permanent magnet materials.

* Joint research among groups within ISSP.

1. Calculating Curie temperatures for rare-earth permanent magnets: *Ab initio* inspection of localized magnetic moments in *d*-electron ferromagnetism: M. Matsumoto and H. Akai, *Phys. Rev. B* **101**, 144402 (2020).
2. Element- and orbital-selective magnetic coherent rotation at the first-order phase transition of a hard uniaxial ferromagnet: Sh. Yamamoto, D. I. Gorbunov, H. Akai, H. Yasumura, Y. Kotani, T. Nakamura, T. Kato, N. V. Mushnikov, A. V. Andreev, H. Nojiri and J. Wosnitza, *Phys. Rev. B* **101**, 174430 (2020).
3. Magnetic Friedel Oscillation at the Fe(001) Surface: Direct Observation by Atomic-Layer-Resolved Synchrotron Radiation ^{57}Fe Mössbauer Spectroscopy: T. Mitsui, S. Sakai, S. Li, T. Ueno, T. Watanuki, Y. Kobayashi, R. Masuda, M. Seto and H. Akai, *Phys. Rev. Lett.* **125**, 236806 (2020).
4. *First-principles calculations of finite temperature electronic structures and transport properties of Heusler alloy Co_2MnSi : H. Shinya, S. Kou, T. Fukushima, A. Masago, K. Sato, H. Katayama-Yoshida and H. Akai, *Appl. Phys. Lett.* **117**, 042402(1-5) (2020).
5. Spin-wave dispersion and exchange stiffness in $\text{Nd}_2\text{Fe}_{14}\text{B}$ and RFe_{11}Ti ($\text{R}=\text{Y}, \text{Nd}, \text{Sm}$) from first-principles calculations: T. Fukazawa, H. Akai, Y. Harashima and T. Miyake, *Phys. Rev. B* **103**, 024418-1–7 (2021).
6. Data assimilation method for experimental and first-principles data: Finite-temperature magnetization of $(\text{Nd}, \text{Pr}, \text{La}, \text{Ce})_2(\text{Fe}, \text{Co}, \text{Ni})_{14}\text{B}$: Y. Harashima, K. Tamai, S. Doi, M. Matsumoto, H. Akai, N. Kawashima, M. Ito, N. Sakuma, A. Kato, T. Shoji and T. Miyake, *Phys. Rev. Materials* **5**, 013806-1–10 (2021).

Miyashita team

We studied temperature dependence of coercivity for permanent magnets as the activity of ESICMM. We also studied subjects for phase transitions and quantum dynamics.

1. Dynamical aspects of magnetization reversal in the neodymium permanent magnet by a stochastic Landau-Lifshitz-Gilbert simulation at finite temperature: Real-time dynamics and quantitative estimation of coercive force: M. Nishino, I. E. Uysal, T. Hinokihara and S. Miyashita, *Phys. Rev. B* **102**, 020413(R) (1-5) (2020).
2. Elastic-frustration-driven unusual magnetoelastic properties in a switchable core-shell spin-crossover nanostructure: Y. Singh, H. Oubouchou, M. Nishino, S. Miyashita and K. Boukheddaden, *Phys. Rev. B* **101**, 054105(1-15) (2020).
3. Magnetic field threshold for nucleation and depinning of domain walls in the neodymium permanent magnet $\text{Nd}_2\text{Fe}_{14}\text{B}$: I. E. Uysal, M. Nishino and S. Miyashita, *Phys. Rev. B* **101**, 094421 (1-9) (2020).
4. Dynamical phase transition in Floquet optical bistable systems: An approach from finite-size quantum systems: T. Shirai, S. Todo and S. Miyashita, *Phys. Rev. E* **101**, 013809(1-7) (2020).
5. Magnetic-Pole Flip by Millimeter Wave: S.-I. Ohkoshi, M. Yoshikiyo, K. Imoto, K. Nakagawa, A. Namai, H. Tokoro, Y. Yahagi, K. Takeuchi, F. Jia, S. Miyashita, M. Nakajima, H. Qiu, K. Kato, T. Yamaoka, M. Shirata, K. Naoi, K. Yagishita and H. Doshita, *Adv. Mater.* **32**, 2004897(1-7) (2020).
6. Construction of quantum dark soliton in onedimensional Bose gas: E. Kaminishi, T. Mori and S. Miyashita, *J. Phys. B: At. Mol. Opt. Phys.* **53**, 095302(1-8) (2020).
7. Role of atomic-scale thermal fluctuations in the coercivity: Y. Toga, S. Miyashita, A. Sakuma and T. Miyake, *npj Computational Materials* **6:67**, 1-7 (2020).
8. Effect of the surface magnetic anisotropy of neodymium atoms on the coercivity in neodymium permanent magnets: M. Nishino, I. E. Uysal and S. Miyashita, *Phys. Rev. B* **103**, 014418(1-9) (2021).
9. Systematic survey of magnetic configurations in multilayer ferromagnet system with dipole-dipole interaction: T. Hinokihara and S. Miyashita, *Phys. Rev. B* **103**, 054421(1-9) (2021).
10. Rapid Faraday Rotation on epsilon-Iron Oxide Magnetic Nanoparticles by Visible and Terahertz Pulsed Light: S.-I. Ohkoshi, K. Imoto, A. Namai, M. Yoshikiyo, S. Miyashita, H. Qiu, S. Kimoto, K. Kato and M. Nakajima, *J. Am. Chem. Soc.* **141**, 1775-1780 (2021).

† Joint research with outside partners.

Laser and Synchrotron Research Center

Kobayashi group

We have supplied some laser systems for applications such as astronomical science and photoemission spectroscopy. Some results related to a laser processing were published in 2020.

1. †Ablation threshold and crater morphology of amorphous and crystalline SiO₂ glass for extreme ultraviolet femto-second pulses: T. Shibuya, K. Sakaue, H. Ogawa, T. -H. Dinh, D. Satoh, E. Terasawa, M. Washio, M. Tanaka, T. Higashiguchi, M. Ishino, Y. Kubota, Y. Inubushi, S. Owada, M. Nishikino, Y. Kobayashi and R. Kuroda, *Jpn. J. Appl. Phys.* **59**, 122004 (2020).
2. †Precision measurement of ablation thresholds with variable pulse duration laser: T. Takahashi, S. Tani, R. Kuroda and Y. Kobayashi, *Appl. Phys. A* **126**, 582 (2020).
3. †Study on nonthermal–thermal processing boundary in drilling of ceramics using ultrashort pulse laser system with variable parameters over a wide range: A. Narazaki, H. Takada, D. Yoshitomi, K. Torizuka and Y. Kobayashi, *Appl. Phys. A* **126**, 252 (2020).
4. レーザーアブレーションの学理解明と次世代レーザー加工に向けた自動計測技術開発：小林 洋平，高橋 孝，谷峻 太郎，*応用物理*，**Vol.89, No.12**, 719-723 (2020).
5. *Q*-switching stability limits of Kerr-lens mode locking: S. Kimura, S. Tani and Y. Kobayashi, *Phys. Rev. A* **102**, 043505 (2020).
6. Neural-network-assisted in situ processing monitoring by speckle pattern observation: S. Tani, Y. Aoyagi and Y. Kobayashi, *Opt. Express* **28**, 26180 (2020).
7. Piezo-electric transducer actuated mirror with a servo bandwidth beyond 500 kHz: T. Nakamura, S. Tani, I. Ito, M. Endo and Y. Kobayashi, *Opt. Express* **28**, 16118 (2020).
8. †Work function seen with sub-meV precision through laser photoemission: Y. Ishida, J. K. Jung, M. S. Kim, J. Kwon, Y. S. Kim, D. Chung, I. Song, C. Kim, T. Otsu and Y. Kobayashi, *Commun Phys* **3**, 158 (2020).
9. Subgigahertz-resolution table-top spectrograph calibrated with a 4-GHz optical frequency comb: M. Endo, T. Sukegawa, A. Silva and Y. Kobayashi, *J. Astron. Telesc. Instrum. Syst.* **6**, 1 (2020).
10. †Ablation thresholds and morphological changes of poly-L-lactic acid for pulse durations in the femtosecond-to-picosecond regime: T. Shibuya, D. Yoshitomi, D. Satoh, K. Sakaue, M. Tanaka, H. Takada, H. Ogawa, K. Torizuka, Y. Kobayashi and R. Kuroda, *Surf Interface Anal* **52**, 1145 (2020).
11. 固体レーザーによる光周波数コム：小林 洋平，木村 祥太，*電子情報通信学会誌*，**Vol.103, No.11**, 1082, 1088 (2020).
12. *Direct generation of sub-picosecond pulse via multi-section gain switching: T. Nakamura, T. Ito, H. Nakamae, C. Kim, Y. Hazama, Y. Kobayashi, R. Kuroda and H. Akiyama, *Opt. Lett.* **46**, 1277 (2021).
13. Coherent control of acoustic phonons in a silica fiber using a multi-GHz optical frequency comb: M. Endo, S. Kimura, S. Tani and Y. Kobayashi, *Commun Phys* **4**, 73 (2021).
14. †Ultrafast laser processing of ceramics: Comprehensive survey of laser parameters: A. Narazaki, H. Takada, D. Yoshitomi, K. Torizuka and Y. Kobayashi, *Journal of Laser Applications* **33**, 012009 (2021).

Harada group

This year, in order to tackle the new coronavirus problem, we analyzed water treatment membranes that can be used as virus removal membranes as part of the project to analyze the solid-liquid interface, which is the main theme of Grant-in-Aid for Scientific Research on Innovative Areas "Aquatic Functional Materials". With the support of the AMED project "Development of Technology for Countermeasures against Infectious Diseases including Viruses," we also promoted research and development on the improvement of coating materials for the inner wall of the tubes for Extra Corporeal Membrane Oxygenation (ECMO), which is mainly used in the treatment of patients with severe pneumonia. In order to develop cathode materials that contribute to the high performance of lithium-ion batteries, we analyzed materials in which the ligand oxygen, rather than transition metals, is involved in the redox reaction. We succeeded in capturing the dimerization of oxygen atoms interacting with metals under high potentials using RIXS.

1. †Revisiting the Phase Diagram of T*-type La_{1-x/2}Eu_{1-x/2}Sr_xCuO₄ Using Oxygen K-edge X-ray Absorption Spectroscopy: S. Asano, K. Ishii, K. Yamagami, J. Miyawaki, Y. Harada and M. Fujita, *J. Phys. Soc. Jpn.* **89**, 075002 (1-2)

* Joint research among groups within ISSP.

(2020).

2. †*Localized character of charge excitations for $\text{La}_{2-x}\text{Sr}_x\text{NiO}_{4+\delta}$ revealed by oxygen K-edge resonant inelastic x-ray scattering: K. Yamagami, K. Ishii, Y. Hirata, K. Ikeda, J. Miyawaki, Y. Harada, M. Miyazaki, S. Asano, M. Fujita and H. Wadati, *Phys. Rev. B* **102**, 165145 (1-7) (2020).
3. †Anisotropic X-Ray Scattering of Transiently Oriented Water: K. H. Kim, A. Späh, H. Pathak, C. Yang, S. Bonetti, K. Amann-Winkel, D. Mariedahl, D. Schlesinger, J. A. Sellberg, D. Mendez, G. van der Schot, H. Y. Hwang, J. Clark, O. Shigeki, T. Tadashi, Y. Harada, H. Ogasawara, T. Katayama, A. Nilsson and F. Perakis, *Phys. Rev. Lett.* **125**, 076002 (1-6) (2020).
4. †Ion Selectivity of Water Molecules in Subnanoporous Liquid-Crystalline Water-Treatment Membranes: A Structural Study of Hydrogen Bonding: R. Watanabe, T. Sakamoto, K. Yamazoe, J. Miyawaki, T. Kato and Y. Harada, *Angew. Chem. Int. Ed.* **59**, 23461-23465 (2020).
5. †Tetragonal Distortion of a $\text{BaTiO}_3/\text{Bi}_{0.5}\text{Na}_{0.5}\text{TiO}_3$ Nanocomposite Responsible for Anomalous Piezoelectric and Ferroelectric Behaviors: W. Zhang, Q. Feng, E. Hosono, D. Asakura, J. Miyawaki and Y. Harada, *ACS Omega* **5**, 22800-22807 (2020).
6. †Multiorbital bond formation for stable oxygen-redox reaction in battery electrodes: T. Sudayama, K. Uehara, T. Mukai, D. Asakura, X.-M. Shi, A. Tsuchimoto, B. M. D. Boisse, T. Shimada, E. Watanabe, Y. Harada, M. Nakayama, M. Okubo and A. Yamada, *Energy Environ. Sci.* **13**, 1492-1500 (2020).

I. Matsuda group

Since the beginning of the year 2020, there has been a serious coronavirus (COVID-19) pandemic over the world and care has been urgently needed for those affected. In living, we have had to stop the spread of the virus by avoiding three Cs: closed spaces, crowded places, and close contact. No exception has been applied for experiments in any facilities or laboratories, including our beamline, SPring-8 BL07LSU. A number of the user-group members and visiting itself have been restricted. After summer, beamtime experiments were carried out normally for domestic users. We have made advanced X-ray magneto-optical experiments of exotic quantum phases and ambient pressure photoemission measurements on surface reactions. In the laboratory, soft X-ray non-linear optical research was made at X-ray free electron laser facility at SACL A.

1. Topological Dirac nodal loops in nonsymmorphic hydrogenated monolayer boron: N. T. Cuong, I. Tateishi, M. Cameau, M. Niibe, N. Umezawa, B. Slater, K. Yubuta, T. Kondo, M. Ogata, S. Okada and I. Matsuda, *Phys. Rev. B* **101**, 195412 (2020).
2. Two-dimensional conducting layer on SrTiO_3 surface induced by hydrogenation: Y. Takeuchi, R. Hobara, R. Akiyama, A. Takayama, S. Ichinokura, R. Yukawa, I. Matsuda and S. Hasegawa, *Phys. Rev. B* **101**, 085422-1,-6 (2020).
3. †Time-resolved X-ray photoelectron diffraction using an angle-resolved time-of-flight electron analyzer: A. K. R. Ang, Y. Fukatsu, K. Kimura, Y. Yamamoto, T. Yonezawa, H. Nitta, A. Fleurence, S. Yamamoto, I. Matsuda, Y. Yamada-Takamura and K. Hayashi, *Jpn. J. Appl. Phys.* **59**, 100902 (2020).
4. *Element-selectively tracking ultrafast demagnetization process in Co/Pt multilayer thin films by the resonant magneto-optical Kerr effect: K. Yamamoto, S. E. Moussaoui, Y. Hirata, S. Yamamoto, Y. Kubota, S. Owada, M. Yabashi, T. Seki, K. Takahashi, I. Matsuda and H. Wadati, *Appl. Phys. Lett.* **116**, 172406-1,-5 (2020).
5. Scanning magneto-optical Kerr effect (MOKE) measurement with element-selectivity by using a soft x-ray free-electron laser and an ellipsoidal mirror: Y. Kubota, H. Motoyama, G. Yamaguchi, S. Egawa, Y. Takeo, M. Mizuguchi, H. Sharma, S. Owada, K. Tono, H. Mimura, I. Matsuda and M. Yabashi, *Appl. Phys. Lett.* **117**, 042405 (2020).
6. *A computational examination of the electric-field-induced proton transfer along the interface hydrogen bond between proton donating and accepting self-assembled monolayers: Y. Kanematsu, H. S. Kato, S. Yoshimoto, A. Ueda, S. Yamamoto, H. Mori, J. Yoshinobu, I. Matsuda and M. Tachikawa, *Chem. Phys. Lett.* **741**, 137091 (2020).
7. 分割型アンジェレータを用いた新しい軟 X 線磁気光学法と次世代光源への展開：久保田 雄也，松田 巖，*放射光* **33**, 206-212 (2020).
8. †*Atomistic-Level Description of GaN/Water Interface by a Combined Spectroscopic and First-Principles Computational Approach: M. Sato, Y. Imazeki, T. Takeda, M. Kobayashi, S. Yamamoto, I. Matsuda, J. Yoshinobu, Y. Nakano and M. Sugiyama, *J. Phys. Chem. C* **124**, 12466 (2020).
9. *Edge-state correlation accelerates metal-insulator transition in topological semimetal nanofilms: S. Ito, M. Arita, J. Haruyama, B. Feng, W. -C. Chen, H. Namatame, M. Taniguchi, C. -M. Cheng, G. Bian, S. -J. Tang, T. -C. Chiang, O. Sugino, F. Komori and I. Matsuda, *Science Advances* **6**, eaaz5015 (7 pages) (2020).

† Joint research with outside partners.

10. *Electronic structure of a (3×3)-ordered silicon layer on Al(111): Y. Sato, Y. Fukaya, M. Cameau, A. K. Kundu, D. Shiga, R. Yukawa, K. Horiba, C.-H. Chen, A. Huang, H.-T. Jeng, T. Ozaki, H. Kumigashira, M. Niibe and I. Matsuda, *Phys. Rev. Materials* **4**, 064005 (2020).
11. Ellipsometer Equipped with Multiple Mirrors for Element-selective Soft X-ray Experiments: M. Araki, J. Meikaku, Y. Kubota, J. Miyawaki, Y. Kosegawa, S. E. Moussaoui, T. Bouillaud, P. Manset, S. Owada, K. Tono, M. Yabashi and I. Matsuda, *e-J. Surf. Sci. Nanotechnol.* **18**, 231 (2020).
12. Geometrical Frustration of B-H Bonds in Layered Hydrogen Borides Accessible by Soft Chemistry: S. Tominaka, R. Ishibiki, A. Fujino, K. Kawakami, K. Ohara, I. Matsuda, H. Hosono and T. Kondo, *Chem* **6**, 406-418 (2020).
13. Recent progresses in spectroscopies using soft X-ray free-electron laser: I. Matsuda and Y. Kubota, *Chem. Lett. Advanced publication*, cl.200881 (2021).
14. †*Femtosecond Charge Density Modulations in Photoexcited CuWO₄: Y. Uemura, A. S. M. Ismail, S. H. Park, S. Kwon, M. Kim, Y. Niwa, H. Wadati, H. Elnaggar, F. Frati, T. Haarman, N. Höppel, N. Huse, Y. Hirata, Y. Zhang, K. Yamagami, S. Yamamoto, I. Matsuda, T. Katayama, T. Togashi, S. Owada, M. Yabashi, U. Halisdemir, G. Koster, T. Yokoyama, B. M. Weckhuysen and F. M. F. D. Groot, *J. Phys. Chem. C* **125**, 7329 (2021).
15. †Valence Fluctuations in Yb(Al,Fe)B₄ Studied by Nanosecond-time-resolved Photoemission Spectroscopy Using Synchrotron Radiation: M. Okawa, K. Akikubo, S. Yamamoto, I. Matsuda and T. Saitoh, *e-J. Surf. Sci. Nanotechnol.* **19**, 20 (2021).

Itatani group

We mainly worked on soft-X-ray attosecond spectroscopy and the upgrade of the attosecond beamline. First, we extended the nitrogen *K*-edge experiments from diatomic molecules (NO) to triatomic molecules (N₂O) and observed intriguing dynamics of 2ω oscillation. The interpretation of this ultrafast oscillation is underway. Second, a new sample-feeding system for organic molecules was introduced. We successfully measured static absorption spectra of benzene, acetone, ethanol, and methanol at the carbon *K* edge around 280 eV. Third, a new soft X-ray spectrometer was developed and installed to improve the energy resolution. In addition, we started to develop new infrastructures in the building E. We constructed a beamline booth next to the existing laser booth, with a clean and temperature-stable environment for ultrafast experiments using EUV and soft-X-ray pulses. A Ti:sapphire laser system was developed as a pump source for an ultrashort-pulse infrared optical parametric chirped pulse amplifier (OPCPA), or as a driver to produce high-flux femtosecond EUV pulses for imaging experiments. We also developed prototype light sources such as a mid-infrared optical parametric amplifier (OPA) and a harmonic-based tunable UV source, both of which are pumped by a high-repetition-rate Yb laser.

1. †*Photoinduced Phase Transition from Excitonic Insulator to Semimetal-like State in Ta₂Ni_{1-x}Co_xSe₅ (x = 0.10): T. Mitsuoka, T. Suzuki, H. Takagi, N. Katayama, H. Sawa, M. Nohara, M. Watanabe, J. Xu, Q. Ren, M. Fujisawa, T. Kanai, J. Itatani, S. Shin, K. Okazaki and T. Mizokawa, *J. Phys. Soc. Jpn.* **89**, 124703 (2020).
2. †Detecting electron-phonon coupling during photoinduced phase transition,: T. Suzuki, Y. Shinohara, Y. Lu, M. Watanabe, J. Xu, K. L. Ishikawa, H. Takagi, M. Nohara, N. Katayama, H. Sawa, M. Fujisawa, T. Kanai, J. Itatani, T. Mizokawa, S. Shin and K. Okazaki, *Phys. Rev. B* **103**, L121105 (2020).
3. *Efficient Terahertz Harmonic Generation with Coherent Acceleration of Electrons in the Dirac Semimetal Cd₃As₂: B. Cheng, N. Kanda, T. N. Ikeda, T. Matsuda, P. Xia, T. Schumann, S. Stemmer, J. Itatani, N. P. Armitage and R. Matsunaga, *Phys. Rev. Lett.* **124**, 117402 (2020).
4. 軟 X 線領域でのアト秒分光：斎藤 成之，*光学* **49**, 249 (2020).
5. 中赤外光パルスを用いた固体高次高調波発生とその偏光特性：石井 順久，金島 圭佑，夏 沛宇，斎藤 成之，金井 輝人，板谷 治郎，*レーザー研究* **49**, 168-173 (2020).
6. †Role of virtual band population for high harmonic generation in solids: Y. Sanari, H. Hirori, T. Aharen, H. Tahara, Y. Shinohara, K. L. Ishikawa, T. Otobe, P. Xia, N. Ishii, J. Itatani, S. A. Sato and Y. Kanemitsu, *Phys. Rev. B (Rapid Communication)* **102**, 041125(R)-1-7 (2020).
7. †Observation of the quantum shift of a backward rescattering caustic by carrier-envelope phase mapping: T. Mizuno, N. Ishii, T. Kanai, P. Rosenberger, D. Zietlow, M. F. Kling, O. I. Tolstikhin, T. Morishita and J. Itatani, *Phys. Rev. A* **103**, 043121 (2021).
8. *Optical parametric amplification of phase-stable terahertz-to-mid-infrared pulses studied in the time domain: N. Kanda, N. Ishii, J. Itatani and R. Matsunaga, *Optics Express* **29**, 3479-3489 (2021).
9. †Time-domain spectroscopy of optical parametric amplification for phase-stable terahertz-to-midinfrared pulses:

* Joint research among groups within ISSP.

Kondo group

We use angle-resolved photoemission spectroscopy (ARPES) with ultrahigh energy resolution. The main findings in 2020 were small pockets in cuprate, Devil's staircase in CeSb, and spin-polarized band in Te.

1. †*Bulk quantum Hall effect of spin-valley coupled Dirac fermions in the polar antiferromagnet BaMnSb₂: H. Sakai, H. Fujimura, S. Sakuragi, M. Ochi, R. Kurihara, A. Miyake, M. Tokunaga, T. Kojima, D. Hashizume, T. Muro, K. Kuroda, T. Kondo, T. Kida, M. Hagiwara, K. Kuroki, M. Kondo, K. Tsuruda, H. Murakawa and N. Hanasaki, Phys. Rev. B **101**, 081104/1-7 (2020).
2. Three-dimensional electronic structure in ferromagnetic Fe₃Sn₂ with breathing kagome bilayers: H. Tanaka, Y. Fujisawa, K. Kuroda, R. Noguchi, S. Sakuragi, C. Bareille, B. Smith, C. Cacho, S. W. Jung, T. Muro, Y. Okada and T. Kondo, Phys. Rev. B **101**, 161114 (2020).
3. *Radial Spin Texture in Elemental Tellurium with Chiral Crystal Structure: M. Sakano, M. Hirayama, T. Takahashi, S. Akebi, M. Nakayama, K. Kuroda, K. Taguchi, T. Yoshikawa, K. Miyamoto, T. Okuda, K. Ono, H. Kumigashira, T. Ideue, Y. Iwasa, N. Mitsuishi, K. Ishizaka, S. Shin, T. Miyake, S. Murakami, T. Sasagawa and T. Kondo, Phys. Rev. Lett. **124**, 136404 (2020).
4. *Observation of small Fermi pockets protected by clean CuO₂ sheets of a high-T_c superconductor: S. Kunisada, S. Isono, Y. Kohama, S. Sakai, C. Bareille, S. Sakuragi, R. Noguchi, K. Kurokawa, K. Kuroda, Y. Ishida, S. Adachi, R. Sekine, T. K. Kim, C. Cacho, S. Shin, T. Tohyama, K. Tokiwa and T. Kondo, Science **369**, 833 (2020).
5. *Devil's staircase transition of the electronic structures in CeSb: K. Kuroda, Y. Arai, N. Rezaei, S. Kunisada, S. Sakuragi, M. Alaei, Y. Kinoshita, C. Bareille, R. Noguchi, M. Nakayama, S. Akebi, M. Sakano, K. Kawaguchi, M. Arita, S. Ideta, K. Tanaka, H. Kitazawa, K. Okazaki, M. Tokunaga, Y. Haga, S. Shin, H. S. Suzuki, R. Arita and T. Kondo, Nat Commun **11**, 2888/1-9 (2020).
6. *Observation and control of the weak topological insulator state in ZrTe₅: P. Zhang, R. Noguchi, K. Kuroda, C. Lin, K. Kawaguchi, K. Yaji, A. Harasawa, M. Lippmaa, S. Nie, H. Weng, V. Kandyba, A. Giampietri, A. Barinov, Q. Li, G. D. Gu, S. Shin and T. Kondo, Nat. Commun. **12**, 406 (2021).

Matsunaga group

We have investigated light-matter interactions and light-induced nonequilibrium phenomena in solids by utilizing terahertz (THz) pulse. We have studied nonlinear THz responses and nonequilibrium dynamics of carriers in Dirac and Weyl semimetals. We have also developed optical parametric amplification of low-frequency infrared pulses in the intermediate region between THz frequency and mid-infrared, 167., from 16.9 to 44.8 THz (6.7–17.8 μm) based on the intra-pulse differential frequency generation in GaSe. The long-term phase drift of the THz-to-MIR pulses after two-stage OPA is as small as 16 mrad during a 6-h operation without any active feedback. Our scheme using the intra-pulse DFG and post-amplification proposes a new route to intense THz-to-MIR light sources with extreme phase stability.

1. *Efficient Terahertz Harmonic Generation with Coherent Acceleration of Electrons in the Dirac Semimetal Cd₃As₂: B. Cheng, N. Kanda, T. N. Ikeda, T. Matsuda, P. Xia, T. Schumann, S. Stemmer, J. Itatani, N. P. Armitage and R. Matsunaga, Phys. Rev. Lett. **124**, 117402 (2020).
2. *Room-temperature terahertz anomalous Hall effect in Weyl antiferromagnet Mn₃Sn thin films: T. Matsuda, N. Kanda, T. Higo, N. P. Armitage, S. Nakatsuji and R. Matsunaga, Nat Commun **11**, 909 (2020).
3. Opening a new route to multiport coherent XUV sources via intracavity high-order harmonic generation: N. Kanda, T. Imahoko, K. Yoshida, A. Tanabashi, A. Amani Eilanlou, Y. Nabekawa, T. Sumiyoshi, M. Kuwata-Gonokami and K. Midorikawa, Light: Sci. Appl. **9**, 168 (2020).
4. *Optical parametric amplification of phase-stable terahertz-to-mid-infrared pulses studied in the time domain: N. Kanda, N. Ishii, J. Itatani and R. Matsunaga, Optics Express **29**, 3479-3489 (2021).

Okazaki group

We have investigated superconducting-gap structures of unconventional superconductors by a low-temperature and high-resolution laser ARPES apparatus and transient electronic structures in photo-excited non-equilibrium states by a time-resolved ARPES apparatus using EUV and SX lasers. In the academic year 2020, we have found that Bose–Einstein condensation (BEC) superconductivity is induced by disappearance of the nematic state in FeSe by high-resolution laser ARPES. In addition, we

† Joint research with outside partners.

have revealed a characteristic electron-phonon coupling during the photo-induced insulator-to-metal transition in Ta₂NiSe₅ by a newly developed analysis method, frequency-domain angle-resolved photoemission spectroscopy (FDARPES), based on the measurements of HHG laser time-resolved ARPES.

1. †*Photoinduced Phase Transition from Excitonic Insulator to Semimetal-like State in Ta₂Ni_{1-x}Co_xSe₅ (x = 0.10): T. Mitsuoka, T. Suzuki, H. Takagi, N. Katayama, H. Sawa, M. Nohara, M. Watanabe, J. Xu, Q. Ren, M. Fujisawa, T. Kanai, J. Itatani, S. Shin, K. Okazaki and T. Mizokawa, *J. Phys. Soc. Jpn.* **89**, 124703 (2020).
2. Massive Suppression of Proximity Pairing in Topological (Bi_{1-x}Sb_x)₂Te₃ Films on Niobium: J. A. Hlevyack, S. Najafzadeh, M. -K. Lin, T. Hashimoto, T. Nagashima, A. Tsuzuki, A. Fukushima, C. Bareille, Y. Bai, P. Chen, R. -Y. Liu, Y. Li, D. Fl'ototto, J. Avila, J. N. Eckstein, S. Shin, K. Okazaki and T. -C. Chiang, *Phys. Rev. Lett.* **124**, 236402 (2020).
3. Bose-Einstein condensation superconductivity induced by disappearance of the nematic state: T. Hashimoto, Y. Ota, A. Tsuzuki, T. Nagashima, A. Fukushima, S. Kasahara, Y. Matsuda, K. Matsuura, Y. Mizukami, T. Shibauchi, S. Shin and K. Okazaki, *Sci. Adv.* **6**, eabb9052 (2020).
4. *Devil's staircase transition of the electronic structures in CeSb: K. Kuroda, Y. Arai, N. Rezaei, S. Kunisada, S. Sakuragi, M. Alaei, Y. Kinoshita, C. Bareille, R. Noguchi, M. Nakayama, S. Akebi, M. Sakano, K. Kawaguchi, M. Arita, S. Ideta, K. Tanaka, H. Kitazawa, K. Okazaki, M. Tokunaga, Y. Haga, S. Shin, H. S. Suzuki, R. Arita and T. Kondo, *Nat Commun* **11**, 2888/1-9 (2020).
5. *Detecting electron-phonon coupling during photoinduced phase transition: T. Suzuki, Y. Shinohara, Y. Lu, M. Watanabe, J. Xu, K. L. Ishikawa, H. Takagi, M. Nohara, N. Katayama, H. Sawa, M. Fujisawa, T. Kanai, J. Itatani, T. Mizokawa, S. Shin and K. Okazaki, *Phys. Rev. B* **103**, L121105 (2021).

Kimura group

Kimura group started in July 2020, and our group works on developing new microscopic imaging technologies using advanced X-ray sources: X-ray free-electron lasers, synchrotron radiation, and high-order harmonics of ultrashort infrared laser pulses. In 2020, we developed a new X-ray microscopic imaging system at BL25SU of SPring-8 and BL1 of SACLA. We designed and fabricated novel X-ray optical components, such as focusing mirror and microfluidic device, by utilizing ultra-precision fabrication, measurement techniques, and semiconductor manufacturing processes.

1. Chi-Feng Huang, Wei-Hau Chang, Ting-Kuo Lee, Yasumasa Joti, Yoshinori Nishino, Takashi Kimura, Akihiro Suzuki, Yoshitaka Bessho, Tsung-Tse Lee, Mei-Chun Chen, Shun-Min Yang, Yeukuang Hwu, Shih-Hsin Huang, Po-Nan Li, Peilin Chen, Yung-Chieh Tseng, Che Ma, Tsui-Ling Hsu, Chi-Huey Wong, Kensuke Tono, Tetsuya Ishikawa, and Keng S. Liang: C.-F. Huang, W.-H. Chang, T.-K. Lee, Y. Joti, Y. Nishino, T. Kimura, A. Suzuki, Y. Bessho, T.-T. Lee, M.-C. Chen, S.-M. Yang, Y. Hwu, S.-H. Huang, P.-N. Li, P. Chen, Y.-C. Tseng, C. Ma, T.-L. Hsu, C.-H. Wong, K. Tono, T. Ishikawa and K. S. Liang, *AIP Advances* **10**, 055219 (2020).
2. Micro-liquid enclosure array and its semi-automated assembling system for x-ray free-electron laser diffractive imaging of samples in solution: T. Kimura, A. Suzuki, Y. Yang, Y. Niida, A. Nishioka, M. Takei, J. Wei, H. Mitomo, Y. Matsuo, K. Niikura, K. Ijro, K. Tono, M. Yabashi, T. Ishikawa, T. Oshima, Y. Bessho, Y. Joti and Y. Nishino, *Review of Scientific Instruments* **91**, 083706 (2020).
3. A highly efficient nanofocusing system for soft x rays: Y. Takeo, H. Motoyama, T. Shimamura, T. Kimura, T. Kume, Y. Matsuzawa, T. Saito, Y. Imamura, H. Miyashita, K. Hiraguri, H. Hashizume, Y. Senba, H. Kishimoto, H. Ohashi and H. Mimura, *Applied Physics Letters* **117**, 151104 (2020).
4. Design of two-stage soft-X-ray nano-focusing system with a ring-focusing mirror and quasi-Wolter mirror: Y. Takeo, H. Motoyama, T. Shimamura, T. Kimura, T. Kume, Y. Matsuzawa, T. Saito, Y. Imamura, H. Miyashita, K. Hiraguri, H. Hashizume, Y. Senba, H. Kishimoto, H. Ohashi and H. Mimura, in: *PROCEEDINGS OF SPIE* (SPIE, 2020), 114920N.
5. Design of ultrashort Kirkpatrick-Baez mirror for soft x-ray nanofocusing: T. Shimamura, Y. Takeo, T. Kimura, H. Hashizume, Y. Senba, H. Kishimoto, H. Ohashi and H. Mimura, in: *PROCEEDINGS OF SPIE* (SPIE, 2020), 114920P.

* Joint research among groups within ISSP.

The Institute for Solid State Physics (ISSP), The University of Tokyo

Address 5-1-5 Kashiwanoha, Kashiwa, Chiba, 277-8581, Japan

Phone +81-4-7136-3207

Home Page <https://www.issp.u-tokyo.ac.jp>